The Effects of Aging and Tooth Loss on the Microstructure of the Mandible in South Africans

by

Charlotte E. G. Theye

A thesis submitted in fulfilment of the requirements for the degree

Doctor of Philosophy (PhD) Anatomy

In the Department of Anatomy, Faculty of Health Sciences,

University of Pretoria, South Africa

2022

Supervisors

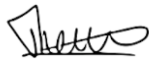Professor Anna C. Oettlé

Professor Maryna Steyn

Declaration of original work

I, <u>Charlotte Eugénie Gabrielle Theye</u>, declare that the thesis entitled,

The Effects of Aging and Tooth Loss on the Microstructure of the Mandible in South Africans

which I hereby submit for the degree of Doctor of Philosophy (PhD) in Anatomy at the University of Pretoria, is my own work and has not previously been submitted by me for a degree at this or any other tertiary institution.

Charlotte EG Theye

02/02/2022

Ethics statement

The author, whose name appears on the title page of this thesis, has obtained, for the research described in this work, the applicable research ethics approval. The author declares that he/she has observed the ethical standards required in terms of the University of Pretoria's Code of ethics for researchers and the Policy guidelines for responsible research.

Institution: The Research Ethics Committee, Faculty Health Sciences, University of Pretoria complies with ICH-GCP guidelines and has US Federal wide Assurance.
- FWA 00002567, Approved dd 22 May 2002 and Expires 03/20/2022.
- IORG #: IORG0001762 OMB No. 0990-0279 Approved for use through February 28, 2022 and Expires: 03/04/2023.

**UNIVERSITEIT VAN PRETORIA
UNIVERSITY OF PRETORIA
YUNIBESITHI YA PRETORIA**

Faculty of Health Sciences

Faculty of Health Sciences Research Ethics Committee

11 November 2021

**Approval Certificate
Annual Renewal**

Dear Ms CEG Theye

Ethics Reference No.: 340/2015
Title: The Effects of Aging and Tooth Loss on the Microstructure of the Mandible in South Africans

The **Annual Renewal** as supported by documents received between 2021-10-25 and 2021-11-10 for your research, was approved by the Faculty of Health Sciences Research Ethics Committee on 2021-11-10 as resolved by its quorate meeting.

Please note the following about your ethics approval:
- Renewal of ethics approval is valid for 1 year, subsequent annual renewal will become due on 2022-11-11.
- Please remember to use your protocol number (340/2015) on any documents or correspondence with the Research Ethics Committee regarding your research.
- Please note that the Research Ethics Committee may ask further questions, seek additional information, require further modification, monitor the conduct of your research, or suspend or withdraw ethics approval.

Ethics approval is subject to the following:
- The ethics approval is conditional on the research being conducted as stipulated by the details of all documents submitted to the Committee. In the event that a further need arises to change who the investigators are, the methods or any other aspect, such changes must be submitted as an Amendment for approval by the Committee.

We wish you the best with your research.

Yours sincerely

_____
On behalf of the FHS REC, Dr R Sommers
MBChB, MMed (Int), MPharmMed, PhD
Deputy Chairperson of the Faculty of Health Sciences Research Ethics Committee, University of Pretoria

The Faculty of Health Sciences Research Ethics Committee complies with the SA National Act 61 of 2003 as it pertains to health research and the United States Code of Federal Regulations Title 45 and 46. This committee abides by the ethical norms and principles for research, established by the Declaration of Helsinki, the South African Medical Research Council Guidelines as well as the Guidelines for Ethical Research: Principles Structures and Processes, Second Edition 2015 (Department of Health)

Research Ethics Committee
Room 4-60, Level 4, Tswelopele Building
University of Pretoria, Private Bag x323
Gezina 0031, South Africa
Tel +27 (0)12 356 3084
Email: deepeka.behari@up.ac.za
www.up.ac.za

Fakulteit Gesondheidswetenskappe
Lefapha la Disaense tša Maphelo

© University of Pretoria

Summary

The Effects of Aging and Tooth Loss on the Microstructure of the Mandible in South Africans

Charlotte E. G. Theye[1]

Supervisors: Professor Anna C. Oettlé[1,2], Professor Maryna Steyn[3]

[1]Department of Anatomy, Faculty of Health Sciences, University of Pretoria, Pretoria, South Africa

[2]Department of Anatomy and Histology, School of Medicine, Sefako Makgatho Health Sciences University, Pretoria, South Africa

[3]Human Variation and Identification Research Unit, School of Anatomical Sciences, Faculty of Health Sciences, University of the Witwatersrand, Johannesburg, South Africa

The mandible plays a crucial role in many biological functions (especially mastication, swallowing and speech) and its efficiency to perform these functions depends on its intactness. Aging and tooth loss are biological processes that may compromise the normal functioning of the mandible by changing its morphology. While many studies address the macroscopic mandibular variations, there is a paucity regarding its microstructure.

The aim was to investigate microstructural mandibular changes, with reference to the macrostructure, with advancing age and across various tooth loss patterns in South Africans. As the reasons why individuals are differently affected (extent, rate) by senescence or tooth loss are unclear, the influence of other biological factors (sex, ancestry) was also considered. Using micro-focus X-ray computed tomography (micro-CT) scans of 333 mandibles, external dimensions, and inner parameters, namely the cortical thickness (CtTh) and cortical density (approximated by histomorphometric parameters, BV/TV) were measured. To assess whether the mandible ages in the same way and rate as the rest of the skeleton, a comparison of

mandibular and femoral cortical BV/TV, using a micro-CT subsample of 68 individuals, was included.

A comprehensive assessment of the mandibular morphology and cortical microstructure of fully dentate individuals highlighted that the smaller the alveolar height is, the thicker and denser the cortical bone. An inner cortical asymmetry between basal, buccal, and lingual areas was described for CtTh, but was absent for BV/TV. Sexual dimorphism and ancestral variations were confirmed for the external distances and CtTh, but not for BV/TV. With tooth loss, a general decrease in external distances (aggravated by edentulism), CtTh and BV/TV was observed, except at the midline where the lingual CtTh increased with edentulism. Sexual dimorphism and ancestral variations of the external dimensions and CtTh were emphasised in edentulous mandibles. The cortical density decreased with aging, corroborating the general decline in bone mass of the skeleton, as noted in the femur. By contrasting the effects of tooth loss and aging, it was concluded that both external distances and CtTh were mainly influenced by tooth loss and not age, whereas the cortical bone density displayed an age-related decrease independent of tooth loss.

To ascertain the applicability of the findings in a dental setting, where cone-beam computed tomography (CBCT) is commonly used, measurements were performed on 24 mandibles scanned by both CBCT and micro-CT (considered as the reference). The accuracy and repeatability of CBCT was confirmed for large-scale measurements, and CtTh in a lesser manner, whereas results were uncertain for BV/TV, revealing a distinct lack of reliability.

In conclusion, this thesis inferred the precise role of aging and tooth loss, but also sex and ancestry, on the variations of the mandibular macro- and microstructure. Not only does knowledge and understanding of these changes have implications in dentistry fields, as cortical thickness and density are essential for many dental procedures; but also in biological anthropology, in which the microstructure of extant human mandibles gives valuable insights into intra- and interspecific variations (e.g., sexual dimorphism), or functional considerations (mastication, diet) of archaeological/fossil specimens.

Acknowledgements

et Remerciements

These PhD years were full of emotions, far from a smooth and quiet journey, but still interesting and exciting. It was a great learning opportunity, scientifically but also personally. The completion of this thesis would not have been possible without the support of many people. However, although the acknowledgements are usually the first thing read, they are one of the last things written, when tiredness is at its worst. I wish to apologise if I have forgotten anyone.

My first acknowledgements go to my supervisors who were always available to help and without whom, the completion of the thesis would not have been possible. I would like to express my deepest gratitude to Prof Anna Oettlé for her continual support, patience, and guidance. She has always made me feel welcome in South Africa, thanks to her selfless time, contagious enthusiasm, and assistance not only in the PhD, but also in all daily things. Thanks for including me in all these interesting projects, from Southern Implants and collaborating with dentists, to Bakeng se Afrika and Dirisana+. I would also like to express my deepest appreciation to Prof Maryna Steyn for accepting to co-supervise the PhD, and always sharing well-advised inputs and invaluable insights. I am particularly grateful for her help, patience, and support throughout the PhD.

I would like to extend my sincere thanks to Prof José Braga, who supervised my MSc and introduced the world of virtual anthropology to me. Without the first funding provided by the Erasmus Mundus Programme AESOP, coordinated by Prof Braga, this South African adventure would not have been possible.

I am particularly grateful to Prof Ericka L'Abbé for helping me at UP and including me in the activities of the Forensic Anthropology Research Centre, as well as in various projects, such as Bakeng se Afrika or Dirisana+.

This research was supported through several other funders that I wish to acknowledge, starting by AESOP and the postgraduate bursaries of the University of Pretoria. I am also particularly grateful to Prof Anna Oettlé, Prof Maryna Steyn and Prof Ericka L'Abbé for providing research funds for various fees or travelling over the years.

I also wish to express my thanks to André Hattingh and Southern Implants (particularly Tamsin Cracknell and Graham Blackbeard) for giving me the opportunity to work with them and explore a bit more in detail one of the possible applications of my thesis.

During the PhD, I was granted access to several facilities allowing my data collection and thus the completion of this research project. First, I would like to acknowledge the assistance and efforts received from the curators of the two osteological collections visited: Gabi Krüger at UP for the Pretoria Bone Collection, Brendon Billings and Jason Hemingway at Wits for the Raymond A. Dart Collection. I also wish to sincerely thank those who donated their bodies to science so that anatomical research could be performed. These donors and their families deserve our highest gratitude.

Necsa is another facility I spent a considerable amount of time, and this would not have been the same without Kobus Hoffman and Lunga Bam. Thank you for your assistance, the good mood, and the, always interesting, discussions. Thanks also to Frikkie de Beer who was always available to help and organise my visits.

I also had great pleasure working with André Uys from the Oral and Dental Hospital at UP, who helped me to have access to CBCT scans but also to the CBCT machine itself and scan bones instead of patients.

Thank you also to Volume Graphics for granting me a full licence of their 3D imaging software, VGStudioMax, for free so I could work directly from the office and from home.

I also would like to thank Marine Cazenave, Anna Oettlé, Clarisa van der Merwe and Clément Zanolli for sharing scans with me. I am particularly grateful to Jean Dumoncel for all the training and advice in 3D imaging and statistics over the years, and his availability for any questions I would have.

These past years would not have been the same without the support and friendship of everyone I met and could get to know in the old bone room or in Tswelopele. Special thanks to Amélie, Alieske, Alison, Clarisa, Clément, Gabi, Jean, Manon, Marie-Christine, Marine, Maritza, Meg-Kyla, Okuhle, Rachel, Reabe, Samuel… Thank you for all the cake days, early morning coffees, or late afternoon endless discussions! One last special thanks to Clarisa and Gabi, who were always available for my questions and willing to help me navigate the SA administrative labyrinth. I cannot wait to welcome you in France for some awesome winter and snowy holidays!

Un grand merci à Alison et Marine avec qui j'ai partagé ce long chemin vers la thèse et un bout de bureau pendant des années. Merci à Alison pour le soutien, les discussions et échanges quotidiens, ainsi que pour tous les moments partagés, particulièrement en conférence ! Marine, je retiendrais particulièrement nos Noëls et vacances ensemble, nos allers-retours à Necsa, le nombre incroyable de fois où l'on a pu se perdre sur les routes sud-

africaines (mais toujours en bonne humeur et souvent en chanson !). Je ne compte plus les aventures que l'on a partagé ensemble, merci !

Un merci tout particulier à Amélie pour son soutien et sa présence constante, ainsi que pour nos longues discussions et échanges portant sur à peu près tout et n'importe quoi ! Sa disponibilité, ses conseils et ses relectures attentives (et drôles !) ont été inestimables à la réalisation de cette thèse.

Merci à tous ceux, amis et famille (Anne-Lucie, Marie et Max, Laeti et Arnaud, Joris et Ludo, Yannick et Céline, Lorenzo et Thomas), qui sont venus et qui nous ont accompagné sur un bout de chemin dans la découverte de ce magnifique pays.

Je ne peux pas ne pas remercier tout particulièrement Anne-Lucie et Marie pour tous ces moments partagés ces dix (voire plus !) dernières années, ces discussions de tout, de rien, jour et nuit, ces appels visio de 8h… avec les milliers de kilomètres qui nous séparent.

À mes parents, car on a beau être adulte, crier haut et fort son indépendance, partir au bout du monde… On reste toujours l'enfant de ses parents. Merci pour la compréhension, le soutien de toujours, croyant parfois bien plus à ma réussite que moi-même. Un merci tout particulier à Carole et Corine, mais aussi Monique (et ses cartes postales !), J-B, et mes neveux et nièces Antoine, Daniel et Sarah pour leurs nombreux encouragements, et conversations toujours bienveillantes et souvent motivantes ! Une très grosse pensée pour Charlye et Sylvia. Sylvia, tu ne t'en souviens peut-être pas, mais je ne pourrais jamais assez te remercier d'avoir convaincu François de partager ce voyage à mes côtés. À très vite pour des supers vacances !

Enfin, merci à cette personne rencontrée il y a un peu plus de 14 ans, François, sans qui rien de ces dernières années n'aurait été possible, si tu ne m'avais pas suivie au bout du monde. Merci pour ton soutien dans les moments difficiles comme dans les moments de joie, tes encouragements permanents, et ton réconfort, même au plus profond de mes doutes. Merci de partager ma vie et de me suivre dans mes rêves les plus fous.

À mes grands-parents,

Table of Contents

3.2. Methods

Chapter 4. Results – Micro-CT analysis of the mandible

4.3. External distances

4.4. Cortical thickness

4.5. Histomorphometric parameters

Chapter 5. Results – Micro-CT analysis of the femur and comparison with the mandible

5.1. Femoral sample

5.2. Comparison between mandibular and femoral sample

Chapter 6. Results – CBCT analysis of the mandible and comparison with micro-CT

6.1. Manual comparison of measurements

6.2. Automatic comparison of volumes

List of Tables

4.5. Histomorphometric parameters

Chapter 5. Results – Micro-CT analysis of the femur and comparison with the mandible

5.1. Femoral sample

5.2. Comparison between mandibular and femoral sample

Chapter 6. Results – CBCT analysis of the mandible and comparison with micro-CT

6.1. Manual comparison of measurements

6.2. Automatic comparison of volumes

Chapter 1. Introduction

1.1. Background and rationale

The mandible participates in several essential biological functions of the human body, such as mastication, swallowing/deglutition, and speech. The "normal" functioning and efficiency of these physiological processes of utmost importance are highly dependent on the condition and "fitness" of the lower jaw (Posnick, 2014; Laguna *et al.*, 2017).

The loss of teeth is for example one of the principal causes of ineffective mastication (Fontijn-Tekamp *et al.*, 2000; Ikebe *et al.*, 2012; Scheid and Weiss, 2012; Bourdiol *et al.*, 2020), as even intermediate degrees of tooth loss may have substantial consequences and often prompts considerable morphological changes to the mandible (Kingsmill, 1999; White *et al.*, 2012). Tooth loss and more particularly edentulism are on the rise in many developing countries (Kailembo *et al.*, 2017; Al-Rafee, 2020). In recent years, middle- and low-income countries have been particularly affected by oral diseases, such as dental caries and periodontal diseases, which are generally considered to be the principal causes of tooth loss (either naturally or by extraction) (Watt *et al.*, 2015; Al-Rafee, 2020). In South Africa for example, the number of cases of dental caries and periodontal disease continues to increase yearly, albeit that they already are the most prevalent oral disease of the country (Bhayat and Chikte, 2019).

The mandible is known to have a continuing "growth" throughout adult life, which is considered as a normal maturational process by many authors (Bishara *et al.*, 1994; Akgül and Toygar, 2002; Albert *et al.*, 2007; Pessa *et al.*, 2008; Oettlé *et al.*, 2016). However, advancing age, even if often associated with tooth loss, is a confounding factor on its own and can independently cause many impairments in the ability to masticate or speak and articulate, notably because of age-related decreases in muscle and bone mass and the emergence of age-related pathologies (Newton *et al.*, 1993; Peyron *et al.*, 2004; Ikebe *et al.*, 2012; Laguna *et al.*, 2017; Park *et al.*, 2017). Due to the general aging of the world population, the number of patients affected by these age-related conditions is rising and is a growing concern for public health globally (United Nations, 2019).

Knowledge of the changes associated with aging, from adulthood to senescence, and understanding the effects of tooth loss on the mandible and its cortical microstructure are important and have implications in clinical fields, such as dentistry. For example, information

on the thickness and density of the cortical bone and their distributions within the mandible is crucial for common dentistry procedures like tooth extraction (Humphries, 2007), or for more complicated procedures, such as oral and maxillofacial surgeries, orthodontic treatments, and dental implants, among others. Besides dentistry fields, the morphology and microstructure of the mandible are also important for biological anthropology, especially in forensic, archaeological, or palaeoanthropological contexts. The mandible is a robust and particularly resistant bone with high rates of preservation and recovery (Standring, 2009; White *et al.*, 2012; Stodder, 2019), leading to a large number of mandibles found worldwide in archaeological and fossil records. A few fossil specimens affected by tooth loss or even edentulism have also been recovered (Russell *et al.*, 2013). In the literature, the archaeological/fossil specimens are usually compared to recent nonhuman and/or human primate samples to give insight into various topics, such as functional and biomechanical purposes (e.g., mastication, diet, speech), or intra- and interspecific variations (e.g., sexual dimorphism, taxonomic hypotheses).

In recent years, virtual exploration of cranial and mandibular structures has been employed extensively for anatomical and anthropological purposes. With the development of imaging technologies, from X-ray Computed Tomography (CT) to more advanced scanning modalities, such as Cone-Beam Computed Tomography (CBCT) or micro-focus X-ray Computed Tomography (micro-CT), researchers are now able to answer many more questions on bone and particularly on the quantification of its microstructure in a non-invasive and non-destructive way. While many studies exist on the external morphology and shape of the human mandible, its microstructure itself has not really garnered much attention, even if changes in the osseous external morphology are related to bone resorption events implying microstructural changes of the bone as well (Dechow *et al.*, 2010; Chrcanovic *et al.*, 2011; Swasty *et al.*, 2011; Williams and Slice, 2014). Furthermore, when finally considering the bone microstructure, the cortical bone seems to be disregarded by researchers, especially when compared to the number of studies on the trabecular bone. Moreover, the methodology often employed for microstructural bone analysis (both for trabecular and cortical bone) is usually based on small bone biopsies (González-García and Monje, 2013a, 2013b; Van Dessel *et al.*, 2013; Panmekiate *et al.*, 2015; Parsa *et al.*, 2015; Van Dessel *et al.*, 2017; Suttapreyasri *et al.*, 2018), which are not always able to capture the range of variations present in the mandible.

Overall, both for the outer and inner morphology of the mandible, many different modalities of measurements are mentioned in the literature and might not all be comparable to each other. For example, in terms of imaging modalities, CBCT, developed for clinical

2

dentistry applications, is widely used because of its many specificities and advantages, such as lower costs, reduced scanning time, and lower radiation doses (Danforth *et al.*, 2003; Scarfe *et al.*, 2006; Cotton *et al.*, 2007; Scarfe and Farman, 2008; Dawood *et al.*, 2009; Benavides *et al.*, 2012; Rios *et al.*, 2017). The accuracy and reproducibility of CBCT-based measurements have been confirmed when compared to traditional digital caliper measurements (Lascala *et al.*, 2004; Loubele *et al.*, 2007; Ludlow *et al.*, 2007; Kamburoglu *et al.*, 2011; Barreto *et al.*, 2020) and CT (Kobayashi *et al.*, 2004; Hilgers *et al.*, 2005; Loubele *et al.*, 2007). However, a lack of agreement and standardisation between the machines was pointed out by several researchers, with results highly dependent on the manufacturer or on the model (Liang *et al.*, 2010a; Parsa *et al.*, 2013; Pauwels *et al.*, 2015; Stimmelmayr *et al.*, 2017; Jacobs *et al.*, 2018; Gaêta-Araujo *et al.*, 2020). Furthermore, CBCT is usually characterised by a limited spatial resolution and artefact issues, which may hinder the analysis of the bone microstructure, especially in the case of small-scale measurements or parameters (Scarfe and Farman, 2008; Liang *et al.*, 2010a, 2010b; Maret *et al.*, 2012, 2014; Forst *et al.*, 2014; Rios *et al.*, 2017). Micro-CT, on the other hand, even if developed initially for industry, is now acknowledged as the reference imaging method for dental and bone research. For instance, contrary to CBCT, micro-CT was found to be very reliable across models and manufacturers (Olejniczak *et al.*, 2007). However, micro-CT is limited to ex-vivo research due to high radiation exposure, and cannot be directly used on living individuals (Burghardt *et al.*, 2011; Andronowski *et al.*, 2018).

In addition to the methodological issues highlighted above, several important limitations often encountered are directly associated to the samples studied and their composition. Many studies, both for the evaluation of the external and internal morphology of the mandible, are for instance limited in sample size with small samples not representative of the population, or samples restricted in their distribution in terms of biological (e.g., dentition status) and demographic factors (e.g., age, sex, ancestry).

One of the major problems encountered in several studies of the mandible is the fact that the dentition status of the individuals is not always comprehensively evaluated, or not even considered and just ignored. This may result in discrepancies and contradictions between findings from different studies. For instance, for studies on the mandible, some authors do not even indicate the general presence/absence of teeth (Bartlett *et al.*, 1992; İlgüy *et al.*, 2014; Ishwarkumar *et al.*, 2017; Motawei *et al.*, 2020), while others will at least detail if the sample is only composed of dentate individuals and exclude individuals with tooth loss (Fukase and Suwa, 2008; Shaw *et al.*, 2010, 2012; Swasty *et al.*, 2011; Cassetta *et al.*, 2013), or do the

opposite and only include edentulous individuals (Schwartz-Dabney and Dechow, 2002; Dutra *et al.*, 2006). However, most of the authors looking especially at the effects of tooth loss on the mandible, usually take into account the number of teeth, which was found to be not enough to reflect on the multiple possible patterns of tooth loss and their consequences (Oettlé *et al.*, 2009a). The precise distribution of the remaining teeth, as well as the occlusion patterns between maxillary and mandibular teeth, are of great importance (Oettlé *et al.*, 2009a; Mays, 2013, 2015a; Oettlé *et al.*, 2016; Parr *et al.*, 2017).

Besides the dentition status, another important limitation related to the sample is often the age of the individuals. It is difficult to discuss changes related to tooth loss without considering advancing age, often directly associated to the loss of teeth. As the precise effects of tooth loss are still debated for certain parameters, the distinction with the consequences of aging is even more complicated to do for a bone like the mandible. For instance, some studies will consider tooth loss only, without any available details on age (Cawood and Howell, 1988; Chrcanovic *et al.*, 2011), while others will outline the composition of their sample but omit age in the analyses or in the interpretations (Kingsmill and Boyde, 1998; Raustia *et al.*, 1998; Merrot *et al.*, 2005; Joo *et al.*, 2013). Furthermore, in articles supposed to focus on the aging process, some researchers based their analyses over a restricted time interval and therefore not covering the entire lifespan of the individuals (Bartlett *et al.*, 1992; Schwartz-Dabney and Dechow, 2003; e.g., Dutra *et al.*, 2004; Deguchi *et al.*, 2006; Swasty *et al.*, 2009; Leversha *et al.*, 2016; Ishwarkumar *et al.*, 2017). Compared to studies with comprehensive age distributions (e.g., von Wowern and Stoltze, 1980; Kingsmill and Boyde, 1998; Shaw *et al.*, 2010; Oettlé *et al.*, 2016; Parr *et al.*, 2017), inconsistencies and contradicting results might appear, both for the mandibular external morphology and the inner structure.

The reasons why some individuals are affected to a greater or lesser degree and at differing rates by tooth loss and/or advancing age are still not clear (Carlsson, 2004). Beyond the dentition status and the age of the individuals, other biological factors, such as sex and ancestry, are essential to consider and thus include all the variations encountered. Indeed, like the rest of the skeleton, the mandible is highly influenced by demographic factors (Albert *et al.*, 2007; Swasty *et al.*, 2009; Ruff, 2019), which are not always properly represented in the literature, particularly when considering the mandibular microstructure in the South African population.

Comprehensive studies considering all these interdependent factors (e.g., tooth loss, aging, sex, ancestry) and their interactions are rare to find in the literature on the mandible. For

instance, even if mandibular sexual dimorphism is well known and studied, most of the studies focusing on it do not really take into consideration tooth loss and often prefer to exclude individuals with high degree of tooth loss or edentulism, even if they represent a substantial part of the population nowadays.

1.2. Aims and objectives

The main aim of this study is to investigate, assess, and evaluate in detail, within a South African population, macrostructural and microstructural changes in the mandible with advancing age and across various patterns of tooth loss. Using high-resolution micro-CT scans, the study employs a unique methodology combining external dimensions with inner distances and 3D parameters, in order to provide a better understanding of the cortical bone microstructure in the mandible. This research focused particularly on the cortical bone with the analysis of its thickness and density, as these parameters reflect two fundamental bone properties, namely the cortical thickness and cortical bone density. Cortical thickness informs on the bone quality (via its geometry and distribution), while the bone density gives an indication of the bone quantity (i.e., the bone mass) (Agarwal, 2019; Ruff, 2019).

In addition, as it is not well known whether the mandible ages in the same way and at the same rate as the rest of the skeleton, the cortical microstructure of the mandible is compared to that of the femur. Used as a proxy for the rest of the skeleton, this gives additional information as to whether mandibular bone loss and changes in morphology are associated purely with tooth loss, or whether it is also associated with a generalised age-related tendency of bone loss in the skeleton.

As CBCT is the most widely used scanning technique in dentistry (and not micro-CT for safety reasons), another aim of the project is to compare the findings between modalities and confirm the feasibility and applicability, or not, of the micro-CT-based measurements in CBCT. While micro-CT is acknowledged as the gold standard modality for dental and bone microstructural research, the accuracy and reliability of CBCT is still questioned regarding small-scale measurements or microstructural parameters.

To achieve the aims mentioned above, several specific objectives were defined:

- To select a relevant sample (mandibles and corresponding maxillae from South African skeletal collections), depicting a wide range of tooth loss patterns – from completely dentate mandibles (category A) to edentulous mandibles (category C), using the Eichner Index. This tooth loss scoring method reflects individual masticatory performances and is based on the presence of occlusal contacts, explaining the importance of having access to each mandible with its associated maxilla.

- To constitute a large micro-CT scan database by imaging the selected mandibles, from which a reproducible data collection protocol is established in order to collect external measurements, cortical thicknesses and cortical densities:

  - To describe and quantify the changes of the external mandibular morphology in various patterns of tooth loss, with advancing age, sex, and ancestry.

  - To describe and quantify the changes in mandibular cortical thickness in various patterns of tooth loss, with advancing age, sex, and ancestry.

  - To describe and quantify the changes in mandibular cortical bone density (using histomorphometric parameters) in various patterns of tooth loss, with advancing age, sex, and ancestry.

  - To discuss these findings to enable reflection of the effects of tooth loss and aging on the mandibular macro- and microstructure within a South African population.

- To constitute a dataset of micro-CT-scanned femora from individuals of which mandibles have already been scanned (Eichner categories A and B only – no extreme tooth loss or edentulous to avoid any tooth loss-related bias):

  - To describe and quantify the changes in cortical density at the level of the femoral neck with advancing age, sex, and ancestry, and compare them with the changes noted in the mandibles of the same individuals.

  - To reflect on the age-related tendency of bone loss in the femur and to consider its relationship with tooth loss in the mandible by integrating these findings.

- To constitute a subsample of mandibles scanned by both micro-CT and CBCT:

  - To assess the accuracy and repeatability of the CBCT modality in measuring external distances, cortical thickness, and density by comparing CBCT-based and micro-CT-based measurements performed on the same skeletonised mandibles, using micro-CT as the reference.

1.3. Layout

This PhD thesis consists of eight chapters with, first, a general introduction in Chapter 1, followed by Chapter 2, a comprehensive review of the literature available on the mandible, its biological functions, its known macro- and microstructure, as well as some technical aspects on the 3D imaging modalities used. This chapter also highlights the knowledge gaps on the specific effects of tooth loss and advancing age on the cortical microstructure of the mandible, as well as the discrepancies in the results obtained. Chapter 3 presents the material selected, and the methodology designed to address the objectives, while Chapters 4 to 6 detail all the results obtained. These results are first presented for the mandible in Chapter 4, followed by results of the comparative study on the mandibular and the femoral microstructure in Chapter 5, and thirdly, results of the comparison between scanning modalities in Chapter 6. Finally, the integration of all these results, their interpretation and their discussion with the literature are done in Chapter 7. This chapter also develops possible implications of the thesis, with a particular focus on two practical applications, in dentistry and palaeoanthropology, of the methodology created during the thesis. Lastly, Chapter 8 concludes the thesis.

Chapter 2. Literature review

In the following literature review, the essential biological functions of the mandible, its known external morphology, as well as its bony microstructure are considered in [2.1]. Technical aspects, such as the two scanning modalities used in the thesis, are then briefly introduced in [2.2]. The expected effects of tooth loss and aging on the mandibular macro- and microstructure are discussed in [2.3], [2.4] and [2.5], along with the influence of non-mechanical factors, such as sex and ancestry. Indeed, the mandible, like the rest of the skeleton, is highly impacted by these systemic factors and their complex relationships (Swasty *et al.*, 2009; Ruff, 2019).

2.1. Functions and anatomy of the mandible

A brief overview of the biological functions of the mandible is first given, followed by a description of its external morphology, which is important to consider as a reference to where assessments of morphological changes are made to be. The muscle attachments are also considered, as biomechanical factors are pivotal in the external anatomy and microstructure of the mandible. Finally, the expected microstructure of bone in general, and of the mandible, is discussed as a starting point for the planned investigations.

2.1.1. Biological functions of the mandible

The mandible is highly involved in various essential physiological and functional processes of the human body, such as mastication and swallowing, but also speech. As detailed later in the Chapter (see section [2.1.2]), several muscles (and associated ligaments, tendons, nerves) have attachments on the mandible, assuring its mobility, and thus its different movements. Their coordinated actions ensure specific sequences of mechanisms, leading to effective masticating, swallowing or speaking abilities (Posnick, 2014; Lucas, 2016; Laguna *et al.*, 2017).

The beginning of the masticatory process is characterised by the opening of the mouth via movements of the mandible, i.e., depression and protrusion followed by elevation and

retraction, allowing the ingestion of food (Lucas, 2016). Mastication is then initiated with a succession of chewing cycles processing food into smaller-sized particles that are blended/mixed with saliva until forming a cohesive bolus, easy to swallow and digest (Lucas, 2016; Laguna *et al.*, 2017; Laird *et al.*, 2020). Each chewing cycle is defined by the opening and closing of the mouth, interrupted by lateral rotating movements. The next step is the swallowing of the bolus, from the mouth to the oesophagus and thus, the digestive apparatus.

Because of the high level of coordination in place during the feeding process, as soon as one mechanism is compromised, the entire masticatory capability is compromised and becomes less efficient (Posnick, 2014; Laguna *et al.*, 2017). For example, one of the principal causes of ineffective mastication is the loss of teeth (Fontijn-Tekamp *et al.*, 2000; Ikebe *et al.*, 2012; Scheid and Weiss, 2012). Indeed, teeth, by their number, occlusion patterns and location in the jaw, have a central role as soon as the masticatory process begins (Fontijn-Tekamp *et al.*, 2000; Herring, 2007; Nakatsuka *et al.*, 2010; Lepley *et al.*, 2011; Ikebe *et al.*, 2012; Posnick, 2014). Teeth are a unique "tool" in the mouth having the capability of efficiently breaking the food in swallowable reduced-sized particles (Posnick, 2014; Lucas, 2016; Laguna *et al.*, 2017). Attached to the mandible, the tongue also has a significant role during mastication, notably by mechanically manipulating the food, pushing and transporting it towards the swallowing step (Posnick, 2014; Lucas, 2016; Laguna *et al.*, 2017). The muscular anatomy, position and motor skills of the tongue have been found to be highly sensitive to tooth loss, particularly in extreme cases, such as edentulism (Bucca *et al.*, 2006). Indeed, as teeth are lost, the tongue starts to fill the empty space previously occupied by the missing teeth and becomes wider (Bucca *et al.*, 2006; Morelli *et al.*, 2011). This abnormal enlargement is called macroglossia and is often associated with an increase in volume of several muscles of the mouth, such as the genioglossus (Morelli *et al.*, 2011), with the accompanying elongation of the mental spines where it attaches (Jindal *et al.*, 2015).

Elderly individuals, apart from being more prone to tooth loss, are also more subjected to other age-related impairments of mastication, including a decline in saliva secretion, in tongue motor skills or even a decrease in bite force, which are not only linked to the general progressive age-related reduction in muscle mass, but additionally linked to the emergence of other age-related pathologies (such as osteoarthritis at the temporomandibular joints) (Newton *et al.*, 1993; Peyron *et al.*, 2004; Ikebe *et al.*, 2012; Laguna *et al.*, 2017; Park *et al.*, 2017; Bourdiol *et al.*, 2020).

9

In addition to the masticatory process, the mechanism of speech is also highly influenced by the mandible, its muscles and ligaments, particularly during the articulation phase (Daegling, 2012; Posnick, 2014). Indeed, the articulation process involves synchronised movements of the upper and lower jaws, tongue, and lips, in order to change the shape of the oral cavity and vocal tract, controlling the articulation of sound. The different components used during speech are impacted by each other's movements and positions, and if one of the components (such as the mandible) is unusually located or shifted forward (due for example to a variation in shape), the articulation can be affected (Posnick, 2014).

2.1.2. External anatomy of the mandible

2.1.2.1. Mandibular bone

The adult human skull, usually comprising 28 bones, can be subdivided into two principal parts: the cranium – with 27 of these 28 bones – and the mandible, the only mobile bone of the entire skull (e.g., White and Folkens, 2005; Standring, 2009; White *et al.*, 2012). The mandible, with its primary function of mastication, is the most inferior, largest, and strongest bone in the face. It consists of three elements (illustrated in Figure 2.1): the body (or corpus) which is horizontal U- or V-shaped, particularly dense and solid; and the two ascending paired rami on both left and right sides, considerably thinner than the body, each bearing a coronoid process (thin and triangular) anteriorly and a condyle (large and rounded) posteriorly. The left and right condyles articulate with the temporal bones of the cranium through the temporomandibular joints (TMJ), conferring its mobility to the mandible.

Borders can be naturally defined inferiorly and superiorly on the body and the ramus, but also anteriorly and posteriorly on the ramus. On the body, the superior border is specifically called the alveolar process and consists of alveoli and their associated teeth (see Figure 2.1). On the ramus, the superior border, often named the mandibular notch, separates the coronoid process from the condyle. On the other hand, the inferior border runs along the base of the body towards each ramus and forms the gonial angle at the intersection with their posterior borders.

A

coronoid processes
mandibular notch
mandibular condyles
mandibular teeth
alveolar bone
mental foramen
mental protuberance
masseteric tuberosities
gonial angle
body
ramus

B

coronoid process
mandibular condyle
condylar neck
mandibular teeth
sublingual fossa
mandibular foramen
mylohyoid groove
submandibular fossa
masseteric tuberosities
lingula
mylohyoid line
digastric fossa
mental spines

C

incisors
canine
premolars
molars
mental foramen
coronoid process
mandibular notch
mandibular condyle

Figure 2.1. Bony features of an adult mandible (3D model reconstructed from a micro-CT scan) in lateral [A], posterior [B] and superior [C] views.

Borders delineate two main surfaces on the mandible: external (also called buccal or lateral) and internal (also called lingual or medial), on which many specific bony features can be observed. First, on the external surface (Figure 2.1 A), the following characteristics are evident: (i) the mandibular symphysis (or midline), a faint ridge on the median line of the body indicating the fusion of the right and left halves of the mandibular bones during the first year of life; (ii) the mental eminence (or protuberance), a triangular shape forming the bony chin, located at the midline and almost on the inferior border; (iii) the mental foramen, an opening lodging the mental vessels and nerve, on both left and right sides, generally below the premolars; (iv) the oblique line, a faint ridge starting at the end of the anterior border of the ramus and running on the external surface of the body under the molar regions. Then, as illustrated in Figure 2.1 B, the following bony features are observed on the internal surface of the mandible: (i) the mylohyoid line, a ridge starting in the anterior part of the ramus (i.e., close to the molars) and descending towards the body; (ii) the submandibular fossa, below the mylohyoid line in the molar region, and impression of the submandibular salivary gland; (iii) the sublingual fossa, above the mylohyoid line, in the premolar region, and impression of the sublingual salivary gland; (iv) the digastric fossa, on the inferior border of the mandible, close to the symphysis; (v) the mental spines, protruding tubercles on the symphysis, almost on the inferior border; (vi) the mandibular foramen, a large opening in the centre of the ramus for the inferior alveolar vessels and inferior alveolar nerve going through the entire mandible via the mandibular canal. Leaving from the edge of the foramen, the mylohyoid groove is descending across the ramus, occupied by the mylohyoid vessels and nerve. The mandibular foramen presents on its edge a vertical bony projection, the lingula, which is the point of insertion of the sphenomandibular ligament.

2.1.2.2. Mandibular muscles

The mandible is a major actor in the masticatory system, particularly because of its unique mobility. To perform a wide range of movements (such as biting, chewing) and ensure the mobility of the mandible, four pairs of primary muscles of mastication have insertions on the mandible (illustrated in orange, Figure 2.2): temporalis, masseter, medial and lateral pterygoids. During the masticatory process, three of them are elevating the mandible (i.e., moving the mandible closer to the maxilla, closing the mouth): the masseter and medial pterygoid muscles particularly, but also the temporalis; while the lateral pterygoid muscle

keeps the temporomandibular joint immobile and stable with its superior head. The lateral pterygoid muscle is also a depressor (i.e., moving the mandible away from the maxilla, opening the mouth) via its inferior head, and is assisted by suprahyoid and infrahyoid muscles, such as the digastric muscle. Other movements are possible: protrusion (i.e., moving the mandible towards the anterior, with the lateral pterygoid muscles) or retrusion of the mandible (i.e., retracting it back, with the temporalis muscle, assisted by the digastric muscle), as well as lateral movements to the sides (by the asynchronous contraction of the masseteric and medial pterygoid muscles).
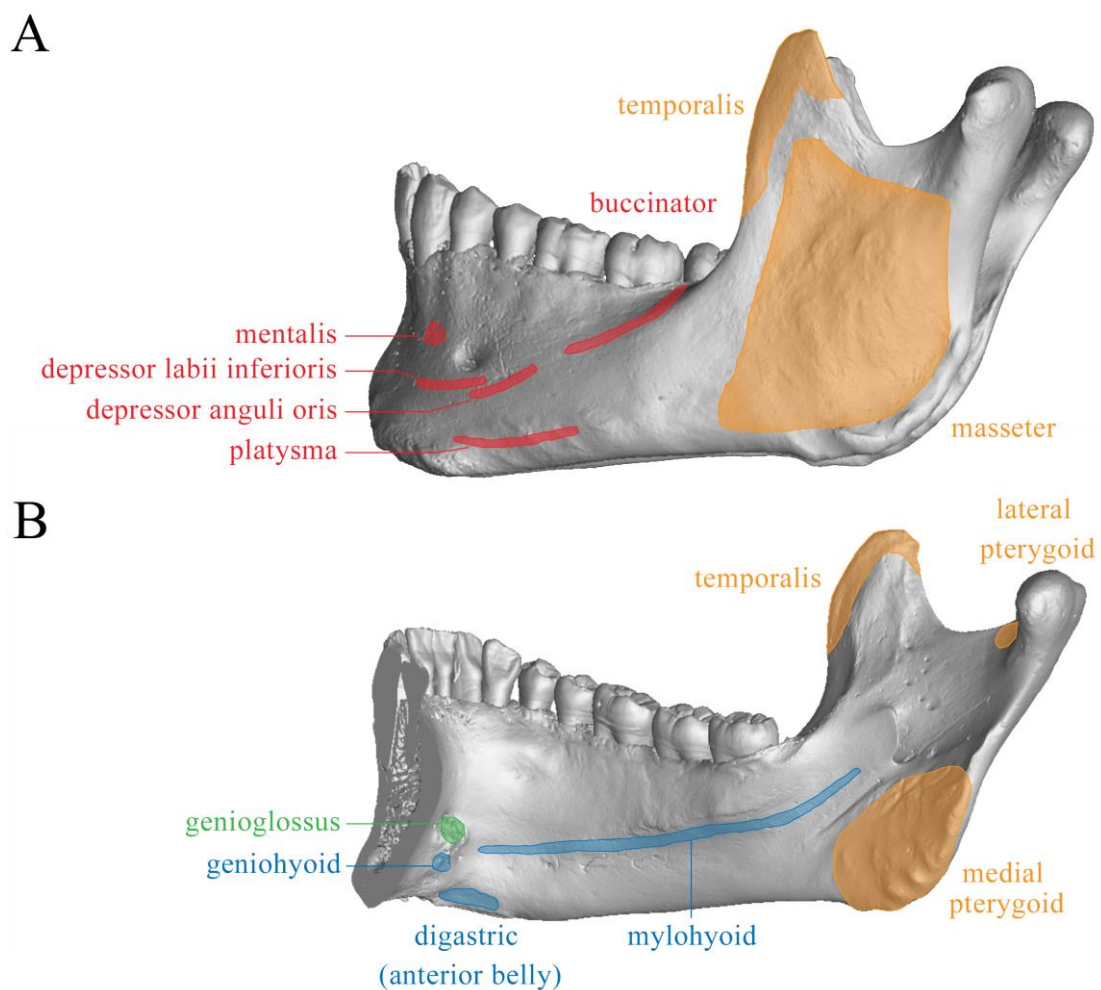
Figure 2.2. Muscle attachments on an adult mandible in buccal [A] and lingual views [B] (3D model reconstructed from a micro-CT scan). Insertions of the primary muscles of mastication are coloured in orange, while origins of facial expression muscles are in red, origins of suprahyoid muscles in blue and origins of the extrinsic muscles of the tongue in green.

The origins and insertions of the four primary muscles are listed below (Standring, 2009; White *et al.*, 2012; Netter, 2014): (i) the temporalis, a large muscle originating from the

temporal fossa of the cranium, and inserting on both external and internal surfaces of the coronoid process; (ii) the masseter, arising from the inferior aspect of the zygomatic arch, and attached to the entire external surface of the ramus and more particularly all along the posterior border of the gonial angle, where it forms the masseteric tuberosity. When the attachments are specifically strong and the tuberosities project laterally, the gonial angle is described as "everted". Still on the external surface of the ramus, but superiorly to the masseteric tuberosity, the attachment of the masseter causes a deepened mark, the masseteric fossa; (iii) the medial pterygoid, inserting on the internal surface of the ramus and more particularly along the posterior border of the ramus, above the gonial angle, where pterygoid tuberosities are found; (iv) the lateral pterygoid, attaching to the condyle in the pterygoid fovea of the condylar neck (area inferior to the rounded articular surface of the condyle).

Apart from the primary muscles of mastication, several other muscles (Standring, 2009; Netter, 2014), all originating on the mandible, can influence the mandibular morphology and are classified in three main groups: muscles of facial expression, suprahyoid muscles and extrinsic muscles of the tongue. Muscles of facial expression (in red, Figure 2.2 A) include: (i) the buccinator, causing the impression of the oblique line by its insertion on the mandibular bone, and compressing the cheeks (for smiling, holding food between teeth during chewing, etc.); (ii) the mentalis, originating in the incisive fossa of the mandible, and protruding the lips; (iii) the depressor labii inferioris and depressor anguli oris depressing the lips and the angle of the mouth; (iv) and the platysma, depressing the mandible by tensing the skin of the neck. The suprahyoid muscles (in blue, Figure 2.2 B), located on the floor of the oral cavity, elevate the tongue and the hyoid bone, while depressing the mandible, and comprise: (i) the mylohyoid muscle, causing the impression of the mylohyoid line with its insertion; (ii) the digastric muscle, and more particularly its anterior belly, attached to the digastric fossa; (iii) and the geniohyoid muscle, inserting on the symphysis and prompting the protrusion of the mental spines. Finally, the extrinsic muscles of the tongue (in green, Figure 2.2 B) include four different muscles altering the position of the tongue, but only one attaches to the mandible itself: the genioglossus, inserting on the mental spines.

2.1.3. Bone microstructure

Despite the great variability in external shape (long, flat, irregular, etc.), the organisation of the inner structure of bones, in general, is similar: a dense outer shell of cortical

(compact) bone surrounding and protecting an inner mass of less dense trabecular (cancellous, spongy) bone, where the bone marrow is stored (Standring, 2009; White *et al.*, 2012). The microstructural organisation of the mandible is not different from the other bones, as illustrated in Figure 2.3. The border between trabecular and cortical bone is delineated by the endosteum, the internal surface of the cortical bone; while on the external surface, the cortical bone is coated by a thin, highly vascularised tissue, the periosteum membrane, nourishing the bone itself during life.
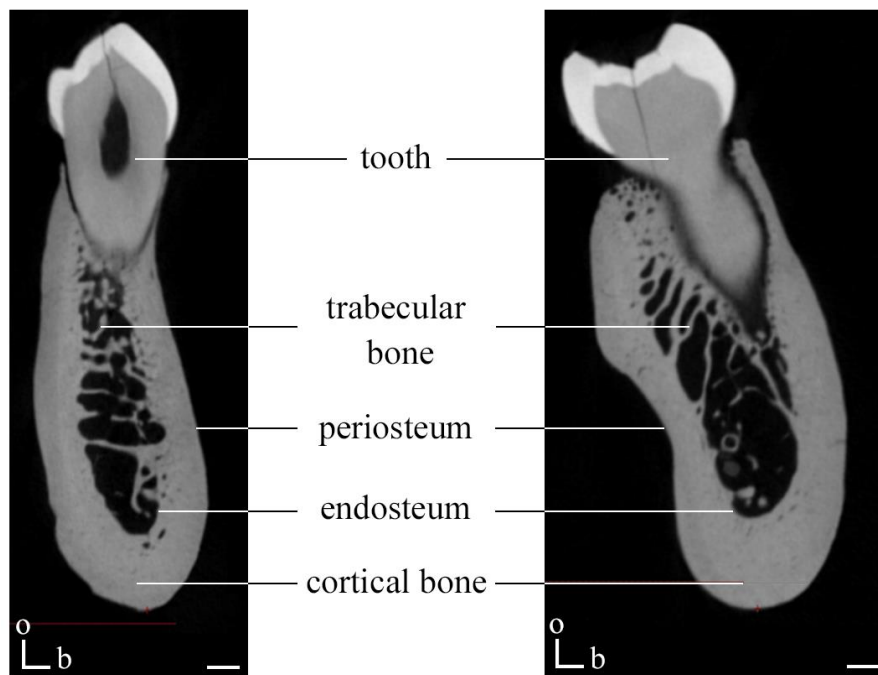
Figure 2.3. Micro-CT cross-sections of the corpus of an adult human mandible, at the level of the incisors (right) and molars (left). Orientation: o: occlusal; b: buccal. Scale bars: 2 mm.

At molecular and cellular levels, both cortical and trabecular bones have a similar composition, but they differ from each other in their physical organisation. Even if they both have a lamellar-type structure, the cortical bone is considerably less porous than the trabecular bone and so dense that it even needs a specific system – called Haversian system – to receive its nutrients from blood, as direct diffusion is not possible. These Haversian systems constitute a network of canals of various sizes, transporting and supplying blood and lymph through the cortical bone down to each osteocyte. The osteocytes have a crucial role in maintaining bone homoeostasis, notably by inducting a remodelling process through mechanotransduction (transmission of signals) (Frost, 2004; Pearson and Lieberman, 2004; Martin *et al.*, 2015; Andronowski, 2016). Two other primary bone cell types are participating in the formation and

renewal of the skeletal tissue: osteoclasts and osteoblasts. The osteoclasts are mainly responsible for the resorption of bone at specified locations, while osteoblasts, intervening after osteoclastic activities during remodelling, will deposit new bone tissue ("packets" of bone) in the same area. Maintaining the equilibrium between resorption and formation is a constant process throughout life and control of the osteoclastic and osteoblastic activities is of paramount importance for bone health and integrity (Martin *et al.*, 2015; Gocha *et al.*, 2019). Indeed, the mechanical functions of bone are maintained by the remodelling process, through the sequential steps of resorption and replacement of non-healthy bone tissue (old, diseased, fractured, micro-damaged, etc.) (Parfitt *et al.*, 1983; Parfitt, 1984; Andronowski, 2016; Barak, 2019). Remodelling is, however, only a microscopic process (at molecular and cellular levels) and does not affect the macroscopic architecture, i.e., the external bone morphology or size (Parfitt, 1984; Frost, 1990a; Andronowski, 2016; Barak, 2019; Gocha *et al.*, 2019). On the other hand, another process, known as bone modelling, can influence the microstructure as well as the outer shape and size of the bone in reaction to non-habitual loading (Frost, 1973, 1990b; Barak, 2019; Gocha *et al.*, 2019). Similarly, as for bone remodelling, the bone modelling process involves similar bone cell types (osteoclasts and osteoblasts), but without following a sequential pattern: bone resorption (or resorptive modelling) and deposition activities are now independent (in terms of time, location, etc.) (Pearson and Lieberman, 2004; Andronowski, 2016; Barak, 2019; Gocha *et al.*, 2019). Modelling is not just to maintain biomechanical functions as in remodelling, but also to adapt and improve the loading resistance of the bone in areas under high strains, for example. The concept of bone functional adaptation responding to an altered mechanical loading (also often referred as "Wolff's law", see Ruff *et al.*, 2006) states that, as loading on a particular bone increases, the bone will adapt over time to become stronger and to have a greater resistance to this particular sort of loading (Pearson and Lieberman, 2004; Ruff *et al.*, 2006; Hansson and Halldin, 2012; Andronowski, 2016; Barak, 2019; Ruff, 2019). Thus, bone modelling cause changes in the external morphology associated with adaptations in the trabecular and cortical microarchitectures (Gocha *et al.*, 2019).

Mastication, but also speech, and more particularly the articulation phase, generate various biomechanical stresses inducing many strains on the maxilla and on the mandible, and more specifically at the insertions of the muscles involved in the movements (Kasai *et al.*, 1996; van Eijden, 2000; Sato *et al.*, 2005; Herring, 2007; Daegling, 2012; Hansson and Halldin, 2012; Posnick, 2014; Toro-Ibacache *et al.*, 2016). The strains, different between these two types of activities (high-amplitude strains during mastication; vs. low-amplitude strains at

higher frequencies during speech), have both a strong influence on the trabecular and cortical microstructures (Kasai *et al.*, 1996; van Eijden, 2000; Herring, 2007; Daegling, 2012; Hansson and Halldin, 2012; Toro-Ibacache *et al.*, 2016). However, while the maxilla can transfer the mechanical loads to the rest of the cranium via its morphological integration, the mandible, due to its relative independence from the rest of the cranium, must sustain the entire force (Bastir and Rosas, 2005; Daegling, 2012; Toro-Ibacache *et al.*, 2016; Roberts, 2020). The lower jaw is, therefore, expected to be more sensitive to changes in biomechanical factors (e.g., tooth loss, diet) and undergo substantial adaptive changes compared to other bones (van Eijden, 2000). Von Cramon-Taubadel (2011) for example showed that the mandibular shape was correlated with diet, while the maxilla was not. Furthermore, the mandible displays an overall cortical and trabecular microstructural arrangement characteristic of bending and torsional loads, especially compared to the maxilla (Roberts, 2020). In other words, while the maxilla has generally a thin cortical bone associated with a fine network of trabeculae, the mandible has thick cortices interconnected by coarse strictly orientated trabeculae (Roberts, 2020). In addition, the mandible itself is subjected to different types of stress and loads depending on the region (i.e., wish-boning effects at the symphysis; bending, twisting, and shearing on the corpus; muscle atonement sites on the ramus), directly influencing the regional microstructure of the cortical and trabecular bone.

Influence of non-biomechanical factors (such as aging, sex, ancestry) is also explored and considered in later sections of this Chapter. Indeed, according to the principle of cellular accommodation (another bone modelling/remodelling theory) (Turner, 1999; Frost and Turner, 2000), bone cells react not only to mechanical changes but also to non-mechanical changes in their environment (such as varying hormone levels) and adapt their activities to face these changes. Several authors confirmed this theory (Pearson and Lieberman, 2004; Ruff *et al.*, 2006; Gocha *et al.*, 2019; Ruff, 2019) proposing that non-mechanical but systemic factors (not just hormones, but also genetics, sex, age, etc.) play a role in the modelling/remodelling process.

2.2. 3D imaging and macro- and microstructural quantification of bone

Three-dimensional (3D) imaging methods are based on the capability of X-rays to penetrate and propagate through an object, which will, according to its particular physical properties, attenuate X-rays to a greater or lesser degree (De Beer, 2018). The differences in attenuation of the beam going through the object are then mapped with different levels of grey values and are projected onto an X-ray sensitive detector system (e.g., an array, a panel…), generating a 2D radiographic projection of the object. The intrinsic characteristics of the panel detector, and particularly its pixel size, define the future resolution of the object imaged (i.e., small pixel sizes will give high-resolution images). The discovery and further refinement of this technology allowed the development of X-ray Computed Tomography (CT) imaging (Hounsfield, 1979), which computes altogether a large number of 2D radiographic projections of the same object. Using specific algorithms, these projections are then reconstructed into a stack of images (slices), from which a volumetric (i.e., 3D) representation of the object can be generated (Scarfe and Farman, 2008; Braga, 2016; De Beer, 2018), both characterised by their particular volumetric pixel (voxel) sizes.

In this thesis, the mandibular external morphology and inner structure are explored in detail thanks to the use of two advanced 3D scanning modalities: cone-beam computed tomography (CBCT) and micro-focus X-ray computed tomography (micro-CT). These two imaging methods, both non-invasive and non-destructive, and their most common applications are detailed in the following sections.

2.2.1. CBCT

As cone-beam computed tomography (CBCT) was first developed for dental and maxillofacial fields, it is entirely dedicated to the imaging of the maxillofacial region (Scarfe *et al.*, 2006; Scarfe and Farman, 2008; Dawood *et al.*, 2009). Since its invention, CBCT has been widely adopted and employed as it provides easier, safer and faster information on patients compared to conventional medical CT (Danforth *et al.*, 2003; Scarfe *et al.*, 2006; Cotton *et al.*, 2007; Scarfe and Farman, 2008; Dawood *et al.*, 2009). CBCT is used nowadays in many aspects of the clinical dental practice and has a particularly great impact in disease prevention, diagnosis, treatment planning, surgical guidance and delivery of patient dental care

(Scarfe and Farman, 2008; De Vos *et al.*, 2009; Benavides *et al.*, 2012; Rios *et al.*, 2017; Jacobs *et al.*, 2018). Indeed, CBCT can be used for the 2D and 3D evaluation and visualisation of various structures in almost all dentistry-associated specialities, such as (in decreasing order of application/use according to Rios *et al.* (2017)) in oral and maxillofacial surgery to locate and characterise the type of injuries/trauma, or to assess the presence and volume of cysts and tumours in oral and maxillofacial pathology (Stoetzer *et al.*, 2013); in endodontics to evaluate the anatomy of the pulp chamber, pulp canals and roots (Cotton *et al.*, 2007; Nair and Nair, 2007; Tyndall and Rathore, 2008); in implant dentistry, where CBCT helps to assess the alveolar bone microstructure, the presence/absence of fenestrations and dehiscences, as well as the pathways of nerves and arteries canals (Benavides *et al.*, 2012; Oettlé *et al.*, 2015; Rios *et al.*, 2017; Jacobs *et al.*, 2018); in orthodontics to evaluate the possible malocclusion or impaction of teeth for instance (Hechler, 2008; De Vos *et al.*, 2009; Lee *et al.*, 2015); in general dentistry and periodontics to detect and characterise caries, periodontal lesions and bony aspects of periodontal disease (Tyndall and Rathore, 2008).

However, compared to conventional CT machines, CBCT follows a peculiar procedure, as the X-ray source and sensors (detectors) themselves rotate around the object (i.e., the patient), which stays immobile (Danforth *et al.*, 2003; Scarfe *et al.*, 2006; Scarfe and Farman, 2008). More detailed information follows in the Materials and Methods Chapter, in which CBCT is discussed within context of the material and scanning procedure used in the thesis.

Due to its specificities, CBCT distinguishes itself from most of the other computed tomography-based modalities and displays several technical advantages: lower costs, easier accessibility and handling, reduced imaging time, and most importantly, lower radiation doses with a higher resolution than in medical CT (Danforth *et al.*, 2003; Scarfe *et al.*, 2006; Cotton *et al.*, 2007; Scarfe and Farman, 2008; Benavides *et al.*, 2012; Rios *et al.*, 2017). Furthermore, as in CT scans, various types of measurements can be performed on 2D sections, or directly on 3D models, extracted and generated from CBCT scans (De Vos *et al.*, 2009). Accuracy and reproducibility of CBCT measurements were tested and confirmed by comparing them to traditional digital caliper measurements performed on dry human skulls or mandibles (Lascala *et al.*, 2004; Loubele *et al.*, 2007; Ludlow *et al.*, 2007; Kamburoglu *et al.*, 2011; Barreto *et al.*, 2020); as well as comparing them to surface areas and diameters of root canals obtained via histologic sections of teeth (Michetti *et al.*, 2010). CBCT measurements were also compared to other imaging techniques such as CT and were found to be accurate and reliable (Kobayashi

et al., 2004; Hilgers *et al.*, 2005; Loubele *et al.*, 2007), even in the case of small-scale measurements, like cortical thicknesses (Loubele *et al.*, 2006; Benavides *et al.*, 2012).

On the other hand, one of the main concerns about CBCT imaging is the lack of agreement and standardisation between the models themselves. Indeed, measurements and outputs obtained from a specific CBCT unit will most likely be slightly different and not be applicable to the ones obtained with another unit from a different manufacturer (Liang *et al.*, 2010a; Parsa *et al.*, 2013; Pauwels *et al.*, 2015; Stimmelmayr *et al.*, 2017; Jacobs *et al.*, 2018; Gaêta-Araujo *et al.*, 2020). Limited spatial resolution, ranging generally between 0.08 mm and 0.4 mm (Scarfe and Farman, 2008; Jacobs *et al.*, 2018), is also a disadvantage when using CBCT, as reconstruction quality and precision of measurements on three-dimensional volumes are resolution-dependent.

2.2.2. Micro-CT

Micro-focus X-ray computed tomography (micro-CT) is a sophisticated X-ray technology rendering high-quality micron-level information of the interior and constitution of samples (Hoffman and De Beer, 2012; De Beer, 2018). Initially, micro-CT was developed for industry and only started to be considered and used for biological applications much later. From the 2000s, micro-CT became a proficient tool commonly used in animal and human studies for both dental and bone research (Swain and Xue, 2009; Burghardt *et al.*, 2011). Currently, the applicability of micro-CT in dental and bone research has evolved to such an extent that it is acknowledged as the gold standard modality not only for dental analysis (Olejniczak and Grine, 2006; Olejniczak *et al.*, 2007; Swain and Xue, 2009; Maret, 2010; Bayle *et al.*, 2011; Marciano *et al.*, 2012; Maret *et al.*, 2012, 2014) but also for bone microstructural assessment (Swain and Xue, 2009; Burghardt *et al.*, 2011; González-García and Monje, 2013a; Kim and Henkin, 2015; Parsa *et al.*, 2015; Andronowski *et al.*, 2018; Andronowski and Cole, 2020). Indeed, contrary to other scanning modalities such as CBCT, where results are highly dependent on the manufacturers or on the models (Gaêta-Araujo *et al.*, 2020), micro-CT was found to be very reliable across models and manufacturers (Olejniczak *et al.*, 2007). Actually, Olejniczak and colleagues (2007) performed various types of dental measurements (surface area, volume, linear measurements) on scans obtained from four different micro-CT machines and obtained comparable, repeatable, and reliable results across all systems.

Micro-CT is characterised by an immobile X-ray source and detector, while a high number of radiographic projections are captured during the rotation of the sample (Hoffman and De Beer, 2012; De Beer, 2018). Furthermore, the flat panel detectors equipping the micro-CT are of very high resolution, allowing the machine to reach much higher spatial resolution and lower voxel sizes than any medical counterparts (CT, CBCT, etc.). More detailed information follows in the Materials and Methods Chapter, in which micro-CT is discussed within context of the material and scanning procedure used.

In different ways than CBCT, micro-CT also has several disadvantages. First and most importantly, it cannot be directly employed on living individuals (for example, in the clinic) because of the high radiation exposure (Burghardt *et al.*, 2011; Hoffman and De Beer, 2012; Andronowski *et al.*, 2018). In addition, micro-CT is generally limited to small ex-vivo samples (teeth, biopsies, small bone, or scan focusing only on one part of a bigger bone, etc.) due to the size and technical restrictions of the machine itself (Burghardt *et al.*, 2011). Running costs as well as rarity of the machines might also impair and limit the access to micro-CT scanning.

2.2.3. Comparison between CBCT and micro-CT

As detailed before, both CBCT and micro-CT allow the visualisation and evaluation of external and internal tissue structures in 2D and 3D, however, CBCT might lack the discriminative abilities required to describe the inner structure of bone or teeth accurately and repeatedly, particularly because of a lower image resolution and artefacts issues (Scarfe and Farman, 2008; Liang *et al.*, 2010a, 2010b; Maret *et al.*, 2012, 2014; Forst *et al.*, 2014; Rios *et al.*, 2017) compared to micro-CT (as seen in Figure 2.4). Indeed, small-scale measurements, like cortical or enamel thicknesses, might not be performed with the best accuracy and repeatability required (Liang *et al.*, 2010a). As the methodology developed in this thesis might have implications in dentistry and associated specialities where CBCT is the preferred scanning modality, comparison of the two imaging techniques is of great importance to confirm the feasibility and applicability, or not, of the micro-CT-based measurements considered.
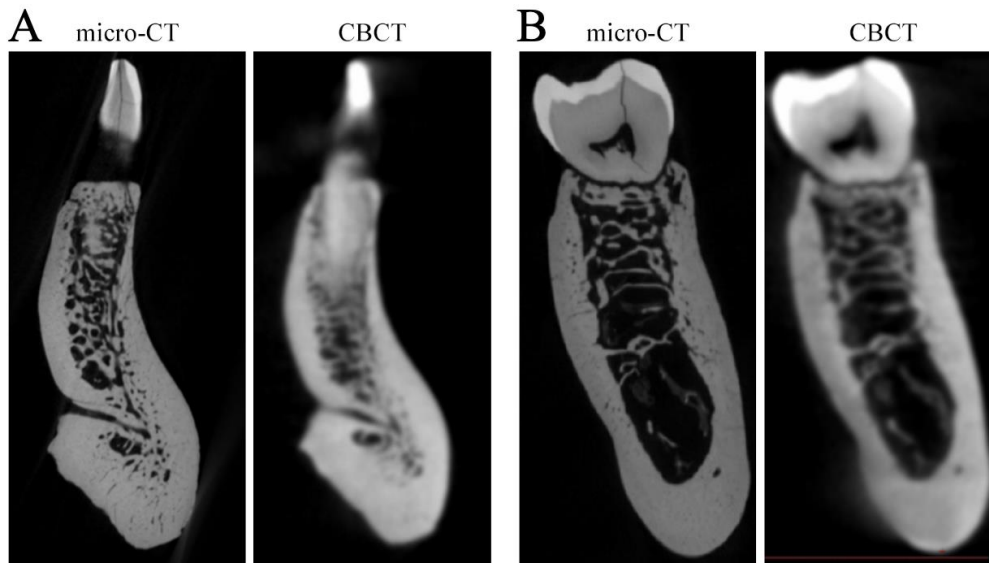
Figure 2.4. Micro-CT and CBCT cross-sections of the corpus of the same adult human mandible at the level of the incisors [A] and molars [B].

Over the last decade, in order to assess the reliability and accuracy of CBCT, many researchers focused on comparing methodologies and measurements, often using micro-CT as the reference. However, most of these studies were performed using dental samples only, and to a lesser extent using bone tissue. Indeed, comparison of CBCT to micro-CT was done extensively on dental samples confirming the accuracy and reliability of CBCT in different types of measurements, such as the volumes of teeth or dental linear distances (Olejniczak and Grine, 2006; Maret *et al.*, 2010, 2012, 2014; Michetti *et al.*, 2010; Wang *et al.*, 2011; Galibourg *et al.*, 2018; Kulczyk *et al.*, 2019). However, when using bone samples, only one study (Suttapreyasri *et al.*, 2018) was found in the literature comparing linear distances performed in CBCT and micro-CT. Indeed, when measuring cortical thicknesses in various regions of the mandible and maxilla using both modalities, Suttapreyasri and colleagues (2018) observed significant correlations between CBCT and micro-CT, and no significant differences between the two modalities. The rest of the literature in general focused on comparing CBCT against 2D techniques (radiographs, cephalograms, etc.) or CT (Kobayashi *et al.*, 2004; Hilgers *et al.*, 2005; Loubele *et al.*, 2007; Ludlow *et al.*, 2007; Barreto *et al.*, 2020); while micro-CT is often compared to the various sorts of CT (conventional CT, multiplanar CT, multislice CT, synchrotron radiation micro-CT [SR-XCT], etc.) or dual X-ray absorptiometry (DXA) (Naitoh *et al.*, 2004; Bodic *et al.*, 2012; Humbert *et al.*, 2016). Compiled together, these evaluations were rather inconclusive as CBCT compared to CT was found to be accurate and reliable even in the case of small-scale measurements (Kobayashi *et al.*, 2004; Hilgers *et al.*, 2005; Loubele *et al.*, 2006, 2007; Benavides *et al.*, 2012); while it was not always the case for CT compared

to micro-CT, especially in the case of small-scale measurements, like cortical thickness (Naitoh *et al.*, 2004; Humbert *et al.*, 2016). In both articles, the differences in cortical thickness between the modalities were hypothesised to be linked to a greater voxel size.

On the other hand, evaluation of trabecular and cortical bone density was performed more extensively and often directly compared between CBCT and micro-CT modalities. Traditionally, in CT, bone density was estimated from grey values which were quantified as absolute Hounsfield units (HU). However, several researchers raised concerns as HU do not seem to apply to CBCT and are not easily comparable, or even correlated to the relative grey values of CBCT voxels (Benavides *et al.*, 2012; Molteni, 2013; Campos, 2014; Cassetta *et al.*, 2014; Pauwels *et al.*, 2015; Vitral *et al.*, 2015; Rios *et al.*, 2017; Jacobs *et al.*, 2018). Researchers then started to evaluate bone density through the use of various bony structural parameters (Parfitt, 1988; Dempster *et al.*, 2013), also called histomorphometric parameters (e.g., BV/TV: bone volume fraction) and commonly used in micro-CT or histology (Pauwels *et al.*, 2015; Jacobs *et al.*, 2018). However, the accuracy and reliability of CBCT still remain uncertain as no real consensus was reached yet for these parameters. For instance, Suttapreyasri and colleagues (2018) directly compared grey values from CBCT to BV/TV values obtained from micro-CT scans of the same bone samples (biopsies) and did not find any significant correlation between them. However, when measuring BV/TV in both CBCT and micro-CT of the same sample, strong correlations were observed (Van Dessel *et al.*, 2013, 2017; Kim *et al.*, 2015; Parsa *et al.*, 2015; Tsai *et al.*, 2020), even if these correlations were accompanied by significant differences between both sets of BV/TV values (Van Dessel *et al.*, 2013, 2017; Kim *et al.*, 2015). Panmekiate and colleagues (2015) also had a moderate conclusion as they observed correlations between BV/TV calculated from CBCT and from micro-CT, but with large ranges of errors and deviations.

Furthermore, microstructural analyses by micro-CT or CBCT are often limited to bone biopsies (González-García and Monje, 2013a, 2013b; Van Dessel *et al.*, 2013, 2017; Panmekiate *et al.*, 2015; Parsa *et al.*, 2015; Suttapreyasri *et al.*, 2018) investigating the trabecular bone structure (Swain and Xue, 2009; Van Dessel *et al.*, 2013, 2017; Panmekiate *et al.*, 2015; Parsa *et al.*, 2015; Andronowski and Cole, 2020; Tsai *et al.*, 2020) and not the cortical bone. The cortical microstructure is perhaps not considered as being influenced by external factors, yet it has important implications for dentistry (Klemetti *et al.*, 1993; De Oliveira *et al.*, 2012; Pauwels *et al.*, 2015) and other relevant fields (Burghardt *et al.*, 2011; Andronowski and Cole, 2020).

2.3. Factors affecting the external morphology of the mandible

External morphological variations of the mandible are important to evaluate and consider to achieve a comprehensive understanding of the inner structural changes. In this thesis, specific external morphological measurements related to the inner parameters are considered, such as the length of the mandibular body (i.e., the distance between the menton and gonion), the midline (symphysis), anterior (around premolars) and posterior (around molars) corpus alveolar heights, as well as height and breadth of the ramus. To better understand the variations in the morphology and their relationship with the internal structure, factors affecting external features of the mandible need to be considered. First, the effects of tooth loss are reviewed, followed by the effects of advancing age, often associated with, and integrated with tooth loss. Finally, a brief overview of the influence of sex and population on the external morphology is presented.

2.3.1. Effects of changes in dentition

Tooth loss, a common pathology in humans, is considered to be one of the most important factors altering the morphology of the mandible during life (Kingsmill, 1999; Standring, 2009; White *et al.*, 2012). To comprehend the precise effects of tooth loss on the morphology of the mandible is pivotal, as even intermediate degrees of tooth loss might have significant consequences. In a substantial review, Kingsmill (1999) defined different factors influencing the remodelling of the mandible caused by tooth loss and classified them in four groups: functional, anatomical/physiological, inflammatory, and systemic. Functional factors were mostly associated with changes in mechanical stress and strain on the bone (e.g., innate muscle tone and activity, absence/presence of dentures, type of diet), whereas anatomical factors were associated to the facial form of each individual and the original size of the mandible (and thus, the size and attachment of muscles), as well as to the local bone quality (alveolar, cortical, trabecular, etc.). Inflammatory factors, on the other hand, are connected to tooth loss itself and its possible causes (such as the presence of periodontal diseases, caries), or its direct consequences (local trauma after tooth extraction, development of an infection, etc.). Eventually, these three types of factors are themselves all related to non-biomechanical systemic factors, such as the skeletal status of each individual, its hormonal and nutritional statuses, age, sex, ancestry, etc. In addition, social inequalities in oral health are well known

and demonstrated in all types of countries, as high-, middle- and low-income countries are all subjected to it (Cunha-Cruz *et al.*, 2007; Watt *et al.*, 2015; Shen and Listl, 2018). In the recent decades, middle- and low-income countries have been intensely affected by an increase in dental caries and in periodontal disease cases (Watt *et al.*, 2015). In South Africa for example, dental caries is the most frequent oral disease among children and adults, followed by periodontal diseases and their prevalence continues to rise every year (Bhayat and Chikte, 2019). The individuals' socioeconomic statuses are also of great importance when accessing professional dental care (Ayo-Yusuf *et al.*, 2013; Watt *et al.*, 2015; Shen and Listl, 2018). As a result, individuals from lower socioeconomic groups generally suffer from tooth loss at an earlier age, leading to consequent premature mandibular morphological changes compared to individuals having easier access to healthcare. Edentulism, the last stage of tooth loss, was for instance observed to be highly prevalent in lower socioeconomic groups (Cunha-Cruz *et al.*, 2007; Kailembo *et al.*, 2017; Al-Rafee, 2020) and on the rise in many developing countries (Al-Rafee, 2020).

Loss of teeth is accompanied by a reduction in strains in specific regions of the bone, and thus in the appearance of localised events of bone resorption (Pearson and Lieberman, 2004; Bodic *et al.*, 2005). The areas, directly impacted by tooth loss, such as the alveolar sockets, undergo a consequent remodelling process and are filled with new bone material instead of teeth. The change in properties leads to an increase in bone stiffness (i.e., its biomechanical strength, its ability to resist deformation) and hence a further reduction in biomechanical strains, resulting in an aggravation of bone loss/resorption (Bodic *et al.*, 2005; Hansson and Halldin, 2012; Mendelson and Wong, 2012). The total loss of teeth, known as edentulism, can lead to the most extreme changes of mandibular morphology (White *et al.*, 2012). In general, the entire mandible is reduced in volume (up to 60% of its initial volume), but the alveolar process is always particularly affected and resorbed (as seen in Figure 2.5) (Ulm *et al.*, 1992; Kingsmill, 1999; Bodic *et al.*, 2005; Chrcanovic *et al.*, 2011; Hansson and Halldin, 2012; Dekker *et al.*, 2018). Several vital structures, such as the mental foramen, are especially affected by edentulism. Indeed, as teeth are lost and the alveolar bone is resorbing, the mental foramen, usually on the lateral surface of the mandibular body, approximates the superior border, and can even be shifted completely onto the superior surface (Standring, 2009; White *et al.*, 2012).
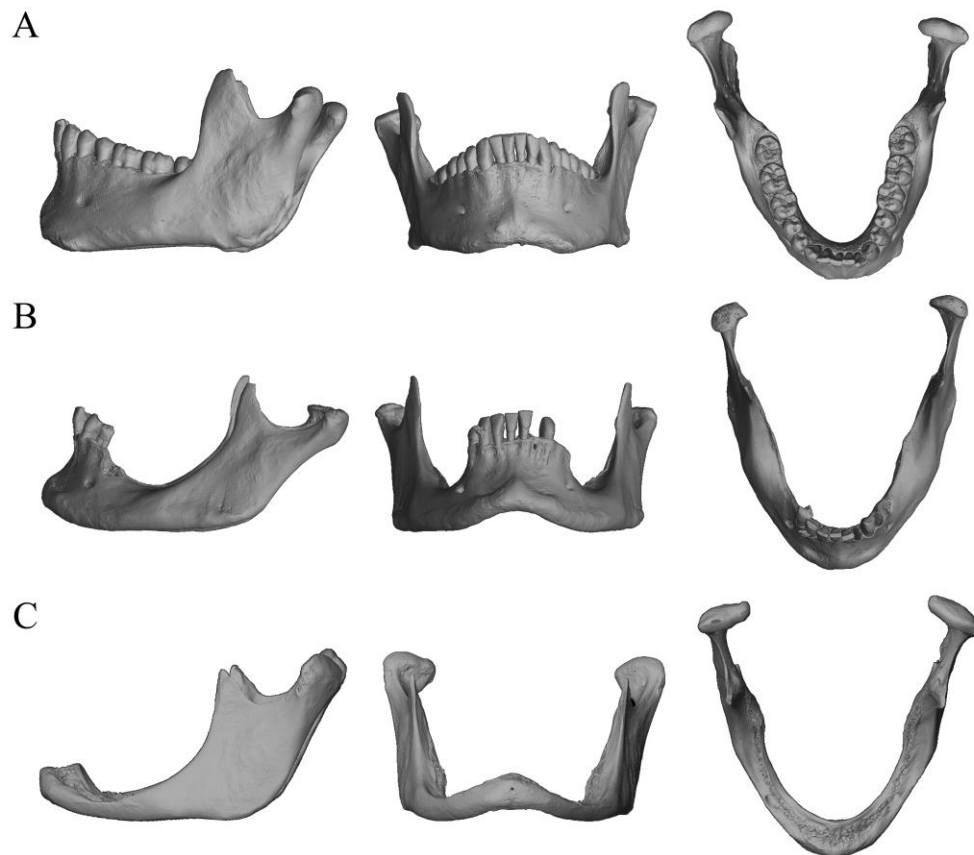
Figure 2.5. 3D models reconstructed from micro-CT scans of adult mandibles in lateral, anterior, and superior views: with complete dentition (Eichner category A) [A], advanced tooth loss (Eichner category B) [B] and edentulism (Eichner category C) [C].

Timing after tooth loss is also a critical parameter. Indeed, the highest rate of bone resorption was observed in the first few months after the loss of a tooth, and the majority of the bone resorption is taking place in the first year after the loss or the extraction of the tooth (Kingsmill, 1999; Bodic *et al.*, 2005). Local severe atrophy is, however, not typically observed during the first five years (Ozan *et al.*, 2013). In the case of total tooth loss, Raustia et *al.* (1998) showed that the duration of edentulism was associated with an increased bone resorption as well as with the alteration of the position of the mandible itself in relation to the glenoid fossa: the longer the individual is edentulous, the more anteriorly the condyle is positioned within the glenoid fossa, facilitating the development of prognathism (Kloss and Gassner, 2006).

When looking at more specific measurements and distances assessing the external morphology of the mandible, the literature is not always in agreement with the possible effects of tooth loss. A first example could be the mandibular body length, which was observed by some authors to increase (Enlow *et al.*, 1976; Parr *et al.*, 2017), decrease (Raustia *et al.*, 1998;

Chrcanovic *et al.*, 2011; Hutchinson *et al.*, 2015; Guevara Perez *et al.*, 2019) or even remain the same (Merrot *et al.*, 2005; Mays, 2013; Ozturk *et al.*, 2013) with tooth loss.

Contradictions were also found in articles looking at the effect of dentition changes on the mandibular angle. Indeed, with tooth loss, major consequences are expected for the mandibular angle area, as several masticatory muscles, such as the elevators, have the main part of their insertions on the ramus and are affected by the loss of teeth. For instance, the size of the masseter and medial pterygoid muscles was found to decrease significantly with tooth loss, due to the lack of occlusion (i.e., resistance) and thus the reduction in strains (Newton *et al.*, 1993; Raustia *et al.*, 1998). Coleman and Grover (2006) also noticed a general coarsening of the bony protuberances located at the insertion of these masticatory muscles, highlighting that significant changes were happening in the area. Most of the authors in the literature researched found that edentulous individuals had particularly obtuse angles compared to dentate individuals (Enlow *et al.*, 1976; Raustia *et al.*, 1998; Xie and Ainamo, 2004; Merrot *et al.*, 2005; Oettlé *et al.*, 2009a; Huumonen *et al.*, 2010; Chrcanovic *et al.*, 2011; Joo *et al.*, 2013; Oettlé, 2014; Hutchinson *et al.*, 2015; Oettlé *et al.*, 2016; Parr *et al.*, 2017), and that even with initial tooth loss, an increased angle was noticed (Oettlé *et al.*, 2016; Parr *et al.*, 2017). While the duration of edentulism does not seem to have an influence on the widening of the angle (Xie and Ainamo, 2004), the absence of particular teeth, such as the molars, was observed to be a very important factor (Oettlé *et al.*, 2009a). A few studies, however, did not find any significant changes to the mandibular angle with the loss of teeth (Israel, 1973; Dutra *et al.*, 2004; Chole *et al.*, 2013; Mays, 2013; Ozturk *et al.*, 2013).

The influence of tooth loss on the ramus itself was also extensively investigated and produced variable results when looking at its breadth or height: either a significant decrease in the ramus breadth was observed (Chrcanovic *et al.*, 2011; Parr *et al.*, 2017; Guevara Perez *et al.*, 2019), or no change at all (Merrot *et al.*, 2005). A similar pattern was seen for the ramus height: a decrease (Chrcanovic *et al.*, 2011; Ozan *et al.*, 2013) or no changes at all with tooth loss (Raustia *et al.*, 1998; Merrot *et al.*, 2005; Ozturk *et al.*, 2013; Parr *et al.*, 2017). One study however (Hutchinson *et al.*, 2015), using distances derived from landmarks, found an increase in ramus height in edentulous individuals compared to the partially dentate and the fully dentate groups.

On the other hand, the literature is generally in agreement with regard to the height of the mandibular body, which was always found to decrease following the loss of teeth. Mandibular body height might change drastically with tooth loss, while is of great importance

for mastication as shown by Fontijn-Tekamp *et al*. (2000), who observed a severe decline in chewing efficiency between individuals having a high symphyseal bone height (>16 mm) and individuals with a low symphyseal bone height (<15 mm). Dekker *et al.* (2018) even observed an association between mandibular height and duration of edentulism. The superior part of the body of the mandible, the alveolar process, is one of the most active sites in the skeleton in terms of bone turnover (Bodic *et al.*, 2005). Cawood and Howell (1988), dividing the mandibular body height horizontally, separately measured the alveolar and the basilar/basal processes, and found that the decrease in body height was only observed in the alveolar process, but not in the basilar process, which height remains unchanged. In the literature researched, the mandibular body height is generally measured at three locations all decreasing with tooth loss: either at the symphysis (or midline) (Merrot *et al.*, 2005; Mays, 2013; Ozturk *et al.*, 2013; Parr *et al.*, 2017); at the level of the mental foramen (Kingsmill and Boyde, 1998; Merrot *et al.*, 2005; Chrcanovic *et al.*, 2011; Hutchinson *et al.*, 2015); or more posteriorly in proximity of the molars (Raustia *et al.*, 1998; Mays, 2017; Parr *et al.*, 2017). Furthermore, depending on the number and position of teeth lost, the alveolar process might end up being very irregular with strong local resorption at each lost tooth location, or almost horizontal with a general and near complete resorption of all the alveoli (Kingsmill, 1999; Chrcanovic *et al.*, 2011; Hansson and Halldin, 2012; Mays, 2013). Mays (2017) particularly observed that the decrease accompanying tooth loss was mostly influenced by the number of lost molars, confirming that the molar region was generally the most affected by bone loss (Ulm *et al.*, 1992). Lastly, in their review, Hansson and Halldin (2012) highlighted the fact that in general, the diminution and the resorption were more important on the buccal side of the alveolar process than on the lingual side.

A first limitation concerning many articles from the literature reviewed previously could be the methodology used to evaluate the dentition status, as most of the authors directly counted teeth. Oettlé *et al.* (2009a) first raised an argument in disfavour of this particular method of only using the number of teeth when highlighting the difference between losing teeth unilaterally or bilaterally. They concluded that not only the number of teeth was important, but also their distribution. Later on, occlusion patterns between maxillary and mandibular teeth were observed to be of great importance, and different studies looking at the influence of tooth loss on the mandibular external morphology started to develop new ways of assessing the dentition status. For instance, Mays (2013, 2015a) considered "units" of teeth comprising of a pair of opposing teeth, while Oettlé *et al.* (2016) constituted dentition groups

according to a more complete pattern of tooth loss (number, location and occlusion). Finally, Parr *et al.* (2017) used the Eichner Index (Eichner, 1990) classifying maxillae and mandibles according to the presence of specific occlusal pairs, considering anterior teeth (incisors and canines), premolars, and molars as distinct occlusal support zones. The Eichner classification method, often used in the dentistry literature, has been proven to be related to masticatory performances, with a lesser number of occlusal contacts correlated to a reduction in bite force (Ikebe *et al.*, 2005, 2012; Nakatsuka *et al.*, 2010; Olofsson *et al.*, 2017), and could thus be a great alternative in anthropological studies.

Finally, the variability in the results might be explained by the fact that certain authors only considered one particular factor (such as tooth loss here), while others included in their analyses other variables possibly influencing the morphology of the mandible. For instance, while some articles did not even have any age data available (Cawood and Howell, 1988; Chrcanovic *et al.*, 2011), others did detail the composition of their sample, but only considered the dentition status as a factor, without including any age-related aspects (Kingsmill and Boyde, 1998; Raustia *et al.*, 1998; Merrot *et al.*, 2005; Joo *et al.*, 2013).

In conclusion, external morphological variations of the mandible are considerably affected by biomechanical changes, particularly when caused by tooth loss, but are also influenced by other types of factors. For instance, since the loss of teeth is usually associated with advancing age, it is difficult to discuss changes related to tooth loss without considering aging, a major confounding factor.

2.3.2. Effects of aging

Even after adulthood has been reached, some age-related changes of the facial skeleton are happening and are considered part of a normal maturational process of bones rather than growth (Bishara *et al.*, 1994; Akgül and Toygar, 2002; Albert *et al.*, 2007). The aging process of the facial skeleton has been extensively studied, mainly for plastic and reconstructive surgery purposes (Doual *et al.*, 1997; Coleman and Grover, 2006; Shaw and Kahn, 2007; Shaw *et al.*, 2010), and a main general pattern emerged: enlargement and expansion of the face with advancing age. Several reviews (Coleman and Grover, 2006; Kloss and Gassner, 2006; Albert *et al.*, 2007; Mendelson and Wong, 2012) highlighted the increasing vertical height of the facial skeleton with age and linked it particularly to changes in the lower region of the face. Indeed, the mandible was found to have a continuing "growth" throughout adult life, as observed in

various longitudinal studies focusing on adult individuals (Bishara *et al.*, 1994; West and McNamara, 1999; Akgül and Toygar, 2002; Pessa *et al.*, 2008). In their extensive review, Albert and colleagues (2007) summarised the age-related changes of the facial skeleton across the adult age span, starting in the 20- to 30-year-old decade with already a slight increase in the height of the lower facial skeleton accompanied by an increase in mandibular length. In the following decades, the mandibular length continued to increase while dento-alveolar regression was increasingly present, with possible remodelling of the alveolar bone and decrease of the dental arch lengths. Although Mendelson and Wong (2012) argued that this resorptive change occurs regardless of dental status, many factors, like tooth loss, are closely intertwined with aging. These factors might be biological (e.g., tooth loss, sex, ancestry, genetics, physiology, pathology, diet), but also environmental (e.g., socioeconomic status, living and working conditions in general), and might influence, or even directly affect, the aging process (Albert *et al.*, 2007).

Several cross-sectional studies also observed that the external mandibular morphology undergoes age-related changes and assessed these changes with specific measurements. As seen before with the longitudinal research, the length of the mandible was often measured and analysed. While some researchers (West and McNamara, 1999) found an increase with age, as stated before, others did not find any significant length changes with age (Ozturk *et al.*, 2013; İlgüy *et al.*, 2014; Hutchinson *et al.*, 2015; Ishwarkumar *et al.*, 2017; Parr *et al.*, 2017), or even observed a decrease (Shaw *et al.*, 2010). In connection with the mandibular length, another measurement, the mandibular/gonial angle, was also extensively investigated. While a few studies observed an increase in the mandibular angle with aging (Shaw *et al.*, 2010; İlgüy *et al.*, 2014; Hutchinson *et al.*, 2015; Leversha *et al.*, 2016), an even greater number did not find any significant change when only considering aging (Israel, 1973; Bartlett *et al.*, 1992; Dutra *et al.*, 2004; Xie and Ainamo, 2004; Dutra *et al.*, 2006; Oettlé *et al.*, 2009a; Chole *et al.*, 2013; Ozturk *et al.*, 2013; Oettlé *et al.*, 2016; Parr *et al.*, 2017). A number of researchers also focused on changes in mandibular body height, mainly because of its importance for mastication (Fontijn-Tekamp *et al.*, 2000). In a review, Kloss and Gassner (2006) observed that, generally, with age, the height of the mandibular body decreased, and that this phenomenon was more common in the posterior than in the anterior area of the body. Even if Bartlett et *al.* (1992) as well as Shaw and colleagues (2010) also found a decrease in body height, results are not in agreement since. For instance, no significant changes in mandibular body height with aging were found when measuring at the midline (chin) (Ozturk *et al.*, 2013; Parr *et al.*, 2017), or

when measuring posteriorly (at the level of the molars) (Mays, 2017). However, Swasty *et al.* (2009) noticed a decrease in mandibular body height, but thanks to a sample stratified in six age groups (from 10- to 65-year-olds), the authors could nuance and detail that, first, an increase was seen (late stages of adolescence, beginning of adulthood) and then, a decrease started to appear in the 40- to 49-year-old group. Finally, the mandibular ramus, also often analysed, was usually described by the assessment of two main features: its breadth and height. When considering only aging, two authors agreed on the absence of change in ramus breadth (Shaw *et al.*, 2010; İlgüy *et al.*, 2014), while Parr *et al.* (2017), measuring the maximum ramus breadth, found a significant increase. Analyses of the ramus height were even more contradicting, as several researchers (Ozturk *et al.*, 2013; Hutchinson *et al.*, 2015; Ishwarkumar *et al.*, 2017; Parr *et al.*, 2017) did not find any significant changes, others a decrease (Shaw *et al.*, 2010; Leversha *et al.*, 2016) or even an increase (West and McNamara, 1999; Motawei *et al.*, 2020).

All the studies reviewed so far, however, are influenced by the fact that many different modalities of measurements (caliper/mandibulometer, microscribe, radiographs, CT, CBCT, etc.) were used and that they might not be all comparable to each other. For example, when measuring the mandibular angle on CBCT, İlgüy and colleagues (2014) obtained different results than Parr *et al.* (2017) using a mandibulometer, or Ozturk *et al.* (2013) using a microscribe. Nonetheless, when assessing the mandibular length, those three authors found similar results despite their different techniques.

The inconsistencies might also be explained by the samples studied and their compositions. Indeed, some researchers claim to study the aging process, but perform age-related analyses on samples not covering the entire lifespan, or even just a very restricted interval. While one study (Ishwarkumar *et al.*, 2017) had a particularly restricted sample with radiographs from patients between 16 and 30 years old only, at least four other study samples had limited age distributions (Dutra *et al.*, 2004; Swasty *et al.*, 2009; Leversha *et al.*, 2016; Motawei *et al.*, 2020) with the youngest individuals of the sample in their forties only or the eldest in their sixties (40 to 79; 10 to 65; 16 to 69; 7 to 58 years old, respectively). Compared to studies such as Shaw *et al.* (2010), Oettlé *et al.* (2016) or Parr *et al.* (2017) having individuals comprehensively distributed until the tenth decade (20 to 93, 18 to 98, and 16 to 99 years old, respectively), discrepancies might occur.

Finally, other factors that might influence the morphology of the mandible were not always considered in studies performed. For example, the presence/absence or number of teeth

was not available at all in some of the studies cited above (Bartlett *et al.*, 1992; İlgüy *et al.*, 2014; Ishwarkumar *et al.*, 2017; Motawei *et al.*, 2020; Costa Mendes *et al.*, 2021) causing uncertainties in the interpretation of the results. The dentition status was briefly discussed in a few articles, but still restricted to certain groups, such as a sample only composed of edentulous individuals (Dutra *et al.*, 2006) or a sample excluding them (Shaw *et al.*, 2010). Recently, however, a larger number of authors studied age-related changes while integrating the dentition status of the individuals in their analyses (Xie and Ainamo, 2004; Chole *et al.*, 2013; Ozturk *et al.*, 2013; Hutchinson *et al.*, 2015; Oettlé *et al.*, 2016; Mays, 2017; Parr *et al.*, 2017). Particularly interesting results were found by Parr *et al.* (2017), as they detected significant changes of external morphology when considering separately tooth loss or aging, but did not find any significant differences at all with the interaction of age and dentition status. They concluded that most of the measurements were affected by tooth loss, while only a few by age.

However, the reasons why some individuals are affected to a greater extent and at a greater rate by the aging process or by tooth loss remain unclear (Carlsson, 2004). Other non-biomechanical factors, and their interactions, may be important and must be considered. For example, aging or tooth loss may not have similar consequences for males and females.

2.3.3. Sex and population variation

Sexual dimorphism is well known in the mandible and is often studied because of forensic archaeological and anthropological applications. Generally, in males, mandibles display larger dimensions, more robust morphological aspects, and more developed muscle insertion sites than in females. Some sex-specific features, like the chin, are often analysed and described as prominent, square-shaped (also bilobed) in males, whereas in females this region is more gracile and rounded (and even pointed) (Thayer and Dobson, 2010; Coquerelle *et al.*, 2011; Garvin and Ruff, 2012; Oettlé, 2014; Fan *et al.*, 2019). The sexual dimorphism in the mental protuberance was hypothesised to be linked to the difference in the mandibular arch: broad in males and much narrower in females (Franklin *et al.*, 2008a; Coquerelle *et al.*, 2011; Ramphaleng, 2015). Dimorphic features of the mandibles are also often located around the ramus, such as an elongated coronoid process, a deeper ante-gonial notch, a more pronounced gonial eversion and flexed ramus in males compared to females (Loth and Henneberg, 1998; Oettlé *et al.*, 2005, 2009b; Franklin *et al.*, 2007; Ramphaleng, 2015). These sex-specific features could be the result of very well-developed insertion sites of the mandibular muscles

on the ramus, such as the masseter and medial pterygoid (Franklin *et al.*, 2006; Bejdová *et al.*, 2013). Indeed, these mandibular muscles are particularly known to be larger in males than in females, causing different bite forces, which are then greater in males (Lavelle, 1988; Ferrario *et al.*, 2004; Mays, 2013; Posnick, 2014). Furthermore, it was confirmed by Sella-Tunis *et al.* (2018) that a significant correlation exists between the force of the mandibular muscles (and more particularly their cross-sectional area) and the overall shape of the mandible.

When assessing the influence of sex on specific measurements capturing the external morphology of the mandible without tooth loss, two patterns were generally observed (even when using different methodologies): either sexual dimorphism was detected with males having greater dimensions than females, or no significant differences between sexes were found. For instance, the mandibular body length was almost always found to be significantly greater in males than in females (Merrot *et al.*, 2005; Franklin *et al.*, 2008b; İlgüy *et al.*, 2014; Dong *et al.*, 2015; Ishwarkumar *et al.*, 2017; Sella-Tunis *et al.*, 2017; Gillet *et al.*, 2020), except for a few authors (Franklin *et al.*, 2006; Kharoshah *et al.*, 2010; Ozturk *et al.*, 2013) who did not find any sex-related difference. In a similar way, the mandibular body height is also in general greater in males than females, especially at the mental symphysis (Franklin *et al.*, 2006, 2008b; Swasty *et al.*, 2011; Ozturk *et al.*, 2013; Mays, 2017; Sella-Tunis *et al.*, 2017; Gillet *et al.*, 2020). However, two studies (Merrot *et al.*, 2005; Chrcanovic *et al.*, 2011) did not find any differences between males and females. On the ramus, and more particularly for the ramus breadth dimension, some authors detected greater values in males than in females (Kharoshah *et al.*, 2010; İlgüy *et al.*, 2014; Dong *et al.*, 2015; Sella-Tunis *et al.*, 2017), while others did not (Merrot *et al.*, 2005; Chrcanovic *et al.*, 2011). Ramus heights, however, were in general longer in males than in females (Merrot *et al.*, 2005; Franklin *et al.*, 2006, 2008b; Huumonen *et al.*, 2010; Joo *et al.*, 2013; Ozturk *et al.*, 2013; Dong *et al.*, 2015; Leversha *et al.*, 2016; Ishwarkumar *et al.*, 2017; Sella-Tunis *et al.*, 2017; Gillet *et al.*, 2020; Motawei *et al.*, 2020); only two studies did not find significant sexual dimorphism (Kharoshah *et al.*, 2010; Chrcanovic *et al.*, 2011). Finally, the mandibular angle, displaying a different pattern than the other measurements, was often found to be greater in females than in males (Xie and Ainamo, 2004; Merrot *et al.*, 2005; Huumonen *et al.*, 2010; Chole *et al.*, 2013; Joo *et al.*, 2013; Mays, 2013; Dong *et al.*, 2015; Leversha *et al.*, 2016; Sella-Tunis *et al.*, 2017), or did not vary between the sexes (Dutra *et al.*, 2004; Oettlé *et al.*, 2009a; Chrcanovic *et al.*, 2011; Ozturk *et al.*, 2013; İlgüy *et al.*, 2014; Gillet *et al.*, 2020).

Most of the literature focusing on mandibular sexual dimorphism and summarised before did not take into consideration tooth loss. Indeed, as the effects of tooth loss on the mandibular morphology and its sex-related differences are not completely understood, a number of authors prefer to exclude individuals with high degree of tooth loss or edentulism, even if they represent a substantial proportion of the population. The literature is not always in agreement, but females might be more affected by tooth loss than males, and even edentulism (Al-Rafee, 2020), as they are for example more prone to periodontal diseases (Kailembo *et al.*, 2017). Thus, even if the mandible appears to maintain a global sexually dimorphic morphology and shape with tooth loss (Oettlé, 2014; Ramphaleng, 2015), some measurements might be affected differently in males and females. For instance, comparing dentate and edentulous individuals, Merrot *et al.* (2005) observed a change in mandibular length with tooth loss, as males and females were significantly different in dentate, but not in edentulous individuals. Almost the opposite result was found by Parr *et al.* (2017) as they detected an increase in length with tooth loss only in males and not in females, increasing the degree of sexual dimorphism. The mandibular body height was also affected by this increase in sexual dimorphism with tooth loss, as the general decrease caused by tooth loss was observed to be more important in females than in males (Mays, 2013, 2017; Parr *et al.*, 2017), which might be explained by the quicker and more important alveolar bone resorption occurring in females compared to males after tooth loss (Mays, 2015b, 2017). When analysing the mandibular angle, Parr *et al.* (2017) observed significant changes with tooth loss only in males, while Xie and Ainamo (2004) found a "loss" of sexual dimorphism with tooth loss, also confirmed by Oettlé *et al.* (2016), who noted that the sexual dimorphism was present as long as tooth loss was limited. The opposite consequence was noticed for the ramus height, where sexual dimorphism appeared in edentulous individuals, but was not present in individuals without any tooth loss (Chrcanovic *et al.*, 2011). This increase in sex-related differences with tooth loss was also reported by Mays (2013) and Joo *et al.* (2013) as they observed significant decreases of ramus height in females, and not in males.

However, to nuance the findings above, several studies comparing dentate and edentulous individuals did not observe changes in sexual dimorphism with tooth loss for some measurements, such as the body height (Merrot *et al.*, 2005; Chrcanovic *et al.*, 2011), the ramus breadth or height (Merrot *et al.*, 2005; Huumonen *et al.*, 2010) and the mandibular angle (Merrot *et al.*, 2005; Huumonen *et al.*, 2010; Chrcanovic *et al.*, 2011).

In addition to tooth loss, the aging process may be a source of variability between males and females. Indeed, as summarised in the review published by Mendelson and Wong (2012), with age, sex-related differences in rates and in extent of change are observed on the facial skeleton. Later on, Gillet *et al.* (2020) confirmed these findings and added that sexual dimorphism increased with aging, as they obtained better accuracy rates of sex estimation from the mandible in older individuals than in the younger groups (<40 years old). Measuring the mandibular angle, Xie and Ainamo (2004) also observed that the sexual dimorphism was more important in older dentate than in younger individuals. Another study (İlgüy *et al.*, 2014) nuanced these results as they found that, with age, the changes in gonial angle were only significant in females, and thus, resulting in a greater sexual dimorphism. Almost similar outcomes were obtained for the mandibular body height by different authors: Parr *et al.* (2017) who observed a significant decrease in body height with age in females only; and Mays (2017) who showed the presence of a significant negative age-related correlation in females only.

In the literature, the sexual dimorphism observed in the mandible was also found to be influenced by the ancestry of the individuals analysed and might be more or less marked depending on the population groups (Humphrey *et al.*, 1999; Franklin *et al.*, 2008a; Garvin and Ruff, 2012; Bejdová *et al.*, 2013; Oettlé, 2014). Franklin *et al.* (2008a) explained that this ancestral variability in the pattern and degree of sexual dimorphism was strongly influenced, and might even be due to many factors (e.g., biological, systemic, environmental, cultural). Interestingly, Bejdová and colleagues (2013) confirmed the influence of external factors but also highlighted the fact that size changes in males reflected the changes in external conditions (environment, climate, diet, etc.) to a lesser degree than in females, which were more sensitive to it.

A large number of studies, mostly for forensic purposes, used virtual methods (e.g., CT, CBCT, surface scanner, microscribe) and analysed sexual dimorphism patterns in different populations worldwide, such as Brazil (Gamba *et al.*, 2016), China (Dong *et al.*, 2015; Zheng *et al.*, 2018), Czech Republic (Bejdová *et al.*, 2013), Egypt (Kharoshah *et al.*, 2010), France (Coquerelle *et al.*, 2011), Israel (Sella-Tunis *et al.*, 2017), the United States (Garvin and Ruff, 2012), but also South Africa (Franklin *et al.*, 2006, 2007, 2008a, 2008b; Nicholson and Harvati, 2006; Oettlé, 2014; Ramphaleng, 2015). In comparison with European populations, Ramphaleng (2015) observed that South Africans showed similar sex-related mandibular shape characteristics, which confirmed what was reported by Franklin *et al.* (2007) with South African and North American populations. They, however, emphasised the fact that

populational variability was seen in the pattern and extent of the expression of these dimorphic features. For instance, Franklin *et al.* (2007) found that South African individuals displayed greater size dimorphism than North Americans. In another article, Franklin and colleagues (2008b) also observed variations albeit rather slight, in expressing sexual dimorphism within South African populations themselves.

While not considering sexual dimorphism at all but studying several worldwide populations, Nicholson and Harvati (2006) observed that the mandibular shape displayed strong geographic patterns, influenced by climatic and functional adaptations (to diet and precise masticatory demands for example). Pooling males and females, Franklin *et al.* (2007) showed shape differences (but not size) between Black individuals from South Africa and White individuals from the United States, particularly regarding the ramus (shorter and broader in South Africans) and the symphysis (higher in South Africans). Within South Africa itself, ancestral variations in the external morphology were observed by several authors and summarised by Oettlé (2014). These variations were especially seen in the breadth and width of the mandible, the shape of the ramus, as well as the shape of the chin. In general, South African individuals of African ancestry had longer and narrower mandibles, more rounded chins with less marked mental tubercles, and displayed more often prognathic features than what was observed in South Africans of European ancestry (Oettlé *et al.*, 2009a; Oettlé, 2014), or in North American of European ancestry (Franklin *et al.*, 2007).

As seen in this entire section, changes in the gross morphology of the mandible are associated with bone resorption events, implying the presence of changes in the microstructure of the bone as well (Dechow *et al.*, 2010; Chrcanovic *et al.*, 2011; Swasty *et al.*, 2011; Williams and Slice, 2014).

2.4. Factors affecting the cortical thickness of the mandible

As seen in the previous section, the external morphology of the mandible is known to be highly variable because of a number of possible factors, but the literature has also shown that its inner structure (cortical and trabecular bone) reflects this variability (Bodic *et al.*, 2005; Swasty *et al.*, 2009, 2011; Dekker *et al.*, 2018; Gocha *et al.*, 2019). Indeed, depending on the biomechanical forces applied on the bone, the trabecular structure will first undergo adaptive changes, followed by the cortical bone (Gocha *et al.*, 2019). One way of assessing these variations in cortical bone is to measure its thickness, which gives a direct indication on the inner geometry of the bone (Ruff, 2019). In the literature, the thickness of the cortical bone is standardly defined as the thickness from periosteum (the outer layer) to endosteum (the endocortical surface) (see Figure 2.3) (Swasty *et al.*, 2009; Dechow *et al.*, 2010).

In this thesis, the cortical bone thickness is considered throughout the entire mandible: corpus (midline or symphysis, anterior, posterior) and ramus, as well as basal, buccal and lingual sides, so as to provide a comprehensive perspective of the mandibular cortical bone distribution. In the following sections, a review of the regional variations in cortical thickness is first provided. The changes accompanying tooth loss are then considered in detail, followed by the effects of advancing age, often associated, and integrated with tooth loss. Finally, a brief overview of the influence of sex and population variation on the thickness of the mandibular cortical bone is done.

2.4.1. Regional variations within the mandible

Several authors showed that the mandibular cortical bone thickness is related to the mechanical loads and strains exerted by mandibular muscles, notably during mastication (Kasai *et al.*, 1996; Daegling, 2007; Holmes and Ruff, 2011; Swasty *et al.*, 2011; Gröning *et al.*, 2013), and thus that variations in cortical thickness at specific locations can provide unique insights about the biomechanical stresses experienced (Swasty *et al.*, 2011; Gröning *et al.*, 2013). Conducting a finite element analysis, Gröning *et al.* (2013) demonstrated that the cortical bone distribution pattern in the mandible reflected the strain distribution, and more particularly that maximum strains were associated with increased thickness.

37

When considering regional variations in cortical bone, the literature agrees on the fact that cortical thickness is similarly and symmetrically distributed when comparing left and right sides of the mandible (Knezović-Zlatarić and Čelebić, 2005; Deguchi *et al.*, 2006; Ono *et al.*, 2008; de Souza Fernandes *et al.*, 2012). However, within one side of the mandible, different types of asymmetries are reported and are thought to be directly linked to the specific distributions of strains during use (Daegling and Hotzman, 2003; Gröning *et al.*, 2013). Firstly, as observed by many authors (Daegling and Grine, 1991; Kasai *et al.*, 1996; Schwartz-Dabney and Dechow, 2003; Fukase, 2007; Humphries, 2007; Swasty *et al.*, 2009, 2011; Cassetta *et al.*, 2013), the thickest cortical bone is located at the base of the mandible (the inferior border), which is an area known to be of depository nature throughout life (Enlow *et al.*, 1976) and subjected to particularly high strains (Gröning *et al.*, 2013).

The second asymmetry often studied concerns the antero-posterior uneven distribution of cortical bone. Indeed, several authors (Carter *et al.*, 1991; Kasai *et al.*, 1996; Masumoto *et al.*, 2001; Katranji *et al.*, 2007; Farnsworth *et al.*, 2011; Al-Jandan *et al.*, 2013; Cassetta *et al.*, 2013; Ko *et al.*, 2017), using several different modalities (caliper, radiograph, CT, CBCT), noticed that the cortical bone was particularly thick in the posterior area of the corpus, below the molars, when compared to the anterior region and even more so to the symphysis. A few articles, however, nuanced this finding, as even if this pattern is always found on the buccal side of the mandible, it is not the case on the lingual side, where the difference is either less clear (Fayed *et al.*, 2010; Kim and Park, 2012; Zhang, 2012; Sathapana *et al.*, 2013; Grover and Gupta, 2021) or absent (Swasty *et al.*, 2011).

Finally, bucco-lingual asymmetrical patterns were also reported in the literature. At the mandibular symphysis, the lingual bone is thicker than the buccal cortex (Kasai *et al.*, 1996; Kingsmill and Boyde, 1998; Daegling and Hotzman, 2003; Fukase, 2007; Katranji *et al.*, 2007; Fukase and Suwa, 2008; Swasty *et al.*, 2009, 2011), most certainly because of the presence of the mental spines in the area (Kingsmill and Boyde, 1998). However, when moving from the symphysis towards the anterior corpus, the lingual thickness gradually decreases until eventually the buccal bone becomes the thickest. For instance, while at the level of the canines, the thickness is still greater lingually than buccally (Kasai *et al.*, 1996; Kingsmill and Boyde, 1998; Daegling and Hotzman, 2003; Katranji *et al.*, 2007); at the level of molars, the buccal cortical bone is thicker than the lingual bone (Enlow *et al.*, 1976; Daegling and Grine, 1991; Kasai *et al.*, 1996; Daegling and Hotzman, 2003; Schwartz-Dabney and Dechow, 2003; Sato *et al.*, 2005; Swasty *et al.*, 2009). Interestingly, the effects of tooth loss on the cortical bone

distribution and its asymmetrical patterns were not studied in particular. While some authors (Schwartz-Dabney and Dechow, 2003; Katranji *et al.*, 2007) reported similar patterns of cortical bone thickness asymmetry in dentate and edentulous individuals, Schwartz-Dabney and Dechow (2002) did not, as they observed a lack of bucco-lingual asymmetry in edentates.

2.4.2. Effects of changes in dentition

Tooth loss was found to affect not only the external morphology of the mandible, but also its cortical microstructure (Dechow *et al.*, 2010). Indeed, the reduction in strains associated with changes in dentition was observed to cause localised events of bone resorption (Martinez-Maza *et al.*, 2013). For instance, on mandibles at various stages of tooth loss, Enlow *et al.* (1976) detected specific remodelling responses affecting the cortical thickness of the basal part of the mandibular body.

Studies focusing on mandibular cortical thickness and considering tooth loss showed a general thinning of the cortical bone accompanying the changes in dentition. However, most of these authors measured the cortical thickness at the gonial angle area (Xie and Ainamo, 2004; Dutra *et al.*, 2005; Joo *et al.*, 2013; Oettlé, 2014), and only a limited number performed measurements elsewhere on the mandible, e.g., at the symphysis or on the corpus (Schwartz-Dabney and Dechow, 2002; Katranji *et al.*, 2007; Oettlé, 2014; McKay, 2019).

On the contrary, in some particular sites of the mandible, such as the lingual side of the symphysis and mental foramen region, a thickening of cortical bone accompanying tooth loss was observed. Enlow et al. (1976) suggested two hypotheses: an increase in bone growth at this specific location or an absence of resorption compared to the rest of the mandibular cortical bone. The first hypothesis was later confirmed by several authors comparing dentate and edentulous individuals directly, and observing a direct increase in lingual cortical thickness with tooth loss (Schwartz-Dabney and Dechow, 2002; Katranji *et al.*, 2007; Oettlé, 2014). This thickening was explained as a secondary adaptation of the bone to localised greater strains, triggered by the changes in morphology (e.g., diminution in corpus height) associated to the reduced global strains and loads following tooth loss (Schwartz-Dabney and Dechow, 2002, 2003). Furthermore, with a specific microscopic analysis allowing mapping of growth modelling activities, Martinez-Maza *et al.* (2013) confirmed later that the lingual side of the symphysis and anterior region of the corpus was indeed characterised by bone formation surfaces.

Most of the literature researched analysed the effects of tooth loss on cortical thickness by comparing dentate to edentulous individuals. Only a few studies considered individuals with various degrees of tooth loss. Dutra *et al.* (2005) for example, observed that, while the cortical thickness was decreasing with edentulism, there were no differences between dentate and partially dentate individuals, which was confirmed by Oettlé (2014), for most of the sites analysed. Nonetheless, at a few sites, such as the buccal side of the midline, the three dentition groups examined (completely inefficient mastication or edentulous; limited occlusions and inefficient mastication; efficient mastication) were all different.

Depending on many factors, such as the degree of edentulism, removable dentures (partial or complete) may be fitted to the alveolar bone to restore important masticatory functions in patients. However, as summarised by Resnik (2020), removable dentures might have adverse consequences, such as changes in the direction of biting (Dechow *et al.*, 2010), or an acceleration of the bone loss normally occurring after the loss/extraction of teeth. The wearing of dentures has thus profound effects on the morphology of the mandible but its impact on the inner structure also needs to be considered. Lestrel *et al.* (1980) found in a cephalometric study that the mandibular cortical bone thickness at the inferior margin or at the symphysis was thinner in denture wearers than in dentate subjects, in groups of young (33-43 years old) and old (54-62 years old) patients. While the authors controlled for the effects of age by comparing the two age groups separately, they, however, compared individuals with tooth loss wearing dentures to dentate patients, making it difficult to exclude the fact that tooth loss directly caused the decrease in cortical thickness and not the wearing of dentures. On the other hand, Knezović-Zlatarić and Čelebić (2005), also measuring the thickness of the cortical bone, compared edentulous individuals wearing complete dentures with individuals with tooth loss wearing removable partial dentures. They found significant differences between both types of patients in all their measurements, and more particularly a thicker cortical bone in patients with removable partial dentures. In contrast to the complete denture wearers, the forces of mastication are diverted to the remaining teeth, avoiding significant bone loss. It was previously shown that individuals with remaining teeth had better performances (bite force, chewing efficiency, less frailty, etc.) compared to complete denture wearers (Fontijn-Tekamp *et al.*, 2000; Hoeksema *et al.*, 2017). Interestingly, implant-supported overdentures also performed well in restoring masticatory functions (even if never at the level of natural dentition), especially compared to the traditional dentures mentioned above (Fontijn-Tekamp *et al.*, 2000; Hoeksema *et al.*, 2017; Resnik and Misch, 2020a). Indeed, osseo-integrated dental

implants were observed to stimulate the surrounding bone and thus mitigate the bone loss in the short-term, and preserve its overall volume and microstructure in the long-term (Watzek *et al.*, 1995; Carlsson, 2004; Hattingh *et al.*, 2020; Resnik, 2020).

Although the literature regarding mandibular cortical thickness and tooth loss is not as extensive as for the external morphology, it shares some limitations, such as the restricted dental status considered, with almost only studies on dentate vs. edentulous individuals. Furthermore, the different modalities used to perform the measurements (caliper, radiograph, CBCT) are not always comparable, or even just accurate enough for small-scale distances. Other factors than tooth loss, such as age, might also influence cortical thickness and are important to consider. For instance, Dutra *et al.* (2005) observed a continuous remodelling in the mandibular cortex with increasing age, which was influenced by dental status, and thus the duration of tooth loss. As for the external morphology of the mandible, as described in section [2.3], it is difficult to discuss changes related to tooth loss without considering aging, a major confounding variable.

2.4.3. Effects of aging

When extrapolating from the postcranial skeleton, age-related changes in the trabecular and cortical bone microstructure are well known. In their review, Chen *et al.* (2013) reported on the effects of age at different skeletal sites (vertebra, radius, femur, tibia), and all were affected by a progressive loss of both bone quantity and quality with increasing age. In other terms and as summarised by Ruff (2019), the cortical bone becomes thinner (i.e., bone quantity) and the bone mass (i.e., bone quality) declines with aging. However, the literature regarding the influence of increasing age on the mandibular microstructure is divided. For instance, although it is clear that the effects of tooth loss or progressive tooth loss will be displayed as a person age, it is less distinct whether aging itself has a predictable effect on the microstructure of the mandible.

More specifically with mandibular cortical thickness, the literature researched is not in agreement with whether it becomes thinner, thicker or stays unaltered with aging. For instance, several researchers noted a decline in cortical thickness associated with senescence, either at the buccal or lingual symphysis, parasymphysis or at the gonion (von Wowern and Stoltze, 1979; Kribbs *et al.*, 1990; Dutra *et al.*, 2005, 2005; McKay, 2019; Grover and Gupta, 2021). Dutra *et al.* (2005), comparing individuals divided in decades, observed that this decrease in

41

cortical thickness was more pronounced in females, particularly from the 40 to 49-year-old decades (40-49 years old > 50-59 > 60-69 > 70-79). In a later article (Dutra *et al.*, 2006), the same authors focused exclusively on edentulous females and also found a decrease in cortical thickness, but were not able to conclude if this diminution was solely due to aging (with its hormonal changes, and associated diseases), or rather caused by edentulism and duration of tooth loss.

On the other hand, a few other articles detected significant age-related differences in some of their measurement locations, but not in the others. In a sample of healthy individuals with teeth, Lestrel *et al.* (1980) for example, observed a decrease in cortical thickness with age at the symphysis, but not at the inferior margin. Oettlé (2014), using CBCT scans, showed that cortical thickness decreased with aging in all the mandibular sites studied, except one, the lingual site at the level of the mental foramen, which displayed an increased thickness. The author hypothesised that this thickening was maybe augmented by tooth loss and not just aging.

Numerous publications have also noted significant increases in cortical thickness with aging, but most of these findings may be attributed to the samples studied (Ono *et al.*, 2008; Fayed *et al.*, 2010; Farnsworth *et al.*, 2011; Cassetta *et al.*, 2013). Indeed, these studies were all comparing juveniles to adults, and not looking at the influence of age among adults. For instance, Ono *et al.* (2008) detected an age-related increase in cortical bone at some sites, but compared a group of adolescents (13-19 years) to a group of adult individuals (20-48 years). Fayed *et al.* (2010) evaluated cortical bone thickness on 34 mandibles within two age groups (13-18 years and 19-27 years). Farnsworth *et al.* (2011) assessed age and regional differences in the maxillary and mandibular cortical bones of 52 patients, also within two age groups: 11-16 years and 20-45 years. Cassetta *et al.* (2013), using CT scans, investigated differences of alveolar cortical bone thickness also between adolescents (12-18 years) and adults (19-50 years). The increase in cortical thickness noted in the above studies was explained by allometry and the continuation of growth processes in the juvenile groups rather than senescence.

Sathapana *et al.* (2013) wanted to clarify whether these changes were not only related to delayed growth processes of the mandible or senescence. They established five different age groups from 11 to 50 years and did not just compare juveniles to adults but looked at the correlations throughout all the ages. They first found an increase between pre-puberty (11-20 years) and post-puberty (11-20 years) groups, followed by a weak decrease in lingual cortical thickness starting from the 11-20 years until the last group (41-50 years). Swasty *et al.* (2009), also using a sample stratified in five age groups, found that the cortical thickness was thinner

in the younger age group (juveniles: 10-19 years) than in the other groups (adults: 20-29, 30-39, 40-49, 50-59, 60-65 years), confirming the continuation of the maturation of the mandibular cortical bone. They, however, also showed that, while the cortical bone maintained its thickness for three decades (20-29, 30-39, 40-49), a decline was noted after the 40 to 49-year-old group, which was particularly significant after 60 years of age.

On the other hand, some other studies could not confirm any of the results mentioned above. For instance, Kingsmill and Boyde (1998) obtained an absence of a significant relationship between age and cortical thickness at the midline and mental foramen. Similarly, Deguchi *et al.* (2006) measured buccal and lingual cortical plate thicknesses around premolars and molars using CT scans and found no differences by age. However, the samples studied in both articles were small: 42 individuals in Kingsmill and Boyde (1998) and only 10 in Deguchi and colleagues (2006), and may have compromised the statistical significance of the results. Furthermore, while, in the first article, age was nicely distributed (with a wide range of ages: 19-96 years) and details available on the sample, only the average age was given for the second study (22.3 years).

Other studies in the literature reviewed so far might be affected by inadequacies in the sample composition. For instance, while some articles were based on samples with adequate age distributions covering the entire lifespan (von Wowern and Stoltze, 1979; Kribbs *et al.*, 1990; Kingsmill and Boyde, 1998; Swasty *et al.*, 2009; Oettlé, 2014), others were more restricted with only a few decades covered (Kribbs *et al.*, 1990; Dutra *et al.*, 2005; Dechow *et al.*, 2010; Grover and Gupta, 2021). Inconsistencies might also be partly explained by the range of modalities used: from calipers (Dechow *et al.*, 2010; McKay, 2019) to radiographs (Lestrel *et al.*, 1980; Kribbs *et al.*, 1990; Kingsmill and Boyde, 1998; Dutra *et al.*, 2005), CT (Kribbs *et al.*, 1990; Deguchi *et al.*, 2006; Ono *et al.*, 2008; Munakata *et al.*, 2011; Cassetta *et al.*, 2013; Sathapana *et al.*, 2013; Grover and Gupta, 2021) or CBCT (Swasty *et al.*, 2009; Fayed *et al.*, 2010; Farnsworth *et al.*, 2011; Oettlé, 2014), which are maybe not all adapted to small measurements like cortical thickness.

Other types of factors, like sex or ancestry, also need to be considered, which was rarely the case in the literature cited above, although a few authors, such as Dutra *et al.* (2005), highlighted the influence of sex on the cortical thickness and on the continuous remodelling associated with aging.

2.4.4. Sex and population variation

As reviewed in section [2.3.3], sexual dimorphism in the general morphology of the mandible is well known, with mandibles in male individuals having more developed muscle insertions, more robust morphological aspects, and larger dimensions than in females. These sex-related differences are associated with the sexual dimorphism of the masticatory muscles themselves, generating greater bite forces in males than females. These differences in the gross morphology and in the muscular activity might be reflected in the cortical microstructure of the mandible.

When analysing the influence of sex on the mandibular cortical thickness, two main patterns were found in the literature: either males had thicker cortical bone than females, or no significant differences between sexes were observed. Indeed, several authors noted a significant sexual dimorphism for various types of cortical thickness: buccal and lingual on the corpus (Fayed *et al.*, 2010; Kim and Park, 2012; Cassetta *et al.*, 2013), or at the angle (Dutra *et al.*, 2005; Joo *et al.*, 2013). On the other hand, some authors reported a lack of sex-related differences and thus similar cortical thickness in females and males (von Wowern and Stoltze, 1979; Daegling and Grine, 1991; Deguchi *et al.*, 2006; Swasty *et al.*, 2011; Oettlé, 2014). Two of these studies (Daegling and Grine, 1991; Deguchi *et al.*, 2006) were, however, based on samples of only 10 individuals (5 males, 5 females in both cases), which may have compromised the significance of the results. In addition, a few other articles (Humphries, 2007; Ono *et al.*, 2008; Farnsworth *et al.*, 2011; Al-Jandan *et al.*, 2013) also reported an absence of sexual dimorphism in cortical thickness, but these samples were restricted in terms of age, as the authors focused particularly on juveniles and young individuals (mean ages of the samples were generally in the twenties). Humphries (2007) however nuanced their results as they observed a trend of thicker cortical bone in males compared to females even though it was not significant.

As seen with the external morphology in section [2.3.3], the sex-related differences in the morphology of the mandible appear to increase with aging. Two studies (Benson *et al.*, 1991; Dutra *et al.*, 2005) highlighted the fact that cortical thickness might follow the same trend. Indeed, Benson *et al.* (1991) observed that sexual dimorphism in cortical thickness was appearing progressively with senescence (young females = young males, but older females < older males). It was also confirmed by Dutra *et al.* (2005), as they detected a significant interaction between sex and age, with older males having a particularly thicker cortical bone

44

than older females. This "late/delayed" sexual dimorphism could be due to the age-related thinning of cortical bone, which was noted to be more important in females than in males. A few authors even focused on female-only samples and analysed for example the influence of menopause (Munakata *et al.*, 2011) or osteoporosis (Kribbs, 1990; Kribbs *et al.*, 1990; Dutra *et al.*, 2006) on the cortical thickness. Both menopause and osteoporosis were found to aggravate or accelerate the age-related diminution in mandibular cortical thickness, and thus accentuate the sexual dimorphism with males of similar ages.

In addition, most of the literature researched was based on samples of individuals not affected by tooth loss (Benson *et al.*, 1991; Daegling and Grine, 1991; Deguchi *et al.*, 2006; Humphries, 2007; Ono *et al.*, 2008; Fayed *et al.*, 2010; Farnsworth *et al.*, 2011; Swasty *et al.*, 2011; Kim and Park, 2012; Al-Jandan *et al.*, 2013; Cassetta *et al.*, 2013). Only a small number of authors studying the mandibular cortical thickness considered different dental status and sex (Dutra *et al.*, 2005; Joo *et al.*, 2013; Oettlé, 2014). For instance, Joo *et al.* (2013) noticed that the cortical bone in edentulous women was more influenced by dental status than in men.

Lastly, a very limited number of studies have investigated the mandibular cortical thickness across different populations. Three of these studies focused on North American individuals, comparing different population groups present in the United States (Benson *et al.*, 1991; Humphries, 2007; Zhang, 2012). They all observed a similar general tendency, with Black American individuals having thicker cortical bone than Asian, Hispanic or White Americans, even if none of these studies had statistically significant results. Two studies focusing on the South African population reported similar findings, with a general non-significant trend of a thicker cortical bone in South African Black individuals compared to their White and Coloured counterparts (Oettlé, 2014; McKay, 2019). This tendency was explained to be associated for instance to the higher incidence of having third molars in Black individuals (Hanihara and Ishida, 2005; Ogawa and Osato, 2013). Indeed, the presence of third molars is usually linked to a higher mandibular body height and a thicker cortical bone, particularly on the buccal side (Swasty *et al.*, 2009; McKay, 2019).

2.5. Factors affecting the cortical density of the mandible

In addition to cortical thickness, which gives an indication of the inner geometry of the bone, bone density, among other parameters, describes its material properties (Ruff, 2019). However, bone density is a wide term, and many different definitions and variables are present in the literature. Furthermore, interpretation of the results and comparisons between studies are complicated by a wide range of techniques employed to assess cortical density.

Historically, actual (or material) density is strictly defined as mass per volume. The apparent density, defined as a mass per unit volume (in g/ml or g/cm^3), is measured by weighing bone with a scale, which is then divided by the specimen external volume. Kingsmill and Boyde (1998) for example measured apparent density by weighting slices of mandibular bone from human cadavers with a balance. For the cortical bone, as it has a compact structure and a small degree of porosity, apparent density and material density are very similar and considered the same (An, 2000; Zioupos *et al.*, 2000). To measure its specific density, Schwartz-Dabney and Dechow (2003) harvested bone cylinders in mandibles and removed the cancellous bone to keep only the cortical part. Then, they determined the apparent density from weight measurements with an analytical balance and a densitometry kit.

With the development of virtual modalities that allowed non-invasive, non-destructive and *in vivo* assessments of bone density, new ways of measuring bone density emerged. The areal Bone Mineral Density (BMD, in g/cm^2) and Bone Mineral Content (BMC, grams of bone) are for example particularly used in clinical settings and measured with dual-energy absorptiometry (DEA) or dual-energy X-ray absorptiometry (DXA or DEXA) (An, 2000). DXA is even considered as the gold standard for osteoporosis and fracture risk diagnosis and monitoring (von Wowern, 2001; Singh and Tripathi, 2010; Dhainaut *et al.*, 2016). However, several authors cautioned against DXA, as it performed poorly when compared to other techniques, and may not always reflect the actual density of the bone, as the BMD obtained is areal (in 2D) and not volumetric (Schwartz-Dabney and Dechow, 2003; Pearson and Lieberman, 2004; Dhainaut *et al.*, 2016; Andronowski *et al.*, 2018, 2018). Furthermore, it is often highlighted in the literature that DXA cannot differentiate cortical from trabecular bone and gives a "general" bone density (Pearson and Lieberman, 2004; Dhainaut *et al.*, 2016).

With the development of specific three-dimensional scanning modalities, like Quantitative Computed-Tomography (QCT) and High-Resolution peripheral Quantitative Computed-Tomography (HR-pQCT) among others, volumetric BMD (in g/cm^3) started to

replace areal BMD in clinical research (Andronowski *et al.*, 2018; Agarwal, 2021). While having several advantages (volumetric measurements, separation of cortical and trabecular bone structures, higher resolution than DXA, etc.), QCT and HR-pCT also have some important limitations: high radiation exposure, high sensitivity to movements of the patient during scanning, poor reproducibility, etc. (Munakata *et al.*, 2011; Dhainaut *et al.*, 2016; Andronowski *et al.*, 2018).

In the dentistry field particularly, bone density has been evaluated using Hounsfield Units (HU) based on the grey value of each voxel of each image of a CT scan, which are directly associated with tissue attenuation coefficients (Gulsahi, 2011; Resnik, 2020; Sharawy, 2020) (see section [2.2] for more details). The Hounsfield scale describes the standardised range of HU from air (-1000), water (0) to enamel (+3000) and is considered as an objective method as HU are directly measured on CT images (Gulsahi, 2011; Sharawy, 2020). Several studies (Shapurian *et al.*, 2006; Merheb *et al.*, 2010) compared HU derived density and more subjective "manual" assessments obtained for instance via the Lekholm and Zarb bone quality classification (Lekholm and Zarb, 1985) or Misch bone density classification (Misch, 1988, 1990). Some researchers even elaborated objective scales of bone density expressed in HU and related it to these bone classifications (Norton and Gamble, 2001; Shapurian *et al.*, 2006). HU are, however, restricted to CT or MSCT modalities and were found to be inapplicable to CBCT (see section [2.2.3]). Since the spreading of CBCT in dental clinics, and the development of advanced imaging techniques like micro-CT, new bony structural parameters, also called histomorphometric parameters and "inspired" by quantitative bone histology techniques, were investigated as to assess bone density, and more particularly cortical bone density (Gocha *et al.*, 2019).

2.5.1. Regional variations within the mandible

Many articles on regional variations of trabecular density in the skull were published, but only a limited number investigates cortical bone density. Furthermore, most of those are focusing only on the cranium and maxilla, and not the mandible, even if regional variations in cortical bone density are suspected, notably because of the functional heterogeneity of the mandible (Bassi *et al.*, 1999; Schwartz-Dabney and Dechow, 2003).

The literature on mandibular cortical bone density seems to agree on two aspects, despite the number of different methodologies used. Firstly, similarly as for cortical thickness,

no record of an asymmetry in cortical bone density between left and right sides of the mandible was found in the literature (Knezović-Zlatarić and Čelebić, 2005; Shapurian *et al.*, 2006; Ozdemir *et al.*, 2014; Goyushov *et al.*, 2020). Secondly, researchers concur on the presence of a denser cortical bone in the basal part of the mandible, especially compared to the crestal cortical bone (Atkinson and Woodhead, 1968; Sato *et al.*, 2005; Park *et al.*, 2008; Cassetta *et al.*, 2013). Cassetta *et al.* (2013) specified that a gradual increase in cortical density was present from crest to base.

However, the literature is inconsistent on other types of regional variations. For example, Kingsmill and Boyde (1998) observed that the apparent cortical density at the midline was greater than at the mental foramen, whereas Schwartz-Dabney and Dechow (2003) found the opposite, with buccal symphyseal sites less dense than buccal sites on the corpus. Similarly, on the corpus, an antero-posterior asymmetry is generally found. However, studies do not agree whether the densest cortical bone is located anteriorly (von Wowern, 1977; Shapurian *et al.*, 2006) or posteriorly (Park *et al.*, 2008; Cassetta *et al.*, 2013). Finally, the bucco-lingual asymmetry, often analysed, is also a source of disagreement. Although most of the authors (Atkinson and Woodhead, 1968; Kingsmill and Boyde, 1998; Sato *et al.*, 2005; Cassetta *et al.*, 2013) detected a denser lingual cortical bone compared to a thinner buccal bone using a wide range of techniques (apparent density by weighting, density with QCT, HU density with CT, respectively), Klemetti *et al.* (1993) found a cortex denser buccally than lingually. Two authors, however, obtained nuanced results depending on the site of measurements. Von Wowern (1977) for instance had a bucco-lingual asymmetry (lingual > buccal) at mid-level of the corpus, while at the alveolar crest, it was not significant (lingual = buccal). On the other hand, Schwartz-Dabney and Dechow (2003) observed a denser lingual than buccal cortical bone at the symphysis, but no asymmetry on the body. While the large number of techniques employed to assess the cortical density does not seem to have an influence in the above studies, the samples used may have affected the results. Some researchers measured cortical bone density in individuals with various dentition status (e.g., von Wowern, 1977; Klemetti *et al.*, 1993) while others, such as Schwartz-Dabney and Dechow (2003) and Cassetta *et al.* (2013), were restricted to dentate individuals only. Interestingly, Schwartz-Dabney and Dechow (2002) assessed the cortical bone density in edentulous individuals and found no significant bucco-lingual variation.

2.5.2. Effects of changes in dentition

Tooth loss has a significant influence on several inner parameters, like cortical thickness, but might also effect the cortical density (Dechow *et al.*, 2010). The reduction in strains caused by the loss of a tooth or even worse, edentulism, is followed by bone resorption, which is associated with local and global, microstructural changes. Using animal models, several studies (Sato *et al.*, 2005; Guerreiro *et al.*, 2013) analysed the consequences of an induced masticatory hypofunction, supposed to simulate the "natural" decreased strains associated with tooth loss. They all observed a decrease in trabecular and cortical bone mineral density.

In the human mandible, however, conflicting results were obtained about the effects of tooth loss on cortical density. One study (Bassi *et al.*, 1999) measured the mean BMD via QCT in dentate and edentulous areas of the same individuals, and found that the mean BMD was higher in dentate than in edentulous areas. These results might be caused by the absence/presence of teeth but might also be influenced by regional variation in density, as the dentate and edentulous areas analysed were located differently (e.g., the dentate area was often in the front close to the incisors and canines, while the edentulous area was located more posteriorly around the molars). On the other hand, with a DXA analysis, Buyukkaplan *et al.* (2013) noticed that edentulous patients had greater BMD than dentate individuals. The authors hypothesised that the cortical bone was maybe becoming denser with edentulism or a long duration of tooth loss to protect the remaining mandible from strong strains caused by the extensive change in morphology.

Instead of showing a decrease or an increase in cortical bone density after tooth loss, an absence of change was observed in a few studies. Measuring the apparent cortical bone density via histology techniques, early studies, like Atkinson and Woodhead (1968) or von Wowern (1977), obtained similar values with or without teeth. Later, Kingsmill and Boyde (1998), also assessing the apparent cortical density by weighing, did not find any significant differences in apparent density between the three dentition categories analysed (completely dentate, partially dentate and edentulous). Schwartz-Dabney and Dechow (2002) confirmed these results, and also completed them by measuring various material properties of the mandibular cortical bone. The authors found several changes with tooth loss and concluded that, although changes in stiffness (i.e., its biomechanical strength, its ability to resist deformation) and anisotropy were present, the cortical density was maintained even in the case of edentulism.

49

Using DXA of patients, von Wowern (1988) evaluated BMC in individuals of different dentition categories while also being able to control variables like the age or sex. Interestingly, they also found non-significant results between dentition groups (e.g., similar BMC values in young dentate women and young edentulous women), confirming the maintenance of mandibular cortical bone density.

2.5.3. Effects of aging

In a review by Chen *et al.* (2013), age-related changes in the trabecular and cortical bone microstructure were found in different skeletal sites (vertebrae, femoral neck, radius, tibia) and were characterised by a progressive loss of both bone quantity and quality with increasing age (Ruff, 2019). As changes with age have an expected effect on several bones and the external shape and size of the mandible, age may also play a role on the modification of the structural properties of the mandibular cortical bone. However, Kingsmill (1999) stressed the uniqueness of a bone like the mandible, and that age-related changes in postcranial bones might be different in the mandible.

The literature on the mandible researched is not always in agreement whether cortical density is influenced by senescence or not. A large part of the studies however noted an age-related decrease in cortical density. First, Atkinson and Woodhead (1968) observed a reduction in apparent cortical density with age, in dentate and edentulous regions of the mandible, which was later confirmed by others (von Wowern and Stoltze, 1979, 1980). Atkinson and Woodhead (1968) also noticed an increase in cortical porosity, correlated with age. This increase was confirmed later by several authors (von Wowern and Stoltze, 1978; Bartlett *et al.*, 1992) at various sites of the mandible (buccal, lingual). Von Wowern and Stolze (1980) even specified that this increase in cortical porosity was particularly important after 50 years. In another study, von Wowern and Melsen (1979) measured the cortical bone mass in different "compartments" of the cortical bone: the subperiosteal layer (first layer from the outside) and the subendosteal layer (between the subperiosteal layer and the trabecular bone). They found an age-related decrease in the two layers, although the subendosteal showed a higher decline in mass, and thus a greater increase in porosity, than in the subperiosteal layer. More recently, an age-related decrease in bone density was also reported while assessing BMD values from DXA (Li *et al.*, 2011; Shaw *et al.*, 2012).

On the other hand, a few authors described an increase in mandibular cortical density with aging. Kingsmill and Boyde (1998) noted a weak increase in apparent bone density only in males and not in the females of the sample; whereas Kribbs *et al.* (1990) observed an increase with age in a female-only sample.

Lastly, several studies did not find any change in cortical bone density (no increase or decrease) related to age. Kribbs (1990) assessing both the mandibular cortical bone mass and bone density, did not notice any age-related association. Schwartz-Dabney and Dechow (2003) found in their study that the apparent cortical density was not significantly correlated with age. Nevertheless, in both Kribbs (1990) and Schwartz-Dabney and Dechow (2003), the samples used were somewhat restricted to older age groups (112 women, 50-85 years; 10 individuals, 48-81 years, respectively). A small number of researchers used CT scans and HU to evaluate the cortical bone density while considering age. Shapurian *et al.* (2006), as well as Cassetta *et al.* (2013), did not find any significant age-related changes in the cortical bone HU. The study by Shapurian and colleagues (2006) focused on edentulous sites of the mandible, which might have influenced the results. On the other hand, Cassetta *et al.* (2013) compared adolescent (12–18 years) to adult (19–50 years) mandibles. One increase in density was, however, detected in the adolescent group and might be attributed to changes associated with growth rather than senescence.

The range of techniques employed, and the different variables used are most probably the main reasons for the discrepancies. Many inconsistencies and uncertainties are still left regarding the influence of tooth loss or aging or both at the same time. Furthermore, no studies using histomorphometric parameters as to evaluate the mandibular cortical bone density, while considering tooth loss or aging, were found in the literature.

2.5.4. Sex and population variation

While sexual dimorphism is clear in the morphology of the mandible, it is less clear for the inner structure. When analysing the influence of sex on the cortical bone density of the mandible, two trends were mainly found in the literature: a similar cortical density in males and females, or a denser cortical bone in males compared to females. Indeed, the absence of sexual dimorphism was observed in several studies, using different techniques or variables assessing the cortical bone density (von Wowern and Stoltze, 1978, 1979; Kingsmill and

Boyde, 1998; Shapurian *et al.*, 2006; Park *et al.*, 2008; Buyukkaplan *et al.*, 2013; Ozdemir *et al.*, 2014).

However, some authors (Bartlett *et al.*, 1992; Bassi *et al.*, 1999; Cassetta *et al.*, 2013), using different techniques (histology, QCT and BMD, CT and HU, respectively), noted the presence of sexual dimorphism in the cortical bone density of the mandible. Bartlett and colleagues (1992) even noted that the increase in cortical porosity with age was weaker in males than in females, and that the greater the ages, the greater the differences. The influence of aging on the sexual dimorphism of the cortical bone density was also observed in several other studies. Von Wowern (1988) for example divided their sample according to the age and dentition status of the individuals. In the young groups (20-43 years, dentate or tooth loss), a higher BMC was always detected in men compared to women. They also observed that the loss in BMC with age was more important in women than men, increasing the sex-related differences with the years. Li *et al.* (2011) studied BMD values derived from DXA and did not find any sexual dimorphism in the young groups of the sample (20-29, 30-39, 40-49 years). However, in the older groups (50-59, 60-69, 70+), a considerable difference in cortical density appeared. Taguchi *et al.* (1996) analysed BMD values obtained with QCT in a women-only sample. As women reach menopause at slightly different ages, the authors compared the mandibular cortical bone density in women of similar ages but in a recent postmenopausal status or a long-term postmenopausal status. They reported that the cortical bone density was higher in the recent postmenopausal status than in the long-term group, even if the ages were similar. Indeed, the cortical bone remodelling process, and its rate, is known to be influenced by sex hormones and is accelerated after the beginning of the menopause (see Gocha *et al.*, 2019 for a review).

The bone remodelling dynamics are also influenced by population variation (Gocha *et al.*, 2019). For instance, rates of cortical bone turnover (in ribs) were shown to differ between African and European Americans, with slower rates in African American individuals (Cho *et al.*, 2006). Similar results were found in studies on the South African population (Pfeiffer *et al.*, 2016), with greater BMD values in South Africans of African ancestry than European ancestry (Micklesfield *et al.*, 2011; Botha *et al.*, 2019). Unfortunately, whereas many clinical studies focusing on the cortical bone density of postcranial bones while considering population variation exist, none could be found on the mandible.

Chapter 3. Materials and methods

3.1. Materials

To investigate the effects of aging and tooth loss on the morphology and microstructure of the mandible, skeletonised mandibles of South African individuals were collected from two modern human skeletal collections: the Pretoria Bone Collection, housed at the University of Pretoria, and the Raymond A. Dart Collection of Modern Human Skeletons, housed at the University of the Witwatersrand. Furthermore, as it is not known whether the mandible ages in the same way and at the same rate as the rest of the skeleton, skeletonised femora were selected from the Pretoria Bone Collection. Used as a proxy for the rest of the skeleton, the analysis of the femur, specifically the femoral neck, will give additional information whether mandibular bone loss is associated purely with tooth loss, or whether it is also associated with a generalised tendency of bone loss in the skeleton with aging.

3.1.1. Skeletal collections

The diversity and genetic heterogeneity of the South African population are unique and mainly due to historical and recent migrations from Africa, Asia and Europe, but also to the political history of the country (Dayal *et al.*, 2009; Petersen *et al.*, 2013; Stull *et al.*, 2016; Krüger *et al.*, 2018). Under racial segregation laws until 1990, South Africans were classified into several categories based on their ancestry (i.e., the geographical origin of an individual's ancestor: individuals of African, European, Asian, or Indian ancestries for example) as to control their life on many different levels (e.g., marriage, education, employment, residence, freedom of movement). Nonetheless, even after the end of the apartheid era, many South Africans continue to refer to themselves according to these categories and self-identify into these groups, notably for governmental and survey purposes (Statistics South Africa, 2016).

The largest part of the sample was collected from the Pretoria Bone Collection (PBC), housed at the Department of Anatomy, University of Pretoria, Pretoria, South Africa. The PBC, initiated in 1943 for medical training, is a well-documented collection with known demographics (L'Abbé *et al.*, 2005). According to the collection curator (G.C. Krüger, personal

communication, November 2018), the PBC includes 1092 South African (SA) adult individuals with complete skulls and mandibles – these comprise mostly males of African ancestry (54.9%), followed by males of European ancestry (21.5%), females of European ancestry (15%) and females of African ancestry (8.6%). SA males of African ancestry are the most numerous and are represented in all age ranges, up to 90 years, while a large number of SA individuals from European ancestry (both male and female) are older than 50 years. The rest of the sample originated from the Raymond A. Dart Collection of Modern Human Skeletons (RADC), housed at the School of Anatomical Sciences, University of the Witwatersrand, Johannesburg, South Africa. Initiated in the early twentieth century (1920s), it is nowadays one of the largest documented human skeletal collections within Africa, with at least 2 226 skulls present with an associated mandible (Dayal *et al.*, 2009). Despite the large sample size of the collection, females (29%) are underrepresented in comparison to males (71%). Furthermore, South African individuals of African ancestry represent the largest proportion (72%) compared to individuals of European ancestry (18%) and individuals from other South African ancestral groups (e.g., individuals of Asian and, Indian ancestries) (Dayal *et al.*, 2009).

Both collections are cadaver-based, originating from two sources: either donated or unclaimed bodies. Permission for research can be given either by family members in the case of donations when possible, or is protected and regulated by the South Africa's National Health Act No. 61 of 2003 (Republic of South Africa, 2004) (and by previous Human Tissues and Anatomy Acts) in the case of donated human remains as well as for unclaimed bodies. The provenance of the cadavers implies different potential socio-economic backgrounds. Most unclaimed individuals in both collections are of African descent and are suspected to have been migrant workers moving from rural areas for economic reasons, and thus, of lower socio-economic status (Keough *et al.*, 2009; L'Abbé and Steyn, 2012). Recently, however, more donations as opposed to unclaimed bodies have been received at both institutions (Kramer *et al.*, 2019), and are starting to contribute increasingly more to the collections. As both institutions actively and continuously accession more skeletons into their collections, a modern sample reflective of the population is ensured.

Only South African individuals from the two major population groups available from these collections (of African and European ancestries) with available demographic information (i.e., age, sex, population affinity, cause of death), were sampled. Thus, the analyses were conducted on four sex/ancestral groups: South African males and females of African ancestry, and South African males and females of European ancestry.

3.1.2. Mandibles

Adult individuals only were selected as to avoid the influence of growth, and according to the following inclusion/exclusion criteria: (i) presence of the entire mandible and maxilla without any damage; (ii) absence of mandibular pathology or abnormalities; (iii) no evidence of significant medical or dental history (e.g., no surgical intervention on the mandible); (iv) no disease or cause of death that might affect the musculoskeletal system and functions; (v) absence of large metal restorations causing artefacts in imaging acquisitions.

In total, 357 mandibles of individuals between 18 and 98 years were identified to be relevant for the research (Table 3.1). The sample comprised of 153 South African (SA) males and 60 SA females of African ancestry (AA), as well as 81 SA males and 63 SA females of European ancestry (EA). A limited number of females (n = 123, i.e., 34.5% for both ancestral groups) was available in comparison to male individuals (n = 234, i.e., 65.5% for both ancestral groups). In the same way, the proportion of individuals of African ancestry (n = 213, i.e., 59.7%) was larger than those from European ancestry (n = 144, i.e., 40.3%).

Table 3.1. Sex/ancestral group distribution in the mandibular sample.

	F	M	**Total**	%
AA	60	153	**213**	59.7
EA	63	81	**144**	40.3
Total	**123**	**234**	357	
%	34.5	65.5		

F: female, M: male; AA: SA of African ancestry, EA: SA of European ancestry.

Individuals were stratified in decades based on their age in order to obtain the most homogeneous and uniformly distributed sample in terms of age (see Table 3.2 and Figure 3.1). African males and females are well represented in most decades. However, young individuals (under 40) of European ancestry are underrepresented in comparison to older decades.

Table 3.2. Age distribution (per decade) of the sex/ancestral groups in the mandibular sample.

| | F | | M | | |
	AA	EA	AA	EA	Total
18-29	7	5	13	2	27
30-39	13	1	24	5	43
40-49	12	10	27	8	57
50-59	10	7	28	11	56
60-69	9	11	25	15	60
70-79	8	12	18	22	60
80-89	1	10	15	10	36
90+	0	7	3	8	18

F: female, M: male; AA: SA of African ancestry, EA: SA of European ancestry.
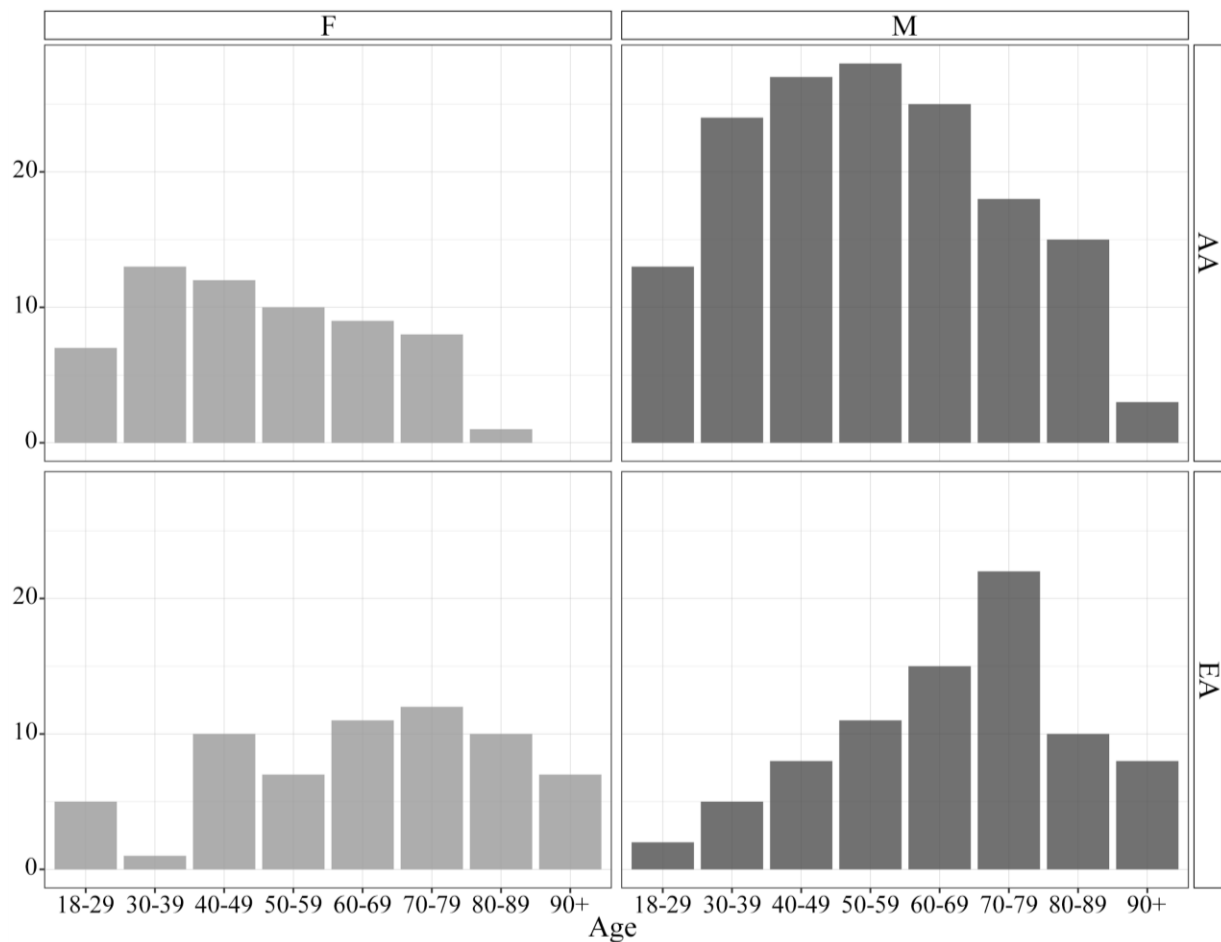
Figure 3.1. Bar plots of the four sex/ancestral groups distributed in function of age (per decade) in the mandibular sample. F: female (light grey), M: male (dark grey); AA: SA of African ancestry (first row), EA: SA of European ancestry (second row).

Individuals were also selected according to their pre-mortem dentition status in order to obtain a wide range of tooth loss patterns: from edentulous mandibles to complete dentition. To control for the different degrees of tooth loss and its consequences on the masticatory performances, the mandibles were classified into different dentition groups according to the Eichner Index (EI) (Eichner, 1990), rather than using the number of teeth present. This tooth loss scoring method is based on the presence of occlusal contacts, explaining the importance of having access to each mandible with its associated maxilla. The EI, mostly used in dentistry because of the validated relation with the masticatory performances (Ikebe *et al.*, 2005, 2010, 2012; Nakatsuka *et al.*, 2010; Olofsson *et al.*, 2017), has also been used in some recent anthropological studies (Parr *et al.*, 2017).

The EI classifies the various dentition patterns into three main groups of tooth loss (A, B, C), but consists of ten subgroups in total (A1, A2, A3, B1, B2, B3, B4, C1, C2, C3) (Figure 3.2). These groups, from A to C, are associated with a loss in occlusal contacts, and thus, a reduction in bite force and masticatory performances. The EI classification is mainly defined by the presence or absence of occlusal contacts/pairs in both premolar and molar regions, also referred to as the four posterior "Occlusal Support Zones" (OSZ). Each OSZ consists of four teeth: upper and lower premolars (P1, P2), or upper and lower molars (M1, M2) – the third molar (M3), erupted or not, is not considered. Within the "A" category, individuals have occlusal contacts in all four OSZs, whereas, in "B", contacts are present in only three to one OSZs, or even in the anterior teeth only (i.e., no posterior OSZ). The last category "C" is characterised by the total absence of occlusal contacts in both posterior and anterior zones. The subgroups for each category are explained further in detail in Figure 3.2.

Category A - Occlusal contacts in all four posterior OSZs

U (upper)

A1 — complete dentition, no missing teeth (U and L)

A2 — at least one missing tooth in one arch (U or L)

A3 — at least one missing tooth in both arches (U and L)

L (lower)

Category B - Occlusal contacts in three to one posterior OSZs or in the anterior region only

B1 — three OSZs

B2 — two OSZs

B3 — one OSZ

B4 — only anterior support

Category C - Absence of occlusal contacts

C1 — at least one tooth in each arch (U and L)

C2 — at least one tooth in one arch (U or L)

C3 — fully edentulous, both arches (U and L)

Figure 3.2. Schematic illustrations of the Eichner Index (redrawn from Ikebe *et al.*, 2010 and Parr *et al.*, 2017). Coloured teeth are in contact with their antagonistic teeth: anterior teeth (I1: central incisor, I2: lateral incisor, C: canine) are in yellow, first and second premolars (P1, P2) in green, first and second molars (M1, M2) in blue; while white teeth are not in occlusion.

58

The sex/ancestral distribution of the individuals according to the EI scoring system is detailed in Tables Table 3.3 and Table 3.4 as well as illustrated in Figure 3.3. As expected, category C is mainly represented in the older decades (over 50) of the four sex/ancestral groups but is more frequent in males and females of European ancestry. However, individuals from category A (especially the subgroup A1) are more often of African ancestry.

Table 3.3. Sex/ancestral group distribution per main dentition category (A, B and C, according to Eichner, 1990).

	A	B	C	Total
F	**32**	**39**	**52**	**123**
AA	22	26	12	60
EA	10	13	40	63
M	**82**	**64**	**88**	**234**
AA	76	35	42	153
EA	6	29	46	81

F: female, M: male; AA: SA of African ancestry, EA: SA of European ancestry.

Table 3.4. Age distribution (per decade) of the sex/ancestral groups divided in the three main dentition categories (A, B, C according to Eichner, 1990).

	F						M					
	AA			EA			AA			EA		
	A	B	C	A	B	C	A	B	C	A	B	C
18-29	4	3	0	4	1	0	12	1	0	0	1	1
30-39	4	8	1	1	0	0	17	5	2	1	2	2
40-49	7	5	0	2	3	5	18	4	5	1	3	4
50-59	4	2	4	1	3	3	13	11	4	1	5	5
60-69	2	3	4	1	2	8	7	7	11	2	8	5
70-79	1	4	3	0	1	11	7	0	11	1	8	13
80-89	0	1	0	1	3	6	2	6	7	0	2	8
90+	0	0	0	0	0	7	0	1	2	0	0	8

F: female, M: male; AA: SA of African ancestry, EA: SA of European ancestry.
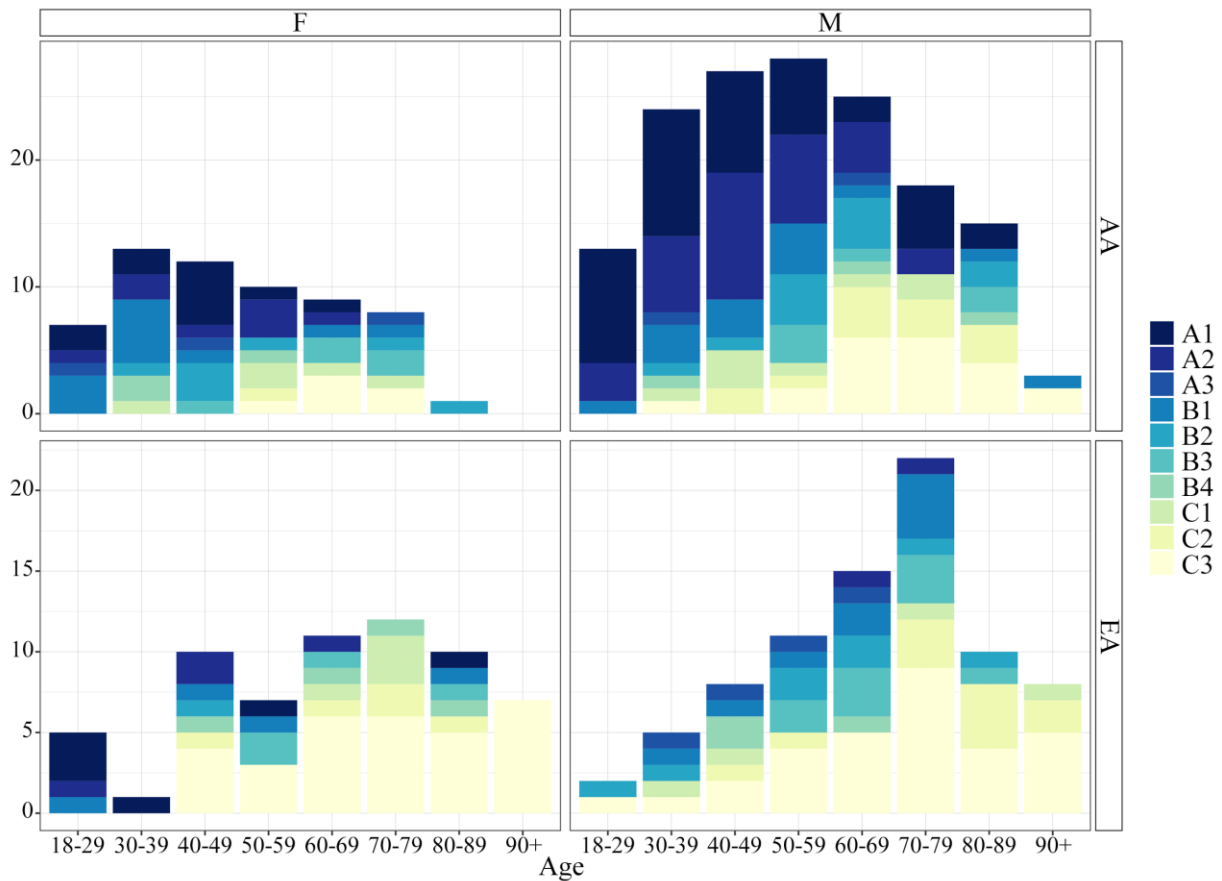
Figure 3.3. Bar plots of the four sex/ancestral groups distributed in function of age (per decade) and divided in the ten dentition subgroups defined by Eichner (1990). F: female, M: male; AA: SA of African ancestry, EA: SA of European ancestry.

3.1.3. Femora

Sixty-eight left femora belonging to the same adult individuals previously selected from the PBC for their mandibles were chosen. The following additional inclusion/exclusion criteria were applied: (i) absence of femoral pathology or abnormalities; (ii) no evidence of surgical interventions (prosthesis, hip replacement, etc.) on the lower limbs; (iii) no signs of trauma. Finally, the femoral sample consisted of 68 SA individuals between 21 and 98 years (summarised in Table 3.5, detailed per decade in Table 3.6): 14 females and 22 males of African ancestry (AA), as well as 15 females and 17 males of European ancestry (EA). The sample distribution between both ancestries, illustrated in Figure 3.4, was well balanced (52.9% AA, 47.1% EA), although the proportion of males (57.4%) was larger than females (42.6%).

Table 3.5. Sex/ancestral group distribution in the femoral sample.

	F	M	Total	%
AA	14	22	**36**	52.9
EA	15	17	**32**	47.1
Total	**29**	**39**	68	
%	42.6	57.4		

F: female, M: male; AA: SA of African ancestry, EA: SA of European ancestry.

Table 3.6. Age distribution (per decade) of the sex/ancestral groups in the femoral sample.

	F		**M**		
	AA	**EA**	**AA**	**EA**	**Total**
18-29	4	2	4	1	**11**
30-39	2	0	2	1	**5**
40-49	1	3	3	1	**8**
50-59	2	2	2	2	**8**
60-69	2	2	3	1	**8**
70-79	3	4	3	2	**12**
80-89	0	1	3	5	**9**
90+	0	1	2	4	**7**

F: female, M: male; AA: SA of African ancestry, EA: SA of European ancestry.
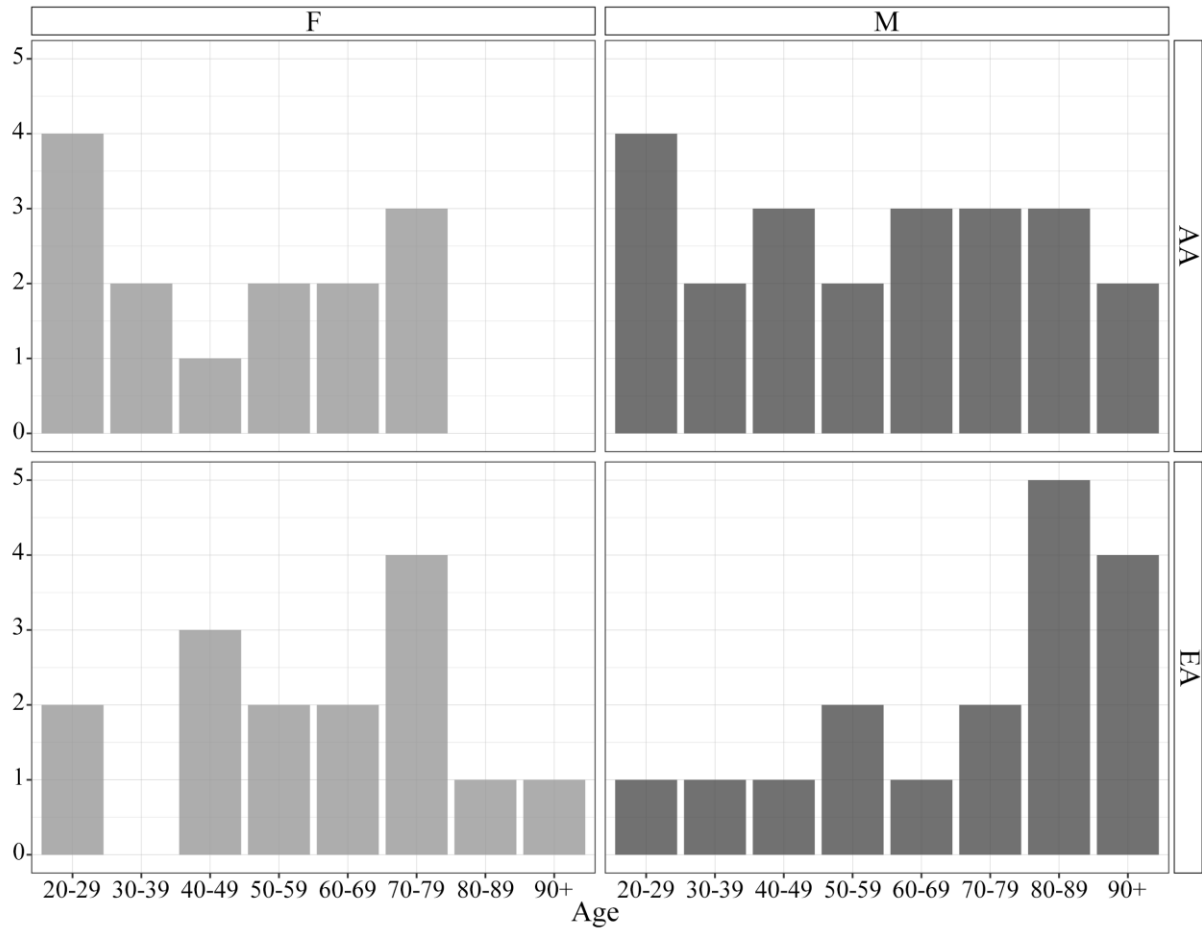
Figure 3.4. Bar plots of the four sex/ancestral groups distributed in function of age (per decade) in the femoral sample. F: female (light grey), M: male (dark grey); AA: SA of African ancestry (first row), EA: SA of European ancestry (second row).

3.2. Methods

The mandibular skeletal material described in the previous section was imaged using two different non-invasive and non-destructive scanning techniques. All mandibles were detailed with Micro-Focus X-ray Computed-Tomography (micro-CT), while a subsample was re-scanned by Cone-Beam Computed-Tomography (CBCT) to compare the findings between modalities. The virtual database acquired was used to assess qualitatively and quantitatively the morphology and cortical microstructure of the mandible, and comparisons to the femur were performed.

The methodology implemented in this thesis is summarised in Figure 3.5. The first part [3.2.1], focusing on the mandible, describes the data acquisition procedures that are specific to both modalities (micro-CT and CBCT), the processing of the images and subsequent measurements. In the second part [3.2.2], the three-dimensional imaging and analysis of the femur are detailed. Finally, the third part [3.2.3] is concerned with all statistical analyses.
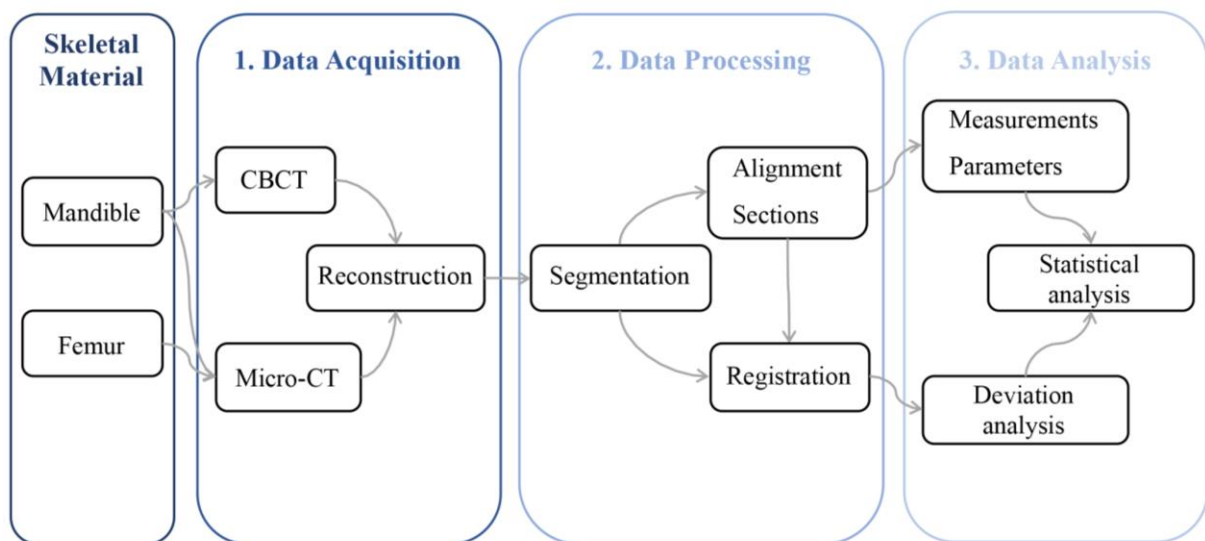
Figure 3.5. Workflow summarising the virtual methods used.

3.2.1. Methods applied to the mandible

3.2.1.1. Micro-CT and CBCT data acquisition

Micro-CT scanning procedure

Each mandible was scanned using the same micro-CT – a Nikon XT H 225L industrial Computed-Tomography system (Nikon Metrology, Belgium) – housed at the Micro-Focus X-ray Radiography and Tomography facility (MIXRAD) of the South African Nuclear Energy Corporation (Necsa, Pelindaba, South Africa) (Hoffman and De Beer, 2012; De Beer, 2018). The system consists of different separate functional units: a cabinet housing the X-ray tube, sample manipulator and flat panel detector, as well as computers for control, acquisition and reconstruction procedures (Figure 3.6 A). During the acquisition, the specimen was placed on the sample manipulator inside the cabinet which is then rotated over 360 degrees, while the X-ray source and the detector stay immobile. The mandible was secured within a squared polystyrene box to avoid any movement or vibration during the process (Figure 3.6 B).
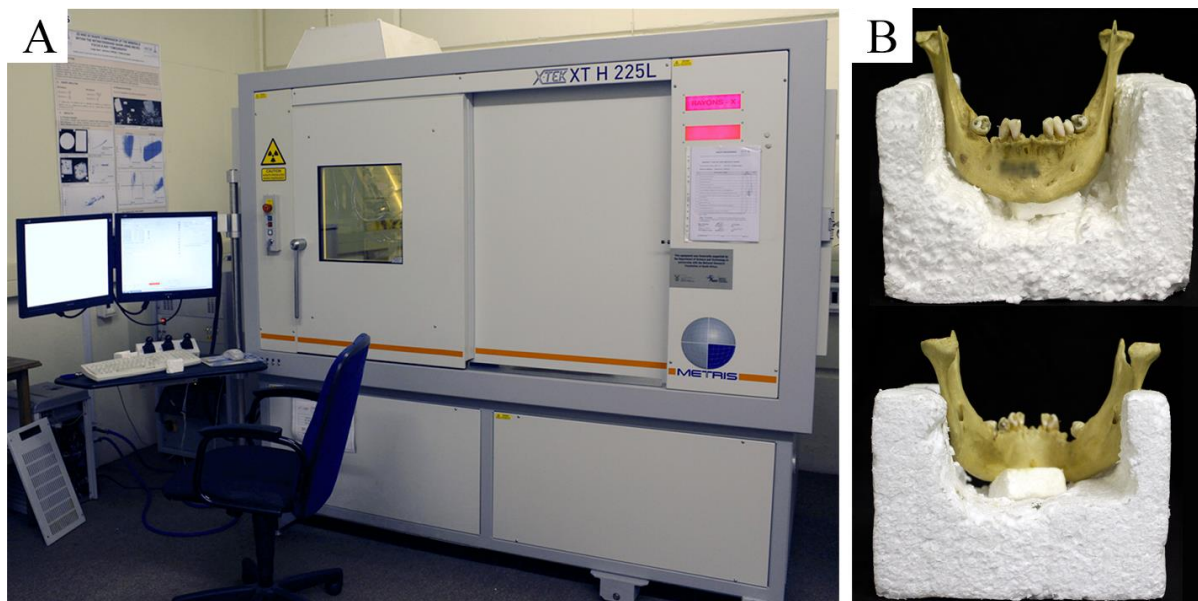
Figure 3.6. Micro-CT system at Necsa (Pelindaba) [A], and experimental settings used for each mandible [B].

During the acquisition, a set of 1 000 two-dimensional (2D) radiographic projection images was created and directly imported into the in-house Nikon CT-Pro software (Nikon Metrology, Belgium), where the reconstruction into a three-dimensional (3D) volume was performed (Figure 3.7), applying automatically optimised transformation parameters, such as

an isotropic resolution adjusted to the size of each specimen. The final volumes were then exported in vol float format or in 16-bit TIFF images.

Figure 3.7. Reconstruction process. Examples of radiographic projections obtained for one micro-CT-scanned mandible [A] and of reconstructed slices constituting the final volume [B].

Two hundred and sixty-five micro-CT scans (i.e., 265 scanned mandibles) were performed with a resolution ranging between 0.066 mm and 0.084 mm, a 100 kV voltage and a beam current of 100 µA or 200 µA. In addition, 92 micro-CT scanned entire mandibles conducted for previous research projects were collected and included in this work (courtesy of A.C. Oettlé and C. Sutherland). The scans were performed at Necsa with the same machine and reconstructed with the following parameters: isotropic voxel sizes ranging from 0.068 mm to 0.106 mm, a 100 kV voltage and a current of 100 µA, 120 µA or 220 µA. Therefore, in total, 357 micro-CT scans of entire mandibles were used, and the acquisition parameters thereof are detailed in Appendix D (Table D.1 andTable D.2).

CBCT scanning procedure

Twenty-four mandibles of male individuals with intact dentition, that have been previously scanned by micro-CT, were randomly selected to be imaged by CBCT – with a

Planmeca ProMax3D® (Planmeca, Finland) – at the Oral and Dental Hospital of the University of Pretoria. The CBCT system consists of a reconstruction computer and an X-ray unit with a movable C-shaped-arm (containing the X-ray source) and sensors (Figure 3.8). During acquisition, the X-ray source moves around the patient's support table to perform a single 360° scan (Scarfe *et al.*, 2006). In order to position the specimen correctly on the patient support table of the unit, the adjustable head support was attached, and the chin support removed. The adaptable arms of this support allowed the researcher to secure a cardboard box containing the mandible in place of the chin support.
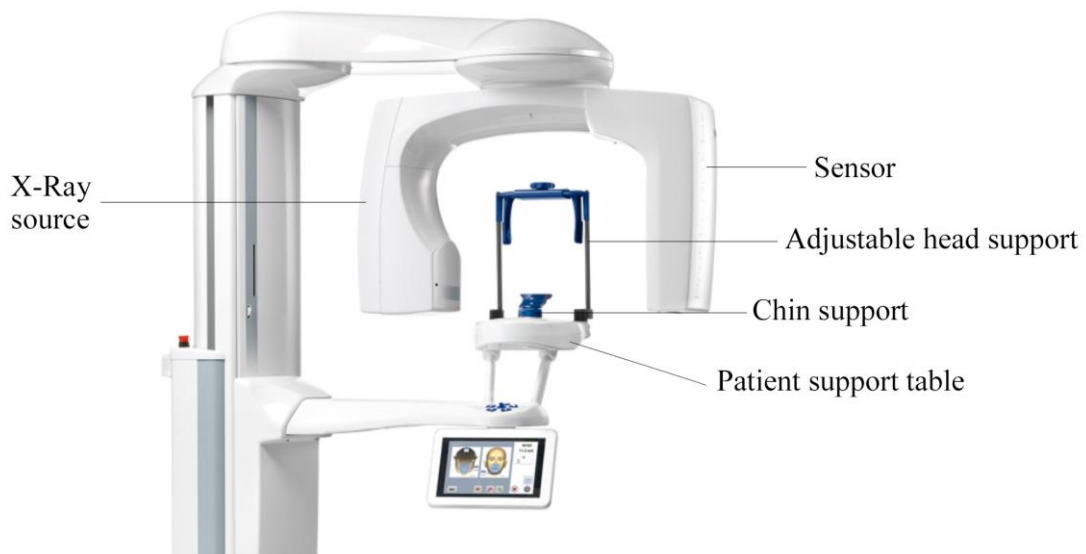
Figure 3.8. General view and description of the Planmeca ProMax3D® CBCT system (Planmeca, Finland), available at the Oral and Dental Hospital from the University of Pretoria.

As with micro-CT, 3D projection images were acquired and reconstructed into 3D volumes using the in-house Planmeca Romexis® software (Planmeca, Finland) with the following settings: 0.200 mm isotropic voxel size, 88 kV voltage and 10–11 mA current. Acquisition parameters are available in Appendix D Table D.3. These volumes were finally exported in DICOM format.

3.2.1.2. Image processing

In order to perform consistent analyses of the images, the same procedure was applied to all the micro-CT and CBCT-based volumes. Each dataset was imported into the analysis and visualisation software VGStudio MAX 3.1. (Volume Graphics GmbH, Germany) for the

following steps: (i) segmentation; (ii) alignment; (iii) definition and extraction of the cross-sections used for measurements. To avoid errors and optimise the importation and analysis time, various importation parameters were verified through the *Loading* module of the software, such as the type of the dataset, resolution, as well as the grey value distribution histogram (Figure 3.9 A). The size of the dataset was also verified and "reduced" by cropping unnecessary surrounding air around the object by defining a region of interest (Figure 3.9 B). This reduces the Random-Access Memory (RAM) use of the computer, and thus accelerates the loading time of the dataset making the analysis easier and faster. Once the dataset is loaded, the software displays the three-dimensional rendering of the specimen, as well as 2D slice views as seen along the x-axis, the y-axis and the z-axis of the original coordinate system (also named the *Scene coordinate system* in VGStudio MAX 3.1.).
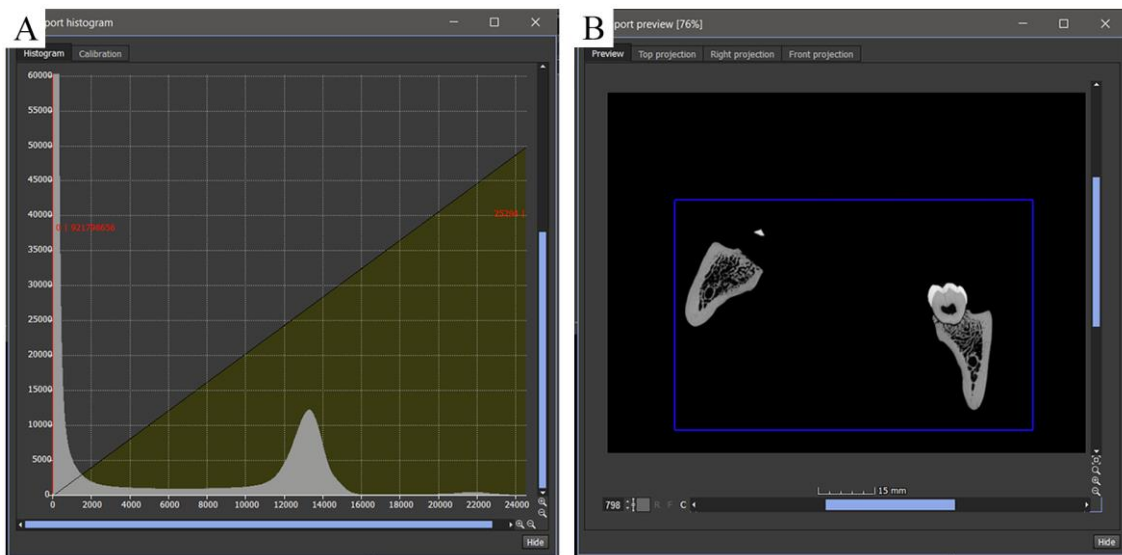
Figure 3.9. Importation process in VGStudio MAX 3.1. Snapshots of the modules displaying the grey value distribution histogram with the peaks corresponding to the different materials/background [A], and the mandibular volume preview with the movable lines (in blue) cropping unnecessary surrounding air [B].

Segmentation

The segmentation procedure is a prerequisite for any analysis on a 3D volume. This essential step allows the user to define and extract regions within the image by delineating the contour of the different structures of interest – e.g., bone and tooth vs. air – based on the greyscale contained in the image. Many different techniques exist (Dawant and Zijdenbos, 2000; Toennies, 2012) but the *Automatic Surface Determination* approach was first selected. This global thresholding method uses the grey value distribution histogram to define and

globally apply one threshold to the volume. Then, the *Advanced Mode* implemented in VGStudio MAX 3.1. was applied. This method re-evaluates and adapts the previously defined contour in function of the grey values of the surrounding voxels (Figure 3.10) (i.e., the same grey value can be processed differently according to the neighbouring voxels) (VGStudio MAX Reference Manual; Dawant and Zijdenbos, 2000). This adaptive local thresholding method provides a high level of accuracy (up to 1/10 of the voxel size) and low measurement error as it minimises user influence and compensates for artefacts (VGStudio MAX Reference Manual; Dawant and Zijdenbos, 2000; Borges de Oliveira *et al.*, 2016).
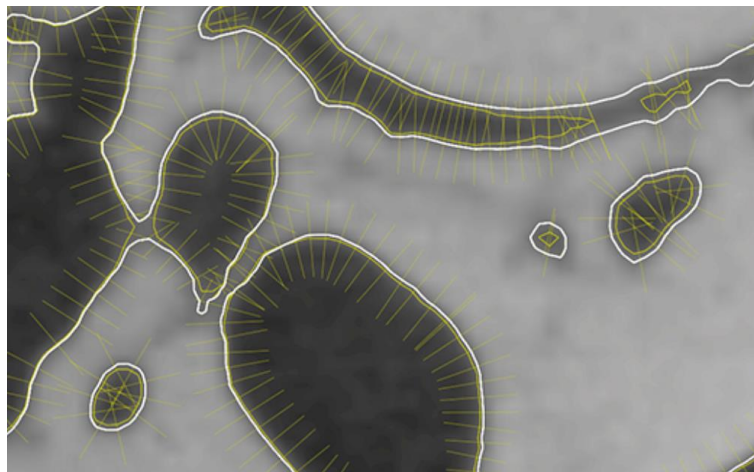
Figure 3.10. Close-up view of a slice with the advanced mode of the surface determination process: white line shows the first contour calculated, yellow hairlines represent the search direction for the local grey values, and bold yellow lines show a preview of the final re-evaluated surface.

Once the surfaces of the segmented structures of interest have been carefully determined, 3D rendering of the volume can be performed with the *Isosurface Renderer* tool (Figure 3.11). However, before starting the analyses, the crucial step of alignment has to be performed.

Alignment

Each mandible was scanned with its own orientation and imported into the software with its own coordinate system, depending on how it was placed in the box or in the scanner, and also depending on the type of modality (micro-CT, CBCT) used. In order to standardise the analyses, all the volumes were aligned following a similar reference coordinate system.

Figure 3.11. Three-dimensional rendering of a mandible (lateral views) with the different materials (cortical and trabecular bones, teeth) in semi-transparency (bottom). Scale bar: 10 mm.

The VGStudio MAX 3.1. *Measurement* menu allows for the creation of different types of geometry elements, such as *Points*, *Plane*… Using *Points,* three anatomical landmarks (defined in İşcan and Steyn, 2013; Caple and Stephan, 2016) were collected on each 3D model: left and right gonions *(go)*, located on the most posterior point of the inferior margin of the mandibular body; and menton *(me)*, the most inferior point of the inferior margin of the body at the mental symphysis. The *Polyline* instrument was then used to fit a spline curve along the inferior margin of the mandibular body, between the left and right gonions and passing through the menton (Figure 3.12 A). A best-fit – reference – plane, positioned under the mandible, was automatically computed from these anatomical landmarks and semi-landmarks (Figure 3.12 B), allowing the creation of a new coordinate system of reference. The installation of this new system generated the three following orthogonal planes: horizontal, parallel to the best-fit plane computed and dividing the mandible into inferior and superior parts; coronal, dividing the anterior and posterior parts of the mandible; and sagittal, dividing the mandible into left and right sides (Figure 3.12 C-D).

The volumes were all realigned allowing the definition of non-oblique and analogous cross-sections independent of the modality (CBCT and micro-CT) and of the individual (regardless of dentition group). The aligned images were saved and exported in TIFF format.
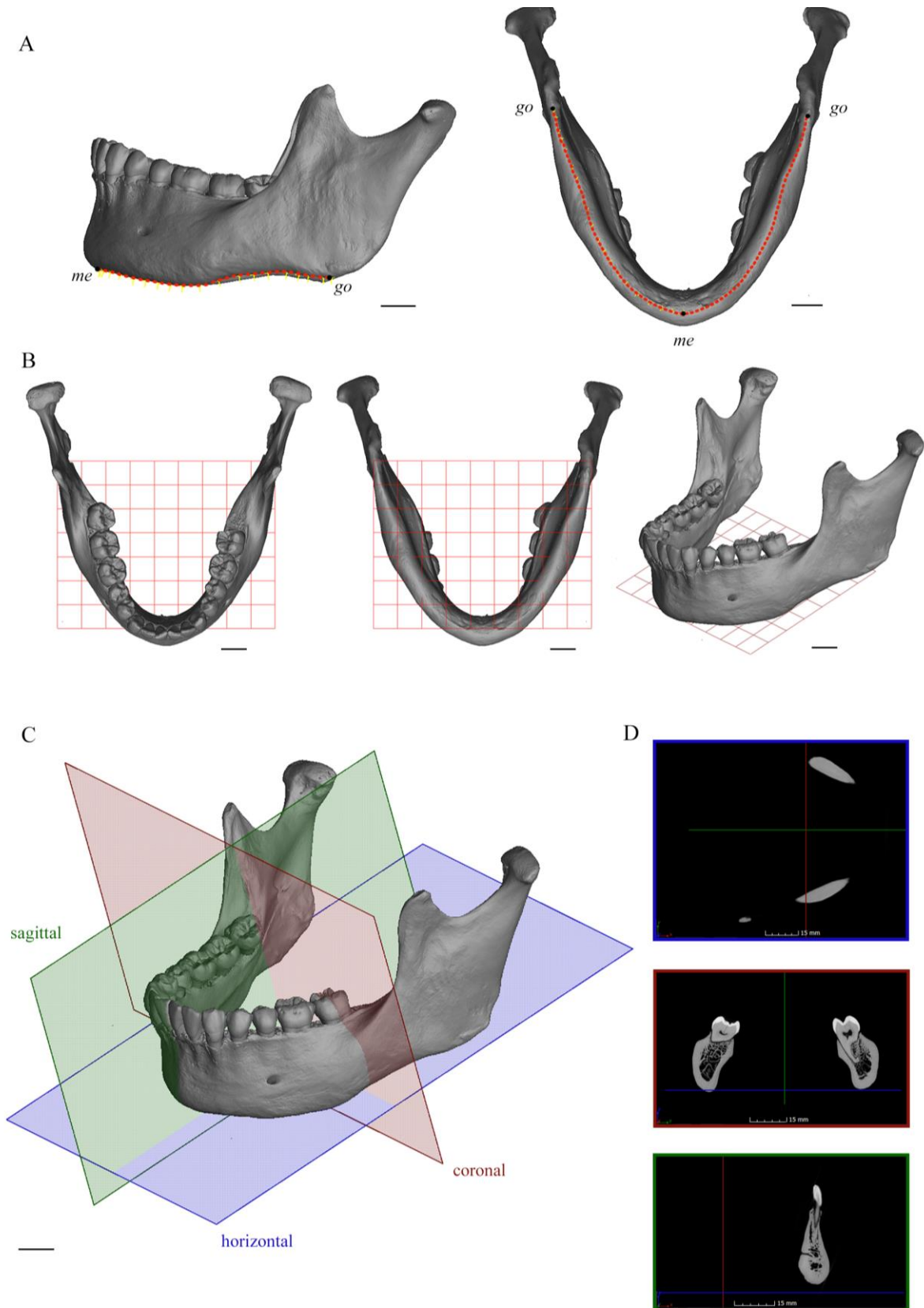
Figure 3.12. Alignment process. Lateral and inferior views of the mandible with the landmarks (black dots, *me*: menton, *go*: gonion) and the spline curve (red and yellow line) [A] allowing the automatic computation of the best-fit plane (red) positioned under the mandible [B]. New reference coordinate system installed generating the horizontal (blue), coronal (red) and sagittal (green) planes [C] and the sections associated [D]. Scale bars: 10 mm.

70

Sections

The first cross-section, the midline *(m)*, was defined in the mid-sagittal plane, i.e., at the mental symphysis passing through several landmarks: menton *(me)*; pogonion *(pg)*, the most anterior projecting point on the mental eminence; and infradentale *(id)*, the projecting point between the two central lower incisors on the buccal surface (Figure 3.13 A-B).

The left side of the mandible was chosen to define the remaining cross-sections of the body, as it was previously shown that no differences in microstructural parameters exist between the sides of the jaws (Schwartz-Dabney and Dechow, 2003; Deguchi *et al.*, 2006). The distance between the menton and the left gonion on the spline curve was recorded and was divided automatically into four equal parts. Two landmarks were defined in precise locations easily reproducible in dentate and edentulous individuals: anterior *(a)* at 1/4th of the menton-gonion distance; posterior *(p)* at 2/4th of the *me-go* distance (midpoint) (Figure 3.13 A). Because of the particular V- or U-shape of the mandible, the cross-sections located at *a* and *p* were oblique relating to the mandibular body. A rotation of the mandible along the vertical axis was achieved in order to have the sagittal (or the coronal) plane tangent to the spline curve (i.e., perpendicular to the surface) at *a* and to obtain the anterior cross-section (shortest distance across) after realignment (Figure 3.13 C). The same process was applied at *p* in order to define the posterior section (Figure 3.13 D). The 3/4th position along the menton-gonion distance was not considered a practical section to do uniform measurements as it inconsistently included the beginning of the anterior part of the ramus.

Finally, two cross-sections were defined on the ramus of the mandible: the minimum height *(rah)* and the minimum breadth *(rab)*. First, to obtain the height section, a *Freeform line* was fitted to the mandibular notch, between the condyle and the coronoid processes (Figure 3.14 A). The *Extract min./max point* tool allowed the automatic extraction of the minimum fit point of the *Freeform line* relative to the *go* landmark. This point, named *no* was usually the deepest point of the mandibular notch. The section containing *no* and *go* was defined as the minimum ramus height section (Figure 3.14 A-B). Then, two other *Freeform lines* were drawn on the anterior and on the posterior margins of the ramus (Figure 3.14 A). Using the *Extract min./max point* tool, the closest point of the anterior margin relative to the posterior margin was extracted and named *cor_min*. The same process was applied to the posterior margin where the *cond_min* point was extracted. The minimum ramus breadth section was defined perpendicularly to the height and passing through *cor_min* and *cond_min* (Figure 3.14 A-C).
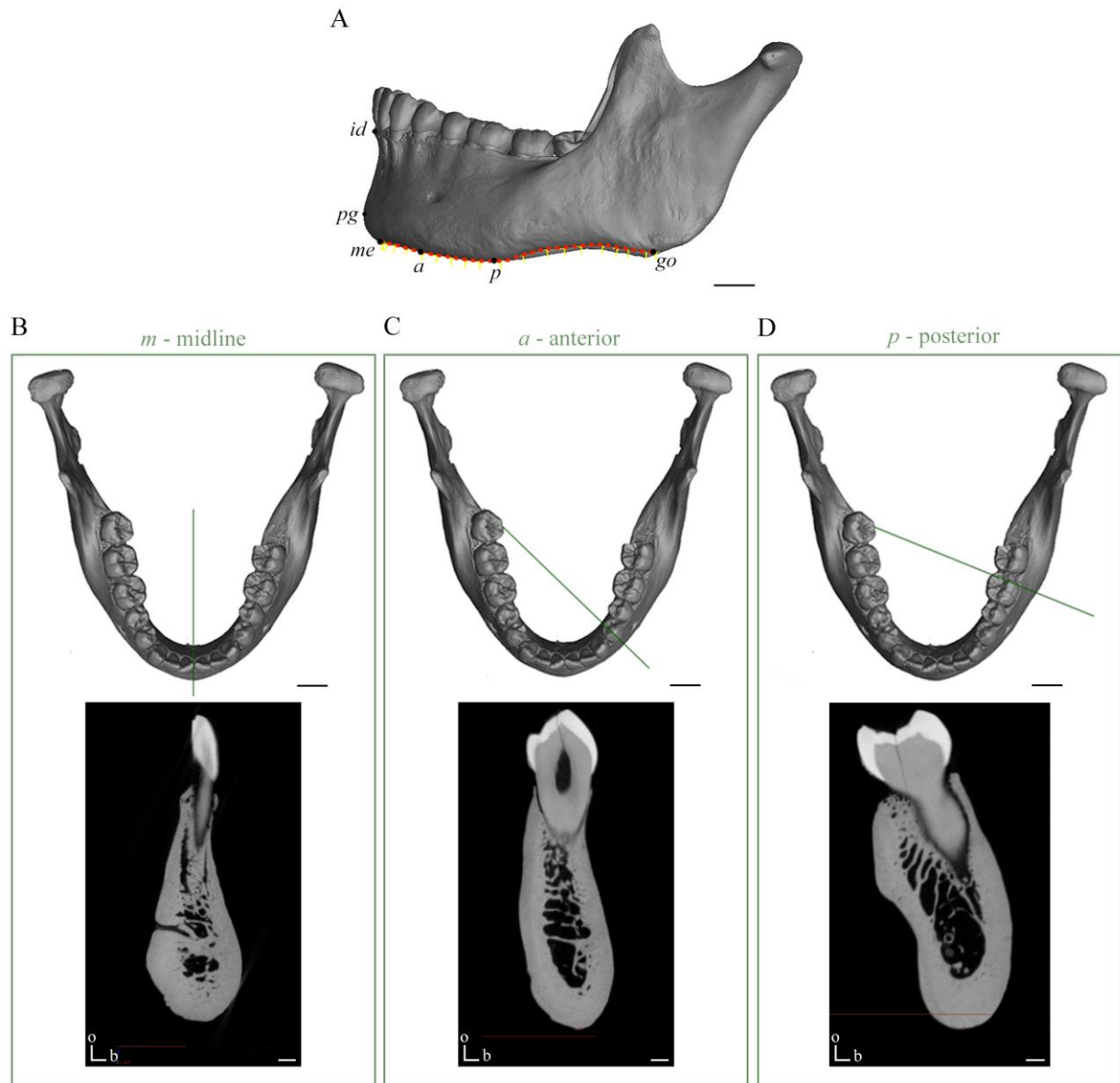
Figure 3.13. Sections on the mandibular body. Lateral view of the mandible with landmarks used (*id*: infradentale, *pg*: pogonion, *me*: menton, *a*: anterior, *p*: posterior, *go*: gonion) [A]. Three-dimensional models (upper row) with the corresponding two-dimensional cross-sections defined on the body (lower row) at the midline [B], anterior [C] and posterior [D] landmarks. Orientation: o: occlusal; b: buccal. Scale bars for the 3D models: 10 mm, and for the sections: 2 mm.
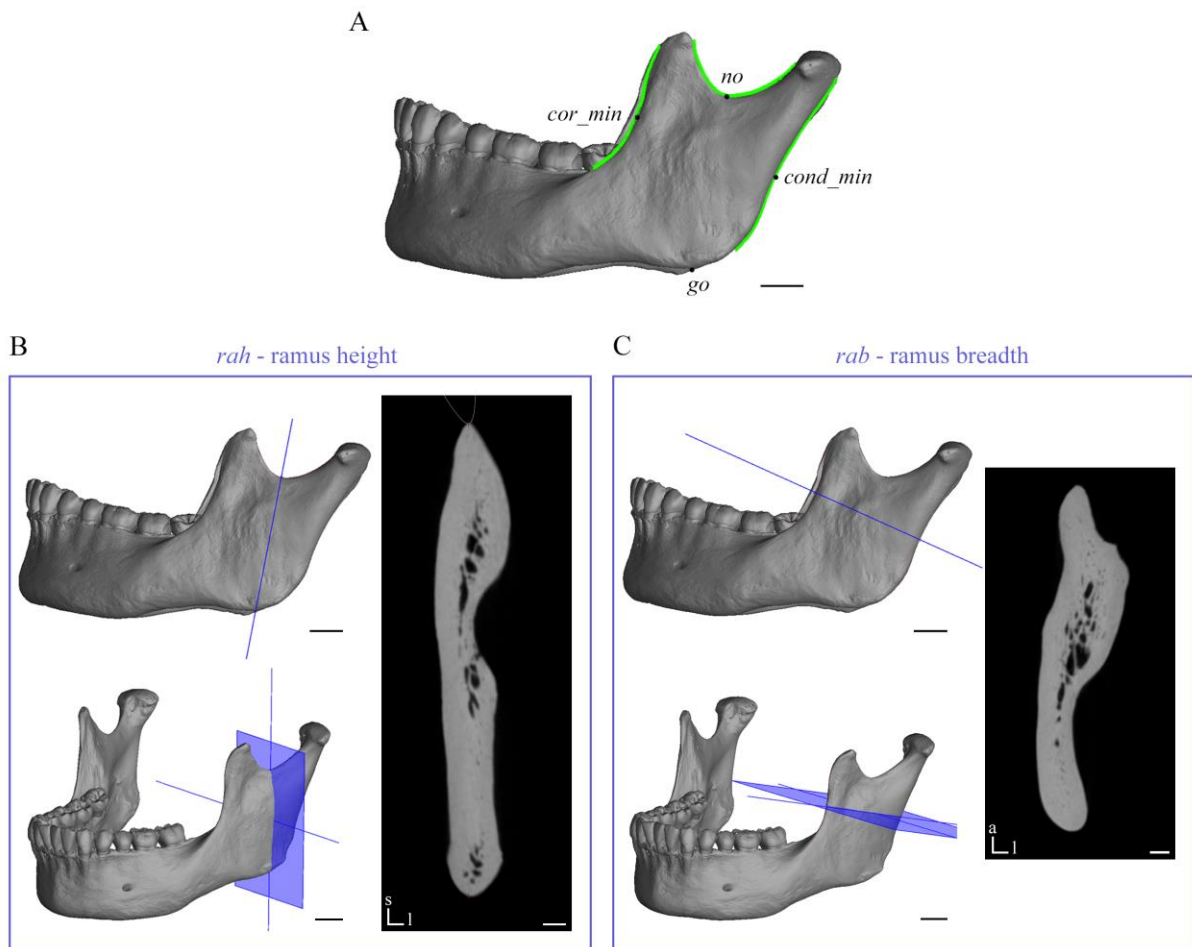
Figure 3.14. Sections on the mandibular ramus. Lateral view of the mandible with the landmarks defined (*no*: notch, *go*: gonion, *cor_min, cond_min*) on the *Freeform lines* (in green) fitted to the mandibular notch, the anterior and posterior margins of the ramus [A]. Three-dimensional models (left) with the corresponding two-dimensional cross-section (right) defined on the minimum ramus height between *no* and *go* [B]; on the ramus breadth between *cor_min* and *cond_min* [C]. Orientation: s: superior; a: anterior; l: lingual. Scale bars for the 3D models: 10 mm, and for the sections: 2 mm.

3.2.1.3. Data analysis

From the 357 micro-CT scans of entire mandibles performed, only 333 were selected for analysis (see Table 3.7 for more details). The 24 remaining scans were not analysed because of either: (i) technical issues during the scanning process, e.g., the mandible was not secured firmly enough and moved during the acquisition, resulting in blurry images; (ii) presence of pathologies; (iii) presence of dental restorations (undetectable with visual inspections) causing significant artefacts.

Table 3.7. Sex/ancestral group distribution of the mandibles analysed.

	F	M	**Total**	%
AA	56	152	**208**	62.5
EA	46	79	**125**	37.5
Total	**102**	**231**	333	
%	30.6	69.4		

F: female, M: male; AA: SA of African ancestry, EA: SA of European ancestry.

The analysis of the mandibular volumes was performed through different types of parameters computed in VGStudio MAX 3.1. software (Volume Graphics GmbH, Germany). First, external distances were recorded on the 3D models in order to quantitatively assess the external morphology of the mandible.

Then, the microstructural properties of the cortical bone were evaluated through the measurement of the cortical thickness on the sections, as well as through histomorphometric parameters, allowing the assessment of the cortical bone density. Each analysis was saved as a vgl project file containing all the information, registered alignment and analyses.

The two imaging modalities (CBCT and micro-CT) were compared with regard to the above 2D and 3D measurements (distances, cortical thickness, histomorphometric parameters), but also with a specific analysis (explained later), i.e., the cartography of the geometric deviations between the two volumes obtained for each specimen.

External distances

As explained previously in [3.2.1.2] *Sections*, the distance (on the spline curve) between the menton and the left gonion was recorded and was used to assess the body length (me-go_length). The *Caliper* instrument provided by VGStudio MAX 3.1. was used to measure the different heights and breadths of the mandibular body and ramus (Figure 3.15 A). The *Snap mode* was activated to automatically position the handles of the instrument on the material boundary defined by the surface determination process. The alveolar height of the body was measured perpendicularly to the reference plane (horizontal) at the location of the three following sections: midline (m_h), anterior (a_h) and posterior (p_h) (Figure 3.15 B-D). On the two sections of the ramus, the height (ra_h) and the breadth (ra_b) were recorded, respectively (Figure 3.15 E-F). All the distances and abbreviations are summarised in Table 3.8.

Cortical thickness

The thickness of the cortical bone was defined as the thickness from periosteum/external surface to the endocortical surface (Schwartz-Dabney and Dechow, 2002; Humphries, 2007), and was not size-adjusted according to each individual. Indeed, the mandibular size variation is often considered minimal and is characterised by a relatively small coefficient of variation.

The mandibular cortical thickness was measured at three sites (basal, buccal and lingual) of each cross-section previously defined (Figure 3.15 B-F). All the names, abbreviations and sites of measurement are summarised in Table 3.8. For example, on the midline section, the basal cortical thickness (m_ba_CtTh) was recorded from the most inferior point of m_h, tangentially to the outer cortical layer. Then, a *caliper* bisecting perpendicularly m_h was positioned. At the intersection sites with the buccal and lingual surfaces, the buccal and lingual cortical thicknesses were measured respectively (m_buc_CtTh, m_ling_CtTh) (Figure 3.15 B). The same process was repeated on the anterior and posterior sections at the respective cortical thickness sites: a_ba_CtTh, a_buc_CtTh, a_ling_CtTh (Figure 3.15 C); and p_ba_CtTh, p_buc_CtTh, p_ling_CtTh (Figure 3.15 D). On the cross-sections located on the ramus, only the buccal and lingual cortical thicknesses were measured. As explained for the corpus sections, the middle of the height and breadth distances were used to locate the four sites: rab_buc_CtTh and rab_ling_CtTh (Figure 3.15 E); rah_buc_CtTh and rah_ling_CtTh (Figure 3.15 F).
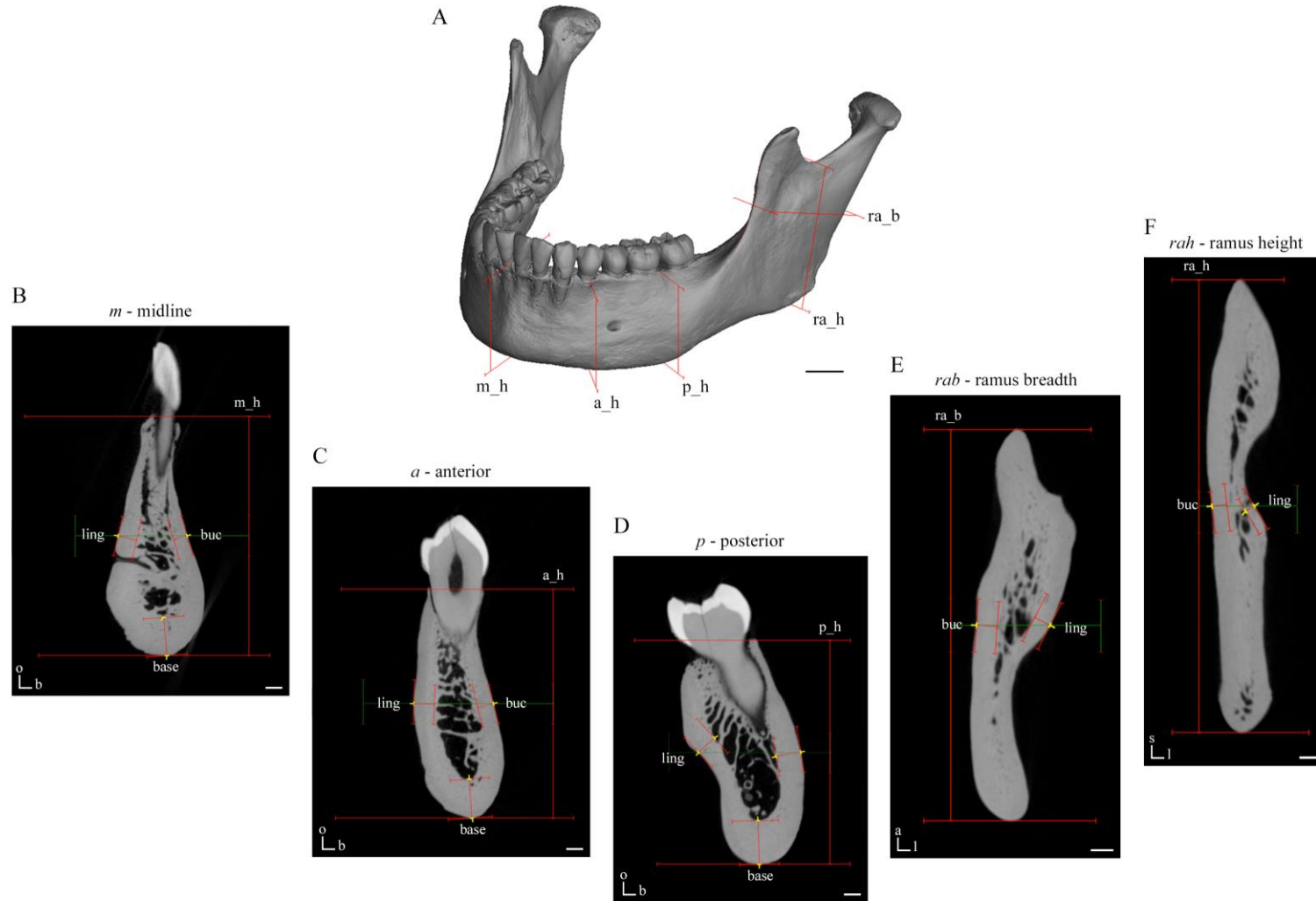
Figure 3.15. Measurements on the mandibular body and ramus. 3D model of the mandible showing the three different alveolar heights and the ramus breadth and height (red lines) [A]. On each corresponding cross-sections of the body – midline [B], anterior [C], posterior [D], ramus breadth [E] and height [F] – basal, buccal and lingual cortical thicknesses are recorded (in red). Orientation: o: occlusal; b: buccal; l: lingual; s: superior; a: anterior. Scale bars for the 3D model: 10 mm, and for the sections: 2 mm.

Table 3.8. List and descriptions of the linear variables recorded on the mandibles.

Section	Abbreviation	Description
Midline	*m*	
	m_h	height of the body at the midline
	m_ba_CtTh	basal cortical thickness at the midline
	m_buc_CtTh	buccal cortical thickness at the midline
	m_ling_CtTh	lingual cortical thickness at the midline
Anterior	*a*	
	a_h	height of the body on the anterior section
	a_ba_CtTh	basal cortical thickness on the anterior section
	a_buc_CtTh	buccal cortical thickness on the anterior section
	a_ling_CtTh	lingual cortical thickness on the anterior section
Posterior	*p*	
	p_h	height of the body on the posterior section
	p_ba_CtTh	basal cortical thickness on the posterior section
	p_buc_CtTh	buccal cortical thickness on the posterior section
	p_ling_CtTh	lingual cortical thickness on the posterior section
Ramus breadth	*rab*	
	ra_b	minimum breadth of the ramus (between *cor_min* and *cond_min*)
	rab_buc_CtTh	buccal cortical thickness on *rab*
	rab_ling_CtTh	lingual cortical thickness on *rab*
Ramus height	*rah*	
	ra_h	minimum height of the ramus (between *no* and *go*)
	rah_buc_CtTh	buccal cortical thickness on *rah*
	rah_ling_CtTh	lingual cortical thickness on *rah*

Histomorphometric parameters

The cortical bone density was assessed through various histomorphometric indices as defined by Parfitt (1988). The *Draw sphere* tool from the *Select* menu in VGStudio MAX 3.1. was used to create and extract spherical 3D volumes of interest (VOIs) from the original volume. These spheres, having a 0.4 mm radius, were placed in the cortical bone of each site of each cross-section previously used for the cortical thickness measurements. Using the automatic surface determination values, the *Properties* menu of the software provides general information on each VOI, such as dimensions (in voxel and mm), total volume (TV, mm^3) taking into account the volume of bone and the volume of the surrounding air (e.g., air in the

porosities for example), and the bone volume itself (BV, mm^3). From these parameters, the software then calculates the bone volumetric fraction (BV/TV, %), an histomorphometric parameter quantifying and accurately estimating the bone density. All the parameters recorded are summarised in Table 3.9.

Table 3.9. List and abbreviations of the mandibular histomorphometric parameters recorded.

Section	Site	BV (mm³) bone volume	TV (mm³) total volume	BV/TV (%) bone volumetric fraction[1]
Midline				
	basal	m_ba_BV	m_ba_TV	m_ba_BV/TV
	buccal	m_buc_BV	m_buc_TV	m_buc_BV/TV
	lingual	m_ling_BV	m_ling_TV	m_ling_BV/TV
Anterior				
	basal	a_ba_BV	a_ba_TV	a_ba_BV/TV
	buccal	a_buc_BV	a_buc_TV	a_buc_BV/TV
	lingual	a_ling_BV	a_ling_TV	a_ling_BV/TV
Posterior				
	basal	p_ba_BV	p_ba_TV	p_ba_BV/TV
	buccal	p_buc_BV	p_buc_TV	p_buc_BV/TV
	lingual	p_ling_BV	p_ling_TV	p_ling_BV/TV
Ramus breadth				
	buccal	rab_buc_BV	rab_buc_TV	rab_buc_BV/TV
	lingual	rab_ling_BV	rab_ling_TV	rab_ling_BV/TV
Ramus height				
	buccal	rah_buc_BV	rah_buc_TV	rah_buc_BV/TV
	lingual	rah_ling_BV	rah_ling_TV	rah_ling_BV/TV

[1] BV/TV: bone volume/total volume ratio.

Micro-CT and CBCT volume registration

As 24 mandibles were scanned with two imaging modalities (see section [3.2.1]), two datasets were obtained for each of the 24 specimens: one from micro-CT and one from CBCT. In order to visualise and quantify the general volumetric discrepancies between the volumes (i.e., to which extent the CBCT volume deviates from the micro-CT reference), a registration process was first performed, followed by a nominal/actual comparison analysis (see section [3.2.3.3]). The registration, conducted in VGStudio MAX 3.1., allows the minimisation of the

distances between the datasets by mapping redundant information and finding correspondence between the two volumes (Toennies, 2012). Using the *Register object* menu (VGStudio MAX Reference Manual), the registration was computed within two steps: a Gaussian *Best-fit registration* of the CBCT volume against the micro-CT; and then, a *Feature-based registration* using the iterative closest point algorithm, with the micro-CT as the reference (Figure 3.16). This superimposition procedure determines significant points on the volume to be registered and matches them to corresponding significant points on the reference object. The quality of the final registration was calculated as a percentage and was repeated if/until necessary (i.e., superior to 95%).
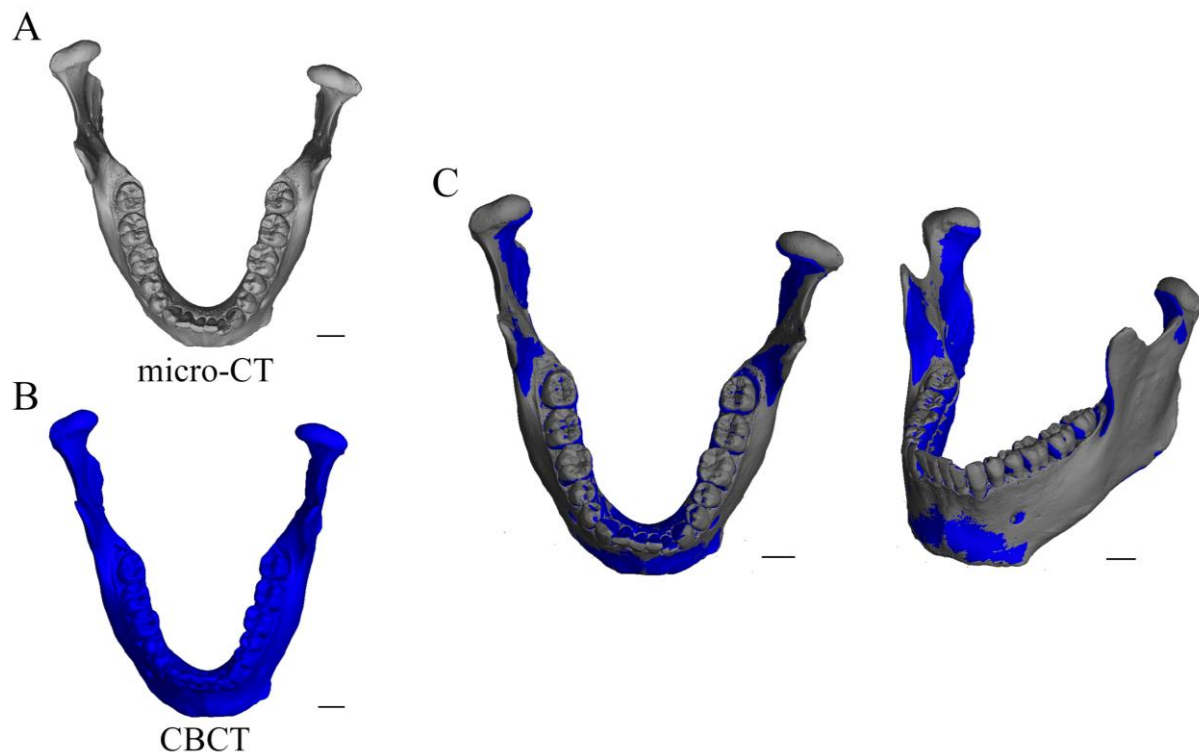
Figure 3.16. Registration process. Superior views of micro-CT-based [A] and CBCT-based [B] three-dimensional mandibular volumes before superimposition, and after [C]. Micro-CT volume is in grey, CBCT in blue. Scale bars: 10 mm.

3.2.2. Methods applied to the femur

3.2.2.1. Micro-CT data acquisition

The femora were scanned at Necsa (Pelindaba) with the same micro-CT system (Nikon Metrology, Belgium) used for the imaging of the mandibles. Following a similar acquisition protocol, each femur was immobilised in a polystyrene tube to avoid any movement and

vibrations during the rotation of the sample manipulator. Because of the large size of the bone, and in order to optimise the resolution, only the proximal end of the femur was scanned (from mid-shaft). In total, 50 micro-CT scans were conducted and 18 were collected from a previous project (courtesy of M. Cazenave), all with the following voltage and current parameters: 100 kV and 100 μA. The reconstruction process of the radiographic projection images into a 3D volume was performed in the Nikon CT-Pro software (Nikon Metrology, Belgium) with optimised parameters, and an isotropic resolution ranging from 0.064 mm to 0.100 mm (all the acquisition parameters are detailed in Appendix D (Table D.4 and Table D.5). The final volumes were then exported in vol float format or in 16-bit TIFF images.

3.2.2.2. Image processing

All the volumes were imported in the VGStudio MAX 3.1. software (Volume Graphics GmbH, Germany). As for the mandibles, the importation parameters, and more particularly the grey value histograms, were checked and followed by the crop of the images to remove the unnecessary surrounding air (Figure 3.17).
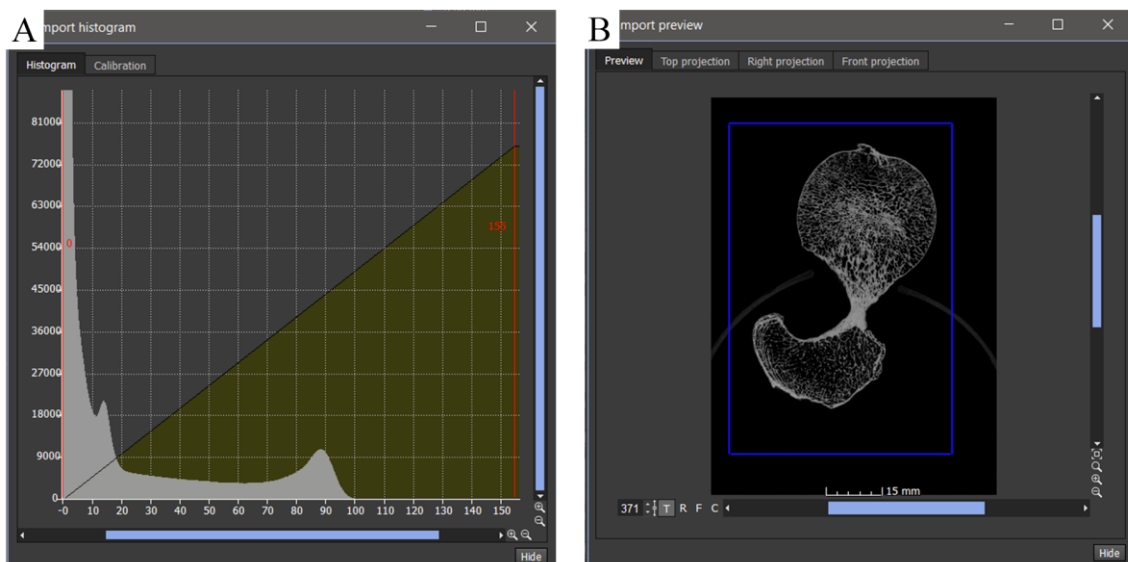
Figure 3.17. Importation process in VGStudio MAX 3.1. Snapshots of the modules displaying the grey value distribution histogram [A], and the volume preview of a femur [B].

Segmentation

The contour of the different types of tissue – cortical and trabecular bone vs. air – were defined following the segmentation procedure, using the grey values' histogram. The process,

like that applied on the mandible, was also divided into two steps: the *Automatic Surface Determination* first, and then the adaptive *Advanced mode.* Once the segmentation was completed, the 3D rendering was computed with the *Isosurface Renderer* tool (Figure 3.18).
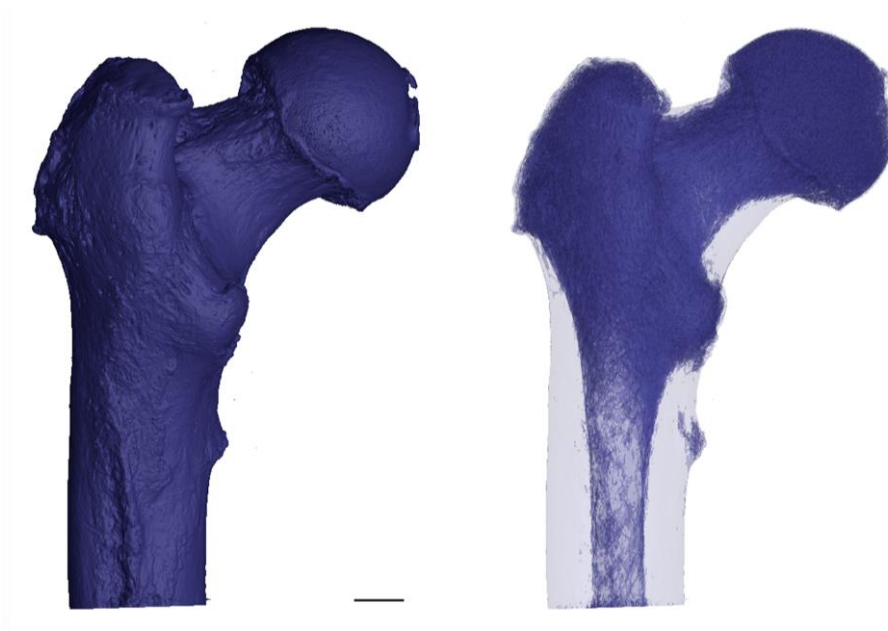
Figure 3.18. Three-dimensional rendering of a left femur (posterior views) with the different materials (cortical and trabecular bones) in semi-transparency (right). Scale bar: 10 mm.

Alignment

Femora were scanned with different positions and angles, affecting the orientation of the slices. To correct this factor and standardise the analyses between individuals, all the scans were aligned following the same coordinate system. A set of sliding landmarks was collected around the femoral head, avoiding the depressed fovea of the ligament of the head. Using the *Sphere* geometrical element from the *Measurement* menu, a best-fit sphere around the femoral head was automatically computed from those landmarks (Figure 3.19 A). A new coordinate system was installed and was used as a reference, with the centre of the sphere situated in the centre of the femoral head. However, the system was rotated in order to obtain the sagittal plane perpendicularly to the femoral neck, the transversal plane parallel to the long axis of the neck, and the coronal plane (Figure 3.19 B). This coordinate system was used as a reference to realign all the images and obtain the following three non-oblique sections: medio-lateral, supero-inferior and antero-posterior, analogously defined in all individuals (Figure 3.19 C). The aligned slices were saved and exported in TIFF format.
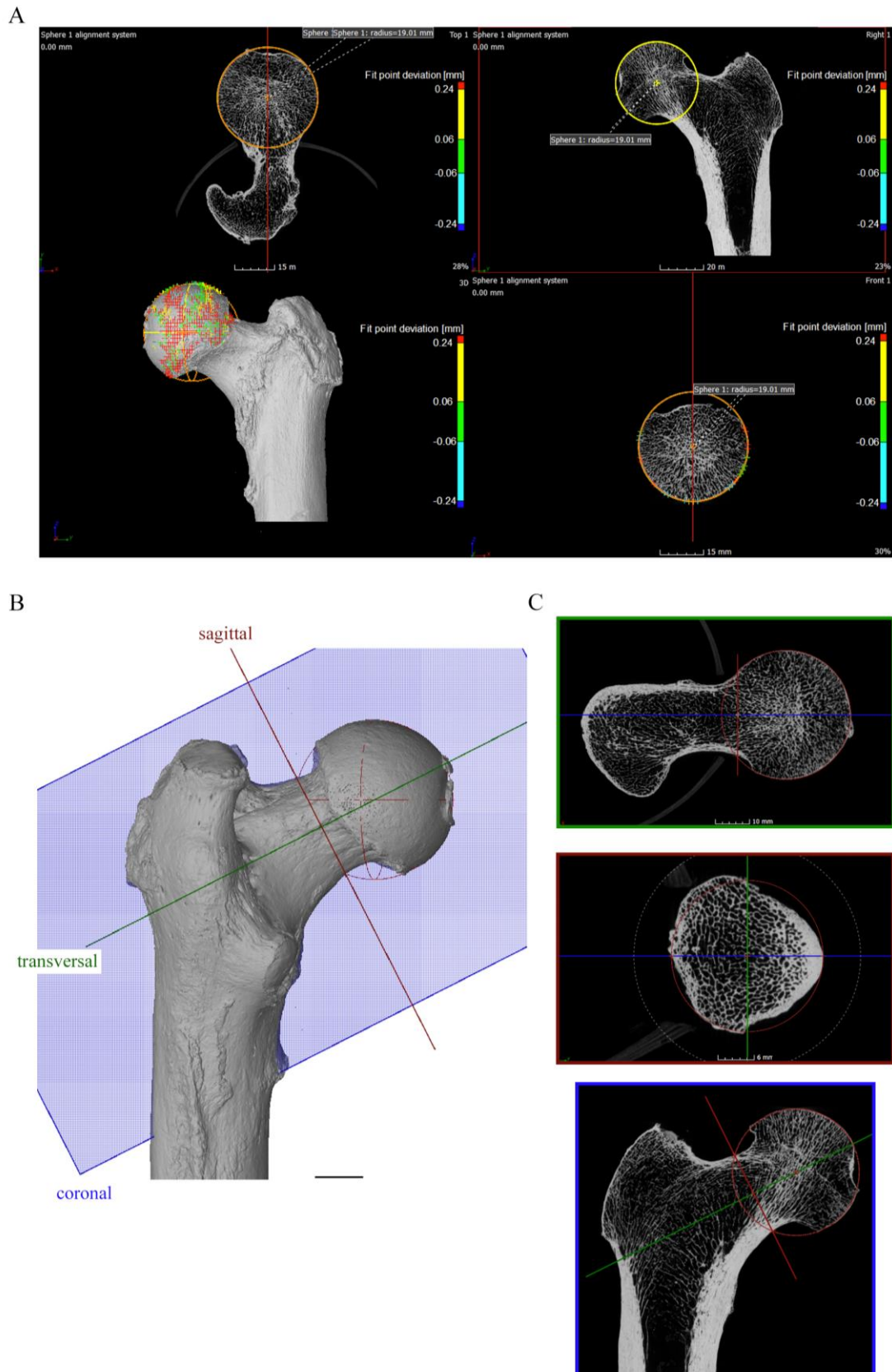
Figure 3.19. Alignment process. Snapshot of the software showing the best-fitted sphere around the femoral head (red, yellow, and green dots) [A]. 3D model of a femur (posterior view) after alignment in the new coordinate system of reference, generating three orthogonal planes: transversal (green), sagittal (red) and coronal (blue) [B]; and the sections associated: supero-inferior (green), medio-lateral (red) and antero-posterior (blue) [C]. Scale bar: 10 mm.

3.2.2.3. Data analysis

Sixty-four scanned femora out of the sixty-eight were selected for analysis (Table 3.10). Four scans were not analysed because of the same type of problems encountered with the micro-CT scans of mandibles: (i) technical issues during the scanning process causing blurry images; (ii) presence of metal inclusions within the bone generating artefacts.

Table 3.10. Sex/ancestral group distribution of the femora analysed.

	F	M	**Total**	%
AA	13	20	**33**	51.6
EA	14	17	**31**	48.4
Total	**27**	**37**	**64**	
%	42.2	57.8		

F: female, M: male; AA: SA of African ancestry, EA: SA of European ancestry.

As for the mandibles, the analyses of the femora were performed in VGStudio MAX 3.1. software (Volume Graphics GmbH, Germany). All the analyses were saved as a vgl project file containing all the information, alignment and measurements. After the alignment of the femur to the new coordinate system described in [3.2.2.2] the medio-lateral section, perpendicular to the maximum femoral axis, and corresponding to the minimum femoral neck diameter was extracted. On this section, the infero-superior (is_n) and antero-posterior (ap_n) neck diameters were traced using the *Caliper* instrument (Figure 3.20) allowing the precise localisation of four sites: inferiorly and superiorly at the most inferior and superior points of is_n, respectively (Figure 3.20 B); anteriorly and posteriorly at the most anterior and posterior points of ap_n, respectively (Figure 3.20 C).

Then, inner cortical parameters (BV/TV) were collected on the 3D models from the sections defined previously. Furthermore, only histomorphometric parameters were compared between the mandible and the femur. Indeed, as cortical thicknesses are two-dimensional linear measurements and highly influenced by the gross morphological features of the bone on which they are recorded, comparing them in the mandible and the femur would not be meaningful. However, the cortical histomorphometric parameters are ratios of three-dimensional parameters (bone volume on total volume, in %) allowing the comparison between two bones, which has

83

been performed by other researchers in the past (such as Hildebrand *et al.*, 1999; Liu *et al.*, 2008).

Three-dimensional spherical VOIs were thus extracted using the *Draw sphere* tool in the four sites of the medio-lateral section defined above. Based on the *Advanced surface determination,* the following structural and textural parameters were computed from each cortical VOI (Table 3.11): total volume (TV, mm^3), bone volume (BV, mm^3) and bone volumetric fraction (BV/TV, %).
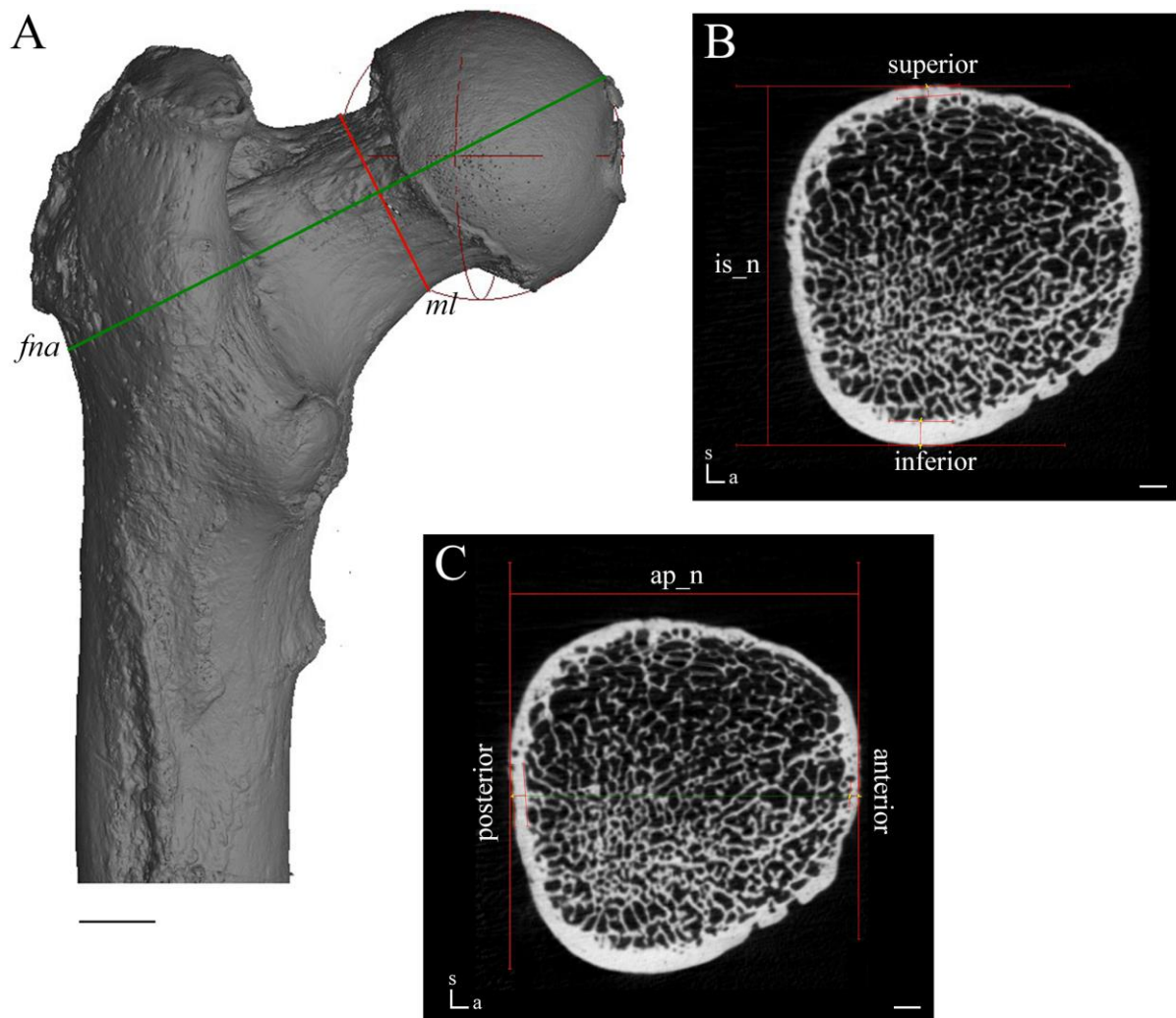
Figure 3.20. Selection of the medio-lateral section of interest. 3D model of a femur, in posterior view, with the femoral neck section (in red, *ml*) and the perpendicular femoral neck axis (in green, *fna*) [A]. Medio-lateral section corresponding to the minimum femoral neck diameter with the infero-superior neck diameter (is_n) and the inferior and superior VOI sites in [B]; and the antero-posterior neck diameter (ap_n) with the anterior and posterior VOI sites in [C]. Orientation: s: superior; a: anterior. Scale bar for the 3D model: 10 mm, and for the sections: 2 mm.

Table 3.11. List and abbreviations of the femoral histomorphometric parameters recorded.

Site	BV (mm³)	TV (mm³)	BV/TV (%)
	bone volume	total volume	bone volumetric fraction[1]
Inferior	i_BV	i_TV	i_BV/TV
Superior	s_BV	s_TV	s_BV/TV
Anterior	a_BV	a_TV	a_BV/TV
Posterior	p_BV	p_TV	p_BV/TV

[1] BV/TV: bone volume/total volume ratio.

3.2.3. Statistical analyses

All statistical analyses were performed using the open-source software R (R Core Team, 2020) and especially the RStudio environment (RStudio Team, 2020). The statistical tests were performed using different packages and functions of R, cited accordingly later, while the graphics and plots were all computed with the *ggplot2* package (Wickham, 2016).

First, basic descriptive statistics were executed using the *R base* package and particularly the *summary ()* function, automatically computing location parameters such as minimum, maximum, mean, median and quartiles. A difference between the mean and the median of a variable suggests the presence of several outliers, and/or a dissymmetry in the distribution of the values. Variances and standard deviations were also calculated (*var ()* and *sd ()* functions) in order to indicate the dispersion of the values. All these descriptive parameters were usually illustrated with plots and boxplots, facilitating the detection of outliers.

3.2.3.1. Repeatability of measurements

The intra-observer reliability was tested by describing the differences between repeated measures performed by one observer (the author) for each scanning modality used in the thesis. Ten micro-CT and ten CBCT scans of mandibles were randomly selected from the entire sample and were analysed twice by the principal investigator (a total of 180 measurements for each modality). Inter-observer repeatability was not practical (volume/number of measurements) or deemed mandatory as the aim of this study was not about advocating a certain method, but mainly descriptive, and data from various researchers were not amalgamated for statistical analyses.

The intra-observer repeatability was firstly assessed by calculating Intraclass Correlation Coefficients (ICCs) using the *icc ()* function from the *irr* package (Gamer *et al.*, 2019). The one-way random model examining consistency (with a 95% tolerance level) was chosen as only the subjects (i.e., the individuals) are random, but not the observers (Koo and Li, 2016). However, as the ICCs are correlation coefficients, only the strength of the relationship between the two measurements is evaluated, but not their magnitude. Thus, absolute and relative technical errors of measurement (TEM, and %TEM) were also calculated, as they give precise values of the magnitude to which repeated measures vary (Knapp, 1992; Bruton *et al.*, 2000; Byrnes *et al.*, 2017).

Although the ICCs are reflecting both consistency and agreement (Bruton *et al.*, 2000), Bland-Altman plots were also computed to illustrate the intra-observer agreement and facilitate the understanding (Bland and Altman, 1986, 1999), especially in complex cases when a high correlation co-exists with a poor agreement (e.g., one scanning modality may always overestimate by 2 mm: the correlation between sets of measurements would be high, but the agreement poor). Systematic bias and outliers are also easily detected on these plots, where the differences between the repeated measurements performed for each individual (vertical y-axis) are plotted against their means (horizontal x-axis). The 95% limits of agreement are calculated as the mean difference ± two standard deviations of the differences, providing the upper and lower limits of a 95% confidence interval (different for each sample). Furthermore, Bland and Altman (1986, 1999) recommended that, for a high agreement, 95% of the points should lie within these limits (i.e., the scatterplot is not extending far from the mean).

3.2.3.2. Exploratory statistics

For each research question (i.e., each statistical test), two statistical hypotheses have to be postulated: H_0, the principal or null hypothesis; and H_1, the alternative hypothesis (Millot, 2018). According to the *p*-value obtained after each test and the significance level/threshold defined ($a = 0.05$ or 0.01 in our case), the null hypothesis was rejected or not: (i) if $p \leq 0.05$, then H_0 is rejected (H_1 is accepted); (ii) if $p > 0.05$, then H_0 cannot be rejected (H_1 cannot be accepted). In the first case (i.e., $p \leq 0.05$), it is said that the *p*-value is significant.

Choosing the appropriate statistical test (i.e., parametric vs. non-parametric) depends on the nature and number of variables analysed. For example, in the case of a quantitative variable (as opposed to a qualitative variable), a parametric test can be used if: (i) the values of the

variable are normally distributed and if the variances are equal (i.e., homoscedasticity); (ii) or if the sample sizes are large enough (N > 30), as their distribution tends to be normal (Millot, 2018). Using the *R stats* package, the distributions of the variables were checked with Shapiro-Wilk tests [*shapiro.test ()*] and were graphically represented with kernel density plots giving a good estimate of each variable distribution in the chosen sample without making any assumption on the probability function. The homogeneity of variances (i.e., homoscedasticity vs. heteroscedasticity) was tested using Fisher-Snedecor or Bartlett tests [*var.test ()* or *bartlett.test ()*] depending on the number of variances observed. Depending on the distribution of the variable and the homogeneity of the variances, parametric or non-parametric tests were chosen.

Micro-CT analysis of the mandible

Several statistical tests were run in order to analyse and compare the effects of tooth loss and advancing age on the mandible, and more particularly: between sexes, among populations, as well as with the location of the section or the VOI.

To compare the means between two independent samples (Millot, 2018), such as between sex (male vs. female) or population (South African of African vs. European ancestries), parametric Student's *t*-tests [*t.test ()*] or its non-parametric counterpart, the Mann-Whitney-Wilcoxon tests [*wilcox.test ()*] were used.

To compare the measurements across more than two groups, such as the sex/ancestral subsamples, the dentition categories, or the location of the measurement/VOI, one-way and two-way ANOVAs [*aov ()*] or MANOVAs [*manova ()*] could be used. Both ANOVAs and MANOVAs use variances to determine whether there are significant differences in the means of groups. However, the assumptions for ANOVAs and MANOVAs include a normal distribution and homoscedasticity. If these assumptions were not met, non-parametric Kruskal-Wallis rank sum tests [*kruskal.test ()*] were run. This test compares the variable's medians, and not the means. Furthermore, when necessary, post-hoc tests [*tukeyHSD ()* or *pairwise.wilcox.test ()*] were run to confirm where the differences occurred between groups (i.e., which pairs of means are significantly different from the rest).

Correlation analyses [*cor.test ()* function] investigated the presence (or not) of linear relationships between the different measurements (external distances, cortical thickness, histomorphometric parameters), but also between the measurements and advancing age. Pearson's correlation coefficient was used when the comparison was performed between two

normally distributed quantitative variables. When this was not the case, Spearman's correlation coefficient was calculated, especially that Pearson's correlation coefficient is very sensitive to extreme values (outliers). In addition, correlation coefficients were adjusted for multiple testing using Holm's correction, because of the high number of comparisons performed on similar variables, which may increase the probability of obtaining Type I errors (i.e., rejecting the null hypothesis, also called a false positive). In both Pearson's and Spearman's correlations, the coefficient quantitatively measures the dependence between two variables and provides the power and direction of the correlation (Rosner, 2016; Millot, 2018). It ranges between -1 and 1, where -1 indicates a strong negative relationship and 1 a strong positive relationship (i.e., the variables are perfectly correlated). Generally, the correlation is interpreted as: very strong if the correlation coefficient ranges between 1 and 0.8 (or -1 and -0.8); strong if between 0.8 and 0.6 (or -0.8 and -0.6); moderate if between 0.6 and 0.4 (or -0.6 and -0.4); weak/low if between 0.4 and 0.2 (or -0.4 and -0.2); very weak if between 0.2 and 0 (or -0.2 and 0). Finally, when the coefficient is close to 0, the relationship is null, or non-existent (Rosner, 2016; Millot, 2018).

The correlation coefficients were provided in tables but also in the form of correlation matrices, illustrated using the *corrplot* package (Wei and Simko, 2017). In these types of matrices, all the variables are presented in the first row and column, and the number at the intersection between each row and column is the coefficient obtained for the correlation of the two corresponding variables. Thus, the central diagonal of the matrix presents the correlation of each variable with itself (i.e., 1).

When correlations against age were significant, linear regression analyses were performed, using two possible types of regression models, i.e., the linear model [*lm ()*] or the generalised linear model [*glm ()*] in the case of non-normal data. Scatterplots with local regression lines were used to illustrate the correlation of each measurement with separated and pooled sexes and ancestries.

Micro-CT analysis of the femur and its comparison with the mandible

In order to bring the mandibular measurements into context with the rest of the skeleton, statistical tests were also performed to compare the measurements collected on the mandible with the ones on the femur. As the measurements were done on the mandible and the femur of the same individuals, the samples are considered paired and not independent as before. Thus, the direct comparisons were made using parametric paired two-samples *t*-tests [*t.test ()*] or its

88

non-parametric counterpart, the paired-samples Wilcoxon test [*wilcox.test ()*], also known as the Wilcoxon signed-rank test.

Correlation and regression analyses were computed between mandibular and femoral parameters as to see if the cortical density in the mandible is correlated to the cortical density in the femur, and reciprocally. Pearson's or Spearman's correlation coefficients [*cor.test ()*], followed by linear model [*lm ()*] or generalised linear model [*glm ()*] analyses were used.

Furthermore, correlations (Pearson's or Spearman's) and regressions (linear or generalised linear models) with advancing age were also performed in the mandible and compared to the femur, as to see if the cortical density of the two bones was similarly influenced by age.

3.2.3.3. Comparison between scanning modalities

As the same 24 mandibles were scanned with both micro-CT and CBCT, the two modalities could be compared. Four complementary statistical techniques were used to evaluate the agreement and the accuracy of CBCT-based measurements in comparison to micro-CT. The concordance was first assessed with Bland-Altman plots, and then through regression analyses. The direct comparison of the measurements was then performed with paired samples tests. Finally, the general volumetric discrepancies between micro-CT and CBCT were visualised and quantified through the deviation analysis.

Agreement between micro-CT and CBCT

Bland-Altman plots were computed for each pair of measurements obtained with both techniques. Furthermore, according to Bland and Altman (1986, 1999; Bruton *et al.*, 2000), correlation coefficients and ICCs are not the most appropriate statistical methods when comparing the reliability of two different instruments in measuring the same variables. However, the Passing-Bablok (1983) regression method is a non-parametric approach especially recommended for studies comparing two different techniques, and was calculated using the *mcr (Method Comparison Regression)* package (Model *et al.*, 2014). For each measurement, the method tested (i.e., CBCT) is regressed against the method of reference (i.e., micro-CT) and illustrated as scatterplots with the regression line and 95% confidence intervals, calculated by means of a resampling method, the bootstrap.

Comparison of measurements

CBCT-based measurements were compared to the micro-CT-based reference using paired sample tests, as each pair of volumes computed is resulting from the same individual. Following assumption testing, paired Student's *t*-tests (parametric) or Wilcoxon signed-rank test (non-parametric) were conducted on each variable using the following functions: *t.test ()* or *wilcox.test ().*

Deviation analysis: comparison of volumes

After the registration of each CBCT volume against its respective micro-CT (see section [3.2.1.3] and Figure 3.16), the *Nominal/Actual Comparison* module of VGStudio MAX 3.1. was applied directly to the registered volumes. The micro-CT volume was defined as the *nominal object*, while the CBCT volume was the *actual object*, i.e., the object for which the comparison was performed. For each specimen, the analysis generated three different types of colour-coded outputs quantifying the extent to which the CBCT volume deviates from the micro-CT reference: a colour map showing the topography of the geometric discrepancies; a histogram of the calculated deviations for the entire surface of the object; a second histogram indicating the cumulated absolute deviation values for the entire surface. In these three outputs, the colours comprised green for a deviation of 0 mm, and then passed through yellow for small deviations, while the largest deviations were coded in red (positive deviations) and blue (negative deviations) (Figure 3.21).

90
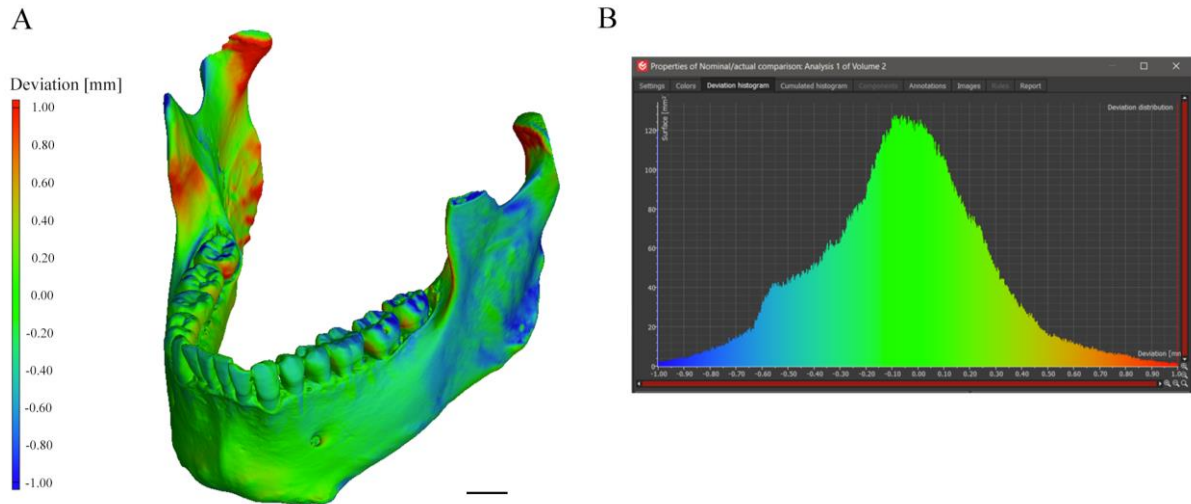
Figure 3.21. Nominal/Actual comparison process. Examples of coloured outputs computed for an individual: deviation map showing the geometric discrepancies on the entire volume [A], and histogram indicating the calculated deviations for the entire surface (in mm) [B]. Scale bar: 10 mm.

Chapter 4. Results: Micro-CT analysis of the mandible

The complete mandibular sample scanned by micro-CT included 333 individuals aged between 18 and 98 years (see Chapter 3. Materials and Methods for more details about the distribution of the sample across sexes, ancestries and dentition groups). As explained in the previous chapter, external distances and cortical thicknesses, as well as histomorphometric parameters, were recorded for all individuals.

In the first part of this section [4.1], the repeatability of micro-CT-based measurements was assessed through three different methods: intraclass correlation coefficients (ICC), technical errors of measurement (TEM and %TEM) and Bland-Altman (BA) plots. The second part [4.2] detailed the process of assumption testing, i.e., all the variables were tested for normality of distributions and homogeneity of variances. The next three parts focused, respectively, on the analyses of the external distances [4.3], cortical thicknesses [4.4] and histomorphometric parameters [4.5]. In each of these three sections, a similar approach was applied (outlined in the workflow Figure 4.1), starting with basic descriptive statistics of the measurements recorded, followed by exploratory statistics investigating the influence of various variables, such as sex, ancestry, tooth loss, location of measurement and aging. Finally, the most substantial results of each section were summarised (see [4.3.6] for the external distances, [4.4.6] for the cortical thickness, and [4.5.6] for the cortical density).

Micro-CT repeatability

ICC
TEM
BA

Assumption testing

normality
homogeneity of variances

1. Descriptive statistics

2. Influence of sex or/and ancestry

sex
F vs. M

ancestry
AA vs. EA

sex/ancestry
FAA vs. FEA vs. MAA vs. MEA

3. Influence of tooth loss

comparing dentition groups

in the entire sample
A vs. B vs. C

while controlling for sex
in F and in M: A vs. B vs. C

while controlling for ancestry
in AA and in EA: A vs. B vs. C

while controlling for sex/ancestry
in FAA, in FEA, in MAA and in MEA:
A vs. B vs. C

controlling for dentition groups

while comparing sexes
in A, in B and in C: F vs. M

while comparing ancestries
in A, in B and in C: AA vs. EA

while comparing sex/ancestries
in A, in B and in C:
FAA vs. FEA vs. MAA vs. MEA

4. Influence of measurement location

sections
midline vs. anterior vs. posterior vs.
ramus height vs. ramus breadth

sites
basal vs. buccal vs. lingual

13 sections/sites

inter-variables correlations

5. Influence of aging

correlations & regressions
entire sample
per sex, per ancestry
per sex/ancestry
per dentition category

Figure 4.1. General workflow followed for the analyses of the external distances, cortical thicknesses and cortical densities recorded on the micro-CT scans of mandibles.

93

4.1. Repeatability of micro-CT-based measurements

Intra-observer reliability was assessed through the repeated analysis of ten micro-CT scans by the same observer. The Intraclass Correlation Coefficients (ICCs) were calculated and resulted in excellent intra-observer reliability, with ICCs between 0.9991 and 1.000 (see Appendix E Table E.1). Both external distances and cortical thicknesses showed very high ICCs.

Following on this, for all the variables, absolute and relative Technical Errors of Measurement (TEM, %TEM) were estimated and are presented in Appendix E (Table E.1). Very low TEMs were found for both external distances (mean TEM at 0.020 mm, range: 0.013 – 0.031 mm) and cortical thicknesses (mean TEM at 0.010 mm, range: 0.007 – 0.014 mm). The mean %TEMs were also particularly small (always less than 0.80%), even if slightly greater for the cortical thicknesses (mean %TEM = 0.505%, range: 0.184 – 0.80%) than for the external distances (mean %TEM = 0.057%, range: 0.036 – 0.094%). The highest %TEMs were calculated for the buccal midline cortical thickness (m_buc_CtTh) and the cortical thicknesses located on the ramus, but were still considered repeatable.

Finally, the intra-observer agreement was examined using the Bland-Altman method. For each plot (i.e., each measurement), the differences between the two analyses performed (observation 1 vs. observation 2) were computed (see Appendix E Figure E.1 for the external distances and Figure E.2 for the cortical thicknesses). All the measurements at all sections showed a very high agreement, with no measuring differences exceeding 0.15 mm for the external distances and even as low as 0.05 mm for the cortical thicknesses. This spread of differences reflects a tendency for the intra-observer agreement of the cortical thicknesses to exceed that of the external distances: the smaller the measurement (cortical thickness vs. external dimensions), the better the agreement.

In summary, both types of mandibular measurements (external distances and cortical thicknesses), presented a very high intra-observer repeatability and agreement, when performed on micro-CT scans.

4.2. Assumption testing

4.2.1. Normality of distributions

Before further statistical analyses, various assumptions, including normality of distributions and homogeneity of variances, must be verified. First, kernel density estimates were calculated and plotted as they give a good estimate of the variable distribution in the chosen sample, without making any assumption on the probability function (e.g., normal distribution or not). These kernel density plots, performed for each variable (age, external distances, cortical thicknesses and densities) are presented in Appendix E, and were followed by Shapiro-Wilk tests.

4.2.1.1. Age

The age variable did not show a normal distribution (see Appendix E Figure E.3) when the entire sample was considered, or when the sample was subdivided by population groups (AA, EA). However, shapes of the age distribution of sex-separated groups were different: females were found to have a normal distribution, while males did not. For sex/ancestral subgroups, the age distribution curves were normal in FAA and approached normality in MAA, while skewed for FEA and MEA. A sampling bias towards older individuals of European ancestry was observed. Age distribution in the different Eichner dentition categories was also tested for normality (Appendix E Figure E.3). As expected, categories A and C were skewed: A towards the left and younger ages, while C was skewed towards older age ranges. However, category B was normally distributed. When the sample was subdivided per sex, males showed a normal distribution only for category B, while females were normally distributed across all three groups (A, B, C).

4.2.1.2. External distances

Kernel density plots of the six external distances are displayed in Appendix E Figure E.4. Within the entire pooled sample, the length of the mandibular body (me-go_length) and the three alveolar heights (m_h, a_h, p_h) showed non-normal distributions. Only the two external distances performed on the ramus (ra_b, ra_h) were following normal distributions.

The length of the body (me-go_length) was normally distributed in all subsamples (Appendix E Figure E.4): in males and females; in African and European individuals (AA, EA); in the four sex/ancestral subgroups (MAA, MEA, FAA, FEA); and in the three dentition categories (A, B, C) (Appendix E Figure E.5). Alveolar heights (m_h, a_h, p_h), however, showed non-normal distributions in both sexes, both ancestries, and in three sex/ancestral subgroups (MAA, MEA, FEA). Ramus breadths (ra_b) and heights (ra_h) were roughly normally distributed in the entire sample and all subgroups except AA. When divided into the three dentition categories (Appendix E Figure E.5 andFigure E.6), all external distances were found to follow a normal distribution in A, while it was more diverse in B and C.

4.2.1.3. Cortical thickness

Most of the cortical thickness measurements (9 of 13) showed non-normal distributions in the entire sample (Appendix E Figure E.7). When divided into subsamples, almost all the CtTh recorded on females were normally distributed, while this was the case in only five males (from the posterior or ramus sections only). A similar pattern was observed in ancestry-separated samples: the CtTh from the midline and anterior sections were not found to follow a normal distribution. The shapes of distribution of the cortical thicknesses were approximately normal in three sex/ancestral subgroups (MEA, FAA, FEA), but not in MAA. When the sample was divided into the three dentition categories (Appendix E Figure E.8 andFigure E.9), most of the CtTh from the midline and anterior sections were not normally distributed. Normality was more frequent posteriorly and on the ramus.

4.2.1.4. Histomorphometric parameters

None of the cortical densities (BV/TV) measured was found to follow a normal distribution in the entire sample, in the two sex-separated groups (M, F), in the two ancestral groups (AA, EA), in the sex/ancestral groups (FAA, FEA, MAA, MEA) or even in the subsamples defined with the three dentition categories (see Appendix E Figure E.10 and Figure E.11).

4.2.2. Homogeneity of variances

Homoscedasticity/heteroscedasticity was assessed on all the measurements taken on the full mandibular sample between sex, ancestry, sex/ancestry and between dentition groups. Homogeneity of variances was detected between sexes for all the external distances except for the mandibular body length and ramus height. However, between ancestries, sex/ancestral groups and dentition categories, the body length (me-go_length), ramus breadth and height showed equal variances, while the alveolar heights (m_h, a_h, p_h) did not. The cortical thicknesses did not present such constant patterns. At the midline, equal variances were only detected between ancestries, but not between sexes, sex/ancestral subsamples or dentition groups, while in the anterior section, homoscedasticity was found between sexes and dentition categories only. The posterior section showed equal variances between sex, ancestry and sex/ancestry, but not between dentition categories. Finally, the cortical thicknesses recorded at the ramus (on the height and breadth) had equal variances between sex, ancestry, and sex/ancestral groups as well as between dentition classes. Homoscedasticity was also tested on the histomorphometric parameters and was detected between sexes in four sites only (m_ba_BV/TV, a_buc_BV/TV, a_ling_BV/TV and rah_ling_BV/TV). All the other cortical densities were not found to have equal variances between ancestries, sex/ancestral groups and between dentition categories.

4.2.3. Conclusion

In conclusion, even if the sizes of the entire sample (N total = 333) and certain subdivided samples were large enough (more than 30 individuals in each of the following groups: M, F, AA, EA, MAA, MEA, FAA, FEA) to assume and tend to normal distributions for the external distances and cortical thicknesses, as soon as the dentition categories were added, the sample sizes were considered too small to approximate normality (e.g., five males of European Ancestry in Eichner category A) – see Appendix E Figure E.9.

To keep a consistent method of analysis for all the variables (external distances, cortical thicknesses, histomorphometric parameters) and because of the absence of normality and homoscedasticity in most of the subsamples, non-parametric statistical tests were selected for the subsequent analyses.

4.3. External distances

4.3.1. Basic descriptive statistics

Means, standard deviations and ranges (minimum – maximum) calculated for the mandibular body length (me-go_length), alveolar heights (m_h, a_h, p_h), ramus heights and breadths are detailed in Table 4.1 and Table 4.2.

As seen in Table 4.1, the lowest mean mandibular body length (me-go_length) and lowest minimal values were found in females (mean ± SD = 81.00 ± 4.79 mm, range: 70.67 – 97.97 mm) or in individuals from European ancestry (mean ± SD = 81.42 ± 4.91 mm, range: 70.67 – 95.55 mm). The FEA subgroup, specifically, showed the lowest mean body length, followed by FAA, MEA and MAA.

The mean alveolar heights were higher at the midline for all subgroups as well as for the pooled group (mean ± SD = 29.12 ± 6.82 mm) than at the posterior location for all subgroups and entire sample (mean ± SD = 23.85 ± 5.77 mm). Between sexes, lower mean values of midline (m_h) and posterior (p_h) heights were recorded in females than in males, but not for the anterior height (a_h). All three alveolar heights were higher in the AA subsample than in the EA subsample. The minimum values were particularly low in EA (e.g., AA range: 17.78 – 45.78 mm vs. EA range: 5.52 – 39.51 mm), showing the degree of resorption in some of the European ancestry individuals. In the sex/ancestral subgroups, the mean alveolar heights of the midline (m_h), anterior (a_h) and posterior sections (p_h) were higher in MAA and FAA than in MEA and FEA especially: MAA > FAA > MEA > FEA. However, high minimum values of m_h, a_h and p_h were found for FAA (18.51 mm, 20.88 mm, 15.41 mm, respectively) compared to the other subgroups, and more particularly compared to FEA (5.52 mm, 6.35 mm, 6.66 mm) and MEA (8.60 mm, 8.10 mm, 7.04 mm). These findings might be related to the difference in edentulism duration of the EA subgroups as compared to the other groups. This aspect will be addressed in later sections.

As expected, ramus breadths were always observed to be smaller than ramus heights in the entire sample, as well as in all the subgroups. When comparing sex groups, mean ramus breadths were found to be greater in males than in females (M mean ± SD = 31.33 ± 4.10 mm vs. F mean ± SD = 34.65 ± 4.58 mm), but the lowest minimum values were detected in males (M range: 21.26 – 50.72 mm vs. F range: 22.93 – 41.47 mm). Furthermore, AA individuals also showed higher mean values than in the EA subgroup. Following the same pattern noticed

98

for the alveolar heights in the sex/ancestral subgroups, the ramus breadths presented the largest mean ra_b in MAA and the lowest in FEA. On the other hand, the ramus heights showed a different pattern. Indeed, even if the mean heights were also smaller in females than in males (F mean $\pm$ SD = 43.05 $\pm$ 4.29 mm vs. M mean $\pm$ SD = 49.03 $\pm$ 5.18 mm), lower mean values were detected in the AA subgroup than in EA (AA mean $\pm$ SD = 45.96 $\pm$ 5.20 mm vs. EA mean $\pm$ SD = 49.32 $\pm$ 5.74 mm). In the sex/ancestral subgroups, the ramus heights were higher in MEA and MAA, than in FEA and FAA particularly.

Basic descriptive statistics were also calculated in each of the three main dentition categories defined with the Eichner Index (Table 4.2). The mandibular body length (me-go_length), the three alveolar heights (m_h, a_h, p_h) and the ramus breadth (ra_b) showed lower mean values in the category C (i.e., edentulous mandibles) than in B and particularly A, in which the values were always the greatest. In addition, particularly low minimum values were recorded in the C category (e.g., m_h range in C: 5.52 – 44.27 mm vs. m_h range in A: 22.71 – 45.70 mm). Furthermore, like the entire sample and the previous subsamples based on demographics (sex, ancestry, sex/ancestry), the posterior section, compared to the midline and anterior sections, consistently displayed the lowest mean alveolar heights in all groups. On the other hand, values recorded on the ramus height were relatively similar in all three dentition categories.

Table 4.1. Descriptive statistics of the external distances (mm) measured on micro-CT scans of mandibles in the entire sample and then separated per sex (F, M), per ancestry (AA, EA) and per sex/ancestral groups (FAA, FEA, MAA, MEA).

		Sex		Ancestry		Sex/ancestry			
	Total	F	M	AA	EA	FAA	FEA	MAA	MEA
	n = 333	n = 102	n = 231	n = 208	n = 125	n = 56	n = 46	n = 152	n = 79
me-go_length									
min – max	70.67 – 101.64	70.67 – 97.97	72.80 – 101.64	72.68 – 101.64	70.67 – 95.55	72.68 – 97.97	70.67 – 87.06	73.39 – 101.64	72.80 – 95.55
mean ± SD	84.68 ± 6.00	81.00 ± 4.79	86.31 ± 5.67	86.65 ± 5.75	81.42 ± 4.91	82.57 ± 4.82	79.09 ± 4.05	88.17 ± 5.31	82.78 ± 4.87
m_h									
min – max	5.52 – 45.70	5.52 – 44.75	8.60 – 45.70	17.78 – 45.70	5.52 – 39.51	18.51 – 44.75	5.52 – 32.92	17.79 – 45.70	8.60 – 39.51
mean ± SD	29.12 ± 6.82	26.93 ± 7.08	30.09 ± 6.49	31.99 ± 4.85	24.35 ± 6.97	30.66 ± 4.15	22.39 ± 7.29	32.48 ± 5.01	25.49 ± 6.56
a_h									
min – max	6.35 – 42.34	6.35 – 40.53	8.10 – 42.34	13.83 – 42.34	6.35 – 39.17	20.88 – 40.53	6.35 – 33.14	13.83 – 42.34	8.10 – 39.17
mean ± SD	28.70 ± 6.53	26.45 ± 6.76	22.69 ± 6.18	31.18 ± 4.54	24.57 ± 7.23	29.64 ± 3.56	22.57 ± 7.68	31.74 ± 4.74	25.74 ± 6.73
p_h									
min – max	6.66 – 34.15	6.66 – 31.73	7.04 – 34.15	14.82 – 34.15	6.66 – 34.15	15.41 – 31.73	6.66 – 29.73	14.82 – 34.15	7.04 – 34.15
mean ± SD	23.85 ± 5.77	22.04 ± 6.12	24.65 ± 5.42	25.84 ± 3.94	20.54 ± 6.74	24.61 ± 3.47	18.91 ± 7.15	26.30 ± 4.01	21.49 ± 6.34
ra_b									
min – max	21.26 – 50.72	22.93 – 41.47	21.26 – 50.72	24.13 – 50.72	21.26 – 40.74	24.13 – 41.47	22.93 – 33.94	28.66 – 50.72	21.26 – 40.74
mean ± SD	33.64 ± 4.69	31.33 ± 4.10	34.65 ± 4.58	35.88 ± 3.89	29.86 ± 3.31	33.86 ± 3.28	28.18 ± 2.55	36.63 ± 3.84	30.86 ± 3.32
ra_h									
min – max	35.00 – 61.49	35.00 – 53.84	35.16 – 61.49	35.00 – 57.28	35.16 – 61.49	35.00 – 50.31	38.70 – 53.84	36.56 – 57.28	35.16 – 61.50
mean ± SD	47.21 ± 5.64	43.05 ± 4.29	49.03 ± 5.18	45.96 ± 5.20	49.32 ± 5.74	41.38 ± 3.72	45.13 ± 4.06	47.64 ± 4.62	51.70 ± 5.17

Table 4.2. Descriptive statistics of the external distances (mm) measured on micro-CT scans of mandibles separated per dentition category, according to the Eichner Index (EI A, B, C: from full dentition to edentulous).

	EI A n = 112	EI B n = 97	EI C n = 124
me-go_length			
min – max	73.39 –101.64	72.68 – 96.89	70.67 –100.13
mean ± SD	86.79 ± 6.13	84.10 ± 5.35	83.23 ± 5.87
m_h			
min – max	22.71 – 45.70	25.00 – 43.48	5.52 – 44.27
mean ± SD	33.16 ± 4.49	31.05 ± 3.71	23.96 ± 7.22
a_h			
min – max	25.37 – 42.34	22.86 – 41.64	6.35 – 37.94
mean ± SD	32.58 ± 3.68	30.69 ± 3.37	23.62 ± 7.15
p_h			
min – max	20.90 – 34.15	13.45 – 34.15	6.66 – 30.61
mean ± SD	27.77 ± 2.93	25.29 ± 3.39	19.18 ± 5.94
ra_b			
min – max	26.09 – 50.72	22.93 – 48.80	21.26 – 44.13
mean ± SD	36.05 ± 4.19	33.38 ± 4.03	31.69 ± 4.65
ra_h			
min – max	35.72 – 61.49	35.16 – 59.30	35.00 – 60.59
mean ± SD	47.08 ± 5.48	47.14 ± 5.78	47.39 ± 5.70

4.3.2. Influence of sex or/and ancestry

4.3.2.1. Sex

Using non-parametric Mann-Whitney Wilcoxon tests, all external distances (me-go_length, m_h, a_h, p_h, ra_b and ra_h) were found to be statistically significantly different between sexes with p-values < 0.001, although some overlap was noticed (Figure 4.2). Measurements recorded on males were always larger than those obtained in females.
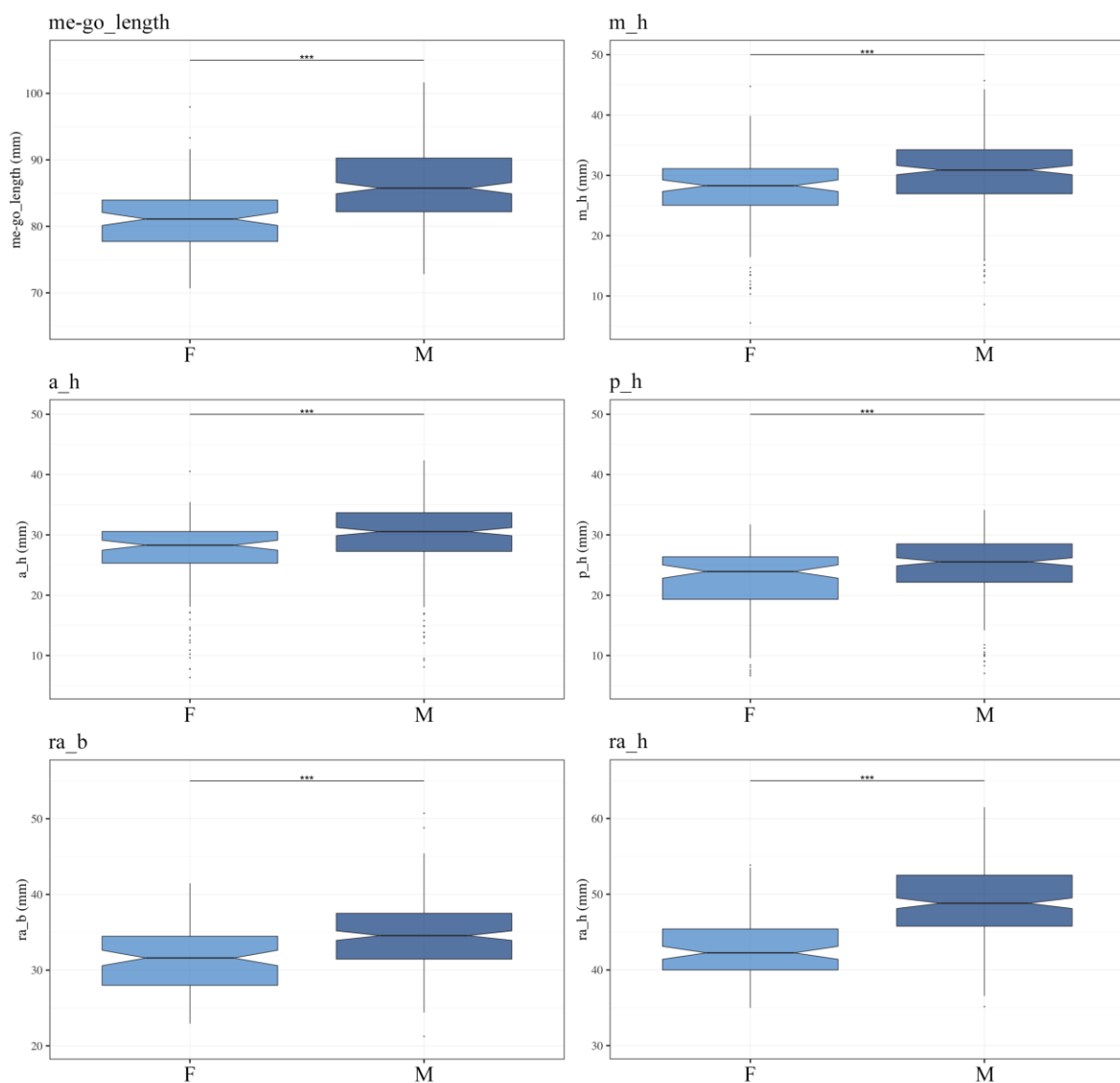
Figure 4.2. Boxplots of external distances (mm) per sex (F: light blue; M: dark blue). Dots depict outliers. Significance: *** $p < 0.001$.

4.3.2.2. Ancestry

As in the sex-separated samples, Mann-Whitney Wilcoxon tests performed on all external distances indicated significant differences between ancestries with p-values < 0.001 (Figure 4.3). South Africans from African ancestry (AA) were found to have significantly larger distances (me-go_length, m_h, a_h, p_h, ra_b) than South African individuals from European ancestry (EA), except for the ramus height, significantly greater in EA.
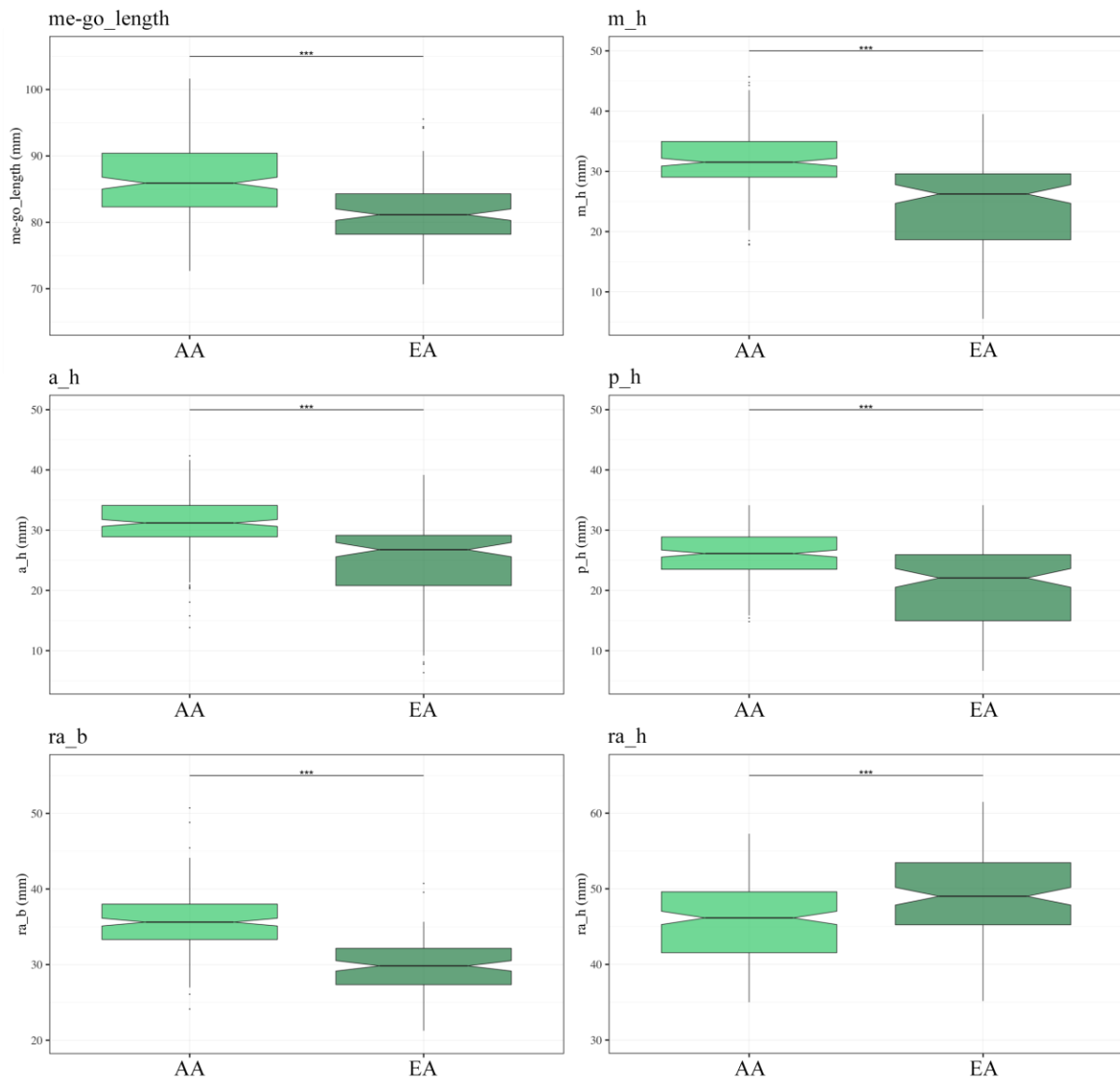
Figure 4.3. Boxplots of external distances (mm) per ancestry (AA: light green; EA: dark green). Dots depict outliers. Significance: *** $p < 0.001$.

103

4.3.2.3. Interaction between sex and ancestry

The sample was then divided into sex/ancestral subgroups (FAA, FEA, MAA, MEA) on which Kruskal-Wallis tests and their associated post-hoc tests (pairwise Wilcoxon) were applied. The different measurements are illustrated for each subgroup in Figure 4.4. For the length of the mandibular body (me-go_length), significant differences were found between all subgroups (with MAA displaying a longer body length, and FEA the shortest), except between FAA and MEA. The midline, anterior and posterior alveolar heights (m_h, a_h and p_h) also showed significant differences between almost all subgroups, excluding between FEA and MEA. Furthermore, unlike m_h and a_h, the posterior alveolar height (p_h) was also found not to be significantly different between FAA and MEA. In these three alveolar heights, MAA always showed the larger mean measurements, while FEA showed the smallest. The ranges of measurement, as seen in Figure 4.4 for m_h, a_h and p_h, were also noticed to be much wider in FEA than in the other subgroups. The distances recorded on the ramus (ra_b and ra_h) were all significantly different between all subgroups. However, while the largest ramus breadth (ra_b) was found in MAA and the smallest in FEA (ra_b: MAA > FAA > MEA > FEA), the largest ra_h was recorded in MEA, and the smallest in FAA (ra_h: **MEA** > MAA > **FEA** > FAA).
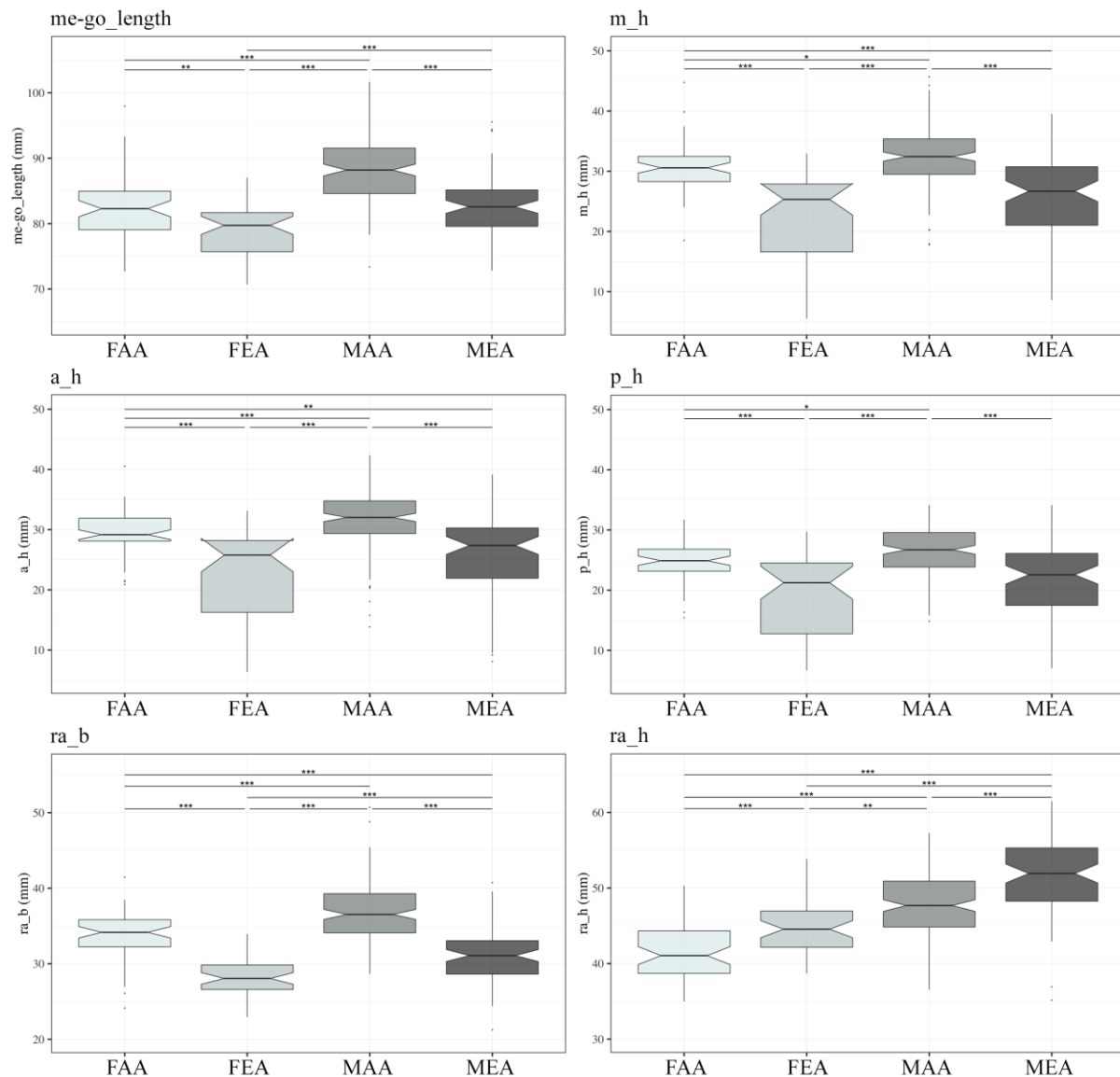
Figure 4.4. Boxplots of external distances (mm) per sex/ancestry (FAA, FEA, MAA, MEA: from light to dark grey). Dots depict outliers. Significance: *** $p < 0.001$, ** $p < 0.01$, * $p < 0.05$.

4.3.3. Influence of tooth loss

In the following section, the influence of tooth loss on the external distances was assessed, using the three dentition categories defined according to the Eichner Index (A, B, C: from full dentition to edentulous) in order to reflect tooth loss. First, the influence of tooth loss was tested in the entire sample, running Kruskal-Wallis tests, followed by pairwise Wilcoxon post-hoc tests when necessary. Then, the influence of tooth loss was analysed while controlling for sex, or ancestry, or their interaction (sex/ancestral subsamples), using Kruskal-Wallis and Wilcoxon post-hoc tests. Finally, the opposite was done, i.e., the influence of sex, ancestry, or

both, was evaluated while tooth loss was controlled for. This was performed using Mann-Whitney Wilcoxon tests for sex and ancestry, while Kruskal-Wallis and Wilcoxon post-hoc tests were applied in the sex/ancestral subsamples.

4.3.3.1. Tooth loss in the entire sample

The complete sample was divided into the three main dentition categories (A, B and C), defined according to the Eichner Index (EI), in order to control for tooth loss and estimate its influence on the external distances recorded on the mandibles. Kruskal-Wallis tests were run and all the external distances (me-go_length, m_h, a_h, p_h, ra_b) except ra_h ($p = 0.9694$), were found to be statistically significantly different between the three categories. Subsequent pairwise Wilcoxon post-hoc tests were used to highlight the differences between A, B and C (see Figure 4.5). The mandibular body length (me-go_length) was found the longest in A and statistically significantly different from B and C, while no significant differences were detected between the B and C categories. The three alveolar heights (m_h, a_h, p_h), however, were statistically significantly different between all three categories, with A consistently the biggest, and C the smallest. Statistically significant differences were also detected in the ramus breadth: ra_b was the widest in A, followed by B and then the smallest in C individuals. It is also interesting to notice that, for most of the measurements, the range of values was much wider in the C category than in the two other categories.
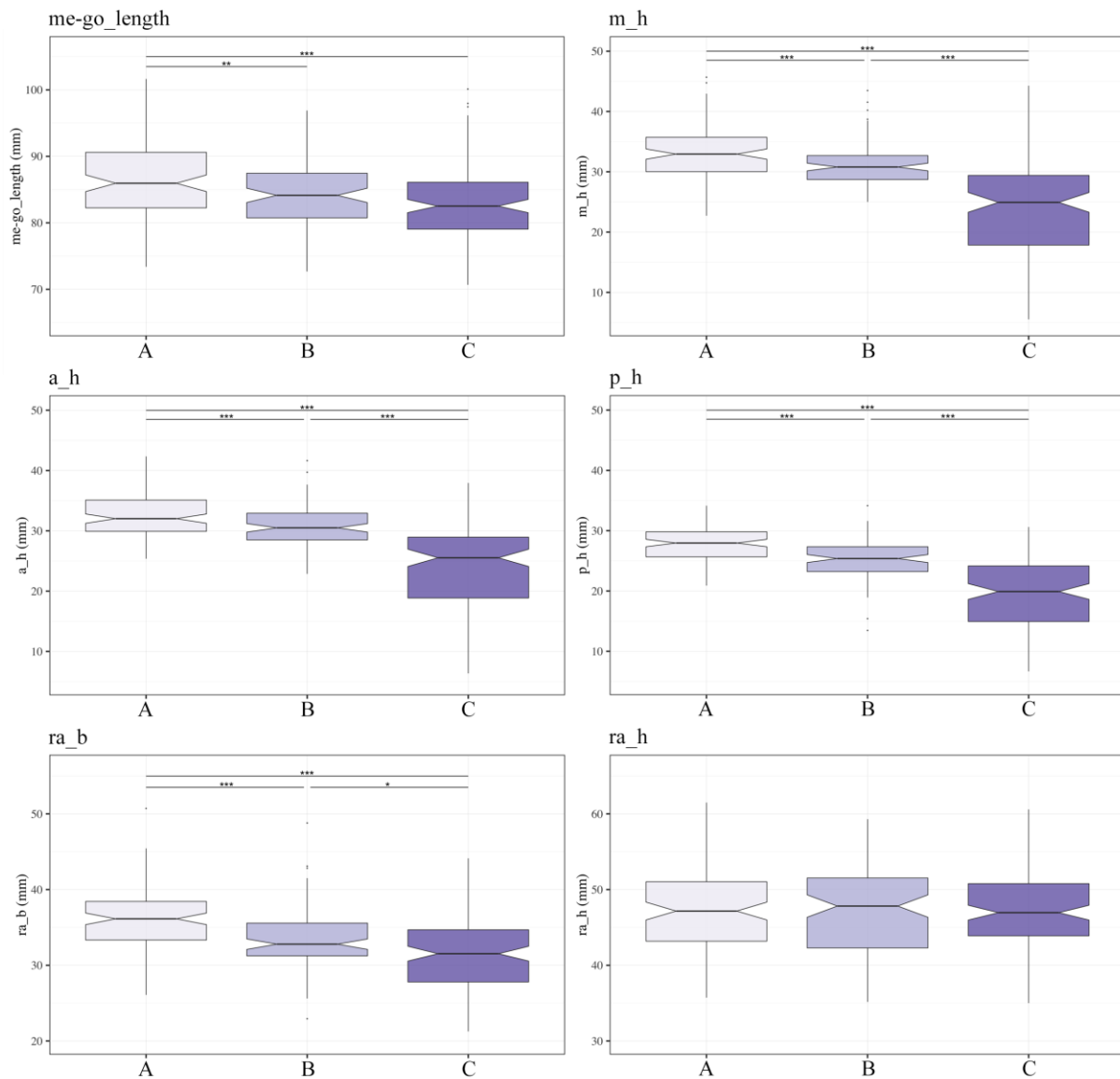
Figure 4.5. Boxplots of external distances (mm) per dentition category (A, B, C: from light to dark purple). Dots depict outliers. Significance: *** $p < 0.001$, ** $p < 0.01$, * $p < 0.05$.

4.3.3.2. Tooth loss per sex

The three dentition categories (A, B, C) were then compared within each sex group as a means to control for sex and assess the influence of tooth loss on the distances (see Figure 4.6 – females A vs. females B vs. females C; males A vs. males B vs. males C). The length of the mandibular body (me-go_length) was noticed to decrease from categories A to C in females and males. However, only males showed statistically significant differences, particularly between categories A and C, and then A and B. The three alveolar heights (m_h, a_h, p_h) and the ramus breadth (ra_b) showed statistically significant decreases with tooth loss within the female subsample and more particularly between dentition groups A and C, or between B and

C. Within males, statistical differences were also detected for the same distances between A and C, between B and C, but also between and A and B. On the other hand, no statistically significant differences were reported in F or M for the ramus height (ra_h).
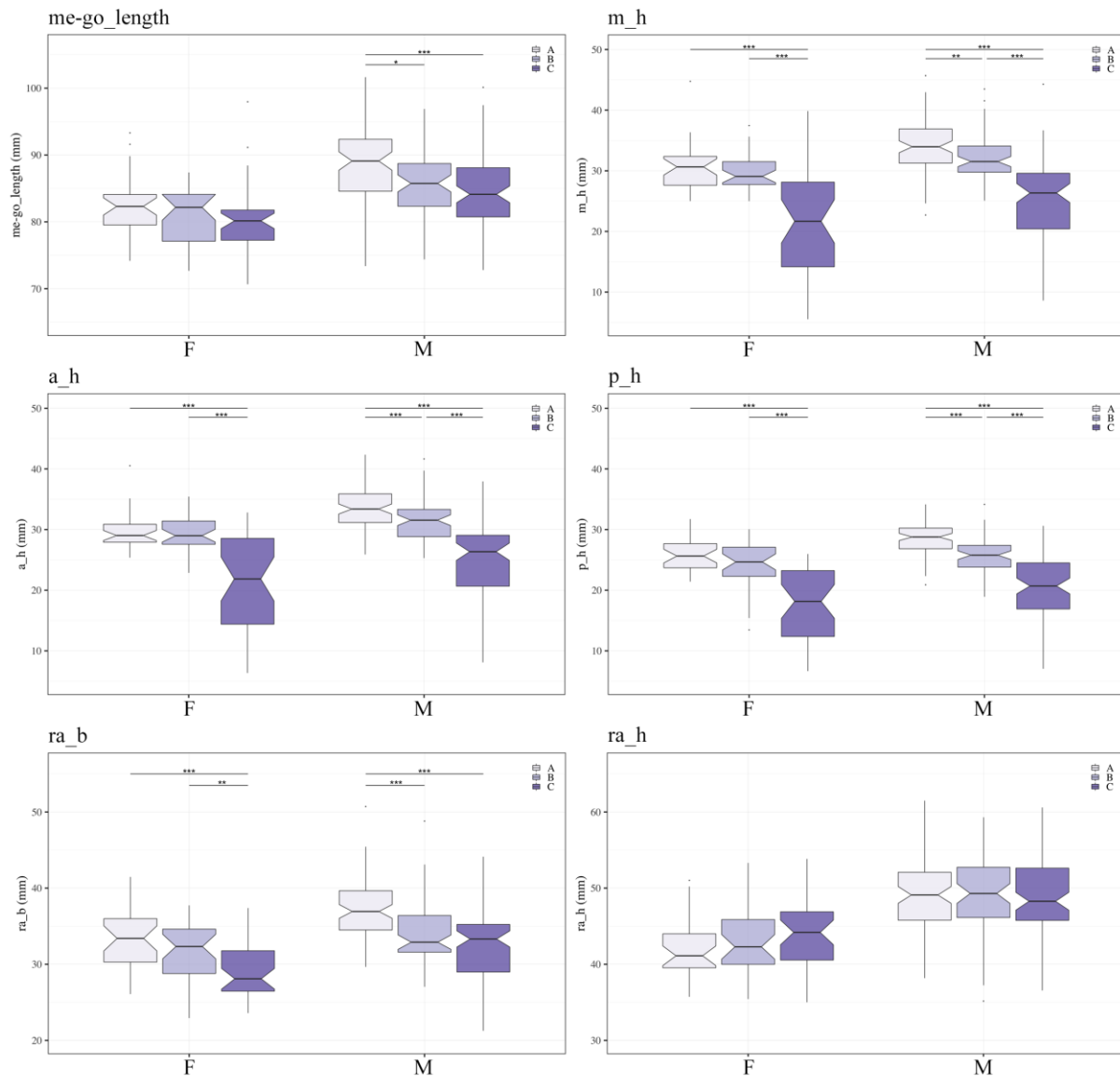
Figure 4.6. Boxplots of external distances (mm) per sex (F, M) and dentition category (A, B, C: from light to dark purple). Dots depict outliers. Significance: *** $p < 0.001$, ** $p < 0.01$, * $p < 0.05$.

4.3.3.3. Tooth loss per ancestry

As performed previously for sex, the influence of tooth loss was now analysed within each ancestral group (see Figure 4.7 – AA A vs. AA B vs. AA C; EA A vs. EA B vs. EA C). The length of the mandibular body (me-go_length) did not show any statistical significance in AA

or EA subsamples. The three alveolar heights (m_h, a_h, p_h), however, showed, in EA, statistically significant decreases with tooth loss, particularly in C compared to the others (significance between A and C, and between B and C). In AA, a less pronounced decrease was detected with tooth loss, even if statistical differences were also detected between A and C, between B and C, as well as between and A and B. The ramus breadth (ra_b) showed a very slight decrease with tooth loss in AA and EA. This decrease was only significant between B and C in EA, while in AA, the significance was found between A and B, and between A and C. On the other hand, for the ramus height (ra_h), no statistically significant differences were found in EA, and was only observed between A and B in AA (with a small decrease in height).
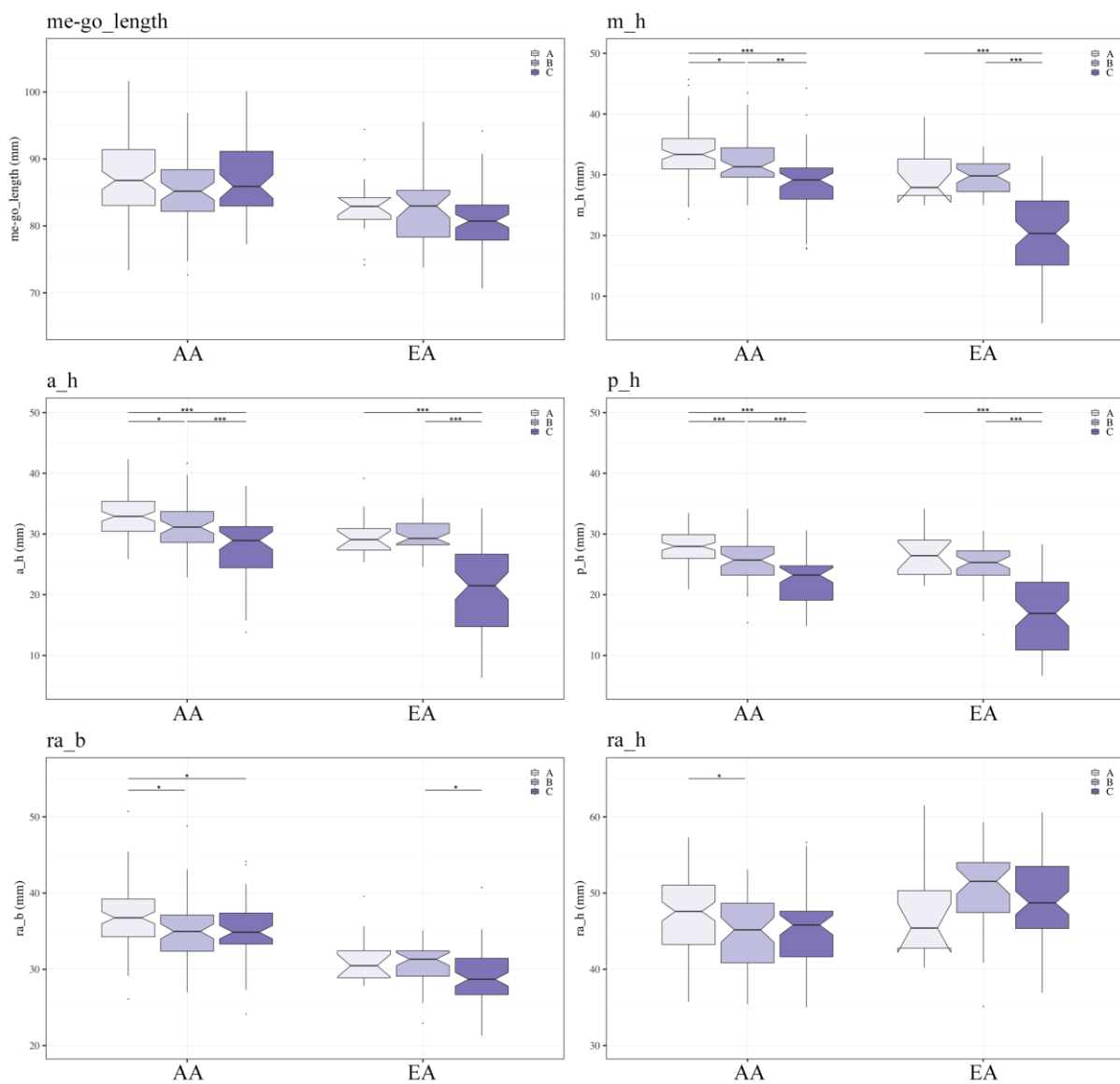
Figure 4.7. Boxplots of external distances (mm) per ancestry (AA, EA) and dentition category (A, B, C: from light to dark purple). Dots depict outliers. Significance: *** $p < 0.001$, ** $p < 0.01$, * $p < 0.05$.

4.3.3.4. Tooth loss per sex/ancestry

Finally, the influence of tooth loss was assessed while controlling for both sex and ancestry, by performing Kruskal-Wallis and Wilcoxon post-hoc tests between the three dentition categories within each sex/ancestral group (see Figure 4.8 – FAA A vs. FAA B vs. FAA C; FEA A vs. FEA B vs. FEA C; MAA A vs. MAA B vs. MAA C; MEA A vs. MEA B vs. MEA C). In AA and EA subsamples, the length of the mandibular body (me-go_length) did not show significant variations between dentition categories in any of the four subgroups. The midline and anterior alveolar heights (m_h, a_h) were significantly decreasing with tooth loss in three subgroups (FEA, MAA, MEA) but not in FAA. The posterior height (p_h), however, showed a decrease from category A to C in all four subgroups. Furthermore, as seen in the entire sample (Figure 4.5), the alveolar height values (i.e., the lengths of the boxplots) were particularly more variable in the C category than in the others, especially in the FEA and MEA subgroups. Interestingly, the ramus height in MAA was consistently decreasing across the dentition loss groups and a statistically significant difference was noted between A and C. This is contrary to the other sex/ancestral groups in which no pattern of changes in this distance could be detected.
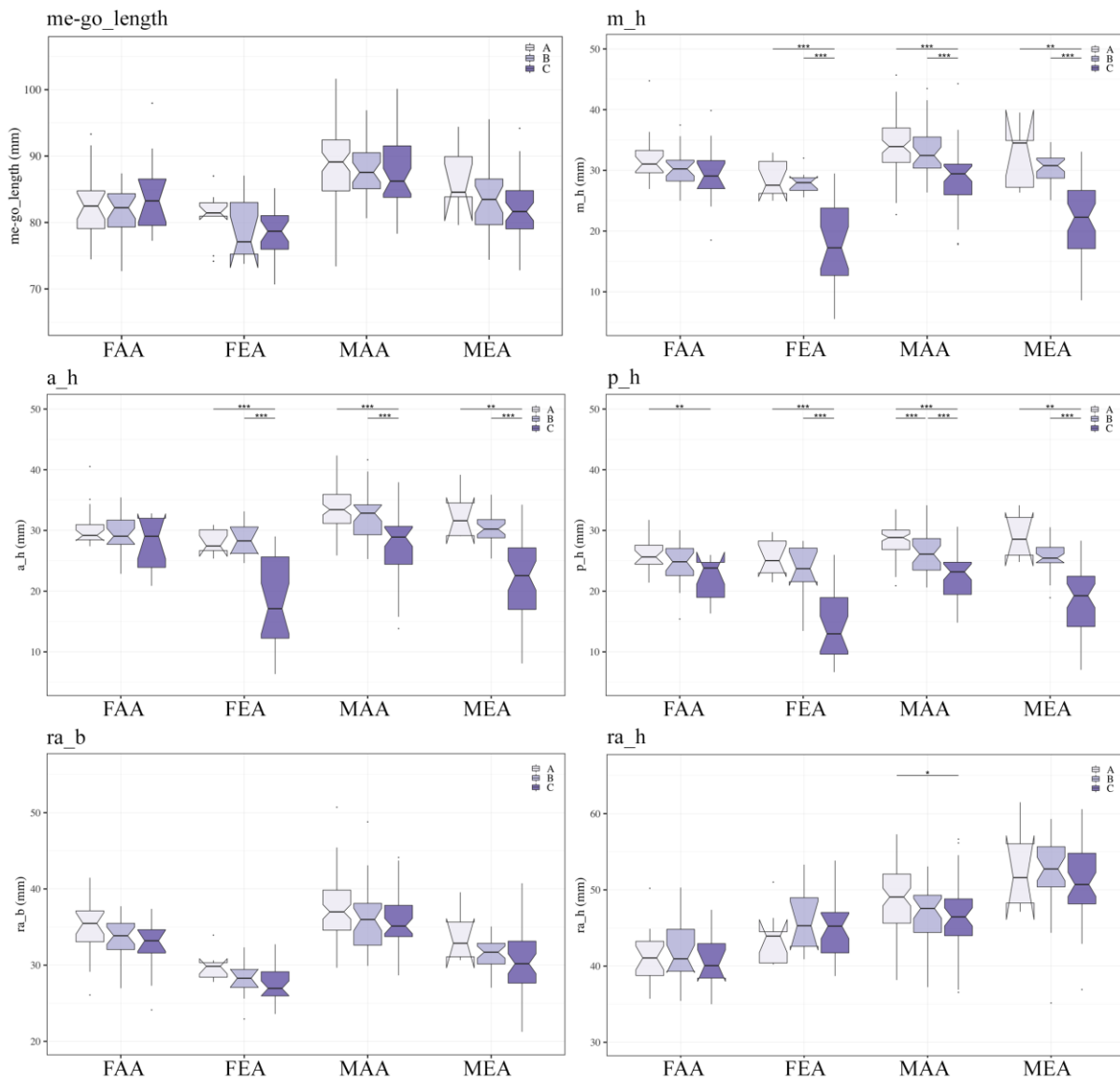
Figure 4.8. Boxplots of external distances (mm) per sex/ancestry (FAA, FEA, MAA, MEA) and dentition category (A, B, C: from light to dark purple). Dots depict outliers. Significance: *** $p <$ 0.001, ** $p < 0.01$, * $p < 0.05$.

4.3.3.5. Influence of sex per dentition category

The influence of sex on the external distances was assessed while controlling for tooth loss, using Mann-Whitney Wilcoxon tests in each dentition category. As illustrated in Figure 4.9, all dimensions were larger in males than in females. In category A, all six distances were statistically significantly different ($p < 0.001$) between sexes. All distances recorded on category C individuals were also significantly different between males and females, but to a lesser extent, particularly for the three alveolar heights ($p < 0.05$), most probably because of

the large spreading of values. Within the B group, significant differences between sexes were detected for me-go_length, m_h, a_h and ra_h, while not for p_h and ra_b ($p > 0.05$).
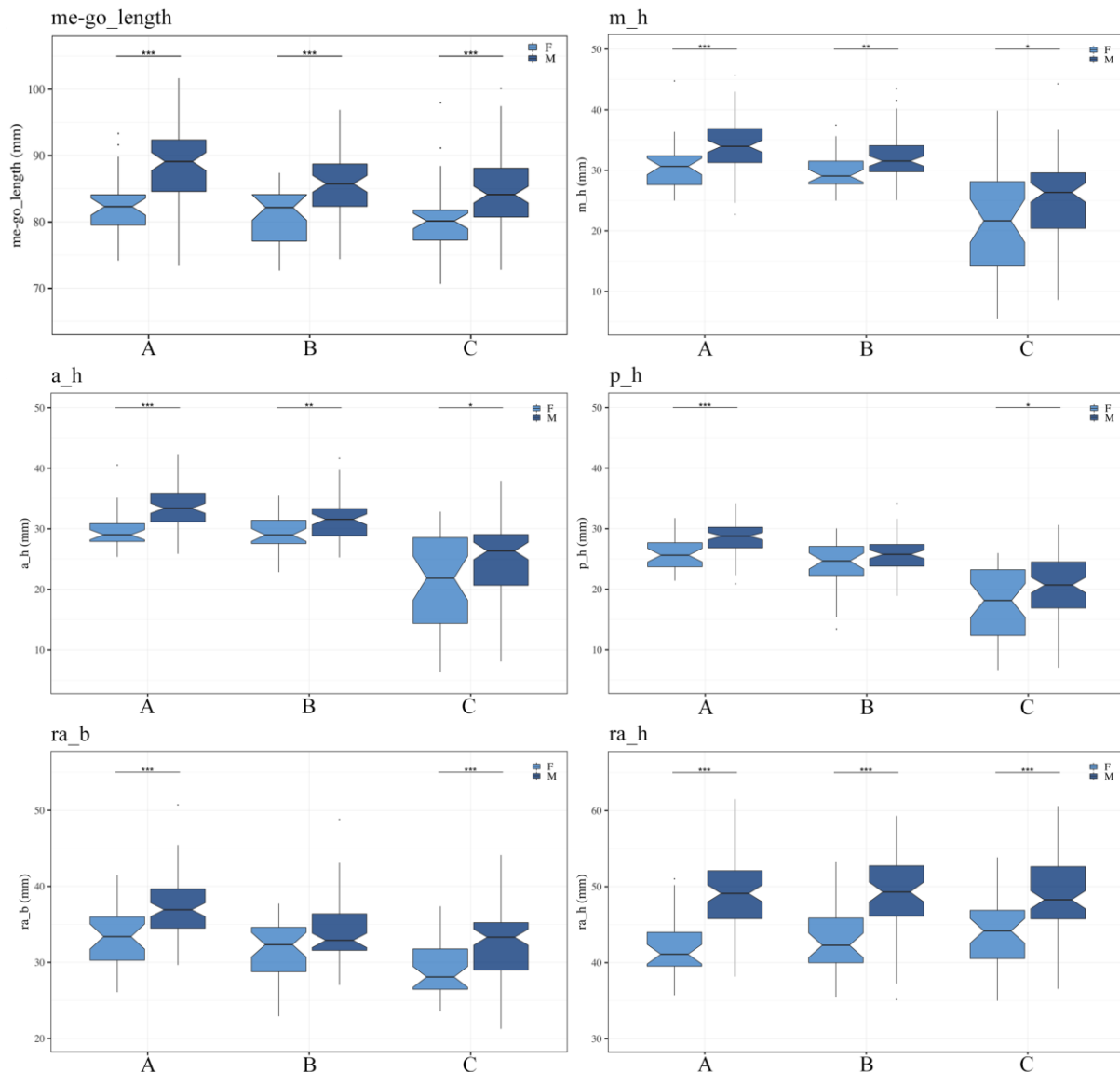
Figure 4.9. Boxplots of external distances (mm) per dentition category (A, B, C) and sex (F: light blue; M: dark blue). Dots depict outliers. Significance: *** $p < 0.001$, ** $p < 0.01$, * $p < 0.05$.

4.3.3.6. Influence of ancestry per dentition category

The influence of ancestry was estimated within A, B and C categories (i.e., controlling for tooth loss), through Mann-Whitney Wilcoxon tests (Figure 4.10). Apart from the ramus height (ra_h) measurements, all the other external distances were larger in AA than in EA. The mandibular body length, the midline and the anterior alveolar heights (m_h and a_h), as well as the ramus breadth, were significantly different between AA and EA subsamples in all three

dentition groups. However, the posterior alveolar height (p_h) was found to differ significantly between category C individuals of African and European ancestries (p < 0.001), but not in A and B ($p = 0.117$ and 0.6065, respectively). The ramus height also was not detected to be significantly different in A ($p = 0.6315$), but was in B and C.
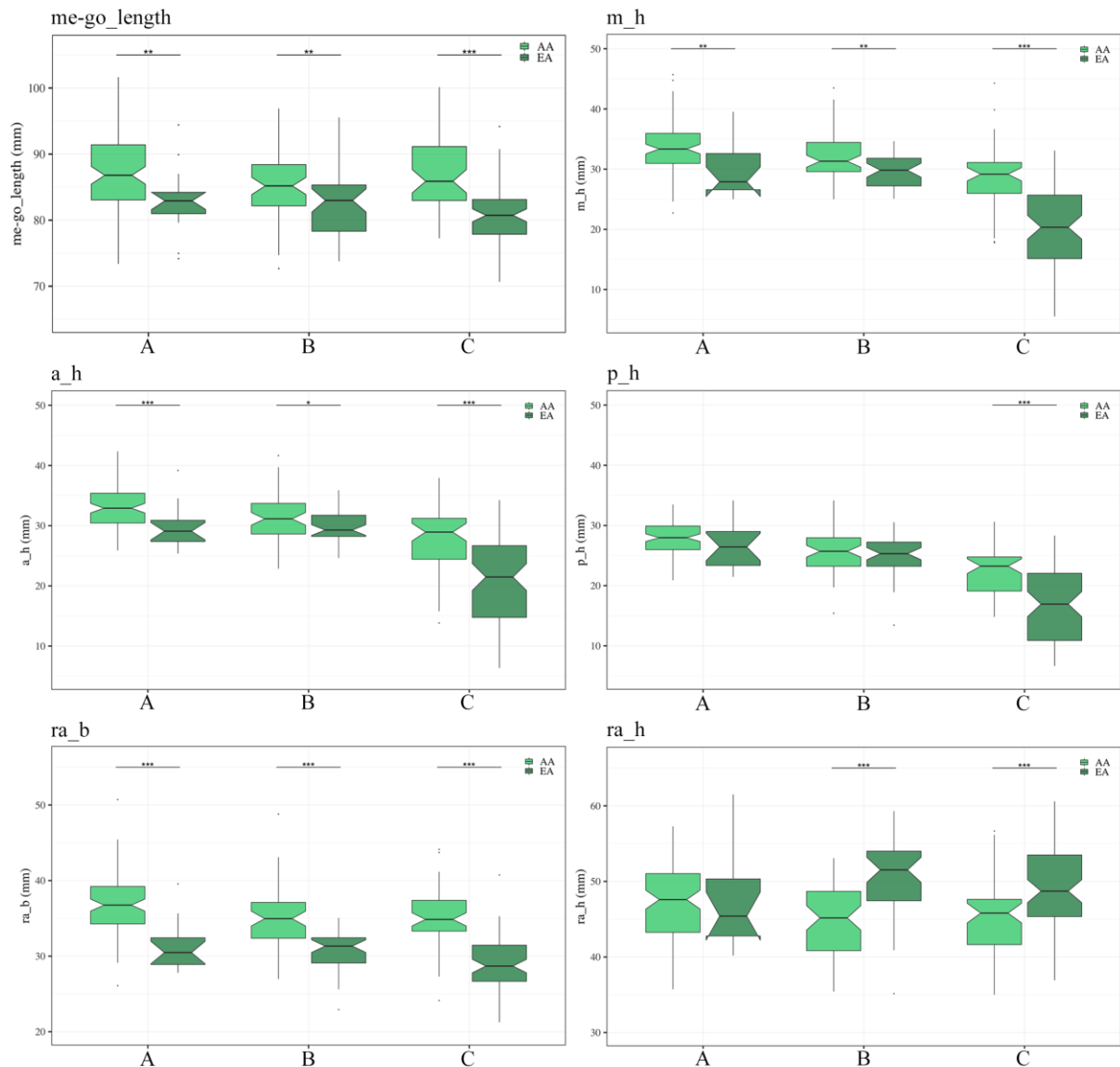
Figure 4.10. Boxplots of external distances (mm) per dentition category (A, B, C) and ancestry (AA: light green; EA: dark green). Dots depict outliers. Significance: *** $p < 0.001$, ** $p < 0.01$, * $p < 0.05$.

4.3.3.7. Influence of sex and ancestry per dentition category

Lastly, within each EI dentition category, the interaction between sex and ancestry was assessed by using the four sex/ancestral subsamples (FAA, FEA, MAA, MEA). Kruskal-Wallis

113

tests, followed by pairwise Wilcoxon post-hoc tests when necessary, were run on all measurements to assess the presence, or not, of differences between the subgroups while controlling for tooth loss. Results are illustrated in Figure 4.11.

Mandibular body length (me-go_length) was previously found to be significantly different between sex (Figure 4.9) and ancestral groups (Figure 4.10) respectively, within dentition categories A, B and C. A similar pattern was noticed when comparing the four sex/ancestral subgroups within the three dentition categories: me-go_length was always longer in MAA, followed by MEA, FAA and then FEA (MAA > MEA > FAA > FEA). More specifically, FEA and MAA individuals were the only individuals found to be statistically significantly different in all three dentition categories, while FAA and MAA were different in A and B but not in C. On the contrary, MAA and MEA were detected to be statistically different in B and C but not in A. Also, FAA and FEA, as well as FEA and MEA, were found to be significantly different within the C category but not in the two others.

Alveolar heights were then compared following the same method, by assessing sex/ancestral subgroups within dentition categories. The midline and the anterior heights (m_h, a_h) had similar patterns of significance: in category A, significance was detected only between MAA and FEA or FAA; in category B, only between MAA and the three other subgroups; while in C, it was detected between all the subgroups. The posterior height (p_h) was slightly different as no significant differences were detected in B (Kruskal-Wallis p-value = 0.339), and fewer in C (only between MAA and the other groups). Furthermore, a pattern (MAA > MEA > FAA > FEA), similar to the one noted with me-go_length, was detected in A and B categories for all three alveolar heights, while a different distribution was noticed in C (MAA > **FAA** > **MEA** > FEA), also consistent for all three heights. It is also worth noting that FEA and MEA were never statistically significantly different in any of the three alveolar heights in A, B or C.

Regarding the ramus measurements (ra_b and ra_h), statistically significant differences between sex/ancestral subgroups were detected in A, B and C categories. The ramus breadth was found to be the biggest in MAA, followed by FAA, MEA and finally FEA (MAA > FAA > MEA > FEA) in all three dentition groups. Significant differences were found between FAA and FEA within A, B and C, as well as between FEA and MAA, and between FEA and MEA. In categories B and C, additional statistically significant differences were detected between MAA and MEA, while significant differences were also found between FAA and MEA in category B only. Unlike all the other distances in which MAA was the greatest, the ramus

height was the longest in MEA, followed by MAA, FEA and then FAA (**MEA** > MAA > **FEA** > FAA), in categories A, B and C. Statistical significances were found between males and females, and more specifically between FAA and MAA, FAA and MEA, FEA and MEA in all three dentition categories as well as between MAA and MEA in the B and C categories. However, FAA and FEA were statistically significantly different only in category C individuals.
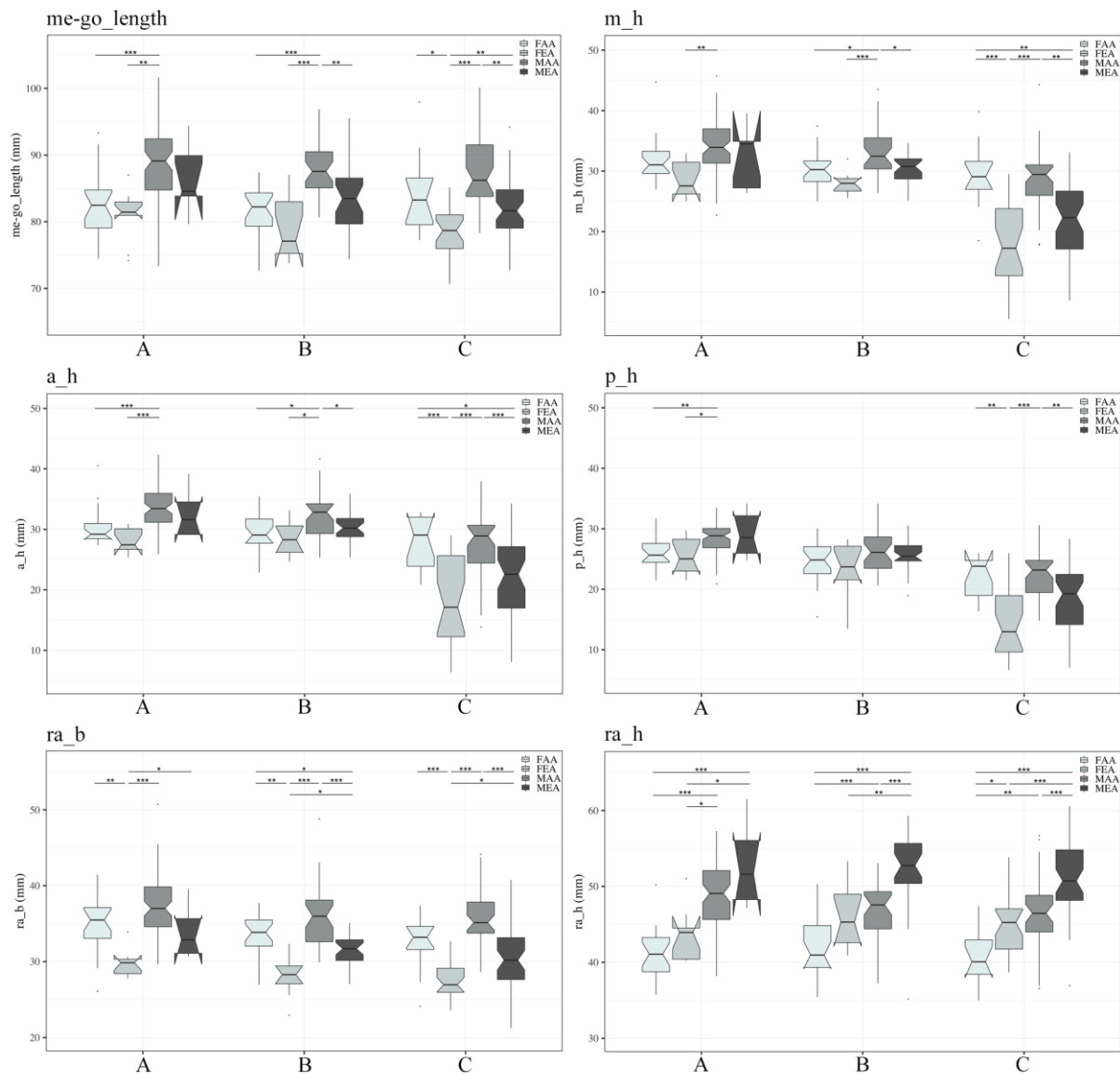
Figure 4.11. Boxplots of external distances (mm) per dentition category (A, B, C) and sex/ancestry (FAA, FEA, MAA, MEA: from light to dark grey). Dots depict outliers. Significance: *** $p < 0.001$, ** $p < 0.01$, * $p < 0.05$.

4.3.4. Inter-variable relationships

Inter-variable relationships were assessed using Spearman's correlations and were illustrated as correlation matrices in the entire sample, the sex and ancestry subsamples, as well as within the sex/ancestral subsamples.

In the entire sample for example, as seen in Figure 4.12, strong statistically significant positive correlations were found between the alveolar heights: between m_h and a_h ($\rho = 0.88$, $p < 0.001$), m_h and p_h ($\rho = 0.74$, $p < 0.001$) and a_h and p_h ($\rho = 0.82$, $p < 0.001$). An interesting pattern was also detected for the distances recorded on the ramus: ra_b was significantly moderately correlated with all the other distances (me-go_length, m_h, a_h, p_h) except ra_h (ns.), while ra_h was only very weakly correlated with each of the alveolar heights ($\rho = 0.14$, 0.19 and 0.24 for ra_h/m_h, ra_h/a_h and ra_h/p_h respectively).
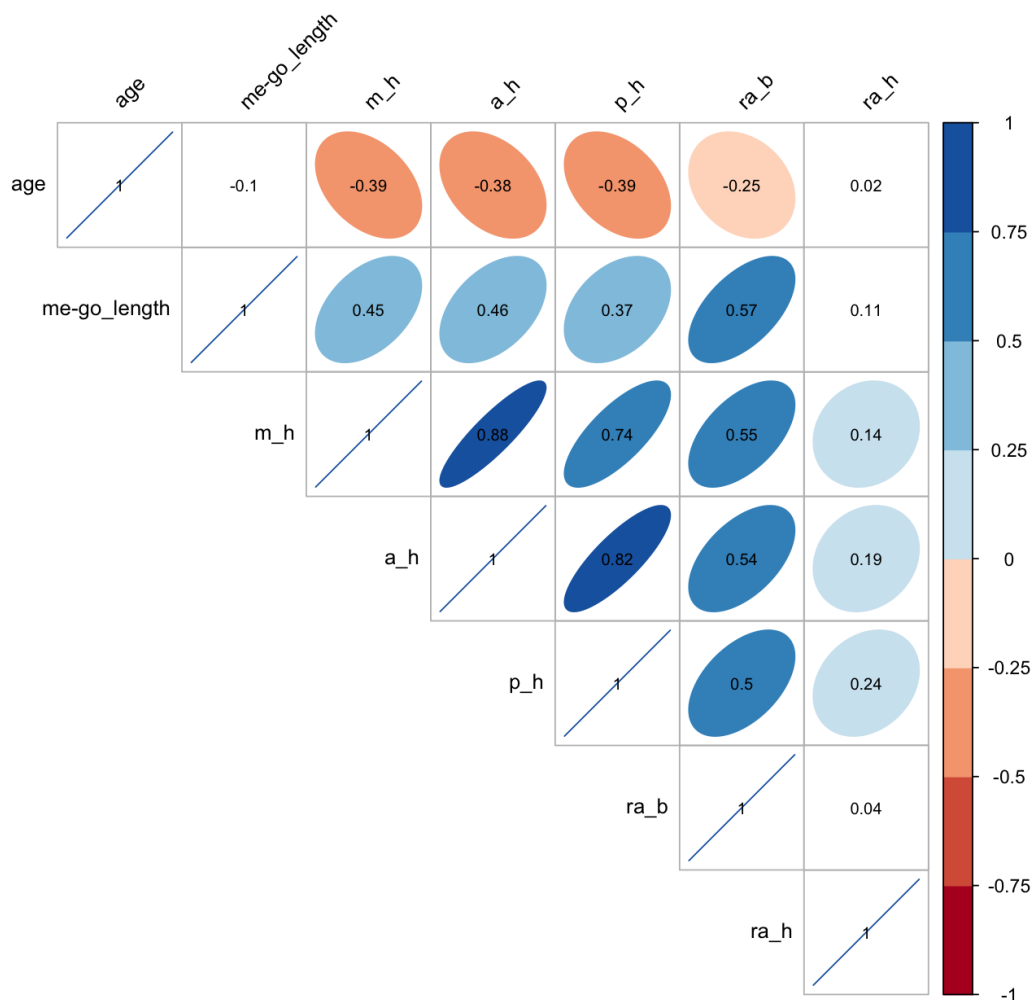
Figure 4.12. Corrplot illustrating inter-variable relationships between all the external distances in the entire sample. Ellipses were removed if the correlation, adjusted with Holm's correction, was not significant ($p > 0.05$). Correlation coefficients ρ are noted within each ellipse (in blue: positive ρ, in red: negative ρ).

116

In sex- and ancestry-separated subgroups (Figure 4.13 and Figure 4.14), similarly to the entire sample, strong significant correlations were found between the three alveolar heights. In females and males, the length of the body (me-go_length), as well as the ramus breadth (ra_b), were moderately correlated to the alveolar heights, while only one correlation linked to the ramus height (ra_h) was significant but weak (in males, between ra_h and p_h, $\rho = 0.18$). In individuals from African and European ancestries (Figure 4.14), a higher number of correlations were detected between the rami measurements (ra_b and ra_h) and the other variables.

Similar inter-distance correlations were also computed within each dentition category (Figure 4.15). In category A, all the distances were all statistically significantly correlated with each other, particularly the three alveolar heights, for which strong correlation coefficients were found ($\rho = 0.85$, 0.75 and 0.61 for m_h/a_h, a_h/p_h and m_h/p_h respectively). Within category B, significant correlations were more sparsely distributed (e.g., ra_h only significantly correlated with p_h), and correlation coefficients were generally weaker (particularly for the alveolar heights). In category C, however, a different pattern of statistically significant correlations was observed with very high correlation coefficients, especially between the three alveolar heights ($\rho = 0.93$, 0.88 and 0.81 for m_h/a_h, a_h/p_h and m_h/p_h respectively).

117
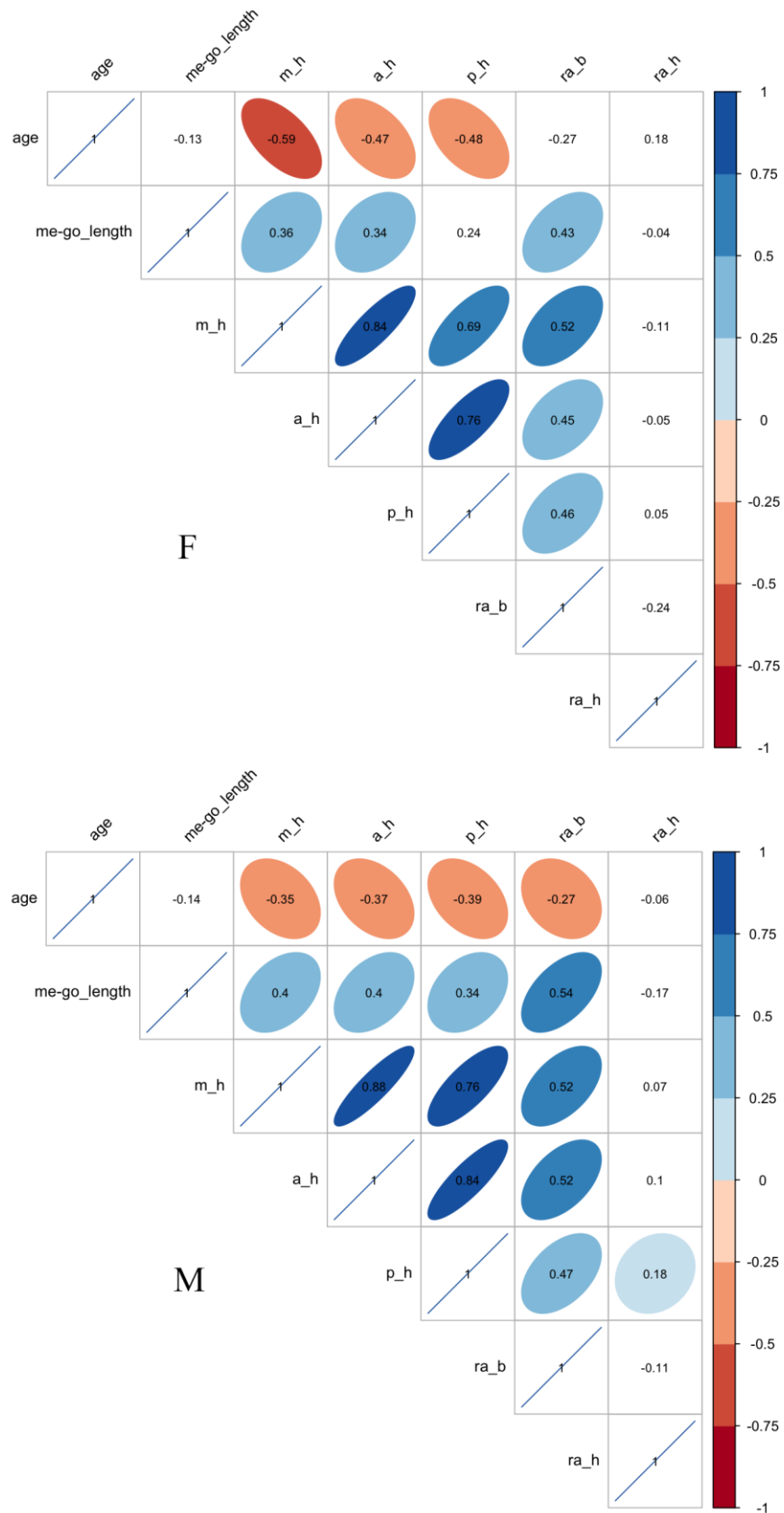
Figure 4.13. Corrplots illustrating inter-variable relationships between all the external distances in each sex-separated subsample (F: upper, M: lower). Ellipses were removed if the correlation, adjusted with Holm's correction, was not significant ($p > 0.05$). Correlation coefficients ρ are noted within each ellipse (in blue: positive ρ, in red: negative ρ).

118
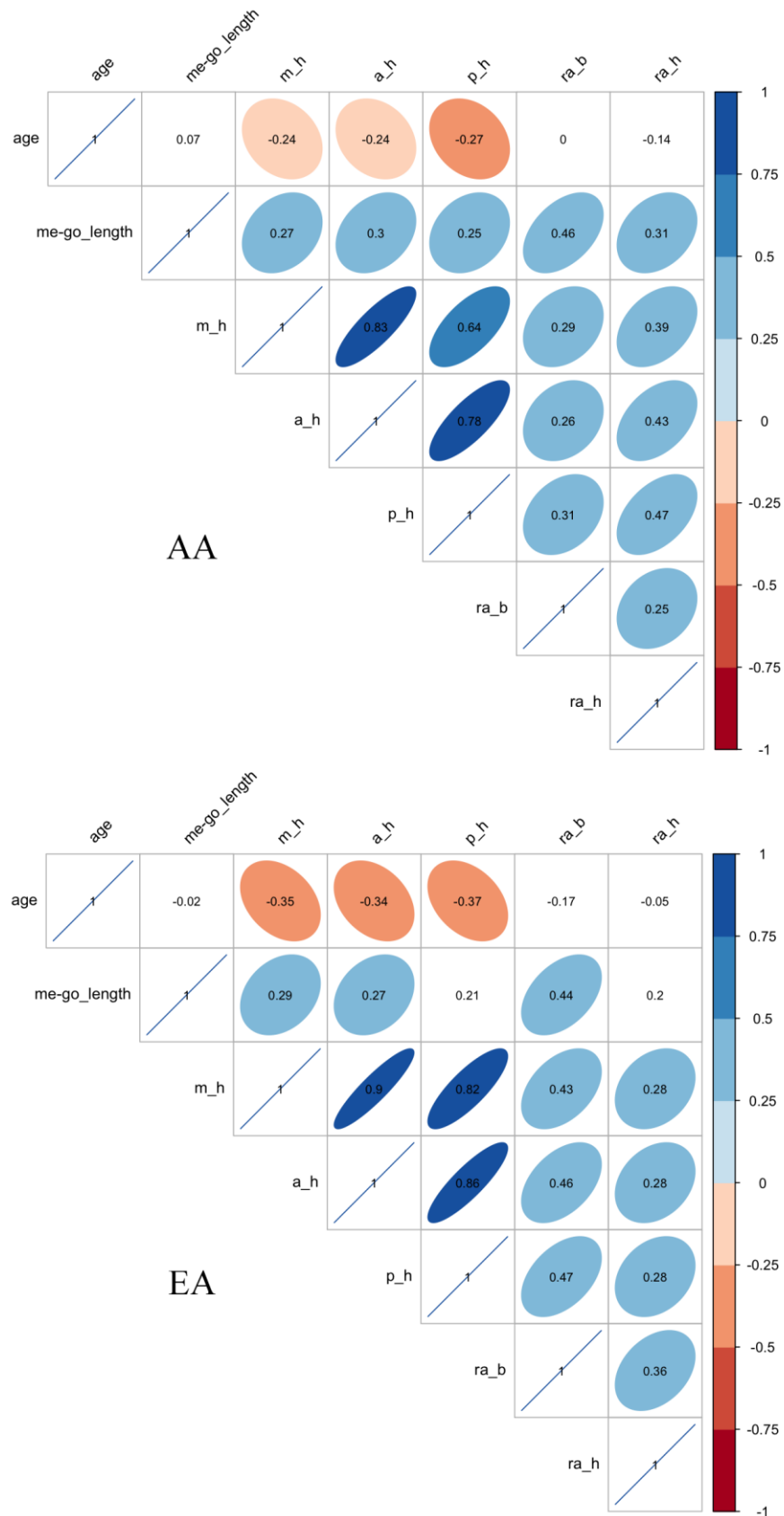
Figure 4.14. Corrplots illustrating inter-variable relationships between all the external distances in the ancestry-separated subsamples (AA: upper, EA: lower). Ellipses were removed if the correlation, adjusted with Holm's correction, was not significant ($p > 0.05$). Correlation coefficients ρ are noted within each ellipse (in blue: positive ρ, in red: negative ρ).

119
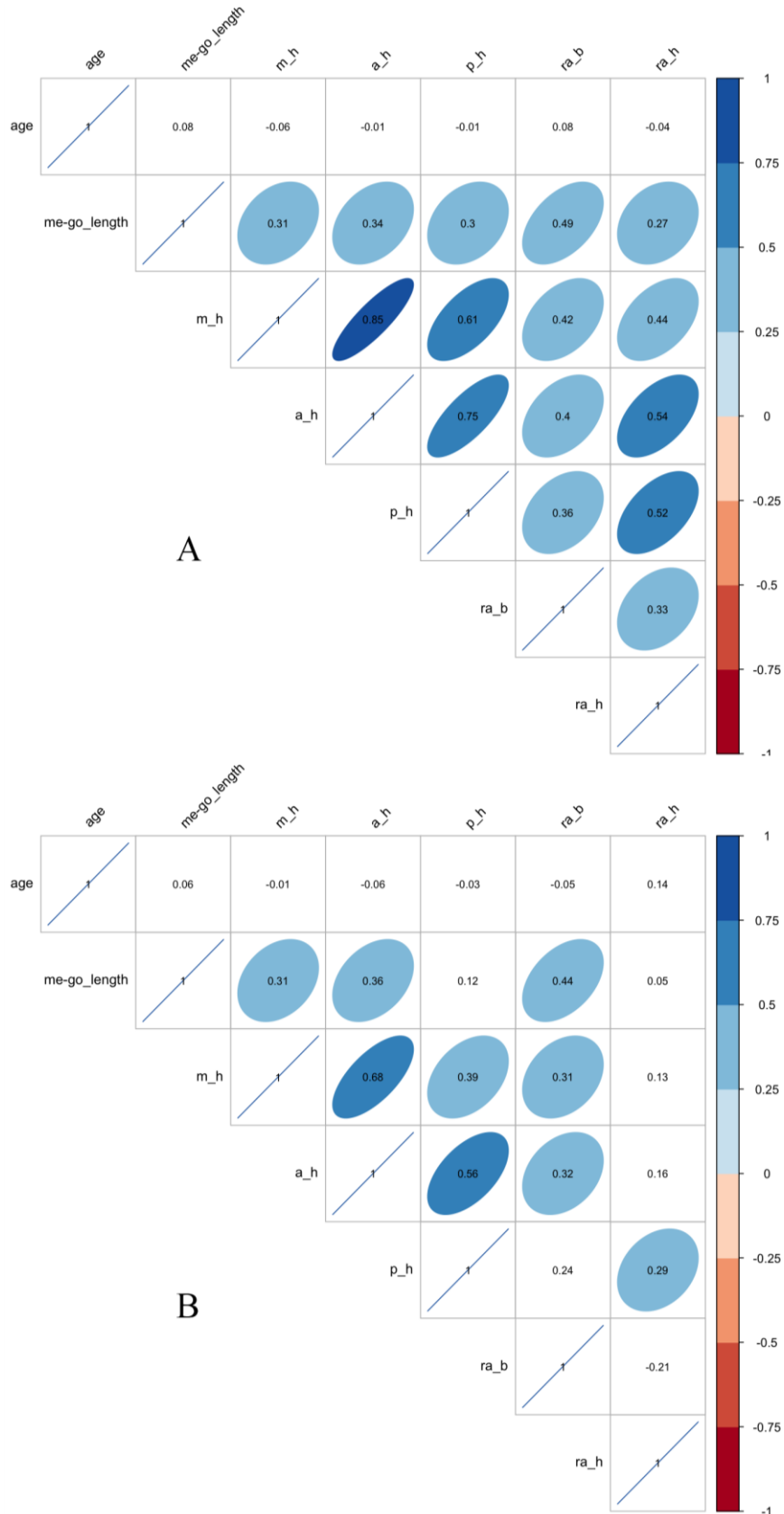
Figure 4.15. Corrplots illustrating inter-variable relationships between all the external distances in each of the three-dentition category (A, B, C). Ellipses were removed if the correlation, adjusted with Holm's correction, was not significant ($p > 0.05$). Correlation coefficients ρ are noted within each ellipse (in blue: positive ρ, in red: negative ρ). (continued on the next page)
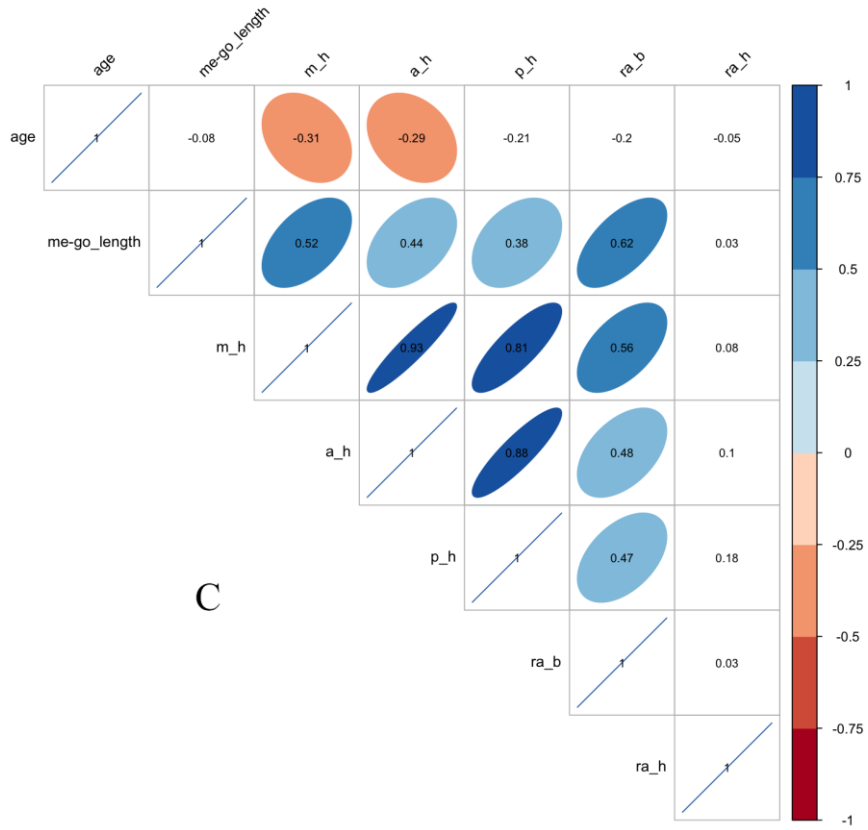
Figure 4.15. (continued)

4.3.5. Influence of aging

The Spearman's correlations between each external distance and aging were computed and are illustrated in the first row of each matrix presented in the previous section (Figures Figure 4.12 to Figure 4.15). For easier reading and comparison, these first rows were duplicated and grouped for the entire sample, the sex- and ancestry-separated samples, as well as within the sex/ancestral subsamples in Figure 4.16. Dentition categories were also analysed and detailed in Figure 4.17 and Figure 4.18.

The mandibular corpus length (me-go_length) was neither significantly correlated with aging in the entire sample nor with any of the subsamples cited above. Statistically significant negative correlations were found between each alveolar height (m_h, a_h, p_h) and advancing age in the entire sample ($p < 0.001$), in females and males ($p > 0.001$), as well as in AA ($p > 0.001$) and EA individuals ($p < 0.01$). The correlation coefficients calculated ranged between $\rho = -0.24$ and $\rho = -0.59$, highlighting stronger correlations within the female subsample than within males; but also, stronger correlations within EA individuals than AA. The ramus breadth (ra_b), however, was only significantly correlated with age in the entire sample and within the male subsample.

As seen in the last four rows of Figure 4.16, correlations with aging were also run within the sex/ancestral subgroups. No statistical significances were detected within FAA and MEA for any of the external distances. However, in FEA and MAA, the three alveolar heights were found to decrease significantly with aging ($p < 0.05$), following weaker correlation coefficients in MAA and stronger in FEA.

The influence of advancing age on the external distances was then tested within each dentition category (see Figure 4.17): A and B categories did not show any statistical significance while in C, which might be restricted to the older age ranges, significant correlations were detected for m_h ($p < 0.01$) and a_h ($p < 0.05$). Furthermore, within C, only females were significantly correlated with aging, once again for m_h ($p < 0.001$) and a_h ($p < 0.05$), while males were not. Correlations with aging within the ancestral subsamples separated in dentition categories (e.g., AA-A, AA-B, AA-C, EA-A, etc. – see Figure 4.18) were also run, but were not found significant for any of the six subgroups.
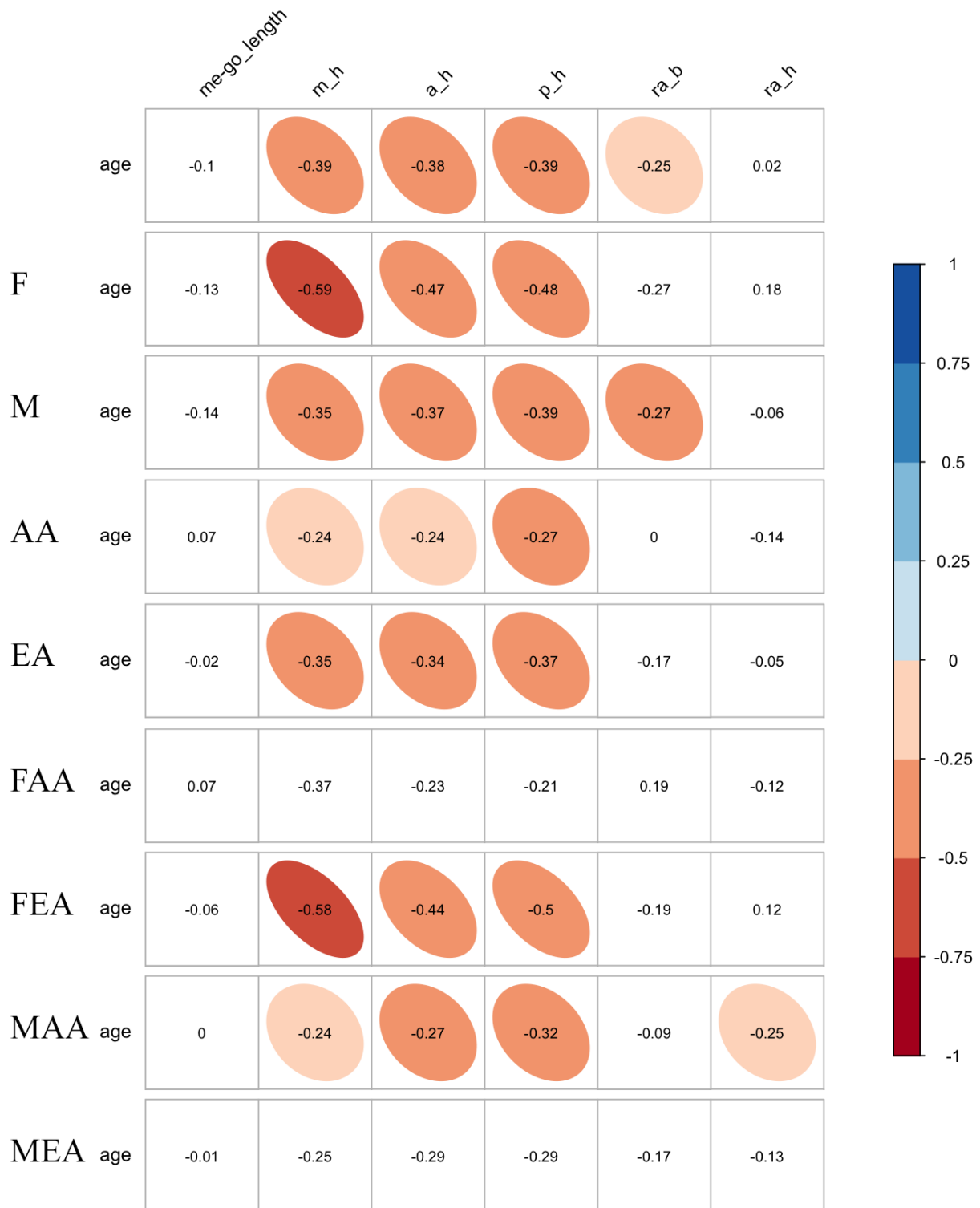
Figure 4.16. Corrplots illustrating correlations between each external distance and age in the entire sample (first row) and then in F, M, AA, EA, FAA, FEA, MAA and MEA subsamples. Ellipses were removed if the correlation, adjusted with Holm's correction, was not significant ($p > 0.05$). Correlation coefficients ρ are noted within each square (in blue: positive ρ, in red: negative ρ).
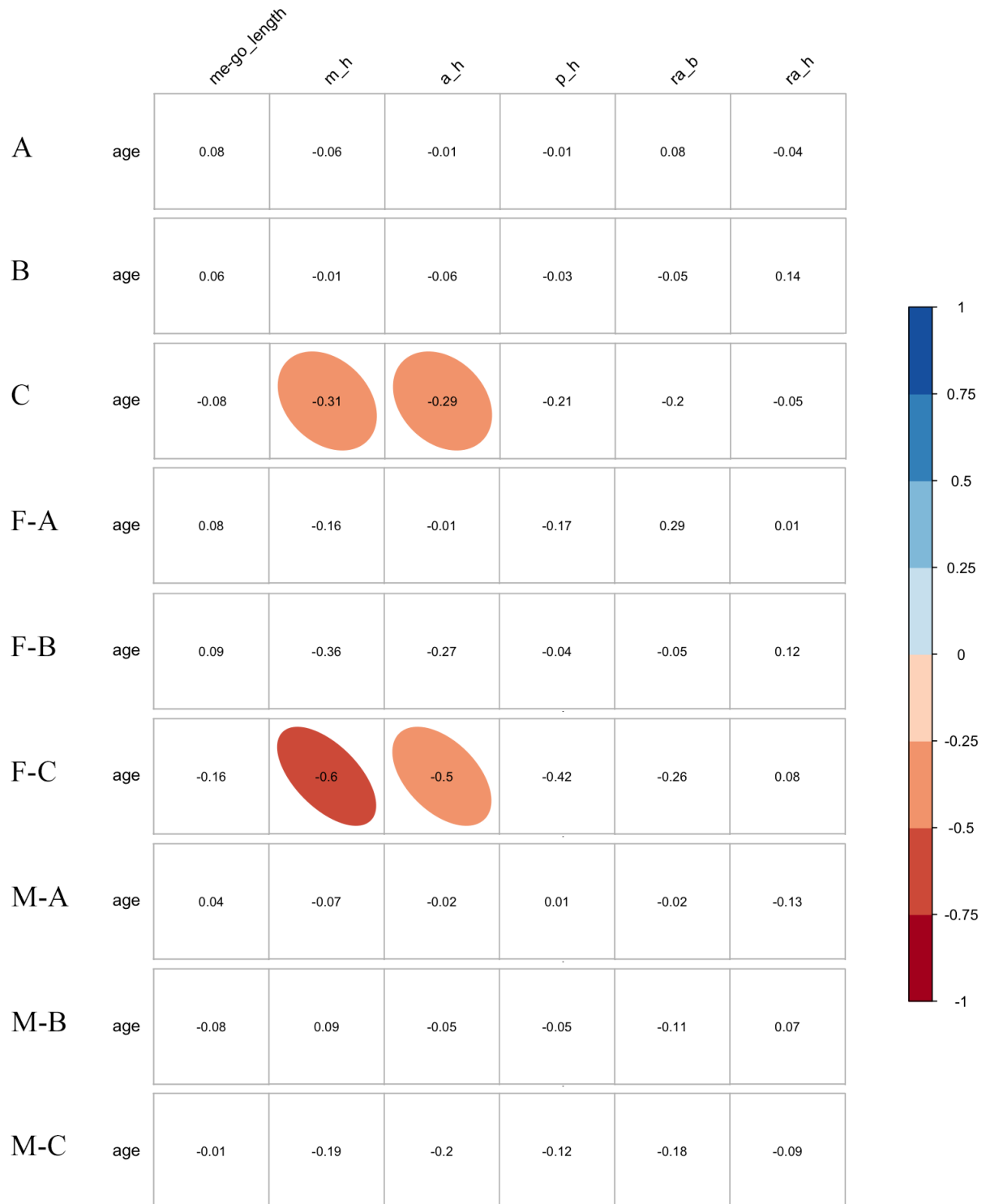
Figure 4.17. Corrplots illustrating correlations between each external distance and age in the entire sample separated per dentition category in the first three rows (A: first row, B: second, C: third), and then per dentition categories within females (F-A, F-B, F-C) or males (M-A, M-B, M-C). Ellipses were removed if the correlation, adjusted with Holm's correction, was not significant ($p > 0.05$). Correlation coefficients ρ are noted within each square (in blue: positive ρ, in red: negative ρ).
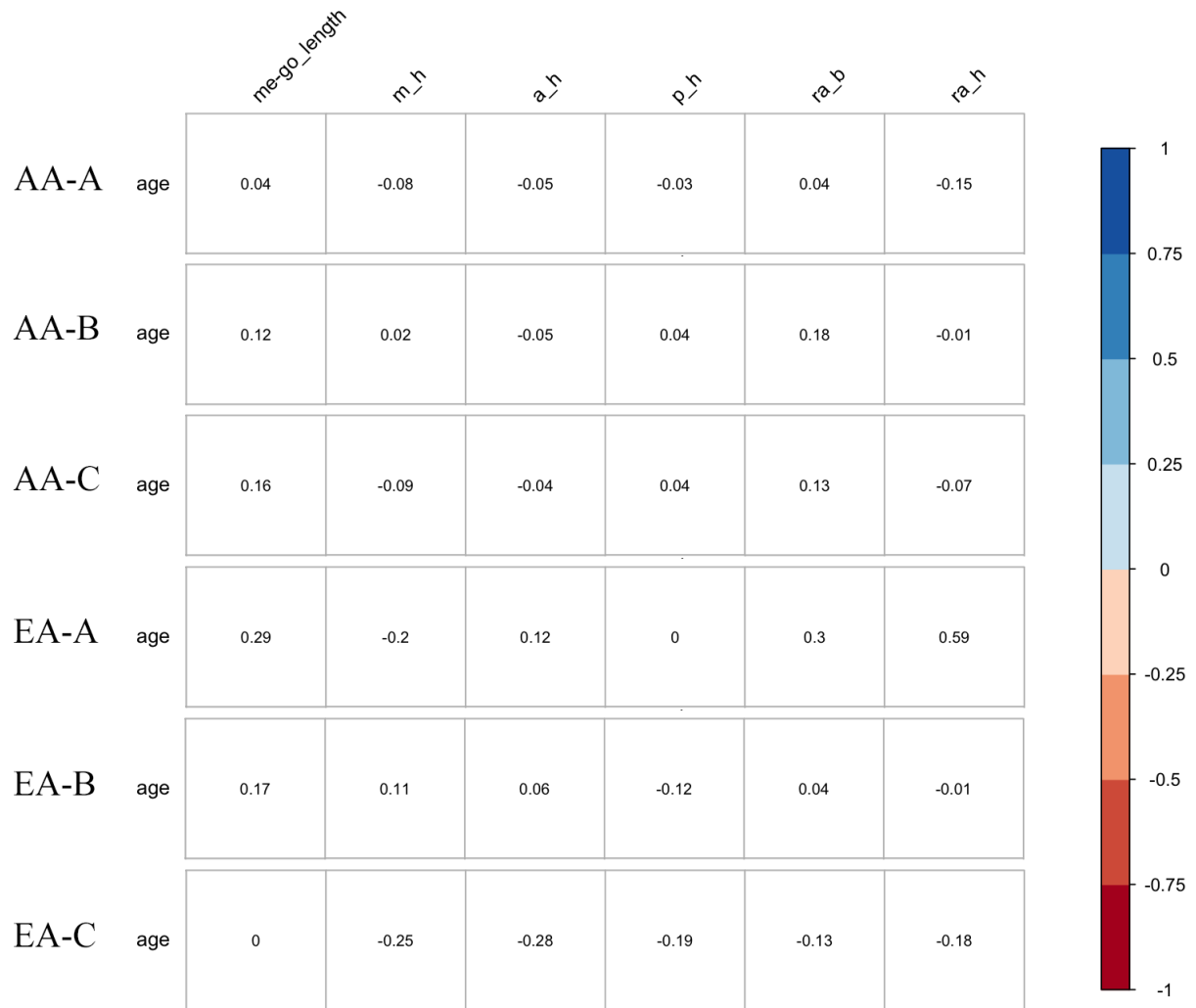
Figure 4.18. Corrplots illustrating correlations between each external distance and age in the entire sample separated per dentition category within the AA (AA-A, AA-B, AA-C) and EA (EA-A, EA-B, EA-C) subgroups. Ellipses were removed if the correlation, adjusted with Holm's correction, was not significant ($p > 0.05$). Correlation coefficients ρ are noted within each square (in blue: positive ρ, in red: negative ρ).

4.3.6. Summary – External distances

In the South African population analysed here, all external mandibular distances showed significant sexual dimorphism (with M > F), and significant differences between ancestries (with AA > EA, except for the ramus height where EA > AA). When grouped per sex/ancestry, two patterns emerged: one where ancestry seemed to be the main cause of difference, with MAA > FAA > MEA > FEA in the three alveolar heights and ramus breadth; and a second pattern, in which sex was the main co-founding factor, with MEA > MAA > FEA > FAA in the ramus height.

When considering tooth loss alone, a decrease in all external distances (except ramus height) was noted as soon as teeth are lost (i.e., significant differences between dentition groups A vs. B), and was even more marked in edentulous individuals (significant differences between A vs. C, and B vs. C). This decrease not only reflects the loss of alveolar bone and the consequent remodelling in height of the mandibular body, but also changes in the gonial angle, as the length of the mandibular body is also reduced. The ramus height, however, did not seem to be impacted by tooth loss.

External distances were then analysed while simultaneously considering tooth loss and demographic parameters, such as sex or ancestry. First, all dimensions, except the ramus height, decreased with tooth loss both in males and females. Sexual dimorphism (M > F) was confirmed in all three categories of tooth loss: strong when fully dentate (A) or when edentulous (C), but less accentuated, or even moderate, in individuals starting to lose teeth (B). The variability in measurements due to asymmetrical tooth loss in B could mask the differences between males and females and make it more difficult to evaluate. Both South Africans of African and European ancestries displayed a decrease associated with tooth loss in most of the dimensions. However, the decrease was more pronounced in EA than in AA, which could reflect either an earlier tooth loss in EA and thus a greater bone loss over time, or a higher sensitivity to tooth loss associated with an accentuated bone loss. Furthermore, tooth loss seemed to accentuate differences between ancestries (AA > EA), as they are present in A and B, but more marked in C (edentulous).

When considering both sex and ancestry, tooth loss, especially edentulism, appeared to increase the differences between the four groups (MAA, MEA, FAA, FEA), even if all individuals showed a decrease in dimensions. South African males of African ancestry always showed the greatest dimensions across all dentition categories, except for the ramus height, in

which South African males of European ancestry were the biggest (also in all three dentition groups). South African females, and particularly of European ancestry, seemed to be more affected by tooth loss as they showed a bigger decrease.

Regarding the dimensions themselves, the three alveolar heights, even if different (midline > anterior > posterior heights), were all highly correlated with each other, while the ramus height was rarely correlated with the other measurements. The mandible could undergo minor or massive morphological changes, without affecting its ramus height, independent of the rest of the body. This integrated and generalised external body morphology was not influenced by sex or ancestry, but present in all individuals, as long as they are fully dentate (category A). Indeed, as soon as tooth loss starts (category B), the correlations and thus, the integrity, became sparse or even absent. However, in edentulous individuals, high correlations between the alveolar heights were detected again. The associated considerable bone remodelling caused generalised morphological changes while re-establishing the interdependency of the dimensions (except for the ramus height). It is also worth noticing that the length of the corpus was also correlated with the alveolar heights, in A and C categories, but not in B.

Finally, the influence of advancing age was also evaluated and showed interesting results. First, the ramus height, as with tooth loss, did not vary with age. Then, the length of the corpus, also found to be independent of age, highlighted the fact that tooth loss might be the only factor causing a shift in the gonial angle, and thus, a reduced length of the body. The other distances, though, and particularly the alveolar heights, were found to decrease with age. This tendency was more stressed in females, especially of European ancestry. However, the decrease in dimensions with age was only significant in the edentulous group, and not in A or B, which might imply that tooth loss is playing a more important role on the external distances than age itself.

4.4. Cortical thickness

4.4.1. Basic descriptive statistics

Cortical thickness descriptive statistics (i.e., means, standard deviations, minimum and maximum) are available in Table 4.3, where they are detailed in the total sample, in each sex- and ancestry-separated subgroup as well as in each sex/ancestral subsample. Descriptive statistics are also detailed per dentition categories in Table 4.4.

In the entire pooled sample (Table 4.3), the thickest mean CtTh were measured in the anterior and posterior sections of the body (such as at the basal anterior site: a_ba_CtTh = 3.32 ± 1.26 mm; or at the posterior basal site: p_ba_CtTh = 3.18 ± 0.99 mm), while the lowest values were found in the ramus (e.g., lingual ramus breadth CtTh: rab_ling_CtTh = 1.23 ± 0.58 mm). The lingual site of the ramus height particularly showed very low mean values (rah_ling_CtTh mean ± SD = 0.87 ± 0.44 mm) as well as very low minimum values (rah_ling_CtTh range: 0.00 – 2.21 mm). When considering all CtTh, the basal sites of the three sections of the body (midline, anterior, posterior) showed higher mean CtTh and higher maximum values than in the buccal and lingual sites. The mean values recorded on the buccal sites were particularly lower than in the two other sites (e.g., m_buc_CtTh mean ± SD = 1.53 ± 0.55 mm vs. m_ba_CtTh mean ± SD = 2.54 ± 1.35 mm vs. m_ling_CtTh mean ± SD = 2.16 ± 0.72 mm).

When separated per sex, all the sites always showed greater mean CtTh and higher maximum values in males than in females. Between the two ancestral subgroups, the midline, anterior and posterior CtTh, as well as the ramus CtTh, were detected to have greater mean and maximum values in AA individuals than in EA.

In the sex/ancestral subsamples, for all the cortical thicknesses measured on the body of the mandible (midline, anterior and posterior sections: basal, buccal, lingual sites), except for m_ling_CtTh, MAA consistently showed higher mean values than the three other subgroups, while FEA displayed the lowest. Furthermore, the maximum values of the cortical thicknesses were particularly high in the MAA. The m_ling_CtTh means, however, were higher in MEA as compared to MAA (MEA mean ± SD = 2.15 ± 0.68 mm vs. MAA mean ± SD = 2.15 ± 0.68 mm) and higher in FEA compared to FAA (FEA mean ± SD = 2.09 ± 0.66 mm vs. FAA mean ± SD = 1.86 ± 0.51 mm). The four cortical thicknesses measured on the ramus breadth and height followed the same trend: lowest mean values in FEA, and highest in MAA. Overall, on the body, the lowest mean values were found in the buccal sites of the

midline (m_buc_CtTh) for FAA, FEA, MAA and MEA (1.36 mm, 1.24 mm, 1.69 mm and 1.51 mm respectively), while the highest values were recorded at the basal site of the anterior section (a_ba_CtTh) in the four subgroups (3.31 mm, 2.71 mm, 3.59 mm and 3.17 mm for FAA, FEA, MAA and MEA).

Descriptive statistics were also calculated for the three dentition categories and are given in Table 4.4. At all sites, except for the lingual site of the midline, higher CtTh values were consistently detected in the A category in comparison to B and C. The midline lingual cortical thickness (m_ling_CtTh) was, in fact, the thinnest in B (1.90 ± 0.51 mm), and the thickest in C (2.52 ± 0.86 mm). The two other lingual sites on the mandibular body (anterior a_ling_CtTh, posterior p_ling_CtTh) also presented thinner values in category B than in categories C or A. In contrast, the six remaining sites – basal and buccal CtTh of the midline, anterior and posterior sections as well as buccal and lingual CtTh of the ramus breadth and height – had the lowest CtTh means in edentulous individuals (C category).

Table 4.3. Descriptive statistics of the cortical thicknesses (CtTh, mm) measured on the micro-CT scans of mandibles in the entire sample, in each sex (F, M), ancestral group (AA, EA) and sex/ancestral group (FAA, FEA, MAA, MEA). (continued on the next page)

| | Total | Sex | | Ancestry | | Sex/ancestry | | | |
| | | F | M | AA | EA | FAA | FEA | MAA | MEA |
	n = 333	n = 102	n = 231	n = 208	n = 125	n = 56	n = 46	n = 152	n = 79
m_ba_CtTh									
min − max	0.45 − 10.54	0.74 − 4.16	0.45 − 10.54	0.45 − 8.18	0.69 − 10.54	0.90 − 4.16	0.74 − 3.85	0.45 − 8.18	0.69 − 10.54
mean ± SD	2.54 ± 1.35	2.15 ± 0.87	2.71 ± 1.48	2.72 ± 1.34	2.24 ± 1.31	2.33 ± 0.94	1.93 ± 0.74	2.86 ± 1.44	2.43 ± 1.52
m_buc_CtTh									
min − max	0.36 − 3.74	0.46 − 2.45	0.36 − 3.74	0.47 − 3.05	0.36 − 3.74	0.47 − 2.29	0.46 − 2.45	0.54 − 3.05	0.36 − 3.74
mean ± SD	1.53 ± 0.55	1.31 ± 0.43	1.62 ± 0.57	1.60 ± 0.52	1.41 ± 0.58	1.36 ± 0.38	1.24 ± 0.48	1.69 ± 0.54	1.51 ± 0.61
m_ling_CtTh									
min − max	0.69 − 4.62	0.70 − 4.06	0.69 − 4.62	0.69 − 4.43	0.96 − 4.62	0.70 − 4.06	0.96 − 3.60	0.69 − 4.43	1.02 − 4.62
mean ± SD	2.16 ± 0.72	1.97 ± 0.59	2.24 ± 0.75	2.07 ± 0.65	2.30 ± 0.79	1.86 ± 0.51	2.09 ± 0.66	2.15 ± 0.68	2.43 ± 0.84
a_ba_CtTh									
min − max	0.58 − 8.11	1.08 − 6.31	0.58 − 8.11	0.58 − 8.11	0.73 − 6.58	1.08 − 6.31	1.15 − 4.86	0.57 − 8.11	0.73 − 6.58
mean ± SD	3.32 ± 1.26	3.04 ± 1.11	3.45 ± 1.31	3.51 ± 1.29	3.00 ± 1.16	3.31 ± 1.15	2.71 ± 0.99	3.59 ± 1.33	3.17 ± 1.22
a_buc_CtTh									
min − max	0.44 − 4.66	0.46 − 3.11	0.44 − 4.66	0.47 − 4.67	0.44 − 3.03	0.47 − 3.11	0.46 − 2.12	0.78 − 4.66	0.44 − 3.03
mean ± SD	1.69 ± 0.54	1.45 ± 0.51	1.79 ± 0.52	1.83 ± 0.54	1.44 ± 0.44	1.59 ± 0.52	1.29 ± 0.45	1.92 ± 0.52	1.54 ± 0.41
a_ling_CtTh									
min − max	0.74 − 5.31	1.12 − 3.52	0.74 − 5.31	1.31 − 5.31	0.74 − 4.23	1.31 − 3.52	1.12 − 3.19	1.38 − 5.31	0.74 − 4.23
mean ± SD	2.47 ± 0.70	2.16 ± 0.55	2.61 ± 0.71	2.71 ± 0.68	2.08 ± 0.54	2.37 ± 0.51	1.92 ± 0.51	2.84 ± 0.69	2.18 ± 0.54

Table 4.3. (continued)

	Total	Sex		Ancestry		Sex/ancestry			
		F	M	AA	EA	FAA	FEA	MAA	MEA
	n = 333	n = 102	n = 231	n = 208	n = 125	n = 56	n = 46	n = 152	n = 79
p_ba_CtTh									
min – max	0.72 – 6.56	0.72 – 5.22	0.78 – 6.56	0.78 – 6.56	0.72 – 5.30	0.79 – 5.22	0.72 – 4.34	0.78 – 6.56	0.93 – 5.30
mean ± SD	3.18 ± 0.99	2.81 ± 1.04	3.34 ± 0.92	3.37 ± 0.96	2.86 ± 0.95	3.09 ± 1.01	2.47 ± 0.98	3.47 ± 0.92	3.08 ± 0.87
p_buc_CtTh									
min – max	0.81 – 4.79	0.81 – 3.07	0.81 – 4.79	0.82 – 4.79	0.81 – 3.11	0.82 – 3.07	0.81 – 3.04	0.93 – 4.79	0.81 – 3.11
mean ± SD	2.11 ± 0.66	1.84 ± 0.55	2.23 ± 0.67	2.30 ± 0.68	1.80 ± 0.49	1.95 ± 0.55	1.71 ± 0.52	2.43 ± 0.68	1.86 ± 0.47
p_ling_CtTh									
min – max	0.81 – 3.79	0.81 – 3.47	0.93 – 3.79	0.94 – 3.79	0.81 – 3.49	0.94 – 2.81	0.81 – 3.47	1.06 – 3.79	0.93 – 3.49
mean ± SD	2.11 ± 0.56	1.90 ± 0.53	2.20 ± 0.54	2.21 ± 0.53	1.93 ± 0.55	1.97 ± 0.47	1.81 ± 0.58	2.30 ± 0.52	2.00 ± 0.53
rab_buc_CtTh									
min – max	0.17 – 3.53	0.44 – 2.62	0.17 – 3.53	0.60 – 3.53	0.17 – 2.51	0.62 – 2.62	0.44 – 2.22	0.60 – 3.53	0.17 – 2.51
mean ± SD	1.58 ± 0.48	1.36 ± 0.41	1.67 ± 0.48	1.73 ± 0.46	1.33 ± 0.42	1.50 ± 0.40	1.19 ± 0.36	1.82 ± 0.45	1.40 ± 0.43
rab_ling_CtTh									
min – max	0.00 – 2.84	0.16 – 2.52	0.00 – 2.84	0.10 – 2.84	0.00 – 2.59	0.21 – 2.52	0.16 – 2.08	0.10 – 2.84	0.00 – 2.59
mean ± SD	1.23 ± 0.58	1.17 ± 0.50	1.25 ± 0.61	1.35 ± 0.57	1.02 ± 0.53	1.30 ± 0.48	1.00 ± 0.49	1.37 ± 0.61	1.03 ± 0.56
rah_buc_CtTh									
min – max	0.42 – 2.76	0.42 – 2.37	0.44 – 2.76	0.44 – 2.76	0.42 – 2.63	0.51 – 2.36	0.42 – 2.37	0.44 – 2.76	0.49 – 2.63
mean ± SD	1.53 ± 0.45	1.38 ± 0.45	1.60 ± 0.43	1.64 ± 0.43	1.36 ± 0.43	1.49 ± 0.40	1.26 ± 0.48	1.69 ± 0.43	1.42 ± 0.39
rah_ling_CtTh									
min – max	0.00 – 2.21	0.00 – 1.67	0.00 – 2.21	0.12 – 2.21	0.00 – 1.88	0.22 – 1.56	0.00 – 1.67	0.12 – 2.21	0.00 – 1.88
mean ± SD	0.87 ± 0.44	0.73 ± 0.38	0.94 ± 0.44	0.94 ± 0.45	0.76 ± 0.39	0.74 ± 0.34	0.70 ± 0.43	1.02 ± 0.46	0.79 ± 0.37

Table 4.4. Descriptive statistics of the cortical thicknesses (CtTh, mm) measured on the micro-CT scans of mandibles, separated per dentition category, according to the Eichner Index (EI A, B, C: from full dentition to edentulous).

	EI A n = 112	EI B n = 97	EI C n = 124
m_ba_CtTh			
min – max	0.51 – 6.39	0.67 – 8.18	0.45 – 10.54
mean ± SD	2.70 ± 0.99	2.47 ± 1.17	2.45 ± 1.70
m_buc_CtTh			
min – max	0.36 – 3.05	0.51 – 3.55	0.46 – 3.74
mean ± SD	1.66 ± 0.50	1.49 ± 0.54	1.44 ± 0.58
m_ling_CtTh			
min – max	0.89 – 3.59	0.80 – 4.06	0.69 – 4.62
mean ± SD	1.97 ± 0.50	1.90 ± 0.51	2.52 ± 0.86
a_ba_CtTh			
min – max	0.63 – 7.76	1.05 – 6.67	0.58 – 8.11
mean ± SD	3.46 ± 1.14	3.25 ± 1.27	3.25 ± 1.36
a_buc_CtTh			
min – max	0.62 – 4.66	0.51 – 3.11	0.44 – 4.16
mean ± SD	1.85 ± 0.51	1.65 ± 0.46	1.56 ± 0.58
a_ling_CtTh			
min – max	1.31 – 4.41	1.12 – 4.57	0.74 – 5.31
mean ± SD	2.54 ± 0.61	2.42 ± 0.64	2.46 ± 0.81
p_ba_CtTh			
min – max	1.57 – 6.56	1.36 – 5.42	0.72 – 5.40
mean ± SD	3.46 ± 0.87	3.24 ± 0.80	2.87 ± 1.13
p_buc_CtTh			
min – max	0.81 – 4.25	1.00 – 4.44	0.81 – 4.79
mean ± SD	2.32 ± 0.58	2.12 ± 0.59	1.92 ± 0.73
p_ling_CtTh			
min – max	1.06 – 3.79	0.81 – 3.22	0.90 – 3.62
mean ± SD	2.24 ± 0.51	2.03 ± 0.51	2.05 ± 0.61
rab_buc_CtTh			
min – max	0.78 – 3.53	0.44 – 2.43	0.17 – 2.73
mean ± SD	1.82 ± 0.45	1.56 ± 0.40	1.38 ± 0.48
rab_ling_CtTh			
min – max	0.10 – 2.67	0.00 – 2.84	0.00 – 2.74
mean ± SD	1.44 ± 0.53	1.21 ± 0.57	1.06 ± 0.57
rah_buc_CtTh			
min – max	0.62 – 2.76	0.55 – 2.63	0.42 – 2.53
mean ± SD	1.70 ± 0.40	1.57 ± 0.40	1.36 ± 0.47
rah_ling_CtTh			
min – max	0.16 – 2.21	0.00 – 1.63	0.00 – 2.07
mean ± SD	0.99 ± 0.46	0.81 ± 0.36	0.81 ± 0.45

4.4.2. Influence of sex or/and ancestry

4.4.2.1. Sex

To assess the influence of sex on the mandibular cortical thicknesses, Mann-Whitney Wilcoxon tests were run on the 13 variables recorded (Figure 4.19): nine on the three sections of the corpus (midline, anterior, posterior); and four on the two sections selected on the ramus (ramus breadth, ramus height). Except for the lingual CtTh of the ramus breadth (rab_ling_CtTh: $p = 0.30$), which was often located near the mandibular foramen (causing many missing values, i.e., NAs), statistically significant sexual dimorphism was detected for all the sites of all sections ($p < 0.05$ for a_ba_CtTh; $p < 0.01$ for m_ba_CtTh and m_ling_CtTh; $p < 0.001$ for the other sites), with males having consistently thicker CtTh than females although some overlap was noted (see Figure 4.19).

4.4.2.2. Ancestry

Influence of ancestry was evaluated by following the same protocol, i.e., Mann-Whitney Wilcoxon tests performed on the 13 cortical thicknesses, of which the results are illustrated with boxplots in Figure 4.20. Although overlap was observed, statistically significant differences in ancestry were detected for all the cortical thicknesses ($p < 0.05$ for m_ling_CtTh; $p < 0.01$ for rah_ling_CtTh; $p < 0.001$ for all the other CtTh), with thicker dimensions in AA than in EA individuals.

133
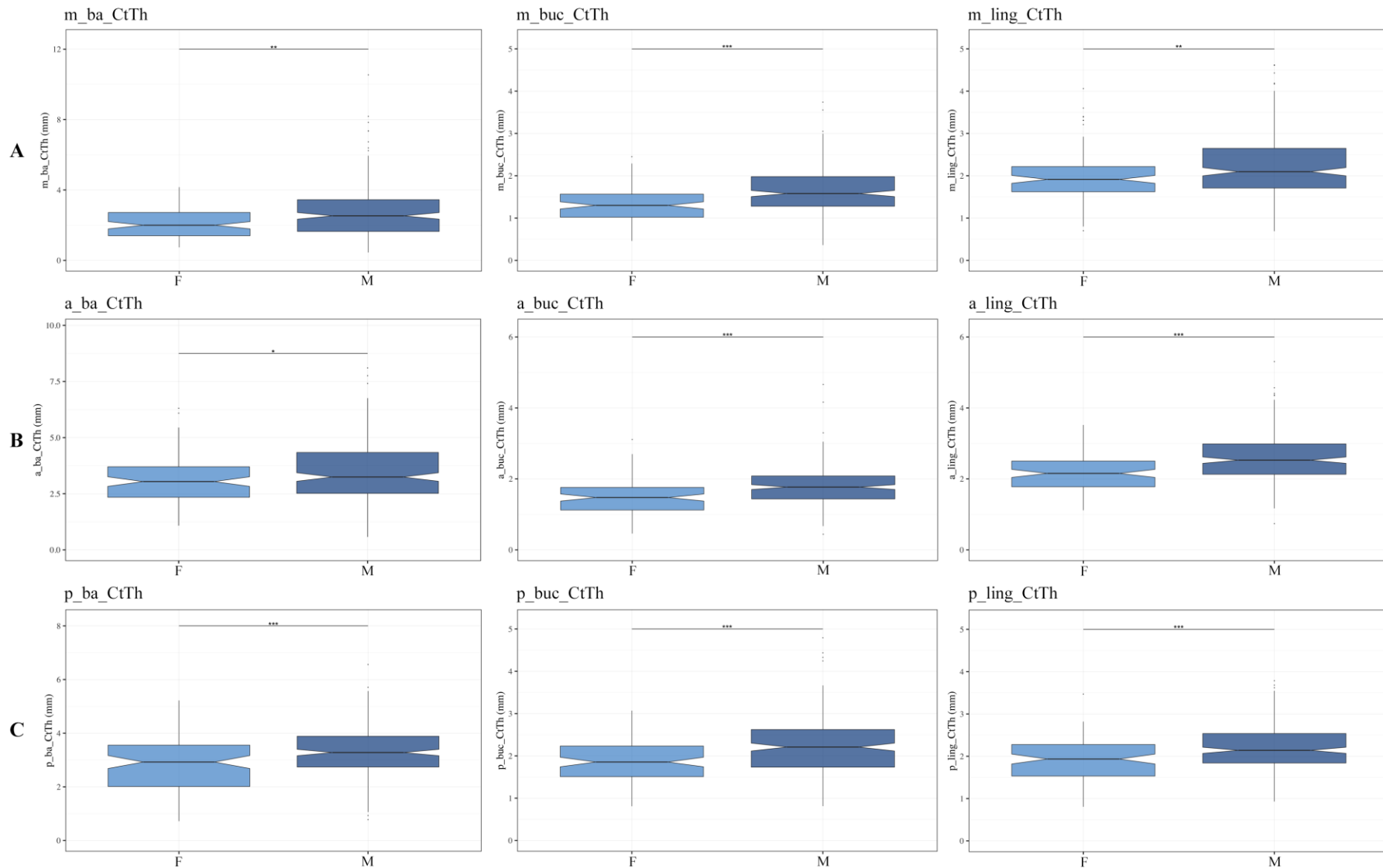
Figure 4.19. Boxplots of CtTh (mm) per sex (F: light blue; M: dark blue), recorded on the midline [A], anterior [B], posterior [C], ramus breadth [D] and height [E] sections. Dots depict outliers. Significance: *** $p < 0.001$, ** $p < 0.01$, * $p < 0.05$. (continued on the next page)
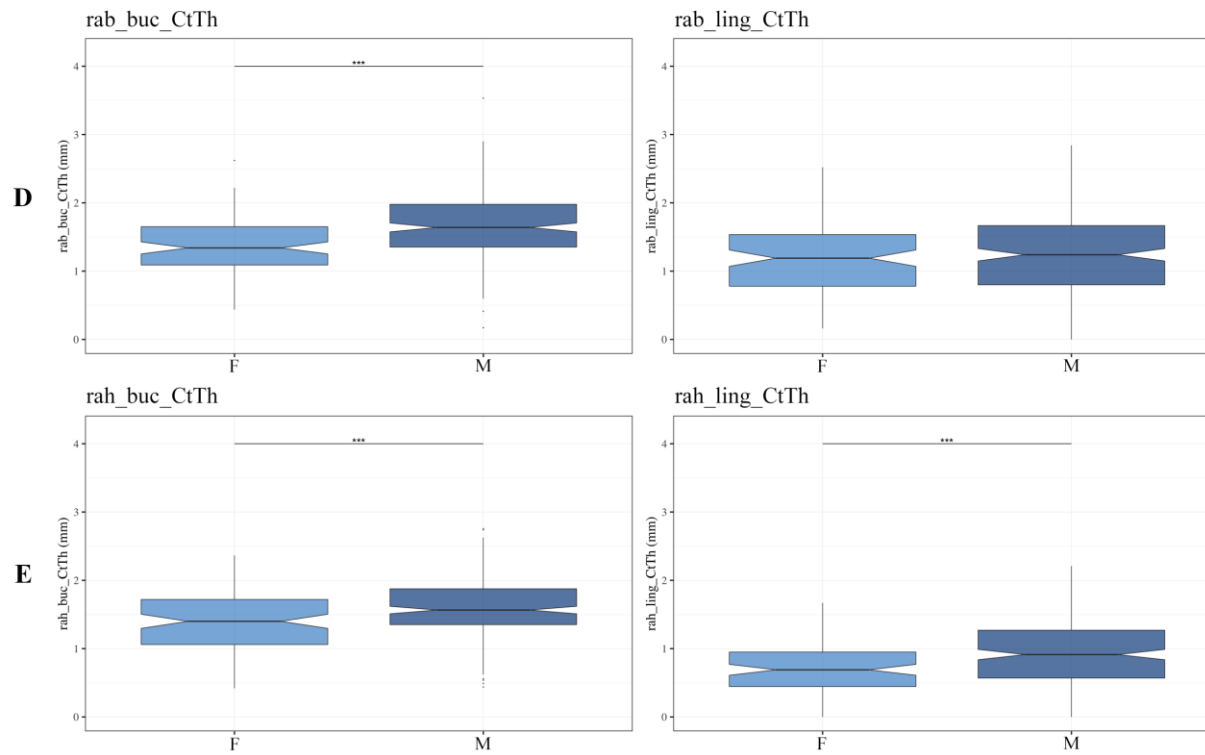
Figure 4.19. (continued)
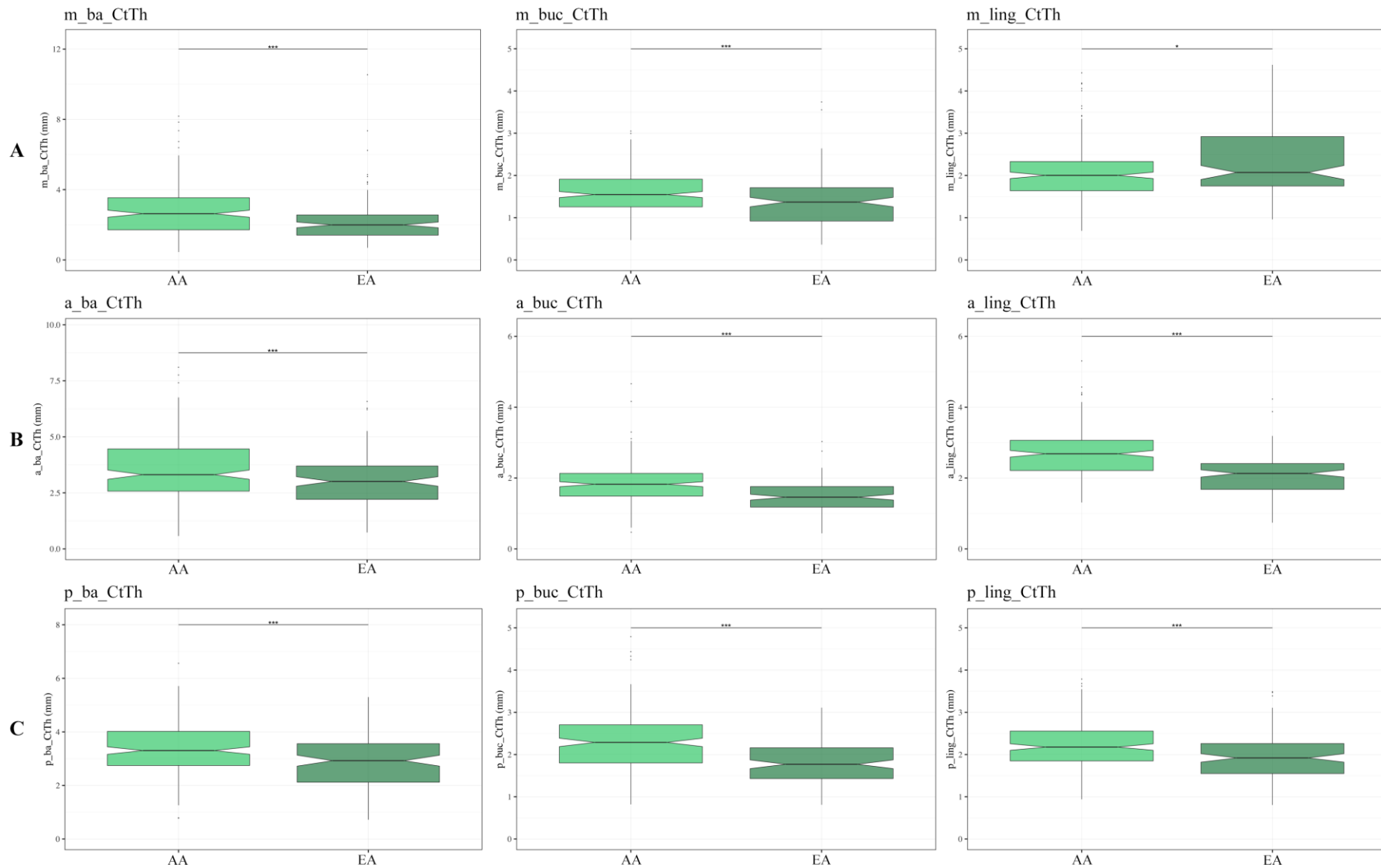
Figure 4.20. Boxplots of CtTh (mm) per ancestry (AA: light green; EA: dark green), recorded on the midline [A], anterior [B], posterior [C], ramus breadth [D] and height [E] sections. Dots depict outliers. Significance: *** $p < 0.001$, ** $p < 0.01$, * $p < 0.05$. (continued on the next page)
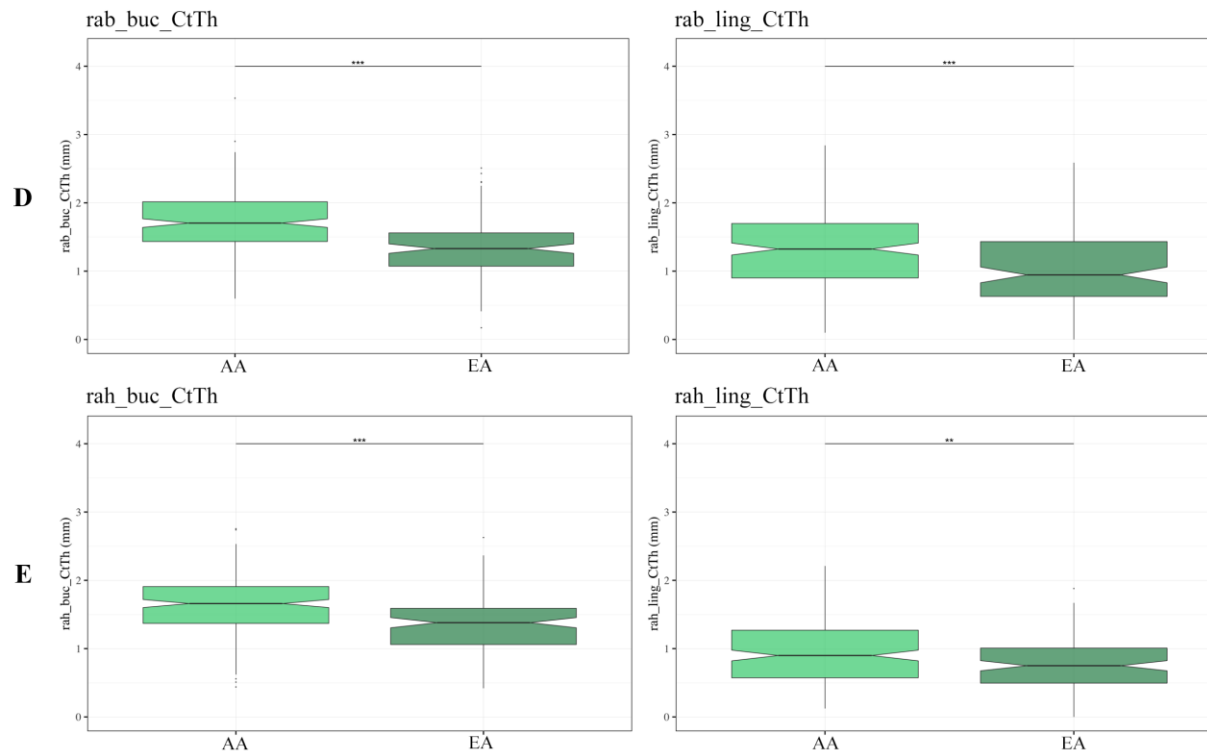
Figure 4.20. (continued)

4.4.2.3. Interaction between sex and ancestry

Kruskal-Wallis tests, run on the sex/ancestral subgroups, were found to be statistically significant for all the cortical thicknesses. Pairwise Wilcoxon post-hoc tests were therefore performed to determine which subgroups differed from the others. For easier reading, the results detailed below are grouped per section: midline (Figure 4.21 A), followed by anterior (Figure 4.21 B), then posterior (Figure 4.21 C), and finally ramus (Figure 4.21 D-E).

Except for the lingual site of the midline (m_ling_CtTh) where MEA demonstrated greater values, MAA individuals consistently had the thickest CtTh, followed by MEA, FAA and FEA: MAA > MEA > FAA > FEA (Figure 4.21 A). However, no statistical differences were detected between MAA and MEA at the buccal and lingual sites. The only other statistically significant differences were identified between MAA and FEA at the basal (m_ba_CtTh p-value < 0.001) and buccal sites (m_buc_CtTh p-value < 0.001), as well as between MAA and FAA at the buccal site (m_buc_CtTh p-value < 0.001). In addition, the lingual site (m_ling_CtTh) showed a unique significant difference between MEA and FAA, partially explained by the different pattern observed: MEA > MAA > FEA > FAA.

A different pattern from the midline was observed on the anterior section (as seen in Figure 4.21 B) – MAA > **FAA** > **MEA** > FEA – where statistically significant differences were detected between MAA (the thickest) and FEA (the thinnest) at all three sites (p < 0.001). While this was the only significant difference detected at the basal site, other significantly different pairings were found at the buccal and lingual sites: MAA-FAA, MAA-MEA, FAA-FEA and MEA-FEA. However, FAA and MEA were never statistically different from each other.

On the posterior section (Figure 4.21 C), a pattern (MAA > **FAA** > **MEA** > FEA), similar to that found in the anterior section, was observed at the basal and buccal sites, while the lingual site was different (MAA > MEA > FAA > FEA), even if no statistically significant differences were found between MEA and FAA at all three sites. However, MAA and FEA, as well as MAA and MEA, were consistently statistically significantly different, with MAA showing the greater CtTh, and FEA, the smallest. Furthermore, significant differences were also found between MAA and FAA at the buccal and lingual sites only, while FAA and FEA were different only at the basal site.

138

The patterns detected in the ramus sections (Figure 4.21 D-E) were similar to that seen in the anterior and posterior sections – MAA > FAA > MEA > FEA – except for the lingual CtTh of the ramus height (rah_ling_CtTh: MAA > MEA > FAA > FEA).
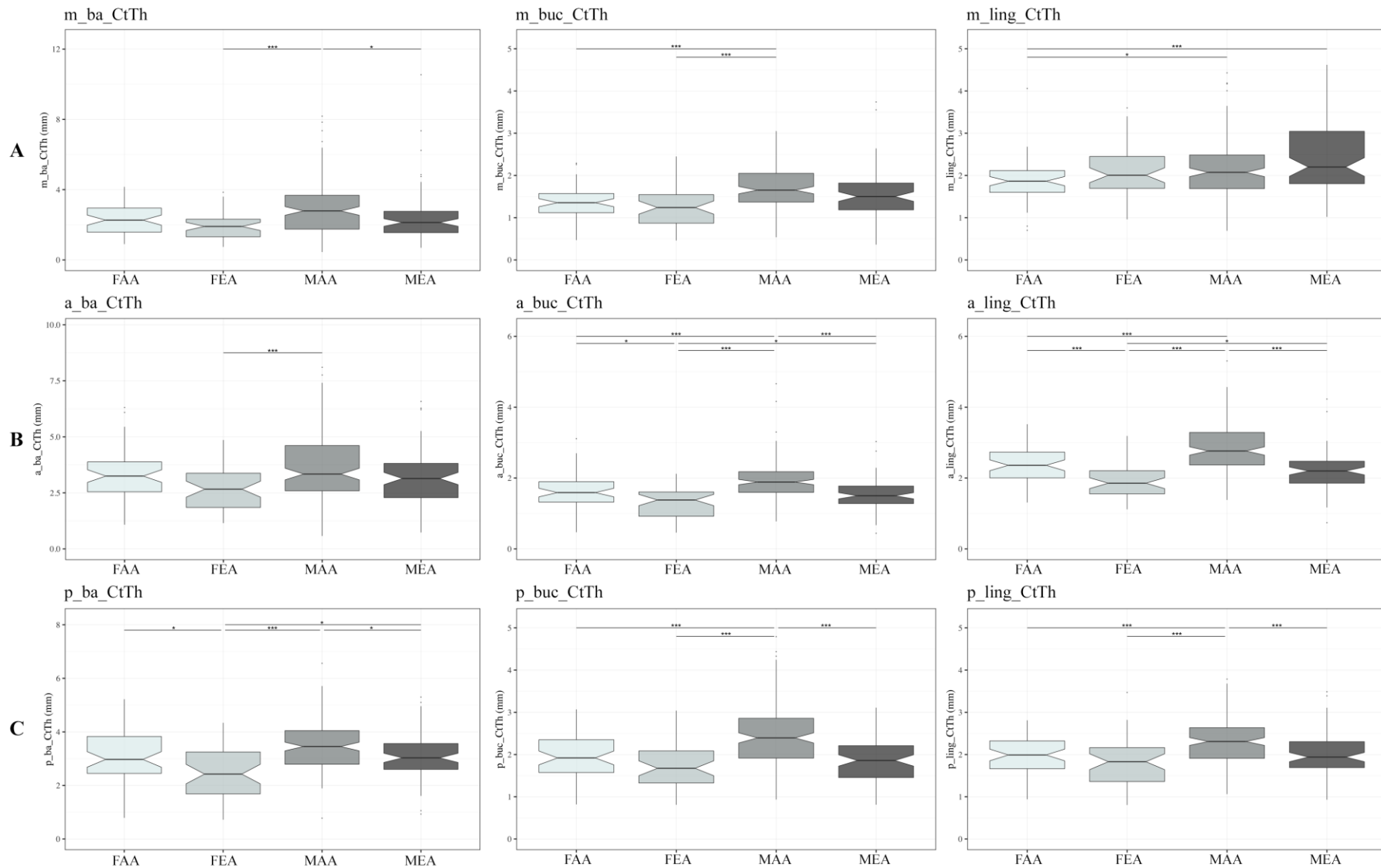
Figure 4.21. Boxplots of CtTh (mm) per sex/ancestry (FAA, FEA, MAA, MEA: from light to dark grey), recorded on the midline [A], anterior [B], posterior [C], ramus breadth [D] and height [E] sections. Dots depict outliers. Significance: *** $p < 0.001$, ** $p < 0.01$, * $p < 0.05$. (continued on the next page)
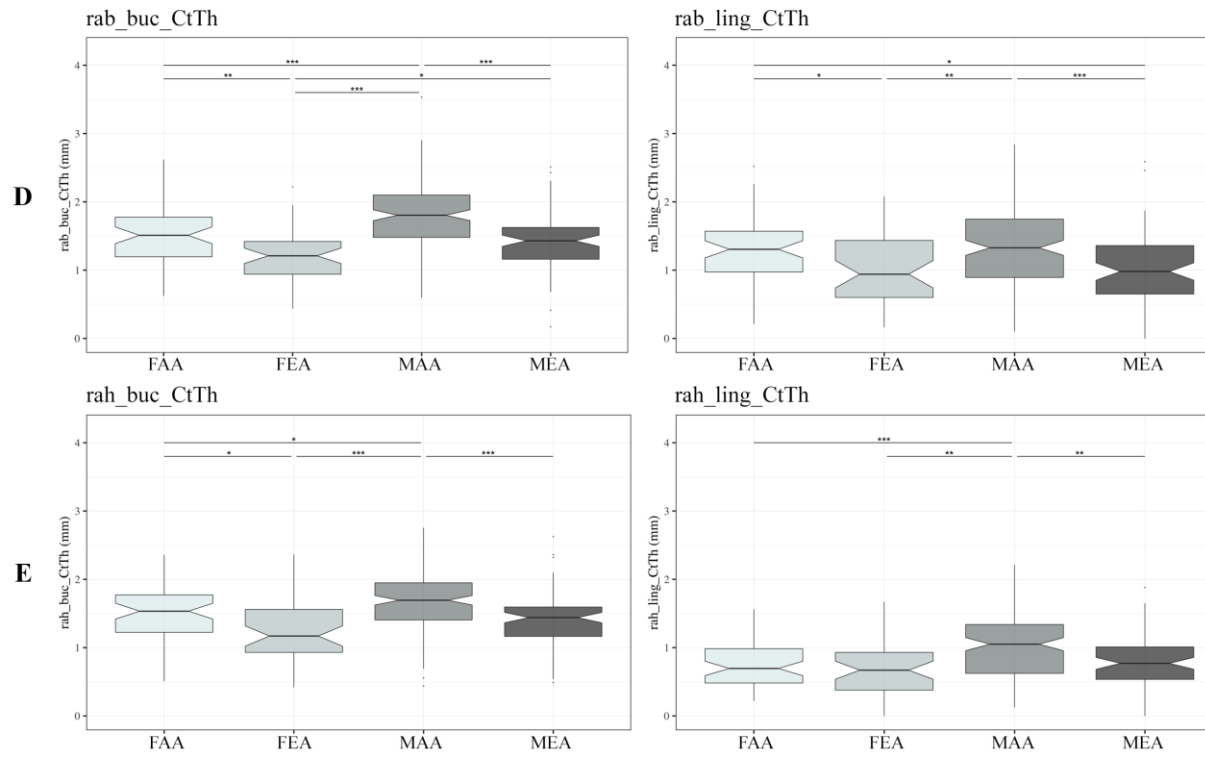
Figure 4.21. (continued)

4.4.3. Influence of tooth loss

The influence of tooth loss (from moderate to extreme) on cortical thickness was first evaluated in the entire sample using Kruskal-Wallis tests, followed by pairwise Wilcoxon post-hoc tests. The influence of tooth loss was then assessed in subsamples separated by sex, ancestry, or sex/ancestry, respectively, to control for these demographic parameters. To do so, Kruskal-Wallis and pairwise Wilcoxon post-hoc tests were also performed. Finally, the influence of sex, ancestry, or both, on the cortical thicknesses was assessed while controlling for tooth loss. Mann-Whitney Wilcoxon tests were done for sex and ancestry, while Kruskal-Wallis and Wilcoxon post-hoc tests were performed for sex/ancestral subsamples.

4.4.3.1. Tooth loss in the entire sample

The cortical thicknesses recorded on the mandibular body and ramus were analysed according to the three dentition categories defined (A, B, C). First, Kruskal-Wallis tests showed that all sites from the midline, posterior and ramus sections had statistically significant differences in CtTh between A, B and C categories, with cortical thicknesses declining with tooth loss. However, in the anterior section, only the buccal site (a_buc_CtTh) displayed significant differences with tooth loss.

Pairwise Wilcoxon post-hoc tests were performed to investigate the differences between each dentition category (A vs. B, A vs. C, B vs. C), as illustrated in Figure 4.22. Individuals from the A category were found to have statistically significantly thicker CtTh than those from the C category in 10 of the 13 sites studied (all sites from all sections except a_ba_CtTh and a_ling_CtTh, where no statistical significances were detected; and m_ling_CtTh). Only four CtTh (m_buc_CtTh, a_buc_CtTh, p_buc_CtTh, p_ling_CtTh) from the nine recorded on the mandibular body were found statistically different between A and B categories, while all four CtTh measured on the ramus (Figure 4.22 D-E) showed a significant decrease with moderate changes in dentition (from A to B categories). Significant differences between B and C were detected in five sites: lingual CtTh of the midline section (m_ling_CtTh), basal (p_ba_CtTh) and buccal (p_buc_CtTh) sites of the posterior section, buccal sites of the ramus breadth (rab_buc_CtTh) and height (rah_buc_CtTh) sections.

142

A specific pattern was noticed at the lingual site of the midline (m_ling_CtTh – Figure 4.22 A), with a statistically significant increase in CtTh (associated with a wider range of values) for the edentulous individuals classified in the C category compared to A, and even B.

4.4.3.2. Tooth loss per sex

The entire sample was then divided into sex subgroups (Figure 4.23), in which CtTh differences between the three dentition categories were analysed. Within the female subsample, statistical significance was detected in cortical thickness between the dentition categories at the basal and buccal sites of the midline, the anterior and posterior sections, as well as in both buccal sites of the ramus sections (breadth and height). These eight measurements (m_ba_CtTh, m_buc_CtTh, a_ba_CtTh, a_buc_CtTh, p_ba_CtTh, p_buc_CtTh, rab_buc_CtTh, rah_buc_CtTh) were all significantly thicker in category A than in C. Within the male subsample, however, only three sites on the mandibular body were displaying statistically significant differences between the dentition categories: midline lingual site (m_ling_CtTh), anterior and posterior buccal sites (a_buc_CtTh, p_buc_CtTh). Although the anterior and posterior buccal sites showed a decreasing CtTh with tooth loss (from A to C), the midline lingual site displayed an important and significant increase of CtTh in the C category ($p < 0.001$ between A and C, as well as between B and C). As in females, the lingual site of the ramus height (rah_ling_CtTh) was the only site on the ramus not displaying any significant differences between dentition categories. Indeed, the three other sites (rab_buc_CtTh, rab_ling_CtTh, rah_buc_CtTh) presented significantly decreasing CtTh with tooth loss (from A to C).

4.4.3.3. Tooth loss per ancestry

Tooth loss was then evaluated within the two ancestry-separated subgroups (Figure 4.24), using Kruskal-Wallis and pairwise Wilcoxon post-hoc tests. Overall, compared to the male and female subgroups analysed above, fewer statistically significant differences were noticed between dentition categories within AA and EA. However, a similar pattern of increased CtTh with tooth loss was noted and was significant in the midline and anterior lingual sites of AA and EA individuals. In contrast, a significant decrease in CtTh, associated with moderate tooth loss (from A to B categories), was detected at only one site (m_buc_CtTh) in

AA individuals, while in the EA subgroup, two other sites (p_ba_CtTh, p_buc_CtTh) were found to decrease significantly between all dentition categories (A vs. C, B vs. C for p_ba_CtTh; A vs. C, A vs. B for p_buc_CtTh).

4.4.3.4. Tooth loss per sex/ancestry

Statistical analyses were then performed within each sex/ancestral subsample to assess the effect of moderate to extreme tooth loss in each of these groups (Figure 4.25). A decrease in CtTh was noted at all sites except lingually and more particularly in the midline, where increases from A to C were detected (which were significant in MAA and MEA). Within FAA and FEA, significant differences between A and C categories were mostly found at similar sites (m_ba_CtTh, p_ba_CtTh, p_buc_CtTh, rab_buc_CtTh), while in MAA and MEA, the differences were less frequent and less predictable.

144
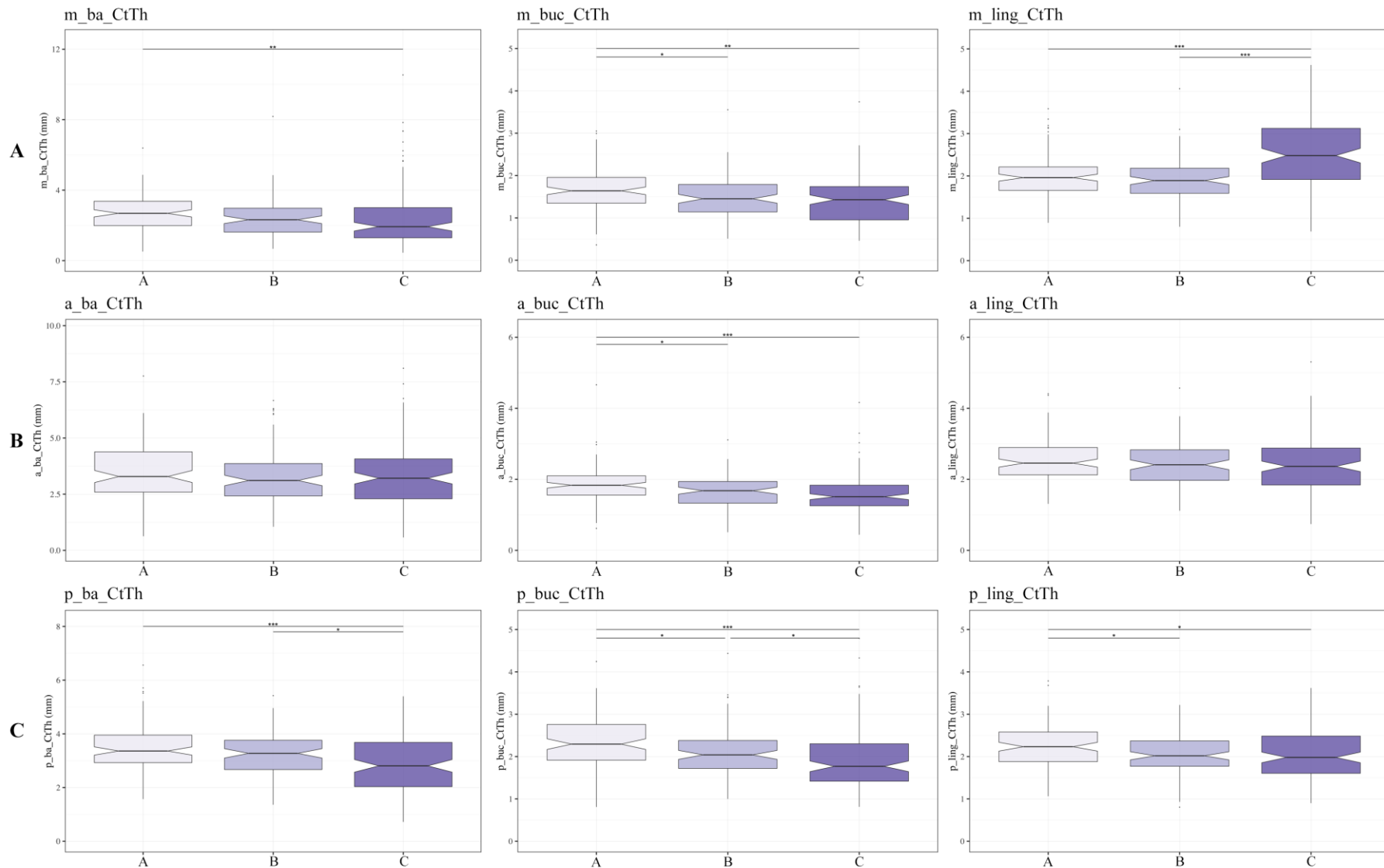
Figure 4.22. Boxplots of CtTh (mm) per dentition category (A, B, C: from light to dark purple), recorded on the midline [A], anterior [B], posterior [C], ramus breadth [D] and height [E] sections. Dots depict outliers. Significance: *** $p < 0.001$, ** $p < 0.01$, * $p < 0.05$. (continued on the next page)
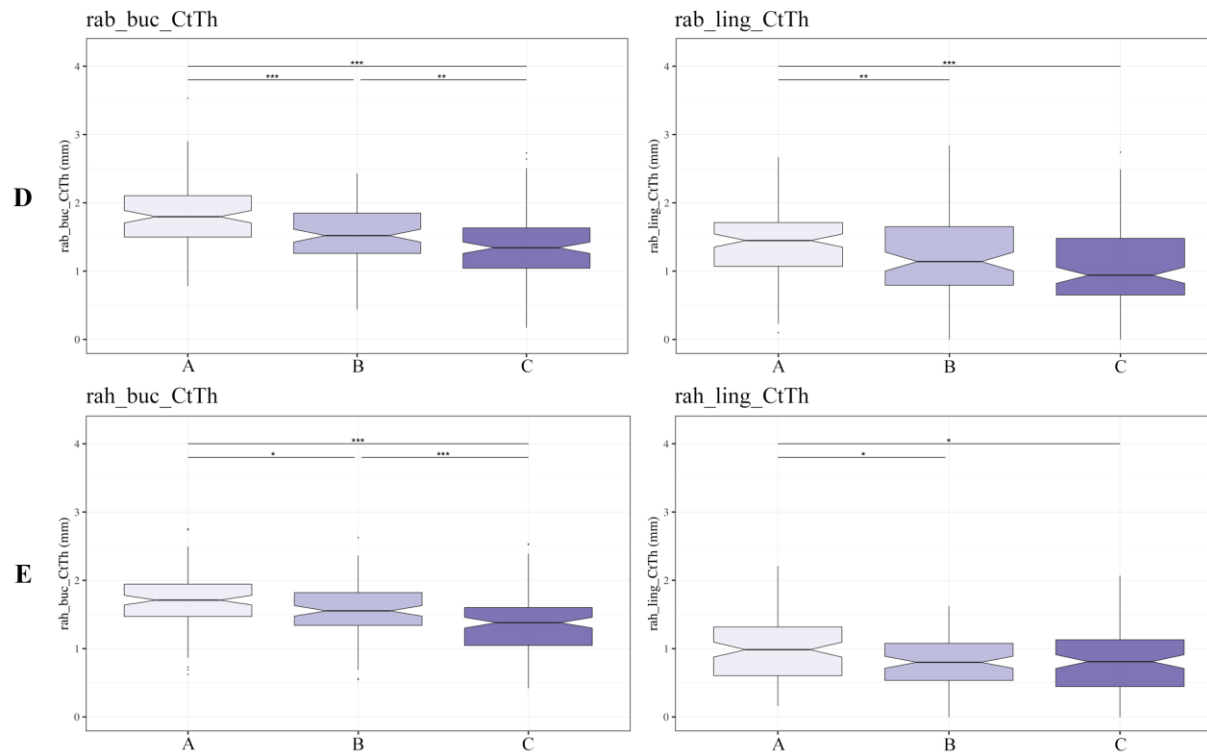
Figure 4.22. (continued)
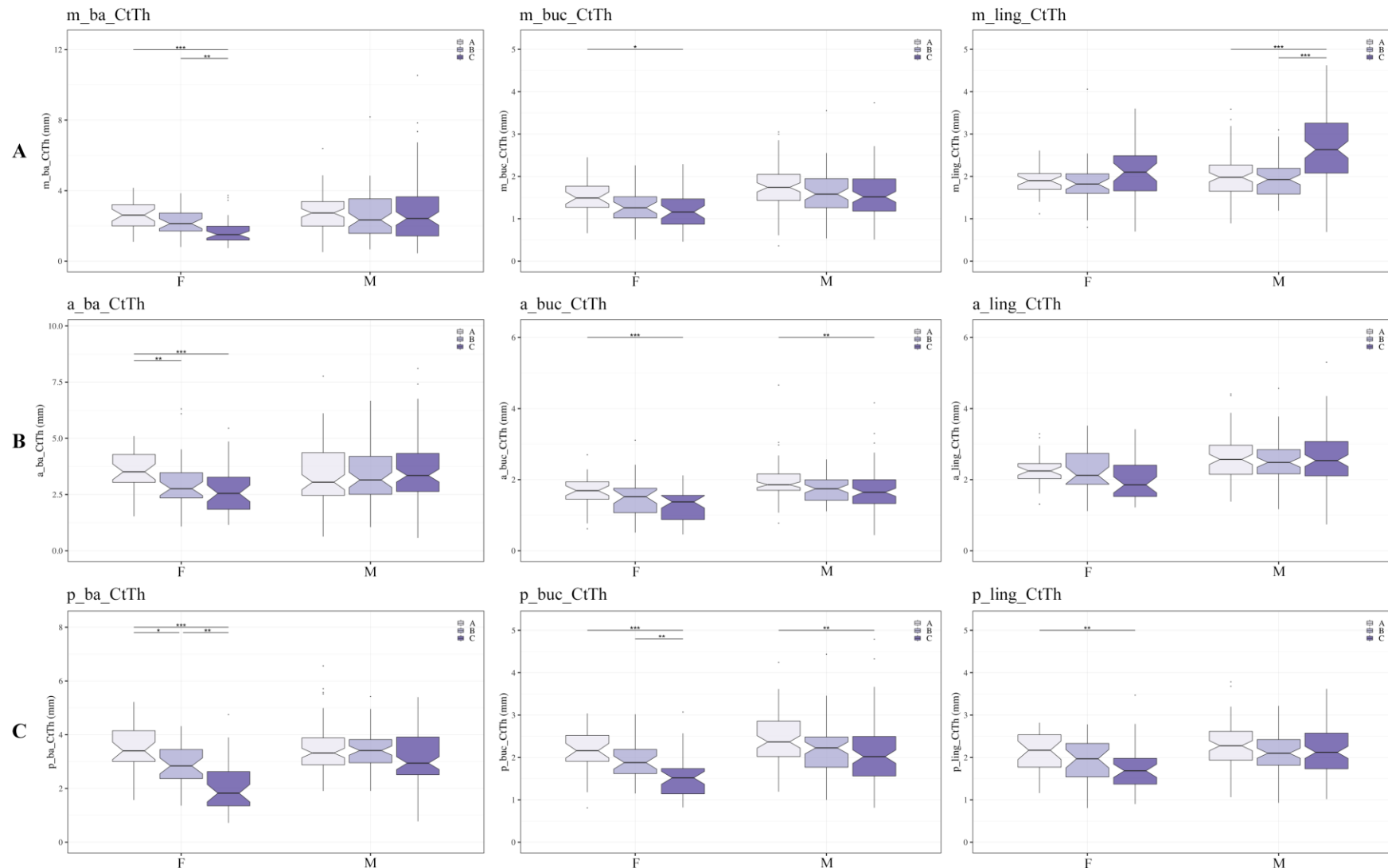
Figure 4.23. Boxplots of CtTh (mm) per sex (F, M) and dentition category (A, B, C: from light to dark purple), recorded on the midline [A], anterior [B], posterior [C], ramus breadth [D] and height [E] sections. Dots depict outliers. Significance: *** $p < 0.001$, ** $p < 0.01$, * $p < 0.05$. (continued on the next page)
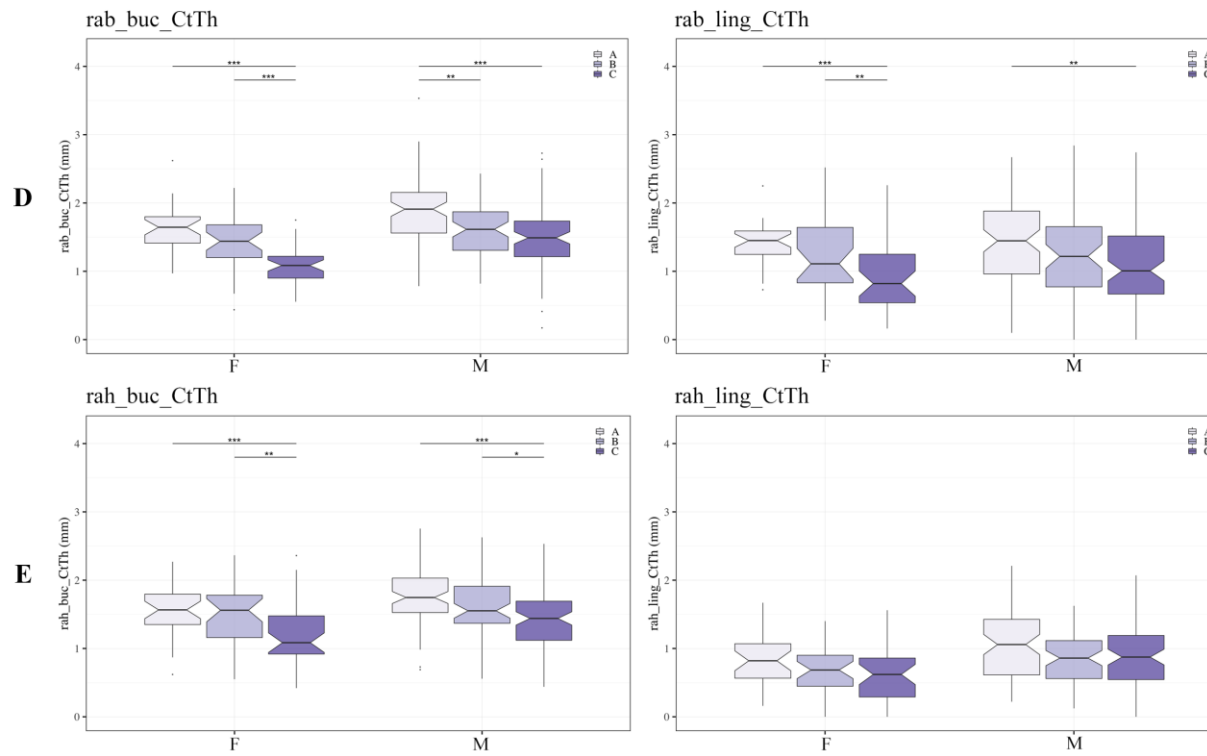
Figure 4.23. (continued)
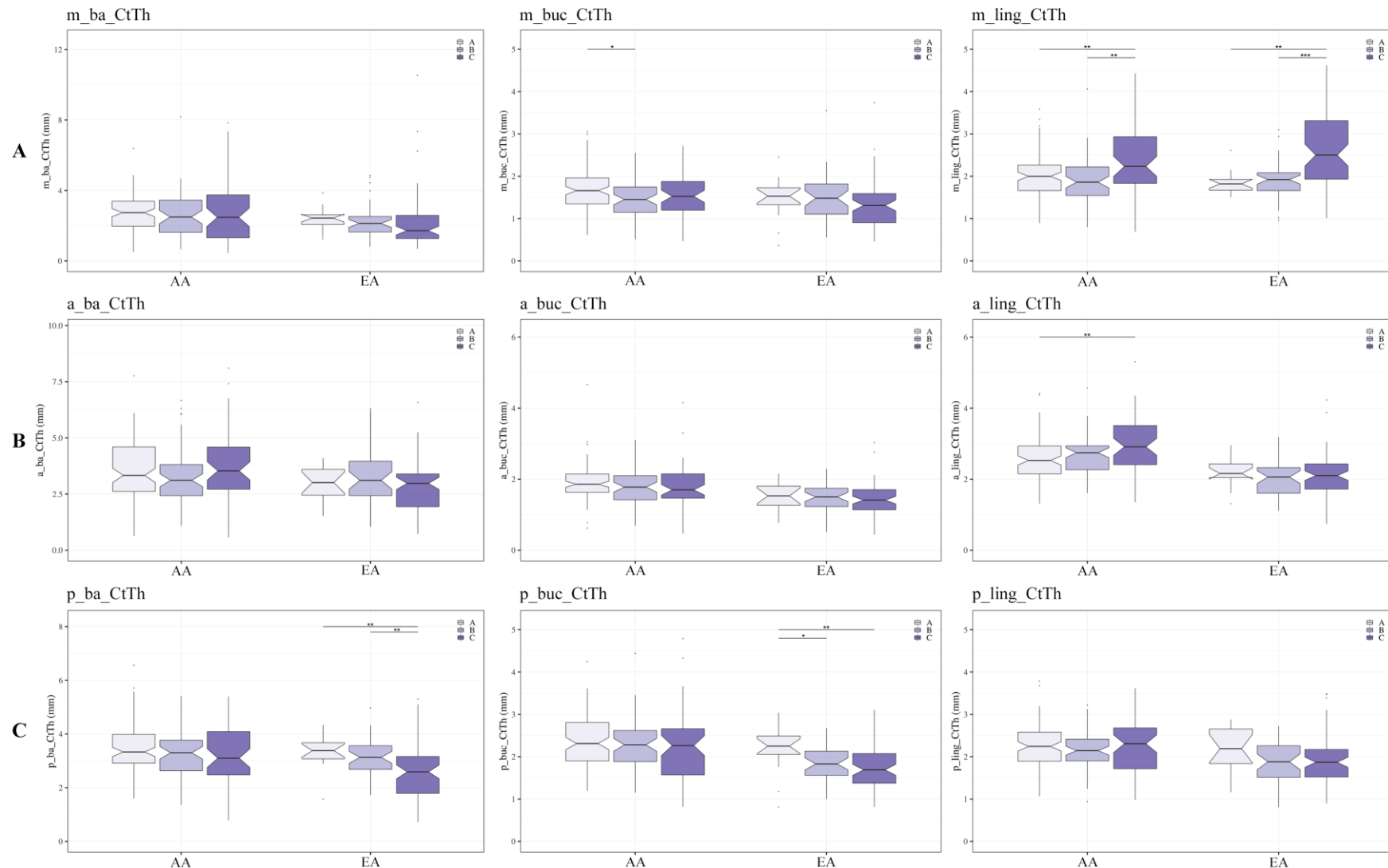
Figure 4.24. Boxplots of CtTh (mm) per ancestry (AA, EA) and dentition category (A, B, C: from light to dark purple), recorded on the midline [A], anterior [B], posterior [C], ramus breadth [D] and height [E] sections. Dots depict outliers. Significance: *** $p < 0.001$, ** $p < 0.01$, * $p < 0.05$. (continued on the next page)
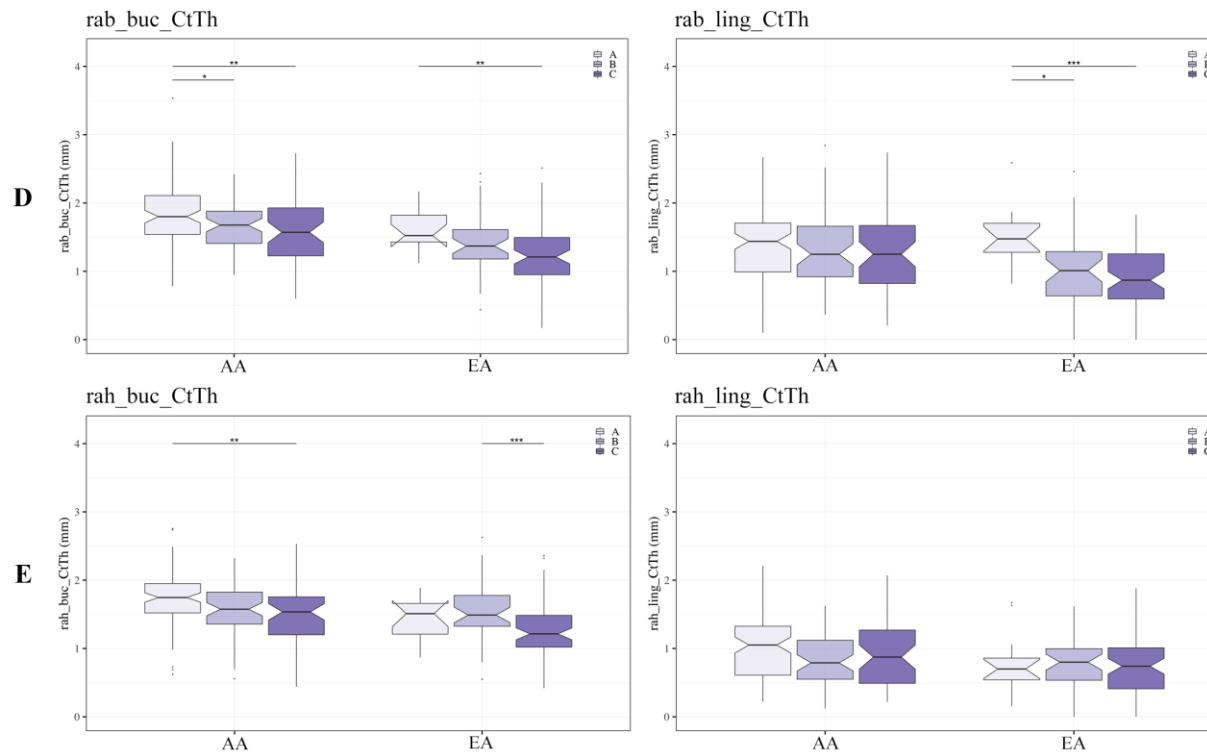
Figure 4.24. (continued)
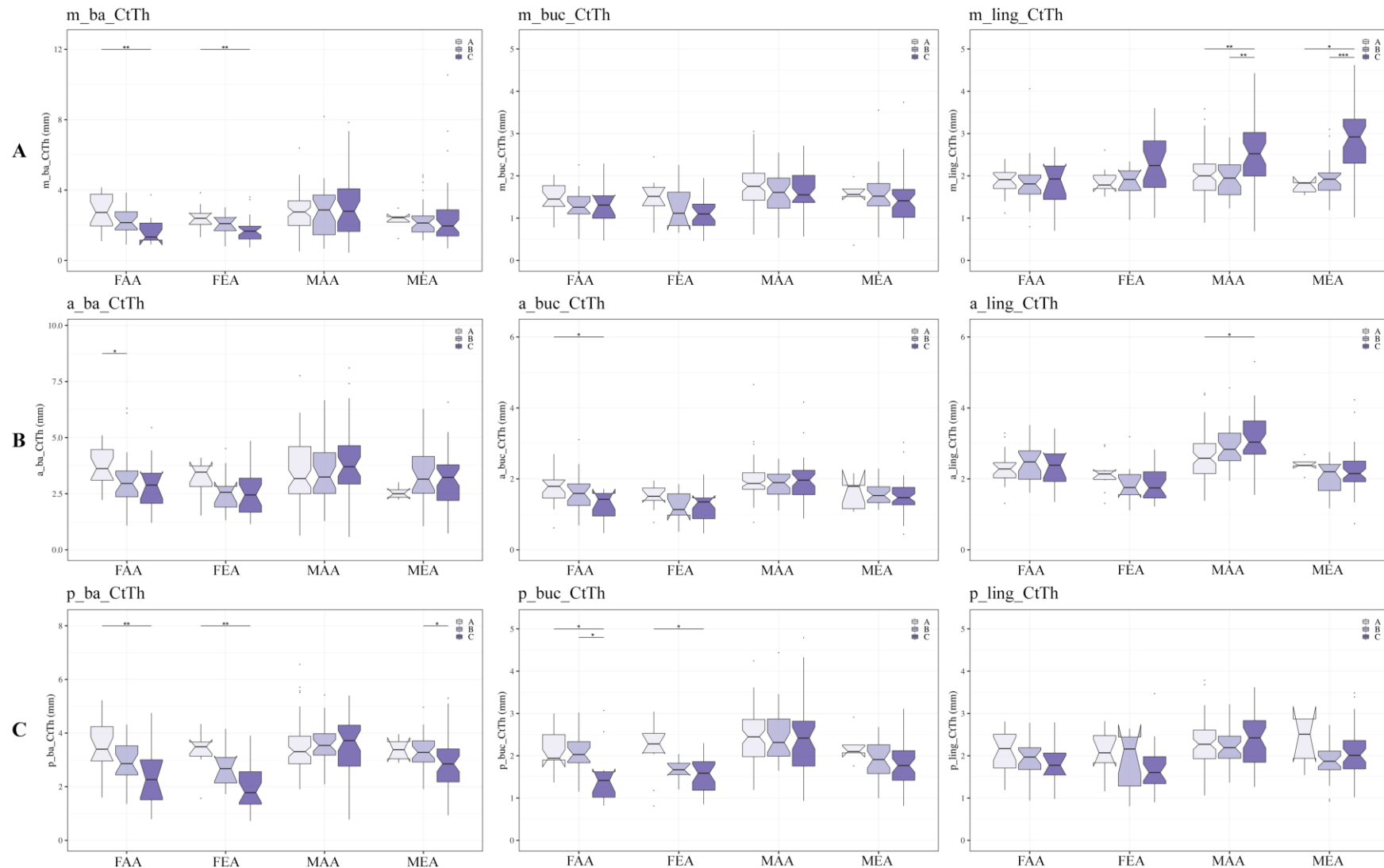
Figure 4.25. Boxplots of CtTh (mm) per sex/ancestry (FAA, FEA, MAA, MEA) and dentition category (A, B, C: from light to dark purple), recorded on the midline [A], anterior [B], posterior [C], ramus breadth [D] and height [E] sections. Dots depict outliers. Significance: *** $p < 0.001$, ** $p < 0.01$, * $p < 0.05$.

(continued on the next page)
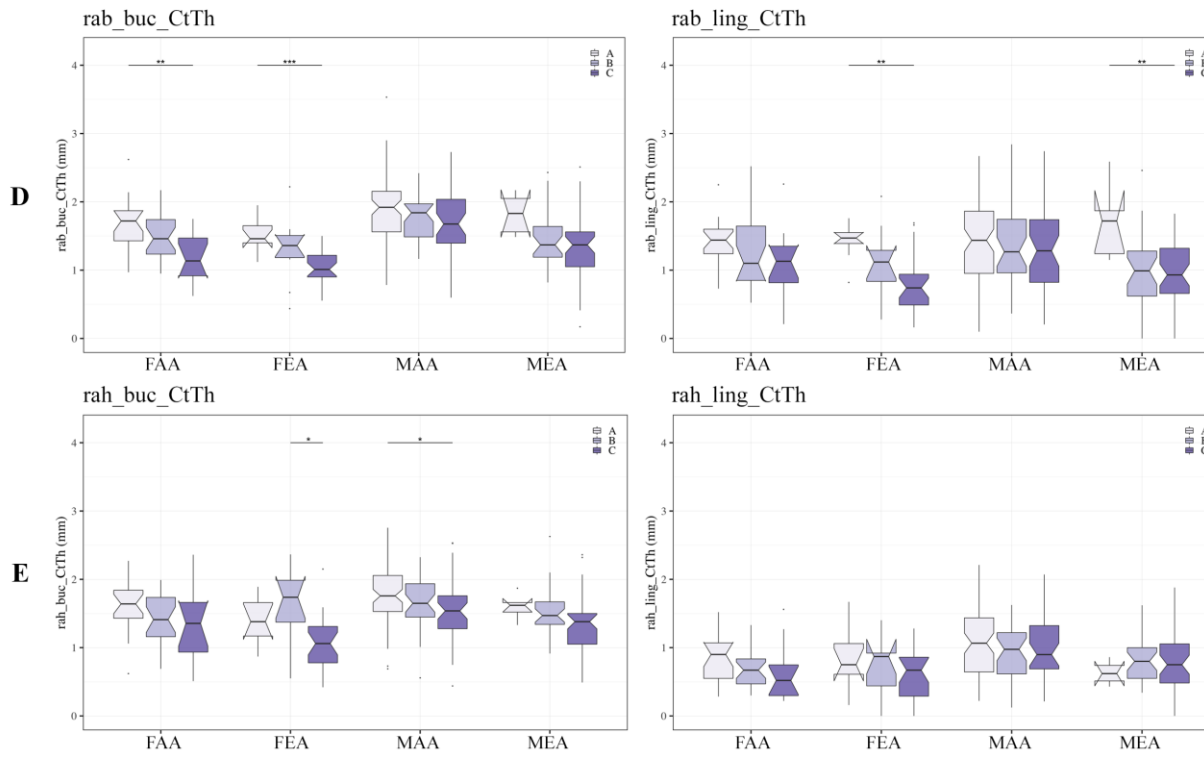
Figure 4.25. (continued)

4.4.3.5. Influence of sex per dentition category

The influence of sex on the mandibular cortical thicknesses was evaluated within each dentition category (A, B, C), in order to control for tooth loss (Figure 4.26). The individuals within the A category showed a greater CtTh in males than in females at all sites, but only statistically significant at one lingual site (a_ling_CtTh), and all buccal sites (m_buc_CtTh, a_buc_CtTh, p_buc_CtTh, rab_buc_CtTh, rah_buc_CtTh). In the B category, most of the CtTh measured at the buccal sites (m_buc_CtTh, a_buc_CtTh, p_buc_CtTh, rab_buc_CtTh) as well as at the anterior lingual site (a_ling_CtTh) remained significantly different between sexes, with males always thicker than females, while the posterior basal site (p_ba_CtTh) also became significantly different. When analysing the C category, statistically significant sexual dimorphism was detected at all sites of all sections, except for the lingual site of the ramus breadth (rab_ling_CtTh), most probably because of the location of the section and the number of missing values. Overall, even if the distribution of the values was wider in the edentulous mandibles (i.e., in category C), the differences between males and females were accentuated and particularly noticeable on the boxplots (Figure 4.26), with the non-overlapping of the boxplot's notches.

In summary, females start off with a thinner CtTh compared to males, which becomes more accentuated and generalised to the whole mandible as teeth are lost.

4.4.3.6. Influence of ancestry per dentition category

Ancestry and its effect on CtTh were investigated while controlling for tooth loss (Figure 4.27). Within A, statistically significant differences between AA and EA were only detected for the buccal and lingual sites of the anterior section (a_buc_CtTh, a_ling_CtTh), as well as for the buccal sites of the ramus breadth and height (rab_buc_CtTh, rah_buc_CtTh): always showing greater CtTh in AA than in EA individuals. In B, however, both buccal and lingual sites of the anterior, posterior and ramus breadth sections (a_buc_CtTh, a_ling_CtTh, p_buc_CtTh, p_ling_CtTh, rab_buc_CtTh, rab_ling_CtTh) were found to have statistically significant greater CtTh in AA than in EA. In other sites, such as the basal site of the anterior and posterior sections (a_ba_CtTh, p_ba_CtTh), no significant differences were found, partly explained because the mean values (centre of the notches) of AA and EA were close. These six sites were also found to differ significantly between ancestries in the edentulous mandibles

(i.e., within the C category), with always thicker CtTh in AA. Other sites also became significant (which were not in A and B): the buccal site of the midline (m_buc_CtTh) and the basal sites of the anterior and posterior sections (a_ba_CtTh, p_ba_CtTh). The lingual site of the midline (m_ling_CtTh) displayed a non-significant but unusual pattern with a particularly wide distribution of values ("long" boxplots) and a mean CtTh greater in EA than in AA. To sum up, a generally thicker CtTh, accentuated by edentulism, was detected in AA individuals compared to EA, except for the lingual site of the mandible where the opposite was noticed.

4.4.3.7. Influence of sex and ancestry per dentition category

The influence of the interaction between sex and ancestry was then assessed within each dentition category, using Kruskal-Wallis tests and pairwise Wilcoxon post-hoc tests when needed (Figure 4.28). Within category A, only the buccal site of the anterior section (a_buc_CtTh), as well as the buccal sites of the ramus breadth and height showed statistically significant differences in CtTh between subgroups, with MAA showing the greater values. Similarly to category A, no significant differences were found at any sites of the midline section in individuals from category B. However, the buccal and lingual sites of the anterior and posterior sections were found to have a significantly greater CtTh in MAA than in the other groups. Finally, within the C category, at least one sex/ancestral subgroup was always significantly different from the others, at any of the sites and always with a thicker MAA. At the midline lingual site, however, CtTh was significantly thicker in MEA than in the other subsamples.
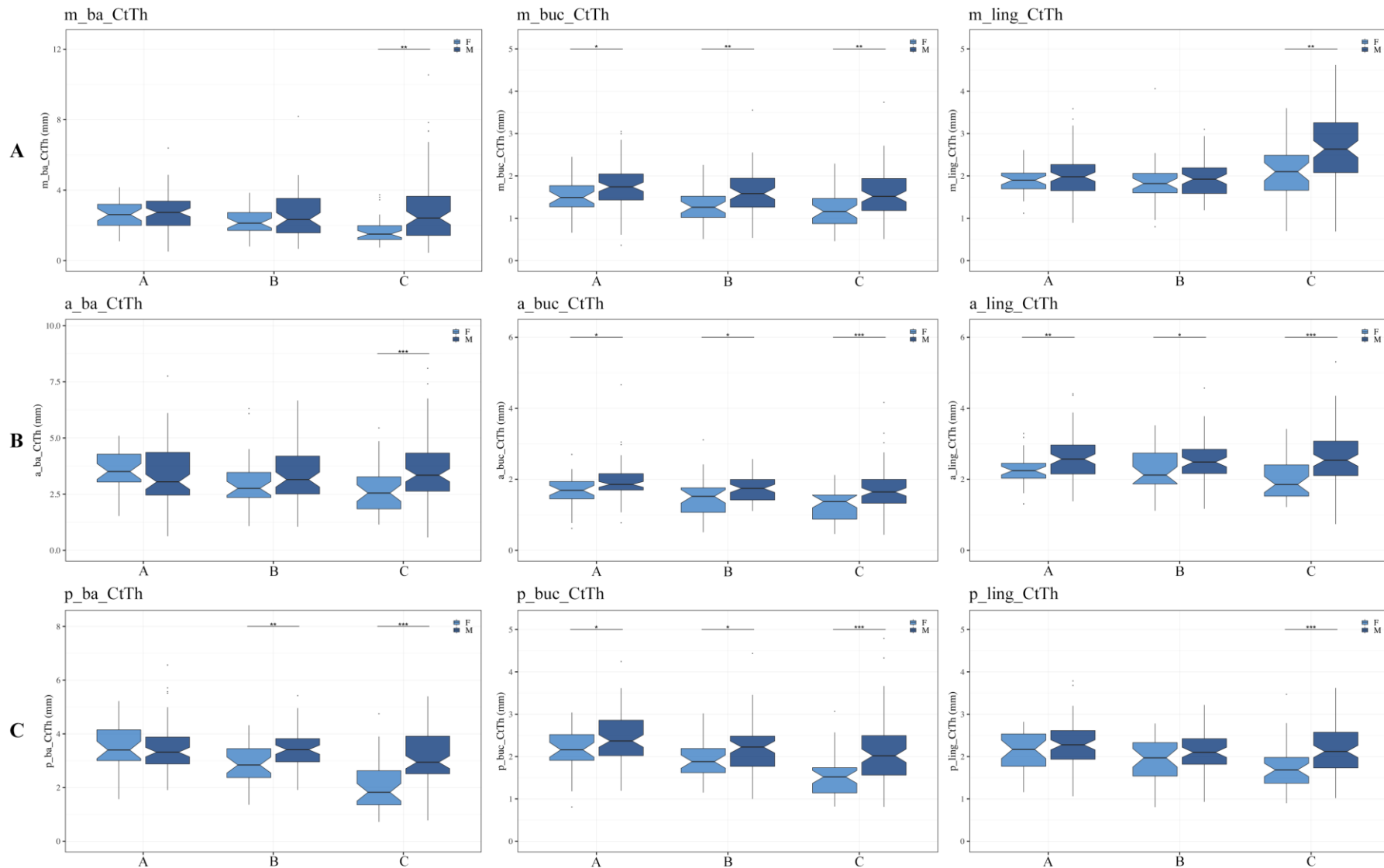
Figure 4.26. Boxplots of CtTh (mm) per dentition category (A, B, C) and sex (F: light blue; M: dark blue), recorded on the midline [A], anterior [B], posterior [C], ramus breadth [D] and height [E] sections. Dots depict outliers. Significance: *** $p < 0.001$, ** $p < 0.01$, * $p < 0.05$. (continued on the next page)
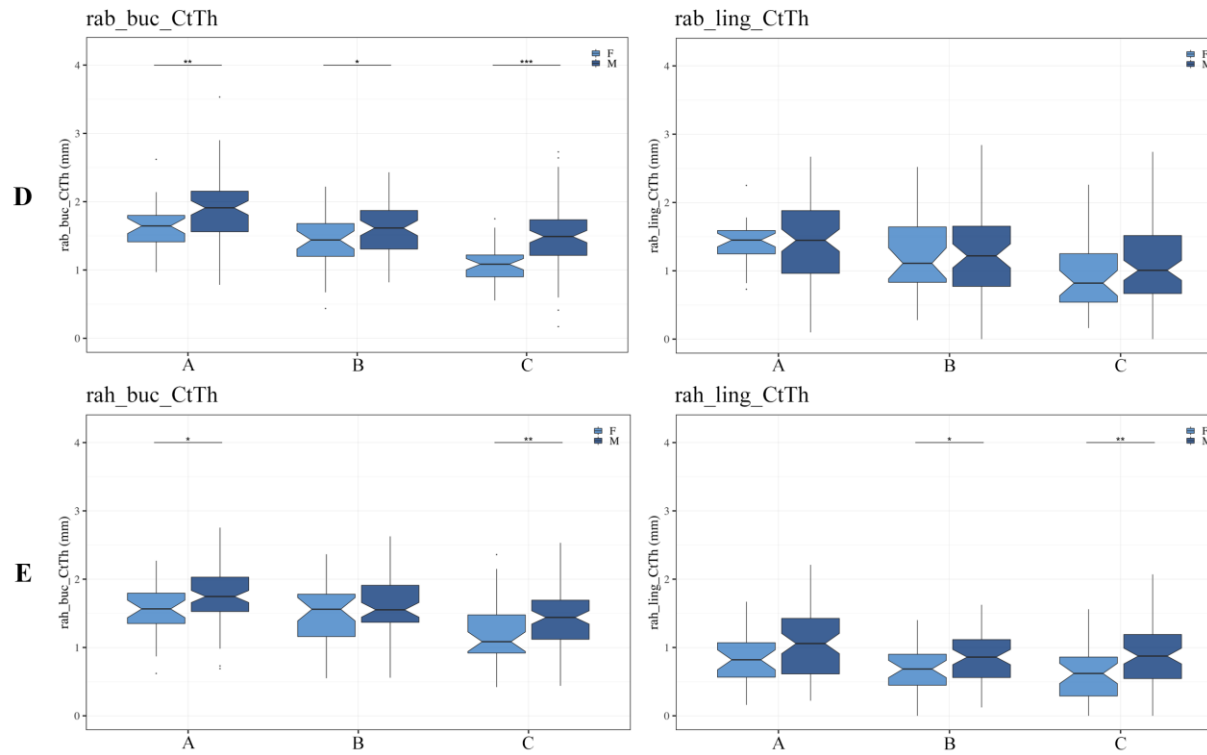
Figure 4.26. (continued)
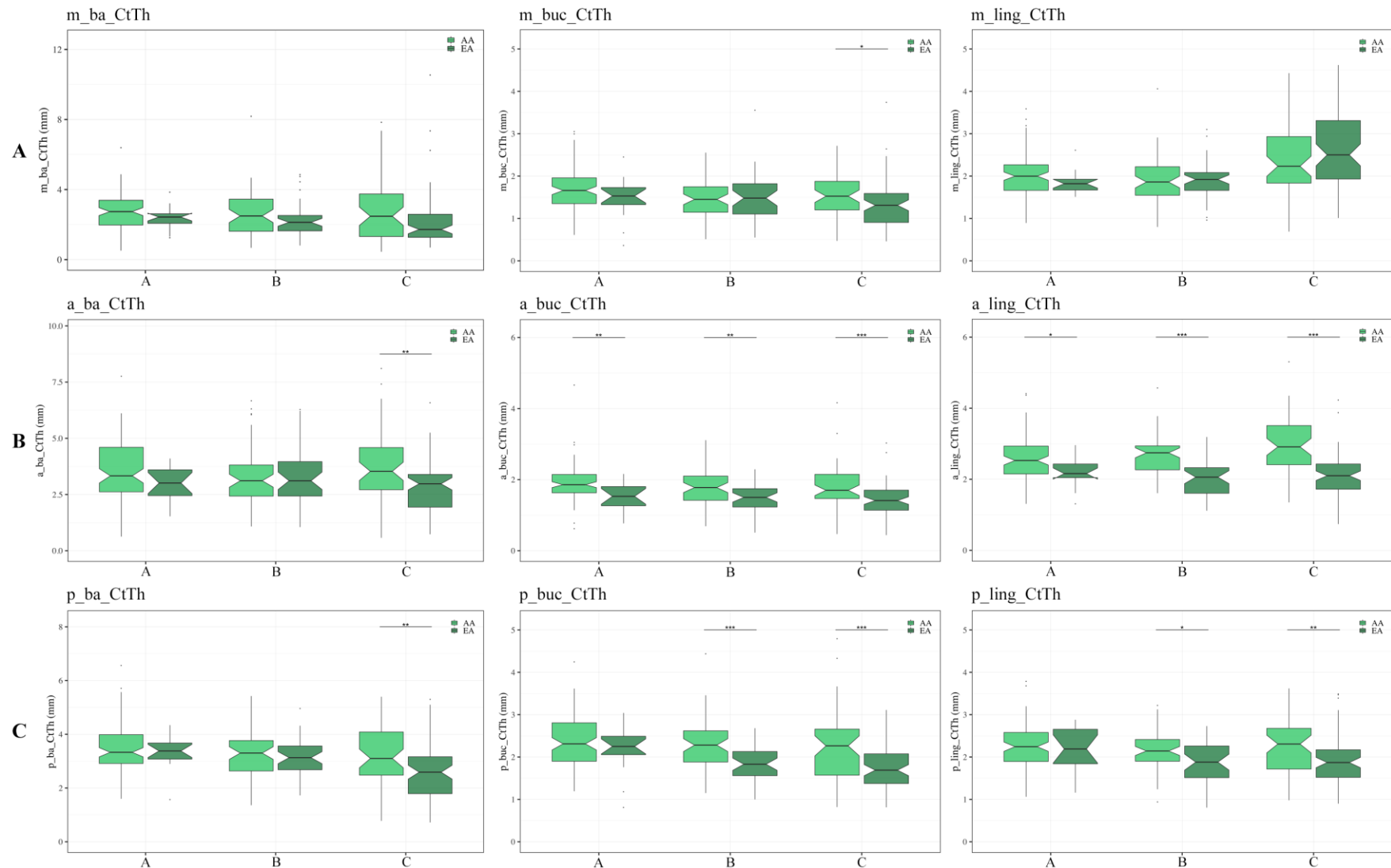
Figure 4.27. Boxplots of CtTh (mm) per dentition category (A, B, C) and ancestry (AA: light green; EA: dark green), recorded on the midline [A], anterior [B], posterior [C], ramus breadth [D] and height [E] sections. Dots depict outliers. Significance: *** $p < 0.001$, ** $p < 0.01$, * $p < 0.05$. (continued on the next page)
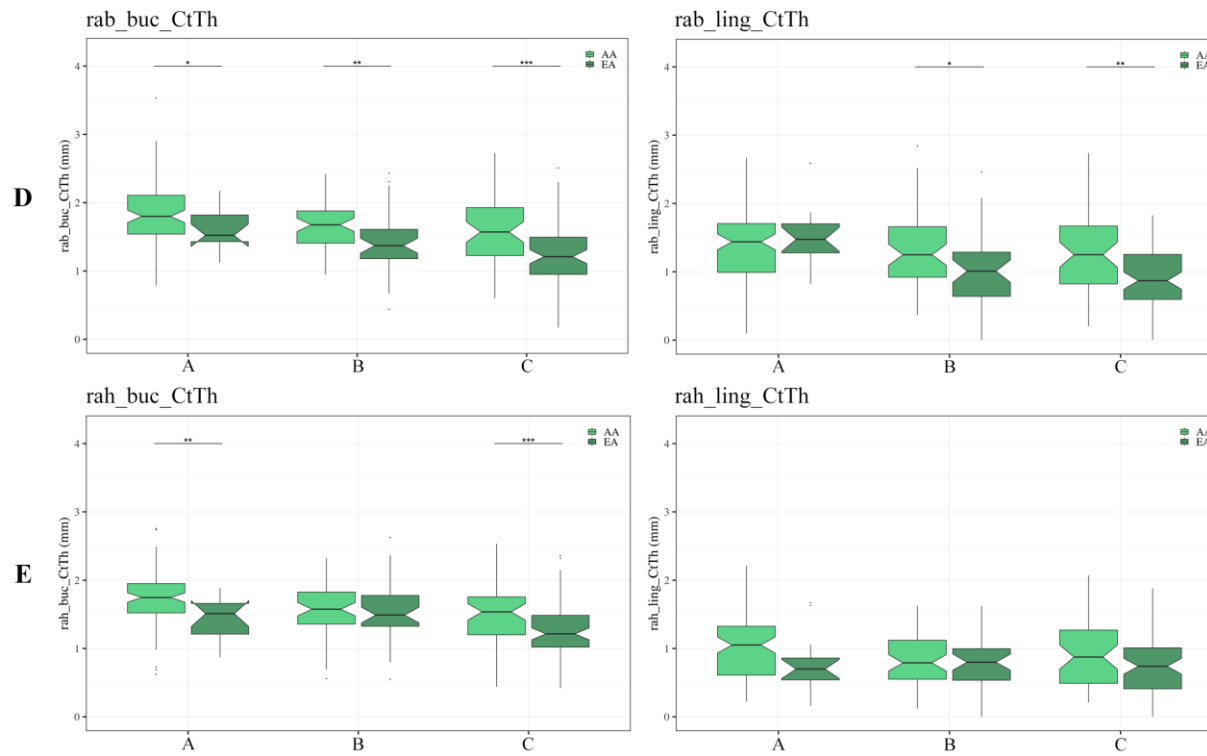
Figure 4.27. (continued)
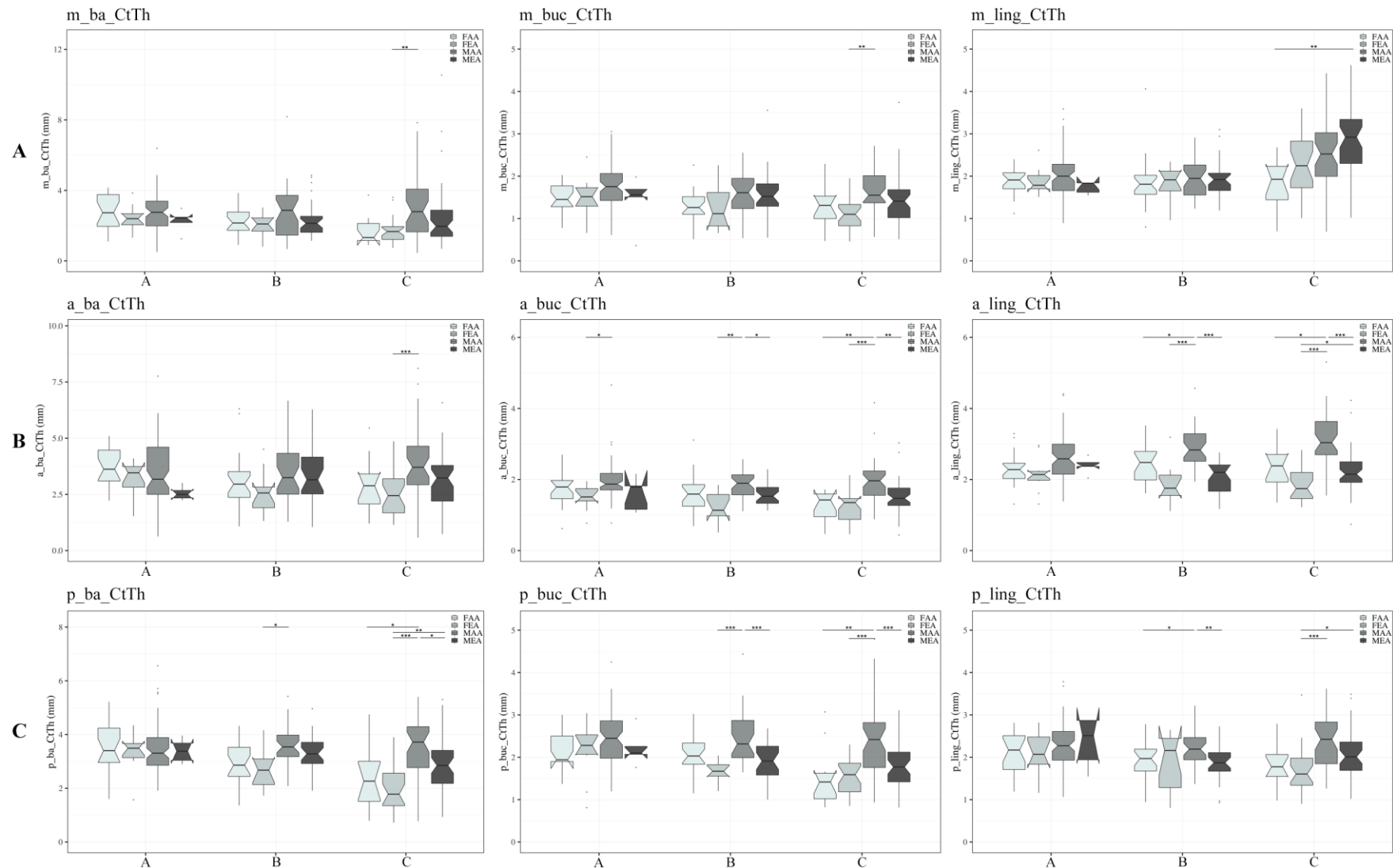
Figure 4.28. Boxplots of CtTh (mm) per dentition category (A, B, C) and sex/ancestry (FAA, FEA, MAA, MEA: from light to dark grey), recorded on the midline [A], anterior [B], posterior [C], ramus breadth [D] and height [E] sections. Dots depict outliers. Significance: *** $p < 0.001$, ** $p < 0.01$, * $p < 0.05$. (continued on the next page)
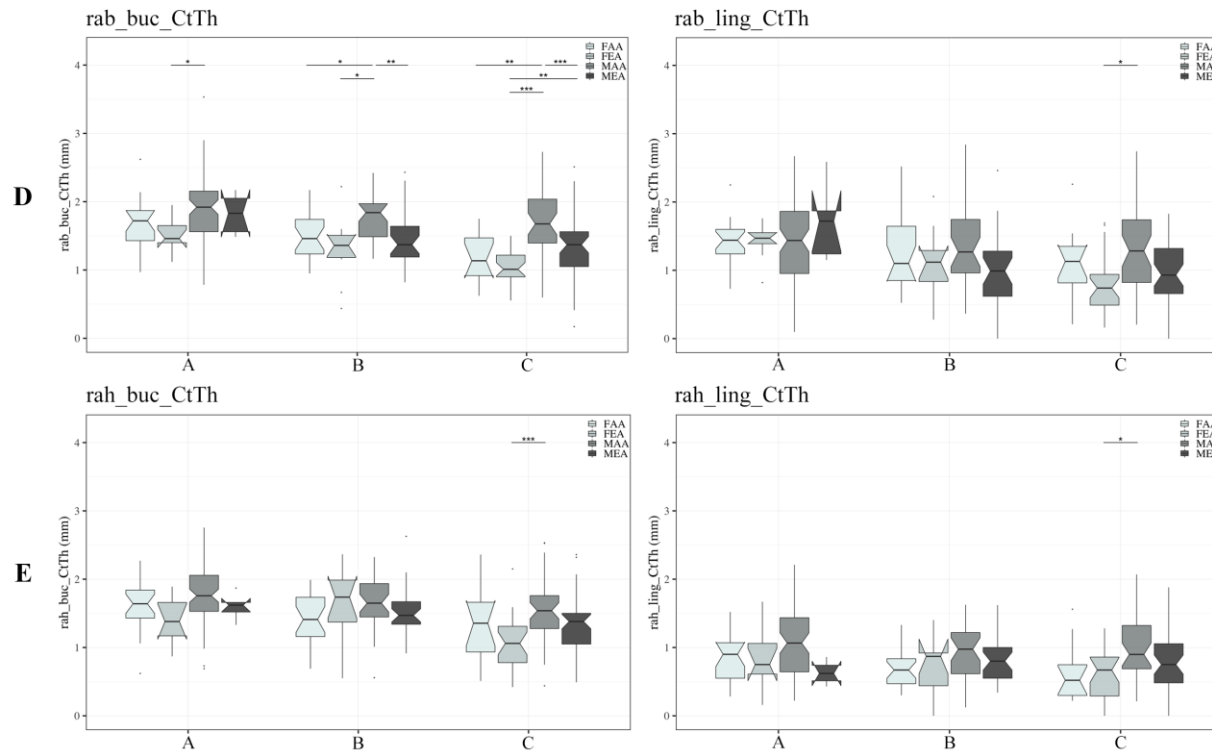
Figure 4.28. (continued)

4.4.4. Section and site location

4.4.4.1. Influence of section and site selection on CtTh recorded

Kruskal-Wallis tests and their associated pairwise Wilcoxon post-hoc tests were performed on the entire sample to investigate the differences in cortical thickness location (where the CtTh was recorded) by exploring the variations (i) between the five sections: midline vs. anterior vs. posterior vs. ramus breadth vs. ramus height (Figure 4.29 A); (ii) between the three sites: basal vs. buccal vs. lingual (Figure 4.29 B); and (iii) between the 13 section/site interactions: midline basal vs. anterior buccal vs. posterior lingual vs. ramus breadth buccal, etc. (Figure 4.30).

Statistically significant differences were detected between all the sections ($p < 0.001$), except between anterior and posterior ($p = 1.00$) (Figure 4.29 A). The midline CtTh was found to be the thinnest CtTh recorded on the mandibular body compared to the anterior and posterior thicknesses. Furthermore, the CtTh recorded on the ramus were found to be the thinnest overall. The three sites, as illustrated in Figure 4.29 B, also displayed significant differences, particularly the basal site, which was significantly thicker (and with a wider value distribution) than the two other sites ($p < 0.001$). Buccal and lingual sites were more similar but still significantly different ($p < 0.01$), with the lingual site slightly thicker and showing more variation. Regarding the 13 locations (i.e., when each section was associated with a site, as seen in Figure 4.30), most of them showed significant differences between each other, with p-values < 0.001. Interestingly, while a significant bucco-lingual asymmetry (buccal < lingual) was found at the midline ($p < 0.001$) and at the anterior section ($p < 0.001$), it was not present at the posterior section ($p = 1.00$).

161

A

B
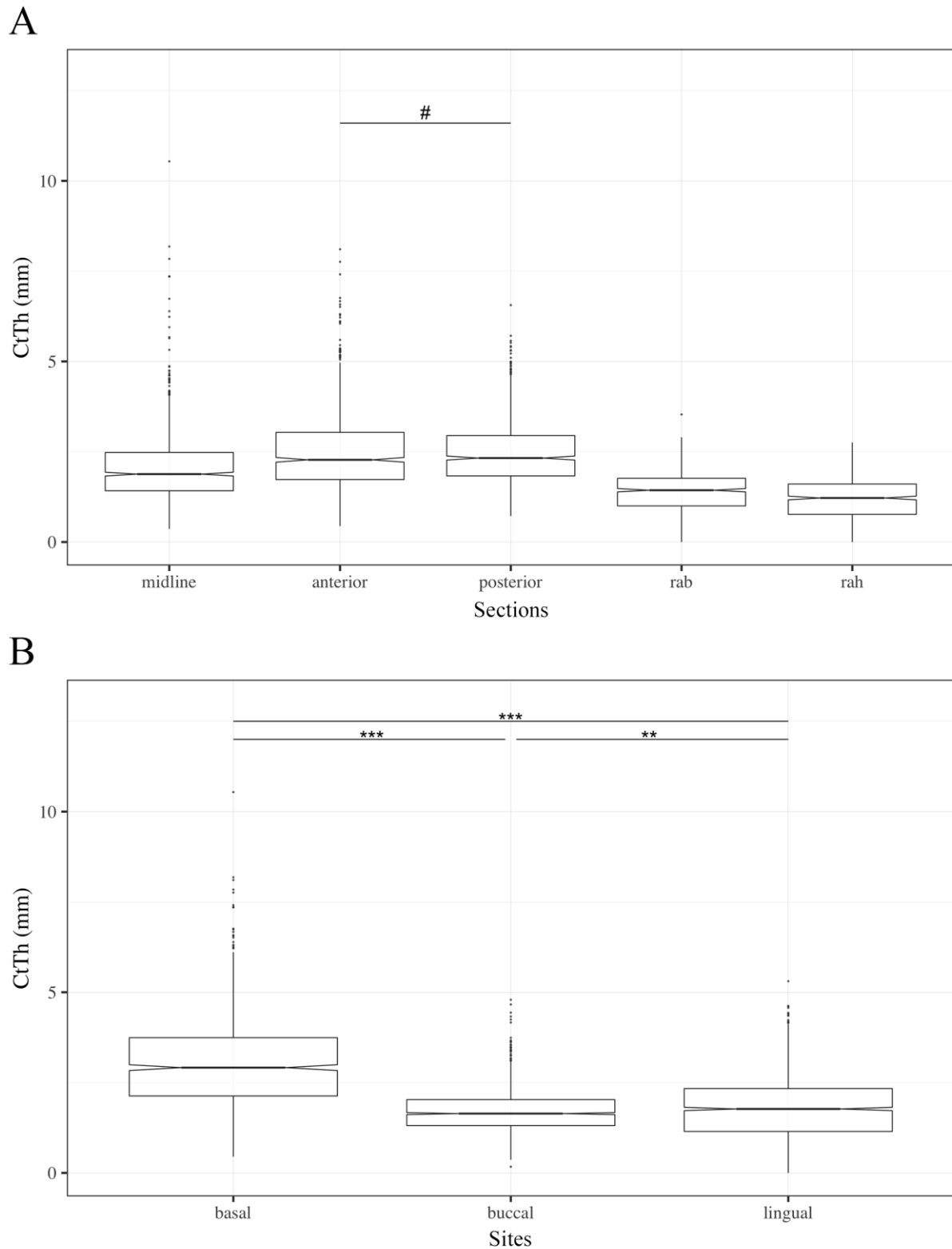
Figure 4.29. Boxplots of CtTh (mm) grouped per section [A] or per site [B].

In A, only the non-significant *p*-value is illustrated, all the other sections are significantly different from each other ($p < 0.001$). Significance: # $p > 0.05$, *** $p < 0.001$, ** $p < 0.01$. Dots depict outliers.
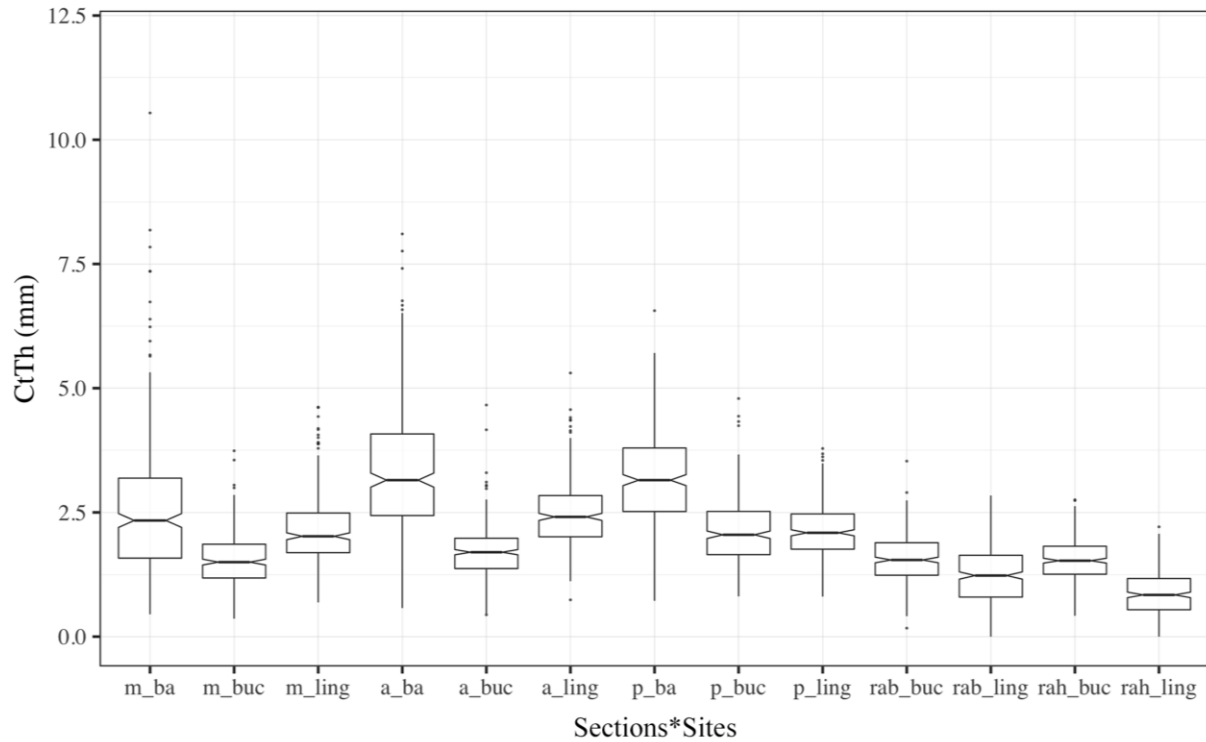
Figure 4.30. Boxplots of CtTh (mm) grouped per section*site interactions and on the next page, table detailing the pairwise Wilcoxon post-hoc test p-values. In the table, non-significant p-values are in bold: $p > 0.05$. (continued on the next page)

163

	m_ba	m_buc	m_ling	a_ba	a_buc	a_ling	p_ba	p_buc	p_ling	rab_buc	rab_ling	rah_buc
m_ba	-	-	-	-	-	-	-	-	-	-	-	-
m_buc	< 2.00E-16	-	-	-	-	-	-	-	-	-	-	-
m_ling	**0.1780**	< 2.00E-16	-	-	-	-	-	-	-	-	-	-
a_ba	1.00E-15	< 2.00E-16	< 2.00E-16	-	-	-	-	-	-	-	-	-
a_buc	< 2.00E-16	0.0051	< 2.00E-16	< 2.00E-16	-	-	-	-	-	-	-	-
a_ling	**1.00**	< 2.00E-16	< 2.00E-16	< 2.00E-16	< 2.00E-16	-	-	-	-	-	-	-
p_ba	2.80E-15	< 2.00E-16	< 2.00E-16	**1.00**	< 2.00E-16	< 2.00E-16	-	-	-	-	-	-
p_buc	0.0368	< 2.00E-16	**1.00**	< 2.00E-16	4.70E-16	2.60E-09	< 2.00E-16	-	-	-	-	-
p_ling	**0.0562**	< 2.00E-16	**1.00**	< 2.00E-16	< 2.00E-16	7.60E-10	< 2.00E-16	**1.00**	-	-	-	-
rab_buc	< 2.00E-16	**1.00**	< 2.00E-16	< 2.00E-16	**0.3970**	< 2.00E-16	< 2.00E-16	< 2.00E-16	< 2.00E-16	-	-	-
rab_ling	< 2.00E-16	1.10E-08	< 2.00E-16	< 2.00E-16	< 2.00E-16	< 2.00E-16	< 2.00E-16	< 2.00E-16	< 2.00E-16	1.30E-13	-	-
rah_buc	< 2.00E-16	**1.00**	< 2.00E-16	< 2.00E-16	0.0136	< 2.00E-16	< 2.00E-16	< 2.00E-16	< 2.00E-16	**1.00**	1.30E-11	-
rah_ling	< 2.00E-16	< 2.00E-16	< 2.00E-16	< 2.00E-16	< 2.00E-16	< 2.00E-16	< 2.00E-16	< 2.00E-16	< 2.00E-16	< 2.00E-16	4.60E-14	< 2.00E-16

Figure 4.30. (continued)

4.4.4.2. Inter-variable correlations

Inter-variable Spearman's correlations, associated with Holm's adjustments, were then performed between the 13 locations in which the cortical thicknesses were recorded. As before, these correlations were graphically represented as correlation matrices and were computed for the entire sample, per sex, per ancestry, per sex/ancestry, as well as within the dentition categories.

In the entire sample (Figure 4.31), the majority of the inter-variable correlations were significant and presented with weak to moderate positive correlations ($0.19 < \rho < 0.64$). Only a few (9%) were not significant and were mostly associated with the midline lingual site (e.g., m_ling_CtTh vs. a_buc_CtTh, m_ling_CtTh vs. rab_buc_CtTh...). The strongest correlations were found between similar sites and not similar sections, e.g., correlations observed between the basal sites were stronger (m_ba_CtTh vs. a_ba_CtTh: $\rho = 0.45$; m_ba_CtTh vs. p_ba_CtTh: $\rho = 0.48$; a_ba_CtTh vs. p_ba_CtTh: $\rho = 0.62$) than those between the CtTh recorded at the midline (m_ba_CtTh vs. m_buc_CtTh: $\rho = 0.47$; m_ba_CtTh vs. m_ling_CtTh: $\rho = 0.09$; m_buc_CtTh vs. m_ling_CtTh: $\rho = 0.19$). Once again, this pattern was not very consistent in the three lingual sites. Overall, the strongest correlation was observed between the buccal sites of the ramus breadth and height ($\rho = 0.64$), which was followed by the relationship between the basal sites of the anterior and posterior sections ($\rho = 0.62$).

Inter-variable correlations were then calculated within the female and male subsamples and can be visualised in Figure 4.32. In both sexes, approximately 60% (F: 61.5%; M: 60.3%) of the correlations were statistically and positively significant, with weak to moderate coefficients, although the strongest were found in females (F: $0.33 < \rho < 0.71$) compared to males (M: $0.23 < \rho < 0.62$). Very few (in males) or no statistically significant relationships at all (in females) between variables were observed in the lingual sites of the midline (m_ling_CtTh) and of the ramus height (rah_ling_CtTh). As in the entire sample, the strongest correlation coefficients observed in females and in males were between sites (F: a_ba_CtTh vs. p_ba_CtTh: $\rho = 0.71$, rab_buc_CtTh vs. rah_buc_CtTh: $\rho = 0.63$; M: a_ba_CtTh vs. p_ba_CtTh: $\rho = 0.57$, rab_buc_CtTh vs. rah_buc_CtTh: $\rho = 0.62$) and not between sections.
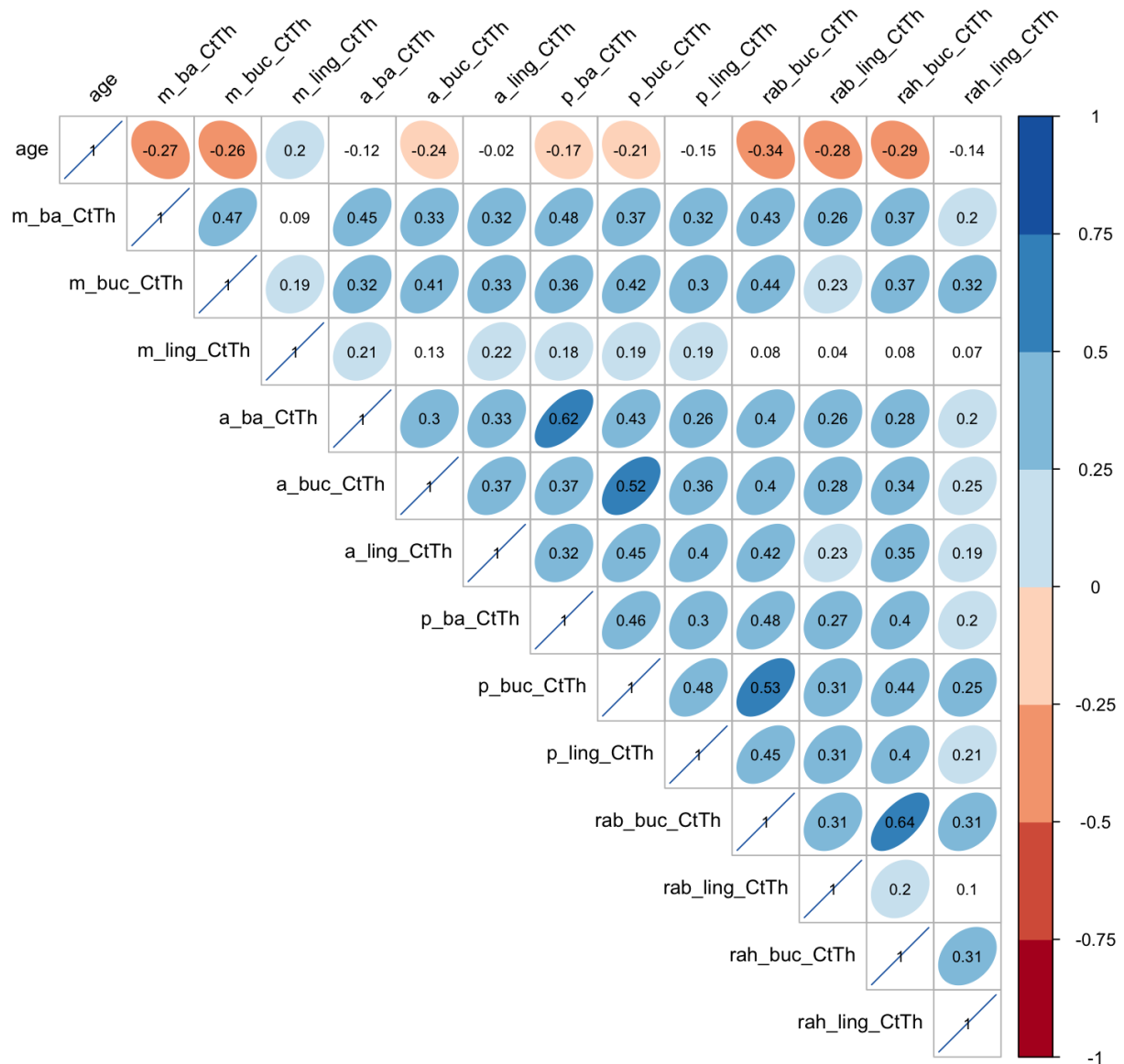
Figure 4.31. Corrplots illustrating inter-variable relationships between all the cortical thicknesses in the entire sample. Ellipses were removed if the correlation, adjusted with Holm's correction, was not significant ($p > 0.05$). Correlation coefficients ρ were noted within each ellipse (in blue: positive ρ, in red: negative ρ).
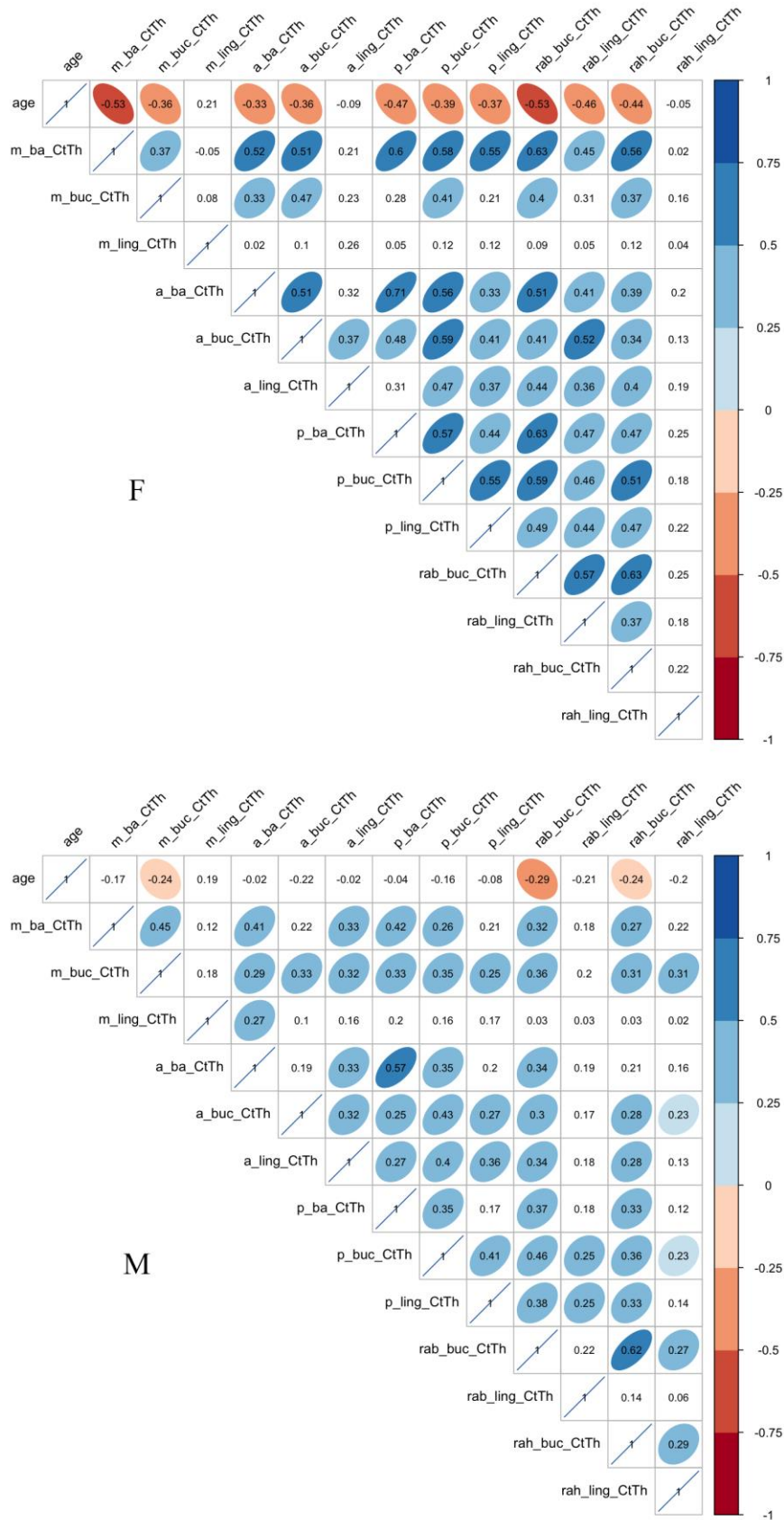
Figure 4.32. Corrplots illustrating inter-variable relationships between all the cortical thicknesses within females (top) and males (bottom). Ellipses were removed if the correlation, adjusted with Holm's correction, was not significant ($p > 0.05$). Correlation coefficients ρ were noted within each ellipse (in blue: positive ρ, in red: negative ρ).

167

The inter-variable correlations were also computed for the two ancestry-separated subsamples (AA, EA) and were all found to be positive (Figure 4.33). While most of the locations (71.8%) were observed to be significantly correlated to each other in AA individuals (except for rab_ling_CtTh), just a few (38.5%) were significant in the EA subsample. As in the entire sample and in the sex-separated subsamples, the strongest correlations were found between sites (AA: a_ba_CtTh vs. p_ba_CtTh: $\rho = 0.62$) and not between sections.

When using sex/ancestral subgroups (Figure 4.34), the number of significant inter-variable correlations decreased: 23.1% in FAA, 30.8% in FEA, 37.2% in MAA, 9% in MEA, probably due to the smaller sample sizes. It was still possible to notice that, as in the sex-separated samples, the coefficients calculated were stronger in females (both FAA and FEA) than in males. Similarly to the entire sample and to the other subsamples, the strongest correlation coefficients were also found between similar sites and not between similar sections – e.g., a_ba_CtTh vs. p_ba_CtTh: $\rho = 0.65$ in FAA, or $\rho = 0.76$ in FEA.

The influence of dentition on the relationships between the CtTh locations was also investigated, and all the inter-variable correlations were represented for each dentition category in Figure 4.35. Some significant correlations were observed in A and C categories (41.0% and 66.7%, respectively) while only 25.6% of them were found in B. The midline lingual site was, however, particularly not significantly correlated to any of the other variables in the C category.
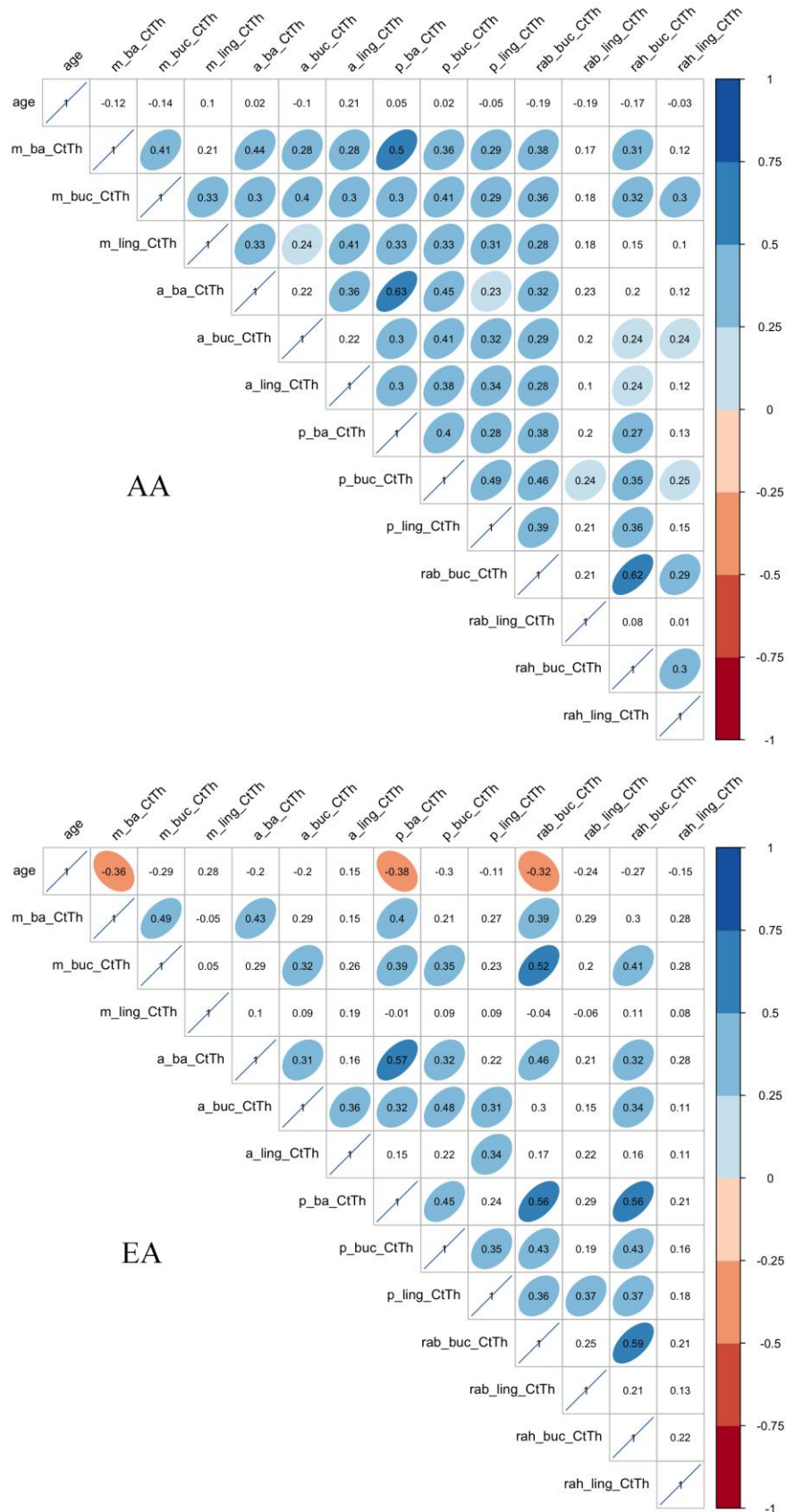
Figure 4.33. Corrplots illustrating inter-variable relationships between all the cortical thicknesses in the ancestry-separated subsamples (AA: upper, EA: lower). Ellipses were removed if the correlation, adjusted with Holm's correction, was not significant ($p > 0.05$). Correlation coefficients ρ were noted within each ellipse (in blue: positive ρ, in red: negative ρ).
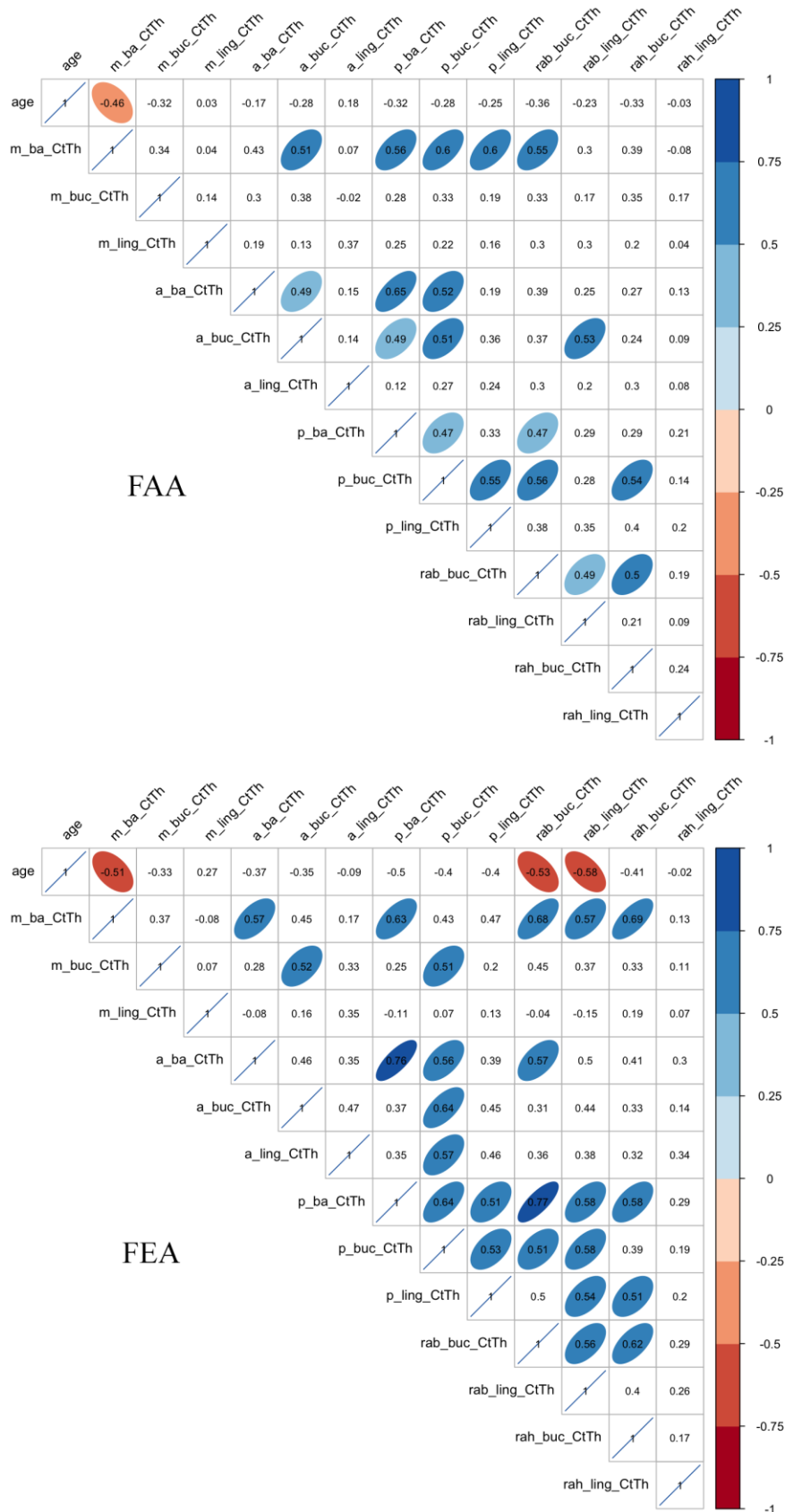
Figure 4.34. Corrplots illustrating inter-variable relationships between all the cortical thicknesses in each sex/ancestral subgroup (FAA, FEA, MAA, MEA). Ellipses were removed if the correlation, adjusted with Holm's correction, was not significant ($p > 0.05$). Correlation coefficients ρ were noted within each ellipse (in blue: positive ρ, in red: negative ρ). (continued on the next page)
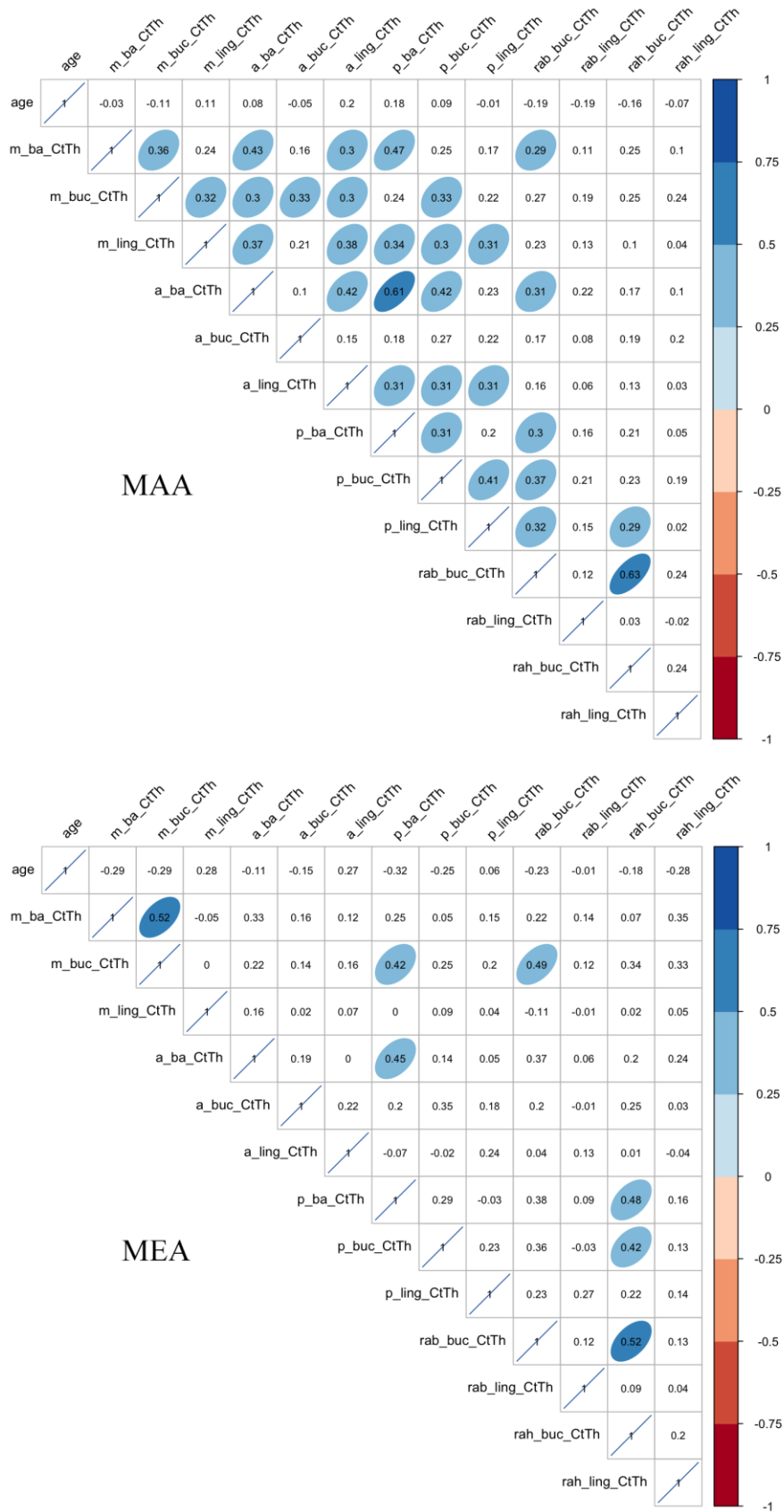
Figure 4.34. (continued)
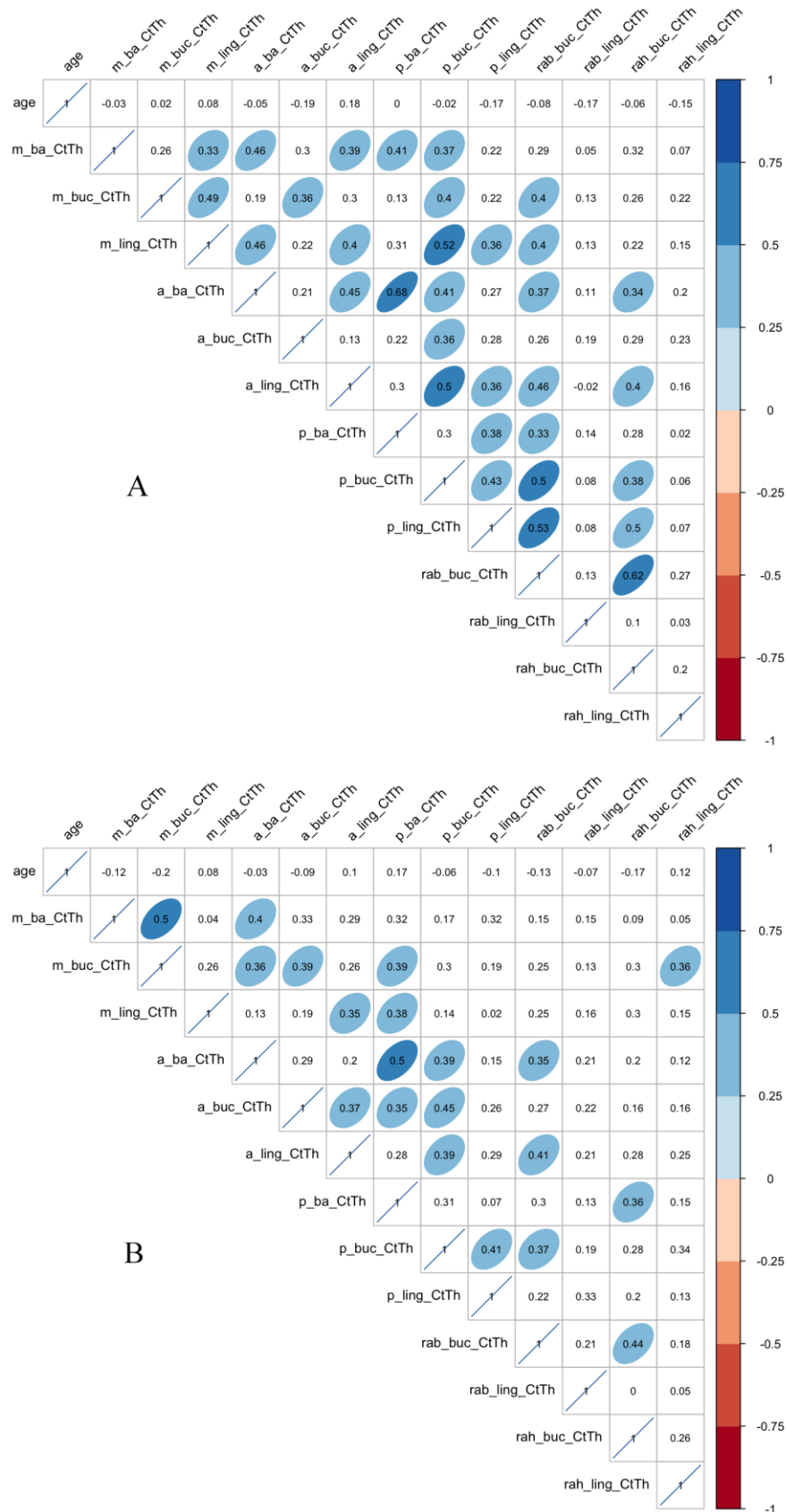
Figure 4.35. Corrplots illustrating inter-variable relationships between all the cortical thicknesses in each dentition category (A, B, C). Ellipses were removed if the correlation, adjusted with Holm's correction, was not significant ($p > 0.05$). Correlation coefficients ρ were noted within each ellipse (in blue: positive ρ, in red: negative ρ). (continued on the next page)

172
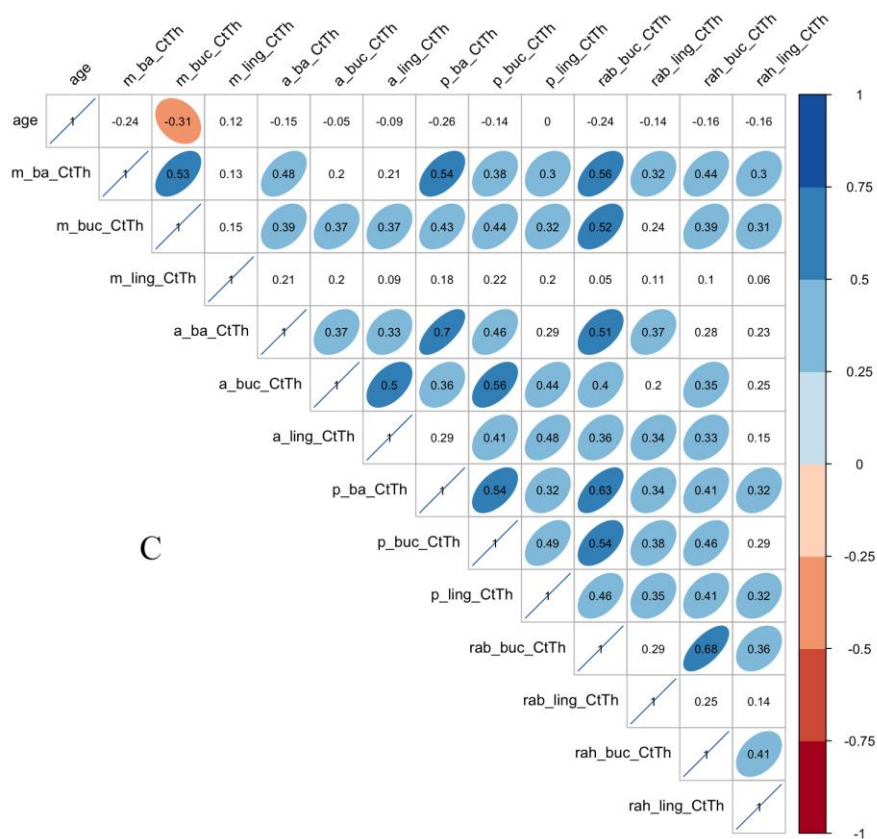
Figure 4.35. (continued)

4.4.5. Influence of aging

4.4.5.1. Correlations

Spearman's correlations, adjusted for multiple comparisons using Holm's correction, were calculated with age for all cortical thicknesses in the entire sample, in the sex and ancestral subsamples as well as in each sex/ancestral subgroup. The correlations obtained were then computed in the form of matrices (Figure 4.36). Subsequently, dentition categories were considered and tested for age correlation in each of these groups and are illustrated in (Figure 4.37).

Within the entire sample (Figure 4.36, first row), nine of the 13 cortical thicknesses recorded on the mandibular body and ramus were significantly correlated with aging: basal, buccal and lingual sites of the midline (m_ba_CtTh, m_buc_CtTh, m_ling_CtTh); buccal site only of the anterior section (a_buc_CtTh); basal and buccal sites of the posterior section (p_ba_CtTh, p_buc_CtTh); buccal and lingual sites of the ramus breadth (rab_buc_CtTh, rab_ling_CtTh); and buccal site of the ramus height (rah_buc_CtTh). Of these nine CtTh, only the lingual site of the midline (m_ling_CtTh) was positively correlated with aging (with a low correlation coefficient $\rho = 0.2$) while all the other significant correlations were negative. Overall, the correlations with aging were weak as the correlation coefficients ranged between $\rho = -0.17$ (p_ba_CtTh) and $\rho = -0.34$ (rab_buc_CtTh).

The correlations between CtTh and advancing age were then tested within each sex-separated sample (Figure 4.36 rows 2 and 3). In females, ten CtTh out of 13 (m_ba_CtTh, m_buc_CtTh, a_ba_CtTh, a_buc_CtTh, p_ba_CtTh, p_buc_CtTh, p_ling_CtTh, rab_buc_CtTh, rab_ling_CtTh, rah_buc_CtTh) were statistically significantly correlated with aging, with weak to moderate correlation coefficients ranging from $\rho = -0.33$ (a_ba_CtTh) to $\rho = -0.53$ (m_ba_CtTh and rab_buc_CtTh). In males, on the other hand, only three sites (m_buc_CtTh, rab_buc_CtTh, rah_buc_CtTh) were detected to have significant but weak correlations with aging ($\rho = -0.24$ for m_buc_CtTh and rah_buc_CtTh; $\rho = -0.29$ for rab_buc_CtTh).

Ancestry-separated subsamples (AA and EA) also displayed different correlation patterns between CtTh and aging (Figure 4.36 rows 4 and 5): no significant correlations were detected at any sites for AA individuals while three were detected within EA (m_ba_CtTh, p_ba_CtTh, rab_buc_CtTh).

174

The correlations between the cortical thicknesses and aging were then investigated within each sex/ancestral subgroup (Figure 4.36 last four rows). No statistically significant correlations were detected in MAA or MEA. In the FAA subsample, only one significant correlation was detected for the basal site of the midline (m_ba_CtTh), with a moderate correlation coefficient of ρ = -0.46. Within the FEA subsample, three correlation coefficients were significant (m_ba_CtTh, rab_buc_CtTh, rab_ling_CtTh), with moderate coefficients (ρ = -0.51, -0.53 and -0.58, respectively)

Spearman's correlations with age were then tested within each dentition category (Figure 4.37). In C, a single site (m_buc_CtTh – see Figure 4.37 third row) was significantly correlated with aging (weak ρ = -0.31), while no other statistically significant correlations between CtTh and aging were detected in categories A or B. Furthermore, none of the correlations calculated in the sex and ancestral subgroups separated per dentition categories (e.g., F-A, F-B, F-C, AA-A, AA-B…) were found significant.

Figure 4.36. Corrplots illustrating correlations between each cortical thickness and age in the entire sample (first row) and then in F, M, AA, EA, FAA, FEA, MAA and MEA subsamples. Ellipses were removed if the correlation, adjusted with Holm's correction, was not significant ($p > 0.05$). Correlation coefficients ρ are noted within each square (in blue: positive ρ, in red: negative ρ).

		m_ba_CtTh	m_buc_CtTh	m_ling_CtTh	a_ba_CtTh	a_buc_CtTh	a_ling_CtTh	p_ba_CtTh	p_buc_CtTh	p_ling_CtTh	rab_buc_CtTh	rab_ling_CtTh	rah_buc_CtTh	rah_ling_CtTh
A	age	-0.03	0.02	0.08	-0.05	-0.19	0.18	0	-0.02	-0.17	-0.08	-0.17	-0.06	-0.15
B	age	-0.12	-0.2	0.08	-0.03	-0.09	0.1	0.17	-0.06	-0.1	-0.13	-0.07	-0.17	0.12
C	age	-0.24	-0.31	0.12	-0.15	-0.05	-0.09	-0.26	-0.14	0	-0.24	-0.14	-0.16	-0.16
F-A	age	-0.25	-0.13	0.06	-0.07	-0.24	0.07	-0.3	-0.22	-0.54	-0.19	-0.18	-0.19	-0.02
F-B	age	-0.45	-0.47	0.24	-0.2	-0.25	0.19	0.05	-0.17	0.02	-0.22	-0.19	-0.26	0.05
F-C	age	-0.15	-0.26	0.16	-0.08	-0.04	-0.03	-0.26	-0.06	-0.1	-0.18	-0.36	-0.26	0.02
M-A	age	0.06	0.04	0.09	-0.01	-0.2	0.2	0.14	0.01	-0.03	-0.07	-0.18	-0.03	-0.21
M-B	age	-0.01	-0.2	-0.03	0.03	-0.11	-0.04	0.16	-0.07	-0.22	-0.15	0	-0.19	0.04
M-C	age	-0.27	-0.31	0.12	-0.15	-0.02	-0.1	-0.21	-0.15	0.08	-0.21	-0.01	-0.09	-0.23
AA-A	age	0	-0.03	0.08	-0.01	-0.17	0.2	0.02	0.02	-0.17	-0.12	-0.18	-0.06	-0.15
AA-B	age	-0.05	-0.13	0.02	0.13	0.01	0.31	0.3	0.13	0.07	-0.05	0	-0.08	0.29
AA-C	age	-0.19	-0.26	0.04	-0.07	0.17	-0.09	0.01	0.09	0.01	-0.05	0.03	-0.06	0.02
EA-A	age	-0.35	0.27	-0.06	-0.37	-0.56	-0.02	-0.07	-0.32	-0.23	0.06	-0.21	-0.16	-0.1
EA-B	age	-0.28	-0.31	0.24	-0.3	-0.11	0.15	-0.01	-0.16	-0.29	-0.21	-0.02	-0.21	-0.12
EA-C	age	-0.21	-0.25	0.06	-0.06	-0.04	0.22	-0.28	-0.13	0.13	-0.17	-0.12	-0.09	-0.19

Figure 4.37. Corrplots illustrating correlations between each cortical thickness and age in the entire sample separated per dentition category in the first three rows (A: first row, B: second, C: third), and then per dentition categories within females (F-A, F-B, F-C), males (M-A, M-B, M-C), individuals from African and European ancestries (AA-A, AA-B, AA-C, EA-A, EA-B, EA-C). Ellipses were removed if the correlation, adjusted with Holm's correction, was not significant ($p > 0.05$). Correlation coefficients ρ are noted within each square (in blue: positive ρ, in red: negative ρ).

4.4.5.2. Regressions

Generalised linear models (GLMs) were computed for each cortical thickness with advancing age. When analysing the entire sample (Figure 4.38), only three sites were found to have a non-significant regression with age (m_ba_CtTh, a_ba_CtTh, a_ling_CtTh) but even if the other cortical thickness regressions were significant, the coefficients of determination calculated were very low ($0.004 < R^2 < 0.096$). Interestingly, the lingual site of the midline (m_ling_CtTh) is the only site showing a significant increased cortical thickness with aging.

As with the Spearman's correlations performed in the sex-separated samples, more CtTh regressions with age were detected to be significant in females than in males (Figure 4.39). Indeed, only two regressions were not significant in females (a_ling_CtTh, rah_ling_CtTh) while five were not in males (m_ba_CtTh, a_ba_CtTh, a_ling_CtTh, p_ba_CtTh, p_ling_CtTh). Furthermore, higher coefficients of determination were found in females than in males or than in the entire sample (e.g., in females: p_ba_CtTh $R^2 = 0.239$, rab_buc_CtTh $R^2 = 0.253$). As in the regressions performed in the entire sample, the midline lingual cortical thickness displayed an increase with advancing age in both females and males.

When the regressions were plotted in each ancestral subsample (Figure 4.40), only a few regressions (decreasing with age) were detected as significant: six within AA and eight within EA individuals, all with very low coefficients of determination. The m_ling_CtTh regressions performed for AA and EA presented once more (i.e., as in the entire sample, in females and males) a significant increase with age. An increased CtTh was also noticed in the anterior lingual site of AA and EA individuals, but was not significant.

Finally, we performed the regressions of CtTh with aging in each dentition category (Figure 4.41). For individuals with complete or almost complete dentition (category A), only three CtTh (a_buc_CtTh, p_ling_CtTh, rab_ling_CtTh) showed significant regressions with age, again with very weak coefficients of determination ($0.030 < R^2 < 0.041$). In the B category, none of the 13 sites displayed any significant regression between CtTh and aging. However, in C, five regressions were detected to be significant: two body sites (m_buc_CtTh $R^2 = 0.026$ and p_ba_CtTh $R^2 = 0.035$) and three ramus sites (rab_buc_CtTh $R^2 = 0.030$, rah_buc_CtTh $R^2 = 0.025$, rah_ling_CtTh $R^2 = 0.026$). Even if some sites showed significant regressions, the coefficients of determination were particularly weak and the slopes almost horizontal. However, at the midline lingual site, only the edentulous category displayed the increased cortical thickness noticed in the entire sample, sex- and ancestry-separated subsamples.

177
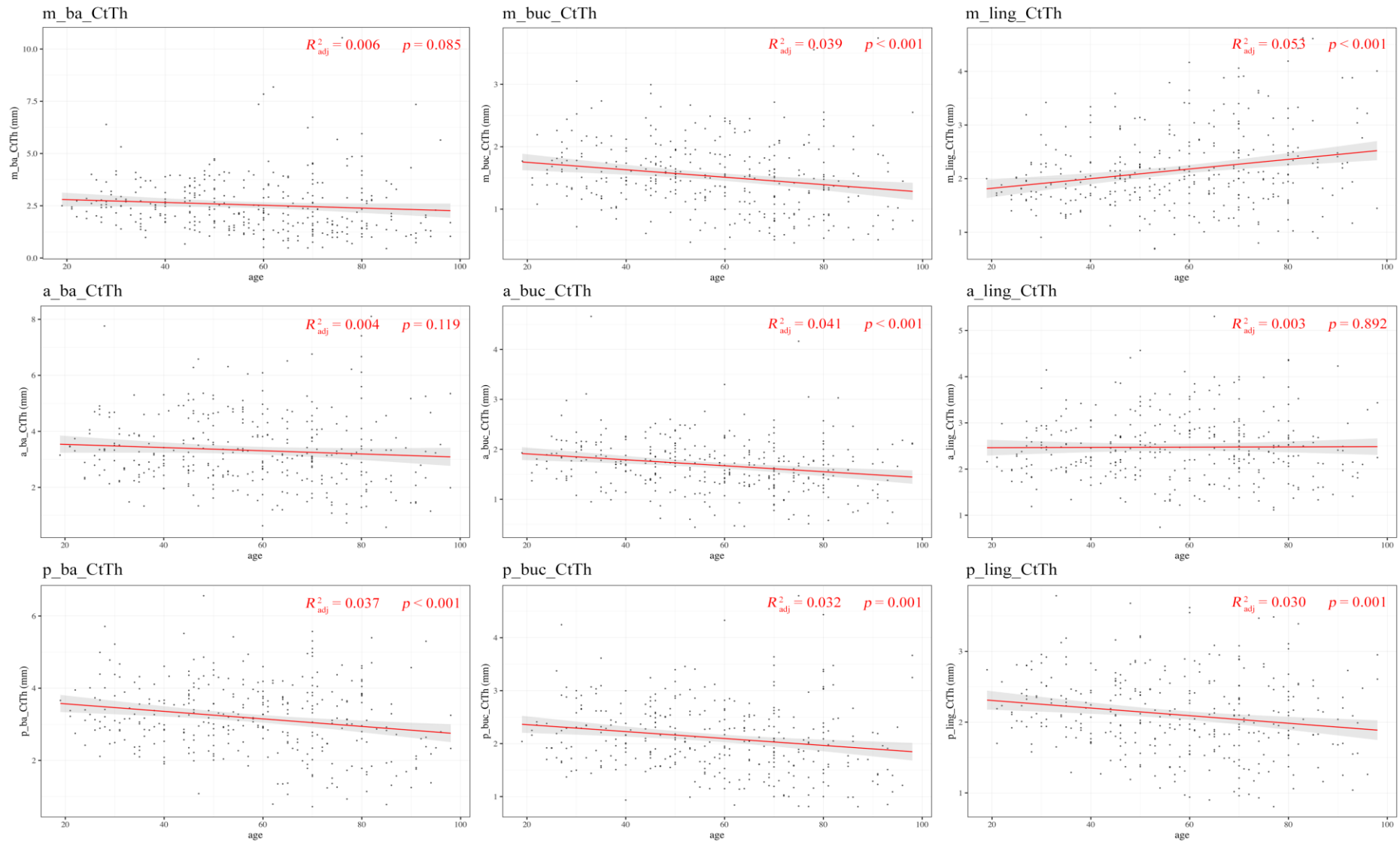
Figure 4.38. Generalised linear models (regressions) between cortical thickness (mm) and age (years) in the entire sample. Grey area represents the 95% confidence interval of each regression. (continued on the next page)
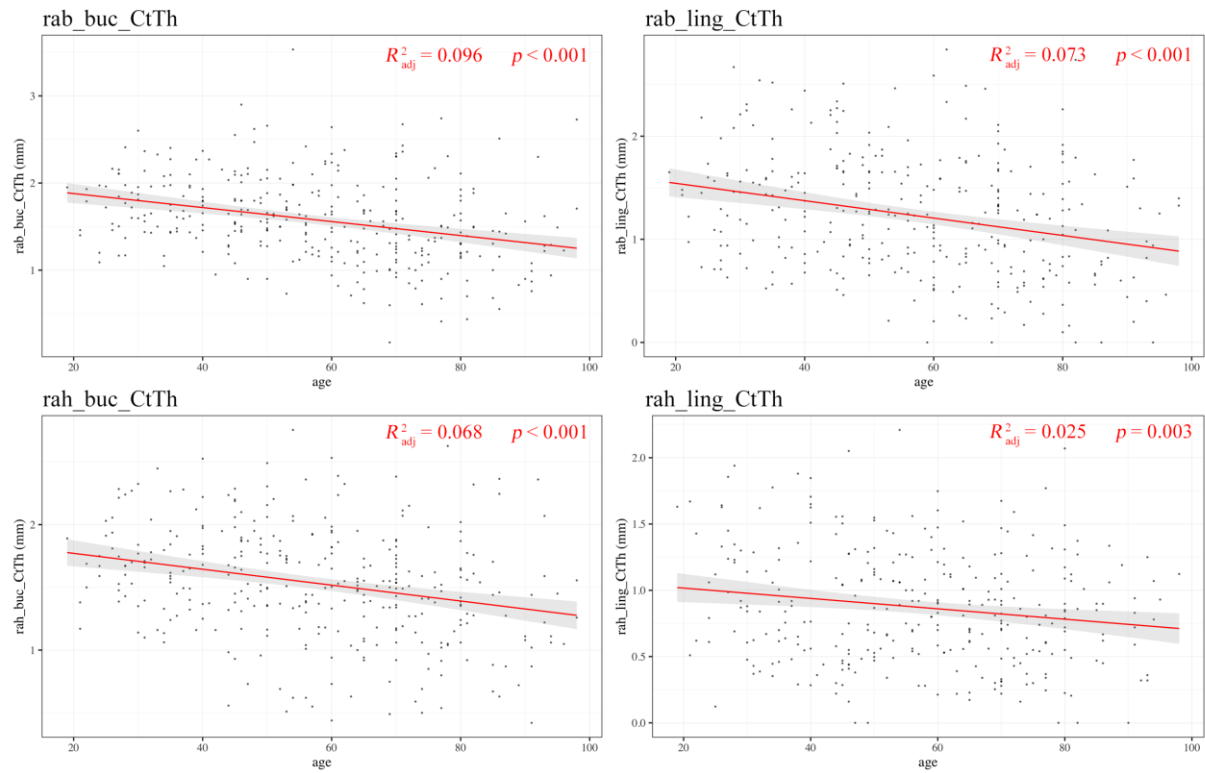
Figure 4.38. (continued)
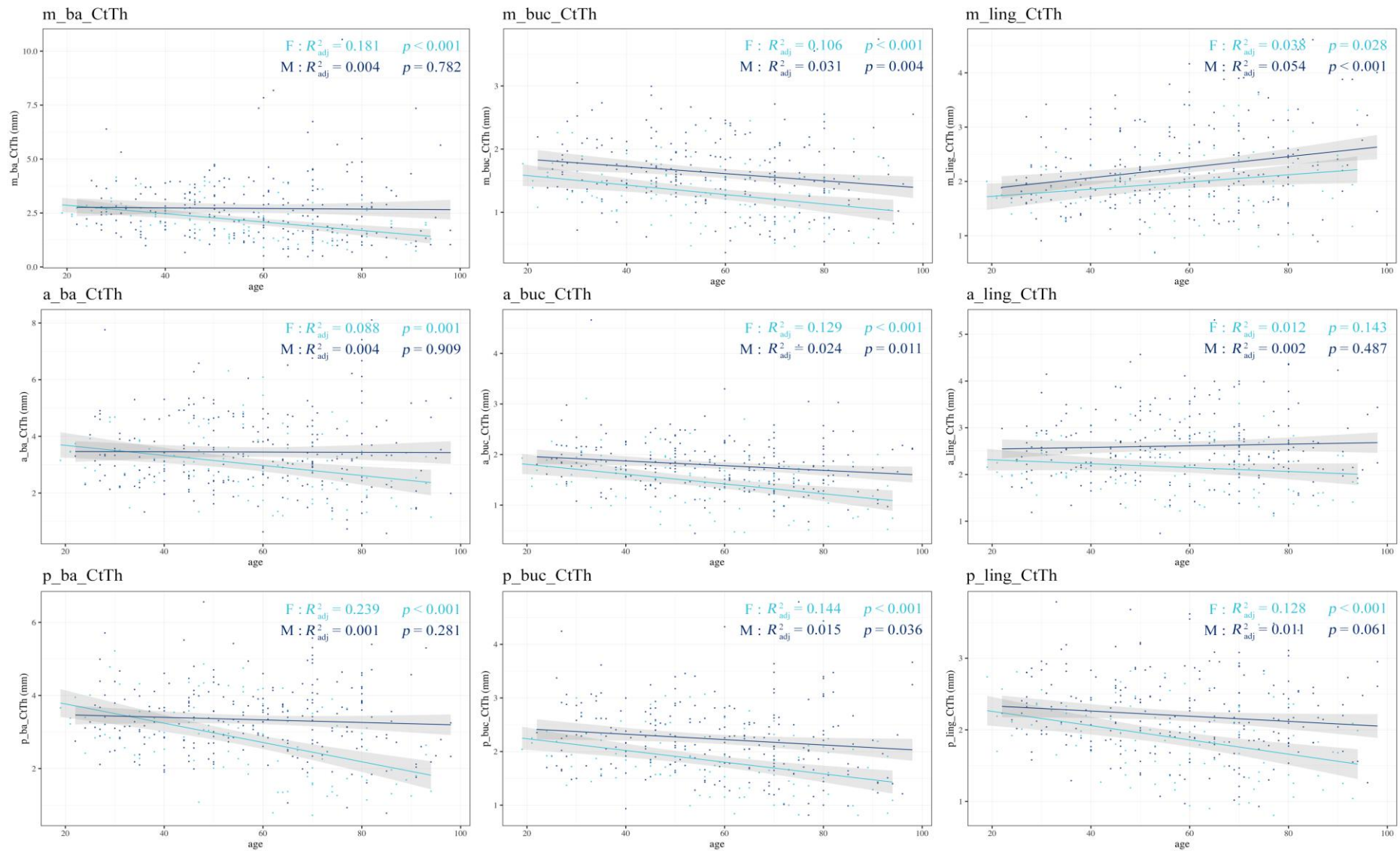
Figure 4.39. Generalised linear models (regressions) between cortical thickness (mm) and age (years) in sex-separated samples (F: light blue, M: dark blue). Grey area represents the 95% confidence interval of each regression. (continued on the next page)
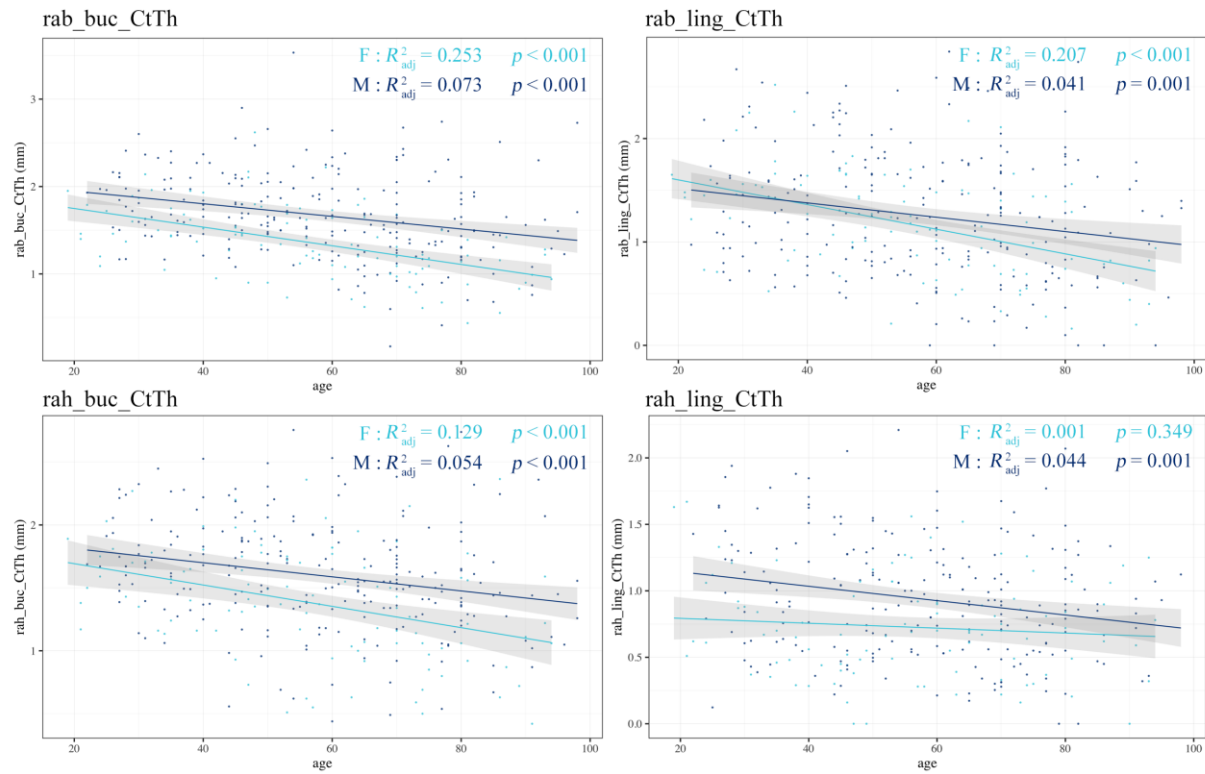
Figure 4.39. (continued)

181
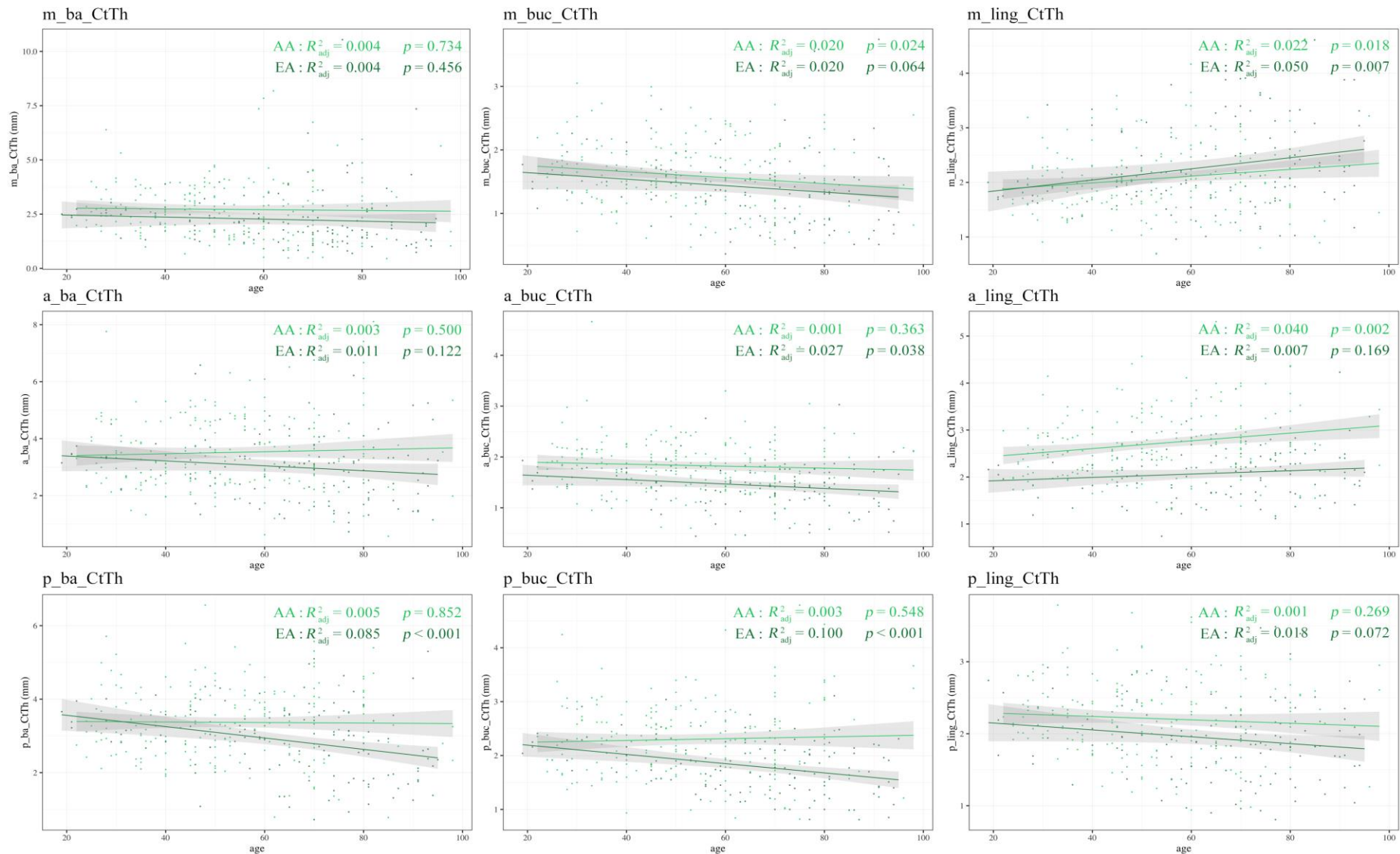
Figure 4.40. Generalised linear models (regressions) between cortical thickness (mm) and age (years) in ancestry-separated samples (AA, EA). Grey area represents the 95% confidence interval of each regression. (continued on the next page)
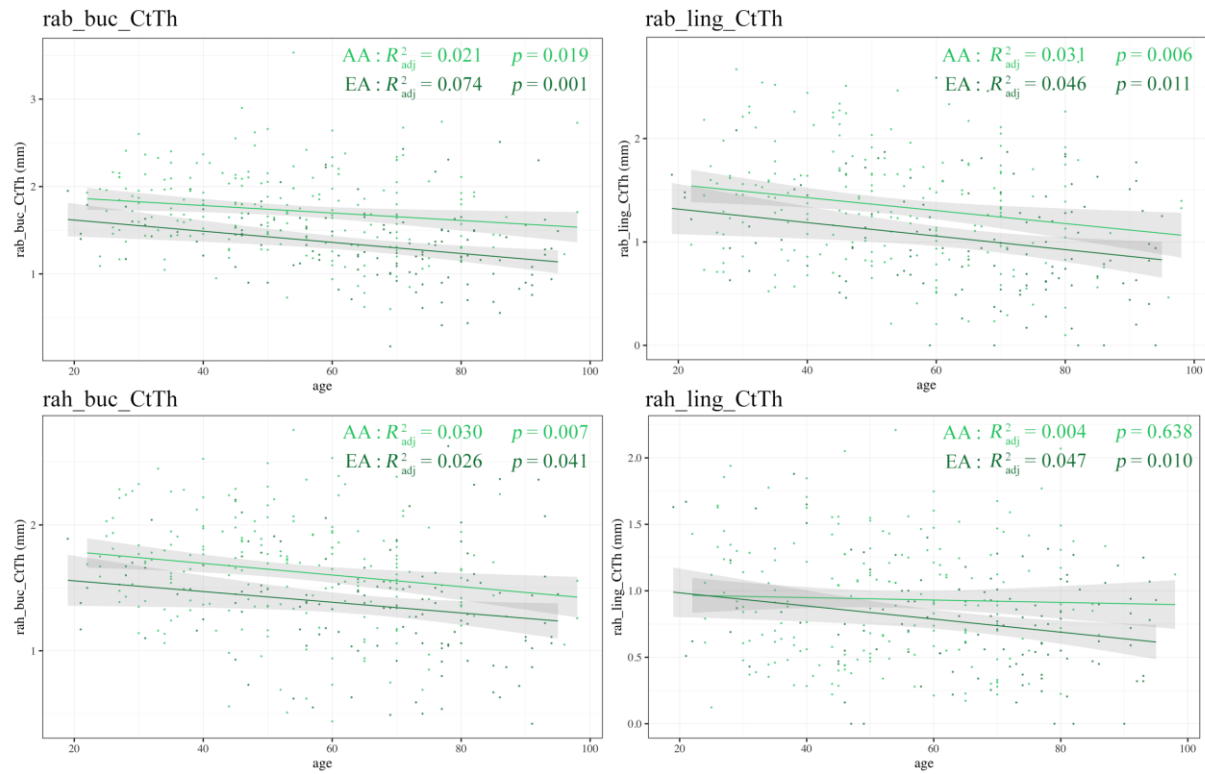
Figure 4.40. (continued)
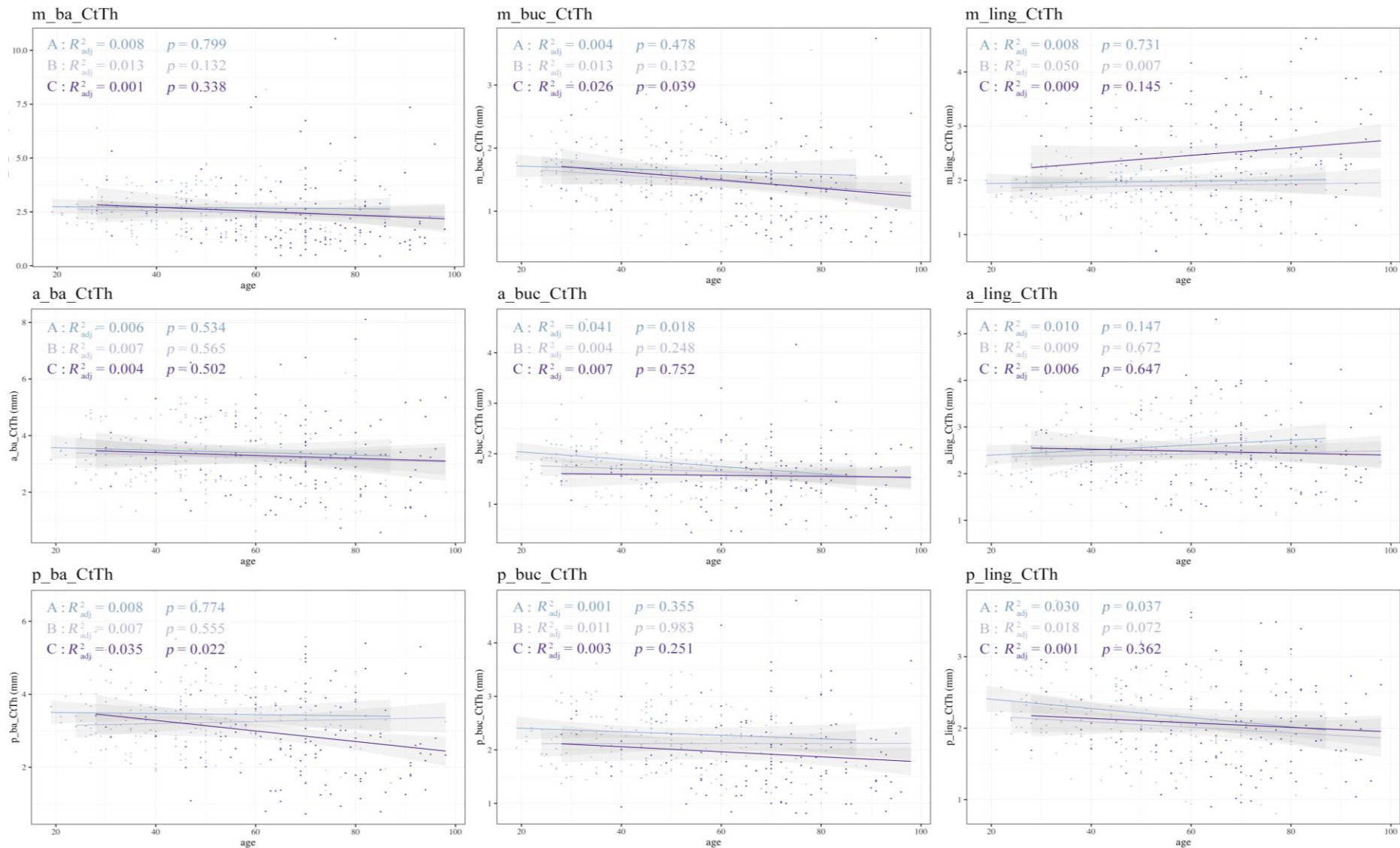
Figure 4.41. Generalised linear models between cortical thickness (mm) and age (years) in each dentition category (A, B, C: from light to dark purple). Grey area represents the 95% confidence interval of each regression. (continued on the next page)

184
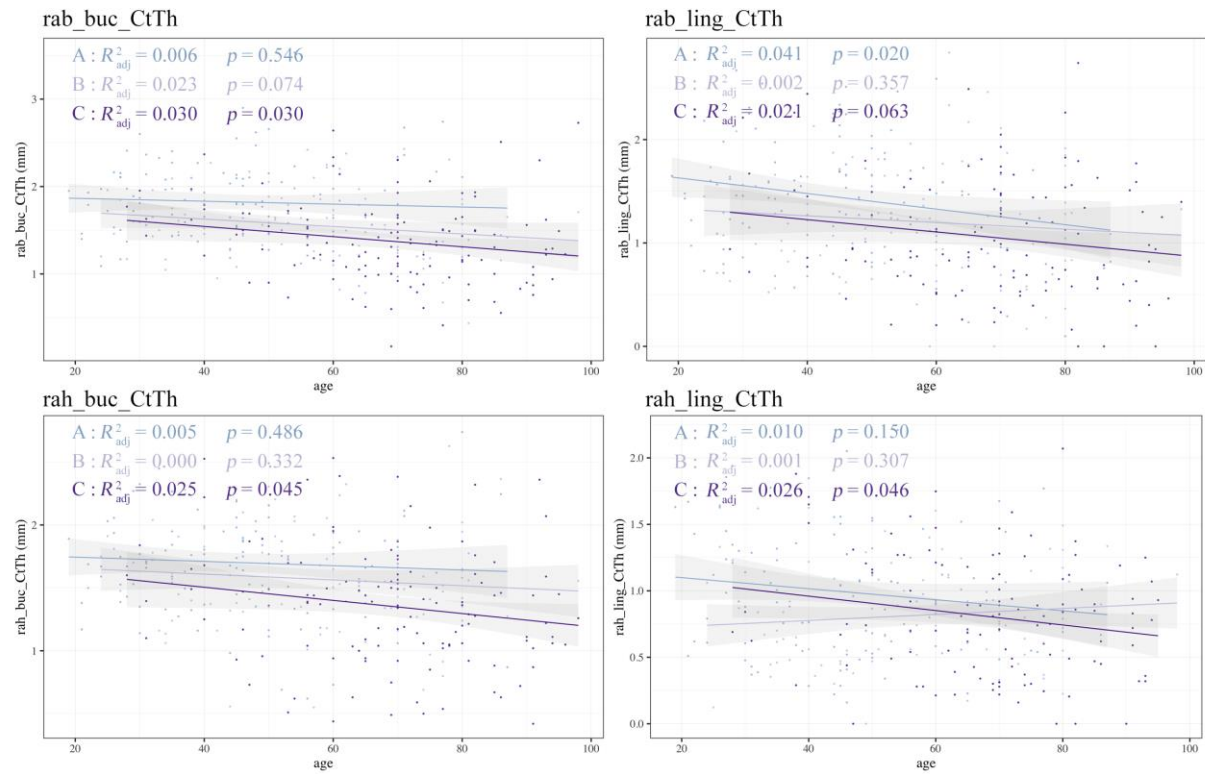
Figure 4.41. (continued)

4.4.6. Summary – Cortical thickness

Mandibular cortical thickness, in general, showed significant sexual dimorphism (with M > F) and significant differences between ancestries (with AA > EA). Sex/ancestral groups also showed differences in cortical thickness, particularly MAA and FEA, who always displayed, respectively, the thickest and thinnest, cortical thicknesses. The lingual site of the midline section, however, was different, with thicker cortical thickness in MEA than in MAA, FEA, or FAA.

Loss of teeth provoked a general decrease in cortical thickness over the whole mandible at both corpus and ramus sites. Most of the sites showed significant differences between fully dentate (category A) and edentulous (C) individuals, with always A > C. However, more sites displayed differences between A and B categories than between B and C, suggesting the fact that even restricted tooth loss and moderate loss of mastication capabilities, are enough to provoke an intense inner bone remodelling, and thus, a decrease in cortical thickness in all the sites of the mandible. Full edentulism, on the other hand, did not accentuate that decrease. However, differences between the posterior section and the other body sections were noticed: the posterior cortical thicknesses appeared to be more affected than the others. Nevertheless, one site, the midline lingual cortical thickness, did show a unique and very different behaviour compared to all the other sites. Indeed, this cortical thickness did not decrease with moderate tooth loss but increased significantly with edentulism (C > B, C > A, while A = B).

Besides tooth loss, sex was then also considered. Sexual dimorphism (M > F) of the cortical thicknesses was present in all three dentition categories, although the sex differences seemed stronger in edentulous (C) than in the other two groups (A and B). Moderate tooth loss (B) did not seem to be enough to accentuate the basal sexual dimorphic pattern observed in A. Furthermore, a decrease in cortical thickness with tooth loss (A > B > C) was noted in both males and females, but the diminution was more generalised in females (i.e., in most of the sites). In summary, females started with a thinner cortical thickness compared to males, which became more accentuated and generalised as teeth are lost. As seen before, the midline lingual cortical thickness increased with edentulism, yet more so in males than in females.

The effects of tooth loss were also analysed while taking ancestry into consideration. First, in all dentition categories, thicker cortical thicknesses were detected in AA compared to EA (AA > EA). A decrease in cortical thickness was observed with tooth loss (A > B > C) in both ancestral groups (AA and EA), although the decrease from A to C seemed more

accentuated in EA than AA (as in the external distances). Furthermore, the anterior and posterior sections showed more differences than the other sections when teeth are lost (in B and C categories), particularly in EA individuals. Again, the midline lingual site showed an increase in cortical thickness in both AA and EA (C > B > A). However, in contrast with earlier findings in males vs. females, the increase was similar in both ancestries, confirming that sex might have a stronger influence on cortical thickness variations due to tooth loss.

The analyses on the effects of tooth loss were then conducted in sex/ancestral groups. As before with sex and ancestry, the cortical thicknesses showed a decrease in all sex/ancestral groups, even if it was less marked in MAA. The loss of thickness was more generalised (more locations affected) in females (FAA and FEA). The greatest cortical thicknesses were always observed in MAA across all dentition groups, while the smallest were often in FAA or FEA. Tooth loss, and especially edentulism, seemed to accentuate the differences between the sex/ancestral groups, and more particularly between MAA and the others. The increase in the lingual midline site was observed again in all groups, and in line with previous observations, i.e., stronger in males than in females, with MEA > MAA > FEA > FAA.

Regarding the locations (i.e., section and site), the cortical thicknesses were distributed differently basally, buccally, and lingually, always displaying a thicker basal cortical bone, followed by lingual, and finally buccal (basal > lingual > buccal) at the midline and anterior sections. However, at the posterior section, while the basal site remained the thickest, buccal and lingual sites did not show differences (basal > buccal = lingual). Even if different, these sites displayed strong correlations between each other, i.e., all the basal sites together, the buccal sites, etc. Within an area, such as the buccal area, for example, cortical thicknesses will be homogeneous, and changes happening anteriorly in the body will reflect posteriorly, or in the midline, and vice versa. This general homogeneous inner morphology was practically not influenced by sex or ancestry, but by tooth loss. Random tooth loss, as represented by category B, showed the lowest number of correlations between the locations, which could be explained by the multiplicity of remodelling patterns (in each of the location affected by tooth loss), and thus, then be associated with the loss of homogeneousness. On the contrary, edentulism, i.e., the generalisation of tooth loss to the whole mandible, allowed to restore the "uniformity". On the other hand, the situation in the midline was particularly different, especially in the midline lingual site, with very few correlations to the rest of the body.

Finally, the influence of advancing age was evaluated alone, and then, in conjunction with sex, ancestry, and loss of teeth through correlations and regressions. All cortical

thicknesses, except the lingual midline, showed negative relationships with aging, indicating that generally, the cortical thicknesses in the mandible decrease while aging increases. The relationship between age and cortical thickness appeared to be mostly influenced by sex, and not ancestry or tooth loss. Indeed, when controlling for sex, i.e., checking the correlations and regressions in female-only or male-only samples, significance was found in most of the sites in females but were practically absent in males. When controlling for ancestry, a very small number of correlations were found in AA or EA individuals, while the decrease was slightly more pronounced in EA than in AA for certain sites. Finally, when dentition categories were considered, no relationships were observed in A and B categories: age alone did not seem to have an effect on individuals without tooth loss, or with moderate tooth loss. In category C, more sites looked affected by age, but caution must be exercised in interpreting these data, as most of the correlation and regression coefficients found were weak. Thus, age alone might not be enough to cause significant diminutions in the mandibular cortical thickness, except in females (of both ancestries), where greater decreases (steeper regression slopes, particularly from 40 years of age) were noticed earlier in comparison to males.

Lastly, as seen earlier, the lingual midline site increased in cortical thickness was found related to age in all groups (F, M, AA, EA, etc.). The increase was, however, not significant in dentition category A, or in B, but was in C, as if only tooth loss, and particularly edentulism, seems to trigger this increase.

4.5. Histomorphometric parameters (cortical BV/TV)

4.5.1. Basic descriptive statistics

The cortical densities were assessed through the recording of BV/TV parameters (bone volume/total volume percentages) within 13 spherical Volumes of Interests (VOIs), extracted from the same 13 locations used for the CtTh [see section 4.4]. Descriptive statistics (such as means, standard deviations, minimum, maximum) were calculated and are provided in Table 4.5 and Table 4.6.

In general, the BV/TV values were very similar in all groups (Table 4.5). In the entire sample, for example, they presented with percentages ranging between 70.81% and 98.74% for VOIs located in the mandibular body. The highest mean values were found in the anterior and posterior sections, while the midline, and more particularly the buccal VOI, had the lowest density. Furthermore, the lowest minimum values were consistently found in all the buccal VOIs (midline min: 70.81%, anterior min: 76.34%, posterior min: 74.29%), with higher standard deviations. On the ramus, BV/TV values were between 48.16% and 98.68%. However, this very low value (48.16%), recorded on the lingual VOI of the ramus breadth in one individual, could be considered as an outlier (mean ± SD = 97.22 ± 3.75% at this site). When separated per sex, no clear patterns were detected: six VOIs showed greater BV/TV values in females while three in males had higher values. Between the two subsamples separated per ancestry, the lowest cortical densities were consistently recorded within EA VOIs. For three of the four sex/ancestral groups (FAA, FEA, MEA), the lowest mean cortical densities (approximating 75%) were found at the buccal site of the midline. Minimum values were also very low at this location (e.g., 70.81% for MEA, 74.17% for FAA, 74.91% for FEA). Overall, in the VOIs recorded on the body, the lowest cortical mean density values were mostly detected in the MEA subsample (six VOIs out of nine) and the highest in FAA. For the ramus VOIs, however, the lowest BV/TV was found in FEA: FAA > MAA > MEA > FEA.

Descriptive statistics were also performed in the three dentition categories (Table 4.6). The highest mean BV/TV values were always measured in category A (individuals with complete dentition), while the lowest mean BV/TV, as well as the lowest minimum values, were found either in B (four VOIs) or C (nine VOIs). In the three dentition categories, the lingual or basal VOIs showed the highest mean BV/TV, while the lowest were consistently measured in the buccal VOIs. As in the other subgroups, larger standard deviations were calculated for these buccal VOIs, and it was particularly noticeable in category B.

189

Table 4.5. Descriptive statistics of the mandibular cortical bone densities (BV/TV, %) recorded on micro-CT scans in the entire sample, in both sexes (F, M), ancestries (AA, EA) and in each sex/ancestral group (FAA, FEA, MAA, MEA). (continued on the next page)

	Total	Sex		Ancestry		Sex/ancestry			
		F	**M**	**AA**	**EA**	**FAA**	**FEA**	**MAA**	**MEA**
	n = 333	n = 102	n = 231	n = 208	n = 125	n = 56	n = 46	n = 152	n = 79
m_ba_BV/TV									
min − max	77.83 − 98.65	85.57 − 98.62	77.83 − 98.65	82.67 − 98.65	77.83 − 98.55	88.72 − 98.62	85.57 − 98.55	82.67 − 98.65	77.83 − 98.49
mean ± SD	97.52 ± 2.21	97.52 ± 2.15	97.53 ± 2.24	97.75 ± 1.80	97.15 ± 2.73	97.70 ± 1.84	97.30 ± 2.48	97.77 ± 1.80	97.07 ± 2.87
m_buc_BV/TV									
min − max	70.81 − 98.64	74.17 − 98.54	70.81 − 98.64	74.17 − 98.64	70.81 − 98.54	74.17 − 98.54	74.91 − 98.54	93.54 − 98.64	70.81 − 98.49
mean ± SD	96.89 ± 4.03	96.07 ± 5.22	97.26 ± 3.31	97.50 ± 2.77	95.88 ± 5.38	96.28 ± 5.01	95.81 ± 5.52	97.95 ± 0.79	95.93 ± 5.33
m_ling_BV/TV									
min − max	88.98 − 98.74	95.68 − 98.74	88.98 − 98.66	91.80 − 98.74	88.98 − 98.54	95.93 − 98.74	95.68 − 98.54	91.80 − 98.66	88.98 − 98.54
mean ± SD	98.05 ± 0.78	98.19 ± 0.50	97.99 ± 0.87	98.10 ± 0.62	97.96 ± 0.98	98.26 ± 0.38	98.10 ± 0.61	98.05 ± 0.68	97.88 ± 1.13
a_ba_BV/TV									
min − max	80.75 − 98.68	92.03 − 98.57	80.75 − 98.68	80.75 − 98.68	96.51 − 98.57	92.03 − 98.51	96.77 − 98.57	80.75 − 98.68	96.51 − 98.50
mean ± SD	98.03 ± 1.17	98.19 ± 0.70	97.96 ± 1.33	97.99 ± 1.45	98.11 ± 0.42	98.20 ± 0.86	98.19 ± 0.44	97.92 ± 1.61	98.06 ± 0.40
a_buc_BV/TV									
min − max	76.34 − 98.63	84.16 − 98.61	76.34 − 98.63	84.16 − 98.63	76.34 − 98.61	84.16 − 98.54	91.69 − 98.61	87.83 − 98.63	76.34 − 98.50
mean ± SD	97.69 ± 2.00	97.63 ± 2.16	97.72 ± 1.94	97.91 ± 1.57	97.33 ± 2.55	97.64 ± 2.57	97.61 ± 1.53	98.01 ± 0.96	97.17 ± 2.99
a_ling_BV/TV									
min − max	94.22 − 98.66	94.22 − 98.58	94.73 − 98.66	96.53 − 98.66	94.22 − 98.58	97.45 − 98.58	94.22 − 98.58	96.53 − 98.66	94.73 − 98.54
mean ± SD	98.10 ± 0.51	98.22 ± 0.53	98.05 ± 0.50	98.13 ± 0.43	98.05 ± 0.62	98.30 ± 0.22	98.11 ± 0.75	98.07 ± 0.47	98.01 ± 0.54

Table 4.5. (continued)

	Total	Sex		Ancestry		Sex/ancestry			
		F	M	AA	EA	FAA	FEA	MAA	MEA
	n = 333	n = 102	n = 231	n = 208	n = 125	n = 56	n = 46	n = 152	n = 79
p_ba_BV/TV									
min − max	94.76 − 98.66	94.76 − 98.61	96.65 − 98.66	95.65 − 98.66	94.76 − 98.61	95.65 − 98.54	94.76 − 98.61	96.84 − 98.66	96.65 − 98.59
mean ± SD	98.10 ± 0.50	98.15 ± 0.63	98.08 ± 0.44	98.14 ± 0.45	98.04 ± 0.58	98.27 ± 0.41	98.00 ± 0.80	98.09 ± 0.45	98.06 ± 0.42
p_buc_BV/TV									
min − max	74.29 − 98.68	94.99 − 98.57	74.29 − 98.68	90.21 − 98.68	74.29 − 98.57	96.81 − 98.57	94.99 − 98.57	90.21 − 98.68	74.29 − 98.56
mean ± SD	97.95 ± 1.61	98.17 ± 0.58	97.86 ± 1.89	98.10 ± 0.69	97.71 ± 2.46	98.29 ± 0.27	98.02 ± 0.80	98.03 ± 0.78	97.53 ± 3.03
p_ling_BV/TV									
min − max	91.32 − 98.68	91.32 − 98.59	94.69 − 98.68	91.32 − 98.68	92.40 − 98.59	91.32 − 98.53	92.40 − 98.59	96.75 − 98.68	94.69 − 98.52
mean ± SD	98.08 ± 0.67	98.10 ± 0.97	98.07 ± 0.48	98.13 ± 0.61	97.99 ± 0.75	98.19 ± 0.96	98.00 ± 1.00	98.10 ± 0.43	97.99 ± 0.56
rab_buc_BV/TV									
min − max	89.03 − 98.68	89.03 − 98.57	96.36 − 98.68	96.36 − 98.68	89.03 − 98.57	97.47 − 98.57	89.03 − 98.57	96.36 − 98.68	96.39 − 98.51
mean ± SD	98.06 ± 0.79	98.06 ± 1.25	98.06 ± 0.47	98.14 ± 0.44	97.93 ± 1.15	98.32 ± 0.20	97.75 ± 1.81	98.07 ± 0.49	98.04 ± 0.44
rab_ling_BV/TV									
min − max	48.16 − 98.64	79.13 − 98.64	48.16 − 98.64	48.16 − 98.64	79.13 − 98.59	91.64 − 98.64	79.13 − 98.54	48.16 − 98.64	84.06 − 98.59
mean ± SD	97.22 ± 3.75	97.15 ± 3.25	97.25 ± 3.95	97.53 ± 3.85	96.67 ± 3.50	97.96 ± 1.32	96.06 ± 4.54	97.36 ± 4.43	97.02 ± 2.71
rah_buc_BV/TV									
min − max	89.02 − 98.66	89.02 − 98.63	94.88 − 98.66	96.06 − 98.66	89.02 − 98.62	97.30 − 98.63	89.02 − 98.62	96.06 − 98.66	94.87 − 98.51
mean ± SD	98.06 ± 0.72	98.10 ± 1.03	98.05 ± 0.53	98.14 ± 0.44	97.93 ± 1.03	98.30 ± 0.25	97.84 ± 1.51	98.08 ± 0.48	97.98 ± 0.62
rah_ling_BV/TV									
min − max	70.07 − 98.62	87.32 − 98.57	70.07 − 98.62	70.07 − 98.62	87.32 − 98.57	90.64 − 98.53	87.32 − 98.57	70.07 − 98.62	90.45 − 98.40
mean ± SD	97.30 ± 2.76	97.22 ± 2.60	97.34 ± 2.84	97.62 ± 2.79	96.74 ± 2.63	97.87 ± 1.46	96.39 ± 3.41	97.53 ± 3.16	96.96 ± 2.01

Table 4.6. Descriptive statistics of the mandibular cortical bone densities (BV/TV, %) recorded on micro-CT scans per dentition category, according to the Eichner Index (EI A, B, C: from full dentition to edentulous).

	EI A n = 112	EI B n = 97	EI C n = 124
m_ba_BV/TV			
min – max	82.67 – 98.65	88.72 – 98.62	77.83 – 98.52
mean ± SD	97.87 ± 1.87	97.59 ± 1.61	97.15 ± 2.79
m_buc_BV/TV			
min – max	79.58 – 98.64	70.81 – 98.54	74.91 – 98.53
mean ± SD	97.70 ± 2.26	96.05 ± 5.42	96.83 ± 3.88
m_ling_BV/TV			
min – max	96.52 – 98.66	88.98 – 98.74	95.93 – 98.55
mean ± SD	98.17 ± 0.42	97.89 ± 1.24	98.08 ± 0.48
a_ba_BV/TV			
min – max	95.39 – 98.68	96.77 – 98.56	97.75 – 98.57
mean ± SD	98.17 ± 0.47	98.10 ± 0.39	97.85 ± 1.83
a_buc_BV/TV			
min – max	90.75 – 98.63	76.34 – 98.61	87.83 – 98.54
mean ± SD	98.03 ± 1.00	97.40 ± 3.08	97.62 ± 1.53
a_ling_BV/TV			
min – max	96.53 – 98.66	96.55 – 98.58	94.22 – 98.54
mean ± SD	98.18 ± 0.42	98.08 ± 0.46	98.05 ± 0.62
p_ba_BV/TV			
min – max	96.84 – 98.66	95.65 – 98.61	94.76 – 98.59
mean ± SD	98.19 ± 0.39	98.07 ± 0.51	98.04 ± 0.58
p_buc_BV/TV			
min – max	95.16 – 98.68	74.29 – 98.57	85.97 – 98.56
mean ± SD	98.16 ± 0.49	97.79 ± 2.49	97.90 ± 1.39
p_ling_BV/TV			
min – max	92.40 – 98.68	96.59 – 98.55	91.32 – 98.59
mean ± SD	98.12 ± 0.68	98.11 ± 0.43	98.01 ± 0.80
rab_buc_BV/TV			
min – max	96.47 – 98.68	94.35 – 98.57	89.03 – 98.50
mean ± SD	98.18 ± 0.43	98.06 ± 0.57	97.96 ± 1.12
rab_ling_BV/TV			
min – max	88.17 – 98.64	84.06 – 98.64	48.16 – 98.54
mean ± SD	97.68 ± 1.79	97.40 ± 2.26	96.59 ± 5.68
rah_buc_BV/TV			
min – max	96.34 – 98.66	96.44 – 98.63	89.02 – 98.58
mean ± SD	98.16 ± 0.45	98.07 ± 0.46	97.97 ± 1.02
rah_ling_BV/TV			
min – max	87.32 – 98.62	88.60 – 98.54	70.07 – 98.57
mean ± SD	97.83 ± 1.59	97.44 ± 1.84	96.63 ± 4.01

4.5.2. Influence of sex or/and ancestry

4.5.2.1. Sex

As in 4.4.2, the influence of sex on the cortical bone density values was assessed using Mann-Whitney Wilcoxon tests (Figure 4.42). Except for the buccal site of the midline (m_buc_BV/TV p-value = 0.22), all other VOIs were statistically significantly different between females and males, with BV/TV values particularly similar. A few outliers (outside the boxplots) can also be noticed, with smaller values in both groups, but more particularly in males.

4.5.2.2. Ancestry

The entire sample was then divided into ancestral subgroups in order to evaluate the influence of ancestry alone on the cortical bone densities. Significant differences were detected between AA and EA in ten VOIs (Figure 4.43), confirming greater BV/TV values in AA than in EA. Furthermore, wider boxplots, and a larger number of outliers, were noticed in EA individuals compared to AA. Three locations – basal and lingual sites of the anterior section (a_ba_BV/TV, a_ling_BV/TV) and basal site of the posterior section (p_ba_BV/TV) – were not found to be significantly different (p = 0.19, 0.08 and 0.06 respectively).

4.5.2.3. Interaction between sex and ancestry

Kruskal-Wallis tests, investigating the differences in cortical bone densities between the four sex/ancestral subsamples, were significant at all 13 locations (p < 0.001). Thus, pairwise Wilcoxon post-hoc tests were performed to observe which subgroup(s) was/were different from the others (Figure 4.44). Almost no differences were detected between females, with no significant differences between FAA and FEA in 12 locations out of 13. Only the lingual site of the ramus breadth (rab_ling_BV/TV – Figure 4.44 D) was found to be significantly different (p-value = 0.03), most probably because of the wide spread of the values in FEA individuals. Males, both MAA and MEA, however, were somewhat more variable: only five locations did not show any statistical differences between their cortical densities (m_ling_BV/TV, a_ba_BV/TV, a_ling_BV/TV, p_ba_BV/TV, rab_buc_BV/TV). In the other

eight locations, BV/TV mean values were consistently and significantly greater in MAA than in MEA, with MEA individuals showing a wide range and very low outlier values.
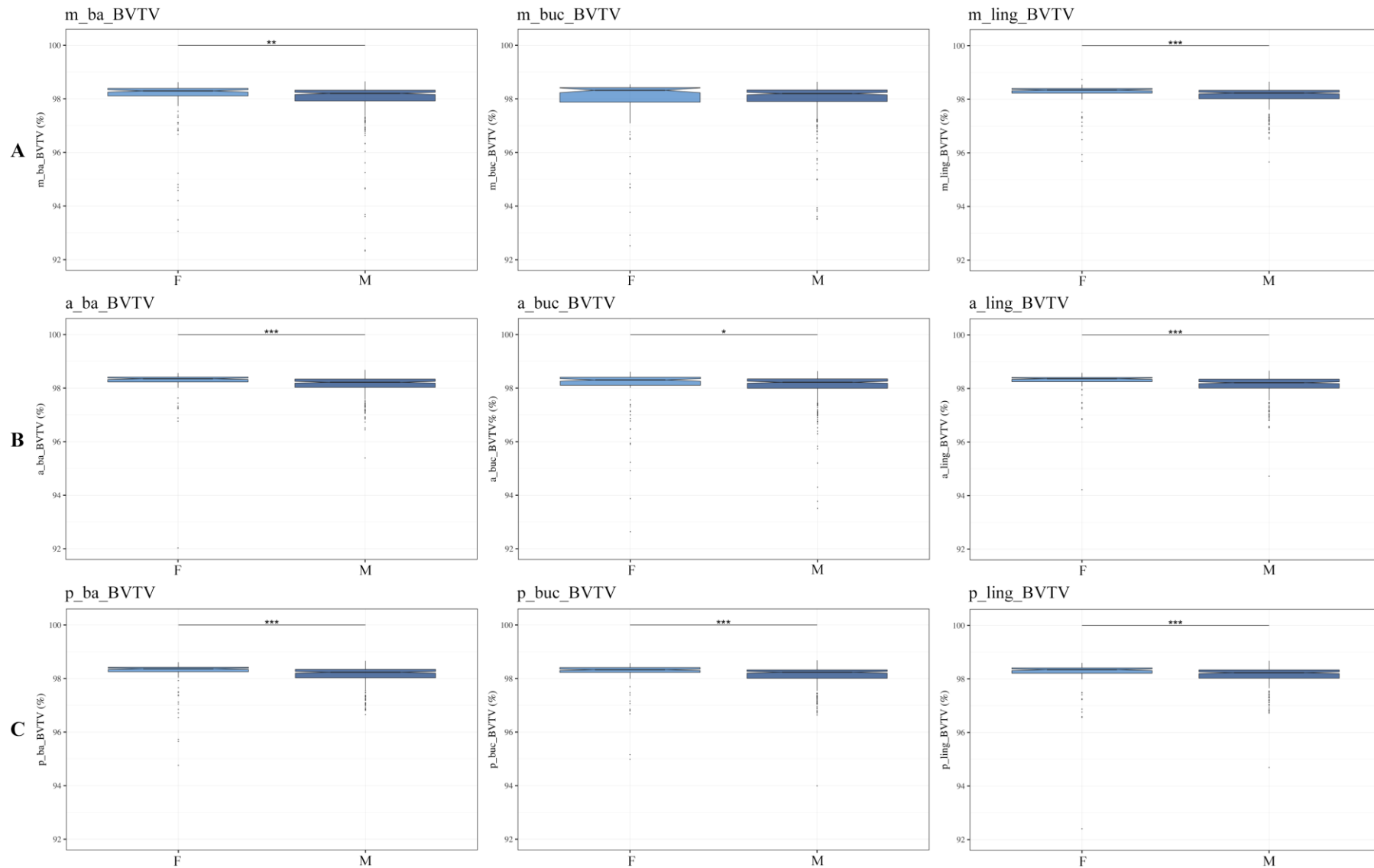
Figure 4.42. Boxplots of cortical BV/TV (%) per sex (F: light blue; M: dark blue), recorded on the midline [A], anterior [B], posterior [C], ramus breadth [D] and height [E] sections. Dots depict outliers. Significance: *** $p < 0.001$, ** $p < 0.01$, * $p < 0.05$. (continued on the next page)
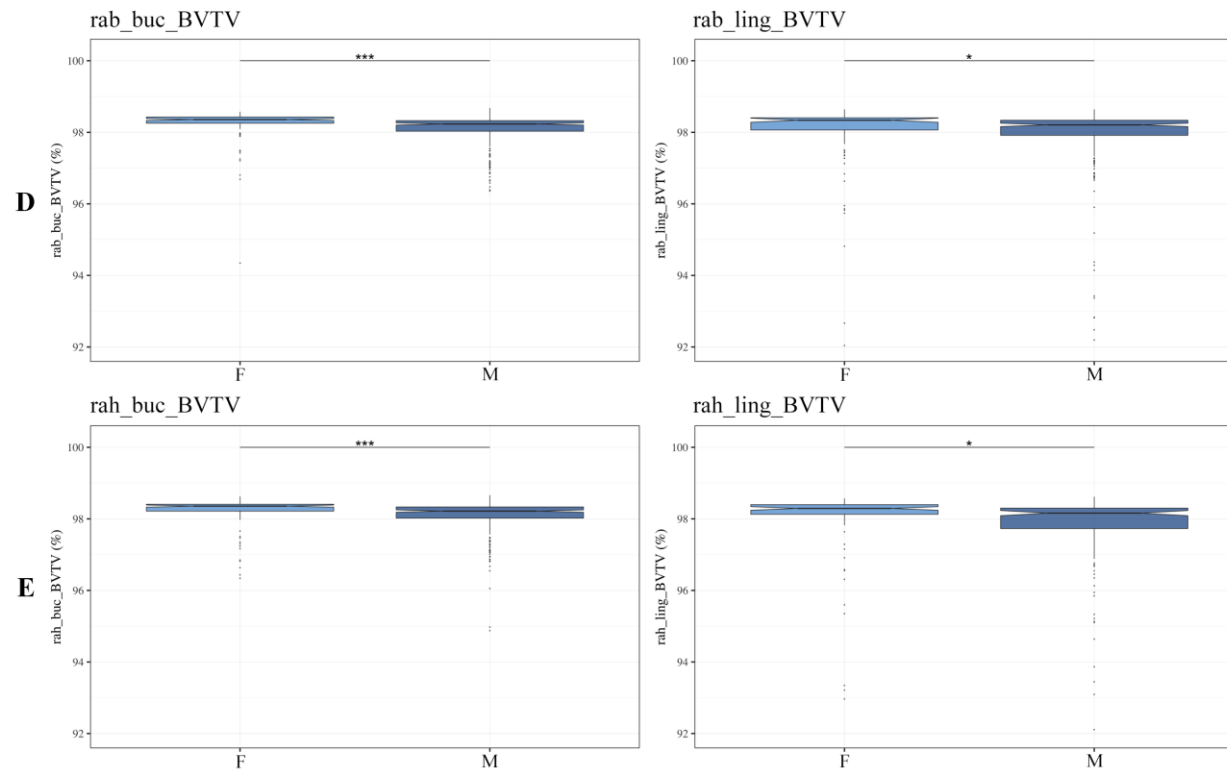
Figure 4.42. (continued)
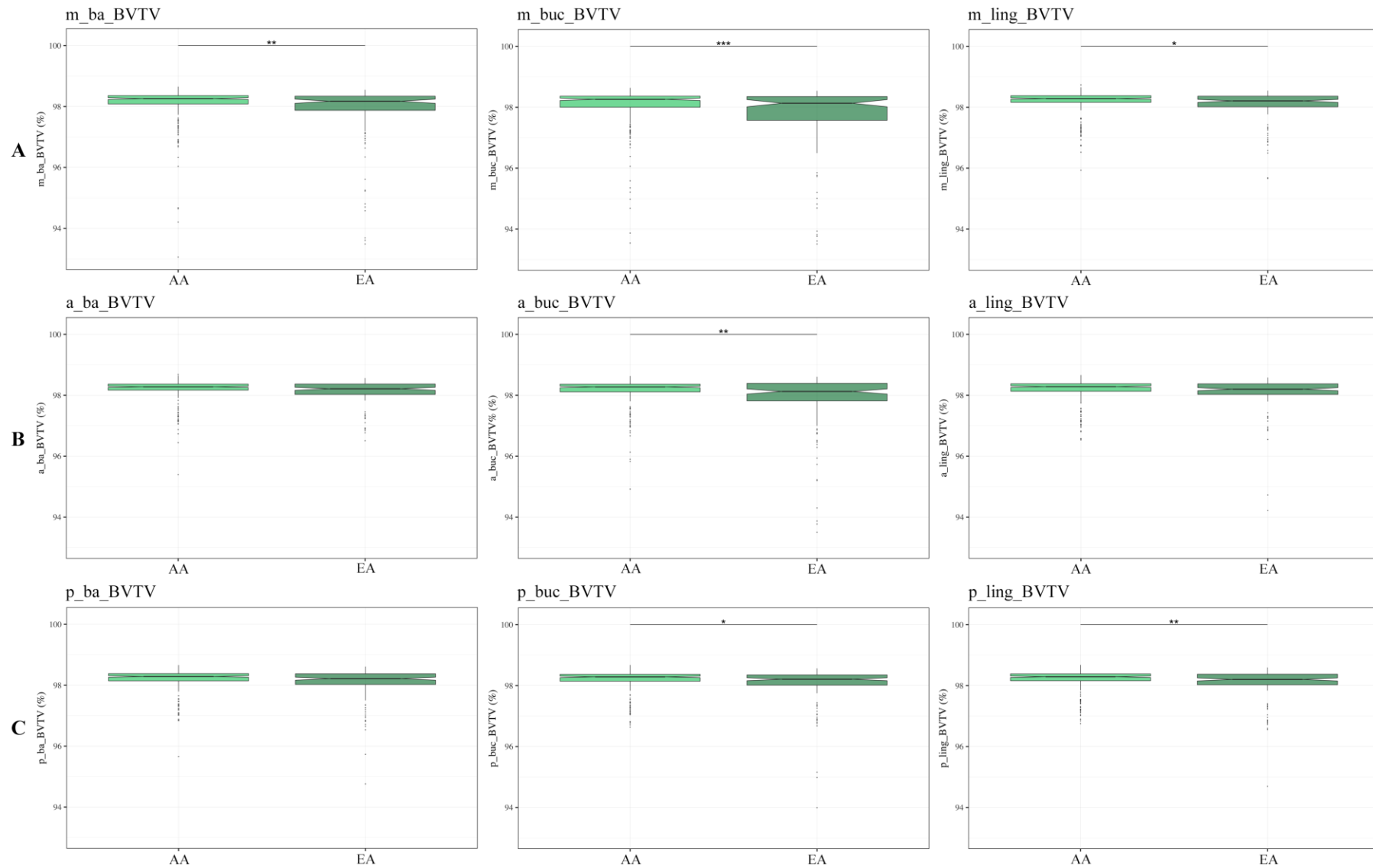
Figure 4.43. Boxplots of cortical BV/TV (%) per ancestry (AA: light green; EA: dark green), recorded on the midline [A], anterior [B], posterior [C], ramus breadth [D] and height [E] sections. Dots depict outliers. Significance: *** $p < 0.001$, ** $p < 0.01$, * $p < 0.05$. (continued on the next page)
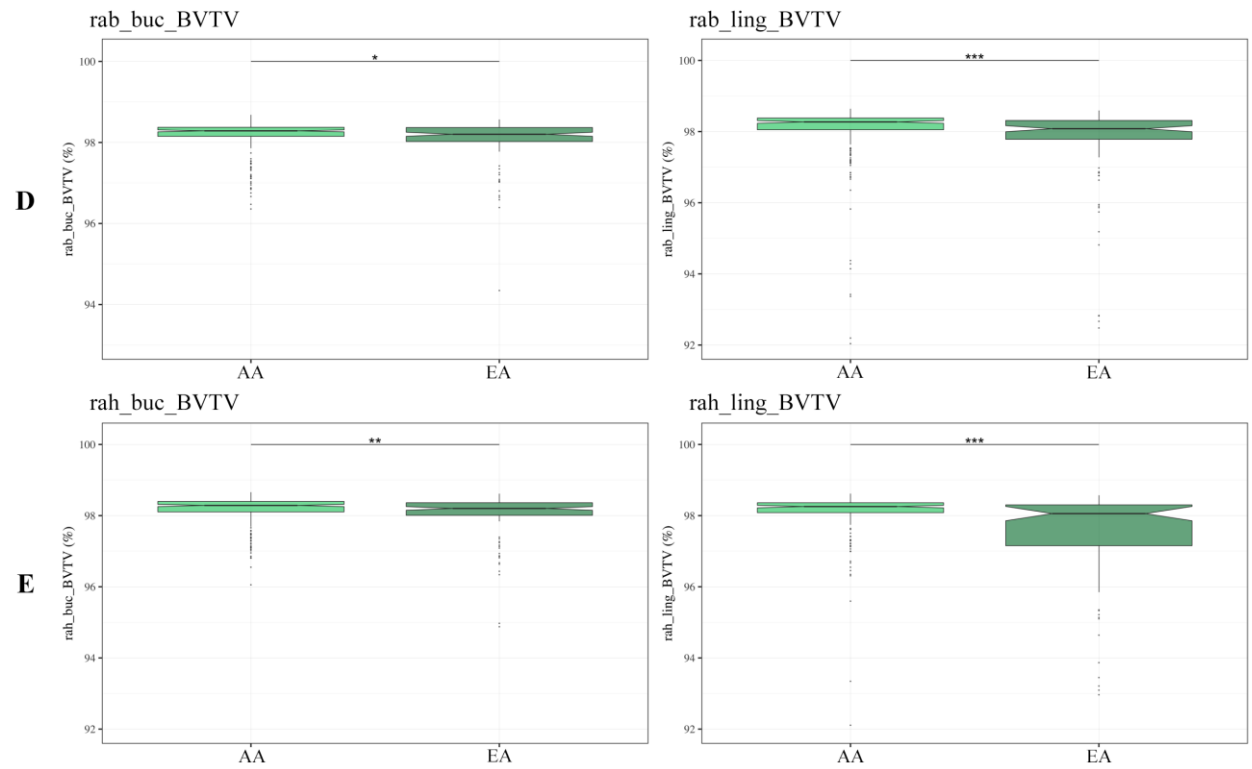
Figure 4.43. (continued)
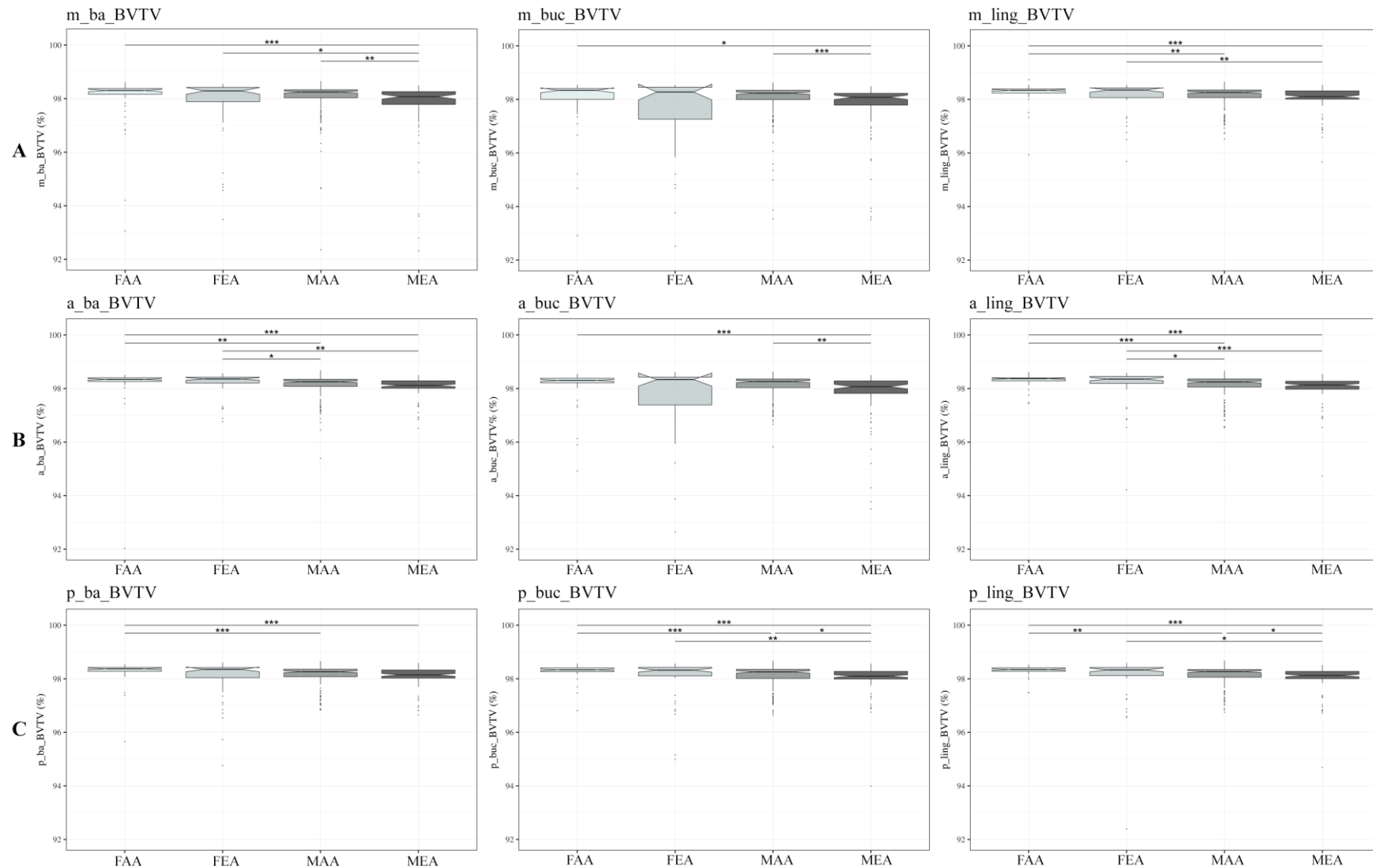
Figure 4.44. Boxplots of cortical BV/TV (%) per sex/ancestry (FAA, FEA, MAA, MEA: from light to dark grey), recorded on the midline [A], anterior [B], posterior [C], ramus breadth [D] and height [E] sections. Dots depict outliers. Significance: *** $p < 0.001$, ** $p < 0.01$, * $p < 0.05$. (continued on the next page)
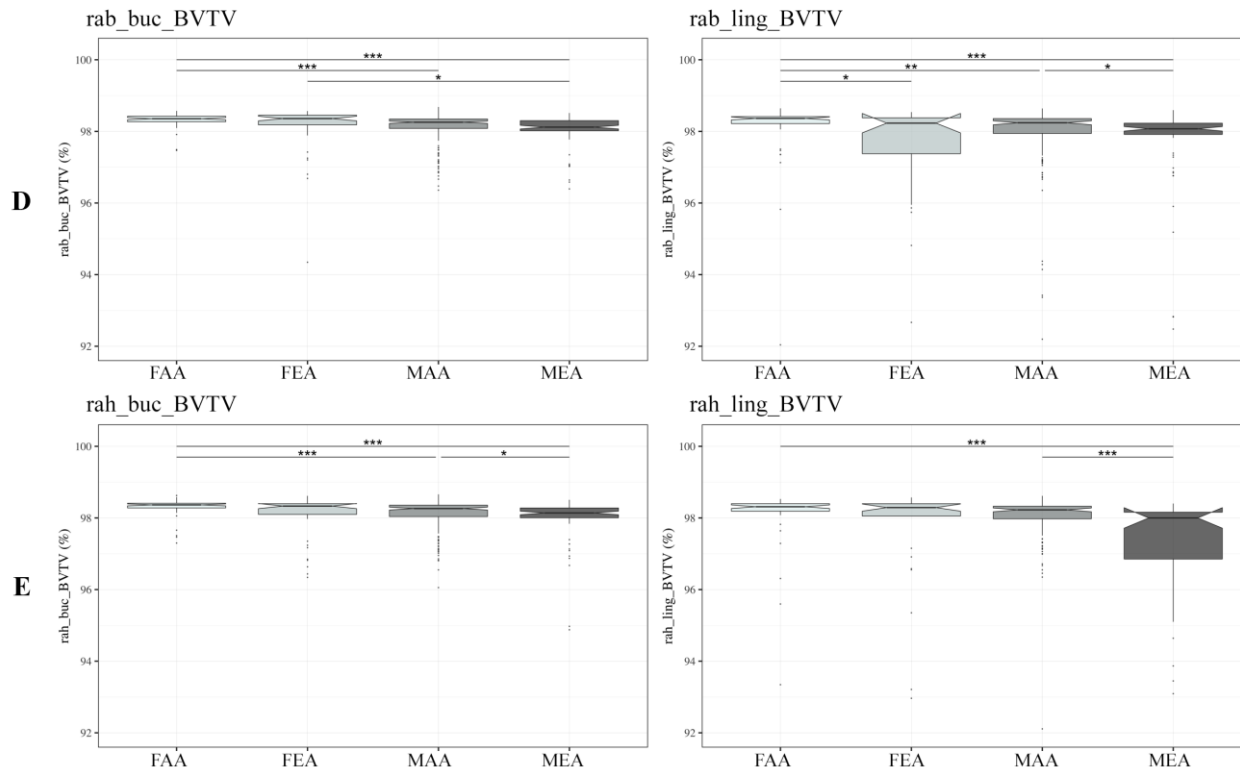
Figure 4.44. (continued)

4.5.3. Influence of tooth loss

4.5.3.1. Tooth loss in the entire sample

The cortical bone densities of the entire sample were analysed according to the three dentition categories (A, B, C) as illustrated in Figure 4.45. First, Kruskal-Wallis tests indicated that only two locations of the 13 did not show any significant differences between the three categories: the lingual sites of the midline (m_ling_BV/TV p = 0.08) and of the posterior section (p_ling_BV/TV p = 0.08). Thus, pairwise Wilcoxon post-hoc tests were run on the previously found 11 significant locations. No statistically significant differences were found between B and C categories in any of the VOIs where the BV/TV was recorded. However, some locations (a_ling_BV/TV, p_ba_BV/TV, rab_buc_BV/TV, rab_ling_BV/TV) showed significant differences only between categories A and C, with the greatest values in A and the smallest in C. Furthermore, other locations were significantly different between A and C as well as between A and B (m_ba_BV/TV, m_buc_BV/TV, a_ba_BV/TV, a_buc_BV/TV, p_buc_BV/TV, rah_ling_BV/TV). It is also interesting to note that individuals in the C category showed a wider range of values and a higher number of outliers than in B, and A more particularly.

4.5.3.2. Tooth loss per sex

The entire sample was then divided into sex subsamples, in which the variations in cortical bone density were investigated with tooth loss (i.e., dentition category A vs. B vs. C within females, and within males) using Kruskal-Wallis tests (Figure 4.46). Firstly, within the female subsample, no statistically significant differences were found between the three dentition categories at any of the 13 VOIs. However, within males, a different pattern was noted: nine VOIs were detected to be statistically significantly different between dentition categories (m_ba_BV/TV, m_buc_BV/TV, a_ba_BV/TV, a_buc_BV/TV, p_buc_BV/TV, p_ling_BV/TV, rab_buc_BV/TV, rab_ling_BV/TV, rah_ling_BV/TV). By running pairwise Wilcoxon post-hoc tests on these nine locations, significant differences were observed between categories A and B, as well as between A and C in six VOIs (m_ba_BV/TV, m_buc_BV/TV, a_ba_BV/TV, a_buc_BV/TV, p_buc_BV/TV), with a significantly greater BV/TV in category A males compared to B and C. The other three VOIs (p_ling_BV/TV, rab_buc_BV/TV,

rab_ling_BV/TV) were found to have a significantly denser BV/TV in A than in C (but no significant differences between A and B).

4.5.3.3. Tooth loss per ancestry

The influence of tooth loss on the cortical bone densities was then investigated within each ancestral group (Figure 4.47) using Kruskal-Wallis and pairwise Wilcoxon post-hoc tests. Within EA, no statistically significant differences were detected at all between the dentition categories while, within AA, statistically significant differences were found in six BV/TV locations. The post-hoc tests performed on these six VOIs (m_ba_BV/TV, m_buc_BV/TV, a_ba_BV/TV, a_buc_BV/TV, p_buc_BV/TV, rab_ling_BV/TV) showed that the BV/TV recorded was consistently and significantly greater in category A than in C. Interestingly, no significant differences were found in the lingual locations of the mandibular body.

4.5.3.4. Tooth loss per sex/ancestry

The cortical bone densities were then analysed within each sex/ancestral subgroup taking into account the three dentition categories (i.e., the differences between A, B and C within FAA, FEA, MAA or MEA). As before, Kruskal-Wallis tests were performed, followed by pairwise Wilcoxon post-hoc tests when necessary. As illustrated in Figure 4.48, all the lingual locations from the body and all the VOIs recorded on the ramus did not show any significant differences with tooth loss in any of the sex/ancestral subsamples. Furthermore, FAA, FEA and MEA individuals showed the same pattern: no statistically significant differences were detected between the three dentition categories (A, B and C) within each subsample, although very long boxplots were particularly observed in FEA. However, within MAA, statistically significant differences were detected in three VOIs (m_ba_BV/TV, m_buc_BV/TV, p_buc_BV/TV), with consistently higher BV/TV in A than in C categories.
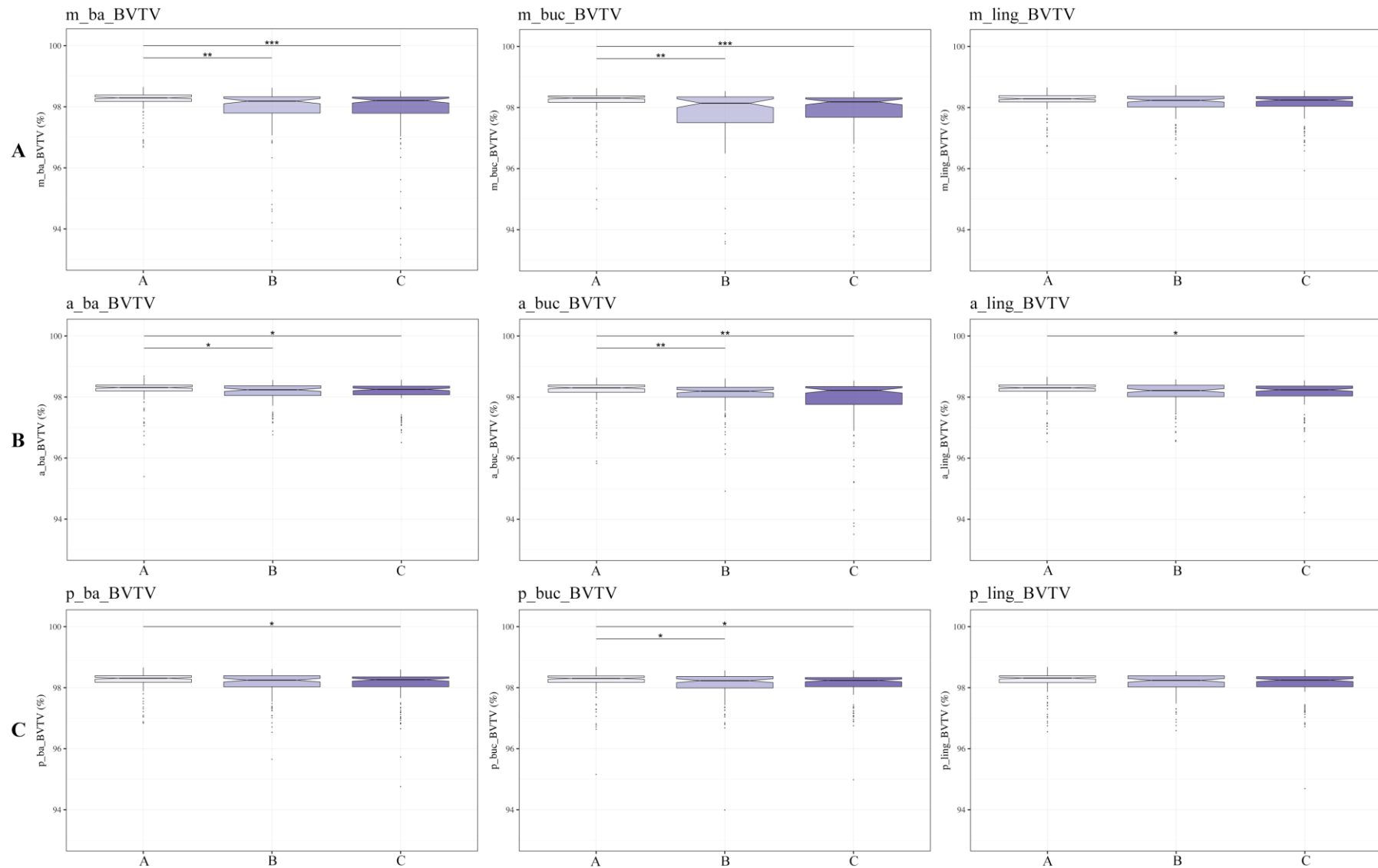
Figure 4.45. Boxplots of cortical BV/TV (%) per dentition category (A, B, C: from light to dark purple), recorded on the midline [A], anterior [B], posterior [C], ramus breadth [D] and height [E] sections. Dots depict outliers. Significance: *** $p < 0.001$, ** $p < 0.01$, * $p < 0.05$. (continued on the next page)
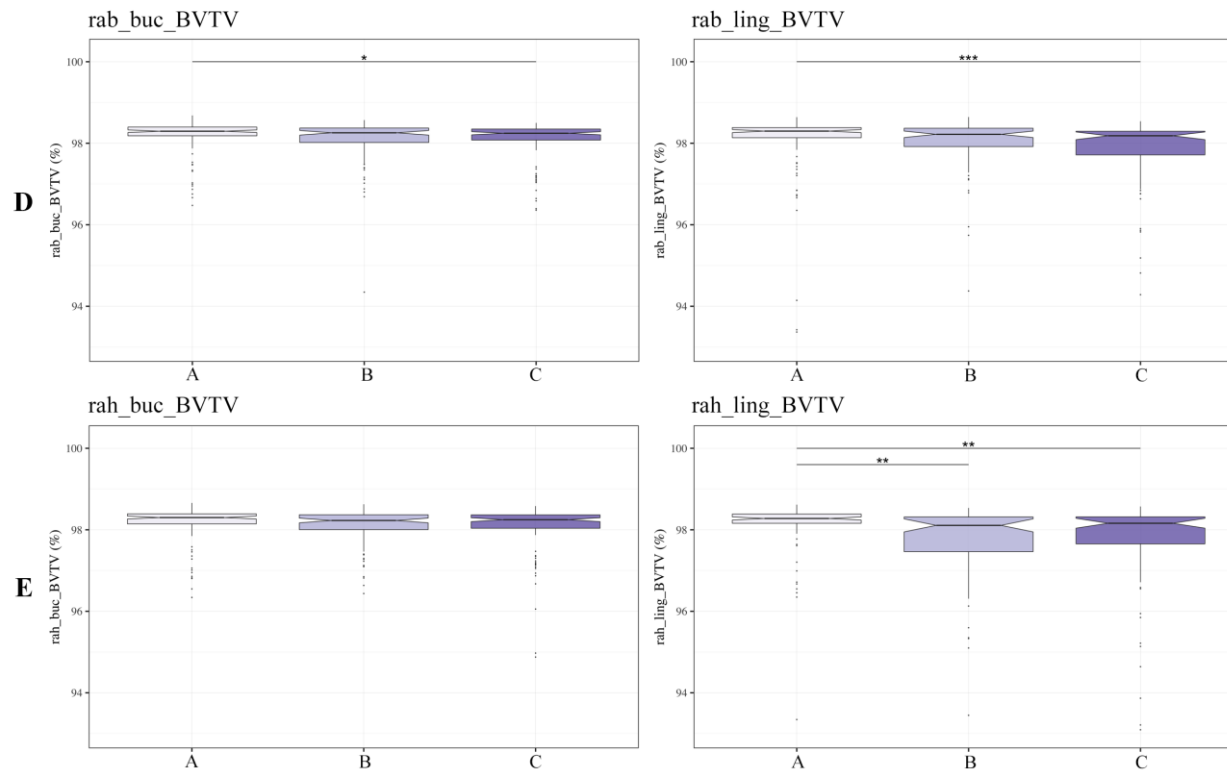
Figure 4.45. (continued)
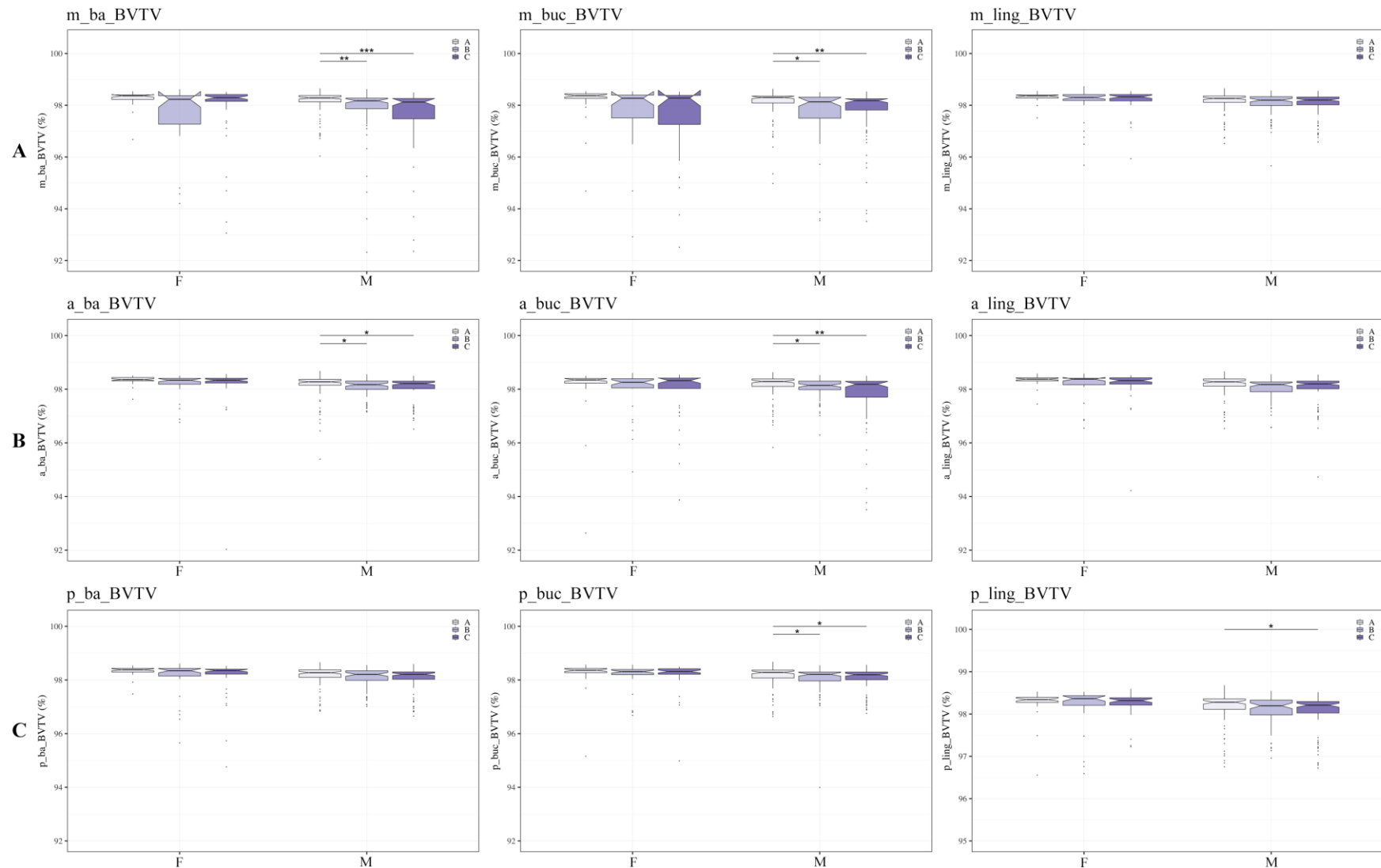
Figure 4.46. Boxplots of cortical BV/TV (%) per sex (F, M) and dentition category (A, B, C: from light to dark purple), recorded on the midline [A], anterior [B], posterior [C], ramus breadth [D] and height [E] sections. Dots depict outliers. Significance: *** $p < 0.001$, ** $p < 0.01$, * $p < 0.05$. (continued on the next page)
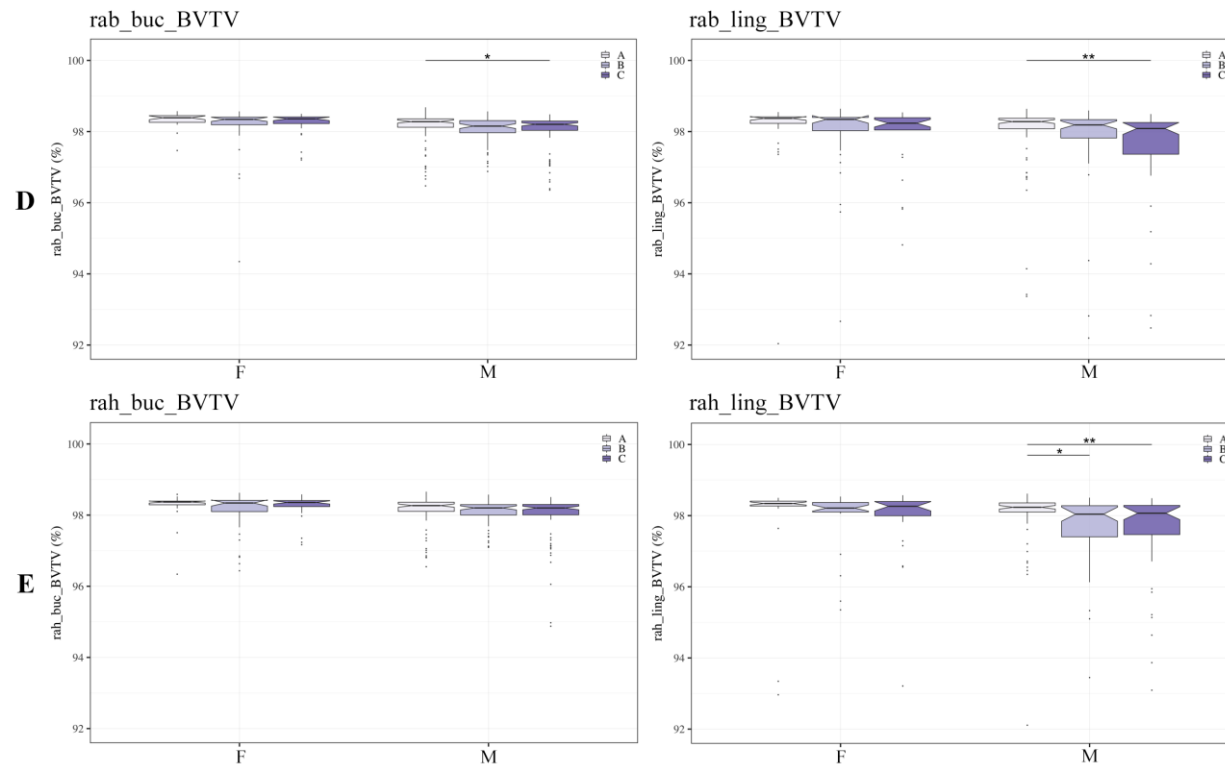
Figure 4.46. (continued)
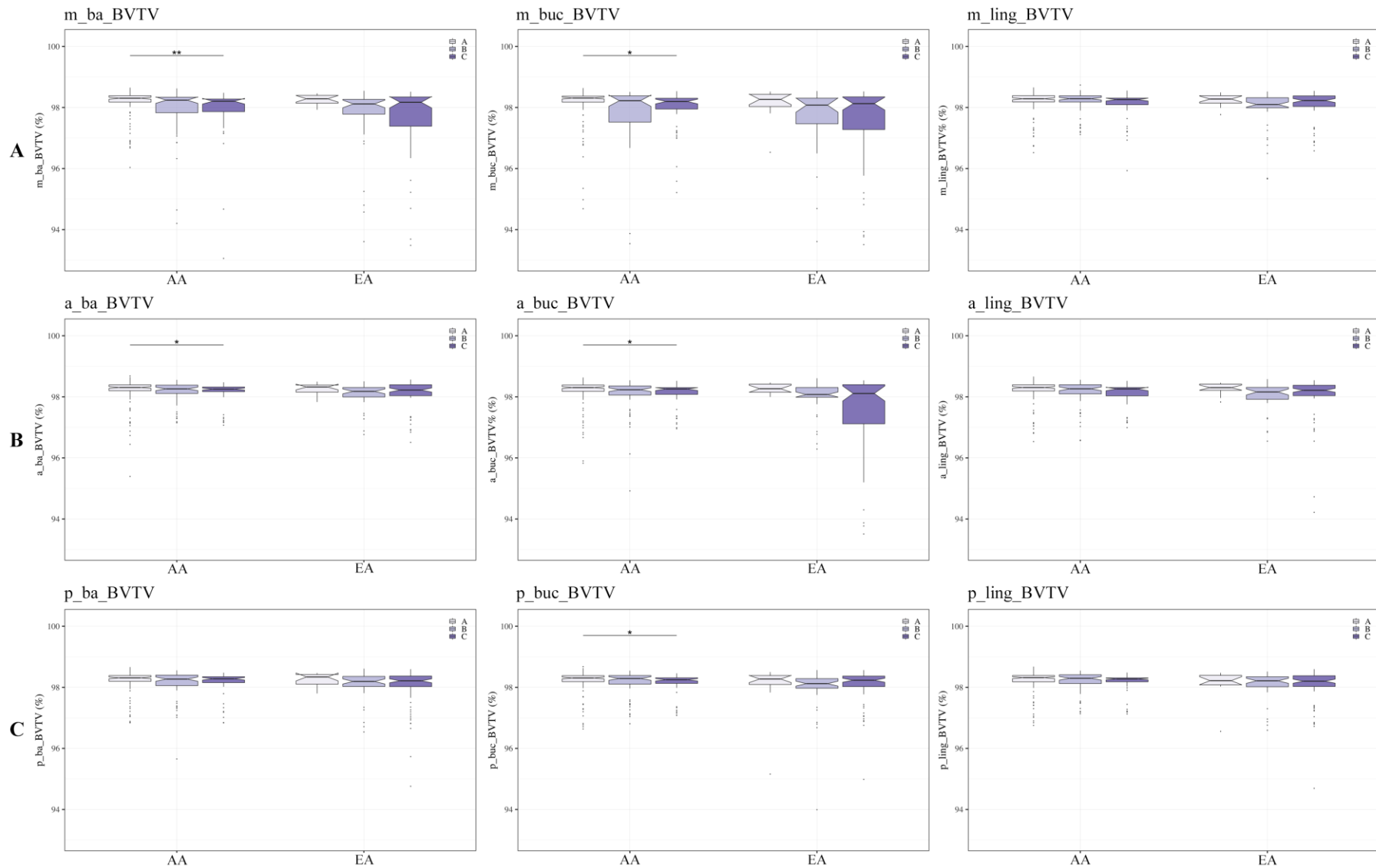
Figure 4.47. Boxplots of cortical BV/TV (%) per ancestry (AA, EA) and dentition category (A, B, C: from light to dark purple), recorded on the midline [A], anterior [B], posterior [C], ramus breadth [D] and height [E] sections. Dots depict outliers. Significance: ** $p < 0.01$, * $p < 0.05$. (continued on the next page)

D

rab_buc_BVTV

rab_ling_BVTV

E

rah_buc_BVTV

rah_ling_BVTV
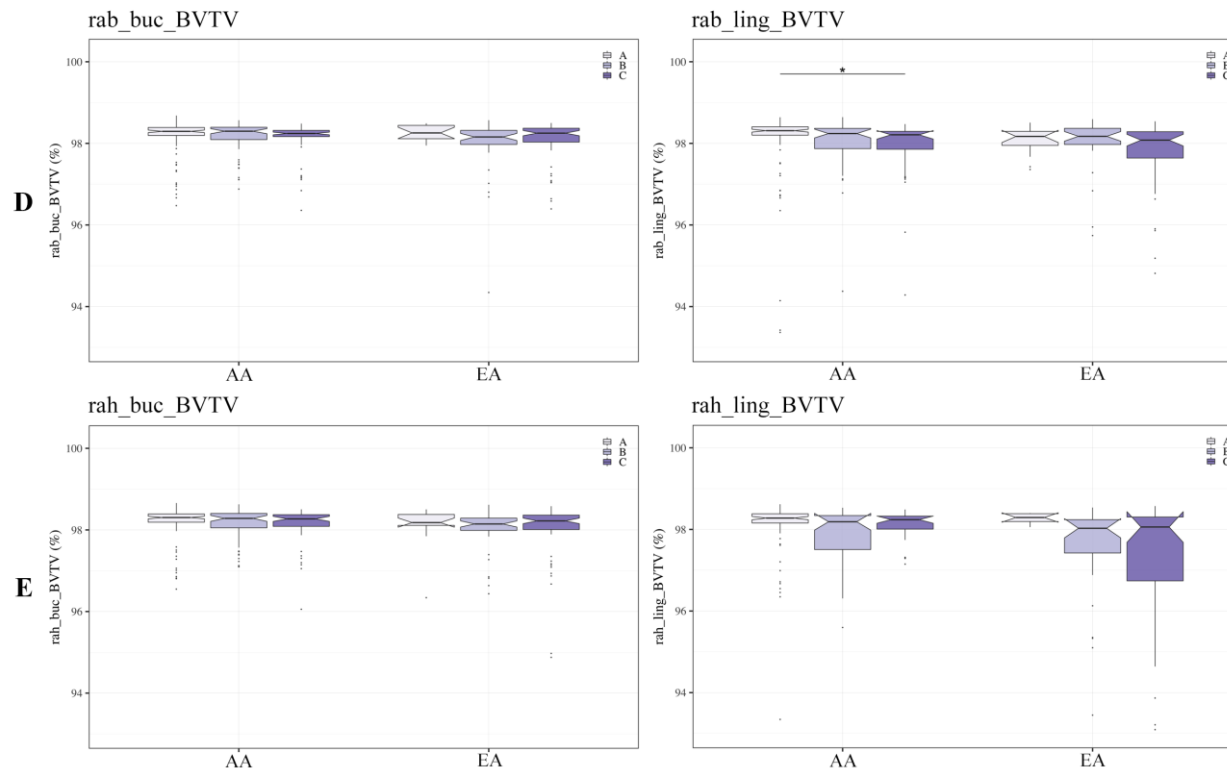
Figure 4.47. (continued)
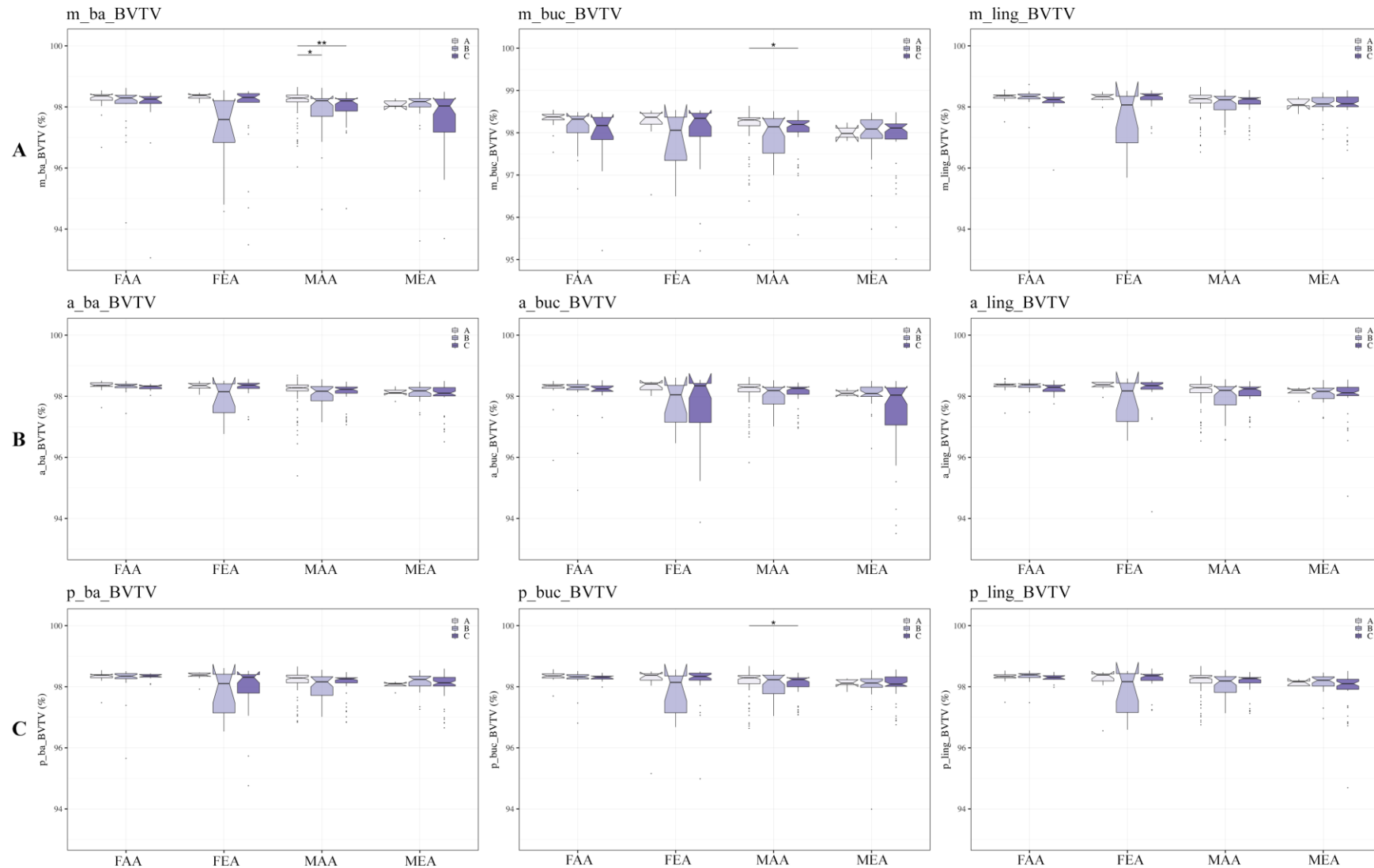
Figure 4.48. Boxplots of cortical BV/TV (%) per sex/ancestry (FAA, FEA, MAA, MEA) and dentition category (A, B, C: from light to dark purple), recorded on the midline [A], anterior [B], posterior [C], ramus breadth [D] and height [E] sections. Dots depict outliers. Significance: ** $p < 0.01$, * $p < 0.05$.

(continued on the next page)

Figure 4.48. (continued)
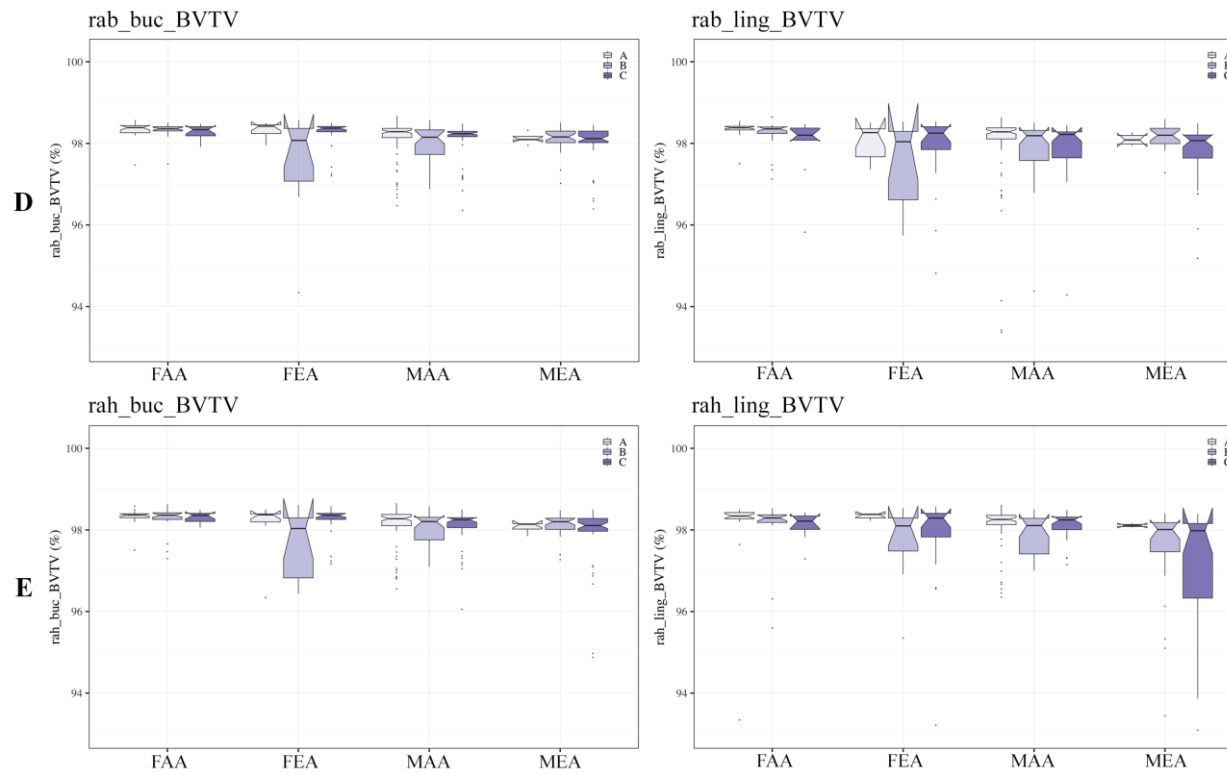
4.5.3.5. Influence of sex per dentition category

While controlling for tooth loss, the influence of sex on the mandibular cortical bone densities was evaluated (Figure 4.49). According to the Mann-Whitney Wilcoxon tests run between males and females within the A category, half of the VOIs did not show differences in density between sexes whereas the other half did (six VOIs out of 13 without differences: m_ba_BV/TV, m_buc_BV/TV, a_buc_BV/TV, p_ling_BV/TV, rab_ling_BV/TV, rah_ling_BV/TV). However, within category B and thus, with moderate tooth loss, most of the VOIs had significant differences in density between males and females (four VOIs out of 13 without differences: m_ba_BV/TV, m_buc_BV/TV, a_buc_BV/TV, rah_ling_BV/TV). In category C, sexual dimorphism was even more frequent, with only three VOIs out of 13 that did not show differences (m_buc_BV/TV, rab_ling_BV/TV, rah_ling_BV/TV). The lingual sites of the midline (m_ling_BV/TV) and anterior sections (a_ling_BV/TV) were consistently significantly denser in females than in males in all categories (A, B, C). In contrast, the buccal site of the midline (m_buc_BV/TV) and the lingual site of the ramus height (rah_ling_BV/TV) were never (i.e., in any of the dentition categories) significantly different between males and females. Furthermore, wider boxplots were observed in individuals with tooth loss (B and C categories) than in A.

4.5.3.6. Influence of ancestry per dentition category

Mann-Whitney Wilcoxon tests were performed between ancestral groups within each dentition category (Figure 4.50). Within A and C categories, no statistically significant differences were detected between AA and EA in any of the locations of the mandibular corpus or ramus (all p-values > 0.05). In category B, however, four sites showed significant differences between AA and EA, with AA individuals always denser than EA (buccal and lingual sites of the midline: m_buc_BV/TV, m_ling_BV/TV, p_buc_BV/TV, rah_buc_BV/TV). Long boxplots with wide ranges of values were particularly observed within edentulous individuals (C category).

4.5.3.7. Influence of sex and ancestry per dentition category

The influence of the interaction between sex and ancestry (FAA, FEA, MAA, MEA) was assessed within each dentition category, using Kruskal-Wallis tests and their associated pairwise Wilcoxon post-hoc tests. Results are illustrated in Figure 4.51.

Within the A category, six VOIs did not show any significant differences between the sex/ancestral subsamples (m_ba_BV/TV, m_buc_BV/TV, a_buc_BV/TV, p_ling_BV/TV, rab_ling_BV/TV, rah_ling_BV/TV), while in the other seven VOIs, significant differences were consistently detected between FAA and MEA individuals ($0.01 < p < 0.05$), displaying respectively the highest and lowest cortical density values.

Within B, five VOIs (m_ba_BV/TV, m_buc_BV/TV, a_buc_BV/TV, p_ba_BV/TV, rah_ling_BV/TV) were not found to show any statistically significant differences between the sex/ancestral groups. As within category A, significant differences were observed between FAA and MEA subsamples in three locations (m_ling_BV/TV, p_buc_BV/TV, rah_buc_BV/TV), with BV/TV values greater in FAA than in MEA. Furthermore, in addition to the differences between FAA and MEA, some VOIs also displayed significant differences between FAA and MAA (a_ba_BV/TV, a_ling_BV/TV, p_ling_BV/TV, rab_buc_BV/TV), still with a higher cortical bone density in FAA than in the other groups.

As in the A category, edentulous individuals (category C) did not show significant differences in the following four VOIs: m_buc_BV/TV, a_buc_BV/TV, rab_ling_BV/TV, rah_ling_BV/TV. The other VOI locations, however, consistently showed significant differences between FEA and MEA (m_ba_BV/TV, m_ling_BV/TV, p_ling_BV/TV) with lower BV/TV in MEA, sometimes also associated with significant differences between FEA and MAA (a_ba_BV/TV, a_ling_BV/TV, p_buc_BV/TV, rab_buc_BV/TV).
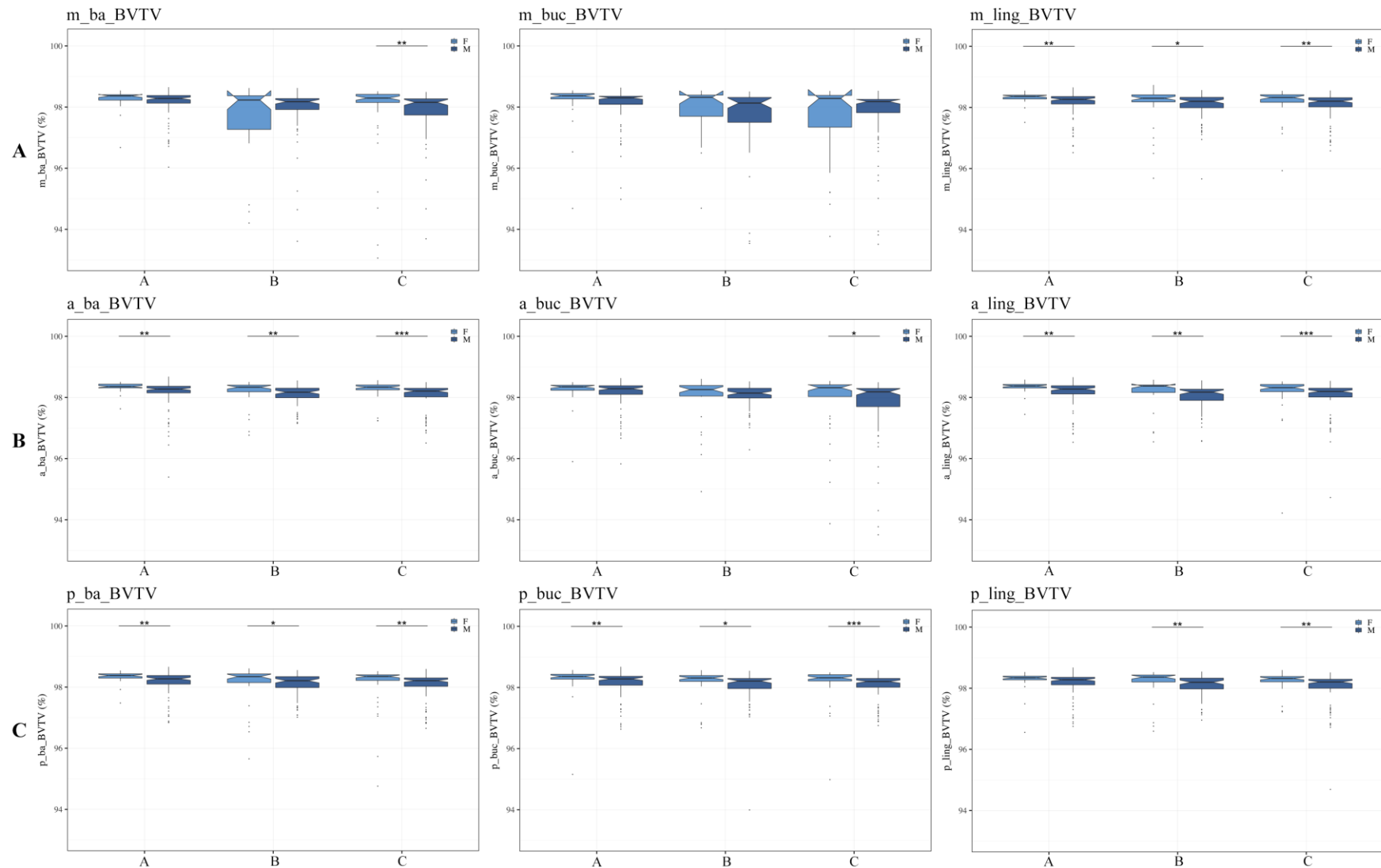
Figure 4.49. Boxplots of BV/TV (%) per dentition category (A, B, C) and sex (F: light blue; M: dark blue), recorded on the midline [A], anterior [B], posterior [C], ramus breadth [D] and height [E] sections. Dots depict outliers. Significance: *** $p < 0.001$, ** $p < 0.01$, * $p < 0.05$. (continued on the next page)

D

E
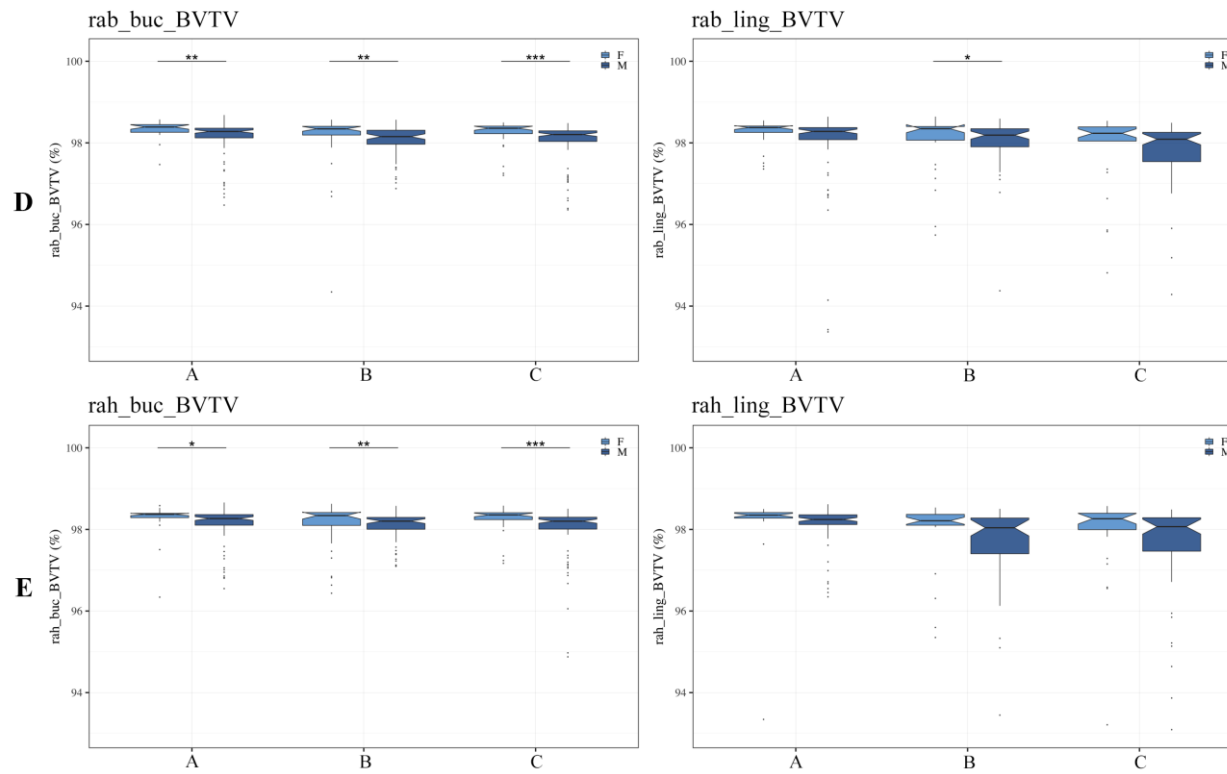
Figure 4.49. (continued)
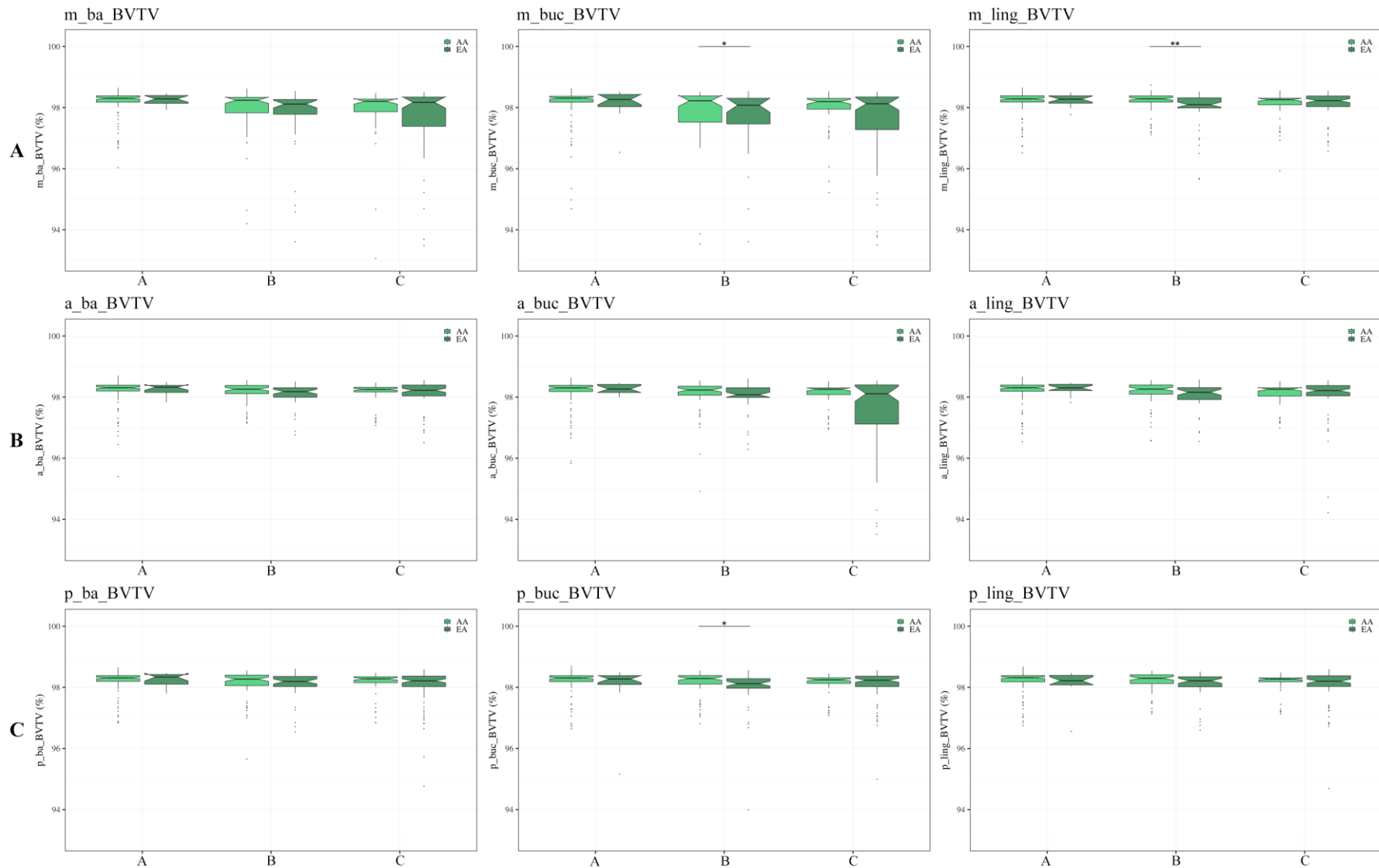
Figure 4.50. Boxplots of BV/TV (%) per dentition category (A, B, C) and ancestry (AA: light green; EA: dark green), recorded on the midline [A], anterior [B], posterior [C], ramus breadth [D] and height [E] sections. Dots depict outliers. Significance: ** $p < 0.01$, * $p < 0.05$. (continued on the next page)
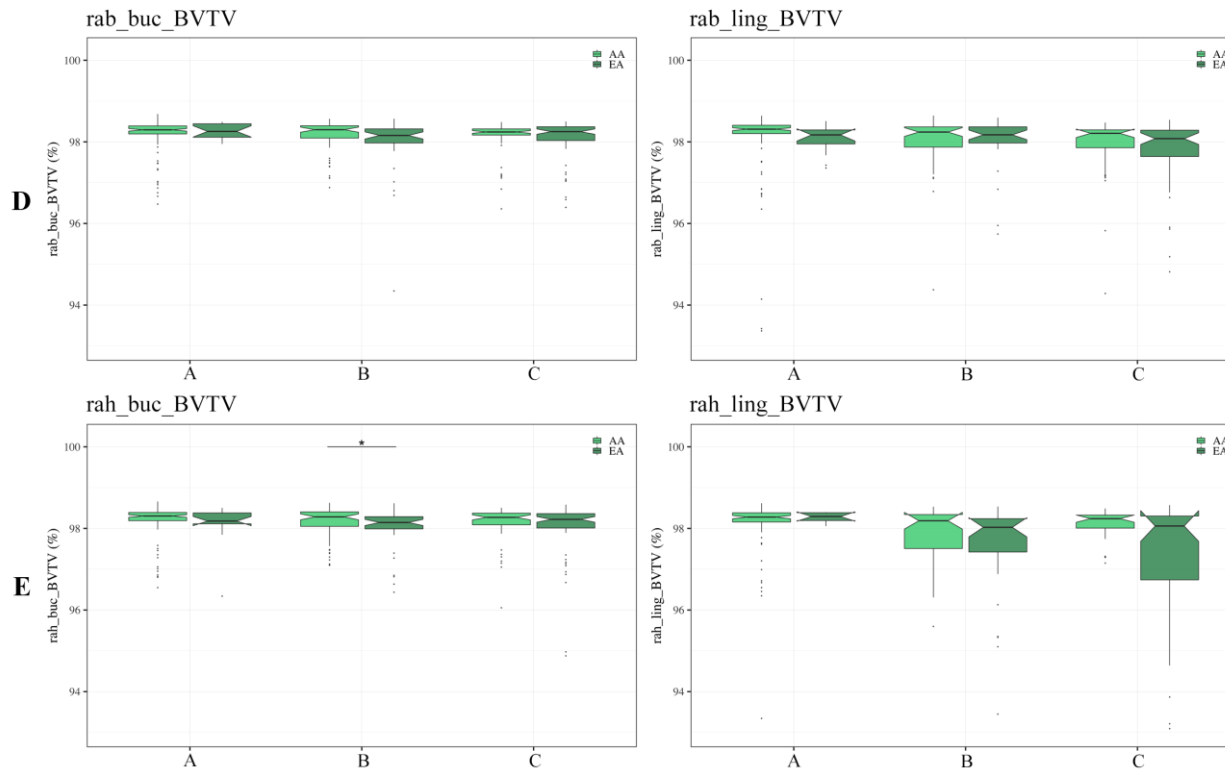
Figure 4.50. (continued)
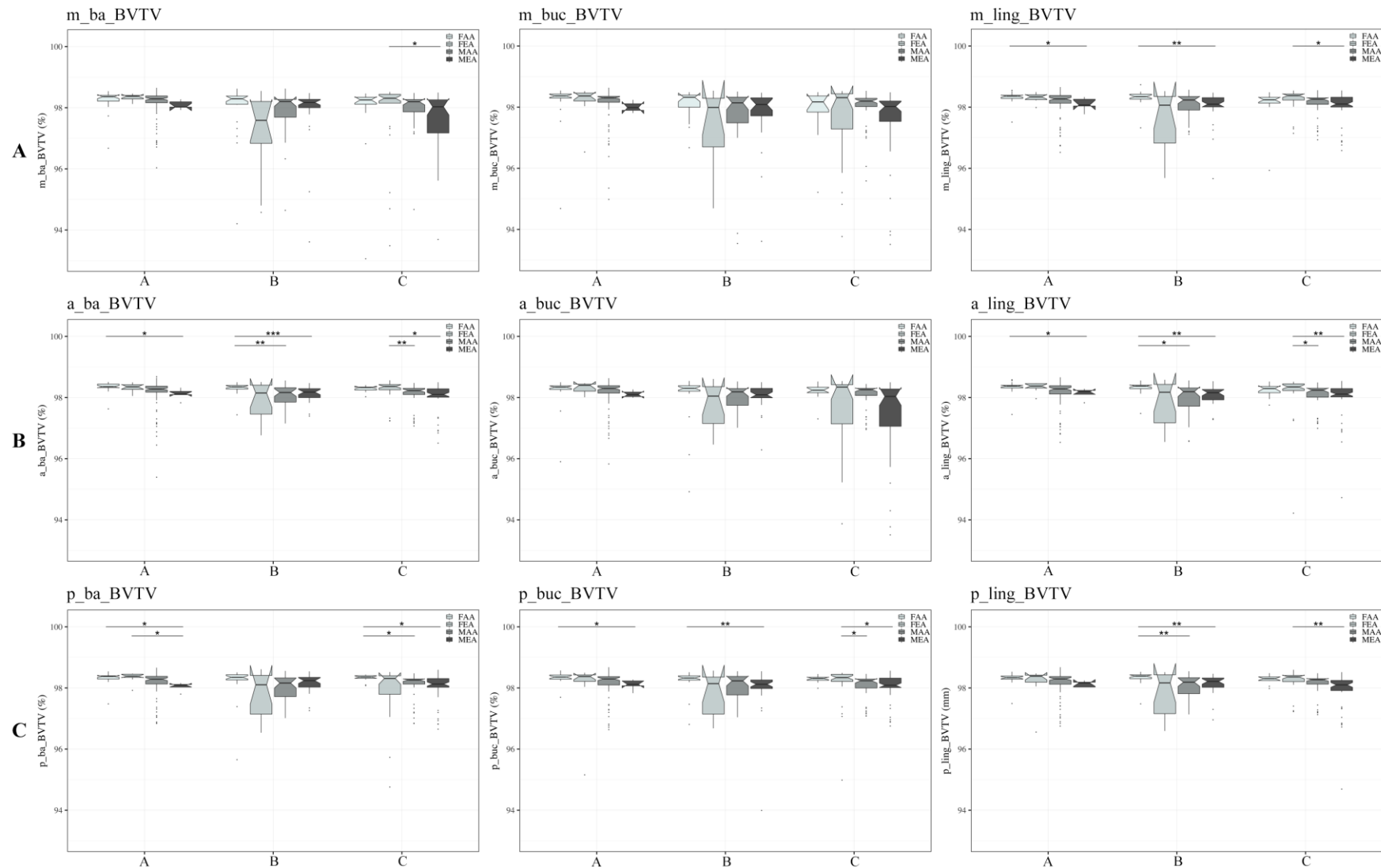
Figure 4.51. Boxplots of BV/TV (%) per dentition category (A, B, C) and sex/ancestry (FAA, FEA, MAA, MEA: from light to dark grey), recorded on the midline [A], anterior [B], posterior [C], ramus breadth [D] and height [E] sections. Dots depict outliers. Significance: *** $p < 0.001$, ** $p < 0.01$, * $p < 0.05$.

(continued on the next page)
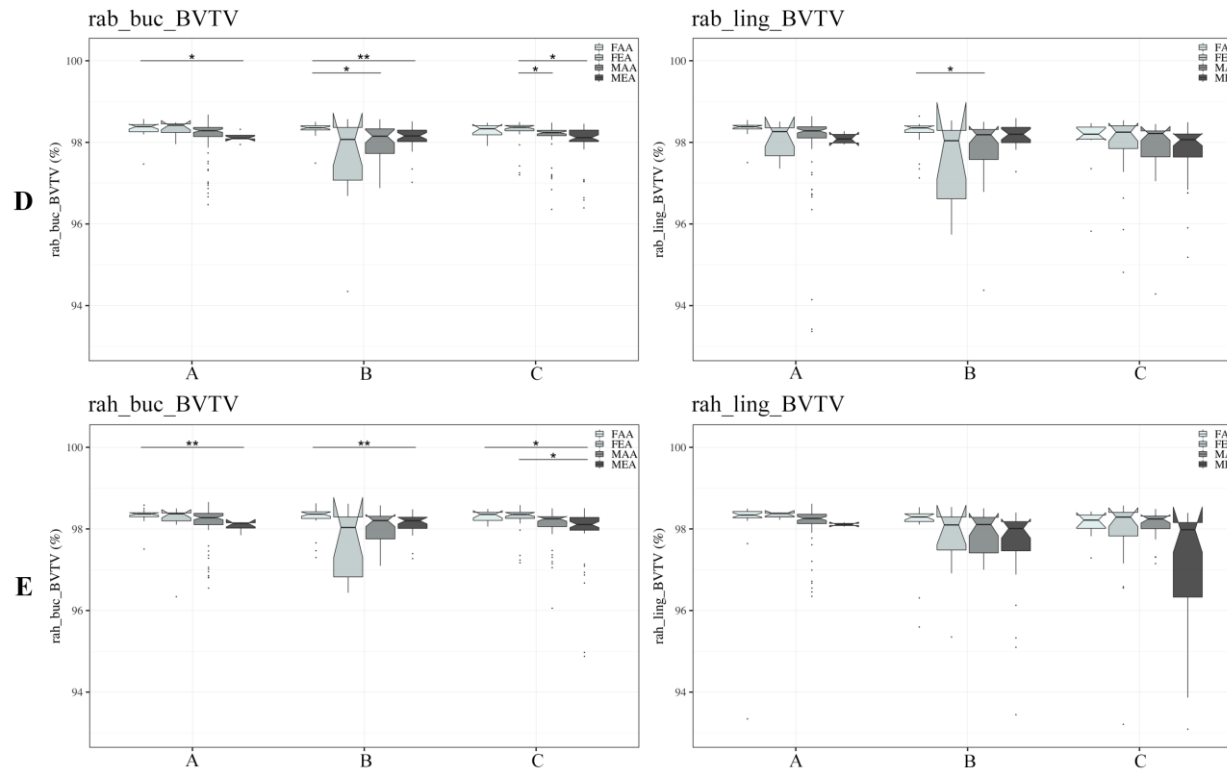
Figure 4.51. (continued)

4.5.4. Location of the VOIs

4.5.4.1. Influence of section and site selection on BV/TV

Variations in the location of the VOIs, at which the cortical bone BV/TV parameters were recorded, were investigated using Kruskal-Wallis tests and pairwise Wilcoxon post-hoc tests (when necessary). The variations in BV/TV were first assessed between the five sections (midline vs. anterior vs. posterior vs. ramus breadth vs. ramus height), then between the three sites (basal vs. buccal vs. lingual) and finally between the 13 section/site locations (midline basal vs. midline buccal vs. anterior basal vs. posterior lingual, etc.).

Statistically significant differences were detected between sections according to the Kruskal-Wallis test ($p < 0.001$), but the post-hoc tests outlined significant differences only between the midline and the anterior section ($p = 0.03$), as well as between the midline and the posterior section ($p = 0.001$). However, as seen in Figure 4.52 A, the absolute differences between these three sections were minimal and were most probably due to the greater number of outliers at the midline (i.e., the lower tail of the boxplot). Furthermore, the three sites did not show any statistically significant differences (Kruskal-Wallis p-value = 0.68) between basal, buccal and lingual VOIs (see Figure 4.52 B). When considering the VOI locations (i.e., section/site, as illustrated in Figure 4.53), only a small number (14 on 78) were statistically significantly different from each other. Of these 14 significant interactions, seven were associated with the buccal site of the midline (m_buc vs. m_ling; vs. a_ba; vs. a_ling; vs. p_ba; vs. p_ling; vs. rab_buc; vs. rah_buc), and seven with the lingual site of the ramus height (rah_ling vs. m_ling; vs. a_ba; vs. a_ling; vs. p_ba; vs. p_ling; vs. rab_buc; vs. rah_buc). Similarly to the significant differences detected between sections, the absolute differences between the VOI locations were minimal (as seen in Figure 4.53).
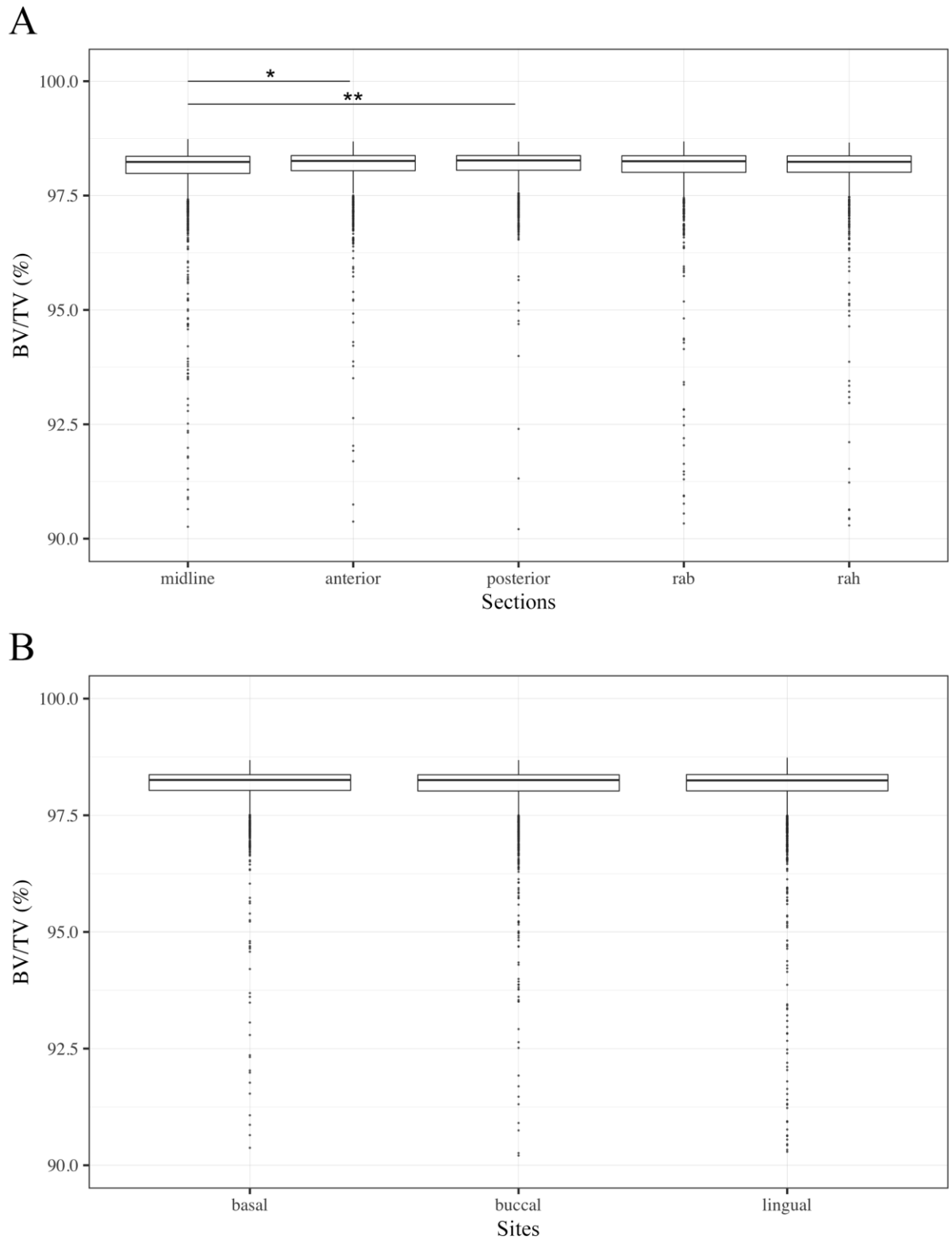
Figure 4.52. Boxplots of BV/TV (%) grouped per section [A] or per site [B]. Dots depict outliers. Significance: ** $p < 0.01$, * $p < 0.05$.
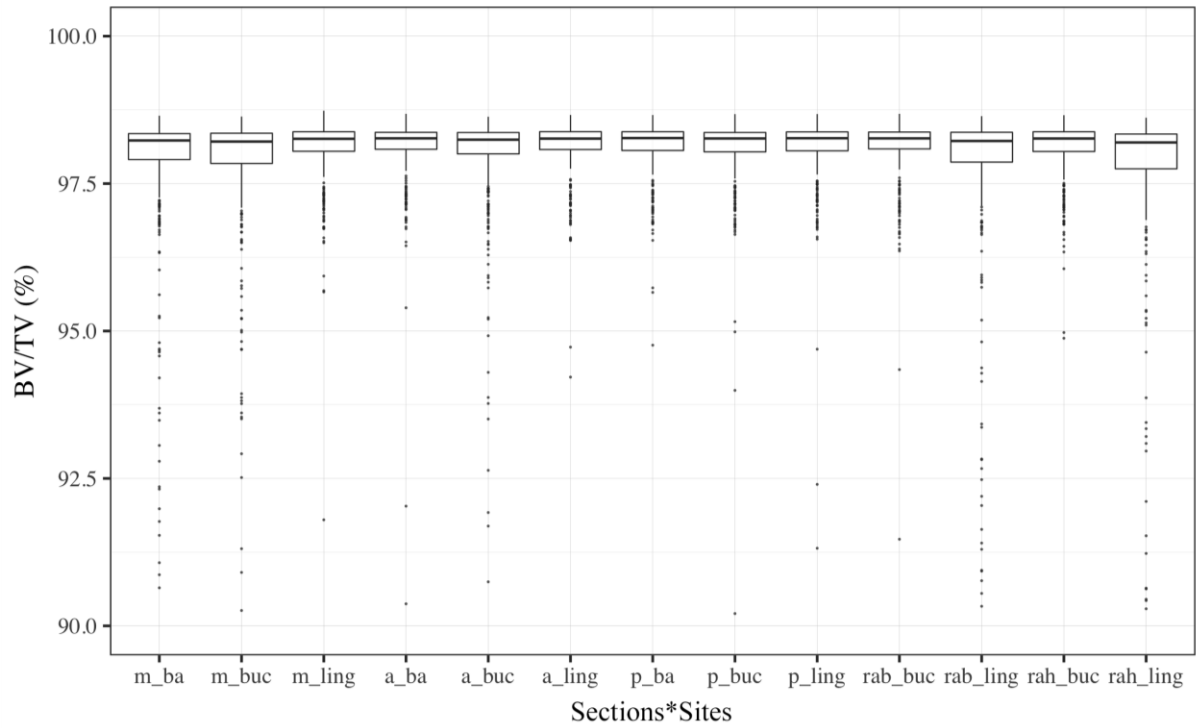
Figure 4.53. Boxplots of BV/TV (%) grouped per section/site interactions (top) and on the next page, table detailing the pairwise Wilcoxon post-hoc test p-values (bottom). Significant p-values are in bold: $p < 0.05$. (continued on the next page)

	m_ba	m_buc	m_ling	a_ba	a_buc	a_ling	p_ba	p_buc	p_ling	rab_buc	rab_ling	rah_buc
m_ba	-	-	-	-	-	-	-	-	-	-	-	-
m_buc	1.00	-	-	-	-	-	-	-	-	-	-	-
m_ling	0.5315	**0.0389**	-	-	-	-	-	-	-	-	-	-
a_ba	0.2414	**0.0157**	1.00	-	-	-	-	-	-	-	-	-
a_buc	1.00	1.00	1.00	1.00	-	-	-	-	-	-	-	-
a_ling	0.1927	**0.0108**	1.00	1.00	1.00	-	-	-	-	-	-	-
p_ba	0.0868	**0.0045**	1.00	1.00	1.00	1.00	-	-	-	-	-	-
p_buc	1.00	0.1122	1.00	1.00	1.00	1.00	1.00	-	-	-	-	-
p_ling	0.2579	**0.0153**	1.00	1.00	1.00	1.00	1.00	1.00	-	-	-	-
rab_buc	0.2577	**0.0197**	1.00	1.00	1.00	1.00	1.00	1.00	1.00	-	-	-
rab_ling	1.00	1.00	0.6755	0.3707	1.00	0.2392	0.1233	1.00	0.3310	0.3551	-	-
rah_buc	0.4879	**0.0326**	1.00	1.00	1.00	1.00	1.00	1.00	1.00	1.00	0.5780	-
rah_ling	1.00	1.00	**0.0453**	**0.0173**	1.00	**0.0138**	**0.0066**	0.12	**0.0182**	**0.0183**	1.00	**0.0395**

Figure 4.53. (continued)

4.5.4.2. Inter-variable correlations

Spearman's correlations, associated with Holm's adjustments, were computed between the 13 VOIs. The inter-VOIs correlations were calculated and illustrated with matrices for the entire sample, for the sex and ancestral subsamples, as well as for each dentition category. As seen in Figure 4.54, the BV/TV values in the thirteen VOIs were all significantly correlated with each other ($p > 0.001$) and showed moderate to strong positive correlations ($0.49 < \rho < 0.85$). The weakest correlations were mainly found between the buccal site of the midline (m_buc) and VOIs in the ramus (such as rab_ling: $\rho = 0.5$; or rah_ling: $\rho = 0.49$). The strongest correlations were detected between mandibular body VOIs, particularly within and between the anterior and posterior sections (e.g., a_ling and p_ba: $\rho = 0.85$).
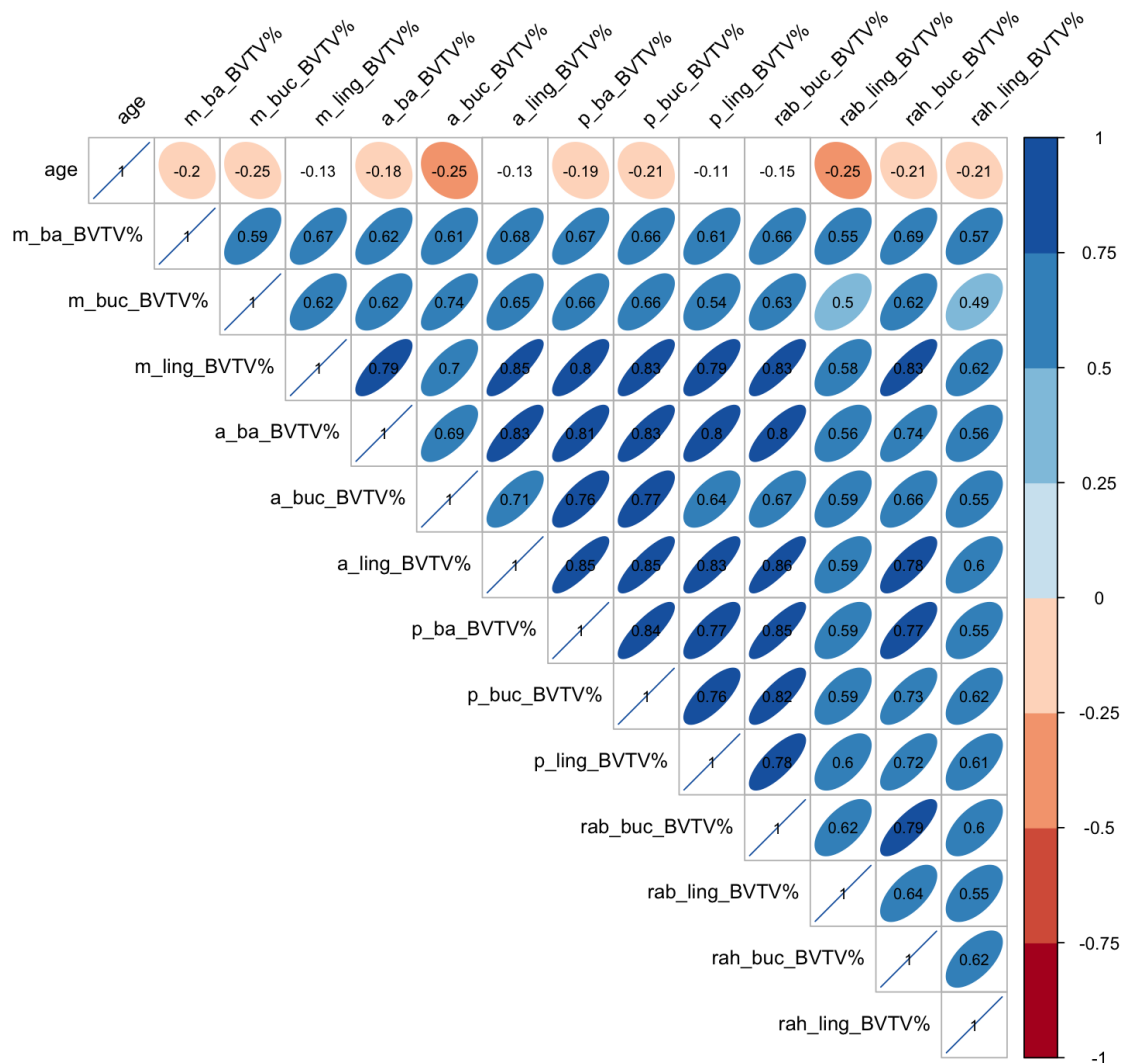
Figure 4.54. Corrplots illustrating inter-variable relationships between all the BV/TV values recorded in the entire sample. Ellipses were removed if the correlation, adjusted with Holm's correction, was not significant ($p > 0.05$). Correlation coefficients ρ were noted within each square (in blue: positive ρ, in red: negative ρ).
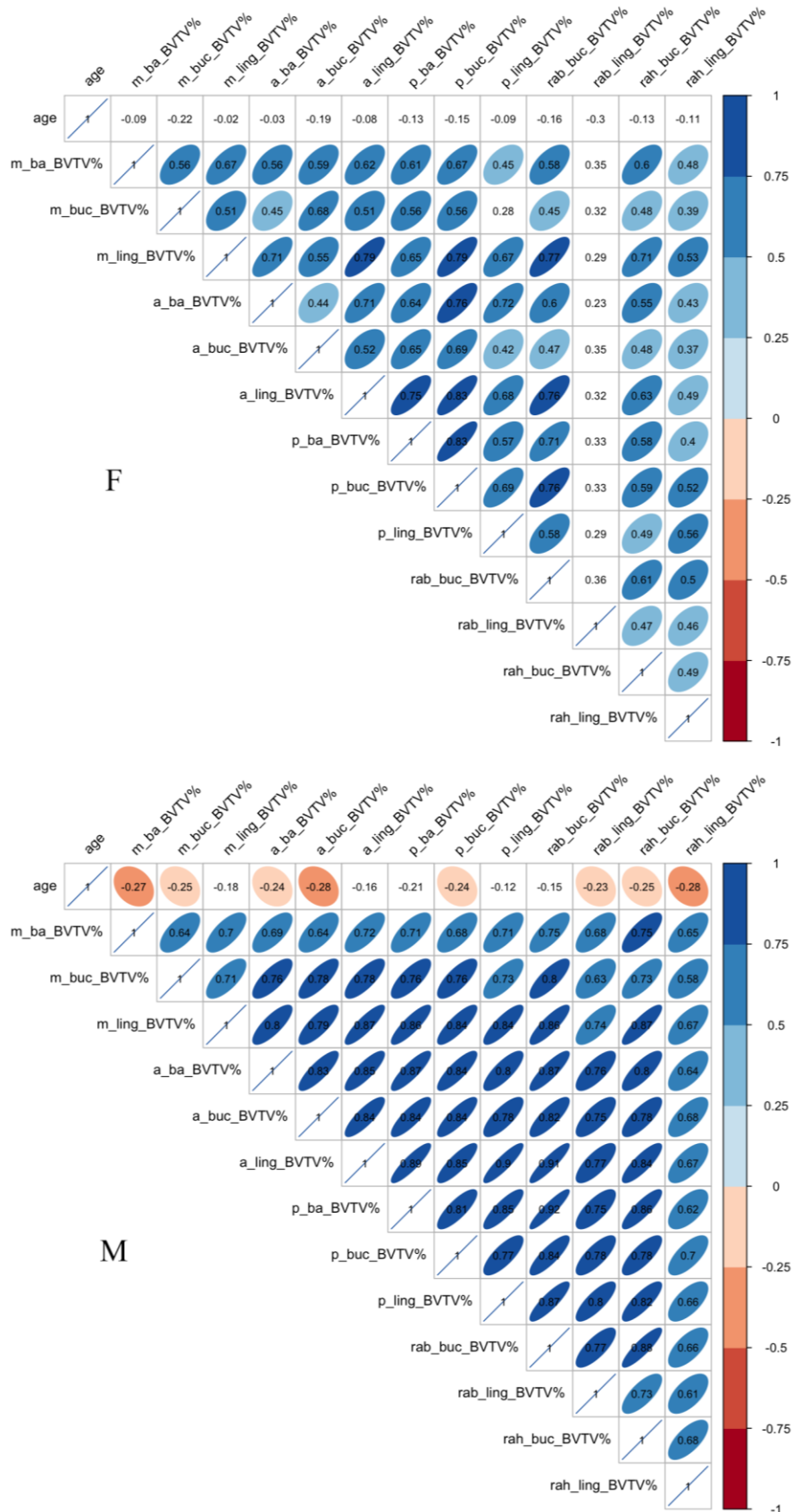
Figure 4.55. Corrplots illustrating inter-variable relationships between all the BV/TV values recorded within females (top) and males (bottom). Ellipses were removed if the correlation, adjusted with Holm's correction, was not significant ($p > 0.05$). Correlation coefficients ρ were noted within each square (in blue: positive ρ, in red: negative ρ).
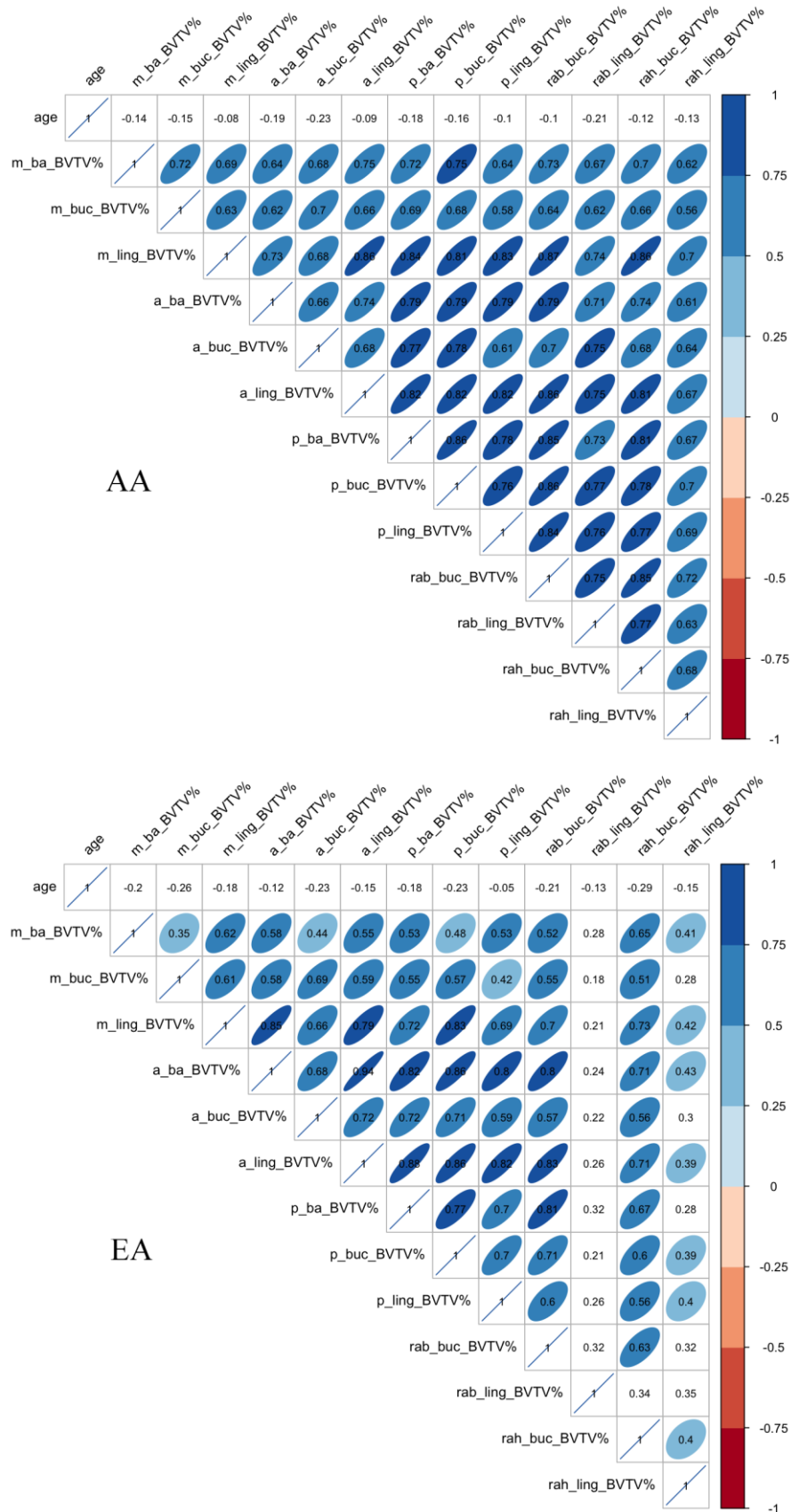
Figure 4.56. Corrplots illustrating inter-variable relationships between all the BV/TV values recorded within the ancestry-separated subsamples (AA: upper, EA: lower). Ellipses were removed if the correlation, adjusted with Holm's correction, was not significant ($p > 0.05$). Correlation coefficients ρ were noted within each square (in blue: positive ρ, in red: negative ρ).
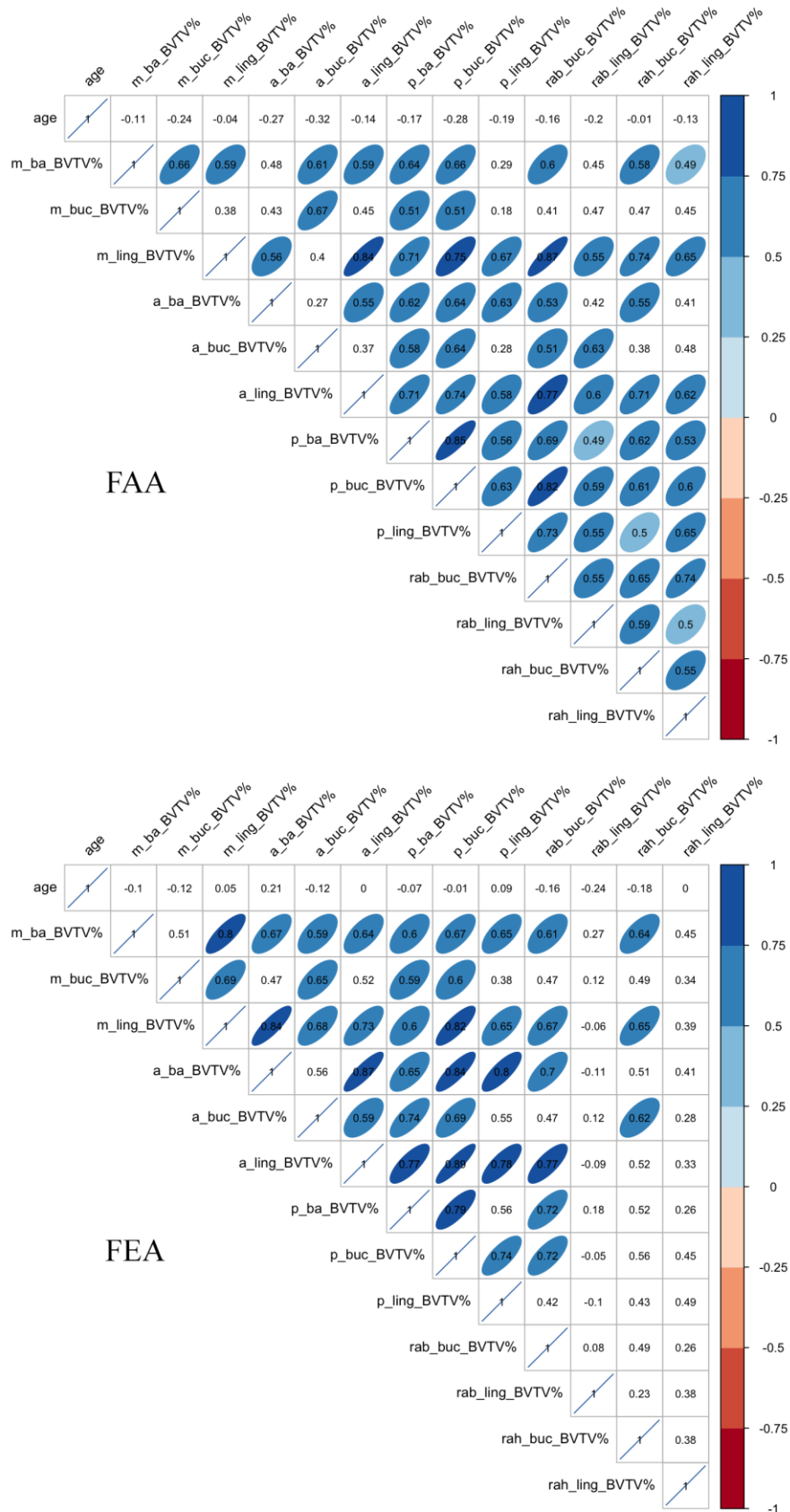
Figure 4.57. Corrplots illustrating inter-variable relationships between all the BV/TV values recorded in each sex/ancestral subgroup (FAA, FEA, MAA, MEA). Ellipses were removed if the correlation, adjusted with Holm's correction, was not significant ($p > 0.05$). Correlation coefficients ρ were noted within each ellipse (in blue: positive ρ, in red: negative ρ). (continued on next page)

MAA

MEA
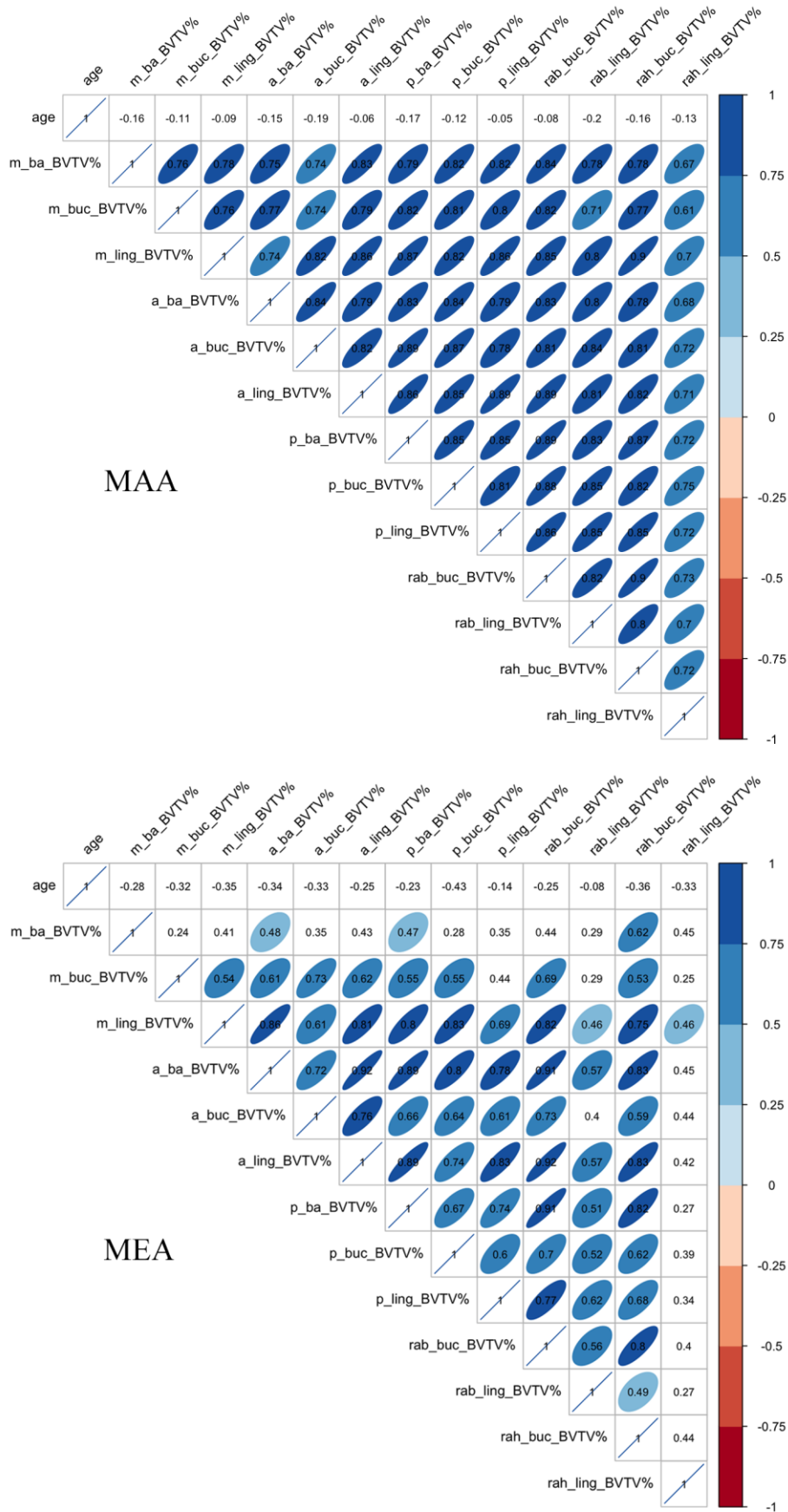
Figure 4.57. (continued)

The influence of tooth loss on the inter-VOIs BV/TV relationships was also investigated and is represented in Figure 4.58. All the BV/TV recorded within the A dentition category, and then within B, showed statistically significant correlations between each other, respectively. All correlations displayed positive and moderate to strong coefficients (A: $0.46 < \rho < 0.88$; B: $0.44 < \rho < 0.94$), even though the correlations within the B category seemed in general weaker than in A. Within the C category, and thus in edentulous mandibles, only approximately 86% of the inter-VOIs correlations were significant. BV/TV VOIs from the mandibular ramus, and most particularly at the lingual sites, were either presenting the weakest correlation coefficients, or no significance at all (rab_ling_BV/TV).
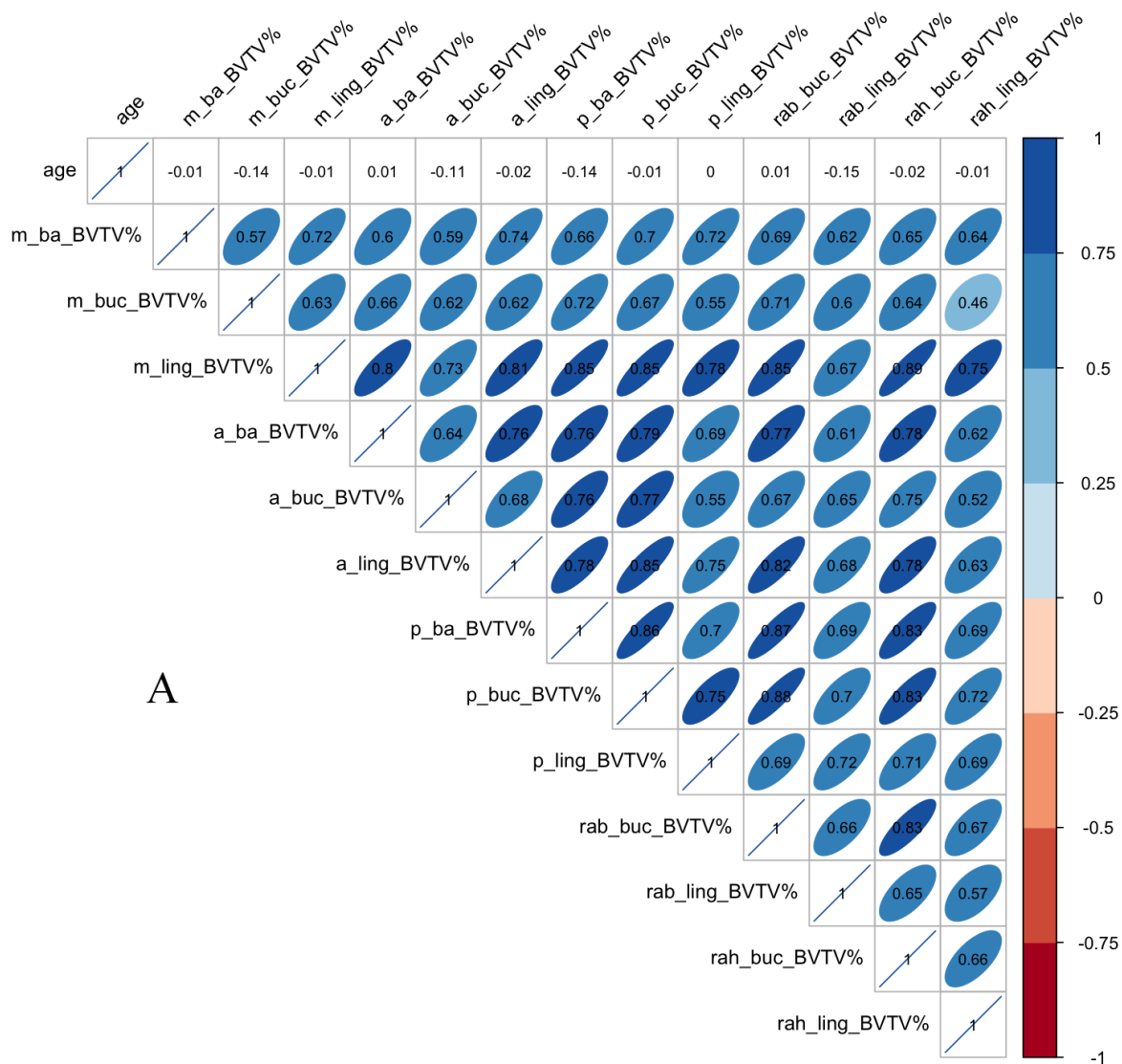
Figure 4.58. Corrplots illustrating inter-variable relationships between all the BV/TV values recorded in each dentition category (A, B, C). Ellipses were removed if the correlation, adjusted with Holm's correction, was not significant ($p > 0.05$). Correlation coefficients ρ were noted within each ellipse (in blue: positive ρ, in red: negative ρ). (continued on next page)
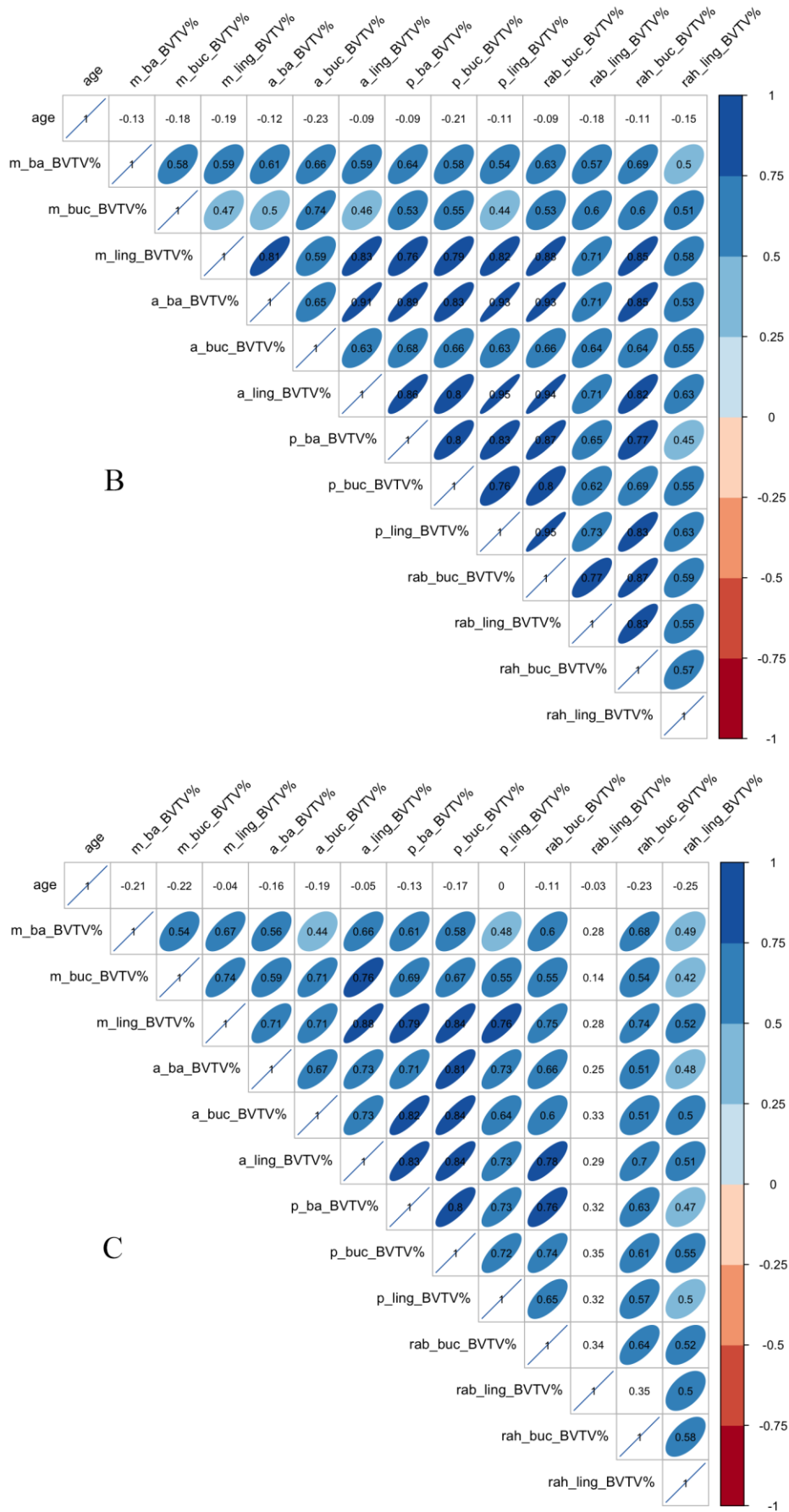
Figure 4.58. (continued)

4.5.5. Influence of aging

4.5.5.1. Correlations per VOI

Influence of advancing age was assessed first through Spearman's correlations, adjusted for multiple comparisons using Holm's corrections. The correlations (Figure 4.59) were calculated against age for each VOI recorded in the entire sample, in the sex and ancestral groups, as well as in each sex/ancestral subsample and dentition category. Within the entire sample (Figure 4.59, first row), nine VOIs displayed significant negative correlations with advancing age – with weak coefficients ($-0.18 < \rho < -0.25$). Of these nine VOIs, six were on the mandibular body (m_ba, m_buc, a_ba, a_buc, p_ba, p_buc) and three on the ramus (rab_ling, rah_buc, rah_ling). It is interesting to note that, of these six significant body VOIs, none was on the lingual side. Except for males, all the other subgroups did not show any significant correlation between any of the 13 BV/TV VOIs and advancing age. In males, however, eight significant correlations were found for almost the same locations as in the entire sample: m_ba, m_buc, a_ba, a_buc, p_buc. The correlation coefficients, still negative, were also similar: $-0.24 < \rho < -0.28$.

		m_ba_BVTV	m_buc_BVTV	m_ling_BVTV	a_ba_BVTV	a_buc_BVTV	a_ling_BVTV	p_ba_BVTV	p_buc_BVTV	p_ling_BVTV	rab_buc_BVTV	rab_ling_BVTV	rah_buc_BVTV	rah_ling_BVTV
	age	-0.2	-0.25	-0.13	-0.18	-0.25	-0.13	-0.19	-0.21	-0.11	-0.15	-0.25	-0.21	-0.21
F	age	-0.09	-0.22	-0.02	-0.03	-0.19	-0.08	-0.13	-0.15	-0.09	-0.16	-0.3	-0.13	-0.11
M	age	-0.27	-0.25	-0.18	-0.24	-0.28	-0.16	-0.21	-0.24	-0.12	-0.15	-0.23	-0.25	-0.28
AA	age	-0.14	-0.15	-0.08	-0.19	-0.23	-0.09	-0.18	-0.16	-0.1	-0.1	-0.21	-0.12	-0.13
EA	age	-0.2	-0.26	-0.18	-0.12	-0.23	-0.15	-0.18	-0.23	-0.05	-0.21	-0.13	-0.29	-0.15
FAA	age	-0.11	-0.24	-0.04	-0.27	-0.32	-0.14	-0.17	-0.28	-0.19	-0.16	-0.2	-0.01	-0.13
FEA	age	-0.1	-0.12	0.05	0.21	-0.12	0	-0.07	-0.01	0.09	-0.16	-0.24	-0.18	0
MAA	age	-0.16	-0.11	-0.09	-0.15	-0.19	-0.06	-0.17	-0.12	-0.05	-0.08	-0.2	-0.16	-0.13
MEA	age	-0.28	-0.32	-0.35	-0.34	-0.33	-0.25	-0.23	-0.43	-0.14	-0.25	-0.08	-0.36	-0.33
A	age	-0.01	-0.14	-0.01	0.01	-0.11	-0.02	-0.14	-0.01	0	0.01	-0.15	-0.02	-0.01
B	age	-0.13	-0.18	-0.19	-0.12	-0.23	-0.09	-0.09	-0.21	-0.11	-0.09	-0.18	-0.11	-0.15
C	age	-0.21	-0.22	-0.04	-0.16	-0.19	-0.05	-0.13	-0.17	0	-0.11	-0.03	-0.23	-0.25

Figure 4.59. Corrplots illustrating correlations between each BV/TV and age in the entire sample (first row), in demographic subsamples and finally in the three dentition categories (A, B, C). Ellipses were removed if the correlation, adjusted with Holm's correction, was not significant (p > 0.05). Correlation coefficients ρ were noted within each square (in blue: positive ρ, in red: negative ρ).

4.5.5.2. Correlations with pooled BV/TV values

The presence of strong inter-variable correlations and very few statistically significant differences between the VOIs suggested a generalised cortical density in the whole mandibular corpus (but not between corpus and ramus). Therefore, using Spearman's correlations, the influence of advancing age was assessed with pooled cortical bone density values, i.e., with a mean BV/TV value for each individual – calculated with all the corpus VOI values but not the ramus VOIs. The correlations, presented in Table 4.7 (p-values and ρ correlation coefficients)

were performed in the entire sample, in the sex- and ancestry-separated groups, as well as in each sex/ancestral subsample. Dentition categories were also considered.

The entire sample, the sex-separated subsamples and the ancestry-separated subsamples were all significantly and negatively correlated with advancing age (p-values < 0.001 in the entire sample, in F, M and EA; p-value < 0.01 in AA). However, the correlation coefficients computed were rather moderate for all these groups: $\rho = -0.35$ in the entire sample and in females, $\rho = -0.34$ in males, $\rho = -0.38$ in EA, $\rho = -0.22$ in AA. Significant correlations with age were also observed in each of the four sex/ancestral subgroups. The correlation coefficients were quite similar to those obtained previously: weak to moderate (MEA: $\rho = -0.38$, FAA: $\rho = -0.34$, FEA: $\rho = -0.32$), particularly for MAA ($\rho = -0.18$). The three dentition categories (A, B, C) also showed significant correlations with aging (p-value < 0.05 in A, p-values < 0.01 in B and C) while the correlation coefficients calculated were quite weak: A: $\rho = -0.21$, B: $\rho = -0.34$ and C: $\rho = -0.27$.

When the influence of aging was assessed within sex or ancestral groups while considering tooth loss, only five of the 12 subgroups had a significant correlation between BV/TV and age: females from category B (with a moderate correlation coefficient $\rho = -0.44$), males from categories B and C ($\rho = -0.27$ and -0.28), as well as EA individuals from categories B and C ($\rho = -0.65$ and -0.27). As expected from the 12 sex/ancestral subgroups associated with tooth loss categories (such as FAA-A, FAA-B, FAA-C…), only two correlations were significant, namely MEA individuals of categories B and C, with a stronger ρ coefficient in B ($\rho = -0.61$) than in C ($\rho = -0.29$).

Table 4.7. Spearman's correlation tests (*p*-values, *ρ* correlation coefficients) between pooled BV/TV (%) and age (years) in the entire sample and in all the subsamples (i.e., separated per sex, ancestry, sex/ancestry, dentition categories in the first column; sex and dentition, ancestry and dentition in the second column; sex/ancestry and dentition in the last column). Significant *p*-values are in bold, correlation coefficients associated with significant *p*-values are in black.

		Correlations	
		p-value	*ρ*
	Total	**7.68E-11**	-0.35
Sex	**F**	**2.82E-04**	-0.35
Sex	**M**	**1.04E-07**	-0.34
Ancestry	**AA**	**0.002**	-0.22
Ancestry	**EA**	**1.57E-05**	-0.38
Sex/ancestry	**FAA**	**0.010**	-0.34
Sex/ancestry	**FEA**	**0.028**	-0.32
Sex/ancestry	**MAA**	**0.026**	-0.18
Sex/ancestry	**MEA**	**0.001**	-0.38
Dentition	**A**	**0.024**	-0.21
Dentition	**B**	**0.001**	-0.34
Dentition	**C**	**0.003**	-0.27

		Correlations	
		p-value	*ρ*
Sex & dentition	**F-A**	0.15	-0.26
Sex & dentition	**F-B**	**0.01**	-0.44
Sex & dentition	**F-C**	0.22	-0.21
Sex & dentition	**M-A**	0.09	-0.19
Sex & dentition	**M-B**	**0.03**	-0.27
Sex & dentition	**M-C**	**0.01**	-0.28
Ancestry & dentition	**AA-A**	0.07	-0.19
Ancestry & dentition	**AA-B**	0.67	-0.06
Ancestry & dentition	**AA-C**	0.38	-0.12
Ancestry & dentition	**EA-A**	0.11	-0.43
Ancestry & dentition	**EA-B**	**7.64E-06**	-0.65
Ancestry & dentition	**EA-C**	**0.02**	-0.27

		Correlations	
		p-value	*ρ*
Sex/ancestry & dentition	**FAA-A**	0.11	-0.36
Sex/ancestry & dentition	**FAA-B**	0.24	-0.26
Sex/ancestry & dentition	**FAA-C**	0.95	-0.02
Sex/ancestry & dentition	**FEA-A**	0.28	-0.38
Sex/ancestry & dentition	**FEA-B**	0.12	-0.53
Sex/ancestry & dentition	**FEA-C**	0.24	-0.24
Sex/ancestry & dentition	**MAA-A**	0.19	-0.15
Sex/ancestry & dentition	**MAA-B**	0.57	-0.10
Sex/ancestry & dentition	**MAA-C**	0.38	-0.14
Sex/ancestry & dentition	**MEA-A**	0.39	-0.50
Sex/ancestry & dentition	**MEA-B**	**0.001**	-0.61
Sex/ancestry & dentition	**MEA-C**	**0.05**	-0.29

4.5.5.3. Regressions with pooled BV/TV values

Generalised linear models (GLMs) were applied on the pooled BV/TV, which was regressed in function of age. The regression (Figure 4.60) computed for the entire sample was significant ($p < 0.001$) and displayed a slow decrease in BV/TV with age, i.e., with a low coefficient of determination: $R^2 = 0.102$.

When performed in females and males separately (Figure 4.61 A), both regressions were significant with low coefficients of determination: $R^2 = 0.089$ and $R^2 = 0.105$. Both regression lines were adjacent and even sometimes overlapped, particularly in the younger ages. The difference between females and males was only accentuated in later ages of life (approximately from 60). As seen on the plot, the confidence interval also appeared to be wider in females than in males, especially in the younger or older ages. In the two ancestry-separated subsamples (Figure 4.61 B), both regressions were also significant, but compared to females and males, the differences were more pronounced from the beginning, and even more

particularly in the older ages. Both groups (AA, EA) showed a decrease in BV/TV with advancing age, but EA individuals specifically showed a faster decrease than in AA (EA R^2 = 0.105 vs. AA R^2 = 0.038).

In each of the four sex/ancestral subsamples (Figure 4.62), except for FAA who did not show significance, the regressions computed with aging displayed significant and similar decreasing patterns with weak determination coefficients (FEA R^2 = 0.101, MAA R^2 = 0.039 and MEA R^2 = 0.096). Even if they had similar and overlapping densities in the first decade (20 – 30), differences were more noticeable in older ages. Overall, MAA showed the highest BV/TV throughout the ages, followed by FAA and FEA, which overlapped. Interestingly, MEA displayed the lowest regression line, with particularly low BV/TV values for some individuals. The non-significance of the FAA subsample was most probably due to the lack of individuals in the older ages (none after 80).
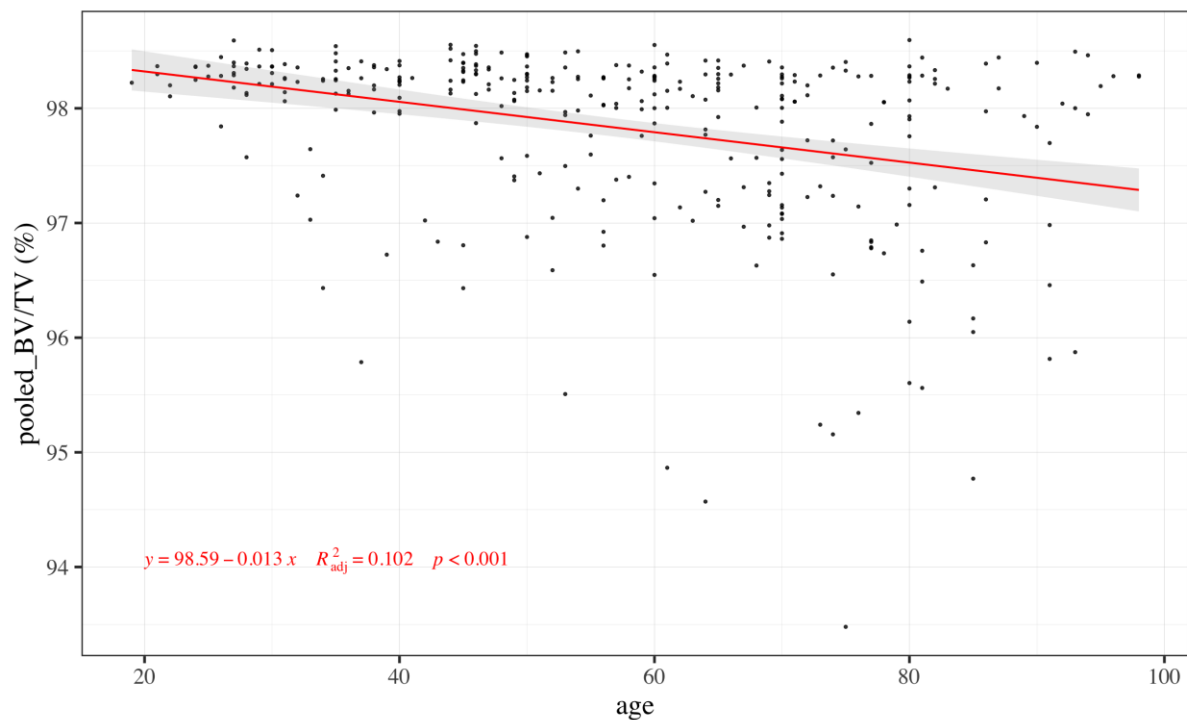
Figure 4.60. Generalised linear models (regressions) between the pooled BV/TV (%) and age (years) in the entire sample. Regression formulae and adjusted R-squared (R^2) values are provided with their respective *p*-values. The grey area represents the 95% confidence interval of each regression.
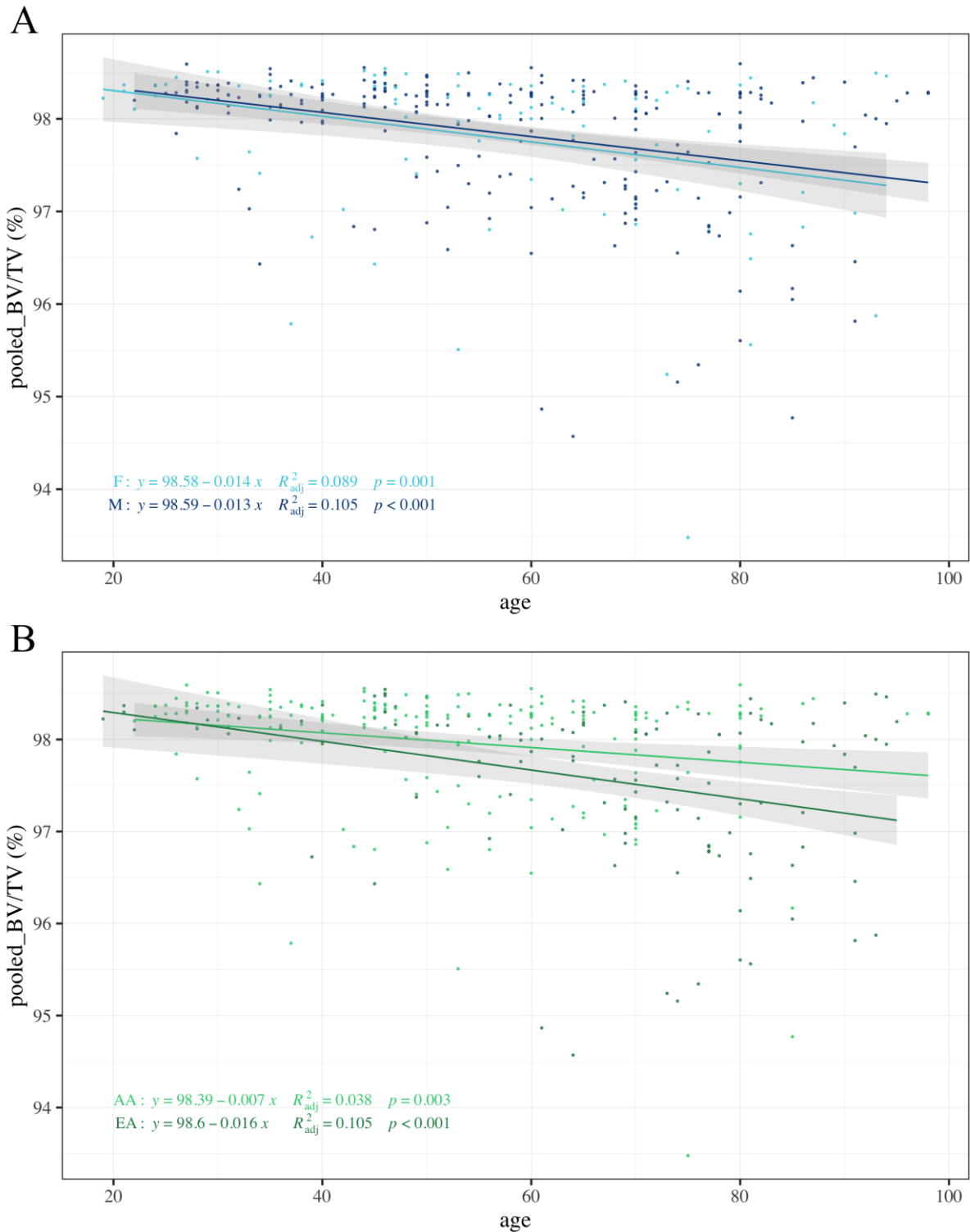
Figure 4.61. Generalised linear models (regressions) between the pooled BV/TV (%) and age (years) per sex [A] and per ancestral [B] subgroup. Regression formulae and adjusted R-squared (R^2) values are provided with their respective p-values. The grey area represents the 95% confidence interval of each regression.

A

FAA: $y = 98.57 - 0.014\,x$ $R^2_{adj} = 0.038$ $p = 0.08$
FEA: $y = 98.56 - 0.014\,x$ $R^2_{adj} = 0.101$ $p = 0.018$
MAA: $y = 98.37 - 0.007\,x$ $R^2_{adj} = 0.039$ $p = 0.008$
MEA: $y = 98.65 - 0.017\,x$ $R^2_{adj} = 0.096$ $p = 0.003$

B
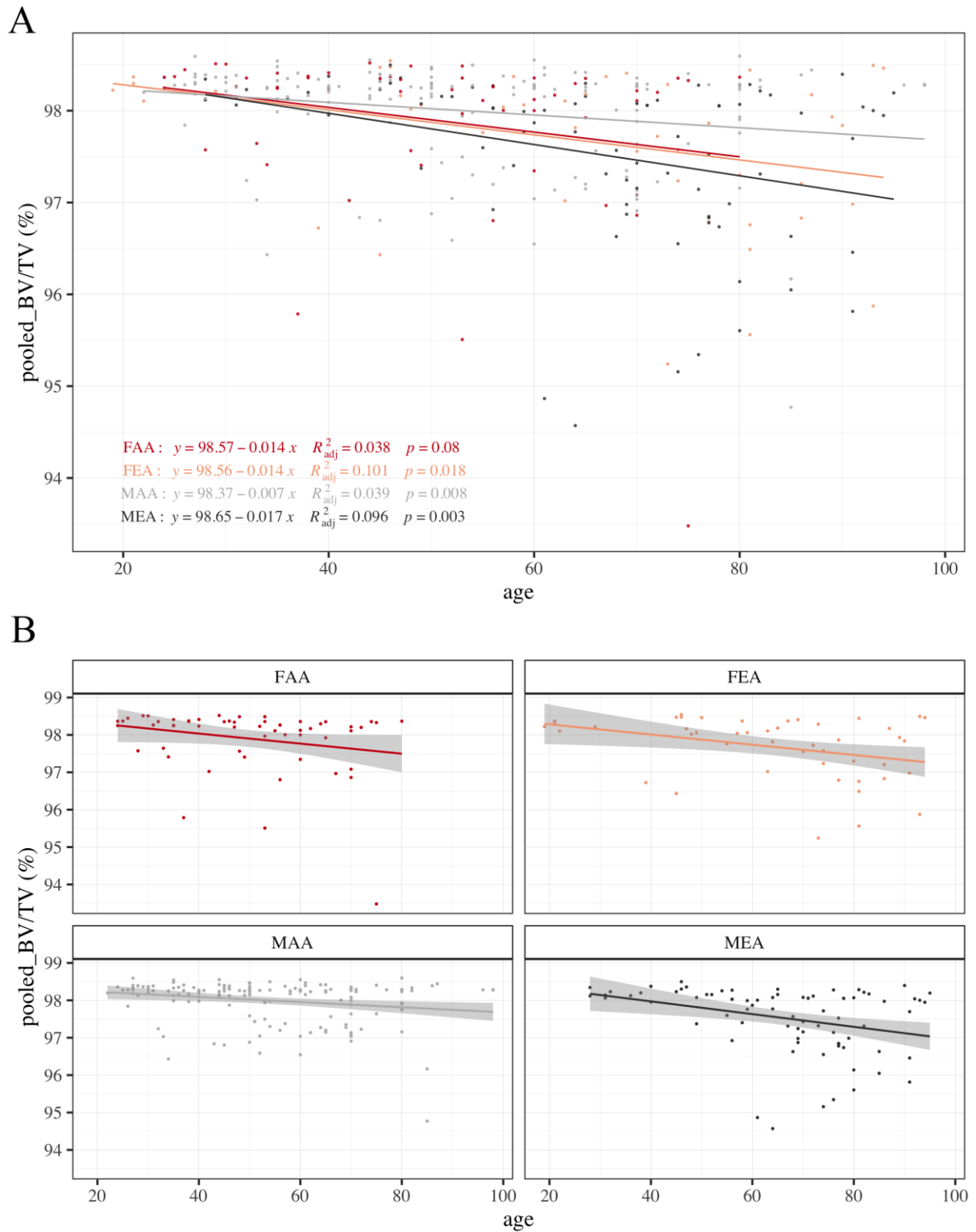
Figure 4.62. Generalised linear models (regressions) between the pooled BV/TV (%) and age (years) in all sex/ancestral subgroups [A] and faceted individually per subgroup [B]. Regression formulae and adjusted R-squared (R^2) values are provided with their respective *p*-values. The grey area represents the 95% confidence interval of each regression.

The regressions in each of the three dentition categories (Figure 4.63) also showed significantly decreasing BV/TV values with aging. Even if the coefficients of determination were again weak (A $R^2 = 0.039$, B $R^2 = 0.083$ and C $R^2 = 0.082$), it is still noticeable that the decrease was much more pronounced in categories C and B than in A.

$A : y = 98.41 - 0.008\,x \quad R^2_{adj} = 0.039 \quad p = 0.021$
$B : y = 98.63 - 0.017\,x \quad R^2_{adj} = 0.083 \quad p = 0.002$
$C : y = 98.69 - 0.014\,x \quad R^2_{adj} = 0.082 \quad p = 0.001$
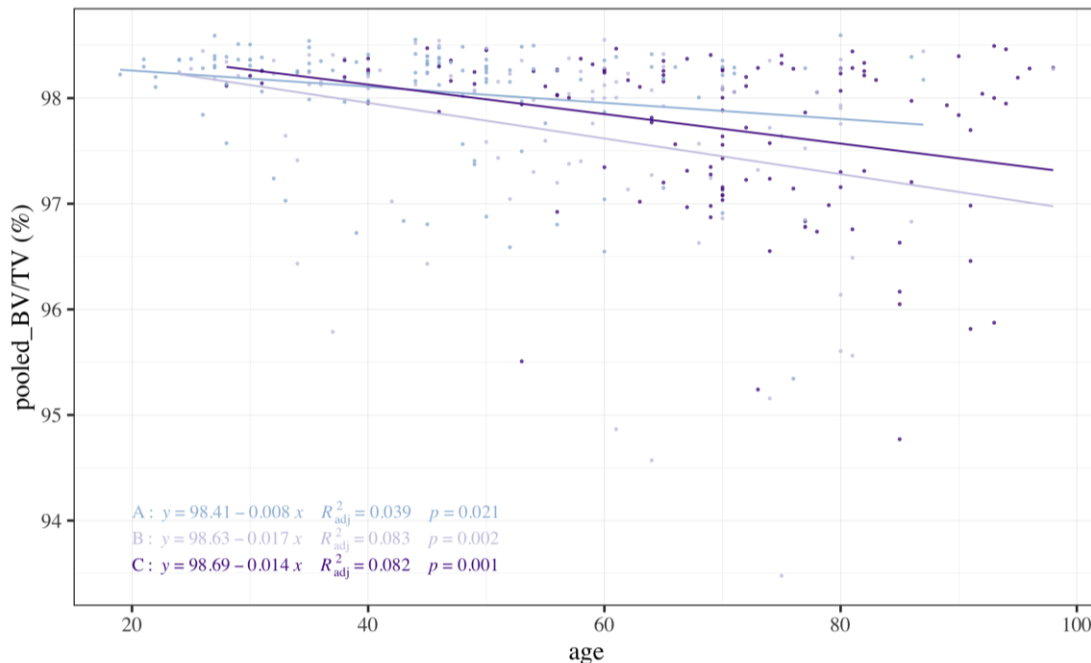
Figure 4.63. Generalised linear models (regressions) between the pooled BV/TV (%) and age (years) in the entire sample separated per dentition category (A, B, C). Regression formulae and adjusted R-squared (R^2) values are provided with their respective *p*-values.

Regressions were finally performed in each dentition category within females and males (Figure 4.64 A), and then within each ancestral subgroup (Figure 4.64 B). When looking at the sexes, only females with intermediate tooth loss (category B) and edentulous males (category C) had significant regression analyses. Even if the coefficients of determination were quite low (e.g., F-B $R^2 = 0.144$ and M-C $R^2 = 0.108$), it was still noticeable that the slopes in B and C were more accentuated. In the subgroups separated per dentition and ancestry (e.g., AA-A, AA-B … in Figure 4.64 B), only two displayed significant regression *p*-values (*p* < 0.01): EA with intermediate tooth loss (category B – $R^2 = 0.235$) or completely edentulous (category C – $R^2 = 0.085$). When looking at the sex/ancestral subgroups separated by dentition categories (Figure 4.64 C), only four regressions with age were found significant: FEA and MEA individuals with intermediate tooth loss, as well as edentulous MAA and MEA – all decreasing with age.

237
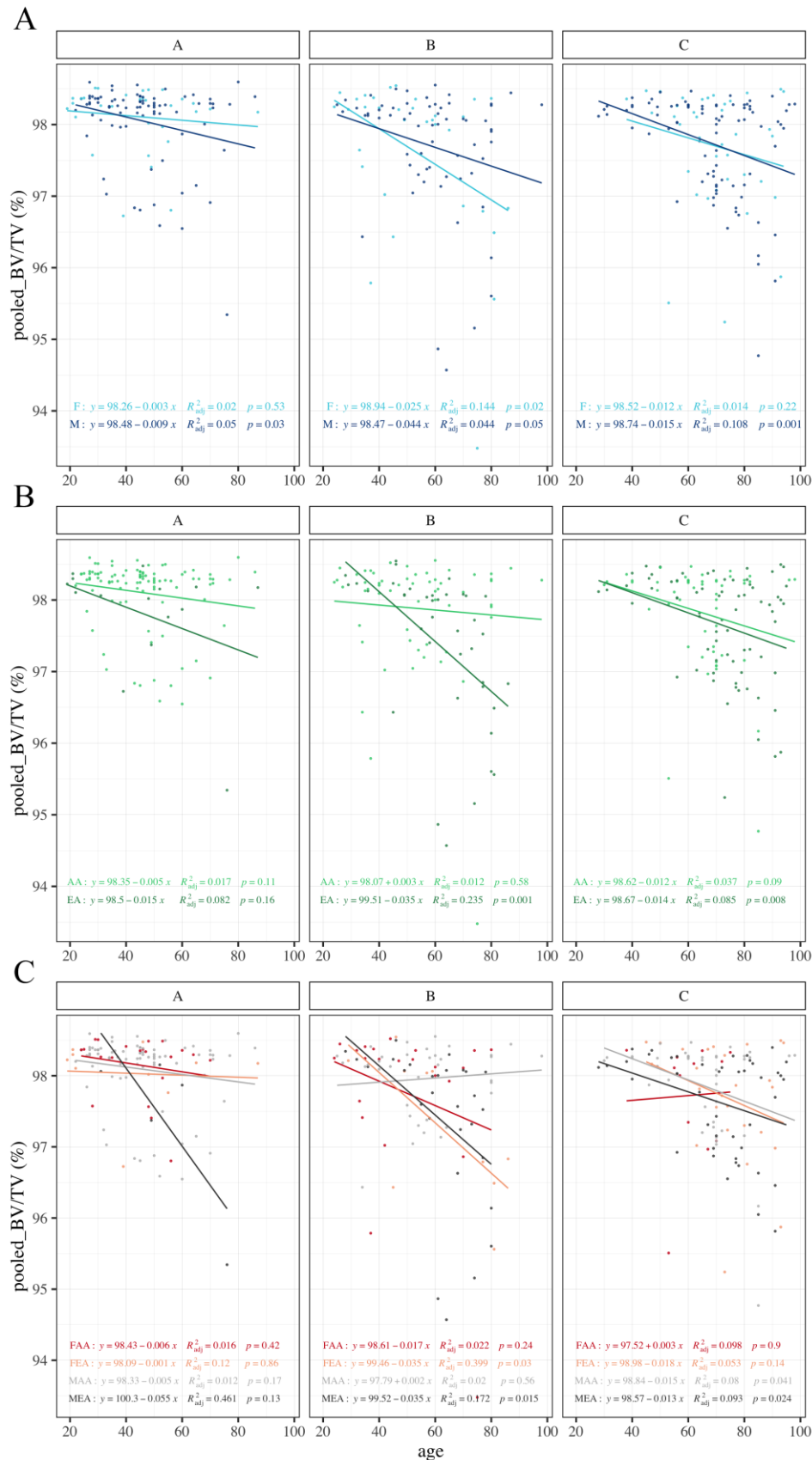
Figure 4.64. Generalised linear models (regressions) between the pooled BV/TV (%) and age (years) in each dentition category (A, B, C), per sex (F, M) [A], per ancestry (AA, EA) [B] and per sex/ancestry (FAA, FEA, MAA, MEA) [C]. Regression formulae and adjusted R-squared (R^2) values are provided with their respective *p*-values.

4.5.6. Summary – Cortical density

Cortical densities were assessed through BV/TV parameters, measured in 13 cortical volumes of interest. Differences between sexes were noted but were not clear. Differences in ancestries were also noticed, as BV/TV parameters were always greater in AA than in EA (AA > EA). When sex and ancestry were both considered, FAA always showed denser cortical densities than the other individuals, even if, FAA and FEA were never different from each other, while MAA and MEA often were.

When tooth loss was analysed, it was noted that loss of teeth, alone and even moderate, caused a decrease in cortical density in the majority of the VOIs (A > B ≥ C). As for the cortical thickness, the midline lingual sites showed a different pattern as no differences between all the dentition categories were detected.

The interaction between tooth loss and sex revealed unusual results about the cortical densities. As for the cortical thickness, sexual dimorphism was present in all three dentition categories, but differences between females and males were stronger in categories B and C than in A. As soon as tooth loss starts, the cortical bone density declines. When analysing females only, BV/TV parameters were not found to be affected by tooth loss: the three dentition categories gave similar results. In males, however, a decrease (A > B > C) was observed in most of the sites, with A and B significantly different in most of the cases, emphasising the fact that even moderate tooth loss caused a decrease in density. The cortical density in the midline lingual VOI was always different between males and females, across all three dentition categories (even A), but was, however, again, not different between the three categories.

When tooth loss was investigated with ancestry, two strong patterns emerged, one for each ancestral group: in AA, half of the VOIs showed a decrease with tooth loss (only with total tooth loss, and not moderate); while in EA, no significance was found at all. However, on the plots, a decrease could still be perceived from A to C and spreading of the values was particularly large in C that it could have caused the non-significance. As with sex, the cortical density in the midline lingual VOI was not affected by tooth loss (no differences between A, B and C) in AA or EA.

Locations of the VOIs were also studied, confirming that the midline section was acting differently than the other sections, and especially more unpredictably compared to the rest of the mandible. Overall, cortical BV/TV parameters were more generalised and homogeneous all over the corpus and even in the ramus (no significant differences between anterior, posterior

and ramus), particularly in comparison to the cortical thicknesses. However, with edentulism, even if the density remains similar in the corpus, it loses its correlation with ramus bone density. The intensive bone remodelling occurring in the corpus because of the complete loss of teeth causes changes that the ramus is not following. The general integrity of the cortical bone density was influenced by sex and ancestry, as it was greater in males (stronger and more frequent correlations) than in females, and in AA than in EA.

Lastly, the influence of age was investigated and showed decreasing densities with increasing age in all individuals and samples (sex, ancestry, tooth loss), with rather moderate coefficients, in contrast to the cortical thicknesses. Even if females tended to have larger confidence intervals, females and males initially, in the younger ages, have an overlapped decrease in BV/TV associated with aging, while later (especially after 40 years of age), the diminution was much faster in females. Compared to AA, EA also displayed a faster decrease in BV/TV, particularly intense after 40 years of age. In sex/ancestral samples, MAA presented the highest cortical densities, with less decrease with age, relative to FAA and FEA (overlapped), and particularly MEA. The differences between the sexes in the different ancestral groups appeared to be accentuated/aggravated in the later ages of life, approximately from 40 years of age.

Once the dentition categories were included in the regression models, it was noteworthy to see that the decrease related to aging noticed earlier, was occurring in all individuals, whether they were affected by tooth loss or not. The decline was, however, surprisingly more important in category B than C.

Chapter 5. Results: Micro-CT analysis of the femur and comparison with the mandible

Micro-CT scanning was performed on 68 femora (proximal parts only), from which 64 individuals were selected for further analysis, as explained in the Materials and Methods (Chapter 3). The sample was constituted of 37 males and 27 females aged between 21 and 98 years (mean age = 58.48 years). For each individual, four cortical densities were recorded in Volumes of Interest (VOIs) located at the inferior (i_BV/TV), superior (s_BV/TV), anterior (a_BV/TV) and posterior (p_BV/TV) sites of the femoral neck section, defined in the Methods section [3.2].

First, in [5.1], the femoral sample was analysed alone to assess the possible influence of demographic parameters or location of the VOIs on the densities. Then, in [5.2], comparisons between femoral and mandibular parameters of the same individuals were performed while controlling for sex, ancestry and age.

5.1. Femoral sample

5.1.1. Assumption testing

Kernel density plots, followed by Shapiro-Wilk tests, were performed to illustrate the shape of the distribution of each variable (age and cortical densities) and are all presented in Appendix F. Finally, variance comparison tests were run.

5.1.1.1. Normality of distributions

Distribution of the individuals' age in the femoral sample (Appendix F Figure F.) was plotted for the entire sample. The Shapiro-Wilk test confirmed that age of the individuals in this sample was not following a normal distribution. As in the mandible, the cortical bone densities were not normally distributed in any of the four sites in the entire sample as well as within the different demographic subgroups (Appendix F Figure F.).

5.1.1.2. Homogeneity of variances

Homogeneity of the variances was then tested for the variables recorded. Histomorphometric parameters showed homoscedasticity (i.e., equal variances) at some sites between sexes and between ancestries, but no consistency was detected.

5.1.1.3. Conclusion

Finally, non-parametric statistical tests were selected for the analysis of the cortical densities, according to the presence of several sites not following a normal distribution or not presenting equal variances, without consistency.

5.1.2. Histomorphometric parameters (cortical BV/TV)

5.1.2.1. Basic descriptive statistics

Descriptive statistics, such as means, standard deviations, minimum and maximum values, were calculated and are detailed below for the entire femoral sample, the subsamples and within the four sex/ancestral subgroups (FAA, FEA, MAA, MEA), and are detailed in Table 5.1. As the density values were all very similar, differences were not clearly noticeable. However, the highest mean cortical densities were always recorded in female individuals and were often accompanied by the highest minimal values (inferior, superior and posterior sites). Furthermore, the lowest mean cortical BV/TV was measured in MEA (e.g., mean s_BV/TV = 90.12%, range: 80.77 – 94.43%).

In terms of differences between sites (inferior, superior, anterior, posterior), the inferior cortical densities (i_BV/TV) showed the highest mean density values in the entire pooled sample, as well as in FEA, MAA and MEA. On the contrary, the lowest minimal values were recorded in the superior sites in FEA, MAA and MEA. The age distribution of the sample could explain the low histomorphometric values, recorded in MEA. Indeed, the mean age of the MEA subgroup is much higher than in the three other subsamples, i.e., MEA: 71.00 years (range: 28 – 94 years); MAA: 57.00 years (range: 26 – 98 years); FEA: 58 years (range: 21 – 91 years); FAA: 44.92 years (range: 22 – 71 years).

Table 5.1. Descriptive statistics of the femoral cortical bone densities (BV/TV, %) recorded on micro-CT scans at the inferior (i_BV/TV), superior (s_BV/TV), anterior (a_BV/TV) and posterior (p_BV/TV) sites of the femoral neck.

| | Total | Sex | | Ancestry | | Sex/ancestry | | | |
| | | F | M | AA | EA | FAA | FEA | MAA | MEA |
	n = 64	n = 27	n = 37	n = 33	n = 31	n = 13	n = 14	n = 20	n = 17
i_BV/TV									
min – max	83.89 – 94.92	83.89 – 94.92	84.49 – 94.30	86.40 – 94.79	83.89 – 94.92	86.67 – 94.79	83.89 – 94.92	86.40 – 94.05	84.49 – 94.30
mean ± SD	91.13 ± 2.63	91.67 ± 2.80	90.73 ± 2.46	90.96 ± 2.34	91.31 ± 2.94	91.81 ± 2.53	91.54 ± 3.12	90.41 ± 2.08	91.12 ± 2.86
s_BV/TV									
min – max	80.51 – 95.12	80.51 – 95.12	80.77 – 94.43	83.89 – 95.11	80.51 – 94.55	88.54 – 95.12	80.51 – 94.55	83.89 – 93.59	80.77 – 94.43
mean ± SD	90.68 ± 3.04	91.32 ± 3.15	90.22 ± 2.91	90.91 ± 2.32	90.44 ± 3.68	91.92 ± 2.10	90.81 ± 3.84	90.30 ± 2.28	90.12 ± 3.62
a_BV/TV									
min – max	74.77 – 95.54	74.77 – 95.54	84.25 – 94.18	74.77 – 95.54	84.25 – 95.13	74.77 – 95.54	86.59 – 95.13	86.96 – 94.12	84.25 – 94.18
mean ± SD	90.52 ± 3.31	90.90 ± 4.24	90.25 ± 2.41	90.28 ± 3.61	90.79 ± 2.98	90.26 ± 5.48	91.49 ± 2.74	90.30 ± 1.71	90.19 ± 3.13
p_BV/TV									
min – max	85.18 – 94.71	86.11 – 94.71	85.18 – 94.47	85.18 – 94.71	87.19 – 94.47	86.11 – 94.71	87.76 – 94.45	85.18 – 94.27	87.19 – 94.47
mean ± SD	90.95 ± 2.53	91.49 ± 2.64	90.56 ± 2.41	90.85 ± 2.61	91.05 ± 2.48	91.68 ± 2.80	91.31 ± 2.57	90.31 ± 2.39	90.85 ± 2.47

5.1.2.2. Influence of sex and/or ancestry

The Mann-Whitney Wilcoxon tests performed between sexes (Figure 5.1), and then between ancestries (Figure 5.2), did not display any significant differences in any of the four VOIs. Moreover, the cortical bone densities did also not differ between any of the sex/ancestral subgroups (Figure 5.3).
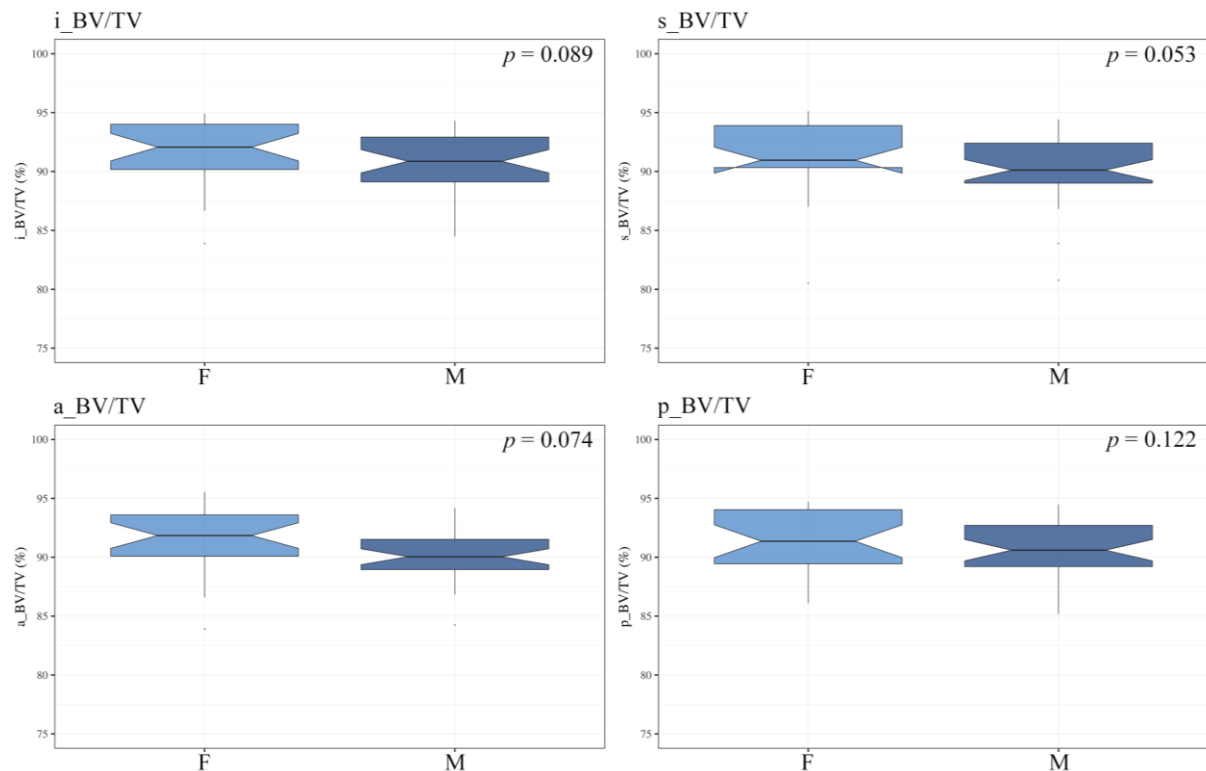
Figure 5.1. Boxplots of cortical BV/TV (%) per sex (F: light blue; M: dark blue), recorded in the inferior (i_BV/TV), superior (s_BV/TV), anterior (a_BV/TV) and posterior (p_BV/TV) femoral VOIs. Dots depict outliers. Mann-Whitney Wilcoxon p-values are indicated.
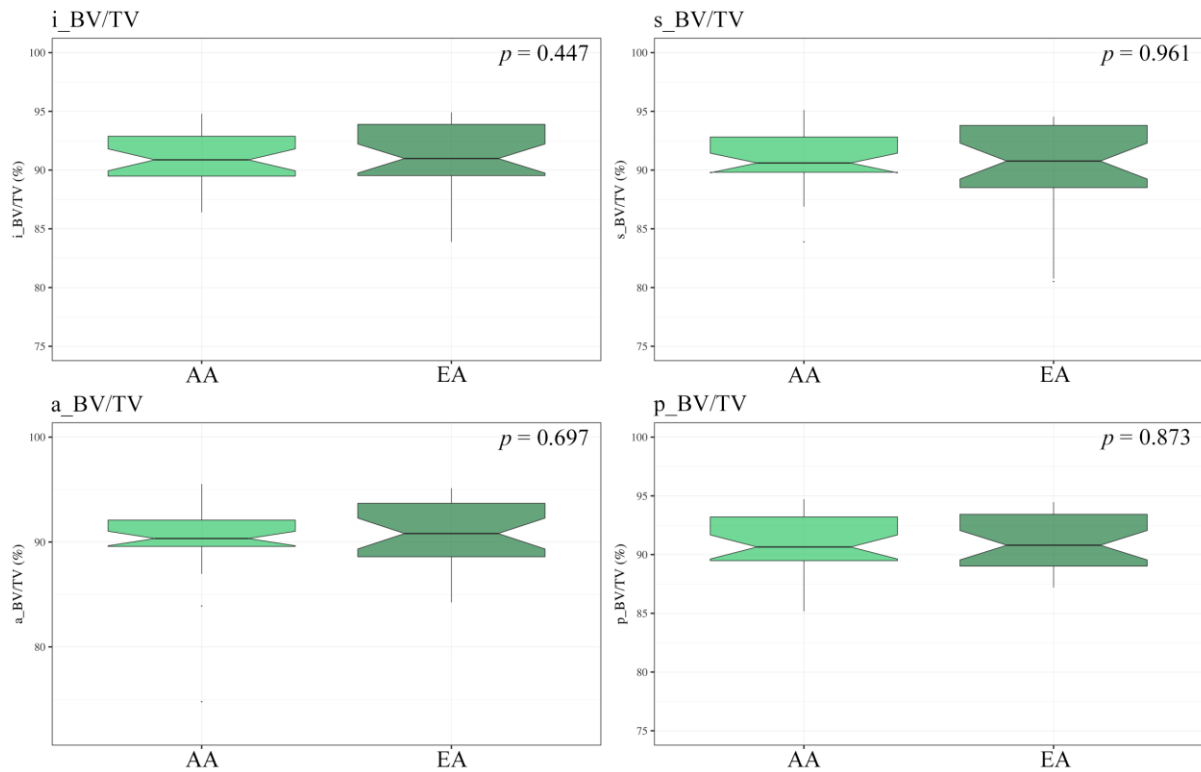
Figure 5.2. Boxplots of cortical femoral BV/TV (%) per ancestry (AA: light green; EA: dark green), recorded in the inferior (i_BV/TV), superior (s_BV/TV), anterior (a_BV/TV) and posterior (p_BV/TV) femoral VOIs. Dots depict outliers. Mann-Whitney Wilcoxon p-values are indicated.
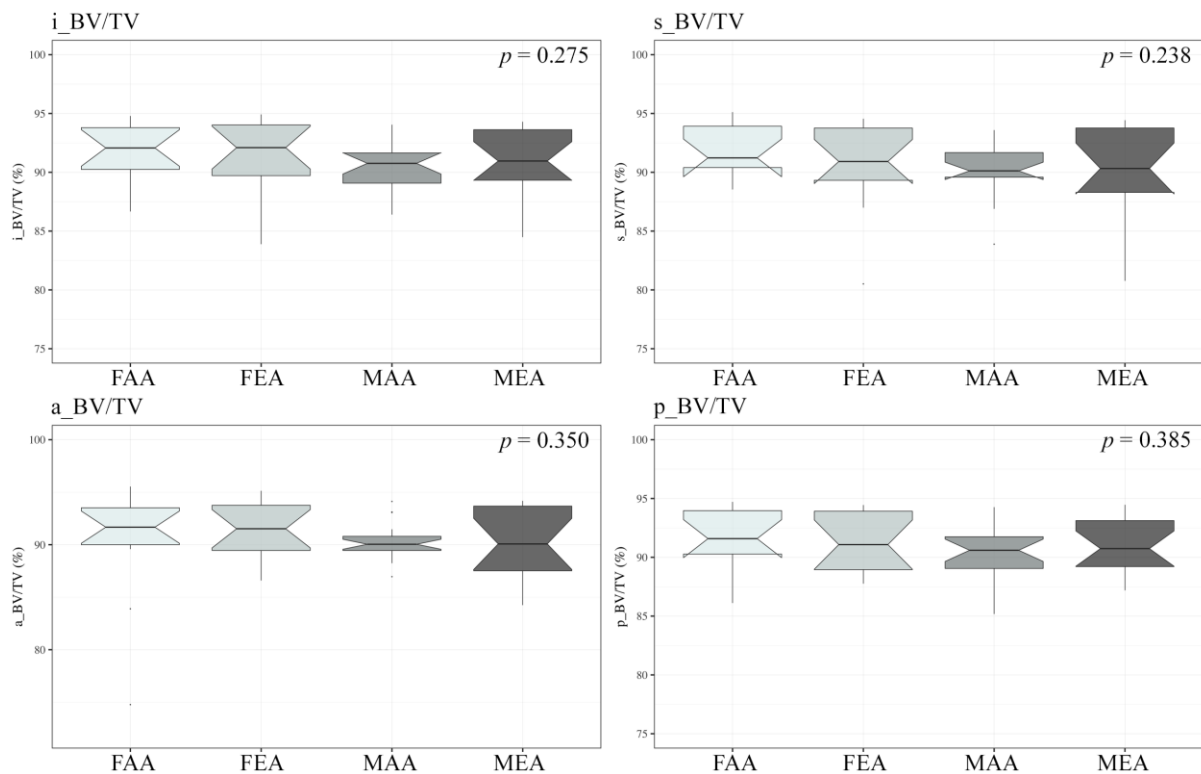
Figure 5.3. Boxplots of cortical BV/TV (%) per sex/ancestry (FAA, FEA, MAA, MEA: from light to dark grey) in the inferior (i_BV/TV), superior (s_BV/TV), anterior (a_BV/TV) and posterior (p_BV/TV) femoral VOIs. Dots depict outliers. Kruskal-Wallis p-values are indicated.

245

5.1.2.3. Influence of VOI location

The four VOIs (inferior, superior, anterior, posterior) in which the histomorphometric parameters were recorded were compared between each other in the entire sample. The Kruskal-Wallis test performed on the densities did not show any significant differences between the four VOIs (Figure 5.4).
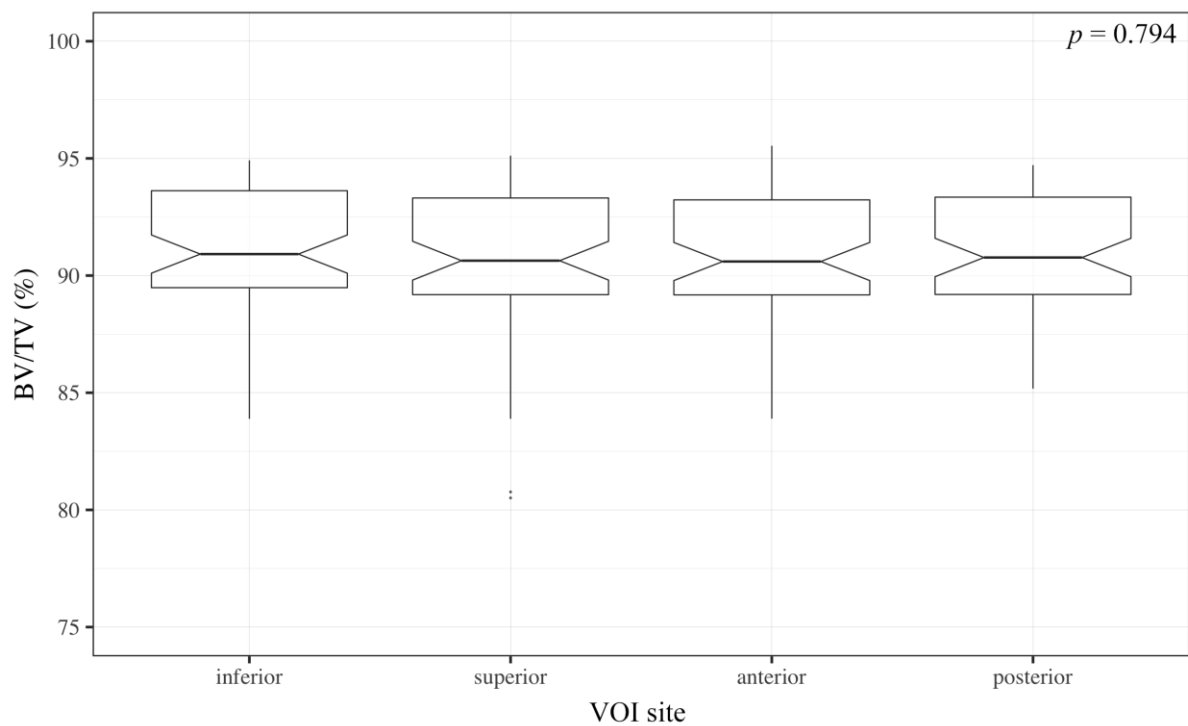
Figure 5.4. Boxplots of cortical BV/TV (%) grouped per VOI site (inferior vs. superior vs. anterior vs. posterior). Dots depict outliers. Kruskal-Wallis p-value is indicated.

5.2. Comparison between mandibular and femoral samples

Comparisons between the two bones were performed between the femoral sample described above, and between a specific mandibular subsample, instead of the entire sample used in the first part of the results in Chapter 4. This subsample was consisted of the same 64 individuals used for the femur, i.e., these individuals had measurements taken on their mandible and their femur.

In a previous section [5.1.2], the four femoral sites (inferior vs. superior vs. anterior vs. posterior), where the histomorphometric parameters were recorded, were compared and were not found to differ from each other. Furthermore, as done in the first part of the results focusing on the mandible (using the complete sample of 333 individuals, in Chapter 4), comparisons of the densities (i) between sections (midline vs. anterior vs. posterior); (ii) between sites (basal vs. buccal vs. lingual); (iii) and between the interaction of the two (e.g., midline basal vs. anterior buccal vs. posterior lingual etc.) were also performed on the smaller mandibular subsample used here. According to the three Kruskal-Wallis tests run, no significant differences were detected at all for any of the three conditions ($p = 0.25$ between sections, $p = 0.19$ between sites, $p = 0.42$ between sections/sites).

Therefore, for the subsequent analyses, cortical bone density values were pooled for the femur and for the mandible. Mean BV/TV values of the four sites of the femur were calculated for each individual, while for the mandible, the mean value of the nine VOI locations were calculated.

5.2.1. Comparison tests

As the cortical density measurements were taken on the mandible and the femur of the same individuals, a non-parametric paired-samples Wilcoxon test (also known as Wilcoxon signed-rank test) was performed. A statistically significant difference was detected between the mandibular and femoral histomorphometric parameters ($p < 0.001$). As illustrated by the boxplots in Figure 5.5, cortical bone density was significantly higher in the mandible than in the femoral neck for the same individuals. The spreading of values was also particularly wider in the femora (mean ± SD = 90.82 ± 2.38% and min – max = 86.43 – 94.74%) than in the mandible (mean ± SD = 97.67 ± 0.90% and min – max BV/TV = 94.57 – 98.51%).
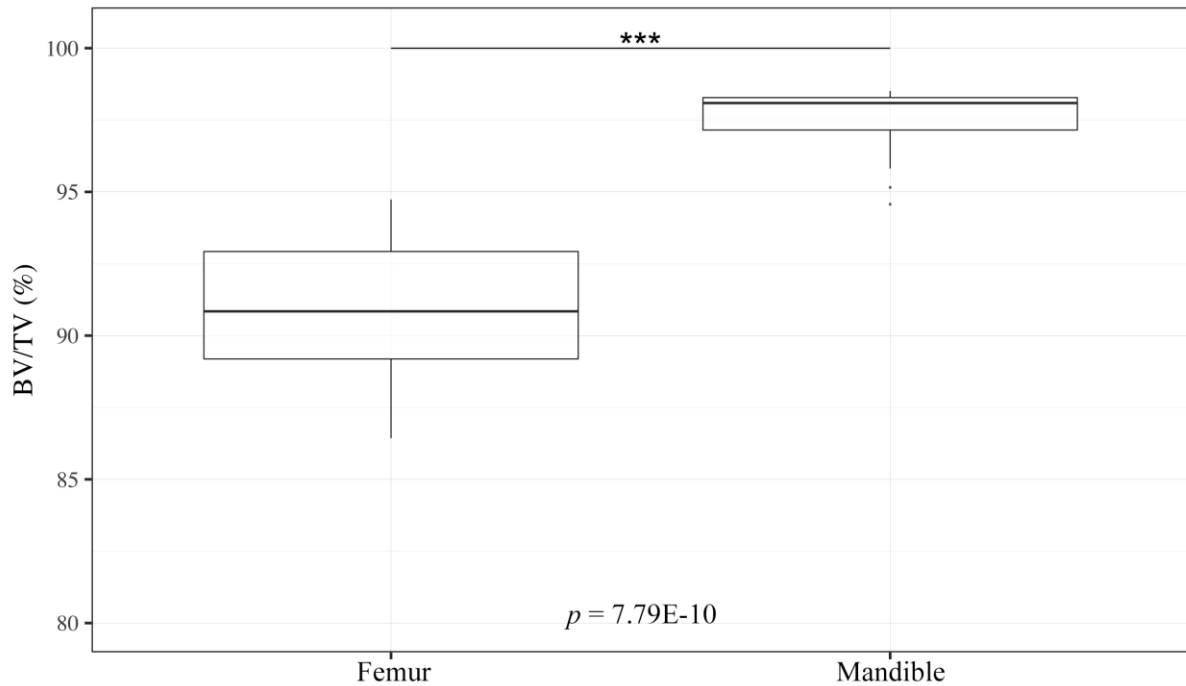
Figure 5.5. Boxplots of cortical BV/TV (%) recorded in the femoral and in the mandibular subsamples. Dots depict outliers. Paired Wilcoxon test *p*-value is indicated. Significance: *** $p <$ 0.001.

Paired Wilcoxon tests were also run on the subsamples separated per sex (Figure 5.6). Within males as well as within females, significant differences ($p < 0.001$) were found between femoral and mandibular densities, with higher cortical densities in the mandible (M mean ± SD = 97.61 ± 1.02% and F mean ± SD= 97.84 ± 0.61%) than in the femur (M mean ± SD = 90.44 ± 2.10% and F mean ± SD= 91.35 ± 2.67%).

The paired Wilcoxon tests were then performed on the subsamples separated per ancestry (Figure 5.7) for which significant differences were found between femoral and mandibular densities in both AA and EA individuals ($p < 0.001$). As before, greater cortical density values were measured in the mandible (AA mean ± SD = 98.06 ± 0.50% and EA mean ± SD = 97.25 ± 1.07%) than in the femur (AA mean ± SD = 90.76 ± 2.21 vs. EA mean ± SD = 90.89 ± 2.58).
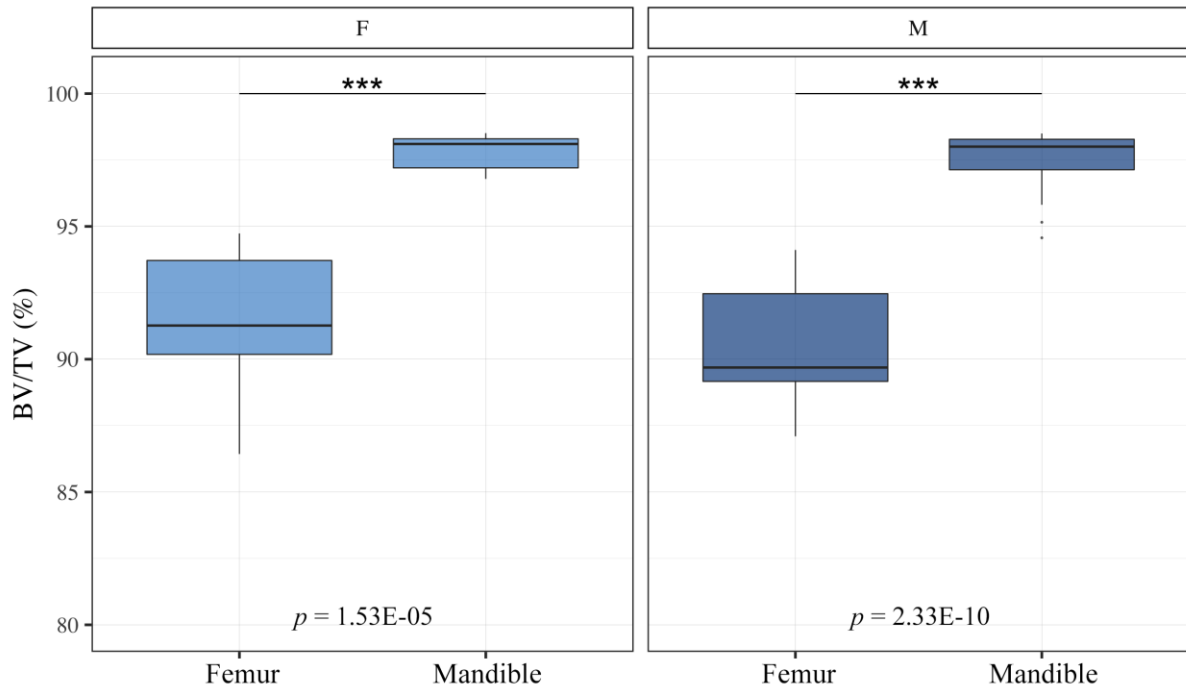
Figure 5.6. Boxplots of cortical BV/TV (%) per sex (F: light blue; M: dark blue), recorded in the femoral and mandibular samples. Dots depict outliers. Paired Wilcoxon tests p-values are indicated. Significance: *** $p < 0.001$.
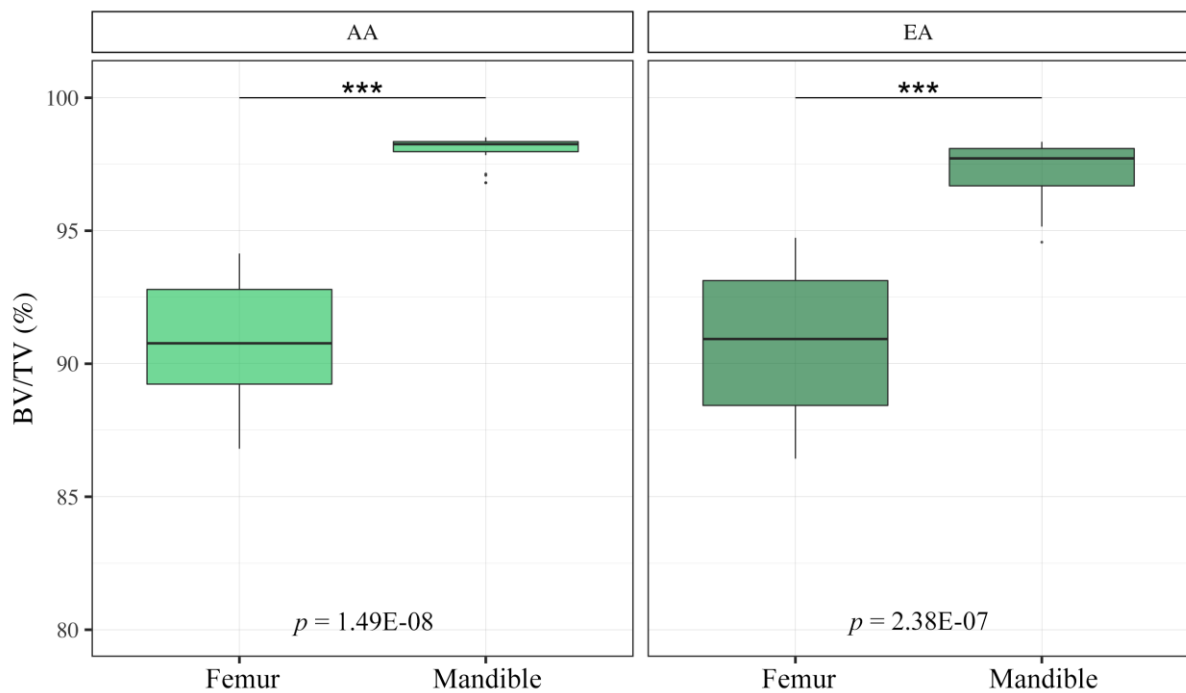
Figure 5.7. Boxplots of cortical BV/TV (%) per ancestry (AA: light green; EA: dark green), recorded in the femoral and mandibular samples. Dots depict outliers. Paired Wilcoxon tests p-values are indicated. Significance: *** $p < 0.001$.

249

Finally, similar tests between femoral and mandibular densities were run within each sex/ancestry and are illustrated in Figure 5.8. As within both sexes and both ancestries, significant differences between femoral and mandibular cortical bone densities were detected within each of the four subgroups ($p < 0.01$ in FAA and FEA, $p < 0.001$ in MAA and MEA), with always greater mean BV/TV in the mandible than in the femur. A pattern regarding the range of BV/TV values was also noticed in all the groups: a wide range of values in one bone was associated with a wide range in the other bone or vice versa. MAA, for example, displayed a restricted range of BV/TV values in the mandible and the femur, while in MEA, wide ranges were detected in both mandible and femur.
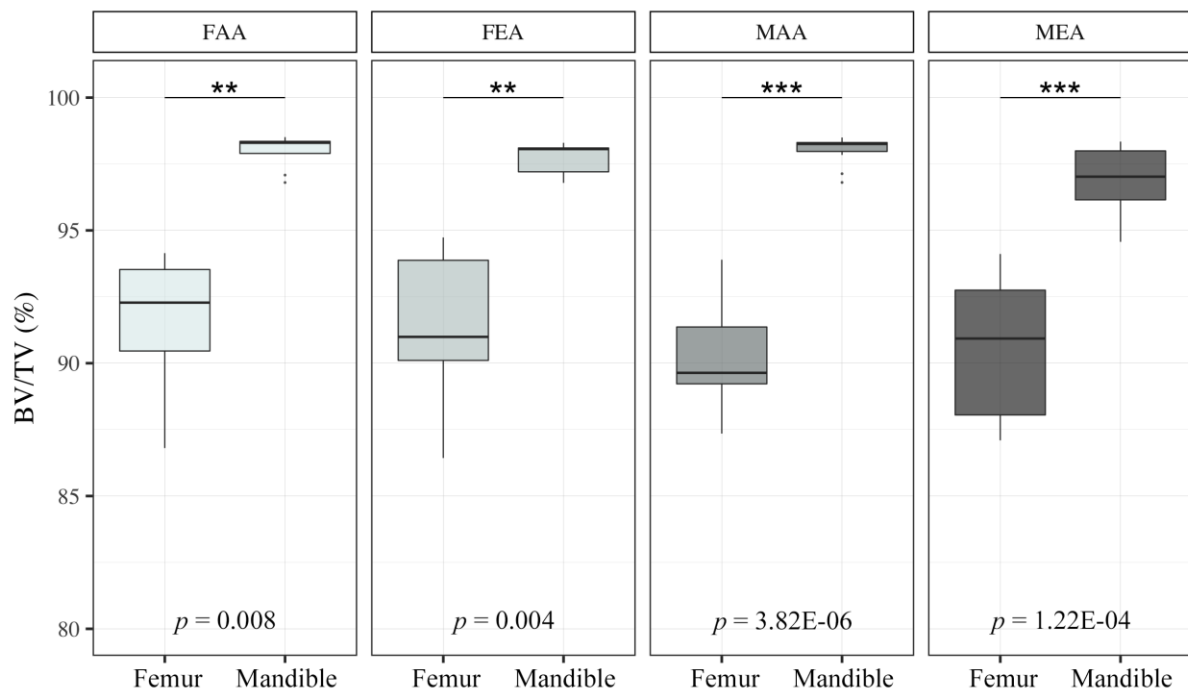
Figure 5.8. Boxplots of cortical BV/TV (%) per sex/ancestry (FAA, FEA, MAA, MEA: from light to dark grey) recorded in the femoral and mandibular samples. Dots depict outliers. Paired Wilcoxon tests p-value are indicated at the bottom of each plot. Significance: *** $p < 0.001$, ** $p < 0.01$.

5.2.2. Correlations and regressions

5.2.2.1. Between femoral and mandibular cortical densities

First, the possible correlation between the two paired samples (mandible vs. femur) was assessed using Spearman's correlation tests. No significant correlations (Table 5.2) were detected in the entire sample nor any of the subsamples (within each sex, ancestry, sex/ancestry). Therefore, cortical densities recorded in the mandible do not appear to be correlated with the cortical densities recorded in the femur.

Table 5.2. Spearman's correlation tests (p-values, ρ correlation coefficients) and generalised linear models (p-values and adjusted R^2 regression coefficients) performed between mandibular and femoral cortical BV/TV (%). Significant p-values are in bold.

	Correlations		Regressions	
	p-value	ρ	p-value	R^2_{adj}
Total	0.73	-0.051	0.80	-0.019
F	0.29	-0.270	0.09	0.125
M	0.72	0.065	0.64	-0.025
AA	0.17	-0.274	0.29	0.006
EA	0.49	0.151	0.88	-0.046
FAA	0.15	-0.571	0.11	0.264
FEA	0.98	-0.017	1.00	-0.083
MAA	0.70	-0.095	0.37	-0.009
MEA	0.65	0.134	0.86	-0.081

To go further, generalised linear models (GLMs) were computed between the mandibular and femoral BV/TV in the complete sample and within the subsamples. GLM p-values and adjusted coefficients of regression (R^2_{adj}) are detailed in Table 5.2. None of the regressions performed was found significant, i.e., the femoral cortical bone density is not increasing or decreasing even if the mandibular cortical bone density is, and reciprocally (see Figure 5.9).
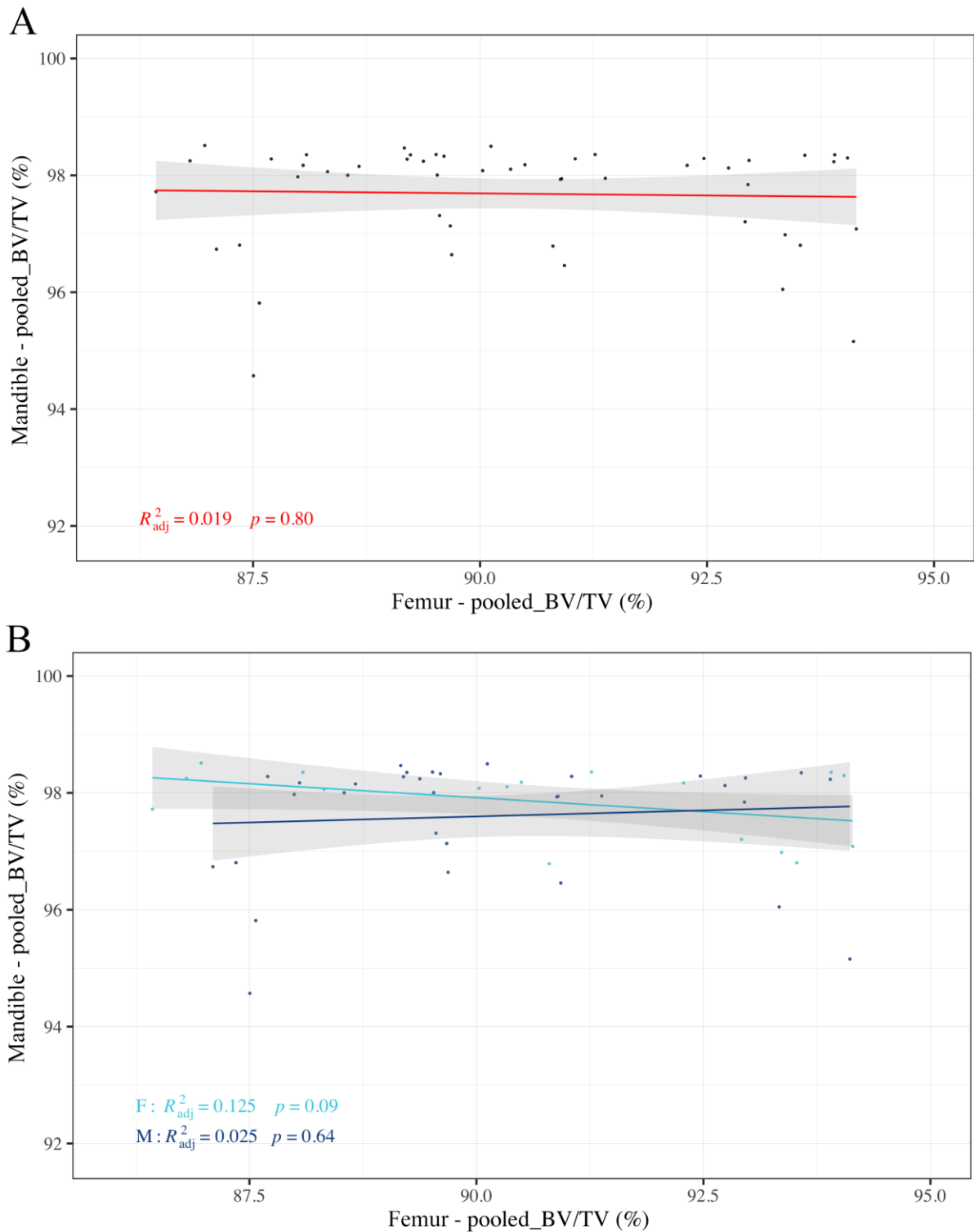
Figure 5.9. Generalised linear models (regressions) between mandibular and femoral cortical BV/TV (%) in the entire sample [A], per sex [B], per ancestry [C] and per sex/ancestry [D]. Grey area represents the 95% confidence interval of each regression. (continued on the next page)

252

C

$$AA: R^2_{adj} = 0.006 \quad p = 0.29$$
$$EA: R^2_{adj} = 0.046 \quad p = 0.88$$

D

$$FAA: R^2_{adj} = 0.264 \quad p = 0.11$$
$$FEA: R^2_{adj} = 0.083 \quad p = 1.00$$
$$MAA: R^2_{adj} = 0.009 \quad p = 0.37$$
$$MEA: R^2_{adj} = 0.081 \quad p = 0.86$$
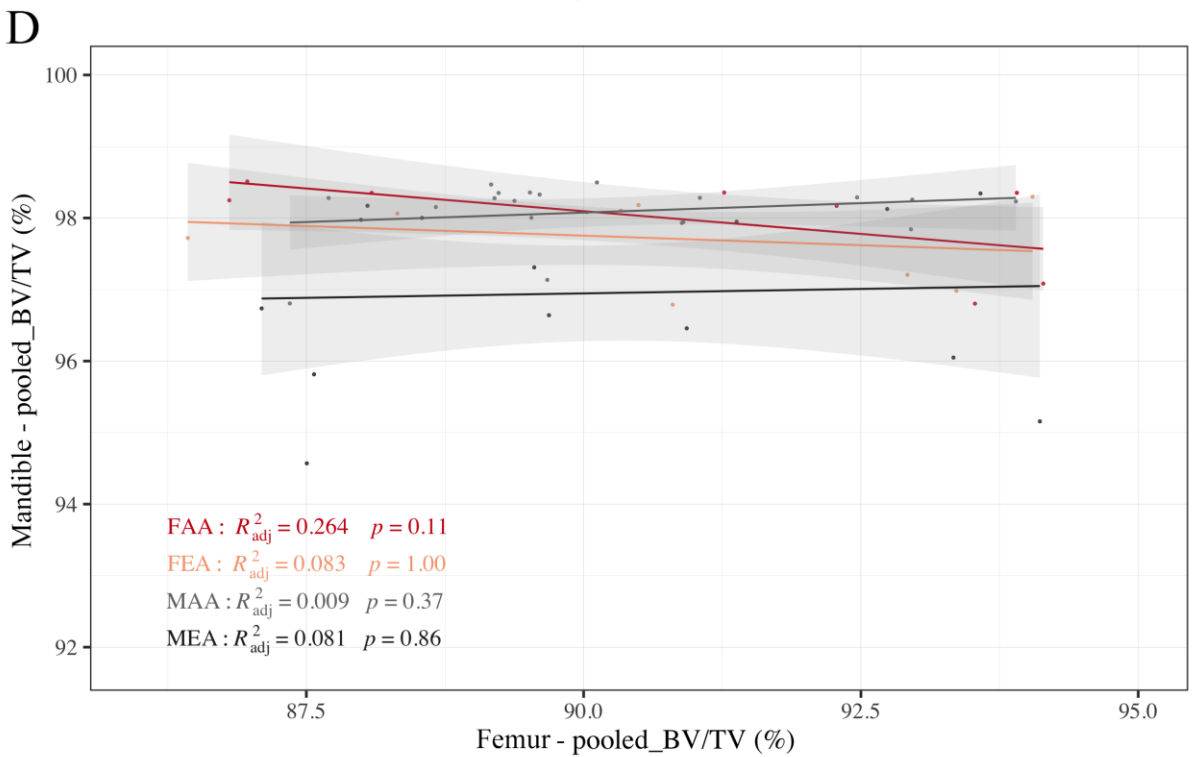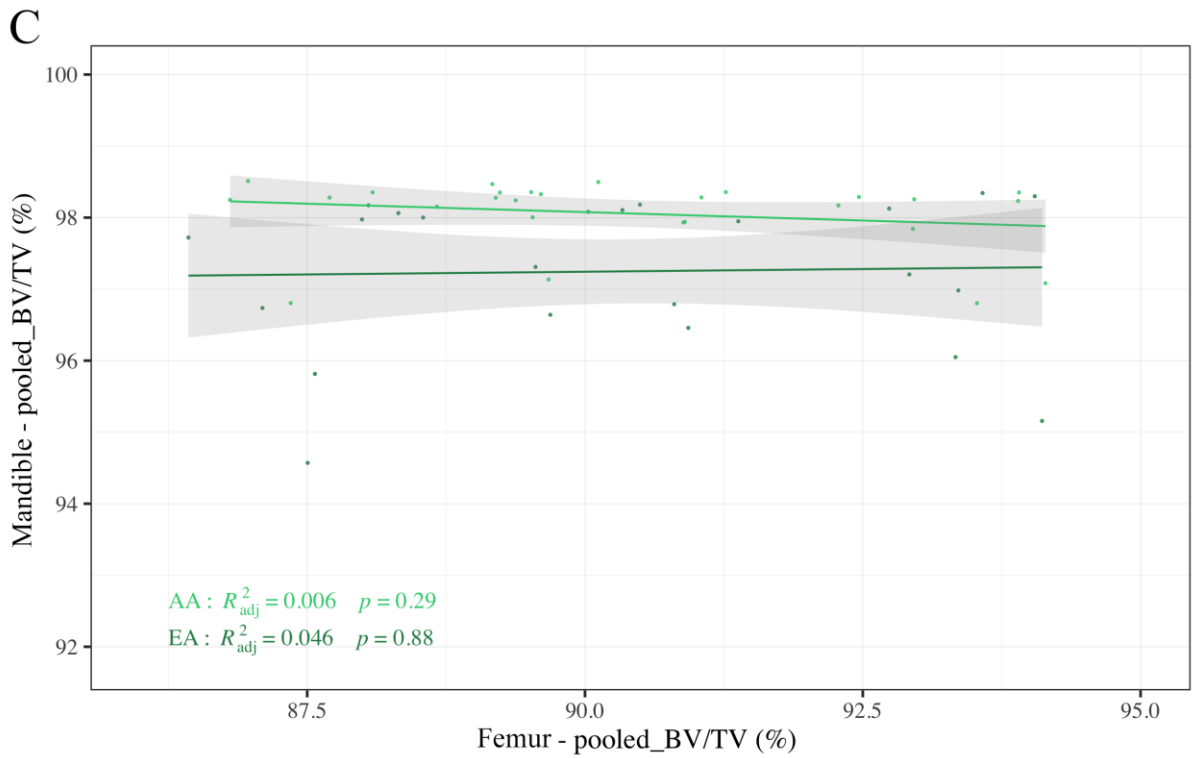
Figure 5.9. (continued)

5.2.2.2. With aging

Correlations with advancing age were investigated in the femoral sample and were compared to the mandibular subsample (Table 5.3). Femoral cortical bone densities did not show any significant correlation with aging, within the entire sample or any of the subgroups. However, as reported previously for the principal mandibular sample [see section 4.5.5], cortical BV/TV values were significantly correlated with aging in the mandibular subsample used here, as well as within females, EA and finally FEA. These significant correlations were associated with strong negative coefficients, particularly in females ($\rho = -0.645$) and FEA ($\rho = -0.867$).

Generalised linear models were performed between these two variables (BV/TV and age) in the femur and the mandibular subsample, consisting of the same individuals (Table 5.3 and Figure 5.10). In the femur, significant regressions were only found within males and MEA, with low regression coefficients. In the mandible, though, three regressions were significant: in the entire sample, females, and FEA, with moderate to strong coefficients.

Table 5.3. Spearman's correlation tests (p-values, ρ correlation coefficients) and generalised linear models (p-values and adjusted R^2 regression coefficients) run between age (years) and cortical BV/TV (%) recorded in mandibles and femora of same individuals. Significant p-values are in bold.

| | Correlations | | | | Regressions | | | |
| | Mandible | | Femur | | Mandible | | Femur | |
	p-value	ρ	p-value	ρ	p-value	R^2_{adj}	p-value	R^2_{adj}
Total	**0.001**	-0.452	0.122	-0.195	**0.009**	0.114	0.105	0.026
F	**0.005**	-0.645	0.848	-0.039	**0.007**	0.351	0.820	-0.038
M	0.052	-0.341	0.066	-0.306	0.116	0.048	**0.040**	0.090
AA	0.415	-0.163	0.644	-0.084	0.694	-0.033	0.583	-0.022
EA	**0.025**	-0.466	0.112	-0.291	0.078	0.099	0.065	0.082
FAA	0.299	-0.429	0.420	0.245	0.239	0.092	0.518	-0.048
FEA	**0.005**	-0.867	0.675	-0.123	**0.028**	0.454	0.858	-0.080
MAA	0.805	-0.061	0.362	-0.215	0.832	-0.056	0.370	-0.008
MEA	0.776	-0.084	0.084	-0.431	0.512	-0.044	**0.024**	0.250

254
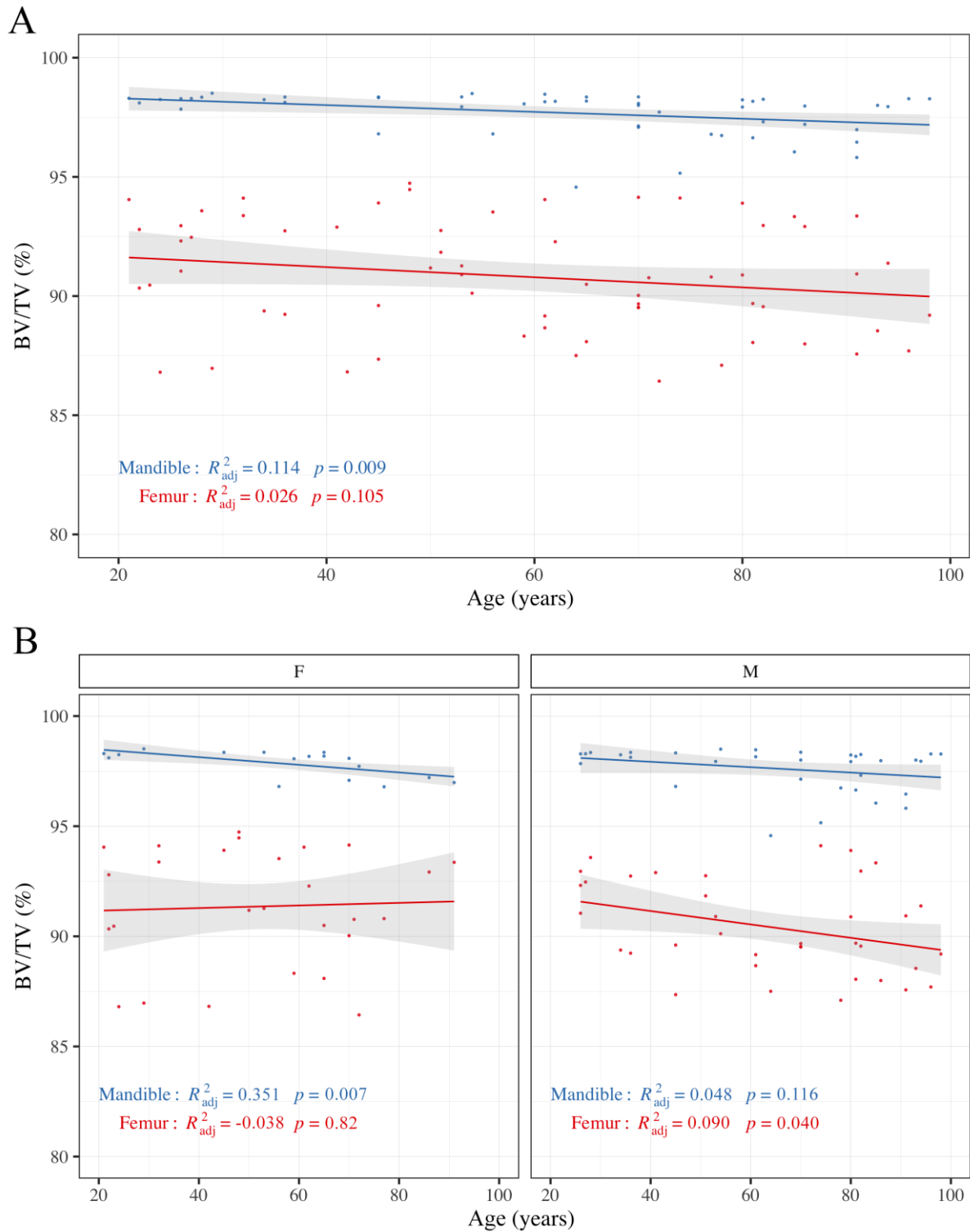
Figure 5.10. Generalised linear models between aging (years) and cortical BV/TV (%) in the mandible (blue regressions) and femur (red regressions) of the entire sample [A], per sex [B], per ancestry [C] and per sex/ancestry [D]. Grey area represents the 95% confidence interval of each regression. (continued on the next page)
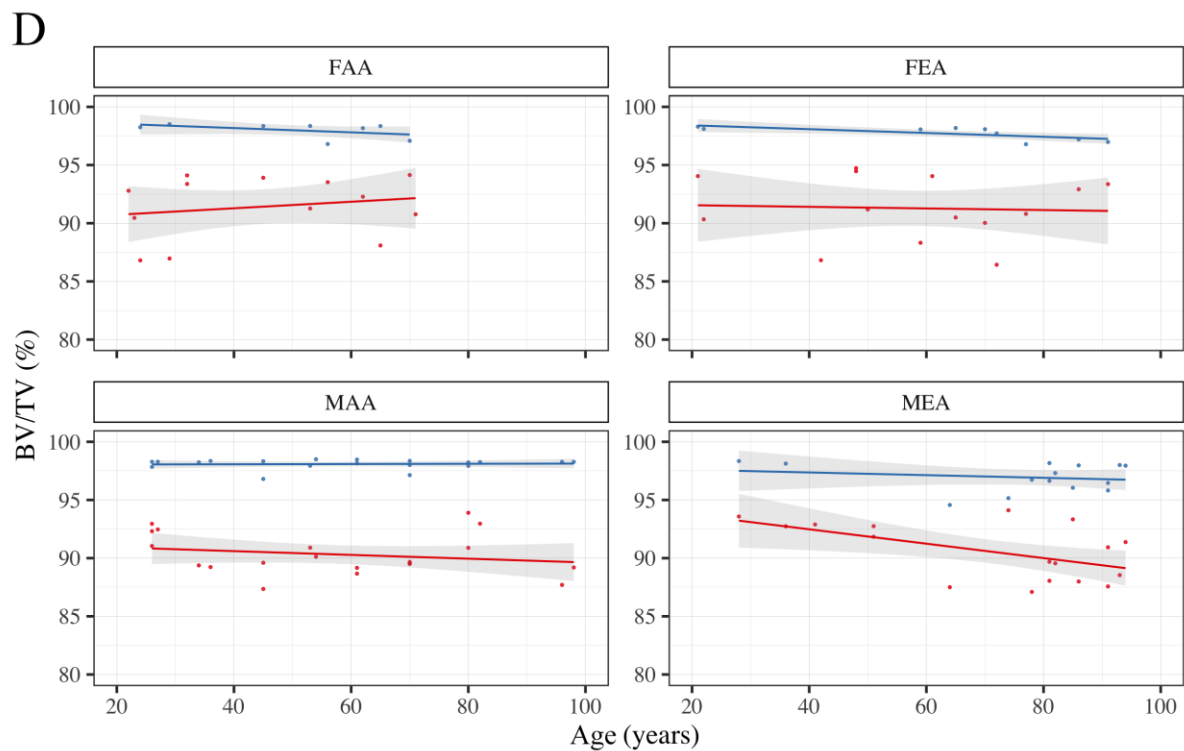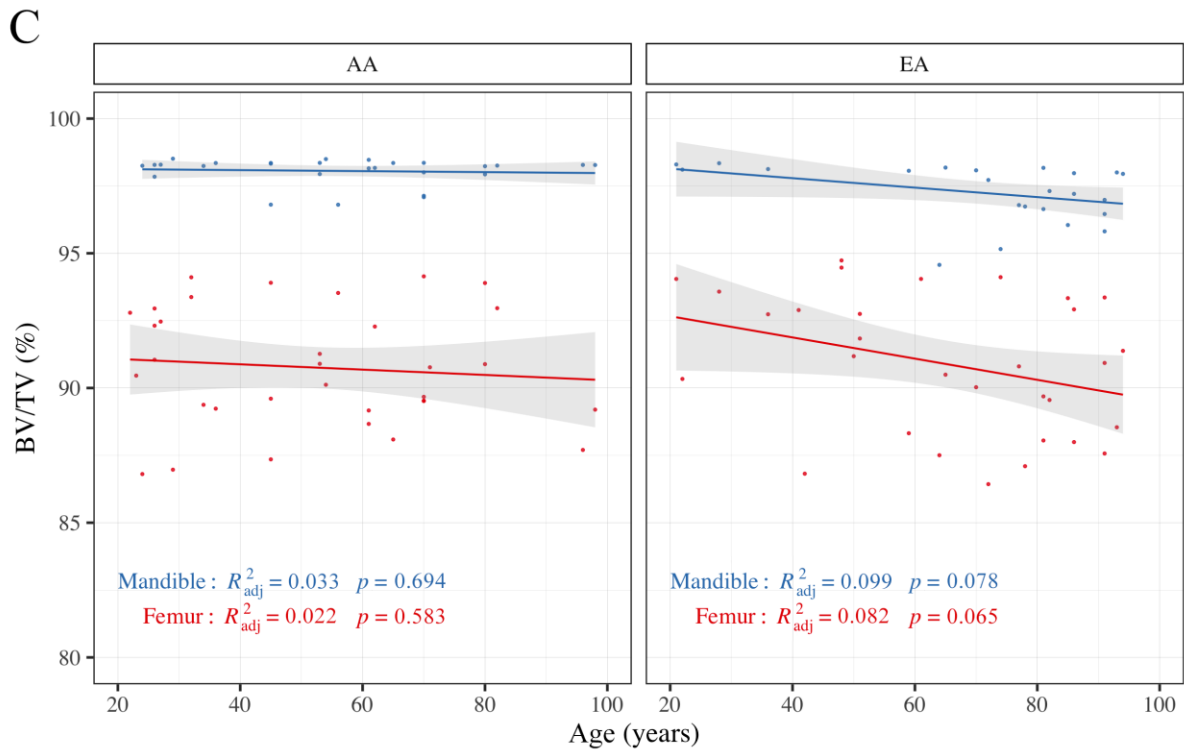
Figure 5.10. (continued)

5.3. Summary

The femoral neck cortical densities displayed surprising results, as no differences in sex and ancestry were detected. Furthermore, no significant differences were observed between the VOI locations (i.e., inferior, superior, anterior, posterior sites).

The cortical densities were then compared across bones: mandible vs. femur. The mandibular BV/TV was found much higher than the femoral BV/TV, in all individuals, whatever the sex or ancestry. However, the spreading of values was larger in the femur than in the mandible, and this spreading appeared to be influenced by sex and ancestry, e.g., MAA showed limited ranges in the mandible and in the femur, while MEA displayed wide ranges in the mandible and in the femur. Moreover, the cortical densities recorded in the femur did not appear to be correlated with the cortical densities recorded in the mandible. The femoral cortical bone density is thus, not increasing or decreasing, when the mandibular cortical bone density is, and reciprocally.

However, once the age of the individuals was considered, the two bones showed similar regression patterns: a decrease in cortical density with advancing age. Although, the decrease was faster in the femur than in the mandible, and not the same in all groups: EA was for example more affected than AA.

Chapter 6. Results: CBCT analysis of the mandible and comparison with micro-CT

A subsample of 24 mandibles was scanned by both micro-CT and CBCT modalities, as explained in Chapter 3 Materials and Methods. This sample included 24 adult males (mean age = 59.2, range: 22 – 98 years) of African ancestry, with similar dentition status (according to the Eichner Index: category A, n = 20; category B: n = 4).

The comparison between the two imaging techniques was performed using two approaches. First, presented in [6.1], the comparison focused on 2D and 3D measurements which were recorded twice (on both modalities). The second approach, in [6.2], considered directly the three-dimensional volumes of entire mandibles (and not specific measurements).

6.1. Manual comparison of measurements

Measurements performed in these 24 individuals were recorded following the same definitions used in Chapter 4: external distances, cortical thickness and histomorphometric parameters. First, before any modality comparison, the repeatability of the CBCT-based measurements was assessed [in 6.1.1]. Then, to evaluate the concordance (or agreement) between both techniques, Bland-Altman plots and regression analyses were performed [in 6.1.2]. Finally, direct comparisons of measurements were conducted through basic descriptive and exploratory statistics [in 6.1.3].

6.1.1. Repeatability of CBCT-based measurements

The intra-observer repeatability of measurements recorded on CBCT scans was assessed through three statistical methods: Intraclass Correlation Coefficients (ICCs), Technical Errors of Measurement (TEM and %TEM) and Bland-Altman plots. To do so, ten CBCT scans were analysed twice. ICCs were calculated first and are presented in Table 6.1. The intra-examiner reproducibility was excellent, with ICCs between 0.847 and 0.999. The alveolar heights (m_h, a_h, p_h) and ramus measurements (ra_b, ra_h) showed the highest ICCs (0.999) while the cortical thicknesses' ICCs were slightly lower. Then, absolute and

relative TEM were estimated for all the variables and showed an overall low intra-observer error rate (Table 6.1). The external distances had a small mean TEM at 0.03 mm (range: 0.01 – 0.07 mm) and a mean %TEM at 0.10% (range: 0.04 – 0.23%). The cortical thicknesses displayed intermediate results with a mean TEM at 0.09 mm (range: 0.01 – 0.15 mm), and more particularly a mean %TEM at 3.64% with a wider range: from 0.56 to 7.09%. Furthermore, as highlighted in bold in Table 6.1, the measurements showing the highest %TEM were associated with the lowest ICCs, such as the midline buccal CtTh (m_buc_CtTh), or the posterior buccal CtTh (p_buc_CtTh).

Table 6.1. Intra-observer errors estimated on CBCT-based measurements: ICCs and 95% Confidence Intervals (CI lower – upper bounds) as well as TEM and %TEM values. Lowest ICCs and largest %TEMs are in bold.

		ICC	95% CI	TEM	%TEM
External distances	m_h	0.999	0.999 – 1.000	0.05	0.14
	a_h	0.999	0.999 – 1.000	0.07	0.23
	p_h	0.999	0.999 – 1.000	0.01	0.04
	ra_b	0.999	0.999 – 1.000	0.02	0.05
	ra_h	0.999	0.999 – 1.000	0.02	0.05
Cortical thicknesses	m_ba_CtTh	0.993	0.975 – 0.998	0.13	3.42
	m_buc_CtTh	**0.847**	0.523 – 0.959	0.15	**7.09**
	m_ling_CtTh	0.985	0.946 – 0.996	0.06	2.78
	a_ba_CtTh	0.988	0.957 – 0.997	0.14	3.21
	a_buc_CtTh	0.944	0.804 – 0.986	0.11	**5.05**
	a_ling_CtTh	**0.913**	0.707 – 0.977	0.11	**4.47**
	p_ba_CtTh	0.973	0.902 – 0.993	0.15	3.25
	p_buc_CtTh	**0.915**	0.714 – 0.978	0.14	**5.62**
	p_ling_CtTh	0.974	0.906 – 0.993	0.05	2.03
	rab_buc_CtTh	**0.910**	0.647 – 0.981	0.10	**5.33**
	rab_ling_CtTh	0.999	0.999 – 1.000	0.01	0.56
	rah_buc_CtTh	0.997	0.987 – 0.999	0.02	1.12
	rah_ling_CtTh	0.981	0.930 – 0.995	0.05	3.33

Finally, Bland-Altman plots were computed for each pair of measurements (CBCT observation 1 vs. CBCT observation 2) and are illustrated in Appendix G Figure G. and Figure G.. All revealed a high agreement, with no measuring differences exceeding 0.2 mm for the external distances and 0.6 mm for the cortical thicknesses. However, the spread of the differences was larger for the cortical thicknesses than for the external distances (approximately between 0.2 mm and -0.2 mm, and between 0.5 mm and -0.5 mm respectively).

To sum up, as high repeatability was found in measurements performed in CBCT, as well as in micro-CT [see 4.1], the comparison between the two modalities could be performed and is presented in the following sections.

6.1.2. Agreement between scanning modalities

The agreement and accuracy of CBCT-based measurements, in comparison to micro-CT, was evaluated using two statistical methods: the Bland-Altman method evaluating their agreement, and the Passing-Bablok regression method, assessing its accuracy.

First, the agreement between CBCT and micro-CT was evaluated visually from the Bland-Altman plots computed. They were computed for each pair of measurements (micro-CT observation vs. CBCT observation), always using micro-CT as the reference. As an example, plots for the variables recorded on the midline section – alveolar height; basal, buccal and lingual cortical thicknesses and densities – are presented in Figure 6.1, while the plots for the mandibular body length (me-go_length) and the other sections (anterior, posterior, ramus) are presented in Appendix G Figure G. toFigure G..

All the measurements showed an overall high degree of agreement between the two modalities, particularly the external distances and cortical thicknesses, with most of the measurements located between the upper and lower limits of the confidence interval. The CBCT as compared to the micro-CT showed a slight underestimation of the measurements, particularly for the external distance (i.e., the means of differences are positive on the Bland-Altman plots). The plots for the densities also showed a distribution of the measurements around the mean but were more peculiar, as they gathered predominantly on one side of the plot. A few outliers were also detected.
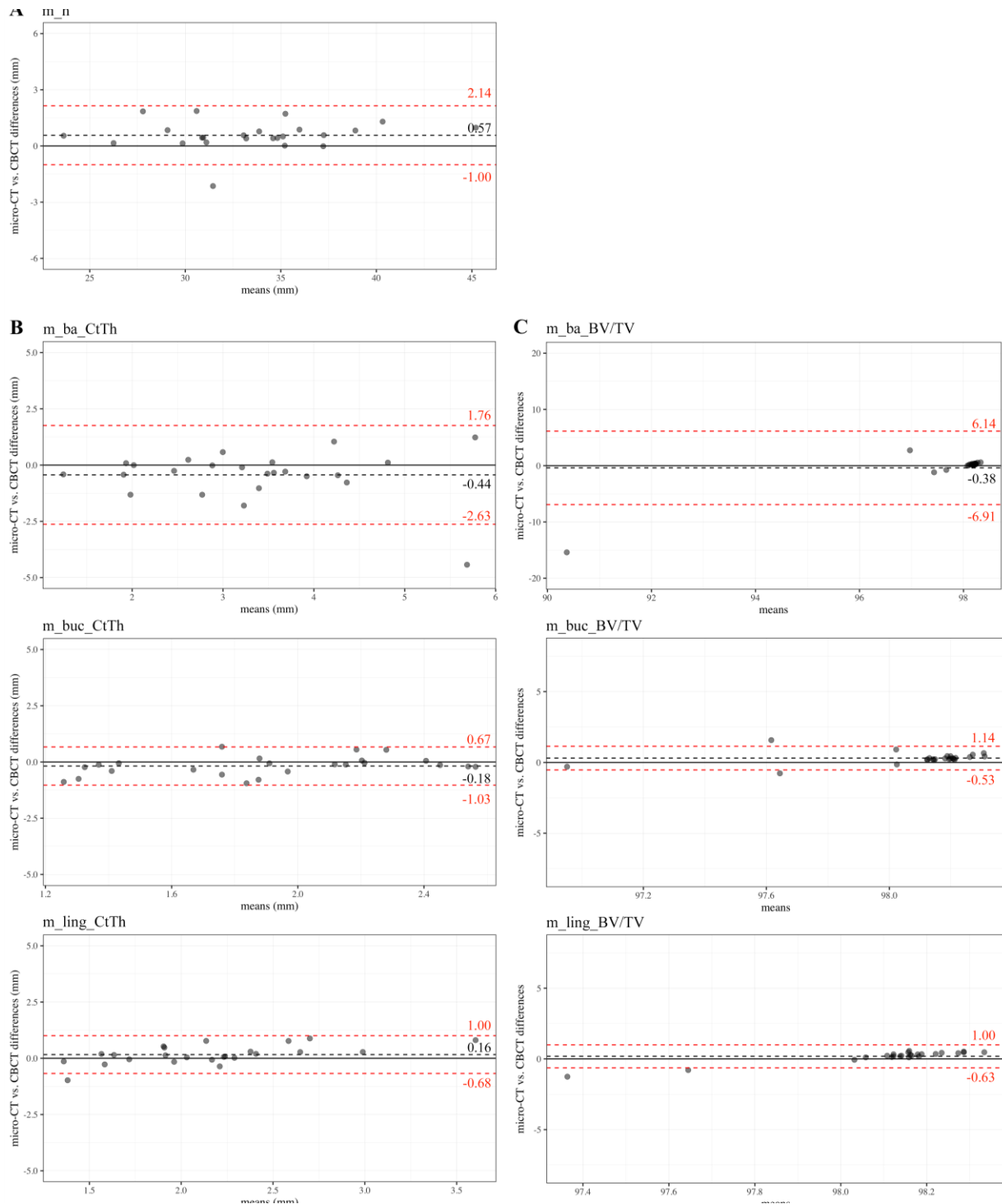
Figure 6.1. Micro-CT vs. CBCT Bland-Altman plots of the midline section: alveolar height m_h [A], basal, buccal and lingual CtTh [B] and BV/TV [C]. 95% of the measurements are located within the upper and lower limits of agreement (red dashed lines), while the mean of differences is illustrated by the horizontal black dashed line. The vertical y-axis scale is relative to the spread of variations.

Then, Passing-Bablok regression analyses, especially recommended for studies comparing different techniques, were performed on the external distances, cortical thicknesses and densities. For each measurement, the method tested (CBCT) is regressed against the reference method (micro-CT), as illustrated in Figure 6.2 for the midline section (other sections are in Appendix G Figure G.Figure G.), with 95% confidence intervals, calculated by means of a resampling method, the bootstrap. Outputs of each regression are presented in Table 6.2, detailing the intercept (a) and slope (b) values, their respective 95% confidence intervals (CI), and final regression coefficients. The interpretation of the results was done as follows: (i) if the intercept CI includes 0, and if the slope CI includes 1, the two methods are comparable and not statistically different; however (ii) if the intercept CI does not include 0, there is a systematic difference; and (iii) if the slope CI does not include 1, there is a proportional difference between the two methods. One way of representing graphically these rules is to plot an identity line (i.e., a line where x = y) with each regression, as seen in Figure 6.2.

First, regarding the external distances, all the regressions, except for the ramus breadth, showed regression and identity lines often in proximity, almost parallel, and always included in the confidence intervals of the regression. As seen in Table 6.2, all the distances (except ra_b) presented confidence intervals for the intercept including 0, and slope CIs including 1, confirming that the two scanning modalities could be considered comparable for this type of distance. The cortical thicknesses showed different profiles, with larger confidence intervals and regression lines intersecting identity lines. In four cortical thicknesses, the identity lines were not even comprised inside the confidence intervals, as confirmed by the values in Table 6.2. The Passing-Bablok regressions for the cortical BV/TV were even more peculiar, with almost perpendicular identity lines, large confidence intervals, often funnel-shaped presenting a narrow area where most of the values were gathered. Eight of the 13 densities did not have 0 included in the intercept CIs, and 1 included in the slope CIs, while the values for the ramus VOIs were particularly large and unusual.

These results are also confirmed by the correlation coefficients calculated with the regressions and given in the last column of Table 6.2: the external distances showed very high coefficients close to 1 (between 0.80 and 0.99); the cortical thickness coefficients were lower and only comprised between 0.33 and 0.87; while the cortical densities presented very low coefficients (between 0.06 and 0.34).

The Bland-Altman plots and Passing-Bablok regression analyses confirmed that micro-CT and CBCT scanning modalities might be comparable methods for linear measurements,

such as the external distances and cortical thicknesses. However, it was also noticed that the smaller the measurement is (such as a cortical thickness), the smaller the agreement and accuracy between the two modalities are. Furthermore, compared to the mandibular corpus, ramus measurements (large distances such as the breadth or height, and cortical thicknesses) done on CBCT scans showed less accuracy and lower correlation coefficients. Finally, these analyses also highlighted that, regarding the BV/TV densities, the two scanning methods were not in agreement and that CBCT might not be accurate to record histomorphometric parameters.
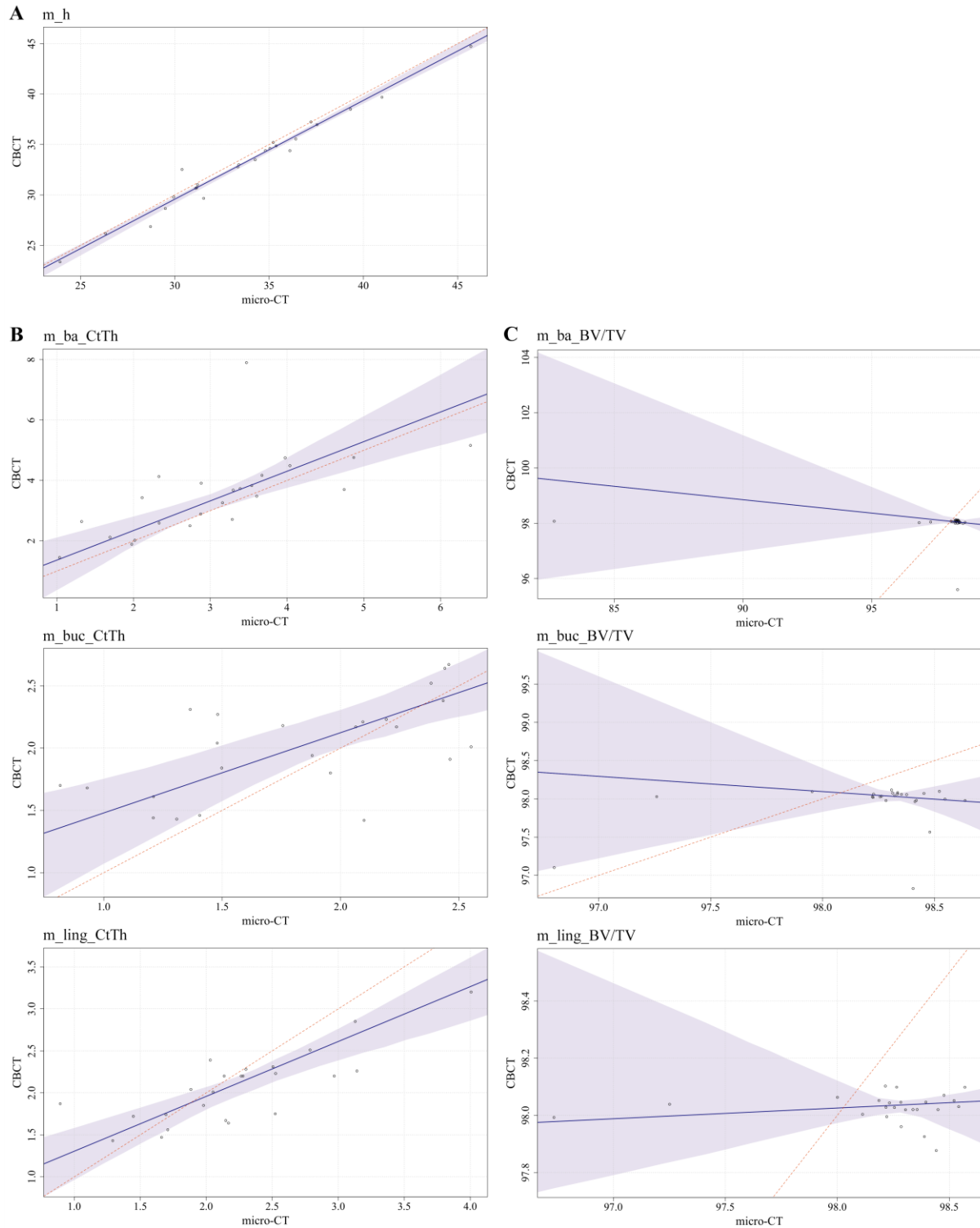
Figure 6.2. Micro-CT vs. CBCT Passing-Bablok regressions for the midline: alveolar height m_h [A], basal, buccal and lingual CtTh [B] and BV/TV [C]. Reference method (x-axis: micro-CT) is plotted against the method tested (y-axis: CBCT) with a regression line (dark purple lines), a 95% confidence area (light purple) and an identity line (x = y, red dashed line).

Table 6.2. Micro-CT vs. CBCT Passing-Bablok regression coefficients (intercept a, slope b) and 95% confidence intervals (95% CI). Intercept CI not including 0, or slope CI not including 1 are in bold.

		Intercept		Slope		Correlation coefficient
		a	95% CI	b	95% CI	
External distances	me-go_length	0.71	-27.95 – 27.13	0.96	0.66 – 1.28	0.80
	m_h	0.21	-2.01 – 1.60	0.98	0.94 – 1.04	0.99
	a_h	-3.86	-9.66 – 2.57	1.10	0.90 – 1.24	0.94
	p_h	-1.26	-13.58 – 2.43	1.03	0.89 – 1.46	0.93
	ra_b	3.68	**0.59 – 8.22**	0.87	**0.76 – 0.96**	0.95
	ra_h	4.11	-5.01 – 15.16	0.90	0.68 – 1.08	0.94
Cortical thicknesses	m_ba_CtTh	0.38	-1.02 – 1.43	0.98	0.65 – 1.41	0.64
	m_buc_CtTh	0.84	**0.09 – 1.32**	0.64	**0.40 – 0.99**	0.61
	m_ling_CtTh	0.65	**0.14 – 1.19**	0.65	**0.41 – 0.85**	0.80
	a_ba_CtTh	1.20	-0.56 – 2.92	0.87	0.41 – 1.23	0.35
	a_buc_CtTh	0.29	-1.07 – 4.67	0.89	-1.17 – 1.57	0.56
	a_ling_CtTh	0.30	-0.19 – 0.64	0.79	**0.62 – 0.98**	0.87
	p_ba_CtTh	0.78	-0.65 – 5.80	0.84	-0.49 – 1.30	0.48
	p_buc_CtTh	0.19	-0.34 – 1.02	0.91	0.53 – 1.14	0.78
	p_ling_CtTh	0.04	-0.77 – 0.94	1.00	0.63 – 1.35	0.73
	rab_buc_CtTh	1.08	**0.15 – 1.92**	0.40	**0.04 – 1.00**	0.44
	rab_ling_CtTh	0.80	-0.47 – 3.42	0.60	-1.11 – 1.15	0.34
	rah_buc_CtTh	0.31	-0.18 – 0.75	0.83	0.58 – 1.10	0.79
	rah_ling_CtTh	0.48	-0.24 – 2.71	0.80	-0.93 – 1.31	0.33
Cortical densities	m_ba_BV/TV	107.59	**89.85 – 140.44**	-0.10	**-0.43 – 0.08**	0.06
	m_buc_BV/TV	117.62	**35.46 – 201.14**	-0.20	**-1.05 – 0.64**	0.34
	m_ling_BV/TV	94.34	**79.89 – 124.82**	0.04	**-0.27 – 0.18**	0.06
	a_ba_BV/TV	109.72	**69.76 – 145.18**	-0.12	**-0.48 – 0.29**	0.12
	a_buc_BV/TV	113.16	**34.22 – 377.83**	-0.15	**-2.85 – 0.65**	0.15
	a_ling_BV/TV	88.68	**49.46 – 113.96**	0.10	**-0.16 – 0.49**	0.08
	p_ba_BV/TV	94.38	**79.36 – 119.74**	0.04	**-0.22 – 0.19**	0.22
	p_buc_BV/TV	76.59	**15.10 – 117.56**	0.22	**-0.20 – 0.84**	0.06
	p_ling_BV/TV	163.16	-102.07 – 1634.59	-0.66	-15.64 – 2.03	0.13
	rab_buc_BV/TV	120.22	-73.37 – 455.02	-0.23	-3.64 – 1.74	0.19
	rab_ling_BV/TV	131.56	-346.52 – 1221.67	-0.34	-11.44 – 4.51	0.03
	rah_buc_BV/TV	73.53	-341.42 – 242.91	0.25	-1.48 – 4.47	0.04
	rah_ling_BV/TV	4958.64	-13911.98 – 8336.25	-49.47	-83.78 – 142.47	0.65

265

6.1.3. Comparison of measurements between scanning modalities

6.1.3.1. Basic descriptive statistics

Basic descriptive statistics, including minimum – maximum values, means and standard deviations, were calculated for all 24 individuals scanned with both imaging modalities, and are detailed in Table 6.3 for the external distances and cortical thicknesses, and in Table 6.4 for the cortical bone densities (BV/TV).

The average external distances measured on micro-CT were always greater than measured on CBCT. However, the cortical thicknesses did not show the same trend (i.e., no general over- or underestimation from one modality to the other). In both micro-CT and CBCT, the standard deviation values were higher for the greatest dimensions such as the body length, or the alveolar heights ($2.97 < SD < 4.75$ mm), than for the cortical thicknesses ($0.33 < SD < 1.41$ mm).

For all the cortical bone densities, except the basal site of the midline (m_ba_BV/TV – Table 6.4), CBCT underestimated the mean BV/TV percentages. However, it is worthwhile to note that m_ba_BV/TV standard deviation was important ($SD = 3.20\%$) compared to the others and thus was maybe influenced by the presence of outliers. All the sections located on the body of the mandible showed similar percentages of cortical BV/TV (micro-CT ranged between $97.57 – 98.24\%$; CBCT ranged between $97.47 – 98.04\%$) and minimal standard deviations. Though the BV/TV measured in the ramus were noticed to be lower, especially the minimum values (e.g., rab_ling_BV/TV = 83.34% or rah_ling_BV/TV = 85.55%).

Table 6.3. Descriptive statistics of the micro-CT and CBCT-based measurements (mm): body length (me-go_length), alveolar heights (midline m_h, anterior a_h, posterior p_h), ramus breadth (ra_b) and height (ra_h), cortical thicknesses on these five sections.

		Micro-CT		CBCT	
		min – max	mean ± SD	min – max	mean ± SD
External distances	me-go_length	79.19 – 99.83	89.23 ± 5.17	78.15 – 86.03	86.03 ± 4.80
	m_h	23.91 – 45.70	33.68 ± 4.75	23.36 – 44.72	33.11 ± 4.66
	a_h	23.74 – 42.34	33.85 ± 3.92	21.22 – 43.71	32.93 ± 4.37
	p_h	20.18 – 33.48	28.65 ± 3.10	19.98 – 33.11	28.00 ± 2.97
	ra_b	29.41 – 45.43	37.61 ± 4.23	29.26 – 41.30	35.83 ± 3.34
	ra_h	40.53 – 56.01	48.19 ± 4.08	37.93 – 54.67	47.43 ± 3.93
Cortical thicknesses	m_ba_CtTh	1.04 – 6.39	3.11 ± 1.21	1.45 – 7.90	3.55 ± 1.35
	m_buc_CtTh	0.82 – 2.55	1.82 ± 0.53	1.42 – 2.67	2.00 ± 0.38
	m_ling_CtTh	0.89 – 4.01	2.23 ± 0.67	1.43 – 3.20	2.07 ± 0.43
	a_ba_CtTh	1.99 – 7.76	3.97 ± 1.41	2.46 – 6.72	4.50 ± 1.15
	a_buc_CtTh	0.78 – 3.05	2.03 ± 0.48	1.04 – 2.93	2.17 ± 0.45
	a_ling_CtTh	1.38 – 4.37	2.78 ± 0.68	1.46 – 3.85	2.44 ± 0.55
	p_ba_CtTh	2.33 – 5.71	3.63 ± 0.82	2.77 – 5.87	4.02 ± 0.80
	p_buc_CtTh	1.19 – 3.67	2.61 ± 0.63	1.69 – 3.60	2.55 ± 0.54
	p_ling_CtTh	1.06 – 3.04	2.35 ± 0.44	1.20 – 3.32	2.41 ± 0.46
	rab_buc_CtTh	0.86 – 3.53	2.00 ± 0.63	1.18 – 2.51	1.97 ± 0.35
	rab_ling_CtTh	0.10 – 2.51	1.39 ± 0.63	0.64 – 2.33	1.54 ± 0.48
	rah_buc_CtTh	1.18 – 2.76	1.86 ± 0.43	1.27 – 2.35	1.83 ± 0.33
	rah_ling_CtTh	0.39 – 2.21	1.14 ± 0.51	0.00 – 2.19	1.37 ± 0.51

267

Table 6.4. Descriptive statistics of the micro-CT and CBCT-based cortical bone density (BV/TV, %), measured in the basal, buccal and lingual VOIs of the three body sections (midline, anterior, posterior), as well as buccal and lingual VOIs of the two ramus sections (breadth, height).

		Micro-CT		CBCT	
		min – max	mean ± SD	min – max	mean ± SD
Cortical densities	m_ba_BV/TV	82.67 – 98.63	97.57 ± 3.20	95.60 – 98.12	97.96 ± 0.50
	m_buc_BV/TV	96.80 – 98.64	98.24 ± 0.40	96.83 – 98.12	97.93 ± 0.32
	m_ling_BV/TV	96.73 – 98.57	98.21 ± 0.41	97.88 – 98.10	98.03 ± 0.05
	a_ba_BV/TV	97.06 – 98.63	98.23 ± 0.37	97.92 – 98.13	98.04 ± 0.06
	a_buc_BV/TV	96.77 – 98.61	98.22 ± 0.39	94.59 – 98.13	97.84 ± 0.72
	a_ling_BV/TV	97.04 – 98.56	98.20 ± 0.38	97.91 – 98.13	98.04 ± 0.06
	p_ba_BV/TV	96.89 – 98.66	98.22 ± 0.39	97.97 – 98.10	98.04 ± 0.04
	p_buc_BV/TV	96.82 – 98.63	98.23 ± 0.39	97.11 – 98.12	97.99 ± 0.20
	p_ling_BV/TV	96.84 – 98.61	98.20 ± 0.38	92.05 – 98.18	97.47 ± 1.42
	rab_buc_BV/TV	96.87 – 98.64	98.23 ± 0.38	95.86 – 98.11	97.88 ± 0.52
	rab_ling_BV/TV	93.37 – 98.50	97.78 ± 1.36	83.34 – 98.14	96.55 ± 3.72
	rah_buc_BV/TV	96.82 – 98.57	98.21 ± 0.38	97.21 – 98.77	97.96 ± 0.29
	rah_ling_BV/TV	92.11 – 98.54	97.91 ± 1.43	85.55 – 98.13	95.33 ± 4.60

6.1.3.2. Assumption testing

Before further statistical analyses, all the variables have to be tested for normality of distributions and homogeneity of variances. According to Shapiro Wilk's normality tests, all the external distances were found to have normal distributions, except for the posterior alveolar height (p_h). Based on further visual examinations of the kernel density plots, p_h was concluded to have a normal distribution. Variances were then analysed and found to be equal in the micro-CT and CBCT samples. Following the same assumption testing protocol, cortical thicknesses were all found to be normally distributed and have equal variances between modality subsamples. On the contrary, the normality and variance tests performed on the histomorphometric parameters revealed non-normal distributions and heteroscedasticity at all sites.

6.1.3.3. External distances

As the variables were normally distributed, parametric paired Student t-tests were performed to compare the modalities. As illustrated in the boxplots (Figure 6.3), significant differences were found between micro-CT and CBCT-based measurements of all three alveolar heights: midline ($p < 0.01$), anterior ($p < 0.01$), posterior ($p < 0.05$); confirming greater distances in micro-CT. The length of the mandibular body (me-go_length) was also found to differ significantly between the two modalities ($p < 0.001$). Finally, on the ramus, the breadth (ra_b) also showed significant differences ($p < 0.05$) while the height (ra_h) did not ($p = 0.06$).
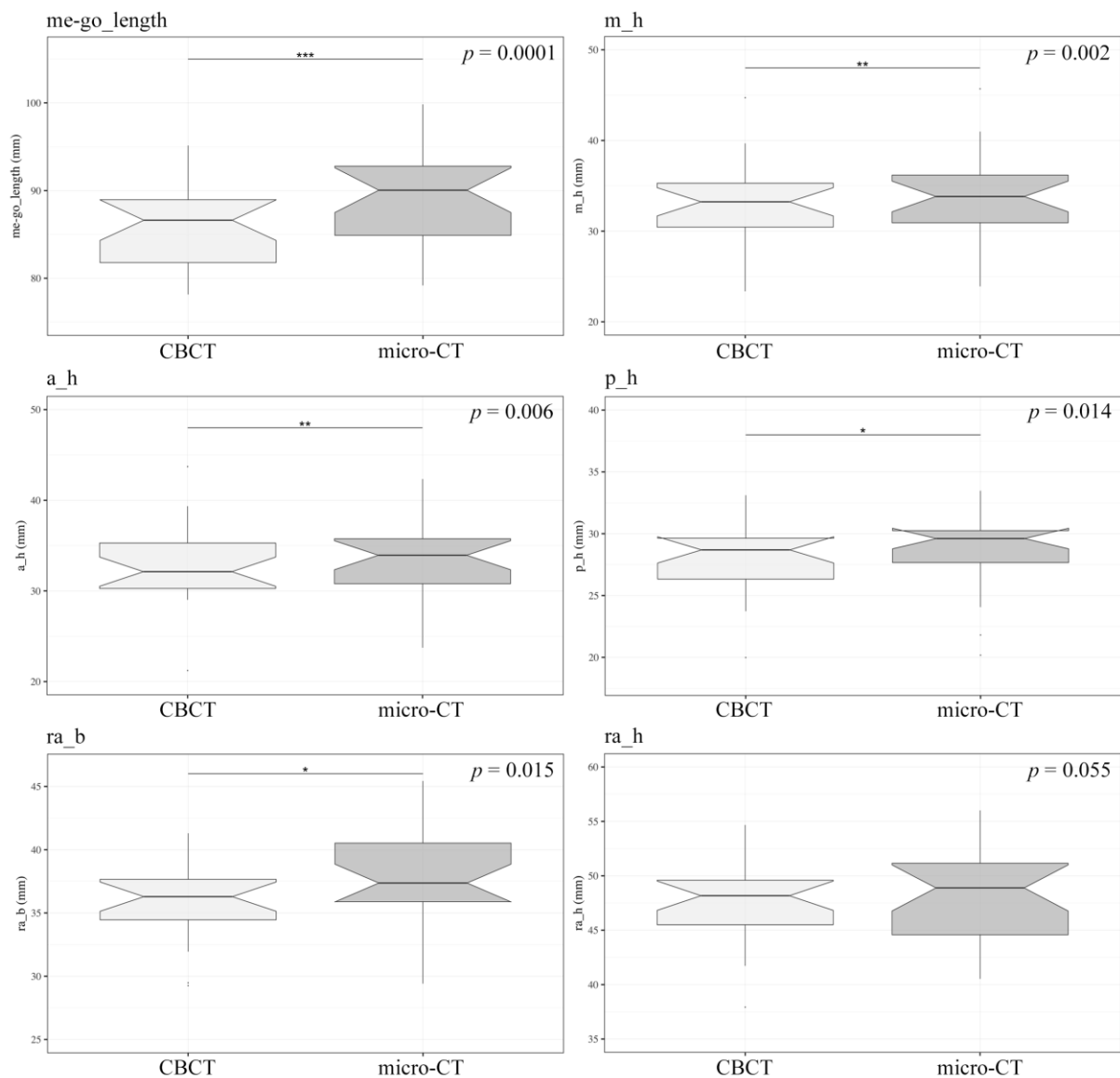
Figure 6.3. Boxplots of external distances (mm) per scanning modality (CBCT vs. micro-CT). Dots depict outliers. Paired Student t-test p-values are indicated for each boxplot. Significance: *** $p < 0.001$, ** $p < 0.01$, * p < 0.05.

6.1.3.4. Cortical thickness

Paired Student t-tests were performed on the 13 cortical thicknesses and showed that only three measurements were significantly different between the two imaging modalities (see Figure 6.4): lingual site of the anterior section (a_ling_CtTh, $p = 0.0001$), basal site of the posterior section (p_ba_CtTh, $p = 0.029$) and finally the lingual site of the ramus height (rah_ling_CtTh, $p = 0.027$). All the other sites did not present any significant differences between micro-CT and CBCT.

6.1.3.5. Histomorphometric parameters

Non-parametric Wilcoxon signed-rank tests were performed between CBCT and micro-CT-based densities (Figure 6.5). Statistically significant differences were found for all thirteen VOIs between the two modalities, with greater BV/TV values in micro-CT VOIs than in CBCT.
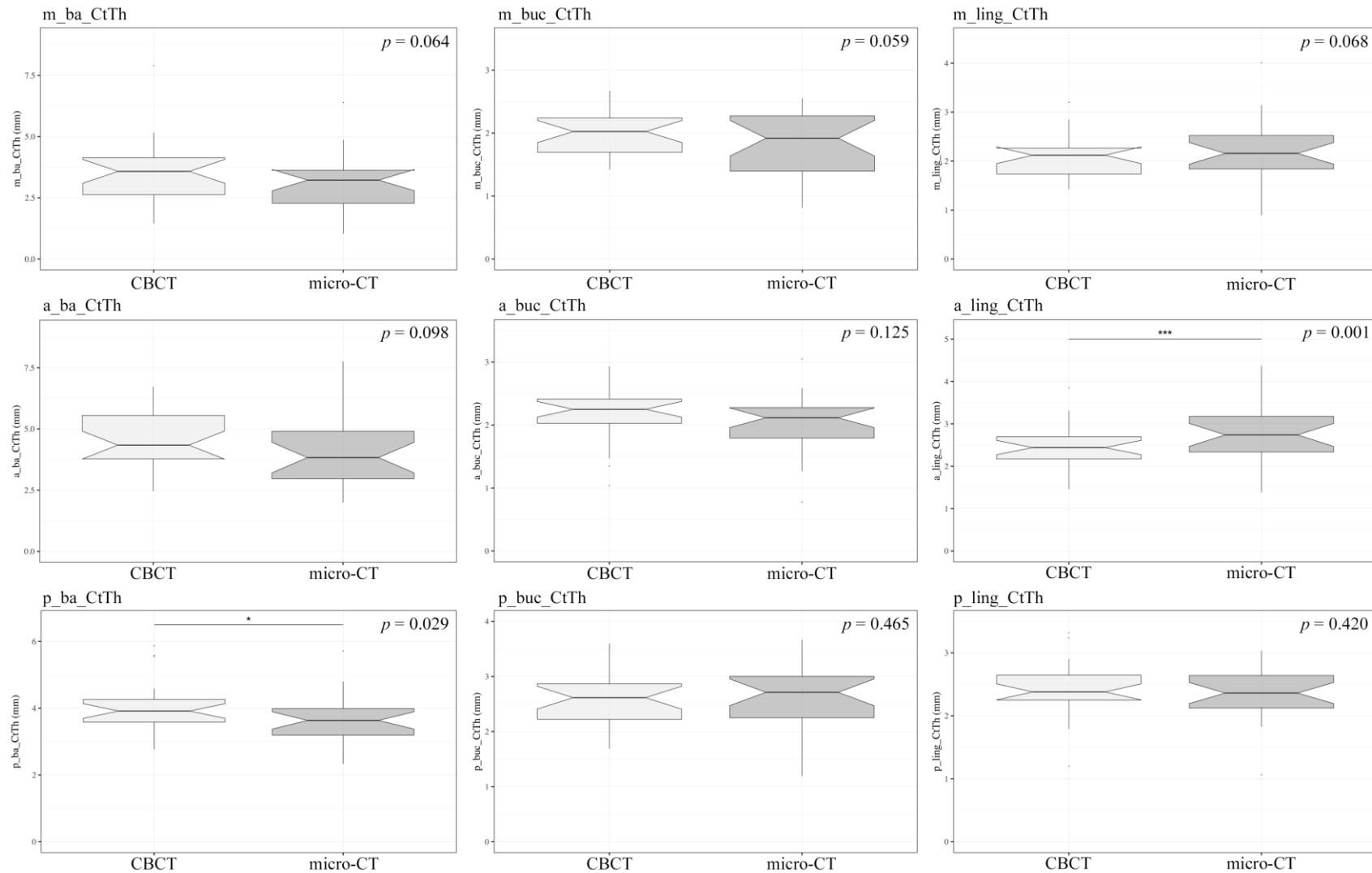
Figure 6.4. Boxplots of CtTh (mm) per modality (CBCT vs. micro-CT), recorded on the midline (first row), anterior (second row), posterior (third row), ramus breadth and height sections. Dots depict outliers. Paired Student *t*-test *p*-values are indicated for each boxplot. Significance: *** *p* < 0.001, * p < 0.05.

(continued on next page)
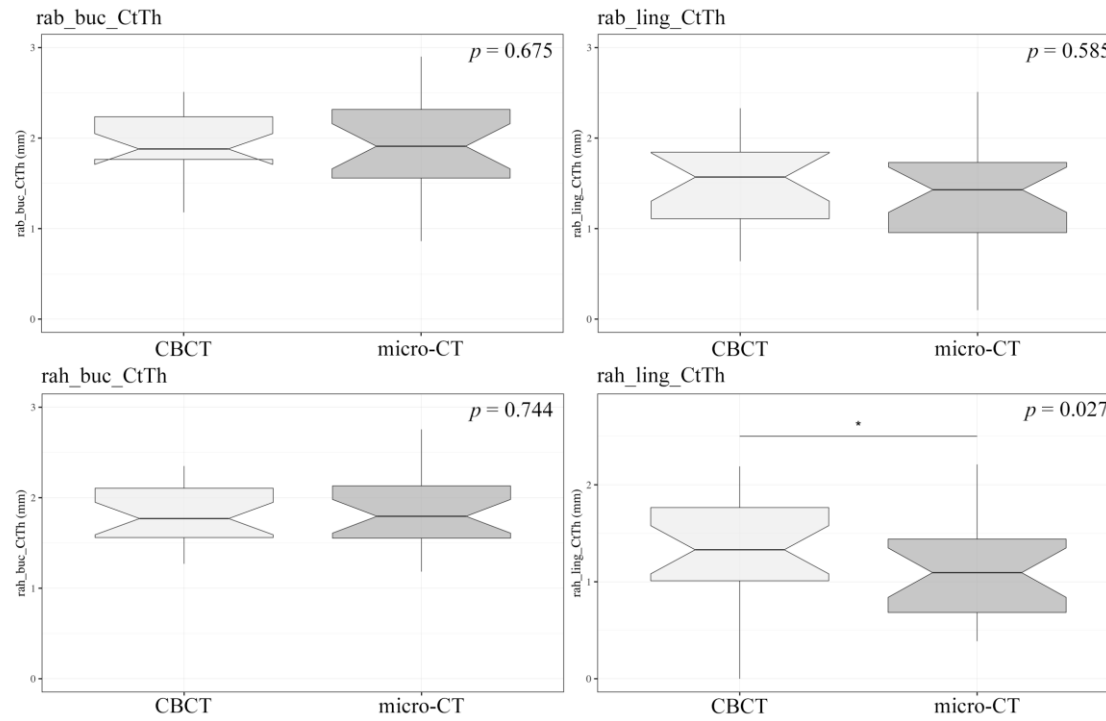
Figure 6.4. (continued)
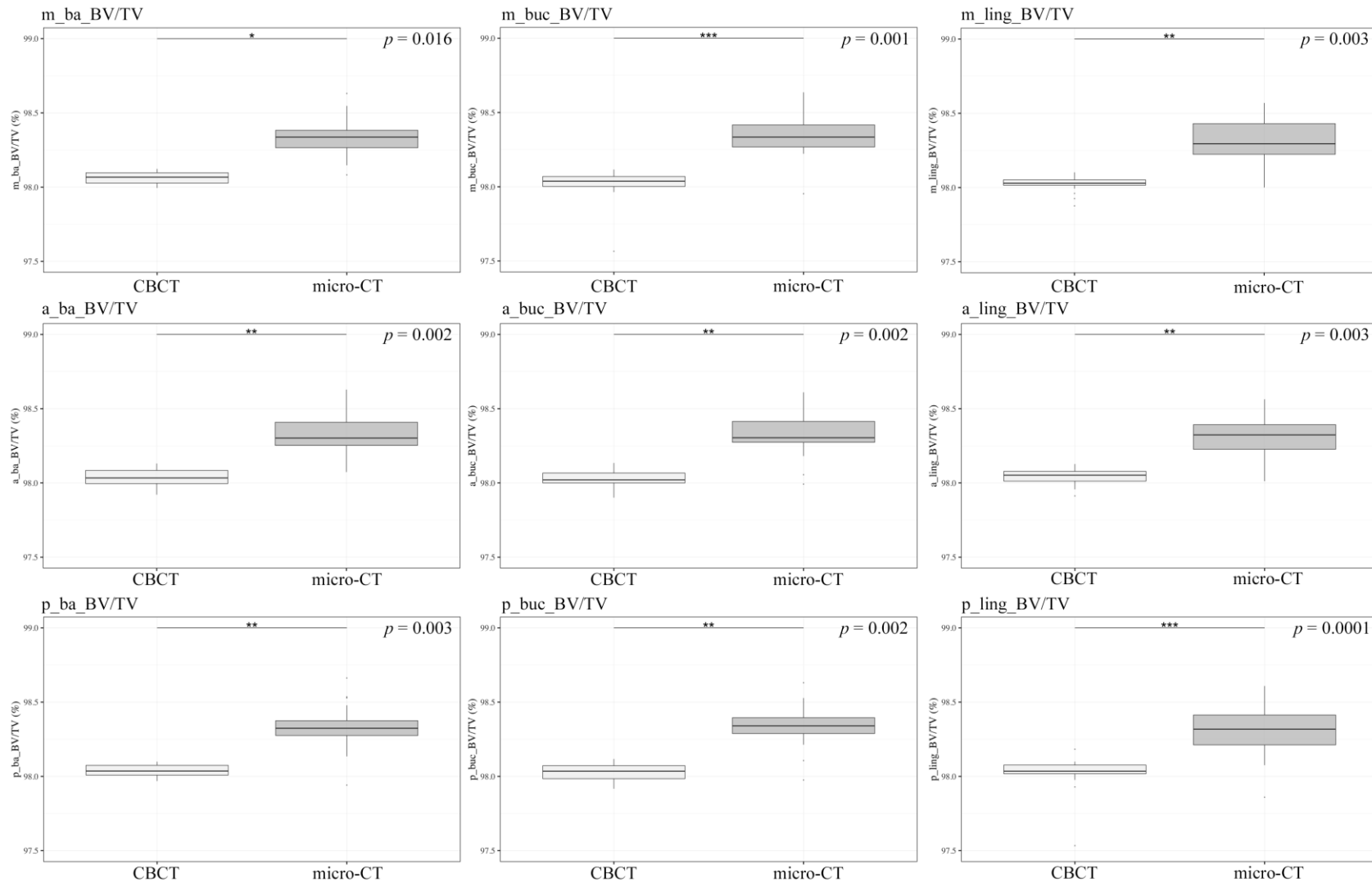
Figure 6.5. Boxplots of BV/TV (%) per modality (CBCT vs. micro-CT), recorded on the midline (first row), anterior (second row), posterior (third row), ramus breadth and height sections. Dots depict outliers. Paired Wilcoxon signed-rank test *p*-values are indicated for each boxplot. Significance: *** *p* < 0.001, ** *p* < 0.01, * p < 0.05. (continued on next page)
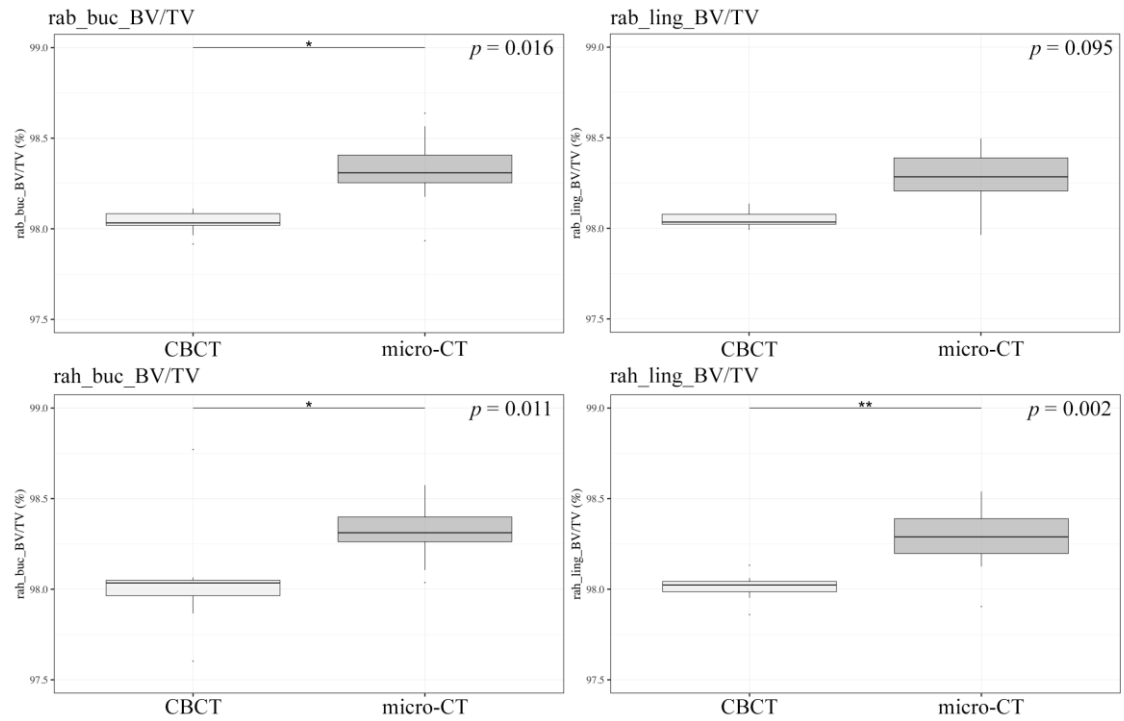
Figure 6.5. (continued)

6.2. Automatic comparison of volumes

Whereas the previous analyses focused on specific measurements and VOIs, this last section considers the mandibular bone as a whole. Comparisons between the two modalities were performed directly on each pair of three-dimensional volumes (CBCT vs. micro-CT) in order to visualise the general discrepancies between the volumes (i.e., to which extent the CBCT volume deviates from the micro-CT reference).

As detailed in Chapter 3 Materials and Methods, first, an automatic best-fit registration process of each CBCT volume onto its respective micro-CT volume was implemented. The quality of each registration was assessed through the automatic calculation of percentages (one for each pair), detailed in Table 6.5. The closer to 100% this percentage is, the better and accurate is the superimposition. Only two individuals showed registration scores lower than 96% (n°6 with 91.43% and n°24 with 87.97%).

Nominal/Actual comparison analyses were then performed generating three-dimensional colour-coded deviation maps (one for each pair) allowing the visualisation of the global topography of the deviations between the two volumes (Figure 6.6). For each pair, analyses were computed four times, using four different maximum deviation distances: 0.2 mm, 0.4 mm, 0.6 mm and 1.0 mm. No maximum deviation distances greater than 1.0 mm were computed as a distance of more than 1.0 mm between the two surfaces would not be considered acceptable. On the other hand, a maximum deviation distance of 0.2 mm is regarded as minimal, and almost insignificant.

Cumulated deviation values (normalised surface in % in function of the absolute deviation in mm) were generated and are summarised in Table 6.5 for all the individuals, where the normalised surface percentages are given per maximum deviation distance (0.2 mm, 0.4 mm, 0.6 mm and 1.0 mm). For example, if a maximum distance deviation of 0.2 mm was accepted, the CBCT and micro-CT volumes of individual n°1 overlapped 53.15% of their surfaces; while in the case of an accepted maximum deviation value of 1.0 mm, 98.66% of their surfaces overlapped, i.e., 98.66% of the surfaces overlapped with less than 1.0 mm of deviation, or in other words, only 1.34% of the CBCT surface deviated from the micro-CT with more than 1.0 mm.

In average (as calculated in the last rows of Table 6.5), the CBCT volume surfaces overlapped the micro-CT reference surfaces at 98.91%, with less than 1.0 mm of deviation, i.e., only 1.09% of the CBCT surfaces were deviating from the micro-CT with more than 1.0 mm.

Even when the maximum deviation distances were lowered to 0.6 mm, 0.4 mm or 0.2 mm, the average overlap amounted to 92.79%, 81.00% or 54.60%, respectively. To sum up, the large majority (98.91%) of the differences between CBCT and micro-CT mandibular surfaces were inferior to 1.0 mm, but more than half (54.60%) was greater than 0.2 mm.

As illustrated in Figure 6.6 with three individuals taken as examples (n°15, 21, 14) and a maximum deviation distance of 1.0 mm, visualisation of the topography of the deviations of all the pairs highlighted that the posterior area of the mandible showed more pronounced errors (blue and red spots) than the rest. These three individuals were chosen because they reflect different degrees of deviations: maximal deviation differences with 96.35% of overlapped surfaces and 3.65% of surfaces deviating more than 1.0 mm (n°15, Figure 6.6 A); average with 98.38% of overlap and 1.62% of errors (n°21, Figure 6.6 B); minimal with 99.47% of overlap and only 0.53% of deviations greater than 1.0 mm (n°14, Figure 6.6 C). The three colour-coded maps, however, confirmed that deviations were mainly observed on the posterior body (around the molar region), on the ramus, including the condyles and coronoid processes. The condylar neck and its posterior border, as well as the internal (or lingual) surfaces of the condyles, were particularly affected. Posterior teeth, like molars, also displayed deviations, especially on their occlusal surfaces. On a last note, differences were not observed between the left and right sides of the same mandible.

In conclusion, CBCT volumes, when compared to micro-CT volumes, seemed to present small geometrical deformations towards the posterior part of the mandible. This could be explained by several factors, such as the different system procedures followed by the two machines (e.g., the object rotates or not during scanning, the size of the field of view), the differences in resolution, in calibration, etc.

Table 6.5. CBCT vs. micro-CT volume comparison statistics: registration quality (%) and nominal/actual comparison analysis results presented as percentages of identical/overlapped normalised surface (%) per absolute deviation distance (at 0.2 mm, 0.4 mm, 0.6 mm or 1.0 mm). The individuals in bold are illustrated in Figure 6.6: n°15 in [A], n°21 in [B] and n°14 in [C].

MD	Best-fit registration (%)	Nominal/actual comparison: normalised surface (%)			
		at 0.2 mm	at 0.4 mm	at 0.6 mm	at 1.0 mm
1	98.91	53.15	79.55	92.33	98.66
2	99.47	60.92	84.51	95.00	99.48
3	99.21	49.74	77.79	92.03	99.15
4	99.05	57.21	79.82	90.46	97.61
5	99.53	54.07	80.76	92.11	99.36
6	91.43	54.60	81.00	92.79	98.91
7	99.43	55.68	83.58	95.00	99.25
8	99.27	58.48	80.47	91.51	99.10
9	99.90	62.93	86.3	95.21	99.83
10	99.14	52.69	79.83	92.57	99.01
11	100.00	59.21	84.41	94.74	99.25
12	99.83	45.5	76.31	91.75	99.05
13	100.00	58.32	84.0	93.94	99.20
14	**100.00**	**57.85**	**84.92**	**95.29**	**99.47**
15	**97.01**	**48.37**	**74.99**	**89.72**	**96.35**
16	98.54	49.35	78.03	91.69	98.55
17	99.38	48.63	81.28	94.64	99.47
18	99.57	57.33	81.24	92.47	99.22
19	99.97	51.19	78.33	90.91	98.18
20	99.44	54.50	80.78	92.45	98.45
21	**99.19**	**58.71**	**84.52**	**93.85**	**98.38**
22	99.34	52.34	78.52	91.35	99.22
23	99.76	52.17	80.46	92.76	99.36
24	87.97	57.41	82.57	92.47	99.35
mean		54.60	81.00	92.79	98.91
min		45.50	74.99	89.72	96.35
max		62.93	86.30	95.29	99.83
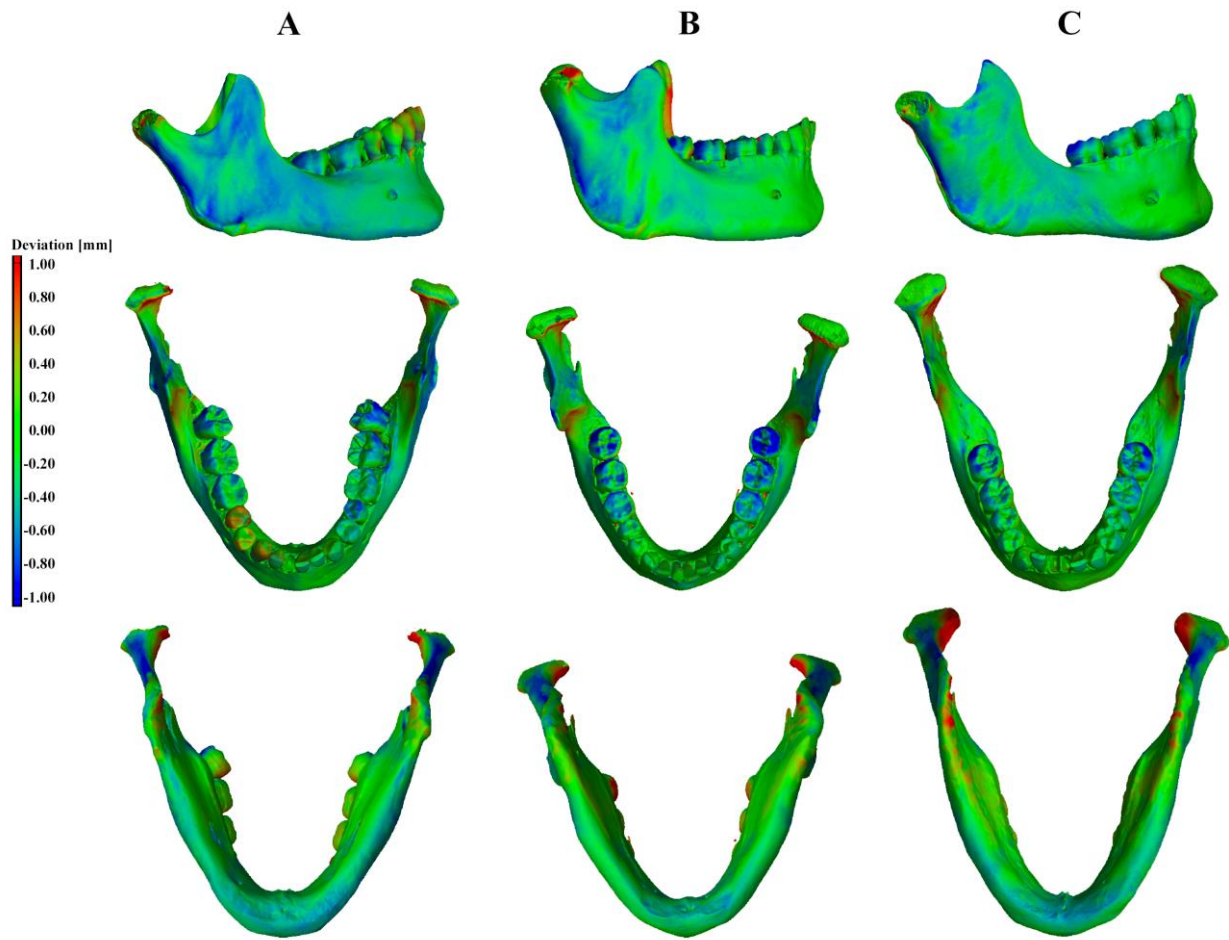
Figure 6.6. Examples of CBCT vs. micro-CT deviation maps obtained for three individuals (left to right: n°15, 21 and 14), illustrating different degrees of deviations: maximal deviation differences with only 96.35% of overlapped surfaces [A]; average with 98.38% [B], minimal with 99.47% [C]. Colour-coded maps depict the geometric discrepancies on the entire volume, on a scale ranging from red (the largest positive deviations), passing through green (no deviations or small), to blue (the largest negative deviations). Mandibles are in lateral (top row), superior (middle) and inferior (bottom) views.

278

Chapter 7. Discussion

This research project is the first attempt to investigate the consequences of tooth loss and advancing age on the mandible in a large adult South African sample, employing very high-resolution scanning modalities (micro-CT and CBCT). While Oettlé (2014) also analysed the effects of tooth loss and age on the mandible in South Africans, her research focused mainly on macroscopic changes using traditional methods and on a preliminary description of the changes in cortical thickness using CBCT scanning. Hutchinson (2017) also studied South African populations using micro-CT scans, but focused on immature mandibles and consequences of growth on the microstructure. On the other hand, this research focused particularly on the mandibular cortical microstructure and microarchitecture, although variations in external mandibular morphology were also noted as they relate closely to the internal structure.

With the current development and continuing advancement of high-resolution imaging technologies, like micro-CT, many questions on the microstructure of the mandibular bone could be answered. The extensive skeletal virtual database acquired, as well as the methodology developed in the thesis whereby external distances and two types of inner parameters (linear and 3D) were combined, gives a better understanding of the mandibular cortical bone microstructure, and its adaptations following tooth loss, or aging. This research is the first providing such a comprehensive review of the mandibular cortical architecture, while also mapping the external changes. Most of the studies found in the literature focused either on one type of measurement (external distance, cortical thickness, cortical density), and one type of influencing variables (such as tooth loss, age, sex, ancestry). For instance, the effects of tooth loss (Raustia *et al.*, 1998; Merrot *et al.*, 2005; Huumonen *et al.*, 2010; Chrcanovic *et al.*, 2011; Hansson and Halldin, 2012; Mays, 2013; Dekker *et al.*, 2018; Guevara Perez *et al.*, 2019), or aging (Kloss and Gassner, 2006; Swasty *et al.*, 2009; Shaw *et al.*, 2010; İlgüy *et al.*, 2014; Ishwarkumar *et al.*, 2017), or both (Xie and Ainamo, 2004; Oettlé *et al.*, 2009a, 2016; Chole *et al.*, 2013; Ozturk *et al.*, 2013; Oettlé, 2014; Hutchinson *et al.*, 2015; Mays, 2017; Parr *et al.*, 2017) on the external morphology of the mandible were extensively studied in the past, but the objectives were often limited to the analysis of sexual dimorphism or ancestral variations.

The methodology created and tested in this thesis addressed two issues which permitted the collection of measurements on mandibles in a consistent manner, even when displaying various degrees of tooth loss (from none to completely edentulous). Firstly, the Eichner Index (Eichner, 1990; Ikebe *et al.*, 2010) used in this study to evaluate each individual's dentition status (instead of just counting teeth as in the majority of the literature), considers several parameters besides the number of teeth, such as the occlusion and the pattern of tooth loss (e.g., unilateral vs. bilateral) and made it possible to reflect on the masticatory abilities of the individuals. Secondly, most of the studies reviewed used mandibular cross-sections defined according to teeth, or even according to the position of the mental foramen, which is known to be highly dependent on the dentition status of the individual. These methods often forced the authors to restrict their sample and exclude individuals with an important degree of tooth loss or even in an edentulous state. In this thesis, however, the placement of the cross-sections of the body was determined according to landmarks positioned along the inferior border of the mandible, which is less influenced by the dentition status and thus, ensured analogous sections between individuals despite the effects tooth loss could have on the mandible. The cross-section at the symphysis for instance was defined using standard anatomical landmarks (such as the menton and pogonion), while the other two cross-sections of the body were defined from the distance along the inferior border delineated by the menton and gonion landmarks. This distance was then automatically divided in several equidistant segments demarcating the anterior and posterior cross-sections.

In this Discussion Chapter, and in order to have a comprehensive assessment of the mandibular changes related to tooth loss and/or aging, the external morphology (assessed with the external distances) is considered in conjunction with the microstructure (evaluated with cortical thickness and density). First, an overview of the external morphology and cortical microstructure of the mandible in a control sample is presented, in which tooth loss or the aging process is excluded and is compared with the literature. Following this, the changes caused by tooth loss only are summarised, followed by a description of the age-related changes and their final co-integration. Several prospective implications are put into perspective, with a particular focus on two practical applications of the methodology developed in the thesis: namely in dentistry (implantology) (see Appendix A), and in palaeoanthropology (see Appendix B). The limitations of the study are also reviewed and are presented with various suggestions for future research.

7.1. Macro- and microstructure of the mandible in a control sample

In order to have a better comprehension of the macro- and microstructural changes of the mandible occurring with tooth loss and aging, an overview of the mandible in a control sample used as reference, i.e., those not affected by tooth loss (mandibles classified as Eichner Index category A only), is presented here. Two important factors of variation (sex and ancestry) are also discussed.

7.1.1. Regional variations within the mandible

Firstly, even if not exposed to biomechanical stresses like tooth loss, variability within different areas of the mandible was confirmed, as the mandibular body height, particularly, was always the greatest at the midline and then decreased gradually towards the posterior areas, as observed in the literature (Kasai *et al.*, 1996; Swasty *et al.*, 2011). Swasty *et al.* (2011) associated this antero-posterior reduction with different facial type categories and their vertical dimensions. "Long-face" individuals, compared to "short-face", were found to display the biggest change between the midline and the other areas. However, in the South African sample analysed in the thesis, all dentate individuals (females and males; individuals of African and European ancestries) showed a similar decreasing height pattern from the midline (or symphysis) to the anterior section (around premolars) and finally to the posterior area (around molars).

The cortical bone thickness, however, was generally thicker in the posterior area of the mandible than in the anterior or even more importantly than at the midline, as observed in several previous studies (Carter *et al.*, 1991; Kasai *et al.*, 1996; Katranji *et al.*, 2007; Swasty *et al.*, 2009, 2011; Fayed *et al.*, 2010; Farnsworth *et al.*, 2011, 2011; Al-Jandan *et al.*, 2013; Cassetta *et al.*, 2013). In terms of the cortical bone density, a similar pattern was observed with lower BV/TV values at the midline compared to the anterior or posterior volumes of interest, which was confirmed by several articles (Schwartz-Dabney and Dechow, 2003; Park *et al.*, 2008; Cassetta *et al.*, 2013). This difference in density between the midline, the anterior and posterior areas of the corpus was also observed in different primate species (macaque, baboons) by Dechow *et al.* (2017). On the other hand, Kingsmill and Boyde (1998), only looking at the area between the midline and the mental foramen, observed that the apparent density was

greater at the midline than at the level of the mental foramen. However, the sample studied comprised individuals with various degrees of tooth loss (from completely dentate individuals to edentulous), which might have influenced the results.

Finally, to summarise, the morphology and microstructure in the anterior and posterior regions of the mandible display similar variations and profiles as they might undergo similar forces and stresses. However, compared to the rest of the mandible, the symphysis shows unique features: a higher alveolar height associated with a thinner and less dense cortical bone. Schwartz-Dabney and Dechow (2003) drew similar conclusions, completed by further information on cortical bone material properties. Indeed, additionally to the lesser density, the symphysis also showed less stiffness (i.e., less ability to resist) in axial loading and shear compared to other regions of the mandible. Eventually, it appears that, for a mandible without tooth loss, the smaller the height of a section, the thicker and denser the cortical bone. Farnsworth *et al.* (2011), who also found this midline/anterior/posterior pattern, explained that it may be due to greater masticatory demands in the region of the molars as there is an increase in bite forces, and more particularly occlusal forces towards the posterior regions (Throckmorton and Dean, 1994; Tortopidis *et al.*, 1998; Masumoto *et al.*, 2001; Ferrario *et al.*, 2004; Gröning *et al.*, 2013). Indeed, not all teeth contribute in the same way to the masticatory process and molars, with their large occlusal contact areas, are often regarded as the most influential (Lepley *et al.*, 2011; Bourdiol *et al.*, 2020).

Regarding the bucco-lingual distribution of cortical bone, no differences in cortical density were noted in the thesis, whereas differences were reported in the literature. Most of the authors (Atkinson and Woodhead, 1968; Kingsmill and Boyde, 1998; Sato *et al.*, 2005; Cassetta *et al.*, 2013) observed that the lingual bone was denser than the buccal cortex, even if a few studies did not find any bucco-lingual density asymmetry on the mandibular corpus, confirming our findings (Schwartz-Dabney and Dechow, 2003). On the other hand, some differences in cortical thickness were noticed between the basal, buccal, and lingual areas of the mandible. In this research, the basal cortical bone was always thicker than lingually or buccally. Several authors assessed the basal bone in addition to buccal and lingual thicknesses and obtained corroborating results (basal >>) in the region of the symphysis (Fukase, 2007; Fukase and Suwa, 2008), of the corpus (Daegling and Grine, 1991; Humphries, 2007) or both (Kasai *et al.*, 1996; Schwartz-Dabney and Dechow, 2003; Swasty *et al.*, 2009, 2011; Cassetta *et al.*, 2013). According to Gröning *et al.* (2013), this thick cortical bone on the inferior border of the mandible reflects the high strains applied to the areas.

In our results, the lingual cortical bone thickness was greater than the buccal thickness (lingual > buccal) at the symphysis and at the anterior section. This buccal vs. lingual cortical thickness asymmetry was also obtained by other authors (Kasai *et al.*, 1996; Kingsmill and Boyde, 1998; Daegling and Hotzman, 2003; Fukase, 2007; Katranji *et al.*, 2007; Fukase and Suwa, 2008). For example, Kingsmill and Boyde (1998) measured cortical thickness at the midline and at the level of the mental foramen, and noticed the difference in thickness between buccal and lingual cortical bone (lingual > buccal). They associated it with the recurrent presence of "extra thick struts" at the level of the mental spines (genial tubercles), which provide insertions for the geniohyoid and genioglossus muscles. These extra protruding spines are indeed present around the midline of the mandible, but not on the rest of the mandibular body.

However, at the posterior section, around the molars, no bucco-lingual thickness asymmetry was detected. Interestingly, several articles (Kasai *et al.*, 1996; Daegling and Hotzman, 2003; Schwartz-Dabney and Dechow, 2003; Sato *et al.*, 2005) found that, at this position, the mandibular body had thicker buccal than lingual cortical bone (buccal > lingual). For instance, Daegling and Grine (1991), measuring the cortical thickness at the level of the first and second molars in a sample composed of great apes and modern humans, found that, while the basal bone was indeed thicker than at any other sites, the buccal cortical bone was thicker than lingually. This was often interpreted as an adaptative effect of stronger buccal than lingual strains applied during mastication (Gröning *et al.*, 2013), and thus also linked to the inclination of the molars towards the lingual side in order to resist to these strains (Masumoto *et al.*, 2001). The difference in results between this thesis and the literature may be influenced by the location of the posterior section, which was not defined according to the position of a specific tooth in our research and thus maybe positioned slightly before the molars in some individuals. In the articles cited before, the cortical thickness was measured on cross-sections directly under the first, second or third molars (Daegling and Grine, 1991; Kasai *et al.*, 1996; Daegling and Hotzman, 2003).

7.1.2. Integrated morphology and microstructure

Mandibles with complete dentition seemed to have had an integrated external morphology with mutually dependent areas. This integration is of utmost importance during growth and continues during adulthood to ensure coordination and proper biological functions

(Bastir and Rosas, 2005; Polanski, 2011). For instance, the three alveolar body heights (midline, anterior, posterior) were strongly correlated to each other, as well as moderately with the body length, or even with the two ramal distances (ramus breadth and height). Mutually dependent areas were also observed for each of the microstructural parameters, as also found by Daegling (2007). Indeed, all the cortical thicknesses measured basally (or buccally, or lingually) were correlated to each other, resulting in an antero-posterior homogeneity of the basal cortical bone (or buccal, or lingual, respectively). In other words, changes occurring in the symphyseal basal cortical bone are reflected anteriorly or posteriorly in the basal area of the body, and reciprocally. The other microstructural parameter measured, the cortical BV/TV, showed an even more generalised and homogeneous distribution of density all over the corpus and to a lesser extent with the ramus, as all the volumes of interest were correlated with each other, with particularly strong relationships between the anterior and posterior areas. Studying cortical bone mass, von Wowern (1977) also found a correlation between the density measured at the premolar and molar cross-sections. Kingsmill and Boyde (1998) observed a significant correlation more anteriorly, between the apparent cortical density measured at the midline and at the mental foramen. Finally, Klemetti *et al.* (1993) found that the buccal and the lingual cortical bone densities, assessed via BMD were strongly correlated.

7.1.3. Sex and population variation

Overall, regarding sexual dimorphism, the observed variations in the external morphology of the mandible followed the literature, using either traditional (Franklin *et al.*, 2006, 2008b; Ozturk *et al.*, 2013; Ishwarkumar *et al.*, 2017; Mays, 2017) or virtual methods (Swasty *et al.*, 2011; İlgüy *et al.*, 2014; Dong *et al.*, 2015; Gillet *et al.*, 2020; Motawei *et al.*, 2020), with males always displaying larger dimensions than females. Strong sexual dimorphism was found for all external measurements (mandibular body length; midline, anterior and posterior body heights; ramus breadth and height), with greater differences at the level of the ramus, or for the mandibular body length, which was also summarised by several authors (Humphrey *et al.*, 1999; Nicholson and Harvati, 2006). The greater level of sexual dimorphism at the ramus confirms what was initially found by Plavcan (2002) on a sample of 82 different primate species, where the author observed that in areas with strong muscles attachments, such as the masseter with the ramus, magnitude of the dimorphism was more pronounced. Besides influencing the external morphology of the mandible, sexual dimorphism

was found to particularly affect one component of the mandibular microstructure as well: the cortical thickness. As in many articles in the literature (Fayed *et al.*, 2010; Kim and Park, 2012; Cassetta *et al.*, 2013; Joo *et al.*, 2013), almost all cortical thicknesses measured were greater in males than in females, except at the three body basal sites in which values were very close. As for the cortical bone density, there was significant sexual dimorphism, but the values for males and females were close, with particularly wide ranges for males. A small number of studies (Bartlett *et al.*, 1992; Cassetta *et al.*, 2013) reported a significant difference in cortical density between fully dentate males and females. On the other hand, majority of the studies analysing a dentate sample noticed the absence of sexual dimorphism in cortical density (von Wowern and Stoltze, 1978, 1979; Kingsmill and Boyde, 1998; Park *et al.*, 2008; Buyukkaplan *et al.*, 2013; Ozdemir *et al.*, 2014).

Focusing only on the South African population, some ancestral variations were also observed, such as a longer mandible with a broader and shorter ramus, and greater body heights in individuals from African ancestry than from European ancestry. These findings confirmed what was found in the literature between South Africans of African and European ancestries (Franklin *et al.*, 2006, 2008b; Oettlé *et al.*, 2009a; Oettlé, 2014), or even when compared to other worldwide populations (Nicholson and Harvati, 2006), such as North Americans of European ancestry (Franklin *et al.*, 2007). Moreover, variations associated with ancestry were also observed on the microstructural level for a few cortical thickness locations (two sites on the body, and two on the ramus), in which greater thicknesses were found in South African individuals of African ancestry compared to European ancestry. Two studies observed a similar trend, although their results were not significant (Oettlé, 2014; McKay, 2019). Regarding the cortical bone density, no significant ancestral variations were observed in this research, although South Africans of African ancestry showed a greater number of outliers, and South Africans of European ancestry had much wider ranges of BV/TV values.

Interactions between sex and ancestry in individuals without tooth loss were also considered, as it was shown that sexually dimorphic features and patterns were themselves often dependent on the population considered. In the South African sample studied in the thesis, the ramus height showed the greatest values in males of European ancestry, followed by males of African ancestry, and then females of both ancestries. However, all the other distances, and particularly the ramus breadth, were always greater in males of African ancestry, confirming the broader ramus observed by several authors (Franklin *et al.*, 2007; Oettlé, 2014). Interestingly, most of the external distances (body length; midline, anterior and posterior body

heights; ramus height) were more influenced by sex than by ancestry, except for the ramus breadth, for which ancestry appeared to be the main co-founding factors. Similarly to the external distances, South African males of African ancestry always displayed the thickest cortical bone, while females, particularly of European ancestry, had the thinnest cortical thicknesses. As seen for sex and ancestry independently, the cortical bone densities were not particularly affected by sex/ancestral variations, as only a very small number of volumes of interest were found to differ, which was always between females of African ancestry (densest cortical bone) and males of European ancestry (less dense). This slight difference may be explained by a confounding factor, aging, discussed more in detail later in section [7.3]. Indeed, the African ancestry female subsample in general comprised younger individuals than the three other subsamples.

7.2. Effects of changes in dentition

As tooth loss is commonly observed in humans, and considering the impact and the alterations it can provoke on the mandible (Kingsmill, 1999; Standring, 2009; White *et al.*, 2012), its precise effects and consequences on the mandibular external morphology and microstructure are important to assess and understand. The analyses detailed in the tooth loss section of Chapter 4 were partitioned in two: (i) comparing the dentition groups while controlling or not for demographic factors (sex, ancestry, sex/ancestry); (ii) and comparing the changes within each demographic factor while controlling for tooth loss. In other words, the first scenario compared the three main dentition groups in the entire sample, in each sex, in each ancestry and in each sex/ancestral subsample. However, in the second scenario, sexual dimorphism and ancestral variations were investigated within each dentition category. This two-step approach permitted isolating and precise evaluation of the influence of each factor on the microstructure of the mandible and are considered in combination in the Discussion.

Firstly, the sole impact of tooth loss on the external morphology of the mandible and on the associated microstructure is considered, followed by the joint discussion of the effects of tooth loss with demographic factors.

7.2.1. Tooth loss as a unique factor

The integrated and generalised morphology and inner structure of the mandible described in section [7.1] are present in all individuals as long as they remain fully dentate. Indeed, individuals with moderate tooth loss (EI category B) displayed a reduction of homogeneity and uniformity (fewer correlations between all the measurements) for both external dimensions, cortical thicknesses and densities. Moderate tooth loss, often random, caused multiple divergent modelling patterns, as if each area affected by tooth loss undergoes its own local resorptive modelling process. The reduction in strains in specific regions of the bone directly impacted by tooth loss causes the appearance of localised independent events of bone resorption (Pearson and Lieberman, 2004; Bodic *et al.*, 2005).

In contrast, extreme tooth loss and edentulism, i.e., the generalisation of tooth loss to the whole mandible, is often followed by considerable bone remodelling causing global external and inner morphological changes, as hypothesised by Dechow *et al.* (2010), while

restoring uniformity and re-establishing the interdependency of most of the measurements (external distances, cortical thicknesses, and densities), particularly on the body. For instance, in this research, the correlations between the cortical densities all over the body were re-established in edentulous individuals, while all the relationships with the volumes of interest in the ramus were lost. The intensive bone modelling occurring in the mandibular body following complete tooth loss causes inner changes that the mandibular ramus is not following. This is aligned with the notion of modularity supporting the fact that the mandibular body and ramus are different developmental modules, and that each unit follows its functional role (Enlow *et al.*, 1976; Klingenberg *et al.*, 2003; Bastir and Rosas, 2005).

It is also worth noticing that individuals with extreme tooth loss or who are completely edentulous, always display a broad range of values (external distances, cortical thicknesses, and densities), much wider than individuals without tooth loss or with moderate tooth loss. Regarding the influence of tooth loss on the measurements themselves, the predominant global pattern is characterised by pronounced decreases which is delineated and discussed below, followed by two area-specific patterns characterised by either an increase in dimensions, or a total absence of change following tooth loss.

7.2.1.1. Global pattern following tooth loss: reduction of dimensions

Confirming the literature, most of the dimensions assessing the external morphology of the mandible showed a diminution associated with tooth loss. The three body heights – midline, anterior and posterior – (Kingsmill and Boyde, 1998; Raustia *et al.*, 1998; Merrot *et al.*, 2005; Chrcanovic *et al.*, 2011; Mays, 2013, 2017; Ozturk *et al.*, 2013; Hutchinson *et al.*, 2015; Parr *et al.*, 2017), the ramus breadth (Chrcanovic *et al.*, 2011; Parr *et al.*, 2017; Guevara Perez *et al.*, 2019), and the mandibular body length (Raustia *et al.*, 1998; Chrcanovic *et al.*, 2011; Hutchinson *et al.*, 2015; Guevara Perez *et al.*, 2019) were reduced in individuals with minimal tooth loss, as well as in edentulism. The diminution in body length, measured between the menton and the gonion, highlights the forward motion of the gonion, and thus confirms the widening of the gonial angle with the loss of teeth, as observed in several studies (Raustia *et al.*, 1998; Oettlé *et al.*, 2009a; Chrcanovic *et al.*, 2011; Oettlé, 2014; Hutchinson *et al.*, 2015).

Regarding the inner structure, tooth loss was accompanied by a general decrease in cortical thickness and density throughout the whole mandible (body and ramus) in individuals with moderate tooth loss and individuals with edentulism. The general thinning in cortical bone

was expected, as most of the studies considering tooth loss reported a reduction of the cortical bone in the body (Schwartz-Dabney and Dechow, 2002; Katranji *et al.*, 2007; Oettlé, 2014; McKay, 2019), and in the gonial angle area (Xie and Ainamo, 2004; Dutra *et al.*, 2005; Joo *et al.*, 2013; Oettlé, 2014). However, the decrease in density was rarely reported in the literature and may reflect the greater sample size and comprehensive distribution of individuals across dentition categories in this research. Indeed, while only one article noted a decrease in bone mineral density with edentulism (Bassi *et al.*, 1999), the majority of them did not find any significant differences between different dentition status (Atkinson and Woodhead, 1968; von Wowern, 1977; Kingsmill and Boyde, 1998; Schwartz-Dabney and Dechow, 2002).

The degree of tooth loss was particularly important when considering changes both in the external morphology and inner structure. The decreases of most external dimensions (body length and heights, ramus breadth), cortical thicknesses and densities were observed as soon as the first teeth were lost (Eichner Index categories A vs. B), suggesting that even a moderate, or a slightly unbalanced, loss of masticatory capabilities is enough to provoke an intense inner bone modelling. According to several reviews, the first couple of months after the loss of a tooth are the most important as this is when bone resorption is at its highest (Kingsmill, 1999; Bodic *et al.*, 2005). However, extreme tooth loss and edentulism had different consequences on the parameters measured in this research. First, the external distances, such as the alveolar heights and ramus breadth, were particularly affected with a stronger decrease and an aggravation of the original diminution. For instance, the midline, anterior and posterior body heights were found to become equal or "smoothed over" (Hillson, 2019) with edentulism, while this was not the case for the early stages of tooth loss, as also observed in Dekker *et al.* (2018). On the other hand, full edentulism did not accentuate the decrease in cortical thickness or in cortical density, but rather generalised the diminution to the entire mandible. On the contrary, Dutra *et al.* (2005) found that there were no differences in cortical thickness between dentate and partially dentate individuals, as they only observed a significant decrease with edentulism. The disagreement between this research and Dutra *et al.* (2005) may be influenced by the way of evaluating the dentition status. Indeed, their main classification criteria were based on the presence (i.e., dentate individuals) or absence of molars (i.e., partially dentate individuals), and did not consider occlusion or other patterns of tooth loss. As the rest of the literature researched only compared dentate to edentulous individuals, no other data are available on how the degree of tooth loss influences mandibular cortical thickness or cortical density.

Additional to the degree of tooth loss, timing and duration of tooth loss are also important parameters. Regarding the external distances, the decrease in posterior corpus height was generally noticed with earlier stages of tooth loss compared to the midline or anteriorly, which was also observed by Mays (2017). Interestingly, when measured posteriorly, the cortical thickness also appeared to be more affected, with greater decreases, than the rest of the body or of the ramus. This could be explained by the proximity of the analysed cross-section to the molars, and more particularly to the first molars. Indeed, molars are often the first teeth to be lost or extracted as they are more subjected to caries and periodontal diseases than any other teeth (and particularly compared to anterior teeth) (Hillson, 2019). Furthermore, molars are considered as the type of tooth contributing the most to mastication, causing greater maximum bite forces in the posterior area compared to the rest of the mandible (Throckmorton and Dean, 1994; Tortopidis *et al.*, 1998; Ferrario *et al.*, 2004; Lepley *et al.*, 2011; Bourdiol *et al.*, 2020). The loss of molars might thus have more serious consequences than the loss of other teeth, with a radical decrease in masticatory forces affecting the bone.

7.2.1.2. Area-specific patterns following tooth loss

As discussed before, reduced measurements associated with tooth loss were mostly similar everywhere in the mandible. However, two specific areas were affected differently by the loss of teeth: the lingual side of the midline, and the ramus (and more particularly the ramus height). Indeed, the midline lingual cortical site did show a unique and quite different behaviour compared to all the other sites, as no decrease in cortical thickness or in cortical density was detected at all, either with moderate or with substantial tooth loss, compared to the rest of the mandible in which both measurements declined. In fact, while the midline lingual cortical density was not affected and did not show any changes with tooth loss (as also found by Kingsmill and Boyde, 1998; Schwartz-Dabney and Dechow, 2002), the midline lingual cortical thickness increased significantly with extreme tooth loss and edentulism, as observed by several authors using different modalities (Lestrel *et al.*, 1980; Schwartz-Dabney and Dechow, 2002; Katranji *et al.*, 2007; Oettlé, 2014). Furthermore, when considering the cortical thickness sites in detail, the thickest-to-thinnest pattern identified in individuals with full dentition (i.e., basal cortical thickness > lingual > buccal, at the midline and anterior sections) was similarly observed in the moderate tooth loss group in these three sections. However, in individuals with extreme tooth loss and total edentulism, this pattern was only found at the anterior section,

while at the midline, the lingual cortical thickness was now greater than the basal and buccal thicknesses.

This increase in midline lingual cortical thickness can be in part explained by the fact that the lingual side of the mandible, particularly at the symphysis and the anterior region of the body, is known to be a bone formation area, while the superior part of the corpus (the alveolar bone) as well as the anterior border of the ramus are resorptive bone (Martinez-Maza *et al.*, 2013). In addition, the midline lingual region is under much strain as Van Eijden (2000) demonstrated that the tensile stresses experienced on the inner (lingual) surface of the mandible are far more important than the compressive stress (due to the lateral bending) exerted on the external (buccal) surface. Furthermore, van Eijden (2000) also highlighted that the magnitude of the lateral bending was at its highest level at the midline, and thus that strains were in general greater at this location than elsewhere in the mandible. These strains are partly due to two particular muscles having insertions there: the geniohyoid (one of the suprahyoid muscles) and the genioglossus (the largest muscle of the tongue) (Lucas, 2016). In order to be able to continue its vital functions (mastication, swallowing, speech), it is usually considered that the tongue is often the first to adapt to changing conditions, like the loss of teeth. Indeed, with tooth loss and even more with edentulism, and the associated changes in bone morphology (e.g., diminution in corpus height), the tongue becomes wider and shorter (macroglossia), and stretches itself to reach extended positions, inducing more strains on the symphysis (Bucca *et al.*, 2006; Morelli *et al.*, 2011; Posnick, 2014; Jindal *et al.*, 2015) and thus bone formation there. Schwartz-Dabney and Dechow (2002, 2003) explained this bone formation (and thus thickening) as a secondary local adaptation to localised greater strains.

Finally, while the minimum breadth of the ramus was influenced by tooth loss and decreased as observed in several studies (Chrcanovic *et al.*, 2011; Parr *et al.*, 2017; Guevara Perez *et al.*, 2019), the height of the ramus was not found to be impacted at all, even by edentulism, confirming a few articles of the literature (Merrot *et al.*, 2005; Ozturk *et al.*, 2013; Oettlé, 2014; Parr *et al.*, 2017), and was also very rarely found to be correlated to the other dimensions. The mandibular body may thus undergo minor or massive morphological changes, without affecting its ramus height. Ramus height therefore seems to be independent from the rest of the body.

7.2.2. Tooth loss and demographic factors

As detailed in Chapter 2 Literature Review and described in the section before, biomechanical factors like tooth loss, are not enough to explain all the external and microstructural changes encountered by the mandible, or in other words, explain why some individuals seem to be affected to a greater extent and at a greater rate than others (Kingsmill, 1999; Carlsson, 2004). Systemic factors for instance, and their interactions, might be important and must be considered, as for example tooth loss may not have similar consequences in males and in females, or sex possibly has an effect on tooth loss patterns.

The interactions between tooth loss and demographic factors, as well as their consequences on the mandible, are discussed in the following four sections. The first one [7.2.2.1] will discuss sex and tooth loss, which will be followed by ancestry and tooth loss in [7.2.2.2]. In the third section [7.2.2.3], both sex and ancestry will be considered with tooth loss. Finally, in [7.2.2.4], a separate discussion is provided for the cortical thickness and density recorded at the midline lingual site because of its unique behaviour associated with the loss of teeth.

7.2.2.1. Tooth loss and sex

The relationships between tooth loss and sex are pondered from two perspectives: the sexual variations during tooth loss (i.e., during tooth loss, are there any changes in sexual dimorphism?); and the consequences of tooth loss itself in each sex (i.e., does tooth loss have similar consequences in females and males?).

Sex has an influence on tooth loss and on its consequences, as females tend to be much more affected (in terms of frequency and magnitude) by the loss of teeth than males, which can be explained by diverse factors. In an extensive review by Russel *et al.* (2013), these factors were detailed and grouped in two categories: those related to "sex" per se, and thus to biological and physiological factors; the others related to the cultural and societal "gender" roles. For instance, in the sex-related factors, the authors cited a general longer life expectancy in females compared to males, and thus a longer period of time to experience tooth loss. This longer life expectancy at birth in females is also present in the South African population with an average age of 68.4 years for females and 62.4 years for males in 2020 (Statistics South Africa, 2021).

292

Russel *et al.* (2013) also addressed hormonal fluctuations, often associated with oral health issues (see also the review by Lukacs, 2011). Indeed, the variations in female hormone levels during menstruation, pregnancy, or menopause, have various repercussions on periodontal health and on the prevalence of periodontal diseases or caries (e.g., frequent gingival inflammation during the menstrual cycle, decreased resistance to oral bacteria and infection during pregnancy, higher rates of caries in females). Parity (number of pregnancies) is also a determinant factor and was found to be highly related to tooth loss in several populations (Russell *et al.*, 2013; Ueno *et al.*, 2013; Oziegbe and Schepartz, 2021). Besides the above sex-related factors, various gender-related factors influence tooth loss, such as the oral hygiene habits (like brushing teeth, flossing, preventive dentist visits), consistently more observed to be followed by women than men (Haikola *et al.*, 2008; Russell *et al.*, 2013). Several reviews (Lukacs, 2011; Russell *et al.*, 2013) also mentioned diet and nutrition as a factor, with different dietary intakes between men and women, because of different physiological requirements and preferences, often linked to diverse cultural and health beliefs.

The consequences of tooth loss observed on the mandibular bone itself were thus as follows. With tooth loss, all external dimensions (body length, alveolar heights, ramus breadth) except the ramus height, were found to decrease in both females and males, while always being greater in males than in females. The decrease in mandibular body length observed in both females and males in the thesis was unique. In the literature researched, Parr *et al.* (2017) obtained an increase in males, while Mays (2013) found non-significant changes in both females and males. The results regarding the alveolar heights confirmed what was found previously (Mays, 2013, 2017; Parr *et al.*, 2017) and even highlighted an increase in sexual dimorphism, which was explained by the more important alveolar bone resorption, and thus decrease in height, in females (Mays, 2015b, 2017).

On the other hand, the degree of tooth loss had different consequences in females and males. Strong sexual dimorphism was detected in fully dentate (EI A) and edentulous individuals (EI C), while it was less accentuated in individuals starting to lose teeth (EI B) (also found in Ramphaleng, 2015). Indeed, only males were affected by moderate tooth loss (EI category B), while extreme tooth loss and edentulism caused significant external changes in both females and males. Females might then require severe tooth loss before showing changes in morphology and decreases in body length, body heights, and ramus breadth. This difference may be linked to the sexual dimorphism in muscle size and force, with males having larger and stronger masticatory muscles than females (Lavelle, 1988; Ferrario *et al.*, 2004; Mays, 2013;

Posnick, 2014). Because there is a significant correlation between their force and the overall shape of the mandible (Sella-Tunis *et al.*, 2018), it is possible to hypothesise that strong masticatory muscles in males will exert more influence on the bone than female muscles. As soon as tooth loss starts, bone will reflect the changes in males, while in females, the smaller and weaker muscles require edentulism to have significant consequences on the external morphology of the mandible.

Like the external distances, the cortical thicknesses decreased with tooth loss in both sexes, while still maintaining sexual dimorphism (i.e., CtTh in males > females), or even increasing it in individuals with edentulism. Indeed, the diminution was stronger and more generalised (i.e., most of the sites were affected) in edentulous females than in edentulous males, as also found in two studies on living individuals (Xie and Ainamo, 2004; Joo *et al.*, 2013). In summary, females started off with a thinner cortical bone thickness compared to males, a difference that became more accentuated as all teeth were lost.

Sexual dimorphism in the cortical densities (i.e., BV/TV in males > females) was also detected in all dentition statuses, although tooth loss and edentulism were found to generalise the differences between males and females from some sites to the entire mandible. Furthermore, while sexual dimorphism was present, the BV/TV parameters recorded in females were not affected at all by tooth loss or edentulism, while within males, the density decreased in most of the sites with moderate tooth loss and with edentulism, even if extreme tooth loss did not seem to affect the decrease or aggravate it. This pattern was also observed by von Wowern (1988) in a study measuring the mandibular Bone Mineral Content (BMC) in 149 Danish patients. Indeed, they observed sexual dimorphism in both dentate and edentulous groups, but the BMC was similar in dentate and edentulous women.

The difference in onset and thoroughness of dental care between females and males might also explain these results. Indeed, women, paying greater attention to their teeth than men, might counteract the negative effects of tooth loss by treating affected regions earlier and in a more effective way with prosthetics, such as dentures or dental implants (Chikte *et al.*, 2020). Removable partial dentures for example, usually worn when a small number of teeth are lost/extracted, are more common in women than in men (Baran *et al.*, 2007). Partial dentures are known to have several advantages, such as the continued presence of high masticatory forces stimulating the surrounding bone and preventing resorption (Knezović-Zlatarić and Čelebić, 2005; Baran *et al.*, 2007), and thus have less impact than the long-term tooth loss (as in males in this research) on the microstructure of the bone (Knezović-Zlatarić

and Čelebić, 2005; Resnik, 2020). In conclusion, even if females started off with a lower cortical bone density than males, their bone microstructure is less affected by tooth loss than males for reasons that are still poorly understood.

7.2.2.2. Tooth loss and ancestry

Similarly than for sex and tooth loss, the interaction between tooth loss and ancestry is considered from two perspectives: the ancestral variations during tooth loss, and the consequences of tooth loss itself in each ancestral group.

Ancestral variations in external dimensions and cortical bone thickness observed between individuals having a full dentition were preserved, or even increased, with tooth loss. Almost all external dimensions (except the body length and the ramus height), as well as all cortical thicknesses, were found to decrease with tooth loss in both ancestral groups. However, South Africans of African ancestry still displayed a longer mandible with a greater body height, a shorter and broader ramus, as well as a thicker cortical bone, when compared to South Africans of European ancestry, and across all dentition statuses (absence of tooth loss, moderate tooth loss, edentulism) (also found by Oettlé, 2014).

When only considering the alveolar body heights, a few differences between the two ancestral groups were noted, depending on the degree of tooth loss. Indeed, even if South African individuals of African ancestry retained at all times the greatest dimensions, they still displayed decreased body heights as soon as tooth loss started, while extreme tooth loss and edentulism were needed before changes were observed in individuals of European ancestry. Inherent morphological differences between the ancestral groups could be accountable for the different reactions to moderate tooth loss. For instance, the differences in dental structure among populations (Hemphill, 2016; Irish, 2016), such as the relative greater size of dental crown or roots in South Africans of African ancestry (Hanihara and Ishida, 2005; Pilloud *et al.*, 2014), could be contributing to a more extensive alveolar bone loss as soon as the tooth is extracted or lost, and thus to a reduction of the mandibular height. The lack of change in alveolar heights with moderate tooth loss might also be the consequence of earlier and more frequent access to dental care in South Africans of European ancestry, for which treatments, including the possibility of dentures, could have been provided as soon as the first teeth are lost, delaying the resorption of the bone to a later period in life. Ayo-Yusuf *et al.* (2013) highlighted that preventive dental visits are a lot more common in South Africans of European

295

ancestry (27.8%) than in South African of African ancestry (3.1%), which was linked to health insurance coverage and other socio-economic factors (like education levels, material wealth).

With edentulism, ancestral variations were accentuated, with a much greater mandibular body height and thicker cortical bone in South Africans of African ancestry compared to European ancestry. Indeed, the decrease in mandibular body height was more important (i.e., greater) in edentulous South Africans of European ancestry than in edentulous South Africans of African ancestry. Similarly, the diminution is cortical thickness was more pronounced and generalised in edentulous individuals of European ancestry than African ancestry. This strong reaction in South Africans of European ancestry could reflect a longer duration of edentulism in these individuals and a greater bone loss over time. Dekker *et al.* (2018) for instance, highlighted the negative influence of the duration of edentulism on the mandibular body height. They observed a strong negative correlation between the body height of the mandible at the level of the mental foramen and the duration of edentulous state recorded in the patients. Furthermore, with earlier edentulism, these individuals might have to switch prematurely from removable partial dentures to complete dentures, which are known to enable bone resorption, and accelerate the thinning of the cortical bone, as opposed to removable partial dentures or implant-supported overdentures stimulating bone growth (only possible with remaining teeth) and thus preventing cortical resorption (Lestrel *et al.*, 1980; Knezović-Zlatarić and Čelebić, 2005).

In addition, cortical thicknesses measured in the posterior section were more affected by tooth loss than the rest of the mandible, particularly in South Africans of European ancestry. As explained earlier when tooth loss was the only factor analysed, the posterior cross-section is closely related to the molars, which are the first teeth typically lost. This might highlight the fact that individuals of European ancestry lose their first teeth earlier in life (or have them extracted) and reach the edentulism state earlier than South Africans of African ancestry, and thus might have indeed a longer duration of edentulism.

As far as mandibular cortical densities are concerned, similar to what was found in fully dentate individuals (see section [7.1]), almost no ancestral variations were observed with tooth loss – only a small number of VOIs showed a faint difference with tooth loss, with greater density values in South Africans of African ancestry. However, the loss of teeth caused different consequences in the two ancestral groups studied. South Africans of African ancestry showed a decrease in density with tooth loss and edentulism, while this change accompanying tooth loss was not significant in individuals from European ancestry. A decrease could still be

perceived with edentulism in the latter, but the distribution of the values was particularly large in edentulous individuals, maybe masking the significance. Another hypothesis, linked with the possible longer duration of edentulism in South Africans of European ancestry, might also be suggested, as this extended period in an edentulous state could cause different, more intense, and durable strains on the mandible than usual. This was hypothesised by Buyukkaplan *et al.* (2013) as well, when they suggested the presence of a denser cortical bone after a long duration of edentulism. As it may be surmised that the mandibular bone has to fulfil the role of teeth in various essential and demanding biological functions (such as mastication) when there are no teeth, the bone is compelled to undergo intensive resorptive modelling to improve its loading resistance and thus balances the destructive effects of random tooth loss. For instance, with edentulism, Schwartz-Dabney and Dechow (2002) observed changes in material properties of the cortical bone, such as a redirection of the maximum stiffness, interpreted as an adaptation to resist effectively the deformation. Furthermore, long-term edentulous individuals would rely on complete dentures to improve mastication, which implies additional functional changes, such as a change in the direction of biting (more vertical to improve denture retention) (Dechow *et al.*, 2010).

7.2.2.3. Interaction of factors: tooth loss, sex and ancestry

In this section, the influence of both sex and ancestry are considered together on individuals with various dentition status. As already observed with sex, and then with ancestry, the external distances measured, and more particularly the alveolar heights, confirmed a decrease in dimensions associated with tooth loss, notably with edentulism, in all four sex/ancestral groups of the South African sample studied. The largest dimensions of the external morphology of the mandible were observed in South African males of African ancestry across all dentition categories, except for the ramus height, in which South African males of European ancestry were the biggest, even with tooth loss or edentulism, confirming what was observed by several authors (Oettlé, 2014). Differences between the four sex/ancestral groups appeared to be accentuated according to the degree of tooth loss, similarly to what was noted for sexual dimorphism or ancestral variation in isolation. For instance, and for most of the measurements, South African females, and particularly of European ancestry, were more affected by tooth loss and showed a more intense decrease (also found in Oettlé, 2014). It was hypothesised by Oettlé (2014) that, additionally to the longer duration of tooth

loss and edentulism, possibly aggravated by the use of complete dentures, the gracility of female mandibles, compared to males, might also contribute to the greater loss with tooth loss.

A similar pattern was noticed with the cortical thicknesses with a diminution associated with tooth loss, and particularly edentulism, in all sex/ancestral groups, even if this decrease was less distinct in South African males of African ancestry. Furthermore, this group always displayed the thickest cortical bone across all dentition categories, compared to females of African and European ancestries which had the thinnest cortices, and a more generalised and frequent decrease.

Both for the external distances and the cortical thicknesses, South African males of African ancestry seemed to be particularly preserved from the influence of tooth loss, or are affected at a more advanced age than the other groups. However, the influence of tooth loss on the cortical bone density of the mandible was less predictable and unexpected, as no change was detected for three of the sex/ancestral groups: only South African males of African ancestry seemed to have their cortical bone densities affected by extreme tooth loss, confirming the decrease in density with tooth loss seen in males (in section [7.2.2.1]) as well as the one seen in individuals from African ancestry in section [7.2.2.2]. Unfortunately, it is difficult to compare these results with the literature, as studies on the mandibular cortical density and tooth loss are scarce, and even non-existent when focusing on the South African population.

As the cortical density seems to be affected by edentulism in only one group, this decrease could be due to a confounding factor, such as aging. Indeed, the subsample affected here (i.e., South African males of African ancestry) comprised individuals particularly well distributed throughout ages in all dentition categories (i.e., young and old in EI A, B or C), while the three other subsamples have more skewed distributions (i.e., younger individuals in EI A, and older in C). This may suggest a stronger influence of aging on the cortical density compared to tooth loss, which will be explored in more detail later (in sections [7.3, 7.4]).

7.2.2.4. Unique changes at the midline lingual site

As described earlier, in section [7.2.1.2], and in the literature (Enlow *et al.*, 1976; Schwartz-Dabney and Dechow, 2002; Katranji *et al.*, 2007; Oettlé, 2014), the lingual side of the midline displayed a strong cortical thickness increase associated with edentulism. This increase was detected in both females and males but was noticed to be much more pronounced in males than females. As explained by Schwartz-Dabney and Dechow (2002, 2003), this

thickening is a secondary adaptation of the bone to localised larger strains happening with edentulism in both males and females. However, the general robusticity displayed in male mandibles and associated muscles (Lavelle, 1988; Mays, 2013; Posnick, 2014; Sella-Tunis *et al.*, 2018) cause greater strains on the muscular insertions present on the lingual side of the symphysis, and thus a more enhanced modelling reaction to edentulism at this location, compared to females.

When considering the ancestry of the individuals, the increase of the midline cortical thickness associated with edentulism was also found in the two South African ancestral groups studied, and in all four South African sex/ancestral groups. However, interestingly, and contrary to the rest of the mandible in which males of African ancestry displayed the thickest cortical bone, the midline lingual cortical thicknesses of South African males of European ancestry were the greatest of all four groups. It could perhaps be explained by the strong increase observed in males, compounded by a longer duration of edentulism in these individuals, compared for instance to South African males of African ancestry.

Cortical bone density measured at the midline lingual site was different between females and males in the control sample but did not change with tooth loss or edentulism, as in other regions of the mandible (see section [7.2.1.2]). No ancestral variations were noted at this location.

7.3. Effects of aging

As described in the Literature Review, the aging process affects the facial skeleton and the resulting changes are considered part of the normal maturational process of bones (Bishara *et al.*, 1994; Akgül and Toygar, 2002; Kloss and Gassner, 2006; Albert *et al.*, 2007). In numerous studies, the lower facial skeleton, and more particularly the mandible, was found to continue "growing" throughout adult life (Bishara *et al.*, 1994; West and McNamara, 1999; Akgül and Toygar, 2002; Pessa *et al.*, 2008; Oettlé *et al.*, 2016), with for example an increase in mandibular length, an intensifying dento-alveolar regression, as well was remodelling and resorption of the alveolar bone. However, it is not always clear if these macro- and microstructural changes are only due to aging and the general progressive reduction in muscle and bone masses, or influenced by other confounding factors (such as tooth loss) (Albert *et al.*, 2007). Thus, in this section, the discussion is based on a sample of reference not affected by tooth loss, as to facilitate the understanding of the changes in the morphology and inner structure of the mandible that are exclusively due to aging, as opposed to what is caused by the loss of teeth.

7.3.1. Aging as a unique factor

In the control sample used here (i.e., not affected by tooth loss, only individuals from EI category A), aging alone did not have an influence on the external structure of the mandible, illustrated by the lack of significant changes in any of the external dimensions. This confirms the findings of other authors for the mandibular body length (Ozturk *et al.*, 2013; İlgüy *et al.*, 2014; Hutchinson *et al.*, 2015; Ishwarkumar *et al.*, 2017; Parr *et al.*, 2017), the alveolar body heights (Ozturk *et al.*, 2013; Mays, 2017; Parr *et al.*, 2017), ramus breadth (Shaw *et al.*, 2010; İlgüy *et al.*, 2014) and height (Ozturk *et al.*, 2013; Hutchinson *et al.*, 2015; Ishwarkumar *et al.*, 2017; Parr *et al.*, 2017).

Likewise, the cortical bone thicknesses (even at the midline lingual site) did not show any significant variation with age alone, verifying what was found by Kingsmill and Boyde (1998) or Deguchi *et al.* (2006) in dentate mandibles. On the other hand, most of the studies on the subject in the literature (von Wowern and Stoltze, 1979; Kribbs *et al.*, 1990; Dutra *et al.*, 2005; Swasty *et al.*, 2009; Sathapana *et al.*, 2013; Oettlé, 2014; McKay, 2019) reported a

decrease in cortical thickness with aging. These changes were hypothesised to be most probably due to the modelling process in reaction to biomechanical strains like tooth loss (Dechow *et al.*, 2010; Oettlé, 2014). Indeed, among these studies, at least three do not mention the dentition status of the individuals analysed, or do not take into account tooth loss in their statistical analyses, even with samples including individuals with tooth loss and edentulism (von Wowern and Stoltze, 1979; Kribbs *et al.*, 1990; Dutra *et al.*, 2005). Oettlé (2014), as well as McKay (2019), looked at the correlations between aging and tooth loss, but do not report on the consequences of aging in dentate individuals separately. In the end, only Swasty *et al.* (2009) and Sathapana *et al.* (2013) analysed cortical thickness with aging in fully dentate individuals. Interestingly, Swasty *et al.* (2009) showed maintenance in cortical thickness between 20 and 49 years old and noticed a decrease only after the 40 to 49-year-old decade. However, only a small number of sites were significant.

Cortical bone densities were particularly sensitive to senescence and showed a diminution in cortical BV/TV with increasing age in individuals not affected by tooth loss, which corroborates the general understanding regarding bone mass declining with aging (also called osteopaenia), even in the mandible. It confirmed the results of several studies on dentate individuals or patients using different definitions for bone density, such as the apparent density (Atkinson and Woodhead, 1968; von Wowern and Stoltze, 1980) or Bone Mineral Density (BMD) (Li *et al.*, 2011; Shaw *et al.*, 2012).

The general understanding of bone mass declining with age was also confirmed by the comparison performed in the thesis between the mandibular and femoral cortical bone densities with both bones showing an age-related decrease. This particular age-related inner bone remodelling is characterised by a shift in the bone resorption/formation balance, as bone resorption will exceed bone formation and cause significant bone loss (Agarwal, 2019). Indeed, it is often noted that with aging, the cortical porosity is increased due to an extensive intracortical remodelling (Agarwal, 2021), even in the mandible (Atkinson and Woodhead, 1968; von Wowern and Stoltze, 1978, 1980; Bartlett *et al.*, 1992). Osteopaenia may evolve in osteoporosis if the diminution in bone mass is particularly strong, or even accelerated, and provokes an increase in bone fragility, and thus a predisposition to fractures. While bone loss is considered as a "normal" age-related process, osteoporosis is a skeletal pathology with a multifactorial aetiology (von Wowern, 2001; Kloss and Gassner, 2006; Agarwal, 2019). According to the results discussed here, the mandibular bone seems to be impacted by osteopaenia like the rest of the skeleton (von Wowern, 1982; Munakata *et al.*, 2011); while,

301

however, there is still no consensus about osteoporosis in the mandible. Indeed, many authors (Kingsmill, 1999; Bodic *et al.*, 2005; Gulsahi, 2015; Coutel, 2018) commented on the various distinct factors of the mandible compared to other bones, e.g., a different embryological origin, presence of teeth and alveolar bone, specific cortico-trabecular repartition, unique biomechanical functions (e.g., mastication, speech) with constant loads and strains throughout life; and thus on its possible "resistance" to osteoporosis.

In this study, when comparing the cortical density of the mandible to the femur within a same individual, no correlations were found between them. The mandibular cortical density is thus not decreasing or increasing when the femoral density is, and reciprocally, suggesting a certain distinctiveness of the mandible. Similar results were reported by Kloss and Gassner (2006) for the mandible vs. vertebrae. In addition, in our results, the cortical bone density of the mandible was noticed to be much greater than in the femur, confirming the very dense nature of the mandible compared to the rest of the skeleton, which may be an explanation to the "resistance" to osteoporosis mentioned earlier.

7.3.2. Aging and demographic factors

Aging affects some individuals to a greater extent and at a greater rate than others. Indeed, similarly to tooth loss (see section [7.2.2]), senescence is influenced by many variables that need to be considered. As summarised by several authors (e.g., Oettlé, 2014; Agarwal, 2021), aging is characterised not only by chronological age, i.e., the number of years since birth, but also by the lifestyle of each individual. For instance, the age-related decrease in bone mass itself is influenced not only by the amount of bone lost, but also by the maximum bone mass gained during growth, which is highly dependent on several intrinsic and extrinsic factors (e.g., hormones, genetics, nutrition, stress) (Agarwal, 2021). From the results obtained with the sample of reference not affected by tooth loss, the influence of age on the mandibular morphology and inner structure is discussed while controlling two demographic factors (sex, ancestry).

When looking at dentate females and males separately, the external morphology (length of the body, alveolar heights, ramus breadth and height) of the mandible as well as the cortical bone thickness were not influenced by aging and maintained a similar pattern of sexual dimorphism throughout the decades (external distances and CtTh: males > females). Regarding the external distances, a few studies showed an increase in sexual dimorphism with aging but

only because of a decrease in dimensions in females (Mays, 2017; Parr *et al.*, 2017), which was not observed in this research. For the cortical thickness, some studies also found an age-related decrease in females, such as Dutra *et al.* (2005), but the samples were in general comprised of individuals of different dental status. This absence of age-related effects on the external distances and cortical thickness were also found in dentate individuals of each of the two ancestries, which retained the ancestral differences in older individuals (external distances and CtTh: AA > EA) observed previously in section [7.1].

However, for the mandibular cortical density in individuals without tooth loss, a slight difference was noted between sexes, as the decrease associated with age was only significant in males and not in females, which is possibly due to the better age distribution of dentate males through the decades. Indeed, in the literature researched, a few studies observed the age-related decrease in cortical bone density in both males and females (von Wowern and Stoltze, 1980; von Wowern, 1988; Li *et al.*, 2011; Shaw *et al.*, 2012). When considering dentate individuals of the two South African ancestral groups analysed in the thesis separately, the tendency of age-related decreasing density was observed in both (even if non-significant), with higher cortical densities in individuals of African ancestry compared to European ancestry, at all ages (from younger to older individuals).

303

7.4. Compounding effects of tooth loss and aging

Senescence is very often accompanied by tooth loss, although aging itself does not cause tooth loss (Haikola *et al.*, 2008; Ruquet *et al.*, 2015). One of the reasons suggested by dentists to explain the onset, or even the acceleration, of tooth loss is based on the presence and age-related development of plaque-related diseases (e.g., dental calculus, caries) and their progressive spreading throughout the dentition with time (Hillson, 2019) is often facilitated by specific health risk behaviour factors. For instance, smoking, and its duration in time, is one important factor that was found to be related to tooth loss, and more particularly edentulism, in many studies (Haikola *et al.*, 2008; Peltzer *et al.*, 2014; Helal *et al.*, 2019).

In the modern era, loss of teeth is rarely "natural" and thus age-related, but most frequently due to extraction of the affected teeth. For instance, in South Africa, extraction, rather than restorations, is the most predominant treatment provided in the public oral health services, causing high percentages of premature tooth loss (Mickenautsch *et al.*, 2007).

Different patterns were highlighted in the results when simultaneously considering the age of the individuals and the degree of tooth loss on the mandibular morphology and cortical microstructure. First, a short summary is given on the features not affected by age but only by tooth loss (moderate or extreme). A focus on variables showing compounding effects of tooth loss and aging (i.e., age-related diminutions depending on the degree of tooth loss) follows. Finally, according to the particular changes discussed in previous sections (see [7.2.1.2] and [7.2.2.4]), the lingual cortical bone of the mandibular symphysis is considered independently from the rest of the mandible. Within each of these four sections, demographic factors are also discussed.

7.4.1. Absence of age-related changes: sole influence of tooth loss

As seen in the previous section, age alone (i.e., individuals without tooth loss) was not observed to have an influence on any of the external distances or on the cortical thicknesses (including the midline lingual cortical thickness). When looking specifically at individuals with moderate tooth loss (EI category B), no further age-related changes were noticed in these distances (external and cortical thickness), even when grouping per sex or ancestry, confirming

304

that only tooth loss, and thus a bone functional adaptation to a variation in loading, is responsible for the decrease observed previously.

When looking specifically at the external morphology in the case of edentulism, aging did not have an influence on some of the external distances, such as the body length, the posterior alveolar height, the ramus breadth and height. This confirms the sole role of tooth loss, independent from aging, on the general reduced aspects of the external morphology. In particular, the diminution in body length observed with moderate tooth loss and edentulism, but not with advancing age in a sample where tooth loss is controlled, confirms the hypothesis stated in section [7.2.1.1] i.e., that the gonion moving forward and thus causing the widening of the gonial angle is only due to the loss of teeth, and is not age-related.

The primary factor of variation in the external morphology of the mandible is thus the loss of teeth, while aging does not have any influence (Oettlé, 2014; Ramphaleng, 2015; Parr *et al.*, 2017). This is in agreement with the bone modelling/remodelling theories, as they usually state that the remodelling process, occurring with senescence for instance, is only microscopic and does not affect the macroscopic architecture, while the modelling (or resorptive modelling) is a reaction against a change in loading and non-habitual strains, like the loss of teeth, and affects the bone microstructure as well as the external morphology (Barak, 2019; Gocha *et al.*, 2019; Ruff, 2019). The alveolar bone is, however, somewhat different from the rest of the mandibular structures (Bodic *et al.*, 2005) and the measurements associated with it (like the body heights) might be influenced by other factors than only tooth loss, as explained in the following section.

7.4.2. Age-related decrease in dimensions with edentulism

Significant diminutions of the midline and anterior alveolar heights were noticed with aging in individuals with extreme tooth loss and edentulism (see also Oettlé, 2014). Indeed, even if already edentulous, these individuals continued to lose alveolar bone in the anterior part of the mandible during life, which might be due to the duration of edentulism, and thus the age of these individuals (as we compared younger edentulous vs. older edentulous individuals), than just edentulism itself. This hypothesis is confirmed in the study by Ruquet *et al.* (2015), in which they linked the loss in alveolar bone (i.e., the body height) to the duration of specific individual and behavioural factors (duration of tooth loss, smoking habits, etc.), rather than to the age of the individuals. The fact that the posterior alveolar height does seem to be only

influenced by tooth loss and not by aging could also confirm this hypothesis. Mechanically, due to the U-shape of the mandible, if there is any loss of occlusion, it can only attempt to restore this occlusion anteriorly, and not posteriorly, as the mandible can only move in that direction. This leads to increased anterior pressure and greater bone resorption over time. Furthermore, the magnitude of the lateral bending is at its highest level in the anterior region, causing greater strains at this location than elsewhere in the mandible (van Eijden, 2000).

In terms of demographic factors, edentulous females, compared to edentulous males, were more affected by this age-related decrease in body height, while no differences were noted between ancestries.

In the case of extreme tooth loss and edentulism, all cortical thicknesses, except the midline lingual site, showed negative relationships with aging, indicating that in edentulous individuals, the mandibular cortical bone becomes thinner while aging increases (as also found by Kribbs *et al.*, 1989; Dutra *et al.*, 2006). Dutra *et al.* (2005) also observed an age-related continuous remodelling of the cortical bone that was influenced by the dentition status of the individuals analysed. Thus, aging alone might not be enough to cause significant decreases in the mandibular cortical thickness, but needs to be accompanied by an advanced pattern of tooth loss. As hypothesised earlier with the midline and anterior body heights, the duration of edentulism contribute to this thinning. In addition, this relationship between age and cortical thickness seemed particularly influenced by sex, but not really by ancestry (even if individuals of European ancestry always had thinner cortical thickness than African ancestry). Females (of both ancestries) showed steeper decreases, particularly after 40 years of age, compared to males. Munakata *et al.* (2011) for instance, showed in a female-only sample that menopause was particularly affecting the mandibular cortical thickness. They found that premenopausal women had a thicker cortical bone than postmenopausal women. However, as most of the correlations and regression coefficients found in this research were weak, caution must be exercised in interpreting this data.

7.4.3. Age-related decrease in density with tooth loss and edentulism

As reported earlier, in section [7.2.1.1], the mandibular cortical bone density was observed to decrease with moderate and extreme tooth loss, compared to fully dentate individuals. As soon as a few teeth are lost, and thus that the masticatory capabilities are slightly changed, an intense bone modelling occurs changing and reducing the cortical bone

density. It was also noted earlier that edentulism only appears to be associated with a generalised decrease in cortical density of the mandible, but not aggravate this diminution (as it was the case for some external distances).

However, when considering the age of the individuals in addition to the different dentition categories (fully dentate, moderate tooth loss and edentulism), new patterns, not observed for any of the linear measurements (external distances, cortical thickness), were noticed. All three dentition categories, analysed separately, displayed age-related decreases in cortical bone density. Senescence, and not only the loss of teeth, could thus be the primary factor causing a decrease in cortical bone density. In addition, the initial age-related decrease occurring even when fully dentate, was aggravated by the degree of tooth loss. The decline was more important with edentulism, which was already more pronounced than with moderate tooth loss. This leads to the hypothesis that the resorptive modelling caused by the loss of teeth, which is more or less intense according to the degree of tooth loss is only a secondary factor and adds to the "normal" bone remodelling associated with aging, causing intense changes into the cortical bone microstructure. Ruff *et al*. (2006) hypothesised that this bone modelling response caused by a change in mechanical loading (tooth loss here) is age-dependent, and thus could change throughout life.

The age-related decrease of the mandibular cortical bone density was particularly sensitive to the influence of two demographic factors: sex and ancestry. In both moderate and edentulous individuals, even if both females and males showed this decrease with aging, females were particularly affected with steeper regressions and faster decreases, as often observed in the literature on the mandible (von Wowern, 1988, 2001) or on the rest of the skeleton (Agarwal, 2021). The differences between females and males were thus particularly accentuated in later ages of life, most probably due to the combined, and thus compounded, influence of menopausal bone loss with aging (von Wowern, 2001; Li *et al.*, 2011). For instance, Taguchi *et al.* (1996) compared BMD values in recent and long-term postmenopausal women of similar ages. They observed that recent postmenopausal women had a denser mandibular cortical bone than the long-term postmenopausal group, highlighting the accelerating and aggravating effect of menopause on the bone remodelling process.

This timing interval could explain why, without taking into account aging, the sexual dimorphism was not less evident for the cortical bone densities than for the other measurements (see for instance in section [7.1]), as it really appears with senescence.

A similar profile was noted with the ancestral groups, with a diminution in cortical bone density with age in both South African individuals of African and European ancestries, even if the latter showed a greater and faster decrease, particularly after 40 years of age. This corroborates the faster cortical bone turnover in South African of European ancestry reported by Pfeiffer *et al*. (2016).

The fact that the cortical thicknesses are more affected by tooth loss than by aging, and that the opposite was found for the cortical bone densities is coherent with the intrinsic nature of these properties. Geometrical properties, like cortical thickness, are more affected by functional bone adaptation, such as tooth loss, than are material properties, like bone density (Ruff, 2019).

7.4.4. Unique changes for the midline lingual cortical thickness

As noted in sections [7.2.1.2] and [7.2.2.4], the cortical thickness measured at the midline lingual site of the mandible reacted differently to tooth loss, and particularly edentulism, compared to the rest of the mandible. With moderate tooth loss, no changes in the midline lingual thickness were noted while a general thinning was observed in the rest of the mandible. However, with extreme tooth loss and edentulism, an important increase, unique in the mandible, was noticed, highlighting that only edentulism might trigger this thickening.

With edentulism, there is a global reduction in strains and loads, causing extreme morphological changes with a loss of up to 60% of its initial volume, like in the alveolar process region, which can be particularly affected by a very strong resorption. To continue mandibular vital functions, such as mastication, adaptation to this changing morphology is required and generally starts with the tongue, which will become wider and shorter. As explained by van Eijden (2000), the midline lingual region is already under a unique set of strains, including a lateral bending of great magnitude, due to the unusual shape of the mandible, and an asymmetric distribution of tensile and compressive stresses (i.e., more important tensile stress lingually than compressive stress buccally). Midline lingual strains, already greater than elsewhere in the mandible, will increase, notably because of macroglossia and its consequences on the geniohyoid and the genioglossus muscles (Bucca *et al.*, 2006; Morelli *et al.*, 2011; Posnick, 2014; Jindal *et al.*, 2015; Lucas, 2016), and cause the local thickening of the cortical bone.

When considering aging in addition to controlling tooth loss, unusual results were observed for this midline lingual site, as a strong age-related thickening was observed in edentulous individuals, confirming what was previously suspected by Oettlé (2014) in a sample including diverse dentition statuses and Schwartz-Dabney and Dechow (2002). Furthermore, while younger edentulous (or almost edentulous) individuals displayed an already thicker than usual midline lingual cortical bone compared to fully dentate individuals or with moderate tooth loss, this thickening was even more important in older age categories (CtTh: old edentulous > young edentulous > fully dentates and moderate tooth loss). Age, and most probably the duration of edentulism, generate a long-term increase in midline lingual strains accentuating the thickening of the lingual cortical bone over time. Moreover, due to the ever-changing morphology of the mandible with edentulism (more and more resorbed and thin), the tongue and its related muscles always have to adapt to the new environment, leading to the maintenance of the increased midline lingual strains.

Furthermore, the cortical thickness increase was present in all edentulous subgroups (females and males, South Africans of African and European ancestries) and always correlated with aging. This local secondary adaptation, compounded by senescence, appears to be independent from demographic factors (sex and ancestry), and common to all individuals with edentulism.

309

7.5. Applications of this study

The comprehensive assessment of the mandibular cortical bone microstructure and its external morphology conducted during this research, considered the effects of biomechanical factors, like tooth loss, as well as the influence of systemic factors, such as aging, sex and ancestry. These findings and the methodology designed may have implications in clinical fields, like dentistry or maxillofacial surgery, but also in biological anthropology, and more particularly in palaeoanthropology, in which they could be used as reference data.

7.5.1. Imaging modalities

In the thesis, micro-CT, considered as the imaging technology of reference in ex-vivo dental and bone research, was the main imaging method employed, notably because of its high micron-level resolution and reliability. However, because of its high radiation exposure and thus its non-usability on patients, comparison of micro-CT and CBCT is of great importance to confirm, or not, the feasibility and applicability of the measurements and parameters assessed in the thesis. As reviewed in the Literature Review (see section [2.2.3]), for linear distances, CBCT and micro-CT were often directly compared using dental samples, but on rare occasions with bone samples. Only one study (Suttapreyasri *et al.*, 2018) was found analysing CBCT vs. micro-CT mandibular and maxillary cortical thicknesses directly, for which they observed significant correlations and no differences between the modalities. Our findings also showed high degrees of agreement and accuracy for external distances and cortical thicknesses, which was confirmed by the automatic volume comparisons performed and displaying general retained shapes and only small deviation errors. However, a small tendency of underestimation was noticed in CBCT measurements – the smaller the measurement was, the lesser the agreement and accuracy between the two modalities were.

CBCT may lack discriminative abilities required to describe the microstructure of the bone because of a lower image resolution and artefacts issues (Scarfe and Farman, 2008; Maret *et al.*, 2012, 2014; Forst *et al.*, 2014; Rios *et al.*, 2017; Sharawy, 2020; Pauwels *et al.*, 2021). This was confirmed by the intra-observer findings we obtained. Indeed, micro-CT and its "clearer" images resulted in very high agreement and repeatability, while it was a bit lower in CBCT measurements. The difference was especially present when measuring small-scale

distances like cortical thickness. The first explanation is, of course, linked to the difference in resolution between the two imaging modalities, which is almost twice in CBCT (0.200 mm) vs. micro-CT (0.068-0.106 mm). Voxel resolution has already been proven to be an essential parameter at multiple occasions for dental or bone samples (Naitoh *et al.*, 2004; Maret *et al.*, 2012, 2014; Humbert *et al.*, 2016). Other explanations might be associated with artefact issues. While several types of artefacts exist in all scanning modalities (Sharawy, 2020), because of similar experimental settings (mandibles secured within a polystyrene box) during micro-CT and CBCT scanning, we can for instance exclude motion-related artefacts, usually caused by movement during the acquisition. However, noise ("graining" of the image) is particularly present in CBCT, notably because of lower amperage settings (in the thesis: CBCT: 10-11 mA vs. micro-CT: 100-120 mA) (Sharawy, 2020).

Additionally, measurements towards the ramus (both external distances and microstructure) displayed less accuracy and lower correlations in CBCT compared to micro-CT. The volume maps corroborated these discrepancies with more frequent geometrical deformations towards the posterior part of the mandible (around the molars, ramus including condyles and coronoid processes). Some technical factors, like the field of view (FOV) of the CBCT machine, may explain these antero-posterior discrepancies. A few authors (Parsa *et al.*, 2013; Ibrahim *et al.*, 2014; de Oliveira Pinto *et al.*, 2021; Pauwels *et al.*, 2021) already reported FOV as a scanning parameter affecting measurement accuracy and repeatability in CBCT systems and all particularly noted differences between the centre of the FOV and its periphery. De Oliveira Pinto *et al.* (2021) observed that measurements done in the centre of the FOV were more specific and accurate, and differed from the lateral positions; which corresponds exactly to what was observed in the thesis (i.e., the ramus is at the periphery of the FOV). This difference between the centre and the periphery is due to the beam collimation causing a difference in intensity between areas and thus a lack in uniformity of the grey values (Ibrahim *et al.*, 2014; Sharawy, 2020).

Even if bone density has been extensively compared between micro-CT and CBCT modalities, uncertainties are still present as no real consensus has been reached yet, even when looking at histomorphometric parameters (such as BV/TV, the bone volume fraction). In the thesis, while the cortical BV/TV values in CBCT and micro-CT followed the same tendencies, significant differences were found between the two scanning techniques. It almost confirmed what was found by several authors in the literature (Van Dessel *et al.*, 2013, 2017; Kim *et al.*, 2015; Parsa *et al.*, 2015; Tsai *et al.*, 2020) as they obtained significant differences as well, but

associated to strong correlations between CBCT and micro-CT BV/TV values. Results observed by Panmekiate and colleagues (2015) were more similar to ours with moderate correlations accompanied by large ranges of errors and deviations. As concluded by Panmekiate *et al.* (2015), this apparent lack of reliability and accuracy of CBCT compared to micro-CT might hinder the direct use of these parameters in clinical applications. However, because the literature is often focused on the trabecular bone structure (Van Dessel *et al.*, 2013, 2017; Panmekiate *et al.*, 2015; Parsa *et al.*, 2015) and not the cortical bone, the comprehensive evaluation of the microstructure of the mandible done in the thesis is still of interest and can be used as a preliminary reference database. Furthermore, while the results obtained with a micro-CT can be generalised to all micro-CTs, it is not the case with CBCT. Indeed, micro-CT measurements were found to be reliable across models and manufacturers (Olejniczak *et al.*, 2007), whereas a lack of standardisation and calibration between manufacturers is often of concern for CBCT (Gaêta-Araujo *et al.*, 2020).

7.5.2. Clinical implications

This research provided a precise and comprehensive set of mandibular measurements (morphological and microstructural) using very high-resolution scanning modalities on a large modern human sample, improving the knowledge of morphological variations, and some of their causes, in South African individuals. Understanding of the morphology and microstructure of the mandible is of great importance for many clinical procedures, such as oral and maxillofacial surgeries, orthodontic treatments, restorative and implant dentistry, among others. Even for common procedures like tooth extraction, information on the cortical bone, such as its thickness and distribution, is often pivotal. Indeed, a thick and dense cortical bone will, for instance, make the extraction more difficult, while a too thin cortical bone makes the extraction more delicate (Humphries, 2007).

7.5.2.1. Oral and maxillofacial surgery

Variations in the mandibular morphology and microstructure are important for treatment of fractures, frequently done by miniplate fixation anchored by screws, for which a good quantity and quality of bone are required (Al-Jandan *et al.*, 2013; McKay, 2019). All over

the world, including South Africa, mandibular fractures are the most common fracture of the entire maxillofacial skeleton in individuals of all ages (children, adults, the elderly) (Ferreira *et al.*, 2005; Yamamoto *et al.*, 2011; Mogajane and Mabongo, 2018). In almost all populations, two age-related incidence peaks are generally detected: one in young adults (15 to 30 years old) and then again after age 70 (Ferreira *et al.*, 2005; Mogajane and Mabongo, 2018; Lalloo *et al.*, 2020). Even if the principles of treatment are the same as in a young population, additional factors need to be considered for the elderly patients (e.g., number of remaining teeth, extended resorption of the alveolar bone, low bone density). In a study focusing on an elderly Japanese population, Yamamoto *et al.* (2011) found that tooth loss and more particularly edentulism had consequences on the type of fractures, with more frequent body fractures. In dentate adults, however, fractures at the angle, condyle, body and symphyseal/parasymphyseal regions are the most common types of mandibular fracture observed (Roode *et al.*, 2007; Yamamoto *et al.*, 2011; Santos *et al.*, 2015; Mogajane and Mabongo, 2018). While in children and young adults, the number of facial and mandibular fractures decreased fractures decreased in the recent years (Ferreira *et al.*, 2005), the incidence particularly increased in the elderly population (Yamamoto *et al.*, 2011), most probably due to the general aging of the world population (United Nations, 2019). Knowledge of the body height and cortical thickness along the body and their variations with age, sex and ancestry gives important insights to develop optimal treatments, with appropriate screw placement and length for stability and safety purposes. For instance, for a good fixation, stability and support of miniplates, a buccal cortical thickness of 3 mm is often recommended with the use of 5-7 mm long screws (Al-Jandan *et al.*, 2013; McKay, 2019). However, many injuries were reported with 6 mm screws, especially in females, which was most certainly due to their general thinner cortical thickness, as reported earlier in the thesis, in section [7.1]. Furthermore, several articles (Katranji *et al.*, 2007; Al-Jandan *et al.*, 2013) and our findings (in fully dentate individuals, anterior CtTh: mean ± SD = 1.85 ± 0.51 mm; posterior CtTh: mean ± SD = 2.32 ± 0.58 mm) highlighted that the buccal cortical thickness is often less than 3 mm, for which 5-7 mm screws would be high risks of injury. Additionally, the cortical thickness in the posterior body of the mandible (around the first and second molars), a site often used for miniplate screws, is particularly affected by tooth loss, with a pronounced decrease (posterior buccal CtTh in individuals without tooth loss: mean ± SD = 2.32 ± 0.58 mm; with moderate tooth loss: mean ± SD = 2.12 ± 0.59 mm; with extreme tooth loss: mean ± SD = 1.92 ± 0.73 mm), especially in females, which intensifies the risk of injuries in this specific group.

7.5.2.2. Orthodontic mini-implants

Similarly than for repairing a fracture, in orthodontics, it is necessary to evaluate the thickness of the mandibular cortical bone, as well as its density, for safe and optimal positioning of Temporary Anchorage Devices (TADs). Among the TADs, mini-implants (also called mini-screw implants), commonly used by orthodontists, are temporarily placed between teeth in various sites of the mandible or maxilla to serve as an anchorage for orthodontic devices in adolescents and adults. Mini-implants are also known to not osseointegrate with the surrounding bone and are thus particularly reliant on cortical bone thickness (Humphries, 2007). The general consensus is that sites with thick and dense cortical bone are the most favourable, as bone quantity and quality will have a direct impact on the primary stability and thus on the implant success rate (Deguchi *et al.*, 2006; Humphries, 2007; Ono *et al.*, 2008; Farnsworth *et al.*, 2011; Sathapana *et al.*, 2013). Several studies (Deguchi *et al.*, 2006; Humphries, 2007; Ono *et al.*, 2008; Park *et al.*, 2008; Fayed *et al.*, 2010; Farnsworth *et al.*, 2011; Cassetta *et al.*, 2013; Sathapana *et al.*, 2013), were conducted to determine the optimal implant sites. However, they are not all in agreement. For instance, while Deguchi *et al.* (2006) did not find any differences in cortical bone thickness between mandibular sites (between premolar and molar areas), the findings in the thesis showed the opposite, which was also confirmed by other authors (Fayed *et al.*, 2010; Farnsworth *et al.*, 2011; Cassetta *et al.*, 2013), particularly between anterior and posterior sites (canine vs. premolar region vs. molar region). Besides sites and location differences, and as explained in various sections of the thesis, variations with sex, age and population should also be considered by clinical professionals. For instance, the cortical bone thickness displaying sexual dimorphism with thicker cortical bone in males than females (see section [7.1]), was also observed in Cassetta *et al.* (2013) and Fayed *et al.* (2010), as well as in Humphries (2007), albeit not significant. However, most of the studies focusing on mini-implant sites did not report any differences between females and males (Deguchi *et al.*, 2006; Ono *et al.*, 2008; Park *et al.*, 2008; Farnsworth *et al.*, 2011; Sathapana *et al.*, 2013), and had particularly small sample sizes (between 10 and 82 individuals). None of the orthodontic studies cited above which analysed cortical thickness or density changes with sex and/or age, were performed in South Africa (e.g., Australia, Italy, Japan, Korea, Switzerland, United States). The measurements done in the thesis, although not always specifically adapted to orthodontic purposes, could thus serve as a preliminary study

314

from which guidelines and placement protocols could be developed for the South African population.

7.5.2.3. Dental implants

Nowadays, one of the most common treatment options to restore dental functions is dental implants (Resnik and Misch, 2020a), which can be performed after natural tooth loss in partially or fully edentulous patients following a delayed approach, or placed directly into a socket after the extraction of a problematic tooth according to the immediate approach. Now implant-fixed prostheses have higher success rates than "traditional" dentures (e.g., fixed or removable partial dentures, complete dentures) and better outcomes thanks to many advantages, like the maintenance of alveolar bone and of masticatory performances, and thus better long-term stability and retention of prostheses (Resnik and Misch, 2020a). Short and long-term success rates of implants are dependent of many factors that are often patient specific and need to be evaluated pre-treatment (Merheb *et al.*, 2010; Chrcanovic *et al.*, 2017; Sharawy, 2020). For instance, the bone quality (i.e., cortical/trabecular densities) is of utmost importance for treatment planning (choice of implant size and design, surgical protocols, etc.), but also post-treatment for the primary stability, anchorage, healing process and osseointegration (Aranyarachkul *et al.*, 2005; Akça *et al.*, 2006; De Oliveira *et al.*, 2012; Chrcanovic *et al.*, 2017; Merheb *et al.*, 2018; Resnik and Misch, 2020b). However, in the implantology literature, bone quantity (e.g., cortical thickness) in the mandible is often overlooked compared to bone quality. Cortical bone thickness, particularly on the buccal side, is in fact a key factor influencing the implant stability, and even appears to contribute more than some implant design characteristics, like the implant length (Miyamoto *et al.*, 2005; Merheb *et al.*, 2010, 2018; Tomasi *et al.*, 2010; Temple *et al.*, 2015; Chrcanovic *et al.*, 2017). Interestingly, bone density continues to be important for stability after healing and osseointegration, while the cortical thickness is only pivotal during implantation and osseointegration (Merheb *et al.*, 2018).

The microstructure of specific areas, like the mandibular symphysis and ramus, is also important to know because of their use as donor sites for autogenous bone grafts (Sharawy, 2020). In order to choose the best possible graft site, inner and morphological variations at these sites need to be described in detail and evaluated (Sharawy, 2020). For example, the midline region has the least dense cortical bone compared to anterior and posterior sites, and

315

this density was observed to decrease even more with tooth loss, which could be a limitation in some patients, particularly in older South African females.

Expanding the knowledge and understanding of the factors affecting the cortical bone are essential for clinicians to choose the ideal implant, the optimal site and thus avoid implant failure (Quirynen *et al.*, 2007; Fugazzotto, 2008; Smith and Tarnow, 2013; Chrcanovic *et al.*, 2017). This knowledge is also important for dental implant manufacturers always aiming to reduce treatment times and improve patient outcomes by designing new and improved products. For example, in Theye *et al.* (2018) (see Appendix A), using micro-CT scans and a subsample of the thesis (i.e., only dentate South African individuals of African ancestry), we provided for the first time, a comprehensive analysis describing and quantifying the morphology of first molars and of the surrounding bone microstructure, with implications for immediate implant placement and design characteristics (e.g., platform width, body shape, taper). Indeed, some of the mandibular cortical measurements of the thesis, supplemented by others on the trabecular bone, were analysed and showed interesting results for the South African population. For instance, the buccal plates in posterior mandibular areas were found to be rarely thinner than 1 mm, which is the threshold recommended by the literature to avoid augmentation procedures and obtain positive predictable outcomes for immediate implant placement (Lazzara, 1989; Tomasi *et al.*, 2010; Matsuda *et al.*, 2016). Furthermore, while aging did not affect the mandibular buccal plate thicknesses, as also found by Temple *et al.* (2015), the cortical densities decreased with advancing age, highlighting the fact that age is of major importance for bone quality, even if the patient does not indicate signs of age-related diseases (like tooth loss or osteoporosis). These results were since confirmed with the bigger sample studied in the thesis (see section [7.3] with individuals not affected by tooth loss).

The possible impact of osteoporosis on dental implant placement and survival is still being debated and no consensus has been reached by the dentistry community yet (von Wowern, 2001; Singh and Tripathi, 2010; Glowacki and Christoph, 2013; de Medeiros *et al.*, 2018; Radi *et al.*, 2018; Temmerman *et al.*, 2019). The diagnostic procedure followed for osteoporosis is generally performed in postcranial bones (such as the vertebrae or the femur), and not on the bones directly involved for the placement of dental implants. As underlined by Kingsmill (1999), changes with aging in the postcranial skeleton are different from changes in the mandible. In the thesis, it was for example observed that, while the cortical bone density showed an age-related decrease in both the mandible and femur, the diminution was more pronounced in the femur. Furthermore, we also noticed that there was a lack of correlation

between the mandibular and femoral cortical bone densities, i.e., the density in the mandible is not increasing or decreasing according to the one in the femur, and reciprocally. This type of result was also found by Guo *et al.* (2020) in an article comparing bone mineral density in the mandible with cervical and lumbar vertebrae without observing predictable relationships between the skeletal sites. To go further, several dentistry professionals suggested to see if individuals at risk of osteoporosis could be directly identified from the mandibular or the maxillary bones using dental radiography, CT or CBCT (Nicopoulou-Karayianni *et al.*, 2009; Gulsahi, 2015; Guerra *et al.*, 2017; Guo *et al.*, 2020; Nakamoto *et al.*, 2020).

In the literature, several authors highlighted that osteoporotic patients presented an age-related decreased bone quality, lower density, and lower primary stability scores, as well as higher implant failure risks in low-density bone (Merheb *et al.*, 2016; de Medeiros *et al.*, 2018). Nonetheless, for most of the authors in the literature, dental implants are not contraindicated in osteoporotic patients (von Wowern, 2001; Singh and Tripathi, 2010; Merheb *et al.*, 2016; de Medeiros *et al.*, 2018; Radi *et al.*, 2018). However, recently, a few authors (Temmerman *et al.*, 2017, 2019; Radi *et al.*, 2018) started to caution on the long-term implant survival (e.g., after several years) and not just on the implant placement and short-term survival as reported in most of the studies. Indeed, Temmerman *et al.* (2019) found that after five years, the survival rate was slightly less in osteoporotic patients, which was also highlighted in a review by Radi *et al.* (2018). Clinicians generally conclude that implant treatments are the best solution for these patients, especially compared to conventional prosthodontic treatments, like partial dentures, which have been found to aggravate the already accelerated bone loss of osteoporotic patients (von Wowern, 2001; Singh and Tripathi, 2010). A more preventive approach with a pre-operative evaluation and an adapted treatment plan, particularly focusing on longer healing times, is generally advised (Merheb *et al.*, 2016; de Medeiros *et al.*, 2018; Radi *et al.*, 2018). This pre-operative assessment of bone quantity and quality is traditionally done using the Lekholm and Zarb classification (1985), which is based on the visual evaluation of radiographs and tactile sensation during surgery. This method is, however, more and more called into question because of its subjectivity, the lack of quantitative data (Merheb *et al.*, 2010; Munakata *et al.*, 2011; Chrcanovic *et al.*, 2017) as well as the lack of information given by 2D images compared to 3D regions (Merheb *et al.*, 2016). The advances and spreading of medical 3D imaging modalities, such as CT or CBCT, allowed the development of new methodologies measuring objectively bone quantity and quality (Merheb *et al.*, 2016; Resnik and Misch, 2020a).

7.5.3. Palaeoanthropological applications

The morphology and cortical microstructure of the mandible are important not only for clinical fields, such as dentistry as seen previously, but also for biological anthropology. The mandible is a particularly resistant bone with high rates of preservation and recovery in forensic, archaeological, and even palaeoanthropological contexts (Standring, 2009; White *et al.*, 2012; Stodder, 2019). While factors of bone preservation are not discussed in detail here, specific intrinsic factors, like size, shape and density, have particular importance for recovery (Stodder, 2019). The mandible, with its size, heaviness, and high density, has greater survival rates than most of the other bones of the skeleton. As illustrated by our findings, the cortical density measured in the mandible was for example much greater than in the femur of the same individuals.

The hominoid fossil record includes many mandibles of adults and juveniles from different taxa ranging from early hominins to modern humans (e.g., Australopithecines, *Homo erectus*, *Homo neanderthalensis,* early and late *Homo sapiens*). In the literature, fossil specimens are usually compared to recent nonhuman and/or human primate samples to provide valuable insights into various topics, such as functional and biomechanical properties (e.g., mastication, diet, speech) or intra- and interspecific variations (e.g., sexual dimorphism, taxonomy). Various morphological and shape parameters, such as mandibular robusticity, are often evaluated as it provides a wealth of information on interspecific relationships and assists in assessing taxonomic affinities (Lague *et al.*, 2008; Mounier *et al.*, 2009; Bermúdez de Castro *et al.*, 2016; Pitirri and Begun, 2019; Balolia *et al.*, 2020). Cortical bone thickness and its distribution in the mandible also are of particular interest to detect possible asymmetrical patterns, and thus attempt to characterise specific local functional demands, such as masticatory and para-masticatory activities (Daegling, 1989, 2007; Daegling and Hotzman, 2003; Zanolli *et al.*, 2017; Fiorenza *et al.*, 2019; Genochio *et al.*, 2019) with caution as highlighted by Ichim and colleagues (2007).

However, several limitations are encountered in most of the articles of the palaeoanthropological literature. One restriction often met is the variety of methods used and protocols followed between studies, or even within a study between specimens, making comparisons difficult or even not always accurate. As the methodology implemented during the present thesis is usable and reliable on mandibles with various morphologies (edentulous or not for example), it could be applied to fossil specimens having diverse dentition status (i.e.,

moderate or complete loss of teeth), which are often deliberately excluded from comparative studies (e.g., in Skinner *et al.*, 2006). Indeed, a few individuals affected by tooth loss or even edentulism were recovered, such as the earliest toothless hominin skull (cranium D3444 and mandible D3900, Early Pleistocene) from Dmanisi (Georgia), which is thought to have lost teeth several years before death and shows extensive resorption and remodelling of the alveolar bone (Lordkipanidze *et al.*, 2005; Margvelashvili *et al.*, 2013); or the Neanderthal "Old Man" La Chapelle-aux-Saints 1 (France), which shows intermediate tooth loss and remodelling (Tappen, 1985; Trinkaus, 1985). In addition to being affected by tooth loss, both individuals were estimated to be elderly individuals. The morphology and internal structure of these fossil specimens could thus be directly compared to the dataset provided in the thesis and interpretations about changes related to either tooth loss or aging in these fossil mandibles could be inferred.

Part of the methodology developed during this thesis was tested and applied to two fossil hominin fragmentary mandibles, with still unclear taxonomic affinities, in Genochio *et al.* (2019) (see Appendix B). In the article, the still unreported cortical structural organisations of two late Early Pleistocene mandible specimens, Tighenif 1 and Tighenif 2 (Tighenif, Algeria), were compared to a small extant human subsample of the thesis. Cortical bone thickness was assessed on two cross-sections at the level of premolars and molars. As expected, the cortical bone was thicker in the two fossils (example of the 2D Relative Cortical Thickness at the molars: 2D RCT Tighenif 1 = 16.4 and 2D RCT Tighenif 2 = 17.3), even if the extant humans presented a high variability (mean 2D RCT = 12.5, range = 9.7 – 18.0). It was also noticed that the cortical bone of the fossil specimens was particularly thick around the right premolars, which was also reflected by an important dental occlusal wear on this side. These results suggested that cortical bone thickness and distribution might be related to biomechanical activities, with specific masticatory and/or para-masticatory strains in the Tighenif specimens. However, some differences between the cortical structural organisations of the two fossils highlighted intraspecific variation, and more particularly possible sexual dimorphism. Furthermore, as several studies have shown the significant influence of sexual dimorphism on intraspecific variations in mandibular size and shape of hominoids (Humphrey *et al.*, 1999; Plavcan, 2002; Taylor, 2006), it is possible to hypothesise similar consequences on the inner structure.

As seen in Genochio *et al.* (2019), in the palaeoanthropological literature, fossil specimens are in general compared to extant human and/or nonhuman primate samples.

However, these comparative samples are often limited (Brown and Vavrek, 2015) and might not be representative of the actual variation detected in the extant human mandible, as observed in our results. The measurements provided in the thesis were obtained from a large extant human sample including several factors of variations, such as different degrees of tooth loss, a broad spectrum of ages, or even sex and ancestry; and thus, could be used in the future as a reference database, particularly when studying fossil specimens affected by tooth loss.

7.6. Limitations and future directions

The principal limitations of this research project were associated with the sample analysed, directly reflecting the unbalanced composition of the two skeletal collections used (L'Abbé *et al.*, 2005; Dayal *et al.*, 2009) with: (i) a general smaller number of females compared to males; (ii) more individuals of European ancestry in the older decades, especially males, compared to the younger age ranges; (iii) fewer females of African ancestry in the older age ranges. However, South African males of African ancestry were well represented in almost all decades and all dentition statuses. Another limitation related to the skeletal sample was the fact that the duration of tooth loss and possible denture wearing was not precisely known restraining the scope of the interpretations and increasing the number of hypotheses explaining some trends. Perhaps a more representative sample of the population and the access to patient records and dental history could have been possible with the use of CT or CBCT scans of patients. However, micro-CT scanning skeletal material was chosen because micro-CT is considered as the gold standard imaging modality and many uncertainties are still surrounding the "clinically accepted" scanning machines (e.g., CT, CBCT), especially for small-scale measurements and microstructural assessments, like the cortical density (BV/TV). Furthermore, despite its biases, the sample size analysed in this thesis surpassed that of many other studies based on 3D imaging, and was comprehensive and representative in terms of dentition status, age, sex and ancestry.

Another type of limitation related to *in vitro* factors of bone preparation and storage needs to be investigated. Indeed, some researchers argue that fresh bone is more appropriate than dry bone for studying mechanical bone properties as certain processes, such as embalming, boiling, freezing storage, or drying, might significantly influence these characteristics (Zioupos *et al.*, 2000). These authors, however, reviewed only studies analysing the effects of these factors on mechanical (e.g., elastic modulus, tensile strength, stiffness) and not microstructural characteristics, like BV/TV, the histomorphometric parameter studied in the thesis. On the other hand, Le Garff (2018) worked on the effects of embalming and freezing on histomorphometric parameters assessed on human trabecular bone by micro-CT. The results highlighted a difference between formalin-based embalming and freezing, with embalming causing significant changes to all histomorphometric parameters of the trabecular bone, while freezing only slightly modified the number of trabeculae. They, however, only focused on trabecular bone biopsies harvested from one type of bone of a unique cadaver. Finally, the

consensus is to use fresh bone, which relies on harvesting bone biopsies in patients or in fresh cadavers, which is not easy to implement and realise. Furthermore, bone biopsies are not always ideal for quantifying microstructural and architectural parameters because of the minimal size of the volume of interest required for the histomorphometric analysis. The way forward would be to evaluate the influence of several conservation methods, like embalming, on cortical bone and on histomorphometric parameters using micro-CT.

Lastly, the methodology itself has encountered some limitations and could be optimised when planning future research. Firstly, only the left side of the mandible was analysed in the thesis. While several authors (Schwartz-Dabney and Dechow, 2003; Deguchi *et al.*, 2006; Swasty *et al.*, 2009) observed that the cortical thickness is symmetric between the left and right sides of the mandible in humans, it might be worthwhile to evaluate this symmetry for the cortical bone density.

Secondly, both the cortical thickness and cortical density were measured at three sites (basal, buccal, lingual) defined on precise sections, which were easily reproducible and not subjected to any changes, like tooth loss. Instead of focusing on these three sites only, the thickness of the cortical bone could be measured on the entire section, by calculating the distances between two curves (one along the periosteum of cortical bone, one along the endosteal border; both from the most superior buccal point to the most superior lingual point), as it was done in Genochio *et al.* (2019) using a subsample of ten individuals (see Appendix B). In a similar way, the cortical density could be assessed with a greater number of VOIs and thus maybe capture more information on the variations – along the mylohyoid line for example, or closer to the alveolar bone, as performed by Wang and colleagues (2010) as well as Dechow *et al.* (2017) on baboon and macaque mandibles, respectively.

Finally, it would be interesting for future research to use the more advanced technology: synchrotron radiation-based micro-CT (SR micro-CT), which is revolutionising 3D imaging with a new way of scanning using an electron beam (Andronowski *et al.*, 2018). SR micro-CT acquisitions can reach a very high resolution approximating traditional histologic techniques, with the additional advantage of the visualisation in 3D and not 2D like in histology. For instance, SR micro-CT allows the assessment of cortical porosity, or very small structures, such as the Haversian systems or osteocytes (Andronowski, 2016; Maggiano *et al.*, 2016; Andronowski *et al.*, 2018).

Chapter 8. Conclusion

The research presented in this thesis was the first attempt to investigate, within South African individuals, microstructural mandibular changes, with reference to macrostructural changes in the mandible, with advancing age and across various patterns of tooth loss. An extensive sample of 333 mandibles was constituted, micro-CT-scanned and analysed with external dimensions and inner cortical parameters, namely cortical thickness and cortical density. From this study, the following conclusions were made:

- The feasibility and applicability of the measurements and parameters assessed in the thesis were tested in CBCT, using micro-CT as the reference. Findings confirmed the accuracy and repeatability of large-size measurements, like the external distances. Agreement and accuracy were more uncertain for smaller types of measurements, like the cortical thickness. CBCT might lack the discriminative abilities required to describe the bone microstructure because of a general lower image resolution and artefact issues. Cortical bone density, assessed with histomorphometric parameters (BV/TV), was significantly different between the two scanning methods. It corroborates the lack of reliability and accuracy of CBCT in measuring these 3D parameters and thus their direct use in clinical settings.

- In fully dentate mandibles, regional mandibular variations were found: between symphyseal, anterior and posterior body heights (midline > anterior > posterior), as well as for the cortical thickness (CtTh: posterior > anterior > midline) and density (BV/TV: posterior and anterior > midline). Thus, for a mandible without tooth loss, the smaller the alveolar height, the thicker and denser the cortical bone. The asymmetry between basal, buccal and lingual areas was confirmed. Even if the basal cortical bone was always the thickest, the cortical thickness was greater lingually than buccally at the midline and anteriorly (CtTh: lingual > buccal), while no bucco-lingual asymmetry was observed posteriorly (CtTh: buccal = lingual). No bucco-lingual asymmetry in cortical density was noted.

- In fully dentate mandibles, sexual dimorphism and ancestral variations were also confirmed in the external distances (M > F; AA > EA, except for ramus height: EA > AA) and in the cortical thicknesses (CtTh: M > F; AA > EA). The cortical bone densities were only slightly

different between males and females (BV/TV: M ≥ F), or between South African of African and European ancestries (BV/TV: AA ≈ EA).

- The precise effects and consequences of tooth loss on the mandible were variable. A general decrease in external distances, cortical thickness (particularly in the posterior mandibular body), and density throughout the entire mandible was observed as soon as tooth loss starts. Extreme tooth loss and edentulism aggravated the decrease in external distances, whereas for the two inner parameters, it rather generalised it to the entire mandible (external distances: A > B >> C; CtTh and BV/TV: A > B > C).

- The reduction in external dimensions and cortical thickness with tooth loss was present in both females and males, with consistently greater measurements in males (external distances and CtTh: M > F), and in South African individuals of African ancestry (external distances and CtTh: AA > EA). Sexual dimorphism, as well as ancestral differences, were emphasised in mandibles with edentulism compared to fully dentate and moderate tooth loss mandibles. Females started off with smaller mandibles and thinner cortical bone compared to males, a difference that became more accentuated with the loss of teeth. Cortical densities stayed similar but generalised across the entire mandible. With tooth loss, females did not show a decrease in cortical BV/TV whereas males did, although sexual dimorphism was present (BV/TV: M > F). Even if the ancestral differences in cortical density were subtle with or without tooth loss (BV/TV: AA ≈ EA), the loss of teeth caused slightly different consequences in the two ancestral groups, with a significant decrease in South Africans of African ancestry with edentulism, but not in individuals of European ancestry. This decrease was, however, suspected of being rather due to a confounding factor, aging, than to tooth loss itself.

- Advancing age was first analysed in fully dentate mandibles to help clarify if any changes are exclusively due to either aging, tooth loss, or a combination of the two. No variations in external distances or cortical bone thickness were observed with aging alone, whereas the cortical bone density decreased with aging, which corroborates the general understanding on bone mass declining with senescence, even in the mandible. The use of the femur as a proxy for the rest of the skeleton confirmed this hypothesis by also revealing a decrease in femoral cortical density with advancing age within the same individuals. However, mandibular and femoral cortical bone densities were not correlated.

- In fully dentate mandibles, no age-related variations in external distances or cortical bone thickness were observed in any of the sex and ancestral groups. Sexual dimorphism

(external distances and CtTh: M > F) and ancestral differences (external distances and CtTh: AA > EA) were thus maintained throughout the decades. Tooth loss alone, and not age, had an influence on the external distances and on the cortical thicknesses. Thus, a bone functional adaptation to a variation in loading is responsible for the decrease. These functional adaptations following tooth loss were nuanced for certain dimensions in individuals affected by edentulism. Even if already edentulous, these individuals continued to have a decrease in alveolar heights, as well as in the cortical thicknesses, which appeared to be due to the duration of edentulism and thus, indirectly, to the age of the individuals. In conclusion, aging alone is not enough to cause significant changes of the mandibular body height or of the cortical thicknesses and needs to be associated with advanced tooth loss.

- Mandibular cortical density was found to decrease with age with or without tooth loss. Senescence, and not only the loss of teeth, could thus be the primary factor of the decreasing density. However, tooth loss, and more particularly edentulism, was observed to aggravate this initial age-related decrease with a more pronounced decline in density. The resorptive modelling caused by the loss of teeth is thus only a secondary factor that, once combined to the standard bone remodelling associated with senescence, provokes intense changes to the density of the cortical bone.

- In fully dentate individuals, the age-related diminution in cortical density was sexually dimorphic, i.e., it was more noticeable in males than in females (which may be an artefact of a better age distribution in males than in females). In individuals with tooth loss or edentulism, the diminution associated with aging affected males and females, but females showed steeper and faster decreases in later stages of life, eliciting the presence of sexual dimorphism for the cortical density in the elderly. The decrease with aging seemed also present in the two ancestral groups (even if non-significant) and revealed higher densities in individuals of African ancestry than in European ancestry at all ages, and more particularly in the older individuals.

- The lingual side of the midline presented an increase in cortical thickness with edentulism, modifying the bone distribution (CtTh: lingual > basal > buccal), and no changes in cortical density (BV/TV: A ≈ B ≈ C). The thickening was linked to the nature of the bone there (bone formation area), but also to the presence of strong muscular insertions and specific increased strains in this region during tooth loss. The increase in cortical thickness was more important in males than females, most probably because of the stronger muscles present in males causing even greater strains on the bone. No differences were noted

between the ancestral groups. This increase was found to be related to advancing age (progressively thicker in the oldest age categories) and may be related to the duration of edentulism.

- Understanding the effects of tooth loss and aging in the mandible, and more particularly in the cortical microstructure, is crucial and has implications in clinical fields. In Theye *et al.* (2018) (see Appendix A), the methodology developed in the thesis was successfully applied to describe and quantify the morphology of the first molars and of the surrounding bone microstructure, such as bone quality (density) and quantity (cortical thickness), having direct implications for immediate dental implant placement and design characteristics (e.g., platform width, body shape, taper).

- Knowledge of the morphology and cortical microstructure of the mandible also has palaeoanthropological applications. In Genochio *et al.* (2019) (see Appendix B), part of the methodology developed during the thesis was successfully adapted to two fossil fragmentary mandibles that had still unreported cortical structural organisations.

326

Chapter 9. References

Agarwal, S.C. 2019. Understanding bone aging, loss, and osteoporosis in the past. In: Katzenberg, M.A. and Grauer, A.L. (eds.). *Biological Anthropology of the Human Skeleton*. Third Edition. Wiley-Blackwell, Hoboken, NJ, United States of America, pp. 385–414.

Agarwal, S.C. 2021. What is normal bone health? A bioarchaeological perspective on meaningful measures and interpretations of bone strength, loss, and aging. *American Journal of Human Biology*, 33(5):e23647.

Akça, K., Chang, T.-L., Tekdemir, I., and Fanuscu, M.I. 2006. Biomechanical aspects of initial intraosseous stability and implant design: a quantitative micro-morphometric analysis. *Clinical Oral Implants Research*, 17(4):465–472.

Akgül, A.A., and Toygar, T.U. 2002. Natural craniofacial changes in the third decade of life: A longitudinal study. *American Journal of Orthodontics and Dentofacial Orthopedics*, 122(5):512–522.

Albert, A.M., Ricanek, K., and Patterson, E. 2007. A review of the literature on the aging adult skull and face: Implications for forensic science research and applications. *Forensic Science International*, 172(1):1–9.

Al-Jandan, B.A., Al-Sulaiman, A.A., Marei, H.F., Syed, F.A., and Almana, M. 2013. Thickness of buccal bone in the mandible and its clinical significance in mono-cortical screws placement. A CBCT analysis. *International Journal of Oral and Maxillofacial Surgery*, 42(1):77–81.

Al-Rafee, M. 2020. The epidemiology of edentulism and the associated factors: A literature review. *Journal of Family Medicine and Primary Care*, 9(4):1841–1843.

An, Y.H. 2000. Mechanical Properties of Bone. In: An, Y.H. and Draughn, R.A. (eds.). *Mechanical Testing of Bone and the Bone-Implant Interface*. CRC Press, Boca Raton, FL, United States of America, pp. 41–63.

Andronowski, J.M. 2016. *Evaluating Differential Nuclear DNA Yield Rates among Human Bone Tissue Types: A Synchrotron Micro-CT Approach*. PhD thesis, University of Tennessee, United States of America.

Andronowski, J.M., and Cole, M.E. 2020. Current and emerging histomorphometric and imaging techniques for assessing age-at-death and cortical bone quality. *WIREs Forensic Science*, 3(2):e1399.

Andronowski, J.M., Crowder, C., and Soto Martinez, M. 2018. Recent advancements in the analysis of bone microstructure: new dimensions in forensic anthropology. *Forensic Sciences Research*, 3(4):294–309.

Aranyarachkul, P., Caruso, J., Gantes, B., Schulz, E., Riggs, M., Dus, I., Yamada, J.M., and Crigger, M. 2005. Bone density assessments of dental implant sites: 2. Quantitative cone-beam computerized tomography. *International Journal of Oral & Maxillofacial Implants*, 20(1):416–424.

Atkinson, P.J., and Woodhead, C. 1968. Changes in human mandibular structure with age. *Archives of Oral Biology*, 13(12):1453–1463.

Ayo-Yusuf, I.J., Ayo-Yusuf, O.A., and Olutola, B.G. 2013. Health insurance, socio-economic position and racial disparities in preventive dental visits in South Africa. *International Journal of Environmental Research and Public Health*, 10(1):178–191.

Balolia, K.L., Jakeman, E.C., Massey, J.S., Groves, C., and Wood, B. 2020. Mandibular corpus shape is a taxonomic indicator in extant hominids. *American Journal of Physical Anthropology*, 172(1):25–40.

Barak, M.M. 2019. Bone modeling or bone remodeling: That is the question. *American Journal of Physical Anthropology*, 172(2):153–155.

Baran, I., Ergün, G., and Semiz, M. 2007. Prevalence of loss of all teeth (edentulism) and associated factors in older adults in China, Ghana, India, Mexico, Russia and South Africa. *European Journal of Dentistry*, 1(2):104–110.

Barreto, M.S., Silva Barbosa, I., Miranda Leite-Ribeiro, P., Araújo, T.M., and Almeida Sarmento, V. 2020. Accuracy of the measurements from multiplanar and sagittal reconstructions of CBCT. *Orthodontics & Craniofacial Research*, 23(2):223–2338.

Bartlett, S.P., Grossman, R., and Whitaker, L.A. 1992. Age-related changes of the craniofacial skeleton: an anthropometric and histologic analysis. *Plastic and Reconstructive Surgery*, 90(4):592–600.

Bassi, F., Procchio, M., Fava, C., Schierano, G., and Preti, G. 1999. Bone density in human dentate and edentulous mandibles using computed tomography. *Clinical Oral Implants Research*, 10(5):356–361.

Bastir, M., and Rosas, A. 2005. Hierarchical nature of morphological integration and modularity in the human posterior face. *American Journal of Physical Anthropology*, 128(1):26–34.

Bayle, P., Bondioli, L., Macchiarelli, R., Mazurier, A., Puymerail, L., Volpato, V., and Zanolli, C. 2011. Three-dimensional imaging and quantitative characterisation of human fossil remains - examples from the NESPOS database. In: Macchiarelli, R. and Weniger, G.-C. (eds.). *Pleistocene Databases: Acquisition, Storing, Sharing*. Neanderthal Museums, Mettmann, Germany, pp. 29–46.

Bejdová, Š., Krajíček, V., Velemínská, J., Horák, M., and Velemínský, P. 2013. Changes in the sexual dimorphism of the human mandible during the last 1200 years in Central Europe. *HOMO - Journal of Comparative Human Biology*, 64(6):437–453.

Benavides, E., Rios, H.F., Ganz, S.D., An, C.-H., Resnik, R., Reardon, G.T., Feldman, S.J., Mah, J.K., Hatcher, D., Kim, M.-J., Sohn, D.-S., Palti, A., Perel, M.L., Judy, K.W.M., Misch, C.E., and Wang, H.-L. 2012. Use of cone beam computed tomography in implant dentistry: the International Congress of Oral Implantologists consensus report. *Implant Dentistry*, 21(2):78–86.

Benson, B.W., Prihoda, T.J., and Glass, B.J. 1991. Variations in adult cortical bone mass as measured by a panoramic mandibular index. *Oral Surgery, Oral Medicine, and Oral Pathology*, 71(3):349–356.

Bermúdez de Castro, J.M., Martín-Francés, L., Modesto-Mata, M., Martínez de Pinillos, M., Martinón-Torres, M., García-Campos, C., and Carretero, J.M. 2016. Brief communication: Virtual reconstruction of the Early Pleistocene mandible ATD6-96 from Gran Dolina-TD6-2 (Sierra De Atapuerca, Spain). *American Journal of Physical Anthropology*, 159(4):729–736.

Bhayat, A., and Chikte, U. 2019. Human resources for oral health care in South Africa: a 2018 update. *International Journal of Environmental Research and Public Health*, 16(10):1668.

Bishara, S.E., Treder, J.E., and Jakobsen, J.R. 1994. Facial and dental changes in adulthood. *American Journal of Orthodontics and Dentofacial Orthopedics*, 106(2):175–186.

Bland, J.M., and Altman, D.G. 1986. Statistical methods for assessing agreement between two methods of clinical measurement. *The Lancet*, 1(8476):307–310.

Bland, J.M., and Altman, D.G. 1999. Measuring agreement in method comparison studies. *Statistical Methods in Medical Research*, 8(2):135–160.

Bodic, F., Amouriq, Y., Gayet-Delacroix, M., Maugars, Y., Hamel, L., Baslé, M.F., and Chappard, D. 2012. Relationships between bone mass and micro-architecture at the mandible and iliac bone in edentulous subjects: a dual X-ray absorptiometry, computerised tomography and microcomputed tomography study. *Gerodontology*, 29(2):e585–e594.

Bodic, F., Hamel, L., Lerouxel, E., Baslé, M.F., and Chappard, D. 2005. Bone loss and teeth. *Joint, Bone, Spine*, 72(3):215–221.

Borges de Oliveira, F., Stolfi, A., Bartscher, M., De Chiffre, L., and Neuschaefer-Rube, U. 2016. Experimental investigation of surface determination process on multi-material components for dimensional computed tomography. *Case Studies in Nondestructive Testing and Evaluation*, 6:93–103.

Botha, D., Lynnerup, N., and Steyn, M. 2019. Age estimation using bone mineral density in South Africans. *Forensic Science International*, 297:307–314.

Bourdiol, P., Hennequin, M., Peyron, M.-A., and Woda, A. 2020. Masticatory adaptation to occlusal changes. *Frontiers in Physiology*, 11:263.

Braga, J. 2016. Non-invasive imaging techniques. In: Irish, J.D. and Scott, G.R. (eds.). *A Companion to Dental Anthropology*. Wiley-Blackwell, Chichester, United Kingdom, pp. 514–527.

Brown, C.M., and Vavrek, M.J. 2015. Small sample sizes in the study of ontogenetic allometry; implications for palaeobiology. *PeerJ*, 3:e818.

Bruton, A., Conway, J.H., and Holgate, S.T. 2000. Reliability: what is it, and how is it measured? *Physiotherapy*, 86(2):94–99.

Bucca, C., Cicolin, A., Brussino, L., Arienti, A., Graziano, A., Erovigni, F., Pera, P., Gai, V., Mutani, R., Preti, G., Rolla, G., and Carossa, S. 2006. Tooth loss and obstructive sleep apnoea. *Respiratory Research*, 7(1):8.

Burghardt, A.J., Link, T.M., and Majumdar, S. 2011. High-resolution computed tomography for clinical imaging of bone microarchitecture. *Clinical Orthopaedics and Related Research*, 469(8):2179–2193.

Buyukkaplan, U.S., Tonguc, M.O., Guldag, M.U., Yildiz, M., and Gumus, B.A. 2013. Comparison of mandibular bone mineral densities in dentate and edentulous patients. *Journal of Prosthodontics*, 22(1):23–27.

Byrnes, J.F., Kenyhercz, M.W., and Berg, G.E. 2017. Examining interobserver reliability of metric and morphoscopic characteristics of the mandible. *Journal of Forensic Sciences*, 62(4):981–985.

Campos, M.J.S. 2014. Bone mineral density in cone beam computed tomography: Only a few shades of gray. *World Journal of Radiology*, 6(8):607.

Caple, J., and Stephan, C.N. 2016. A standardized nomenclature for craniofacial and facial anthropometry. *International Journal of Legal Medicine*, 130(3):863–879.

Carlsson, G.E. 2004. Responses of jawbone to pressure. *Gerodontology*, 21(2):65–70.

Carter, T.B., Frost, D.E., Tucker, M.R., and Zuniga, J.R. 1991. Cortical thickness in human mandibles: clinical relevance to the sagittal split ramus osteotomy. *International Journal of Adult Orthodontics and Orthognathic Surgery*, 6(4):257–260.

Cassetta, M., Sofan, A.A.A., Altieri, F., and Barbato, E. 2013. Evaluation of alveolar cortical bone thickness and density for orthodontic mini-implant placement. *Journal of Clinical and Experimental Dentistry*, 5(5):e245–e252.

Cassetta, M., Stefanelli, L.V., Pacifici, A., Pacifici, L., and Barbato, E. 2014. How accurate is CBCT in measuring bone density? A comparative CBCT-CT in vitro study: bone density assessment. *Clinical Implant Dentistry and Related Research*, 16(4):471–478.

Cawood, J.I., and Howell, R.A. 1988. A classification of the edentulous jaws. *International Journal of Oral and Maxillofacial Surgery*, 17(4):232–236.

Chen, H., Zhou, X., Fujita, H., Onozuka, M., and Kubo, K.Y. 2013. Age-related changes in trabecular and cortical bone microstructure. *International Journal of Endocrinology*, 2013(213234):1–9.

Chikte, U., Pontes, C.C., Karangwa, I., Kimmie-Dhansay, F., Erasmus, R., Kengne, A.P., and Matsha, T.E. 2020. Dental caries in a South African adult population: findings from the Cape Town Vascular and Metabolic Health Study. *International Dental Journal*, 70(3):176–182.

Cho, H., Stout, S.D., and Bishop, T.A. 2006. Cortical bone remodeling rates in a sample of African American and European American descent groups from the American

Midwest: Comparisons of age and sex in ribs. *American Journal of Physical Anthropology*, 130(2):214–226.

Chole, R.H., Patil, R.N., Balsaraf Chole, S., Gondivkar, S., Gadbail, A.R., and Yuwanati, M.B. 2013. Association of mandible anatomy with age, gender, and dental status: a radiographic study. *ISRN Radiology*, 2013:1–4.

Chrcanovic, B., Albrektsson, T., and Wennerberg, A. 2017. Bone Quality and Quantity and Dental Implant Failure: A Systematic Review and Meta-analysis. *International Journal of Prosthodontics*, 30(3):219–237.

Chrcanovic, B.R., Abreu, M.H.N.G., and Custodio, A.L.N. 2011. Morphological variation in dentate and edentulous human mandibles. *Surgical and Radiologic Anatomy*, 33(3):203–213.

Coleman, S., and Grover, R. 2006. The anatomy of the aging face: Volume loss and changes in 3-dimensional topography. *Aesthetic Surgery Journal*, 26(1):S4–S9.

Coquerelle, M., Bookstein, F.L., Braga, J., Halazonetis, D.J., Weber, G.W., and Mitteroecker, P. 2011. Sexual dimorphism of the human mandible and its association with dental development. *American Journal of Physical Anthropology*, 145(2):192–202.

Costa Mendes, L., Delrieu, J., Gillet, C., Telmon, N., Maret, D., and Savall, F. 2021. Sexual dimorphism of the mandibular conformational changes in aging human adults: A multislice computed tomographic study by geometric morphometrics. *PLoS ONE*, 16(6):e0253564.

Cotton, T.P., Geisler, T.M., Holden, D.T., Schwartz, S.A., and Schindler, W.G. 2007. Endodontic applications of Cone-Beam Volumetric Tomography. *Journal of Endodontics*, 33(9):1121–1132.

Coutel, X. 2018. *Bone microstructure and bone marrow adiposity in the mandible: experimental study in the adult ovariectomiezed rat model*. Thèse de doctorat, Université du Droit et de la Santé Lille II, France.

von Cramon-Taubadel, N. 2011. Global human mandibular variation reflects differences in agricultural and hunter-gatherer subsistence strategies. *Proceedings of the National Academy of Sciences*, 108(49):19546–19551.

Cunha-Cruz, J., Hujoel, P.P., and Nadanovsky, P. 2007. Secular trends in socio-economic disparities in edentulism: USA, 1972–2001. *Journal of Dental Research*, 86(2):131–136.

Daegling, D.J. 1989. Biomechanics of cross-sectional size and shape in the hominoid mandibular corpus. *American Journal of Physical Anthropology*, 80(1):91–106.

Daegling, D.J. 2007. Relationship of bone utilization and biomechanical competence in hominoid mandibles. *Archives of Oral Biology*, 52(1):51–63.

Daegling, D.J. 2012. The human mandible and the origins of speech. *Journal of Anthropology*, 2012:1–14.

Daegling, D.J., and Grine, F.E. 1991. Compact bone distribution and biomechanics of early hominid mandibles. *American Journal of Physical Anthropology*, 86(3):321–339.

Daegling, D.J., and Hotzman, J.L. 2003. Functional significance of cortical bone distribution in anthropoid mandibles: An in vitro assessment of bone strain under combined loads. *American Journal of Physical Anthropology*, 122(1):38–50.

Danforth, R.A., Dus, I., and Mah, J. 2003. 3-D volume imaging for dentistry: a new dimension. *Journal of the California Dental Association*, 31(11):817–823.

Dawant, B.M., and Zijdenbos, A.P. 2000. Image Segmentation. In: Sonka, M. and Fitzpatrick, J.M. (eds.). *Handbook of Medical Imaging Volume 2. Medical Image Processing and Analysis*. SPIE Press, Bellingham, WA, United States of America, pp. 71–127.

Dawood, A., Patel, S., and Brown, J. 2009. Cone Beam CT in dental practice. *British Dental Journal*, 207(1):23–28.

Dayal, M.R., Kegley, A.D.T., Štrkalj, G., Bidmos, M.A., and Kuykendall, K.L. 2009. The history and composition of the Raymond A. Dart Collection of Human Skeletons at the University of the Witwatersrand, Johannesburg, South Africa. *American Journal of Physical Anthropology*, 140(2):324–335.

De Beer, F.C. 2018. *Neutron and X-Ray Tomography as Research Tools for Applied Research in South Africa*. PhD thesis, North-West University, South Africa.

De Oliveira, R.C.G., Leles, C.R., Lindh, C., and Ribeiro-Rotta, R.F. 2012. Bone tissue microarchitectural characteristics at dental implant sites. Part I: Identification of clinical related parameters. *Clinical Oral Implants Research*, 23(8):981–986.

De Vos, W., Casselman, J., and Swennen, G.R.J. 2009. Cone-Beam Computerized Tomography (CBCT) imaging of the oral and maxillofacial region: A systematic review of the literature. *International Journal of Oral and Maxillofacial Surgery*, 38(6):609–625.

Dechow, P.C., Panagiotopoulou, O., and Gharpure, P. 2017. Biomechanical implications of cortical elastic properties of the macaque mandible. *Zoology*, 124:3–12.

Dechow, P.C., Wang, Q., and Peterson, J. 2010. Edentulation alters material properties of cortical bone in the human craniofacial skeleton: functional implications for craniofacial structure in primate evolution. *The Anatomical Record*, 293(4):618–629.

Deguchi, T., Nasu, M., Murakami, K., Yabuuchi, T., Kamioka, H., and Takano-Yamamoto, T. 2006. Quantitative evaluation of cortical bone thickness with computed tomographic scanning for orthodontic implants. *American Journal of Orthodontics and Dentofacial Orthopedics*, 129(6):721.e7-721.e12.

Dekker, H., Schulten, E.A.J.M., ten Bruggenkate, C.M., Bloemena, E., van Ruijven, L., and Bravenboer, N. 2018. Resorption of the mandibular residual ridge: A micro-CT and histomorphometrical analysis. *Gerodontology*, 35(3):221–228.

Dempster, D.W., Compston, J.E., Drezner, M.K., Glorieux, F.H., Kanis, J.A., Malluche, H., Meunier, P.J., Ott, S.M., Recker, R.R., and Parfitt, A.M. 2013. Standardized nomenclature, symbols, and units for bone histomorphometry: A 2012 update of the report of the ASBMR Histomorphometry Nomenclature Committee. *Journal of Bone and Mineral Research*, 28(1):2–17.

Dhainaut, A., Hoff, M., Syversen, U., and Haugeberg, G. 2016. Technologies for assessment of bone reflecting bone strength and bone mineral density in elderly women: an update. *Women's Health*, 12(2):209–216.

Dong, H., Deng, M., Wang, W., Zhang, J., Mu, J., and Zhu, G. 2015. Sexual dimorphism of the mandible in a contemporary Chinese Han population. *Forensic Science International*, 255:9–15.

Doual, J.M., Ferri, J., and Laude, M. 1997. The influence of senescence on craniofacial and cervical morphology in humans. *Surgical and Radiologic Anatomy*, 19:175–183.

Dutra, V., Devlin, H., Susin, C., Yang, J., Horner, K., and Fernandes, A.R.C. 2006. Mandibular morphological changes in low bone mass edentulous females: evaluation of panoramic radiographs. *Oral Surgery, Oral Medicine, Oral Pathology, Oral Radiology, and Endodontology*, 102(5):663–668.

Dutra, V., Yang, J., Devlin, H., and Susin, C. 2004. Mandibular bone remodelling in adults: evaluation of panoramic radiographs. *Dentomaxillofacial Radiology*, 33(5):323–328.

334

Dutra, V., Yang, J., Devlin, H., and Susin, C. 2005. Radiomorphometric indices and their relation to gender, age, and dental status. *Oral Surgery, Oral Medicine, Oral Pathology, Oral Radiology, and Endodontology*, 99(4):479–484.

Eichner, K. 1990. Renewed examination of the group classification of partially edentulous arches by Eichner and application advices for studies on morbidity statistics. *Stomatologie der DDR*, 40(8):321–325.

van Eijden, T.M. 2000. Biomechanics of the mandible. *Critical Reviews in Oral Biology and Medicine*, 11(1):123–136.

Enlow, D.H., Bianco, H.J., and Eklund, S. 1976. The remodeling of the edentulous mandible. *Journal of Prosthetic Dentistry*, 36(6):685–693.

Fan, Y., Penington, A., Kilpatrick, N., Hardiman, R., Schneider, P., Clement, J., Claes, P., and Matthews, H. 2019. Quantification of mandibular sexual dimorphism during adolescence. *Journal of Anatomy*, 234(5):709–717.

Farnsworth, D., Rossouw, P.E., Ceen, R.F., and Buschang, P.H. 2011. Cortical bone thickness at common miniscrew implant placement sites. *American Journal of Orthodontics and Dentofacial Orthopedics*, 139(4):495–503.

Fayed, M.M.S., Pazera, P., and Katsaros, C. 2010. Optimal sites for orthodontic mini-implant placement assessed by cone beam computed tomography. *The Angle Orthodontist*, 80(5):939–951.

Ferrario, V.F., Sforza, C., Serrao, G., Dellavia, C., and Tartaglia, G.M. 2004. Single tooth bite forces in healthy young adults. *Journal of Oral Rehabilitation*, 31(1):18–22.

Ferreira, P.C., Amarante, J.M., Silva, P.N., Rodrigues, J.M., Choupina, M.P., Silva, Á.C., Barbosa, R.F., Cardoso, M.A., and Reis, J.C. 2005. Retrospective study of 1251 maxillofacial fractures in children and adolescents: *Plastic and Reconstructive Surgery*, 115(6):1500–1508.

Fiorenza, L., Benazzi, S., Kullmer, O., Zampirolo, G., Mazurier, A., Zanolli, C., and Macchiarelli, R. 2019. Dental macrowear and cortical bone distribution of the Neanderthal mandible from Regourdou (Dordogne, Southwestern France). *Journal of Human Evolution*, 132:174–188.

Fontijn-Tekamp, F.A., Slagter, A.P., Van Der Bilt, A., Van 'T Hof, M.A., Witter, D.J., Kalk, W., and Jansen, J.A. 2000. Biting and chewing in overdentures, full dentures, and natural dentitions. *Journal of Dental Research*, 79(7):1519–1524.

Forst, D., Nijjar, S., Flores-Mir, C., Carey, J., Secanell, M., and Lagravere, M. 2014. Comparison of in vivo 3D cone-beam computed tomography tooth volume measurement protocols. *Progress in Orthodontics*, 15(1):69.

Franklin, D., O'Higgins, P., and Oxnard, C.E. 2008a. Sexual dimorphism in the mandible of indigenous South Africans: A geometric morphometric approach. *South African Journal of Science*, 104:101–106.

Franklin, D., O'Higgins, P., Oxnard, C.E., and Dadour, I. 2006. Determination of sex in South African Blacks by discriminant function analysis of mandibular linear dimensions: a preliminary investigation using the Zulu local population. *Forensic Science, Medicine and Pathology*, 2(4):263–268.

Franklin, D., O'Higgins, P., Oxnard, C.E., and Dadour, I. 2008b. Discriminant function sexing of the mandible of Indigenous South Africans. *Forensic Science International*, 179(1):84.e1-84.e5.

Franklin, D., Oxnard, C.E., O'Higgins, P., and Dadour, I. 2007. Sexual dimorphism in the subadult mandible: quantification using geometric morphometrics. *Journal of Forensic Sciences*, 52(1):6–10.

Frost, H.M. 1973. *Bone Modeling and Skeletal Modeling Errors*. Charles C. Thomas, Springfield, IL, United States of America.

Frost, H.M. 1990a. Skeletal structural adaptations to mechanical usage (SATMU): 2. Redefining Wolff's Law: The remodeling problem. *The Anatomical Record*, 226(4):414–422.

Frost, H.M. 1990b. Skeletal structural adaptations to mechanical usage (SATMU): 1. Redefining Wolff's Law: The bone modeling problem. *The Anatomical Record*, 226(4):403–413.

Frost, H.M. 2004. A 2003 update of bone physiology and Wolff's Law for clinicians. *The Angle Orthodontist*, 74(1):3–15.

Frost, H.M., and Turner, C.H. 2000. Toward a mathematical description of bone biology: the principle of cellular accommodation. *Calcified Tissue International*, 67(2):184–187.

Fugazzotto, P.A. 2008. Implant placement at the time of maxillary molar extraction: treatment protocols and report of results. *Journal of Periodontology*, 79(2):216–223.

Fukase, H. 2007. Functional significance of bone distribution in the human mandibular symphysis. *Anthropological Science*, 115(1):55–62.

Fukase, H., and Suwa, G. 2008. Growth-related changes in prehistoric Jomon and modern Japanese mandibles with emphasis on cortical bone distribution. *American Journal of Physical Anthropology*, 136(4):441–454.

Gaêta-Araujo, H., Alzoubi, T., Vasconcelos, K. de F., Orhan, K., Pauwels, R., Casselman, J.W., and Jacobs, R. 2020. Cone beam computed tomography in dentomaxillofacial radiology: a two-decade overview. *Dentomaxillofacial Radiology*, 49(8):20200145.

Galibourg, A., Dumoncel, J., Telmon, N., Calvet, A., Michetti, J., and Maret, D. 2018. Assessment of automatic segmentation of teeth using a watershed-based method. *Dentomaxillofacial Radiology*, 47(1):20170220.

Gamba, T.O., Alves, M.C., and Haiter-Neto, F. 2016. Mandibular sexual dimorphism analysis in CBCT scans. *Journal of Forensic and Legal Medicine*, 38:106–110.

Gamer, M., Lemon, J., and Singh, I.F.P. 2019. *Irr: Various Coefficients of Interrater Reliability and Agreement*. Available at: https://CRAN.R-project.org/package=irr [Accessed: 21 February 2019].

Garvin, H.M., and Ruff, C.B. 2012. Sexual dimorphism in skeletal browridge and chin morphologies determined using a new quantitative method. *American Journal of Physical Anthropology*, 147(4):661–670.

Genochio, L., Mazurier, A., Dumoncel, J., Theye, C.E.G., and Zanolli, C. 2019. Inner structural organization of the mandibular corpus in the late Early Pleistocene human specimens Tighenif 1 and Tighenif 2. *Comptes Rendus Palevol*, 18:1073–1082.

Gillet, C., Costa-Mendes, L., Rérolle, C., Telmon, N., Maret, D., and Savall, F. 2020. Sex estimation in the cranium and mandible: a multislice computed tomography (MSCT) study using anthropometric and geometric morphometry methods. *International Journal of Legal Medicine*, 134:823–832.

Glowacki, J., and Christoph, K. 2013. Gender differences in the growing, abnormal, and aging jaw. *Dental Clinics of North America*, 57(2):263–280.

Gocha, T.P., Robling, A.G., and Stout, S.D. 2019. Histomorphometry of human cortical bone: applications to age estimation. In: Katzenberg, M.A. and Grauer, A.L. (eds.). *Biological Anthropology of the Human Skeleton*. Third Edition. Wiley-Blackwell, Hoboken, NJ, United States of America, pp. 145–187.

González-García, R., and Monje, F. 2013a. Is micro-computed tomography reliable to determine the microstructure of the maxillary alveolar bone? *Clinical Oral Implants Research*, 24(7):730–737.

González-García, R., and Monje, F. 2013b. The reliability of cone-beam computed tomography to assess bone density at dental implant recipient sites: a histomorphometric analysis by micro-CT. *Clinical Oral Implants Research*, 24(8):871–879.

Goyushov, S., Dursun, E., and Tözüm, T.F. 2020. Mandibular cortical indices and their relation to gender and age in the cone-beam computed tomography. *Dentomaxillofacial Radiology*, 49(3):20190210.

Gröning, F., Fagan, M., and O'Higgins, P. 2013. Comparing the distribution of strains with the distribution of bone tissue in a human mandible: a finite element study. *The Anatomical Record*, 296(1):9–18.

Grover, R., and Gupta, R. 2021. Anthropometric analysis of the human mandibular cortical bone in Indian population as assessed by dental Computed Tomography (DentaScan). *World Journal of Dentistry*, 12(1):42–49.

Guerra, E.N.S., Almeida, F.T., Bezerra, F.V., Figueiredo, P.T.D.S., Silva, M.A.G., De Luca Canto, G., Pachêco-Pereira, C., and Leite, A.F. 2017. Capability of CBCT to identify patients with low bone mineral density: a systematic review. *Dentomaxillofacial Radiology*, 46(8):20160475.

Guerreiro, F. da S., Diniz, P., Carvalho, P.E.G., Ferreira, E.C., Avancini, S.R.P., and Ferreira-Santos, R.I. 2013. Effects of masticatory hypofunction on mandibular morphology, mineral density and basal bone area. *Brazilian Journal of Oral Sciences*, 12(3):205–211.

Guevara Perez, S.V., Behr, M., and Thollon, L. 2019. Exploratory study of the three-dimensional morphological variation of the jaw associated to teeth loss. *Journal of Stomatology, Oral and Maxillofacial Surgery*, 120(6):523–528.

Gulsahi, A. 2011. Bone quality assessment for dental implants. In: Turkyilmaz, I. (ed.). *Implant Dentistry - The Most Promising Discipline of Dentistry*. InTech.

Gulsahi, A. 2015. Osteoporosis and jawbones in women. *Journal of International Society of Preventive and Community Dentistry*, 5(4):263.

Guo, Z., Du, X., Wang, L., Li, K., Jiao, J., Guglielmi, G., Zhurakivska, K., Lo Muzio, L., Blake, G.M., and Cheng, X. 2020. Measurements of volumetric bone mineral density in the

mandible do not predict spinal osteoporosis. *Dentomaxillofacial Radiology*, 49(3):20190280.

Haikola, B., Oikarinen, K., Söderholm, A.-L., Remes-Lyly, T., and Sipilä, K. 2008. Prevalence of edentulousness and related factors among elderly Finns. *Journal of Oral Rehabilitation*, 35(11):827–835.

Hanihara, T., and Ishida, H. 2005. Metric dental variation of major human populations. *American Journal of Physical Anthropology*, 128(2):287–298.

Hansson, S., and Halldin, A. 2012. Alveolar ridge resorption after tooth extraction: A consequence of a fundamental principle of bone physiology. *Journal of Dental Biomechanics*, 3(1758736012456543):1–8.

Hattingh, A., De Bruyn, H., Van Weehaeghe, M., Hommez, G., and Vandeweghe, S. 2020. Contour changes following immediate placement of ultra-wide implants in molar extraction sockets without bone grafting. *Journal of Clinical Medicine*, 9(8):2504.

Hechler, S.L. 2008. Cone-beam CT: Applications in orthodontics. *Dental Clinics of North America*, 52(4):809–823.

Helal, O., Göstemeyer, G., Krois, J., Fawzy El Sayed, K., Graetz, C., and Schwendicke, F. 2019. Predictors for tooth loss in periodontitis patients: Systematic review and meta-analysis. *Journal of Clinical Periodontology*, 46(7):699–712.

Hemphill, B.E. 2016. Assessing odontometric variation among populations. In: Irish, J.D. and Scott, G.R. (eds.). *A Companion to Dental Anthropology*. Wiley-Blackwell, Chichester, United Kingdom, pp. 311–336.

Herring, S.W. 2007. Masticatory muscles and the skull: A comparative perspective. *Archives of Oral Biology*, 52(4):296–299.

Hildebrand, T., Laib, A., Müller, R., Dequeker, J., and Rüegsegger, P. 1999. Direct Three-Dimensional morphometric analysis of human cancellous bone: microstructural data from spine, femur, iliac crest, and calcaneus. *Journal of Bone and Mineral Research*, 14(7):1167–1174.

Hilgers, M.L., Scarfe, W.C., Scheetz, J.P., and Farman, A.G. 2005. Accuracy of linear temporomandibular joint measurements with cone beam computed tomography and digital cephalometric radiography. *American Journal of Orthodontics and Dentofacial Orthopedics*, 128(6):803–811.

Hillson, S. 2019. Dental pathology. *Biological Anthropology of the Human Skeleton*. Third Edition. Wiley-Blackwell, Hoboken, NJ, United States of America, pp. 295–333.

Hoeksema, A., Spoorenberg, S., Peters, L., Meijer, H., Raghoebar, G., Vissink, A., Wynia, K., and Visser, A. 2017. Elderly with remaining teeth report less frailty and better quality of life than edentulous elderly: a cross-sectional study. *Oral Diseases*, 23(4):526–536.

Hoffman, J.W., and De Beer, F.C. 2012. Characteristics of the micro-focus X-ray tomography facility (MIXRAD) at Necsa in South Africa. *18th World Conference on Non-Destructive Testing*. Durban, South Africa.

Holmes, M.A., and Ruff, C.B. 2011. Dietary effects on development of the human mandibular corpus. *American Journal of Physical Anthropology*, 145(4):615–628.

Hounsfield, G.N. 1979. Computed Medical Imaging - Nobel Award Address. *Medical Physics*, 7(4):283–290.

Humbert, L., Hazrati Marangalou, J., del Río Barquero, L.M., van Lenthe, G.H., and van Rietbergen, B. 2016. Technical Note: Cortical thickness and density estimation from clinical CT using a prior thickness-density relationship. *Medical Physics*, 43(4):1945–1954.

Humphrey, L.T., Dean, M.C., and Stringer, C.B. 1999. Morphological variation in great ape and modern human mandibles. *Journal of Anatomy*, 195(4):491–513.

Humphries, S.M. 2007. *Comparison of Cortical Bone Thickness between Second Premolars and First Molars in the Maxilla and Mandible in Four Ethnic Groups*. MSc Thesis, University of Southern California, United States of America.

Hutchinson, E.F. 2017. *Morphology and Function: Aspects of Mandibular Development and Growth at Different Stages across the Lifespan*. PhD thesis, University of the Witwatersrand, South Africa.

Hutchinson, E.F., Farella, M., and Kramer, B. 2015. Importance of teeth in maintaining the morphology of the adult mandible in humans. *European Journal of Oral Sciences*, 123(5):341–349.

Huumonen, S., Sipilä, K., Haikola, B., Tapio, M., Söderholm, A., Remes-Lyly, T., Oikarinen, K., and Raustia, A.M. 2010. Influence of edentulousness on gonial angle, ramus and condylar height. *Journal of Oral Rehabilitation*, 37(1):34–38.

Ibrahim, N., Parsa, A., Hassan, B., van der Stelt, P., Aartman, I.H.A., and Nambiar, P. 2014. Influence of object location in different FOVs on trabecular bone microstructure

measurements of human mandible: a cone beam CT study. *Dentomaxillofacial Radiology*, 43(2):20130329.

Ichim, I., Kieser, J.A., and Swain, M.V. 2007. Functional significance of strain distribution in the human mandible under masticatory load: Numerical predictions. *Archives of Oral Biology*, 52(5):465–473.

Ikebe, K., Matsuda, K., Kagawa, R., Enoki, K., Okada, T., Yoshida, M., and Maeda, Y. 2012. Masticatory performance in older subjects with varying degrees of tooth loss. *Journal of Dentistry*, 40(1):71–76.

Ikebe, K., Matsuda, K., Murai, S., Maeda, Y., and Nokubi, T. 2010. Validation of the Eichner index in relation to occlusal force and masticatory performance. *International Journal of Prosthodontics*, 23(6):521–524.

Ikebe, K., Nokubi, T., Morii, K., Kashiwagi, J., and Furuya, M. 2005. Association of bite force with ageing and occlusal support in older adults. *Journal of Dentistry*, 33(2):131–137.

İlgüy, D., İlgüy, M., Ersan, N., Dölekoğlu, S., and Fişekçioğlu, E. 2014. Measurements of the foramen magnum and mandible in relation to sex using CBCT. *Journal of Forensic Sciences*, 59(3):601–605.

Irish, J.D. 2016. Assessing dental nonmetric variation among populations. In: Irish, J.D. and Scott, G.R. (eds.). *A Companion to Dental Anthropology*. Wiley-Blackwell, Chichester, United Kingdom, pp. 265–286.

İşcan, M.Y., and Steyn, M. 2013. *The Human Skeleton in Forensic Medicine*. Third Edition. Charles C. Thomas, Springfield, IL, United States of America.

Ishwarkumar, S., Pillay, P., Haffajee, M.R., and Satyapal, K.S. 2017. Morphometric analysis of the mandible in the Durban Metropolitan population of South Africa. *Folia Morphologica*, 76(1):82–86.

Israel, H. 1973. Recent knowledge concerning craniofacial aging. *The Angle Orthodontist*, 43(2):176–184.

Jacobs, R., Salmon, B., Codari, M., Hassan, B., and Bornstein, M.M. 2018. Cone beam computed tomography in implant dentistry: recommendations for clinical use. *BMC Oral Health*, 18(1):88.

Jindal, G., Jindal, S., Sharma, P., and Singla, A. 2015. Rare enlargement of genial tubercles and its management: a case report. *Journal of clinical and diagnostic research*, 9(11):23–24.

Joo, J.-K., Lim, Y.-J., Kwon, H.-B., and Ahn, S.-J. 2013. Panoramic radiographic evaluation of the mandibular morphological changes in elderly dentate and edentulous subjects. *Acta Odontologica Scandinavica*, 71(2):357–362.

Kailembo, A., Preet, R., and Stewart Williams, J. 2017. Common risk factors and edentulism in adults, aged 50 years and over, in China, Ghana, India and South Africa: results from the WHO Study on global AGEing and adult health (SAGE). *BMC Oral Health*, 17(1):29.

Kamburoglu, K., Kolsuz, E., Kurt, H., Kilic, C., Ozen, T., and Paksoy, C.S. 2011. Accuracy of CBCT measurements of a human skull. *Journal of Digital Imaging*, 24(5):787–793.

Kasai, K., Enomoto, Y., Ogawa, T., Kawasaki, Y., Kanazawa, E., and Iwasawa, T. 1996. Morphological characteristics of vertical sections of the mandible obtained by CT scanning. *Anthropological Science*, 104(3):187–198.

Katranji, A., Misch, K., and Wang, H.L. 2007. Cortical bone thickness in dentate and edentulous human cadavers. *Journal of Periodontology*, 78(5):874–878.

Keough, N., L'Abbé, E.N., and Steyn, M. 2009. The evaluation of age-related histomorphometric variables in a cadaver sample of lower socioeconomic status: implications for estimating age at death. *Forensic Science International*, 191:114.e1-114.e6.

Kharoshah, M.A.A., Almadani, O., Ghaleb, S.S., Zaki, M.K., and Fattah, Y.A.A. 2010. Sexual dimorphism of the mandible in a modern Egyptian population. *Journal of Forensic and Legal Medicine*, 17(4):213–215.

Kim, J.-E., Yi, W.-J., Heo, M.-S., Lee, S.-S., Choi, S.-C., and Huh, K.-H. 2015. Three-dimensional evaluation of human jaw bone microarchitecture: correlation between the microarchitectural parameters of cone beam computed tomography and micro-computer tomography. *Oral Surgery, Oral Medicine, Oral Pathology and Oral Radiology*, 120(6):762–770.

Kim, J.-H., and Park, Y.-C. 2012. Evaluation of mandibular cortical bone thickness for placement of temporary anchorage devices (TADs). *The Korean Journal of Orthodontics*, 42(3):110.

Kim, Y.J., and Henkin, J. 2015. Micro-computed tomography assessment of human alveolar bone: bone density and three-dimensional micro-architecture. *Clinical Implant Dentistry and Related Research*, 17(2):307–313.

342

Kingsmill, V.J. 1999. Post-extraction remodeling of the adult mandible. *Critical Reviews in Oral Biology & Medicine*, 10(3):384–404.

Kingsmill, V.J., and Boyde, A. 1998. Variation in the apparent density of human mandibular bone with age and dental status. *Journal of Anatomy*, 192(2):233–244.

Klemetti, E., Vainio, P., Lassila, V., and Alhava, E. 1993. Cortical bone mineral density in the mandible and osteoporosis status in postmenopausal women. *European Journal of Oral Sciences*, 101(4):219–223.

Klingenberg, C.P., Mebus, K., and Auffray, J.-C. 2003. Developmental integration in a complex morphological structure: how distinct are the modules in the mouse mandible? *Evolution and Development*, 5(5):522–531.

Kloss, F.R., and Gassner, R. 2006. Bone and aging: Effects on the maxillofacial skeleton. *Experimental Gerontology*, 41(2):123–129.

Knapp, T.R. 1992. Technical error of measurement: A methodological critique. *American Journal of Physical Anthropology*, 87(2):235–236.

Knezović-Zlatarić, D., and Čelebić, A. 2005. Comparison of mandibular bone density and radiomorphometric indices in wearers of complete or removable partial dentures. *Oral Radiology*, 21(2):51–55.

Ko, Y.-C., Huang, H.-L., Shen, Y.-W., Cai, J.-Y., Fuh, L.-J., and Hsu, J.-T. 2017. Variations in crestal cortical bone thickness at dental implant sites in different regions of the jawbone. *Clinical Implant Dentistry and Related Research*, 19(3):440–446.

Kobayashi, K., Shimoda, S., Nakagawa, Y., and Yamamoto, A. 2004. Accuracy in measurement of distance using limited cone-beam computerized tomography. *International Journal of Oral & Maxillofacial Implants*, 19(2):228–231.

Koo, T.K., and Li, M.Y. 2016. A guideline of selecting and reporting intraclass correlation coefficients for reliability research. *Journal of Chiropractic Medicine*, 15(2):155–163.

Kramer, B., Hutchinson, E.F., Brits, D.M., and Billings, B.K. 2019. Making the ethical transition in South Africa: acquiring human bodies for training in anatomy. *Anatomical Sciences Education*, 12(3):264–271.

Kribbs, P.J. 1990. Comparison of mandibular bone in normal and osteoporotic women. *Journal of Prosthetic Dentistry*, 63(2):218–222.

Kribbs, P.J., Chesnut, C.H., Ott, S.M., and Kilcoyne, R.F. 1989. Relationships between mandibular and skeletal bone in an osteoporotic population. *Journal of Prosthetic Dentistry*, 62(6):703–707.

Kribbs, P.J., Chesnut, C.H., Ott, S.M., and Kilcoyne, R.F. 1990. Relationships between mandibular and skeletal bone in a population of normal women. *Journal of Prosthetic Dentistry*, 63(1):86–89.

Krüger, G.C., Liebenberg, L., Myburgh, J., Meyer, A., Oettlé, A.C., Botha, D., Brits, D.M., Kenyhercz, M.W., Stull, K.E., Sutherland, C., and L'Abbé, E.N. 2018. Forensic anthropology and the biological profile in South Africa. In: Latham, K.E., Bartelink, E.J. and Finnegan, M. (eds.). *New Perspectives in Forensic Human Skeletal Identification*. Elsevier/Academic Press, London, United Kingdom; San Diego, CA, United States of America, pp. 313–321.

Kulczyk, T., Rychlik, M., Lorkiewicz-Muszyńska, D., Abreu-Głowacka, M., Czajka-Jakubowska, A., and Przystańska, A. 2019. Computed tomography versus optical scanning: a comparison of different methods of 3D data acquisition for tooth replication. *BioMed Research International*, 2019:1–7.

L'Abbé, E.N., Loots, M., and Meiring, J.H. 2005. The Pretoria Bone Collection: a modern South African skeletal sample. *HOMO - Journal of Comparative Human Biology*, 56(2):197–205.

L'Abbé, E.N., and Steyn, M. 2012. The establishment and advancement of forensic anthropology in South Africa. In: Dirkmaat, D. (ed.). *A Companion to Forensic Anthropology*. Wiley-Blackwell, Chichester, United Kingdom, pp. 626–638.

Lague, M.R., Collard, N.J., Richmond, B.G., and Wood, B.A. 2008. Hominid mandibular corpus shape variation and its utility for recognizing species diversity within fossil Homo. *Journal of Anatomy*, 213(6):670–685.

Laguna, L., Sarkar, A., and Chen, J. 2017. Eating capability assessments in elderly populations. In: Watson, R.R. (ed.). *Nutrition and Functional Foods for Healthy Aging*. Elsevier/Academic Press, London, United Kingdom; San Diego, CA, United States of America, pp. 83–98.

Laird, M.F., Ross, C.F., and O'Higgins, P. 2020. Jaw kinematics and mandibular morphology in humans. *Journal of Human Evolution*, 139:102639.

Lalloo, R., Lucchesi, L.R., Bisignano, C., Castle, C.D., Dingels, Z.V., Fox, J.T., Hamilton, E.B., Liu, Z., Roberts, N.L.S., Sylte, D.O., Alahdab, F., Alipour, V., Alsharif, U., Arabloo, J., Bagherzadeh, M., Banach, M., Bijani, A., Crowe, C.S., Daryani, A., Do, H.P., Doan, L.P., Fischer, F., Gebremeskel, G.G., Haagsma, J.A., Haj-Mirzaian, A., Haj-Mirzaian, A., Hamidi, S., Hoang, C.L., … James, S.L. 2020. Epidemiology of facial fractures: incidence, prevalence and years lived with disability estimates from the Global Burden of Disease 2017 study. *Injury Prevention*, 26(Supp 1):i27–i35.

Lascala, C., Panella, J., and Marques, M. 2004. Analysis of the accuracy of linear measurements obtained by cone beam computed tomography (CBCT-NewTom). *Dentomaxillofacial Radiology*, 33(5):291–294.

Lavelle, C.L.B. (Ed.) 1988. *Applied Oral Physiology*. Second Edition. Wright, London.

Lazzara, R.J. 1989. Immediate implant placement into extraction sites: surgical and restorative advantages. *International Journal of Periodontics & Restorative Dentistry*, 9(5):332–343.

Le Garff, E. 2018. *Taphonomie osseuse humaine au micro-scanner*. Thèse de doctorat, Université de Lille, France.

Lee, R.J., Weissheimer, A., Pham, J., Go, L., de Menezes, L.M., Redmond, W.R., Loos, J.F., Sameshima, G.T., and Tong, H. 2015. Three-dimensional monitoring of root movement during orthodontic treatment. *American Journal of Orthodontics and Dentofacial Orthopedics*, 147(1):132–142.

Lekholm, U., and Zarb, G.A. 1985. Patient selection and preparation. In: Brånemark, P.I., Zarb, G.A. and Albrektsson, T. (eds.). *Tissue-Integrated Prostheses: Osseointegration in Clinical Dentistry*. Quintessence. Chicago, United States of America, pp. 199–209.

Lepley, C.R., Throckmorton, G.S., Ceen, R.F., and Buschang, P.H. 2011. Relative contributions of occlusion, maximum bite force, and chewing cycle kinematics to masticatory performance. *American Journal of Orthodontics and Dentofacial Orthopedics*, 139(5):606–613.

Lestrel, P.E., Kapur, K.K., and Chauncey, H.H. 1980. A cephalometric study of mandibular cortical bone thickness in dentulous persons and denture wearers. *Journal of Prosthetic Dentistry*, 43(1):89–94.

Leversha, J., McKeough, G., Myrteza, A., Skjellrup-Wakefiled, H., Welsh, J., and Sholapurkar, A. 2016. Age and gender correlation of gonial angle, ramus height and bigonial width

in dentate subjects in a dental school in Far North Queensland. *Journal of Clinical and Experimental Dentistry*, 8(1):e49–e54.

Li, N., Jing, H., Li, J., Zhou, F., Bu, L., and Yang, X. 2011. Study of mandible bone mineral density of Chinese adults by dual-energy X-ray absorptiometry. *International Journal of Oral and Maxillofacial Surgery*, 40(11):1275–1279.

Liang, X., Jacobs, R., Hassan, B., Li, L., Pauwels, R., Corpas, L., Souza, P.C., Martens, W., Shahbazian, M., Alonso, A., and Lambrichts, I. 2010a. A comparative evaluation of Cone Beam Computed Tomography (CBCT) and Multi-Slice CT (MSCT). Part I: On subjective image quality. *European Journal of Radiology*, 75(2):265–269.

Liang, X., Lambrichts, I., Sun, Y., Denis, K., Hassan, B., Li, L., Pauwels, R., and Jacobs, R. 2010b. A comparative evaluation of Cone Beam Computed Tomography (CBCT) and Multi-Slice CT (MSCT). Part II: On 3D model accuracy. *European Journal of Radiology*, 75(2):270–274.

Liu, X.S., Huang, A.H., Zhang, X.H., Sajda, P., Ji, B., and Guo, X.E. 2008. Dynamic simulation of three dimensional architectural and mechanical alterations in human trabecular bone during menopause. *Bone*, 43(2):292–301.

Lordkipanidze, D., Vekua, A., Ferring, R., Rightmire, G.P., Agusti, J., Kiladze, G., Mouskhelishvili, A., Nioradze, M., de León, M.S.P., Tappen, M., and Zollikofer, C.P.E. 2005. The earliest toothless hominin skull. *Nature*, 434(7034):717–718.

Loth, S.R., and Henneberg, M. 1998. Mandibular ramus flexure is a good indicator of sexual dimorphism. *American Journal of Physical Anthropology*, 105:91–92.

Loubele, M., Guerrero, M.E., Jacobs, R., Suetens, P., and van Steenberghe, D. 2007. A comparison of jaw dimensional and quality assessments of bone characteristics with cone-beam CT, spiral tomography, and multi-slice spiral CT. *International Journal of Oral & Maxillofacial Implants*, 22:446–454.

Loubele, M., Maes, F., Schutyser, F., Marchal, G., Jacobs, R., and Suetens, P. 2006. Assessment of bone segmentation quality of cone-beam CT versus multislice spiral CT: a pilot study. *Oral Surgery, Oral Medicine, Oral Pathology, Oral Radiology, and Endodontology*, 102(2):225–234.

Lucas, P.W. 2016. The masticatory system and its function. In: Irish, J.D. and Scott, G.R. (eds.). *A Companion to Dental Anthropology*. Wiley-Blackwell, Chichester, United Kingdom, pp. 108–119.

Ludlow, J.B., Laster, W.S., See, M., Bailey, L. 'Tanya J., and Hershey, H.G. 2007. Accuracy of measurements of mandibular anatomy in cone beam computed tomography images. *Oral Surgery, Oral Medicine, Oral Pathology, Oral Radiology, and Endodontology*, 103(4):534–542.

Lukacs, J.R. 2011. Sex differences in dental caries experience: clinical evidence, complex etiology. *Clinical Oral Investigations*, 15(5):649–656.

Maggiano, I.S., Maggiano, C.M., Clement, J.G., Thomas, C.D.L., Carter, Y., and Cooper, D.M.L. 2016. Three-dimensional reconstruction of Haversian systems in human cortical bone using synchrotron radiation-based micro-CT: morphology and quantification of branching and transverse connections across age. *Journal of Anatomy*, 228(5):719–732.

Marciano, M.A., Duarte, M.A.H., Ordinola-Zapata, R., Del Carpio Perochena, A., Cavenago, B.C., Villas-Bôas, M.H., Minotti, P.G., Bramante, C.M., and Moraes, I.G. 2012. Applications of micro-computed tomography in endodontic research. In: Méndez-Vilas (ed.). *Current Microscopy Contributions to Advances in Science and Technology*. pp. 782–788.

Maret, D. 2010. *Morphométrie haute résolution des germes dentaires : Évaluation du Cone Beam CT en tant qu'outil de mesure*. Thèse de doctorat, Université Toulouse III Paul Sabatier, France.

Maret, D., Molinier, F., Braga, J., Peters, O.A., Telmon, N., Treil, J., Inglèse, J.-M., Cossié, A., Kahn, J.-L., and Sixou, M. 2010. Accuracy of 3D reconstructions based on cone beam computed tomography. *Journal of Dental Research*, 89(12):1465–1469.

Maret, D., Peters, O.A., Galibourg, A., Dumoncel, J., Esclassan, R., Kahn, J.-L., Sixou, M., and Telmon, N. 2014. Comparison of the accuracy of 3-dimensional cone-beam computed tomography and micro-computed tomography reconstructions by using different voxel sizes. *Journal of Endodontics*, 40(9):1321–1326.

Maret, D., Telmon, N., Peters, O.A., Lepage, B., Treil, J., Inglèse, J.-M., Peyre, A., Kahn, J.-L., and Sixou, M. 2012. Effect of voxel size on the accuracy of 3D reconstructions with cone beam CT. *Dentomaxillofacial Radiology*, 41(8):649–655.

Margvelashvili, A., Zollikofer, C.P.E., Lordkipanidze, D., Peltomaki, T., and Ponce de Leon, M.S. 2013. Tooth wear and dentoalveolar remodeling are key factors of morphological

variation in the Dmanisi mandibles. *Proceedings of the National Academy of Sciences*, 110(43):17278–17283.

Martin, R.B., Burr, D.B., Sharkey, N.A., and Fyhrie, D.P. 2015. *Skeletal Tissue Mechanics*. Second Edition. Springer, New York, NY, United States of America.

Martinez-Maza, C., Rosas, A., and Nieto-Díaz, M. 2013. Postnatal changes in the growth dynamics of the human face revealed from bone modelling patterns. *Journal of Anatomy*, 223(3):228–241.

Masumoto, T., Hayashi, I., Kawamura, A., Tanaka, K., and Kasai, K. 2001. Relationships among facial type, buccolingual molar inclination, and cortical bone thickness of the mandible. *European Journal of Orthodontics*, 23(1):15–23.

Matsuda, H., Borzabadi-Farahani, A., and Le, B.T. 2016. Three-dimensional alveolar bone anatomy of the maxillary first molars: a cone-beam computed tomography study with implications for immediate implant placement. *Implant Dentistry*, 25(3):367–372.

Mays, S. 2013. Loss of molar occlusion and mandibular morphology in adults in an ancient human population consuming a coarse diet. *American Journal of Physical Anthropology*, 152(3):383–392.

Mays, S. 2015a. Mandibular morphology in two archaeological human skeletal samples from northwest Europe with different masticatory regimes. *HOMO - Journal of Comparative Human Biology*, 66(3):203–215.

Mays, S. 2015b. The effect of factors other than age upon skeletal age indicators in the adult. *Annals of Human Biology*, 42(4):332–341.

Mays, S. 2017. A test of a skeletal ageing method based on resorption of the alveolar crest following tooth loss using a skeletal population of documented age at death. *American Journal of Physical Anthropology*, 163(2):242–251.

McKay, C. 2019. *Mandibular Morphological Variation: Implications for Fracture Repair*. MSc Thesis, Stellenbosch University.

de Medeiros, F.C.F.L., Kudo, G.A.H., Leme, B.G., Saraiva, P.P., Verri, F.R., Honório, H.M., Pellizzer, E.P., and Santiago Junior, J.F. 2018. Dental implants in patients with osteoporosis: a systematic review with meta-analysis. *International Journal of Oral and Maxillofacial Surgery*, 47(4):480–491.

Mendelson, B., and Wong, C.-H. 2012. Changes in the facial skeleton with aging: implications and clinical applications in facial rejuvenation. *Aesthetic Plastic Surgery*, 36(4):753–760.

Merheb, J., Temmerman, A., Rasmusson, L., Kübler, A., Thor, A., and Quirynen, M. 2016. Influence of skeletal and local bone density on dental implant stability in patients with osteoporosis. *Clinical Implant Dentistry and Related Research*, 18(2):253–260.

Merheb, J., Van Assche, N., Coucke, W., Jacobs, R., Naert, I., and Quirynen, M. 2010. Relationship between cortical bone thickness or computerized tomography-derived bone density values and implant stability. *Clinical Oral Implants Research*, 21(6):612–617.

Merheb, J., Vercruyssen, M., Coucke, W., and Quirynen, M. 2018. Relationship of implant stability and bone density derived from computerized tomography images. *Clinical Implant Dentistry and Related Research*, 20(1):50–57.

Merrot, O., Vacher, C., Merrot, S., Godlewski, G., Frigard, B., and Goudot, P. 2005. Changes in the edentate mandible in the elderly. *Surgical and Radiologic Anatomy*, 27(4):265–270.

Michetti, J., Maret, D., Mallet, J.-P., and Diemer, F. 2010. Validation of Cone Beam Computed Tomography as a tool to explore root canal anatomy. *Journal of Endodontics*, 36(7):1187–1190.

Mickenautsch, S., Van't Hof, M.A., and Frencken, J.E. 2007. Oral health service systems in Gauteng Province, South Africa. *East African Medical Journal*, 84(4):178–182.

Micklesfield, L.K., Norris, S.A., and Pettifor, J.M. 2011. Ethnicity and bone: a South African perspective. *Journal of Bone and Mineral Metabolism*, 29(3):257–267.

Millot, G. 2018. *Comprendre et réaliser les tests statistiques à l'aide de R: Manuel de Biostatistique*. Quatrième Édition. De Boeck Supérieur, Louvain-la-Neuve, Belgique.

Misch, C.E. 1988. Bone character: second vital implant criterion. *Dentistry Today*, 7:39–40.

Misch, C.E. 1990. Density of bone: effect on treatment plans, surgical approach, healing, and progressive boen loading. *International Journal of Oral Implantology: Implantologist*, 6(2):23–31.

Miyamoto, I., Tsuboi, Y., Wada, E., Suwa, H., and Iizuka, T. 2005. Influence of cortical bone thickness and implant length on implant stability at the time of surgery—clinical, prospective, biomechanical, and imaging study. *Bone*, 37(6):776–780.

Model, F., Manuilova, E., and Schuetzenmeister, A. 2014. *Mcr: Method Comparison Regression*. Available at: https://CRAN.R-project.org/package=mcr [Accessed: 24 February 2019].

Mogajane, B.M., and Mabongo, M. 2018. Epidemiology of maxillofacial fractures at two maxillofacial units in South Africa. *South African Dental Journal*, 73(3).

Molteni, R. 2013. Prospects and challenges of rendering tissue density in Hounsfield units for cone beam computed tomography. *Oral Surgery, Oral Medicine, Oral Pathology and Oral Radiology*, 116(1):105–119.

Morelli, D.L., Jackson, N., Gislason, T., Arnardottir, E.S., Benediktsdottir, B., Juliusson, S., Einarsdottir, H., Thorarinsson, G.H., Maislin, G., Kim, C., and Schwab, R. 2011. The effect of edentulism on ahi, odi, and tongue morphology in iceland sleep apnea cohort (isac). *B72. Determinants of Upper Airway Size and Function*. American Thoracic Society, Denver, Colorado, United States of America, pp. A3676–A3676.

Motawei, S.M., Helaly, A.MN., Aboelmaaty, W.M., Elmahdy, K., Shabka, O.A., and Liu, H. 2020. Length of the ramus of the mandible as an indicator of chronological age and sex: A study in a group of Egyptians. *Forensic Science International: Reports*, 2:100066.

Mounier, A., Marchal, F., and Condemi, S. 2009. Is Homo heidelbergensis a distinct species? New insight on the Mauer mandible. *Journal of Human Evolution*, 56(3):219–246.

Munakata, M., Tachikawa, N., Honda, E., Shiota, M., and Kasugai, S. 2011. Influence of menopause on mandibular bone quantity and quality in Japanese women receiving dental implants. *Archives of Osteoporosis*, 6(1–2):51–57.

Nair, M.K., and Nair, U.P. 2007. Digital and advanced imaging in endodontics: a review. *Journal of Endodontics*, 33(1):1–6.

Naitoh, M., Katsumata, A., Mitsuya, S., Kamemoto, H., and Ariji, E. 2004. Measurement of mandibles with microfocus x-ray computerized tomography and compact computerized tomography for dental use. *International Journal of Oral & Maxillofacial Implants*, 19(2):239–246.

Nakamoto, T., Hatsuta, S., Yagi, S., Verdonschot, R.G., Taguchi, A., and Kakimoto, N. 2020. Computer-aided diagnosis system for osteoporosis based on quantitative evaluation of mandibular lower border porosity using panoramic radiographs. *Dentomaxillofacial Radiology*, 49(4):20190481.

Nakatsuka, Y., Yamashita, S., Nimura, H., Mizoue, S., Tsuchiya, S., and Hashii, K. 2010. Location of main occluding areas and masticatory ability in patients with reduced occlusal support. *Australian Dental Journal*, 55(1):45–50.

Netter, F.H. 2014. *Atlas of Human Anatomy*. Sixth Edition. Saunders/Elsevier, Philadelphia, PA, United States of America.

Newton, J.P., Yemm, R., Abel, R.W., and Menhinick, S. 1993. Changes in human jaw muscles with age and dental state. *Gerodontology*, 10(1):16–22.

Nicholson, E., and Harvati, K. 2006. Quantitative analysis of human mandibular shape using three-dimensional geometric morphometrics. *American Journal of Physical Anthropology*, 131(3):368–383.

Nicopoulou-Karayianni, K., Tzoutzoukos, P., Mitsea, A., Karayiannis, A., Tsiklakis, K., Jacobs, R., Lindh, C., van der Stelt, P., Allen, P., Graham, J., Horner, K., Devlin, H., Pavitt, S., and Yuan, J. 2009. Tooth loss and osteoporosis: the osteodent study. *Journal of Clinical Periodontology*, 36(3):190–197.

Nikon Metrology *XT H 225 ST | Computed Tomography | X-Ray and CT Inspection*. Available at: https://www.nikonmetrology.com/en-gb/product/xt-h-225-st [Accessed: 19 November 2018].

Norton, M.R., and Gamble, C. 2001. Bone classification: an objective scale of bone density using the computerized tomography scan. *Clinical Oral Implants Research*, 12(1):79–84.

Oettlé, A.C. 2014. *Effects of Dental Loss and Senescence on Aspects of Adult Mandibular Morphology in South Africans*. PhD thesis, University of Pretoria, South Africa.

Oettlé, A.C., Becker, P.J., de Villiers, E., and Steyn, M. 2009a. The influence of age, sex, population group, and dentition on the mandibular angle as measured on a South African sample. *American Journal of Physical Anthropology*, 139(4):505–511.

Oettlé, A.C., Ehlers, R., and Steyn, M. 2016. Changes in the mandibular angle during adulthood in South Africans. *American Journal of Human Biology*, 28(5):681–686.

Oettlé, A.C., Fourie, J., Human-Baron, R., and van Zyl, A.W. 2015. The midline mandibular lingual canal: importance in implant surgery. *Clinical Implant Dentistry and Related Research*, 17(1):93–101.

Oettlé, A.C., Pretorius, E., and Steyn, M. 2005. Geometric morphometric analysis of mandibular ramus flexure. *American Journal of Physical Anthropology*, 128(3):623–629.

Oettlé, A.C., Pretorius, E., and Steyn, M. 2009b. Geometric morphometric analysis of the use of mandibular gonial eversion in sex determination. *HOMO - Journal of Comparative Human Biology*, 60(1):29–43.

Ogawa, T., and Osato, S. 2013. Growth changes of the mandibular body with eruption of mandibular third molars: Analysis of anatomical morphometry and quantitative bone mineral content by using radiography. *Annals of Anatomy - Anatomischer Anzeiger*, 195(2):143–150.

Olejniczak, A.J., and Grine, F.E. 2006. Assessment of the accuracy of dental enamel thickness measurements using microfocal X-ray computed tomography. *The Anatomical Record Part A: Discoveries in Molecular, Cellular, and Evolutionary Biology*, 288A(3):263–275.

Olejniczak, A.J., Tafforeau, P., Smith, T.M., Temming, H., and Hublin, J.-J. 2007. Technical note: Compatibility of microtomographic imaging systems for dental measurements. *American Journal of Physical Anthropology*, 134(1):130–134.

de Oliveira Pinto, M.G., Melo, S.L.S., Suassuna, F.C.M., Marinho, L.E., Leite, J.B. da S., Batista, A.U.D., Bento, P.M., and Melo, D.P. 2021. Influence of size of field of view (FOV), position within the FOV, and scanning mode on the detection of root fracture and observer's perception of artifacts in CBCT images. *Dentomaxillofacial Radiology*, 50(6):20200563.

Olofsson, J., Ljungqvist, O., Stjernfeldt, P.E., Wardh, I., and Odlund Olin, A. 2017. Relationships between oral health-related quality of life and objective and subjective masticatory ability in geriatric patients: a pilot study. *Journal of Dental and Oral Health*, 3(1):1–5.

Ono, A., Motoyoshi, M., and Shimizu, N. 2008. Cortical bone thickness in the buccal posterior region for orthodontic mini-implants. *International Journal of Oral and Maxillofacial Surgery*, 37(4):334–340.

Ozan, O., Orhan, K., Aksoy, S., Icen, M., Bilecenoglu, B., and Sakul, B.U. 2013. The effect of removable partial dentures on alveolar bone resorption: A retrospective study with Cone-Beam Computed Tomography. *Journal of Prosthodontics*, 22(1):42–48.

Ozdemir, F., Tozlu, M., and Germec Cakan, D. 2014. Quantitative evaluation of alveolar cortical bone density in adults with different vertical facial types using cone-beam computed tomography. *The Korean Journal of Orthodontics*, 44(1):36.

Oziegbe, E.O., and Schepartz, L.A. 2021. Association between parity and tooth loss among northern Nigerian Hausa women. *American Journal of Physical Anthropology*, 174(3):451–462.

Ozturk, C.N., Ozturk, C., Bozkurt, M., Uygur, H.S., Papay, F.A., and Zins, J.E. 2013. Dentition, bone loss, and the aging of the mandible. *Aesthetic Surgery Journal*, 33(7):967–974.

Panmekiate, S., Ngonphloy, N., Charoenkarn, T., Faruangsaeng, T., and Pauwels, R. 2015. Comparison of mandibular bone microarchitecture between micro-CT and CBCT images. *Dentomaxillofacial Radiology*, 44(5):20140322.

Parfitt, A.M. 1984. The cellular basis of bone remodeling: The quantum concept reexamined in light of recent advances in the cell biology of bone. *Calcified Tissue International*, 36(S1):S37–S45.

Parfitt, A.M. 1988. Bone histomorphometry: Standardization of nomenclature, symbols and units (summary of proposed system). *Bone*, 9(1):67–69.

Parfitt, A.M., Mathews, C.H., Villanueva, A.R., Kleerekoper, M., Frame, B., and Rao, D.S. 1983. Relationships between surface, volume, and thickness of iliac trabecular bone in aging and in osteoporosis. Implications for the microanatomic and cellular mechanisms of bone loss. *Journal of Clinical Investigation*, 72(4):1396–1409.

Park, H.S., Kim, D.-K., Lee, S.Y., and Park, K.-H. 2017. The effect of aging on mastication and swallowing parameters according to the hardness change of solid food. *Journal of Texture Studies*, 48(5):362–369.

Park, H.S., Lee, Y.J., Jeong, S.H., and Kwon, T.G. 2008. Density of the alveolar and basal bones of the maxilla and the mandible. *American Journal of Orthodontics and Dentofacial Orthopedics*, 133(1):30–37.

Parr, N.M., Passalacqua, N.V., and Skorpinski, K. 2017. Investigations into age-related changes in the human mandible. *Journal of Forensic Sciences*, 62(6):1586–1591.

Parsa, A., Ibrahim, N., Hassan, B., Motroni, A., van der Stelt, P., and Wismeijer, D. 2013. Influence of cone beam CT scanning parameters on grey value measurements at an implant site. *Dentomaxillofacial Radiology*, 42(3):79884780.

Parsa, A., Ibrahim, N., Hassan, B., van der Stelt, P., and Wismeijer, D. 2015. Bone quality evaluation at dental implant site using multislice CT, micro-CT, and cone beam CT. *Clinical Oral Implants Research*, 26(1):e1–e7.

Passing, H., and Bablok, W. 1983. A new biometrical procedure for testing the equality of measurements from two different analytical methods. Application of linear regression procedures for method comparison studies in clinical chemistry, Part I. *Journal of Clinical Chemistry and Clinical Biochemistry*, 21(11):709–720.

Pauwels, R., Jacobs, R., Singer, S.R., and Mupparapu, M. 2015. CBCT-based bone quality assessment: are Hounsfield units applicable? *Dentomaxillofacial Radiology*, 44(1):20140238.

Pauwels, R., Pittayapat, P., Sinpitaksakul, P., and Panmekiate, S. 2021. Scatter-to-primary ratio in dentomaxillofacial cone-beam CT: effect of field of view and beam energy. *Dentomaxillofacial Radiology*, 50(8):20200597.

Pearson, O.M., and Lieberman, D.E. 2004. The aging of Wolff's law?: Ontogeny and responses to mechanical loading in cortical bone. *American Journal of Physical Anthropology*, 125(S39):63–99.

Peltzer, K., Hewlett, S., Yawson, A., Moynihan, P., Preet, R., Wu, F., Guo, G., Arokiasamy, P., Snodgrass, J., Chatterji, S., Engelstad, M., and Kowal, P. 2014. Prevalence of loss of all teeth (edentulism) and associated factors in older adults in China, Ghana, India, Mexico, Russia and South Africa. *International Journal of Environmental Research and Public Health*, 11(11):11308–11324.

Pessa, J.E., Slice, D.E., Hanz, K.R., Broadbent, T.H., and Rohrich, R.J. 2008. Aging and the shape of the mandible: *Plastic and Reconstructive Surgery*, 121(1):196–200.

Petersen, D.C., Libiger, O., Tindall, E.A., Hardie, R.-A., Hannick, L.I., Glashoff, R.H., Mukerji, M., Indian Genome Variation Consortium, Fernandez, P., Haacke, W., Schork, N.J., and Hayes, V.M. 2013. Complex patterns of genomic admixture within Southern Africa. *PLoS Genetics*, 9(3):e1003309.

Peyron, M.-A., Blanc, O., Lund, J.P., and Woda, A. 2004. Influence of age on adaptability of human mastication. *Journal of Neurophysiology*, 92(2):773–779.

Pfeiffer, S., Heinrich, J., Beresheim, A., and Alblas, M. 2016. Cortical bone histomorphology of known-age skeletons from the Kirsten collection, Stellenbosch university, South Africa. *American Journal of Physical Anthropology*, 160(1):137–147.

Pilloud, M.A., Hefner, J.T., Hanihara, T., and Hayashi, A. 2014. The use of tooth crown measurements in the assessment of ancestry. *Journal of Forensic Sciences*, 59(6):1493–1501.

Pitirri, M.K., and Begun, D. 2019. A new method to quantify mandibular corpus shape in extant great apes and its potential application to the hominoid fossil record. *American Journal of Physical Anthropology*, 168(2):318–328.

Planmeca *ProMax3D® | Key Features and User's Manual*. Available at: http://www.planmeca.com/na/Imaging/3D-imaging---Key-features/ [Accessed: 19 November 2018a].

Planmeca *Romexis® / Imaging Software*. Available at: https://www.planmeca.com/Software/Desktop/Planmeca-Romexis/ [Accessed: 19 November 2018b].

Plavcan, J.M. 2002. Taxonomic variation in the patterns of craniofacial dimorphism in primates. *Journal of Human Evolution*, 42(5):579–608.

Polanski, J.M. 2011. Morphological integration of the modern human mandible during ontogeny. *International Journal of Evolutionary Biology*, 2011.

Posnick, J.C. 2014. Speech, Mastication, and Swallowing Considerations in the Evaluation and Treatment of Dentofacial Deformities. *Orthognathic Surgery*. Elsevier, pp. 227–263.

Quirynen, M., Van Assche, N., Botticelli, D., and Berglundh, T. 2007. How does the timing of implant placement to extraction affect outcome? *International Journal of Oral & Maxillofacial Implants*, 22(7):203–226.

R Core Team 2020. *R: A Language and Environment for Statistical Computing. R Foundation for Statistical Computing*. Available at: https://www.R-project.org/.

Radi, I.A.-W., Ibrahim, W., Iskandar, S.M.S., and AbdelNabi, N. 2018. Prognosis of dental implants in patients with low bone density: A systematic review and meta-analysis. *The Journal of Prosthetic Dentistry*, 120(5):668–677.

Ramphaleng, T. 2015. *The Effect of Tooth Loss on Accurately Estimating Sex from Mandibular Features of South Africans*. MSc Thesis, University of the Witwatersrand, South Africa.

Raustia, A., Pirttiniemi, P., Salonen, M., and Pyhtinen, J. 1998. Effect of edentulousness on mandibular size and condyle-fossa position. *Journal of Oral Rehabilitation*, 25(3):174–179.

Republic of South Africa 2004. *Government Gazette | National Health Act | No. 61 of 2003*. Available at: https://www.gov.za/documents/national-health-act [Accessed: 3 December 2018].

Resnik, R.R. (Ed.) 2020. *Misch's Contemporary Implant Dentistry*. Fourth edition. Elsevier, St. Louis.

Resnik, R.R., and Misch, C.E. 2020a. Rationale for Dental Implants. In: Resnik, R.R. (ed.). *Misch's Contemporary Implant Dentistry*. Fourth edition. Elsevier, pp. 450–466.

Resnik, R.R., and Misch, C.E. 2020b. Bone Density: A Key Determinant for Treatment Planning. In: Resnik, R.R. (ed.). *Misch's Contemporary Implant Dentistry*. Fourth edition. Elsevier, pp. 450–466.

Rios, H.F., Borgnakke, W.S., and Benavides, E. 2017. The use of cone-beam computed tomography in management of patients requiring dental implants: an american academy of periodontology best evidence review. *Journal of Periodontology*, 88(10):946–959.

Roberts, W.E. 2020. Bone physiology, metabolism, and biomechanics. In: Resnik, R.R. (ed.). *Misch's Contemporary Implant Dentistry*. Fourth Edition. Elsevier, pp. 69–107.

Roode, G.J., van Wyk, P.J., and Botha, S.J. 2007. Mandibular fractures: an epidemiological survey at the Oral and Dental Hospital, Pretoria. *South African Dental Journal*, 62(6):270, 272–274.

Rosner, B. 2016. *Fundamentals of Biostatistics*. Eighth Edition. Cengage Learning, Boston, MA, United States of America.

RStudio Team 2020. *RStudio: Integrated Development for R*. Available at: http://www.rstudio.com/.

Ruff, C.B. 2019. Biomechanical analyses of archaeological human skeletons. In: Katzenberg, M.A. and Grauer, A.L. (eds.). *Biological Anthropology of the Human Skeleton*. Third Edition. Wiley-Blackwell, Hoboken, NJ, United States of America, pp. 189–224.

Ruff, C.B., Holt, B., and Trinkaus, E. 2006. Who's afraid of the big bad Wolff?: 'Wolff's law' and bone functional adaptation. *American Journal of Physical Anthropology*, 129(4):484–98.

Ruquet, M., Saliba-Serre, B., Tardivo, D., and Foti, B. 2015. Estimation of age using alveolar bone loss: forensic and anthropological applications. *Journal of Forensic Sciences*, 60(5):1305–1309.

Russell, S.L., Gordon, S., Lukacs, J.R., and Kaste, L.M. 2013. Sex/gender differences in tooth loss and edentulism. *Dental Clinics of North America*, 57(2):317–337.

Santos, L.S. de M., Rossi, A.C., Freire, A.R., Matoso, R.I., Caria, P.H.F., and Prado, F.B. 2015. Finite-element analysis of 3 situations of trauma in the human edentulous mandible. *Journal of Oral and Maxillofacial Surgery*, 73(4):683–691.

Sathapana, S., Forrest, A., Monsour, P., and Naser-ud-Din, S. 2013. Age-related changes in maxillary and mandibular cortical bone thickness in relation to temporary anchorage device placement. *Australian Dental Journal*, 58(1):67–74.

Sato, H., Kawamura, A., Yamaguchi, M., and Kasai, K. 2005. Relationship between masticatory function and internal structure of the mandible based on computed tomography findings. *American Journal of Orthodontics and Dentofacial Orthopedics*, 128(6):766–773.

Scarfe, W.C., and Farman, A.G. 2008. What is Cone-Beam CT and how does it work? *Dental Clinics of North America*, 52(4):707–730.

Scarfe, W.C., Farman, A.G., and Sukovic, P. 2006. Clinical applications of cone-beam computed tomography in dental practice. *Journal of the Canadian Dental Association*, 72(1):75–80.

Scheid, R.C., and Weiss, G. 2012. *Woelfel's Dental Anatomy*. Eighth Edition. Lippincott, Williams and Wilkins (eds.). Philadelphia, PA, United States of America.

Schwartz-Dabney, C.L., and Dechow, P.C. 2002. Edentulation alters material properties of cortical bone in the human mandible. *Journal of Dental Research*, 81(9):613–617.

Schwartz-Dabney, C.L., and Dechow, P.C. 2003. Variations in cortical material properties throughout the human dentate mandible. *American Journal of Physical Anthropology*, 120(3):252–277.

Sella-Tunis, T., Pokhojaev, A., Sarig, R., O'Higgins, P., and May, H. 2018. Human mandibular shape is associated with masticatory muscle force. *Scientific Reports*, 8(1):6042.

Sella-Tunis, T., Sarig, R., Cohen, H., Medlej, B., Peled, N., and May, H. 2017. Sex estimation using computed tomography of the mandible. *International Journal of Legal Medicine*, 131(6):1691–1700.

Shapurian, T., Damoulis, P.D., Reiser, G.M., Griffin, T.J., and Rand, W.M. 2006. Quantitative evaluation of bone density using the Hounsfield index. *International Journal of Oral & Maxillofacial Implants*, 21(2):290–297.

Sharawy, M. 2020. Applied Anatomy for Dental Implants. In: Resnik, R.R. (ed.). *Misch's Contemporary Implant Dentistry*. Fourth edition. Elsevier, pp. 331–340.

Shaw, R.B., and Kahn, D.M. 2007. Aging of the midface bony elements: a three-dimensional computed tomographic study: *Plastic and Reconstructive Surgery*, 119(2):675–681.

Shaw, R.B., Katzel, E.B., Koltz, P.F., Kahn, D.M., Girotto, J.A., and Langstein, H.N. 2010. Aging of the mandible and its aesthetic implications. *Plastic and Reconstructive Surgery*, 125(1):332–342.

Shaw, R.B., Katzel, E.B., Koltz, P.F., Kahn, D.M., Puzas, E.J., and Langstein, H.N. 2012. Facial bone density: effects of aging and impact on facial rejuvenation. *Aesthetic Surgery Journal*, 32(8):937–942.

Shen, J., and Listl, S. 2018. Investigating social inequalities in older adults' dentition and the role of dental service use in 14 European countries. *The European Journal of Health Economics*, 19(1):45–57.

Singh, S.V., and Tripathi, A. 2010. An overview of osteoporosis for the practising prosthodontist. *Gerodontology*, 27(4):308–314.

Skinner, M.M., Gordon, A.D., and Collard, N.J. 2006. Mandibular size and shape variation in the hominins at Dmanisi, Republic of Georgia. *Journal of Human Evolution*, 51(1):36–49.

Smith, R.B., and Tarnow, D.P. 2013. Classification of molar extraction sites for immediate dental implant placement: technical note. *International Journal of Oral & Maxillofacial Implants*, 28(3):911–916.

de Souza Fernandes, A.C., de Quadros Uzeda-Gonzalez, S., Mascarenhas, M.L., Machado, L.A., and de Moraes, M. 2012. Direct and tomographic dimensional analysis of the inter-radicular distance and thickness of the vestibular cortical bone in the parasymphyseal region of adult human mandibles. *British Journal of Oral and Maxillofacial Surgery*, 50(4):350–355.

Standring, S. 2009. *Gray's Anatomy: The Anatomical Basis of Clinical Practice*. Fortieth Edition. Elsevier, London, United Kingdom.

Statistics South Africa 2016. Community Survey | Census 2016 / *Statistical release P0301*. Available at: http://cs2016.statssa.gov.za/ [Accessed: 12 December 2018].

Statistics South Africa 2021. Mid-year population estimates / *Statistical release P0302*. Available at: https://www.statssa.gov.za/publications/P0302/P03022021.pdf [Accessed: 7 January 2022].

Stimmelmayr, M., Denk, K., Erdelt, K., Krennmair, G., Mansour, S., Beuer, F., and Güth, J.-F. 2017. Accuracy and reproducibility of four cone beam computed tomography devices using 3D implant-planning software. *International Journal of Computerized Dentistry*, 20(1):21–34.

Stodder, A.L.W. 2019. Taphonomy and the nature of archaeological assemblages. In: Katzenberg, M.A. and Grauer, A.L. (eds.). *Biological Anthropology of the Human Skeleton*. Third Edition. Wiley-Blackwell, Hoboken, NJ, United States of America, pp. 73–115.

Stoetzer, M., Nickel, F., Rana, M., Lemound, J., Wenzel, D., von See, C., and Gellrich, N.-C. 2013. Advances in assessing the volume of odontogenic cysts and tumors in the mandible: a retrospective clinical trial. *Head & Face Medicine*, 9(14):1–5.

Stull, K.E., Kenyhercz, M.W., Tise, M.L., L'Abbé, E.N., and Tuamsuk, P. 2016. The craniometric implications of a complex population history in South Africa. In: Pilloud, M.A. and Hefner, J.T. (eds.). *Biological Distance Analysis: Forensic and Bioarchaeological Perspectives*. Elsevier/Academic Press, London, United Kingdom; San Diego, CA, United States of America, pp. 245–263.

Suttapreyasri, S., Suapear, P., and Leepong, N. 2018. The accuracy of cone-beam computed tomography for evaluating bone density and cortical bone thickness at the implant site: micro-computed tomography and histologic analysis. *Journal of Craniofacial Surgery*, 29(8):2026–2031.

Swain, M.V., and Xue, J. 2009. State of the art of micro-ct applications in dental research. *International Journal of Oral Science*, 1(4):177–188.

Swasty, D., Lee, J., Huang, J.C., Maki, K., Gansky, S.A., Hatcher, D., and Miller, A.J. 2011. Cross-sectional human mandibular morphology as assessed in vivo by cone-beam computed tomography in patients with different vertical facial dimensions. *American Journal of Orthodontics and Dentofacial Orthopedics*, 139(4):e377–e389.

Swasty, D., Lee, J.S., Huang, J.C., Maki, K., Gansky, S.A., Hatcher, D., and Miller, A.J. 2009. Anthropometric analysis of the human mandibular cortical bone as assessed by cone-

beam computed tomography. *Journal of Oral and Maxillofacial Surgery*, 67(3):491–500.

Taguchi, A., Tanimoto, K., Suei, Y., Ohama, K., and Wada, T. 1996. Relationship between the mandibular and lumbar vertebral bone mineral density at different postmenopausal stages. *Dentomaxillofacial Radiology*, 25(3):130–135.

Tappen, N.C. 1985. The dentition of the "old man" of La Chapelle-aux-Saints and inferences concerning Neandertal behavior. *American Journal of Physical Anthropology*, 67(1):43–50.

Taylor, A.B. 2006. Size and shape dimorphism in great ape mandibles and implications for fossil species recognition. *American Journal of Physical Anthropology*, 129(1):82–98.

Temmerman, A., Rasmusson, L., Kübler, A., Thor, A., Merheb, J., and Quirynen, M. 2019. A prospective, controlled, multicenter study to evaluate the clinical outcome of implant treatment in women with osteoporosis/osteopenia: 5-year results. *Journal of Dental Research*, 98(1):84–90.

Temmerman, A., Rasmusson, L., Kübler, A., Thor, A., and Quirynen, M. 2017. An open, prospective, non-randomized, controlled, multicentre study to evaluate the clinical outcome of implant treatment in women over 60 years of age with osteoporosis/osteopenia: 1-year results. *Clinical Oral Implants Research*, 28(1):95–102.

Temple, K.E., Schoolfield, J., Noujeim, M.E., Huynh-Ba, G., Lasho, D.J., and Mealey, B.L. 2015. A cone beam computed tomography (CBCT) study of buccal plate thickness of the maxillary and mandibular posterior dentition. *Clinical Oral Implants Research*, 27(9):1072–1078.

Thayer, Z.M., and Dobson, S.D. 2010. Sexual dimorphism in chin shape: Implications for adaptive hypotheses. *American Journal of Physical Anthropology*, 143(3):417–425.

Theye, C.E.G., Hattingh, A., Cracknell, T.J., Oettlé, A.C., Steyn, M., and Vandeweghe, S. 2018. Dento-alveolar measurements and histomorphometric parameters of maxillary and mandibular first molars, using micro-CT. *Clinical Implant Dentistry and Related Research*, 20(4):550–561.

Throckmorton, G.S., and Dean, J.S. 1994. The relationship between jaw-muscle mechanical advantage and activity levels during isometric bites in humans. *Archives of Oral Biology*, 39(5):429–437.

Toennies, K.D. 2012. *Guide to Medical Image Analysis - Methods and Algorithms*. Springer, London, United Kingdom.

Tomasi, C., Sanz, M., Cecchinato, D., Pjetursson, B., Ferrus, J., Lang, N.P., and Lindhe, J. 2010. Bone dimensional variations at implants placed in fresh extraction sockets: a multilevel multivariate analysis. *Clinical Oral Implants Research*, 21(1):30–36.

Toro-Ibacache, V., Zapata Muñoz, V., and O'Higgins, P. 2016. The relationship between skull morphology, masticatory muscle force and cranial skeletal deformation during biting. *Annals of Anatomy*, 203:59–68.

Tortopidis, D., Lyons, M.F., Baxendale, R.H., and Gilmour, W.H. 1998. The variability of bite force measurement between sessions, in different positions within the dental arch. *Journal of Oral Rehabilitation*, 25(9):681–686.

Trinkaus, E. 1985. Pathology and the posture of the La Chapelle-aux-Saints Neandertal. *American Journal of Physical Anthropology*, 67(1):19–41.

Tsai, M.-T., He, R.-T., Huang, H.-L., Tu, M.-G., and Hsu, J.-T. 2020. Effect of scanning resolution on the prediction of trabecular bone microarchitectures using dental cone beam computed tomography. *Diagnostics*, 10(6):368.

Turner, C.H. 1999. Toward a mathematical description of bone biology: the principle of cellular accommodation. *Calcified Tissue International*, 65(6):466–471.

Tyndall, D.A., and Rathore, S. 2008. Cone-beam CT diagnostic applications: caries, periodontal bone assessment, and endodontic applications. *Dental Clinics of North America*, 52(4):825–841.

Ueno, M., Ohara, S., Inoue, M., Tsugane, S., and Kawaguchi, Y. 2013. Association between parity and dentition status among Japanese women: Japan public health center-based oral health study. *BMC Public Health*, 13(1):993.

Ulm, C., Solar, P., Blahout, R., Matejka, M., and Gruber, H. 1992. Reduction of the compact and cancellous bone substances of the edentulous mandible caused by resorption. *Oral Surgery, Oral Medicine, Oral Pathology*, 74(2):131–136.

United Nations, Department of Economic and Social Affairs, Population Division 2019. *World Population Ageing 2019: Highlights (ST/ESA/SER.A/430)*.

Van Dessel, J., Huang, Y., Depypere, M., Rubira-Bullen, I., Maes, F., and Jacobs, R. 2013. A comparative evaluation of cone beam CT and micro-CT on trabecular bone structures in the human mandible. *Dentomaxillofacial Radiology*, 42(8):20130145.

Van Dessel, J., Nicolielo, L.F.P., Huang, Y., Coudyzer, W., Salmon, B., Lambrichts, I., and Jacobs, R. 2017. Accuracy and reliability of different cone beam computed tomography (CBCT) devices for structural analysis of alveolar bone in comparison with multislice CT and micro-CT. *European Journal of Oral Implantology*, 10(1):95–105.

Vitral, R.W.F., Fraga, M.R., and da Silva Campos, M.J. 2015. Use of Hounsfield units in cone-beam computed tomography. *American Journal of Orthodontics and Dentofacial Orthopedics*, 148(2):204.

Volume Graphics GmbH | *VGStudio MAX 3.1.* | *Three-Dimensional Volume Rendering Software*. Available at: http://www.volumegraphics.com/en/products/vgstudio-max/basic-functionality/ [Accessed: 6 November 2018].

Wang, Q., Ashley, D.W., and Dechow, P.C. 2010. Regional, ontogenetic, and sex-related variations in elastic properties of cortical bone in baboon mandibles. *American Journal of Physical Anthropology*, 141:526–549.

Wang, Y., He, S., Yu, L., Li, J., and Chen, S. 2011. Accuracy of volumetric measurement of teeth in vivo based on cone beam computer tomography: Accuracy of volumetric measurement of teeth. *Orthodontics & Craniofacial Research*, 14(4):206–212.

Watt, R.G., Listl, S., Peres, M., and Heilmann, A. (Eds.) 2015. *Social Inequalities in Oral Health: From Evidence to Action*. International Centre for Oral Health Inequalities Research&Policy. University College London, London, United Kingdom.

Watzek, G., Haider, R., Mensdorff-Pouilly, N., and Haas, R. 1995. Immediate and delayed implantation for complete restoration of the jaw following extraction of all residual teeth: a retrospective study comparing different types of serial immediate implantation. *International Journal of Oral & Maxillofacial Implants*, 10(5):561–567.

Wei, T., and Simko, V. 2017. *R Package 'Corrplot': Visualization of a Correlation Matrix*. Available at: https://github.com/taiyun/corrplot.

West, K.S., and McNamara, J.A. 1999. Changes in the craniofacial complex from adolescence to midadulthood: A cephalometric study. *American Journal of Orthodontics and Dentofacial Orthopedics*, 115(5):521–532.

White, T.D., Black, M.T., and Folkens, P.A. 2012. *Human Osteology*. Third Edition. Academic Press, San Diego, CA, United States of America.

White, T.D., and Folkens, P.A. 2005. *The Human Bone Manual*. Elsevier/Academic Press, San Diego, CA, United States of America.

Wickham, H. 2016. *Ggplot2: Elegant Graphics for Data Analysis*. Second Edition. Springer-Verlag, New York, NY, United States of America.

Williams, S.E., and Slice, D.E. 2014. Influence of edentulism on human orbit and zygomatic arch shape. *Clinical Anatomy*, 27(3):408–416.

von Wowern, N. 1977. Variations in bone mass within the cortices of the mandible. *European Journal of Oral Sciences*, 85(6):444–455.

von Wowern, N. 1982. Microradiographic and histomorphometric indices of mandibles for diagnosis of osteopenia. *European Journal of Oral Sciences*, 90(1):47–63.

von Wowern, N. 1988. Bone mineral content of mandibles: Normal reference values—Rate of age-related bone loss. *Calcified Tissue International*, 43(4):193–198.

von Wowern, N. 2001. General and oral aspects of osteoporosis: a review. *Clinical Oral Investigations*, 5(2):71–82.

von Wowern, N., and Melsen, F. 1979. Comparative bone morphometric analysis of mandibles and iliac crests. *European Journal of Oral Sciences*, 87(5):351–357.

von Wowern, N., and Stoltze, K. 1978. Sex and age differences in bone morphology of mandibles. *European Journal of Oral Sciences*, 86(6):478–485.

von Wowern, N., and Stoltze, K. 1979. Comparative bone morphometric analysis of mandibles and 2nd metacarpals. *European Journal of Oral Sciences*, 87(5):358–364.

von Wowern, N., and Stoltze, K. 1980. Pattern of age related bone loss in mandibles. *European Journal of Oral Sciences*, 88(2):134–146.

Xie, Q.-F., and Ainamo, A. 2004. Correlation of gonial angle size with cortical thickness, height of the mandibular residual body, and duration of edentulism. *The Journal of Prosthetic Dentistry*, 91(5):6.

Yamamoto, K., Matsusue, Y., Murakami, K., Horita, S., Sugiura, T., and Kirita, T. 2011. Maxillofacial fractures in older patients. *Journal of Oral and Maxillofacial Surgery*, 69(8):2204–2210.

Zanolli, C., Schillinger, B., Beaudet, A., Kullmer, O., Macchiarelli, R., Mancini, L., Schrenk, F., Tuniz, C., and Vodopivec, V. 2017. Exploring Hominin and Non-hominin Primate Dental Fossil Remains with Neutron Microtomography. *Physics Procedia*, 88:109–115.

Zhang, N. 2012. *Cortical Bone Thickness of Black and White American Adolescents*. MSc Thesis, Saint Louis University, United States of America.

Zheng, J., Ni, S., Wang, Y., Zhang, B., Teng, Y., and Jiang, S. 2018. Sex determination of Han adults in Northeast China using cone beam computer tomography. *Forensic Science International*, 289:450.e1-450.e7.

Zioupos, P., Smith, C.W., and An, Y.H. 2000. Factors Affecting Mechanical Properties of Bone. In: An, Y.H. and Draughn, R.A. (eds.). *Mechanical Testing of Bone and the Bone-Implant Interface*. CRC Press, Boca Raton, FL, United States of America, pp. 65–85.

Appendices

Appendix A. Published article (Theye *et al.,* 2018)

Theye, C.E.G., Hattingh, A., Cracknell, T.J., Oettlé, A.C., Steyn, M. and Vandeweghe, S. 2018. Dento-alveolar measurements and histomorphometric parameters of maxillary and mandibular first molars, using micro-CT. *Clinical Implant Dentistry and Related Research*, 20(4): 550–561.

ORIGINAL ARTICLE

WILEY 367

Dento-alveolar measurements and histomorphometric parameters of maxillary and mandibular first molars, using micro-CT

Charlotte E. G. Theye MSc[1] [ORCID] | André Hattingh MChD[2] |
Tamsin J. Cracknell BEng Mech[3] | Anna C. Oettlé MBBCh, PhD[1,4] |
Maryna Steyn MBChB, PhD[5] | Stefan Vandeweghe DDS, PhD[2]

[1]Department of Anatomy, Faculty of Health Sciences, University of Pretoria, Pretoria, Gauteng, South Africa

[2]Department of Periodontology, Oral Implantology, Removable and Implant Prosthetics, Dental School, Faculty of Medicine and Health Sciences, Ghent University, Ghent, Belgium

[3]Southern Implants (Pty) Ltd, Irene, Gauteng, South Africa

[4]Department of Anatomy and Histology, School of Medicine, Sefako Makgatho Health Sciences University, Pretoria, Gauteng, South Africa

[5]Human Variation and Identification Research Unit, School of Anatomical Sciences, Faculty of Health Sciences, University of the Witwatersrand, Johannesburg, Gauteng, South Africa

Correspondence
Charlotte E. G. Theye, Department of Anatomy, Faculty of Health Sciences, University of Pretoria, Private Bag X323, Arcadia 0007, South Africa.
Email: charlotte.theye@gmail.com

Funding information
University of Pretoria Postgraduate Research Support Bursary (CT); National Research Foundation of South Africa (MS)

Abstract

Background: Micro-CT is a high-resolution, non-invasive, and non-destructive imaging technique, currently acknowledged as a gold standard modality for assessing quantitatively and objectively dental morphology and bone microarchitecture parameters.

Purpose: The aim of this study was to analyze critical dental and periodontal measurements characterizing the mandibular (MandFM) and maxillary (MaxFM) first molar architecture, as well as the corresponding bony socket, using micro-CT.

Materials and Methods: Thirty-eight human dried skulls (22-76 years) were scanned to enable the virtual analysis of 61 first molars. Depending on the type of measurement, the parameters were recorded on two-dimensional sections or directly on three-dimensional models. Tooth morphology was described by four aspects (e.g., tooth width, trunk length, root length, and root span), while the socket architecture was assessed by buccal plate thicknesses and bone density measurements.

Results: Minimum, maximum, and mean distances as well as cortical and trabecular bone densities were recorded in MandFM and MaxFM. It is noteworthy that the buccal plate thickness was found to be less than 1 mm in more than 55% of cases in MaxFM, whereas only in 20.8% of cases in MandFM (and even 0% at two sites). A wide range of bone densities was observed and the comparison between MandFM and MaxFM did not show a significant difference. Furthermore, cortical densities were negatively correlated with aging, while trabecular densities were not influenced.

Conclusions: Using micro-CT, three-dimensional aspects of the human first molar morphology and microstructural parameters of the surrounding bone were evaluated in the mandible and in the maxilla. These comprehensive measurements and their correlation with aging may be of great importance for the use of immediate implant placement in molar extraction sockets and thus the potential long-term success of this treatment modality.

KEYWORDS
buccal plate, bone density, extraction socket, first molars, immediate implant, implant stability, mandible, maxilla, micro-CT

367

1 | INTRODUCTION

Generally, molars are reported to be the most frequently extracted teeth.[1,2] First molars are the first teeth to permanently erupt and are therefore prone to decay (e.g., caries) at an earlier age than other tooth types.[3] Loss of first molars has severe consequences on the mastication process and its efficiency, as first molars are the largest and strongest teeth, located near the center of the dental arches. Furthermore, first molars play a major role in maintaining continuity within the arch and keeping the teeth in a proper alignment.[4] Thus, the replacement of lost first molars is of particular importance, and should be performed without much delay.

The placement of dental implants at the time of tooth extraction was introduced in 1989 and is now well established.[5,6] However, immediate implant placement into a molar socket is still a challenge for the clinician,[7,8] mainly because of the increased peripheral dimensions but also because of the residual interradicular bone hindering primary stability, and so the critical positioning of the implant.[6,8-13] Other possible anatomical shortcomings include inadequate buccal plate thickness and poor bone density.[14-18] Moreover, as for delayed implant placement, the close proximity of the maxillary sinus, the inferior alveolar nerve, and/or the mandibular lingual canal may be of concern as well.[19-24] Parameters describing and quantifying the three-dimensional morphology of the tooth and of the socket and microstructure of the surrounding bone could provide vital information for clinicians.[9,10,13]

Analysis of the microstructure of the maxillary and mandibular periodontal bone as well as dental parameters may be performed on three-dimensional (3D) models computed from Micro-focus X-ray computed-tomography (micro-CT) scans. Furthermore, even if micro-CT cannot be employed in a daily clinical dental setting, this imaging technique is often used as a gold standard modality for dental research[25-29] and for osseous microstructure assessment[17,30,31] as it renders high-resolution results non-invasively and non-destructively.[25,32,33] Different types of variables can be obtained from micro-CT scans: linear measurements between landmarks on 3D models, or on 2D sections, assessing tooth or bone morphology; and histomorphometric parameters evaluating bone density and microarchitecture. These parameters, such as bone volumetric fraction (BV/TV), bone volume (BV), and total volume (TV) previously defined by Parfitt,[34] provide automatic and objective bone density information.[17,35]

Several studies have used micro-CT to assess bone density and microarchitecture of alveolar bone in human maxillae and mandibles on biopsies from cadaver specimens[17,31,36-38] or from patients.[15,30,33] However, in the literature researched, the cadaver-based studies were all performed on less than 30 specimens,[17,31,36] or even on a single specimen only.[37,38] Moreover, both patient and cadaver-based studies analyzed biopsies extracted from edentulous sites only. In a comparative study between CBCT and micro-CT techniques, Van Dessel et al[39] measured histomorphometric parameters at non-edentulous sites. However, the study focused on single-rooted teeth and was performed on a single cadaver specimen.

Thus, to date, very limited data is available on the microstructure of the cortical and trabecular bone surrounding the first molars, or even density of the interradicular bone. Furthermore, none of these studies have been done on South African individuals, whereas population affinity may influence the parameters. In terms of dental morphology, for example, Pilloud et al[40] showed that external tooth crown measurements varied sufficiently among populations to be used as an additional tool in forensic anthropology for the assessment of ancestry.

The aim of this study is to provide a quantitative analysis of the microstructural anatomy of the first maxillary (MaxFM) and mandibular (MandFM) molar extraction sockets in a South African population. To achieve this objective, critical dento-alveolar parameters characterizing and describing the molar morphology (e.g., tooth width, trunk length, root length, root span) and the corresponding bony socket (e.g., buccal plate thickness, bone density) were assessed on micro-CT scans. We also explored the possible correlation of the various parameters with aging.

2 | MATERIALS AND METHODS

2.1 | Sample

Thirty-eight modern human skulls (with known age, sex, and population affinity) were sourced from the Pretoria Bone Collection (PBC), housed in the Department of Anatomy (University of Pretoria).[41] This collection contains modern skeletal remains of known individuals from South Africa whose bodies have been donated willfully or by local hospitals (i.e., unclaimed bodies). Several population affinities are represented in the collection, with more than half (69%) of the skeletal remains with complete skulls are of African ancestry. Ethics clearance was obtained from the Research Ethics Committee of the Faculty of Health Sciences of the University of Pretoria (Protocol no. 57/2017).

The study sample consisted of adult individuals of African ancestry between 22 and 76 years (mean age: 39.7 years), with thirty males between 24 and 76 years (mean age: 39.5 years) and eight females between 22 and 70 years (mean age: 40.4 years). Individuals were selected according to the following inclusion/exclusion criteria: (1) presence of at least one maxillary and one mandibular first molar; (2) a good state of preservation of the teeth (e.g., no enamel defects and complete roots); (3) no evidence of significant medical or dental history (e.g., sinus pathology, periodontal disease or bone trauma); and (4) absence of metal restorations causing artifacts in imaging acquisitions. Overall, dental and periodontal measurements were performed on 61 teeth: 37 maxillary first molars (MaxFM) and 24 mandibular first molars (MandFM).

2.2 | Scanning procedure and data collection

The selected specimens were scanned by micro-CT at the South African Nuclear Energy Corporation (Necsa, Pelindaba). The acquisitions were performed with a Nikon XTH 225L industrial CT system (Nikon Metrology, Leuven, Belgium) according to the following parameters: 100 kV voltage, 100 µA current, and 2.00 s exposition time per projection.[32] The final volumes were then reconstructed
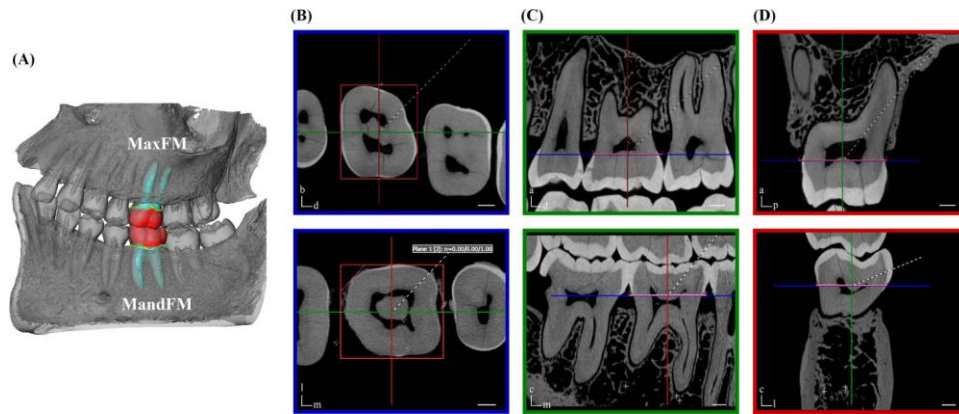
FIGURE 1 (A) Three-dimensional (3D) model of the maxilla and mandible in semi-transparency (buccal view) with the left first molars virtually rendered (the crown, in red, is delineated from the root, in green, by the best-fitted cervical plane). (B) occlusal, (C) mesiodistal, and (D) buccopalatal/lingual sections used to perform the measurements in MaxFM (upper row) and MandFM (lower row). *a*: apical, *b*: buccal, *c*: coronal, *d*: distal, *l*: lingual, *m*: mesial, and *p*: palatal. Scale bars: 2 mm

with an isotropic voxel size ranging from 40 to 48 μm, using Nikon CT Pro software (Nikon Metrology). Subsequently, alignment, measurements and automatic segmentations processes were done with the visualization software VGStudio MAX-3.0 (Heidelberg, Germany).[42] To overcome the introduction of bias, for example, due to oblique planar sections,[43] all the scans were re-oriented following a

TABLE 1 List and descriptions of the variables recorded in MandFM and MaxFM.

	MandFM	MaxFM
Buccal plate thickness		
At 1 mm from buccal crest: b	buccolingual section	buccopalatal section
At L_{mb}: b_{mb}	occlusal section	occlusal section
At L_{db}: b_{db},	occlusal section	occlusal section
Tooth width		
Minimum width: w	mesiodistal section	mesiodistal section
At 1 mm from buccal crest: w_{md}	mesiodistal section	mesiodistal section
At 1 mm from buccal crest: w_{bl}	buccolingual section	buccopalatal section
Root length		
between l and root apices centroid	l_c	l_c
between l and each root apex	$l–L_{mb}$ / $l–L_{db}$ / $l–L_{ml}$ / $l–L_{dl}$	$l–L_{mb}$ / $l–L_{db}$ / $l–L_p$
between CEJ and each root apex	$CEJ–L_{mb}$ / $CEJ–L_{db}$ / $CEJ–L_{ml}$ / $CEJ–L_{dl}$	$CEJ–L_{mb}$ / $CEJ–L_{db}$ / $CEJ–L_p$
Trunk length		
between l and CEJ	$l–CEJ$	$l–CEJ$
Root span		
Between each root apex	$L_{mb}–L_{db}$ / $L_{mb}–L_{ml}$ / $L_{db}–L_{ml}$ / $L_{db}–L_{dl}$ / $L_{mb}–L_{dl}$ / $L_{ml}–L_{dl}$	$L_{mb}–L_{db}$ / $L_{mb}–L_p$ / $L_{db}–L_p$
Surface defined by all the root apices		
Bone density		
Cortical BV/TV	buccal plates: l, L_{db}, L_{mb}	palatal plates: l, L_p
Trabecular BV/TV	interradicular bone l	interradicular bone l

reference plane commonly used in the literature: the cervical plane, ignoring the occlusal aspect of the crown.[44-47] A set of anatomical landmarks was collected on the 3D model, forming a continuous line along the cementum-enamel junction (CEJ) of the first molar. A best-fit plane (referred then as the cervical plane) was automatically computed through those selected landmarks and was used as a reference to re-align the micro-tomographic image stacks (Figure 1A). Therefore, non-oblique precisely chosen sections (mesiodistal, buccolingual, and occlusal) enabled the assessment of linear measurements, analogous between individuals (Figure 1B-D).

Landmarks, characterizing the external morphology of the first molar, were collected on (1) MaxFM: L_{mb} at mesiobuccal apex, L_{db} at distobuccal apex, and L_p at palatal apex; and on (2) MandFM: L_{mb} at mesiobuccal apex, L_{db} at distobuccal apex, L_{ml} at mesiolingual apex (9 of 24 MandFM had a mesiolingual root), and L_{dl} at distolingual apex (2 of 24 MandFM had a distolingual root). Two other landmarks characterizing the surrounding bone were defined, on both MaxFM and MandFM, at the buccal crest (A) and at the deepest point of interradicular bone (I), before the division of the roots from the tooth trunk. Several linear, surface, and volumetric measurements describing the molar morphology and the corresponding bony socket

were virtually collected and are detailed in Table 1. The buccal plate thickness (Figure 2A-C) was measured on sections at three different sites: at 1 mm from the buccal crest (b), and adjacent to the buccal roots (b_{mb} at L_{mb}, and d_{db} at L_{db}). Then, three types of tooth widths (Figure 2A, D) were recorded: the minimum width (w) on the mesiodistal section, the mesiodistal (w_{md}) and the buccolingual (w_{bl}) widths at 1 mm from the buccal crest. The following measurements were not assessed on sections but directly on the 3D models (between landmarks), and assisted us in the appreciation of the (1) root length (Figure 2E): distance (l_c) between I and the centroid of the root apex plane, distances between I and each apex, and distances between CEJ and each apex; (2) trunk length: distance I-CEJ; (3) root span, or degree of divergence of the roots (Figure 2F, G): distances between each root apex, and calculation of the surface defined by all the root apices.

Bone density in the maxilla and the mandible was also automatically assessed with VGStudioMAX-3.0 software from spherical volumes of interest (VOIs) and through histomorphometric parameters such as bone volumetric fraction (BV/TV, %), bone volume (BV, mm^3), and total volume (TV, mm^3). The cortical bone density was evaluated in VOIs located in the palatal plate of MaxFM and in the buccal plate of
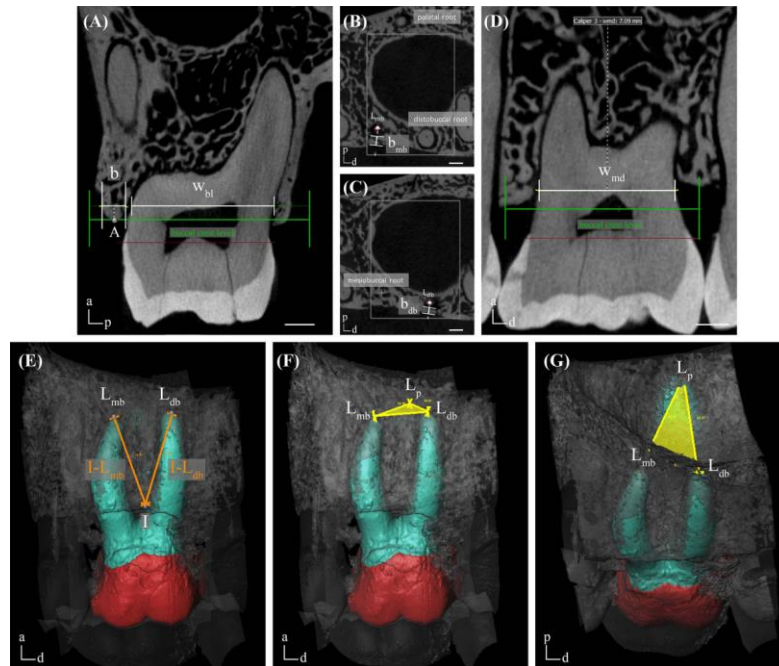
FIGURE 2 Examples of MaxFM measurements on sections and on the 3D model. Sections: (A) b, and w_{bl}, measured at 1 mm from crest on buccopalatal section, (B) b_{mb}, and (C) b_{db}, on the corresponding occlusal sections, (D) w_{md}, measured at 1 mm from crest on the mesiodistal section. The 3D measurements: (E) root lengths from I shown in orange, (F) and (G) root span dimensions and apex surface drawn in yellow. A: buccal bone crest landmark, I: deepest landmark of interradicular bone, L_{mb}: mesiobuccal root apex, L_{db}: distobuccal root apex, L_p: palatal root apex, a: apical, d: distal and p: palatal. Scale bars: 2 mm

TABLE 2 Molar morphology variables: tooth width (mm), root length (mm), trunk length (mm), root span (mm) and surface (mm^2) recorded in MandFM and MaxFM.

	MandFM		MaxFM	
	min - max	mean ± SD	min - max	mean ± SD
Tooth width				
w	07.88 - 9.55	8.79 ± 0.49	6.11 - 7.94	7.09 ± 0.46
w_{md}	07.13 - 9.57	8.80 ± 0.54	5.47 - 8.56	7.05 ± 0.67
w_{bl}	05.71 - 9.10	7.24 ± 0.96	9.51 - 13.33	11.58 ± 1.08
Root length				
I_c	8.48 - 11.07	9.94 ± 0.85	5.58 - 10.91	8.60 ± 1.27
$I-L_{mb}$	7.40 - 12.18	10.09 ± 1.03	6.26 - 12.37	9.55 ± 1.32
$I-L_{db}$	8.06 - 13.39	10.91 ± 1.05	6.76 - 12.67	9.95 ± 1.38
$I-L_{ml}$ / $I-L_p$	8.60 - 10.70	9.89 ± 0.70	5.35 - 12.26	10.37 ± 1.44
$I-L_{dl}$	8.28 - 10.57	9.43 ± 1.62		
$CEJ-L_{mb}$	12.76 - 15.98	14.36 ± 0.88	10.83 - 15.50	13.50 ± 1.06
$CEJ-L_{db}$	11.84 - 15.74	13.92 ± 1.07	10.57 - 14.92	12.78 ± 1.11
$CEJ-L_{ml}$ / $CEJ-L_p$	13.05 - 15.26	14.06 ± 0.86	11.56 - 16.34	13.74 ± 1.13
$CEJ-L_{dl}$	11.87 - 13.37	12.62 ± 1.06		
Trunk length				
I–CEJ	3.23 - 6.54	4.62 ± 0.67	3.41 - 7.17	5.13 ± 0.74
Root span				
$L_{mb}-L_{db}$	2.16 - 10.57	5.98 ± 1.70	1.65 - 7.52	4.33 ± 1.91
$L_{db}-L_{ml}$ / $L_{db}-L_p$	2.64 - 9.47	6.24 ± 1.86	5.54 - 13.62	10.55 ± 1.74
$L_{mb}-L_{ml}$ / $L_{mb}-L_p$	1.14 - 6.75	3.10 ± 1.34	7.06 - 13.36	10.04 ± 1.49
$L_{db}-L_{dl}$	2.56 - 5.48	4.02 ± 2.06		
$L_{dl}-L_{mb}$	2.67 - 7.68	5.18 ± 3.54		
$L_{dl}-L_{ml}$	1.97 - 5.61	3.79 ± 2.57		
Surface	3.52 - 36.36	10.61 ± 8.93	2.95 - 47.13	21.34 ± 8.84

I: deepest landmark of interradicular bone, L_{mb}: mesiobuccal root apex, L_{db}: distobuccal root apex, L_{ml}: mesiolingual root apex, L_{dl}: distolingual root apex, L_{ml}: mesiolingual root apex, L_p: palatal root apex, CEJ: cervical plane.

MandFM. The interradicular trabecular bone density was recorded in both MandFM and MaxFM.

2.3 | Statistical analysis

Data analysis was performed using the software R v.3.3.2.[48] and statistical significance was accepted at $P < .05$. Descriptive statistics, including means and standard deviations (expressed as mean ± SD) were used to have a better understanding of the measurements. Following the results obtained by normality and homoscedasticity tests, differences between measurements and sites were assessed by Kruskal-Wallis analyses, and subsequent pairwise comparisons. To compare the results between maxilla versus mandible, t-tests, and/or Kruskal-Wallis analyses were conducted. Spearman's correlation coefficient was also used to study the influence of the age on the variables.

3 | RESULTS

Data from 61 maxillary and mandibular molars were analyzed. The results of the variables assessing the molar morphology are reported in Table 2, the buccal plate thicknesses are detailed in Table 3, and the bone density parameters are in Table 4.

3.1 | Molar morphology

The results for the tooth width are summarized in Figure 3 for the mandible and the maxilla. In MandFM and MaxFM, w_{bl} was

TABLE 3 Buccal plate thicknesses (mm) and frequency distributions (%) in MandFM and MaxFM.

Thickness	MandFM		MaxFM	
	min - max	mean ± SD	min - max	mean ± SD
b	0.44 - 3.10	1.46 ± 0.58	0.00 - 2.31	1.00 ± 0.53
b_{mb}	1.26 - 4.30	2.51 ± 0.94	0.00 - 3.98	0.99 ± 0.98
b_{db}	1.25 - 5.42	3.29 ± 1.18	0.00 - 3.78	0.99 ± 0.99
Frequency	b < 1	1 < b < 2	b > 2	b < 1	1 < b < 2	b > 2
b	20.83	66.67	12.50	62.16	35.14	2.70
b_{mb}	0.00	45.83	54.17	56.76	35.14	8.11
b_{db}	0.00	16.67	83.33	66.67	16.67	16.67

Frequencies separated in three groups according to the thickness: <1 mm, between 1 and 2 mm, and >2 mm.

significantly different from w and w_{md} ($P < .01$): w_{bl} was thinner than w and w_{md} in MandFM, whereas it was thicker in MaxFM. The three types of tooth widths were also significantly different between the maxilla and the mandible ($P < .01$): w and w_{md} were thicker in MandFM than in MaxFM, while w_{bl} was thinner in MandFM than in MaxFM. As far as root length is concerned, it was found that the distance l_c was significantly greater ($P < .01$) in MandFM than in MaxFM (Figure 4A). Significant differences ($P < .05$) between MandFM and MaxFM were also reported for the distances between l, or CEJ, and each apex landmark, with greater distances in the mandible. The distance l–CEJ, appreciating the trunk length, was significantly smaller ($P < .05$) in MandFM than in MaxFM (Figure 4B). The root span was estimated via the measurement of the distances between all apices and was found to

TABLE 4 Cortical and trabecular bone densities (BV/TV, %) in MandFM and MaxFM.

	min - max	mean ± SD
MandFM		
Cortical VOIs		
buccal plate - l	0.00 - 99.78	70.28 ± 33.45
buccal plate - L_{db}	93.53 - 99.96	99.44 ± 1.42
buccal plate - L_{mb}	91.01 - 99.95	98.58 ± 2.40
Trabecular VOI		
interradicular - l	19.29 - 75.30	49.74 ± 15.38
MaxFM		
Cortical VOIs		
palatal plate - l	0.00 - 99.65	82.49 ± 33.89
palatal plate - L_p	50.72 - 99.72	92.46 ± 11.97
Trabecular VOI		
interradicular - l	19.06 - 83.25	54.13 ± 14.97

be significantly different ($P < .001$) between MandFM and MaxFM. The surface calculated between the apex landmarks confirmed that the spreading of the roots is significantly larger ($P < .001$) in MaxFM than in MandFM (Figure 4C). In MaxFM, the surface averaged 21.34 ± 8.84 mm^2, whereas in MandFM, the mean surface was only 10.61 ± 8.93 mm^2.

3.2 | Bony socket architecture

The mean maxillary buccal plate thickness (Figure 5A) was less than 1 mm in most of the cases: 62.16% at b, 56.76% at b_{mb}, and 66.67% at b_{db}, whereas in the mandible (Figure 5B), only 20.83% of the individuals at b, and none at both apices were less than 1 mm. Furthermore, 83.33% (at distobuccal apex) and 54.17% (at mesiobuccal apex) of the MandFM buccal plates were thicker than 2 mm, while at MaxFM, only 16.67% and 8.11% were thicker, respectively. No significant differences between the sites (b, b_{mb}, and b_{db}) were reported at MaxFM while the three sites were all significantly different ($P < .01$) from each other at MandFM. Significant differences ($P < .01$) were also found between the maxillary and mandibular buccal plate thicknesses, with a constantly thicker MandFM buccal plate at all sites.

Cortical and trabecular bone density were assessed in the maxilla and the mandible by histomorphometric parameters. In MandFM, a wide range of bone densities was observed in the trabecular and cortical bones (Figure 6A). In the interradicular VOI, the BV/TV ranged from 19.29% to 75.30%, whereas in the buccal cortical bone (at l level), the range was from 0% (absence of buccal plate) to 99.78%. Mean cortical bone density at the buccal plates of the apices were 98.58% at L_{mb} and 99.44% at L_{db}. All sites (cortical or trabecular) were statistically significantly different from each other ($P < .001$) for these parameters. Regarding MaxFM (Figure 6B), the BV/TV ranged from 19.06% to 83.25% in the interradicular trabecular bone, whereas in the palatal cortical bone (at l level), the range was from 0% (absence of buccal plate) to 99.65%. Mean cortical bone density of the palatal plate (at L_p level) was 92.46%. The bone density differed significantly between trabecular and cortical sites ($P < .001$), but no differences were detected between the two maxillary cortical sites. The comparison between MandFM and MaxFM interradicular trabecular densities did not show a significant difference.

3.3 | Correlation with aging

Correlations between each variable (tooth width, root length, trunk length, root span, buccal plate thickness, and bone density) and aging were assessed. Only bone density showed significant correlations with age. A significant decrease ($P < .05$) was found in MandFM between age and cortical bone density of the buccal plate at l level (Figure 7A). In MaxFM, significant decreases ($P < .001$) with aging were also found in the two cortical sites (Figure 7B, C), but not in the trabecular site.
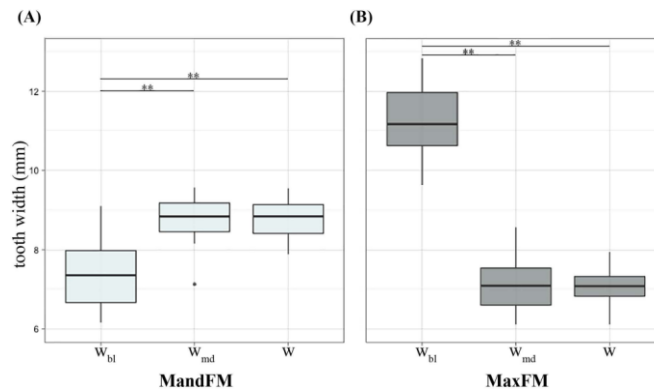
FIGURE 3 Boxplots of tooth width (mm) in (A) MandFM (light gray) and (B) MaxFM (dark gray), separated by tooth width type (w_{bl}, w_{md}, w). Circles depict outliers, ** $P < .01$

3.4 | Comparison with buccal plate

Relationships between the buccal plate thickness and the other measurements (tooth width, root length, trunk length, root span, and bone density) were also investigated, but no significant correlations were detected.

4 | DISCUSSION

To the best of our knowledge, this is the first micro-CT-based study exploring the anatomy of human first molar sockets at this level of detail, and more particularly, for dental implant related purposes. As a gold standard modality for bone microstructure assessment, micro-CT

offers quantitative, and objective parameters. Our research provides anatomical measurements at dental implant sites, including minimum, maximum, and mean distances, characterizing the first molars (e.g., tooth width, trunk length, root length, and root span) and their intact extraction sockets (e.g., buccal plate thickness and bone density).

The external shape and outline of the tooth are the main features in defining the three-dimensional bony structure of the socket. Variables assessing the tooth width, the trunk length, the root length, and the root span are relevant in estimating parameters of the implant design, as well as the height, depth, and width of bone available for safe implant placement.[13] However, to date, few studies have performed similar measurements (Table 5). For example, Smith and Tarnow[13] assembled from the literature[4,49] anatomical dimensions, such as tooth
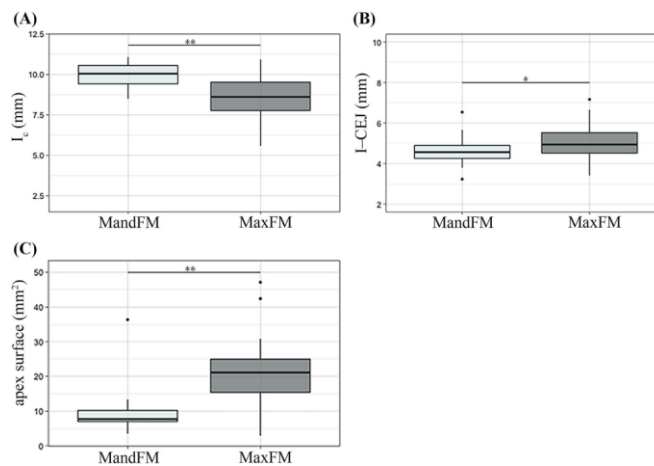
FIGURE 4 Boxplots of dimensions, performed between landmarks, in MandFM (light gray) and MaxFM (dark gray). (A) l_c (mm) appreciating the root length, (B) l–CEJ (mm) assessing the trunk length, (C) apex surface area (mm^2). Circles depict outliers. ** $P < .01$, * $P < .05$
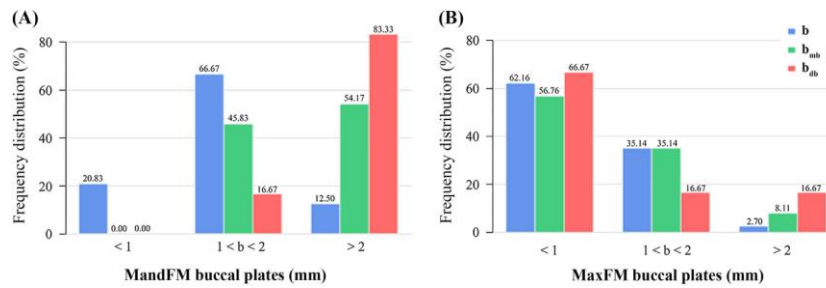
FIGURE 5 Frequency distribution of buccal plate thickness (mm) in (A) MandFM and (B) MaxFM. Frequencies classified by buccal plate type (b in blue, b_{mb} in green, b_{db} in red) and separated in three groups according to the thickness: <1 mm, between 1 and 2 mm, and >2 mm

width, root, and trunk lengths, serving as a basis for many statements in dentistry, but our findings were found to be smaller than those of previous studies. These differences could possibly be explained by the differences in the techniques used. For instance, Kerns et al[49] performed their measurements on extracted teeth with calipers while our study used dimensions performed on embedded teeth micro-CT-scanned in their bony sockets. Nevertheless, we could confirm some general trends, for example, the trunk length is shorter in mandibular first molars than in maxillary molars caused by a closer distance between the root furcation and the CEJ. Matsuda et al[24] measured the distances between the apices on CBCT scans to assess the spreading of the roots or the degree of divergence of the roots—equivalent to the root span in our study. They stated that for the stability of the implant, more than 5 mm is necessary. For this reason, all of our sites could be considered adequate as the minimum distances between the mandibular or maxillary apices were systematically greater than 5 mm.

The buccal plate thickness is known to be one of the most important measurements when it comes to dental implant survival and success.[14,16,21,24,50] If the buccal plate is absent, an immediate implant placement is precarious due to a higher risk for poor stability and a reduced potential for bone fill on the buccal side of the implant as well as implant thread exposure in the long-term. Previous findings[5,24,50] stated that sites with thick bony walls (>1mm) usually had better bone fill after immediate implantation compared with sites with a thin plate. In the mandible, only 20.83% of the sites showed a buccal plate thickness of less than 1 mm. However, in the maxilla, we found that at 1 mm from crest, 62.16% of the sites had a buccal plate thinner than 1 mm, and only 2.7% of the plates were thicker than 2 mm. Huynh-Ba et al[14] also found thin buccal walls (<1 mm) in the majority of their maxillary extraction sites. In contrast to our findings and using CBCT, Matsuda et al[24] showed that 92% of maxillary first molars sites had a buccal plate thickness greater than 1 mm, and that 20% of the sites were thicker than 2 mm. Temple et al[16] measured buccal thicknesses on CBCT scans of maxillary and mandibular first molars, and their results were found to be slightly smaller than reported in our study. However, some trends are similar, for example, the mandibular buccal plate adjacent to the mesial root apex is thinner than in the distal root. Thus, the mandibular sites, with a greater thickness compared with the maxillary sites, may allow more predictable outcomes for immediate implant placement. The limited and non-significant effect of aging on
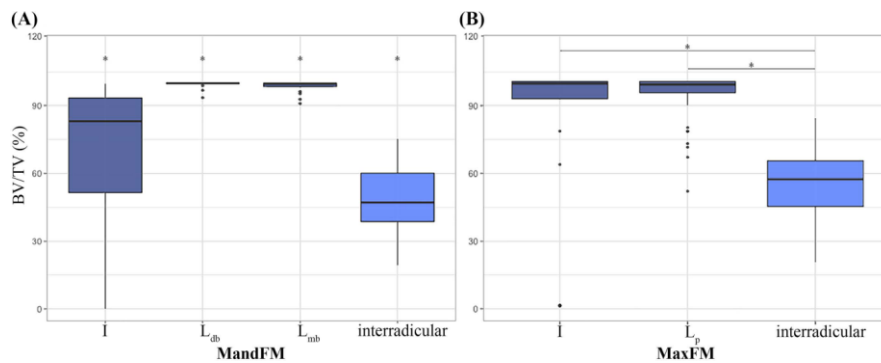
FIGURE 6 Boxplots of (A) mandibular and (B) maxillary BV/TV (%) separated by VOI site (l, L_{db}, L_{mb}, L_p, interradicular) and according to bone type (cortical density in dark blue, trabecular density in light blue). Circles depict outliers, * $P < .001$
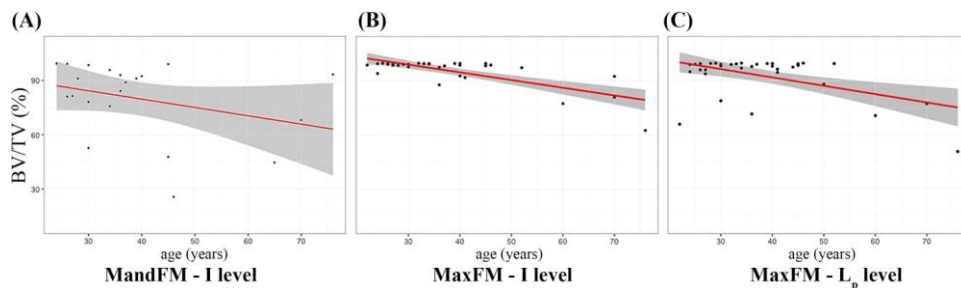
FIGURE 7 Linear regressions of BV/TV (%) with age. (A) At *I*, in the mandibular buccal cortical bone, (B) at *I*, in the maxilla, and (C) L_p, in the maxillary palatal cortical bone

the buccal wall, confirmed by this study, was also demonstrated by Temple et al.[16] The main difference between the maxilla and the mandible in our study was partly a reflection of fenestrations or dehiscences at the mesiobuccal and distobuccal apices of a few maxillary molars with no buccal plate at all, while fenestrations were absent in the mandible. Although minor fenestrations may not have a negative impact on implant placement or success, it is worthwhile to know that they are likely to occur, and if they are of significant dimensions, one may need to consider an alternative treatment protocol. This could include a simultaneous augmentation or a delayed placement protocol.

Histomorphometric parameters, evaluated in various locations of the periodontal and alveolar bones, give a quantitative and objective insight into the microstructural anatomy of the maxillary and mandibular sockets.[15,17,30,33] Kim and Henkin[17] in a micro-CT based study on biopsies from maxillae and mandibles of 12 cadaver specimens, obtained a mean trabecular BV/TV of 14.59% and a range from 2.4% to 48.2%. Their values were lower than what we could observe, with a mean BV/TV of 54.13% in the maxilla and 49.74% in the mandible. Other micro-CT-based studies[15,30] however, obtained values approximating ours: De Oliveira et al[15] had a mean BV/TV of 35.5% (range: 11.1%-67.9%) and González-Garcia and Monje[30] had a mean BV/TV of 48.70% (range: 13.22%-72.99%). Nevertheless, none of these studies measured the density in the interradicular bone, but in a different location of the alveolar bone. Higher values observed in our study might reflect variations in trabecular density between sites, with a denser interradicular bone than in the rest of the trabecular bone. This variation could be an indication of the specific mechanical competence of the interradicular bone in tooth retention. In our sample, we also noticed that the mandibular and the maxillary trabecular bones had similar densities, while the cortical bone densities were higher in the mandible than in the maxilla. Similar results have been observed previously.[30,51] The cortical as well as the trabecular bone density influence the primary stability of an implant, the anchorage and therefore the success of the implantation.[18,38,52] Aranyarachkul et al[52] stated that the clinical success of implants is influenced by the bone quality and density of the implantation site. Furthermore, as bone density varies from site to

site, and from patient to patient, several previous studies[15,30,39,52,53] recommend performing a bone density evaluation using CBCT prior to implant placement. The age of the patient is also of major importance as we found that the cortical bone densities of the buccal and palatal/lingual plates were decreasing with advancing age.

In the present study, we obtained three-dimensional dental and periodontal measurements describing and quantifying the morphology and the microstructure of the first maxillary and mandibular molars and sockets in South African skulls. These population-based reference values, and their correlation with advancing age, may be of great importance for the use of immediate implant placement in molar extraction sockets and thus the potential long-term success of this treatment modality. They also may enable the optimization of the implant design with more precise and specific constraints in order to obtain the best and optimal fit within the multirooted socket. The variables assessed are relevant in estimating parameters of the implant design and position, such as the width of the implant platform, the body shape, and taper of the implant.

CONFLICT OF INTEREST

CT, AH, ACO, and MS have nothing to disclose. TC reports personal fees from Southern Implants (employee), outside the submitted

TABLE 5 Characteristics of selected studies. Buccal plate thicknesses and molar morphology variables are in mm, trabecular bone densities are in %. (NA: variable not available or not recorded in the study).

Study		Sample Type (tooth)	N	Age (mean)	Modality		min-max maxilla	min-max mandible	mean ± SD maxilla	mean ± SD mandible
Buccal plate										
Huynh-Ba et al.[14]	2010	Patient (PM)	93	NA	Caliper	At 1 mm from crest	0.5 - 3.0	NA	1.1 ± 0.50	NA
Jung & Cho[19]	2012	Patient (M1)	83	20 - 53 (28.8)	CBCT	At apex, mesial root	NA	NA	1.23 ± 0.96	NA
						At apex, distal root	NA	NA	1.91 ± 1.18	NA
Kang et al.[21]	2015	Patient (M1)	132	21 - 59 (31)	CBCT	At apex, mesial root	NA	NA	3.00 ± 1.57	NA
						At apex, distal root	NA	NA	3.13 ± 1.48	NA
Temple et al.[16]	2015	Patient (M1)	265	20 - 85 (55.9)	CBCT	At 1 mm from crest, mesial root	0.19 - 2.26	0.11 - 3.31	0.914	0.587
						At 1 mm from crest, distal root	0.40 - 2.81	0.27 - 4.37	1.262	0.673
Matsuda et al.[24]	2016	Patient (M1)	95	18 - 76 (37.2)	CBCT	At 2 mm from crest	NA	NA	1.58 ± 0.6	NA
Molar morphology										
Smith and Tarnow[13]	2013	Extracted teeth (M1)	NA	NA	Caliper	Mesiodistal tooth width at CEJ	9.20	NA	7.90	NA
						Buccolingual tooth width at CEJ	9.00	NA	10.70	NA
						Root length	13.50	NA	13.00	NA
						Trunk length	3.27	NA	4.10	NA
Bone Density (BV/TV)										
Akça et al.[38]	2006	Cadaver	1	NA	Micro-CT	Biopsies of trabecular bone in edentulous sites	NA	NA	26.95	69.95
De Oliveira et al.[15]	2012	Patient	32	25 - 67 (42)	Micro-CT	36 biopsies of trabecular bone in edentulous sites	11.1 - 67.9		35.5 ± 14.3	
González-García & Monje[30]	2013	Patient	31	20 - 79 (51.6)	Micro-CT	39 biopsies of trabecular bone in edentulous sites	13.22 - 72.99		48.7 ± 17.85	
Kim & Henkin[17]	2015	Cadaver	12	NA	Micro-CT	34 biopsies of trabecular bone in edentulous sites	2.4 - 48.2	NA	14.59 ± 7.68	27.28 ± 10.19
Parsa et al.[31]	2015	Cadaver	20	NA	Micro-CT	Trabecular VOIs in edentulous sites	NA	2.24 - 75.83	NA	32.35 ± 18.81

PM and M1: pre-molars and first molars, CEJ: cervical plane, VOIs: Volumes of Interest.

ORCID

Charlotte E. G. Theye http://orcid.org/0000-0002-4756-8854

REFERENCES

[1] McCaul LK, Jenkins WMM, Kay EJ. The reasons for the extraction of various tooth types in Scotland: a 15-year follow up. *J Dent.* 2001;29(6):401–407.

[2] Zadik Y, Sandler V, Bechor R, Salehrabi R. Analysis of factors related to extraction of endodontically treated teeth. *Oral Surg Oral Med Oral Pathol Oral Radiol Endodontol.* 2008;106(5):e31–e35.

[3] Broadbent JM, Thomson WM, Poulton R. Progression of dental caries and tooth loss between the third and fourth decades of life: a birth cohort study. *Caries Res.* 2006;40(6):459–465.

[4] Scheid RC, Weiss G. *Woelfel's Dental Anatomy*. 8th ed. Philadelphia, PA: Lippincott, Williams, & Wilkins; 2012.

[5] Lazzara RJ. Immediate implant placement into extraction sites: surgical and restorative advantages. *Int J Periodont Restor Dent.* 1989;9(5):332–343.

[6] Schwartz-Arad D, Chaushu G. The ways and wherefores of immediate placement of implants into fresh extraction sites: a literature review. *J Periodontol.* 1997;68(10):915–923.

[7] Ketabi M, Deporter D, Atenafu EG. A systematic review of outcomes following immediate molar implant placement based on recently published studies. *Clin Implant Dent Relat Res.* 2016;18(6):1084–1094.

[8] Acocella A, Bertolai R, Sacco R. Modified insertion technique for immediate implant placement into fresh extraction socket in the first maxillary molar sites: a 3-year prospective study. *Implant Dent.* 2010;19(3):220–228.

[9] Quirynen M, Van Assche N, Botticelli D, Berglundh T. How does the timing of implant placement to extraction affect outcome? *Int J Oral Maxillofac Implants.* 2007;22(7):203–226.

[10] Fugazzotto PA. Implant placement at the time of maxillary molar extraction: treatment protocols and report of results. *J Periodontol.* 2008;79(2):216–223.

[11] De Rouck T, Collys K, Cosyn J. Single-tooth replacement in the anterior maxilla by means of immediate implantation and provisionalization: a review. *Int J Oral Maxillofac Implants.* 2008;23(5):897–904.

[12] Vandeweghe S, Hattingh A, Wennerberg A, De Bruyn H. Surgical protocol and short-term clinical outcome of immediate placement in molar extraction sockets using a wide body implant. *J Oral Maxillofac Res.* 2011;2(1):e1.

[13] Smith RB, Tarnow DP. Classification of molar extraction sites for immediate dental implant placement: technical note. *Int J Oral Maxillofac Implants.* 2013;28(3):911–916.

[14] Huynh-Ba G, Pjetursson BE, Sanz M, et al. Analysis of the socket bone wall dimensions in the upper maxilla in relation to immediate implant placement. *Clin Oral Implants Res.* 2010;21(1):37–42.

[15] De Oliveira RCG, Leles CR, Lindh C, Ribeiro-Rotta RF. Bone tissue microarchitectural characteristics at dental implant sites. Part I: identification of clinical related parameters. *Clin Oral Implants Res.* 2012;23(8):981–986.

[16] Temple KE, Schoolfield J, Noujeim ME, Huynh-Ba G, Lasho DJ, Mealey BL. A cone beam computed tomography (CBCT) study of buccal plate thickness of the maxillary and mandibular posterior dentition. *Clin Oral Implants Res.* 2016;27(9):1072–1078.

[17] Kim YJ, Henkin J. Micro-computed tomography assessment of human alveolar bone: bone density and three-dimensional microarchitecture. *Clin Implant Dent Relat Res.* 2015;17(2):307–313.

[18] Merheb J, Temmerman A, Rasmusson L, Kübler A, Thor A, Quirynen M. Influence of skeletal and local bone density on dental implant stability in patients with osteoporosis. *Clin Implant Dent Relat Res.* 2016;18(2):253–260.

[19] Jung Y-H, Cho B-H. Assessment of the relationship between the maxillary molars and adjacent structures using cone beam computed tomography. *Imaging Sci Dent.* 2012;42(4):219–224.

[20] Massey ND, Galil KA, Wilson TD. Determining position of the inferior alveolar nerve via anatomical dissection and micro-computed tomography in preparation for dental implants. *J Can Dent Assoc.* 2013;79(d39):1–7.

[21] Kang SH, Kim BS, Kim Y. Proximity of posterior teeth to the maxillary sinus and buccal bone thickness: a biometric assessment using Cone-Beam Computed Tomography. *J Endod.* 2015;41(11):1839–1846.

[22] Oettlé AC, Fourie J, Human-Baron R, van Zyl AW. The midline mandibular lingual canal: importance in implant surgery. *Clin Implant Dent Relat Res.* 2015;17(1):93–101.

[23] Tian X-M, Qian L, Xin X-Z, Wei B, Gong Y. An analysis of the proximity of maxillary posterior teeth to the maxillary sinus using cone-beam computed tomography. *J Endod.* 2016;42(3):371–377.

[24] Matsuda H, Borzabadi-Farahani A, Le BT. Three-dimensional alveolar bone anatomy of the maxillary first molars: a cone-beam computed tomography study with implications for immediate implant placement. *Implant Dent.* 2016;25(3):367–372.

[25] Marciano MA, Duarte MAH, Ordinola-Zapata R, et al. Applications of micro-computed tomography in endodontic research. In: Méndez-Vilas A, ed. *Current Microscopy Contributions to Advances in Science and Technology*. Badajoz, Spain, FORMATEX Research Center; 2012:782–788.

[26] Olejniczak AJ, Tafforeau P, Smith TM, Temming H, Hublin J-J. Technical note: Compatibility of microtomographic imaging systems for dental measurements. *Am J Phys Anthropol.* 2007;134(1):130–134.

[27] Maret D, Molinier F, Braga J, et al. Accuracy of 3D reconstructions based on cone beam computed tomography. *J Dent Res.* 2010;89(12):1465–1469.

[28] Maret D, Peters OA, Galibourg A, et al. Comparison of the accuracy of 3-dimensional cone-beam computed tomography and micro-computed tomography reconstructions by using different voxel sizes. *J Endod.* 2014;40(9):1321–1326.

[29] Maret D, Telmon N, Peters OA, et al. Effect of voxel size on the accuracy of 3D reconstructions with cone beam CT. *Dentomaxillofac Radiol.* 2012;41(8):649–655.

[30] González-García R, Monje F. The reliability of cone-beam computed tomography to assess bone density at dental implant recipient sites: a histomorphometric analysis by micro-CT. *Clin Oral Implants Res.* 2013;24(8):871–879.

[31] Parsa A, Ibrahim N, Hassan B, van der Stelt P, Wismeijer D. Bone quality evaluation at dental implant site using multislice CT, micro-CT, and cone beam CT. *Clin Oral Implants Res.* 2015;26(1):e1–e7.

[32] Hoffman JW, De Beer FC. Characteristics of the micro-focus X-ray tomography facility (MIXRAD) at Necsa in South Africa. In: *18th World Conference on Non-Destructive Testing*. Durban, South Africa; 2012.

[33] González-García R, Monje F. Is micro-computed tomography reliable to determine the microstructure of the maxillary alveolar bone? *Clin Oral Implants Res.* 2013;24(7):730-737.

[34] Parfitt AM. Bone histomorphometry: standardization of nomenclature, symbols and units (summary of proposed system). *Bone.* 1988; 9(1):67-69.

[35] Burghardt AJ, Link TM, Majumdar S. High-resolution computed tomography for clinical imaging of bone microarchitecture. *Clin Orthop.* 2011;469(8):2179-2193.

[36] Panmekiate S, Ngonphloy N, Charoenkarn T, Faruangsaeng T, Pauwels R. Comparison of mandibular bone microarchitecture between micro-CT and CBCT images. *Dentomaxillofac Radiol.* 2015; 44(5):20140322-20140327.

[37] Fanuscu MI, Chang T-L. Three-dimensional morphometric analysis of human cadaver bone: microstructural data from maxilla and mandible. *Clin Oral Implants Res.* 2004;15(2):213-218.

[38] Akça K, Chang T-L, Tekdemir I, Fanuscu MI. Biomechanical aspects of initial intraosseous stability and implant design: a quantitative micro-morphometric analysis. *Clin Oral Implants Res.* 2006;17(4): 465-472.

[39] Van Dessel J, Nicolielo LFP, Huang Y, et al. Accuracy and reliability of different cone beam computed tomography (CBCT) devices for structural analysis of alveolar bone in comparison with multislice CT and micro-CT. *Eur J Oral Implantol.* 2017;10(1):95-105.

[40] Pilloud MA, Hefner JT, Hanihara T, Hayashi A. The use of tooth crown measurements in the assessment of ancestry. *J Forensic Sci.* 2014;59(6):1493-1501.

[41] L'Abbé EN, Loots M, Meiring JH. The Pretoria Bone Collection: a modern South African skeletal sample. *HOMO - J Comp Hum Biol.* 2005;56(2):197-205.

[42] VolumeGraphics GmbH. VGStudioMAX 3.0. [Internet]. http://www.volumegraphics.com/en/products. Accessed March 16, 2015.

[43] Suwa G, Kono RT. A micro-CT based study of linear enamel thickness in the mesial cusp section of human molars: reevaluation of methodology and assessment of within-tooth, serial, and individual variation. *Anthropol Sci.* 2005;113(3):273-289.

[44] Skinner MM, Gunz P, Wood BA, Hublin J-J. Enamel-dentine junction (EDJ) morphology distinguishes the lower molars of Australopithecus africanus and Paranthropus robustus. *J Hum Evol.* 2008;55 (6):979-988.

[45] Benazzi S, Fornai C, Bayle P, et al. Comparison of dental measurement systems for taxonomic assignment of Neanderthal and modern human lower second deciduous molars. *J Hum Evol.* 2011;61(3): 320-326.

[46] Benazzi S, Panetta D, Fornai C, Toussaint M, Gruppioni G, Hublin J-J. Technical note: guidelines for the digital computation of 2D and 3D enamel thickness in hominoid teeth. *Am J Phys Anthropol.* 2014; 153(2):305-313.

[47] Bauer CC, Bons PD, Benazzi S, Harvati K, Technical N. Using elliptical best fits to characterize dental shapes. *Am J Phys Anthropol.* 2016;159(2):342-347.

[48] R Core Team. *R: A Language and Environment for Statistical Computing.* R Foundation for Statistical Computing, Vienna, Austria. [Internet]. https://www.R-project.org/. Accessed March 16, 2018.

[49] Kerns DG, Greenwell H, Wittwer JW, Drisko C, Williams JN, Kerns LL. Root trunk dimensions of 5 different tooth types. *Int J Periodont Restor Dent.* 1999;19(1):82-91.

[50] Tomasi C, Sanz M, Cecchinato D, et al. Bone dimensional variations at implants placed in fresh extraction sockets: a multilevel multivariate analysis. *Clin Oral Implants Res.* 2010;21(1):30-36.

[51] Park HS, Lee YJ, Jeong SH, Kwon TG. Density of the alveolar and basal bones of the maxilla and the mandible. *Am J Orthod Dentofacial Orthop.* 2008;133(1):30-37.

[52] Aranyarachkul P, Caruso J, Gantes B, et al. Bone density assessments of dental implant sites: 2. Quantitative cone-beam computerized tomography. *Int J Oral Maxillofac Implants.* 2005;20(1): 416-424.

[53] Miguel-Sánchez A, Vilaplana-Vivo J, Vilaplana-Vivo C, Vilaplana-Gómez JÁ, Camacho-Alonso F. Accuracy of quantitative computed tomography bone mineral density measurements in mandibles: a cadaveric study. *Clin Implant Dent Relat Res.* 2015;17(4):693-699.

Appendix B. Published article (Genochio *et al.*, 2019)

Genochio L., Mazurier A., Dumoncel J., <u>Theye C.E.G.,</u> and Zanolli C. 2019. Inner structural organization of the mandibular corpus in the late Early Pleistocene human specimens Tighenif 1 and Tighenif 2. Organisation structurale interne du corps mandibulaire chez les spécimens humains Tighenif 1 et Tighenif 2 du Pléistocène inférieur final. *Comptes Rendus Palevol*, 18: 1073–1082.

Contents lists available at ScienceDirect

Comptes Rendus Palevol

www.sciencedirect.com

Human Palaeontology and Prehistory (Palaeoanthropology)/Paléontologie humaine et préhistoire (Palaeoanthropologie)

Inner structural organization of the mandibular corpus in the late Early Pleistocene human specimens Tighenif 1 and Tighenif 2

Organisation structurale interne du corps mandibulaire chez les spécimens humains Tighenif 1 et Tighenif 2 du Pléistocène inférieur final

Lisa Genochio [a,b], Arnaud Mazurier [c], Jean Dumoncel [a], Charlotte E.G. Theye [d], Clément Zanolli [e,*]

[a] UMR 5288 CNRS, Université Toulouse-3-Paul-Sabatier, 31062 Toulouse, France
[b] Department of Archaeology and Hull York Medical School, University of York, York, UK
[c] Institut IC2MP 7285 CNRS, Université de Poitiers, 86022 Poitiers, France
[d] Department of Anatomy, University of Pretoria, Pretoria, South Africa
[e] UMR 5199 CNRS, Université de Bordeaux, 33615 Pessac, France

ABSTRACT

The present study investigates the inner structural organization of the two mandible specimens Tighenif 1 and Tighenif 2 from the late early Pleistocene site of Tighenif, Algeria. Using (micro)tomographic scans, we built a new protocol to investigate the cortical bone topography at the post-canine level. We selected two cross-sectional slices placed between the P3/P4 and M1/M2 on the right and left sides and assessed the cortical bone thickness topography (CBT) on each slice. Our analyses demonstrate that the mandibles from Tighenif exhibit higher CBT and a different topographic distribution pattern at the molar level than in modern humans, resulting in a proportionally more robust inner structure, while a similar signal is observed between the fossil and extant specimens at the premolar level. Further studies need to be done in order to determine if this feature is related to functional constraints during mastication or paramasticatory activities; or if it is related to any independent evolutionary process.

© 2019 Académie des sciences. Published by Elsevier Masson SAS. This is an open access article under the CC BY-NC-ND license (http://creativecommons.org/licenses/by-nc-nd/4.0/).

RÉSUMÉ

Cette étude examine l'organisation structurale interne des deux spécimens mandibulaires Tighenif 1 et Tighenif 2 du site du début du Pléistocène inférieur final de Tighenif, en Algérie. En utilisant des scans (micro)tomographiques, nous avons construit un nouveau protocole, afin d'étudier la topographie de l'os cortical au niveau des dents jugales. Deux coupes transversales ont été sélectionnées et placées entre les P3/P4 et M1/M2 gauches et droites afin d'y évaluer l'épaisseur de l'os cortical (CBT). Nos résultats montrent que les deux fossiles de Tighenif présentent une épaisseur d'os cortical plus élevée et une distribution de l'os cortical différente au niveau des molaires par rapport aux humains modernes, se traduisant

---

* Corresponding author.
E-mail address: clement.zanolli@gmail.com (C. Zanolli).

L. Genochio et al. / C. R. Palevol 18 (2019) 1073–1082

par une structure interne proportionnellement plus robuste, tandis qu'un signal similaire est observé entre les spécimens fossiles et actuels au niveau des prémolaires. Cependant, des études complémentaires seront nécessaires pour déterminer si cette caractéristique est liée à des adaptations aux contraintes fonctionnelles exercées lors de la mastication ou à des activités para-masticatoires, ou bien si cela est dû à des processus évolutifs indépendants.

1. Introduction

The locality of Tighenif (formerly Ternifine) is situated in northwestern Algeria, in the province of Mascara. The site, a sand quarry near the village of Palikao, was discovered in 1870. Between 1954 and 1956, Arambourg(1954, 1955, 1957; Arambourg and Hoffstetter, 1954) carried out large-scale excavations that led to the discovery of human fossil remains associated with a lithic assemblage of Acheulean tools. The human fossil record consists of nine isolated teeth, two nearly complete adult mandibles (Tighenif 1 and 3), one adult hemi-mandible (Tighenif 2), and a parietal fragment (Tighenif 4). As a whole, the dental record suggests a minimum of five individuals, including four adults and one juvenile (Arambourg and Hoffstetter, 1963; Schwartz and Tattersall, 2003; Tillier, 1980). Based on biostratigraphy and paleomagnetic dating, the site was originally estimated to be c. 700 ka old (Geraads et al., 1986). However, a recent revision of the faunal list compared with those from East African sites suggests a late early Pleistocene age, close to 1 Ma as more likely (Geraads, 2016; Sahnouni and Van der Made, 2009). Accordingly, the fossil human assemblage from Tighenif would currently represent the earliest recovered so far from Northwest Africa, even if the region was certainly inhabited by humans since at least c. 2.4–1.9 Ma (Sahnouni et al., 2018).

The Tighenif human assemblage was originally attributed to *Atlanthropus mauritanicus* (Arambourg, 1954, 1955). However, because of some similarities with the Chinese dentognathic material from Zhoukoudian (Antón, 2003; Antón et al., 2007; Howell, 1960; Schwartz and Tattersall, 2003; Tillier, 1980), the assemblage was later integrated into the *Homo erectus* hypodigm. Based on archaeological and paleontological evidence, some authors have considered the possibility of relationships between the North African human groups represented at Tighenif and those peopling southern Europe at some points during the early–middle Pleistocene (Arribas and Palmqvist, 1999; Finlayson, 2002). However, while direct comparisons of the fossils from Tighenif with three late Early Pleistocene mandibles from the site of Gran Dolina-TD6, Spain, revealed a number of similarities, they have been interpreted as plesiomorphic for the genus *Homo* (Bermúdez de Castro et al., 1997, 2007, 2016). Given the particularly robust morphology of the Tighenif mandibles, Bermúdez de Castro et al. (2007) have suggested to consider these specimens as representatives of a *Homo ergaster* subspecies: *Homo ergaster mauritanicus*. More recently, the mandibles from Tighenif were compared with the Mauer specimen and found to be compatible with the *H. heidelbergensis* hypodigm, the latter being considered as

an Afro-European species (Mounier, 2011; Mounier et al., 2009). However, the anterior symphyseal morphology of the Tighenif specimens as well as some Neanderthal-like features present in these specimens continue to raise some questions about their relationship with the anatomically modern humans and Neanderthal lineages (Mounier et al., 2009). Additionally, the microtomographic-based analysis of the inner structural organization of some deciduous and permanent teeth from the Algerian assemblage highlighted a complex pattern with a combination of unique, primitive, Neanderthal-like and modern human-like features (Macchiarelli et al., 2013; Zanolli and Mazurier, 2013; Zanolli et al., 2010). Thus, partly due to the robustness of the mandibles and to the rare comparative evidence available so far for human fossils sampling this chrono-geographical range, the taxonomic affinities of Tighenif specimens are still unclear.

Combined with the signal from the external morphology, the internal structure of the mandible potentially holds a blend of functional and taxonomic information useful in the study of the human fossil record (Daegling and Hotzman, 2003; Fiorenza et al., 2019; Grine and Daegling, 2017; Zanolli et al., 2017). A common assumption in biomechanical studies on craniofacial morphology is that there is a functional link between the mandibular structure and the forces triggered by mastication and other feeding behaviors (Daegling and Grine, 2006; Godinho et al., 2018; Holmes and Ruff, 2011; Hylander, 2006; Sella-Tunis et al., 2018; Toro-Ibacache et al., 2016). In fact, it is widely accepted that, under strain variations, the mandibular bone is remodeled in areas where it faces higher loads, i.e. where strain magnitude is above a particular threshold (Frost, 1987, 2003; Martinez-Maza et al., 2011; Pearson and Lieberman, 2004; Ruff et al., 2006; Schwartz-Dabney and Dechow, 2003). Thus, local variation in bone organization is, at least partly, linked with differences in functionally-related strain magnitude, and strain analysis can be employed to investigate whether cortical asymmetry is related to biomechanical demands (Fiorenza et al., 2019; Gröning et al., 2012; but see Ichim et al., 2006).

In the mandible, an asymmetric pattern of post-canine cortical bone thickness (CBT) distribution is documented in all anthropoids, where the lingual aspect of the corpus exhibits thinner cortical bone compared to the lateral aspect (Daegling, 1992; Daegling and Grine, 1991; Demes et al., 1984). This asymmetric pattern, which seems to transcend phylogenetic, allometric or ecological aspects, has been explained as resulting from the combined effects of vertical occlusal forces and torsions of the corpus during mastication (Daegling and Hotzman, 2003; Dechow and Hylander, 2000; Demes et al., 1984). This interpretation is

also supported by studies based on Finite Element Analysis (FEA) showing that high strain areas fit well with regions bearing higher CBT, thus highlighting a thicker buccal CBT in the posterior mandibular region (Gröning et al., 2012). However, the role and interpretation of this asymmetric mandibular CBT distribution is still debated. Ichim et al. (2006), for example, have suggested that the asymmetric pattern in modern human is not directly related to masticatory strains, i.e. strictly functionally-related, but rather the genetically-controlled result of a long-term modeling/remodeling balance process achieved during evolution. Asymmetry in cortical bone topography across the mandible could also reflect handedness, as it has been suggested for the Neanderthal specimen from Regourdou (Fiorenza et al., 2019; Volpato et al., 2012). With this respect, also the Algerian fossil specimen Tighenif 1 exhibits an asymmetric occlusal wear pattern of the post-canine dentition (Arambourg and Hoffstetter, 1963; Zanolli and Mazurier, 2013).

In the present study, we quantitatively assess the still unreported internal structural organization of the post-canine corpus of Tighenif 1 and Tighenif 2. Given the especially robust morphology of the two mandibles and their macrodont dentition (Arambourg, 1957; Bermúdez de Castro et al., 2007; Zanolli and Mazurier, 2013), we predict that these fossils will have an absolutely thicker cortical bone compared to extant humans. In addition, we also evaluate whether, and to what extent, buccal vs. lingual relative asymmetry in CBT distribution in the two fossils is affected by their robust morphology, i.e. if a larger size of the mandibular corpus tends to lower, or magnify, the pattern commonly measured in recent humans (Daegling and Hotzman, 2003; Demes et al., 1984).

2. Materials and methods

2.1. Materials

In the analyses, we uniquely considered the two specimens Tighenif 1 and Tighenif 2 because of the relatively poor preservation conditions of the partial mandible Tighenif 3, whose corpus is affected by numerous post-mortem breaks. To assess cortical bone post-canine distribution, we used X-ray microtomographic (μCT) records of the two Algerian fossil specimens performed in 2010 at the University of Poitiers using a X8050-16 Viscom AG equipment (microfocus directional X-ray source with an imaging system comprising a 9-inch triple-field intensifier coupled with a 12 bits, 1004×1004-pixel CCD). The parameters were as follows: voltage, 120 and 130 kV; current, 0.60 and 0.50 mA; a projection each 0.30° and 0.25°, respectively, for Tighenif 1 and Tighenif 2. The final volumes were reconstructed using the Feldkam algorithm with DigiCT v.2.3.3 (Digisens SA, France) in 8-bit format, with a final isotropic voxel size of 115.3 μm and 98.5 μm, respectively. The virtual reconstructions of these two specimens are represented in Fig. 1 A–B.

For comparison, we also used the mandibles of 10 (5 females and 5 males) adult modern humans (MH) selected from the Pretoria Bone Collection housed in the Department of Anatomy of the University of Pretoria, South Africa

(L'Abbé et al., 2005). These materials were scanned at the microfocus X-ray tomography facility (MIXRAD) of the South African Nuclear Energy Corporation SOC Ltd (Necsa), Pelindaba, South Africa, using a Nikon XTH 225 ST (Metris). The parameters were as follows: voltage, 100 kV; current, 0.10 mA; a projection each 0.36°. Depending on their size, the final volumes of the 10 comparative specimens were reconstructed with an isotropic voxel size ranging from 66.5 μm to 79.6 μm. Ethical clearance for using this comparative sample was obtained from the Faculty of Health Sciences Research Ethics committee of the University of Pretoria (Ref. No. 340/2015).

3. Methods

A semi-automatic threshold-based segmentation of the virtual slices of all investigated specimens was preliminarily carried out using Avizo 8.1 (Visualization Science Group Inc) and ImageJ 1.51k (Schneider et al., 2012) following the half-maximum height methods (HMM; Spoor et al., 1993) and the region of interest thresholding methods (ROI-Tb protocol, Fajardo et al., 2002). In processing the record of the two fossil specimens Tighenif 1 and Tighenif 2, some manual corrections were locally necessary to virtually fill the cracks and reliably separate bone from matrix infill and air. On the Tighenif 1 mandible, major breaks are found on the left side, especially at the P3 level, at the inferior aspect of the mandible (Fig. 1C). This Algerian fossil was consolidated and reconstructed with plaster; however, the cortical and trabecular bone is still preserved and well-distinguished. The Tighenif 2 specimen presents local bone micro-breaks, but is better preserved than the one of Tighenif 1 (Fig. 1D). In fact, considering the estimated chronology of this material around 1 Ma, despite some cracks and larger fractures affecting the bone locally, the internal bony structure is well preserved. However, because of the variable positions of the fractures and local taphonomic alterations, a bi-dimensional analytical strategy was preferred to extract the maximum of information directly comparable between the two specimens.

We developed a specific protocol to estimate the CBT between the two premolars (P3/P4) and between the first and second molars (M1/M2) for both sides on each specimen. Firstly, a reference plane was defined as the plane fitting a set of semilandmarks along the most inferior line of the mandible corresponding to the inferior maximum of curvature of the (right or left) mandibular corpus (Fig. 2A). The posteriormost landmarks were placed distally to the M3. Then, CBT was assessed across four coronal slices manually oriented perpendicularly in the *XY* and *XZ* planes to the reference plane and to the alveolar arcade axis, respectively located between the P3 and P4 and between the M1 and M2 (Fig. 2B). We used tpsDig32 2.30 (Rohlf, 1997) to place semilandmarks on the four extracted slices of each specimen (two left and two right slices if available). We then defined a lingual and a buccal compartment on each slice: a line tangential to the alveolar margin has been drawn as the upper limit and the lingual and buccal compartments were created by drawing a second perpendicular line passing by
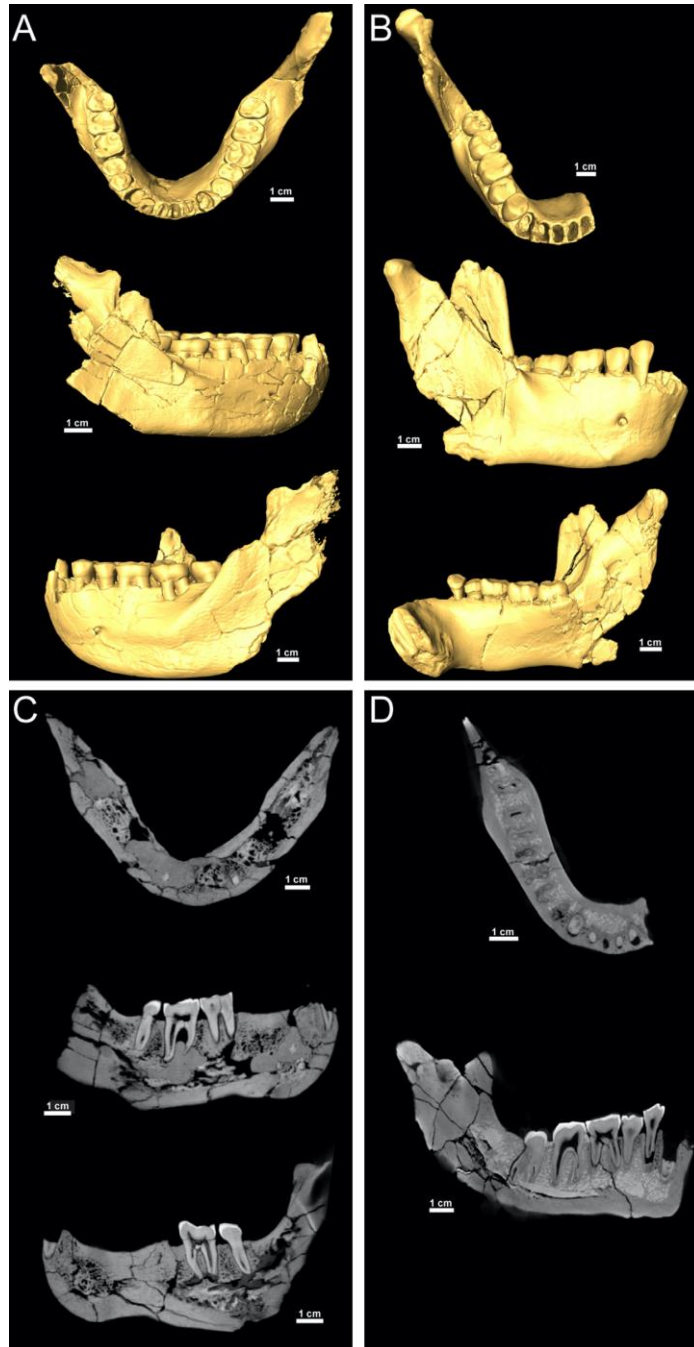
Fig. 1. Virtual renderings of the mandible Tighenif 1 (A) and of the hemi-mandible Tighenif 2 (B) in superior and lateral views. The longitudinal virtual cross-sections along the corpus of Tighenif 1 (C) and Tighenif 2 (D) illustrate the degree of preservation of the internal bone structure.
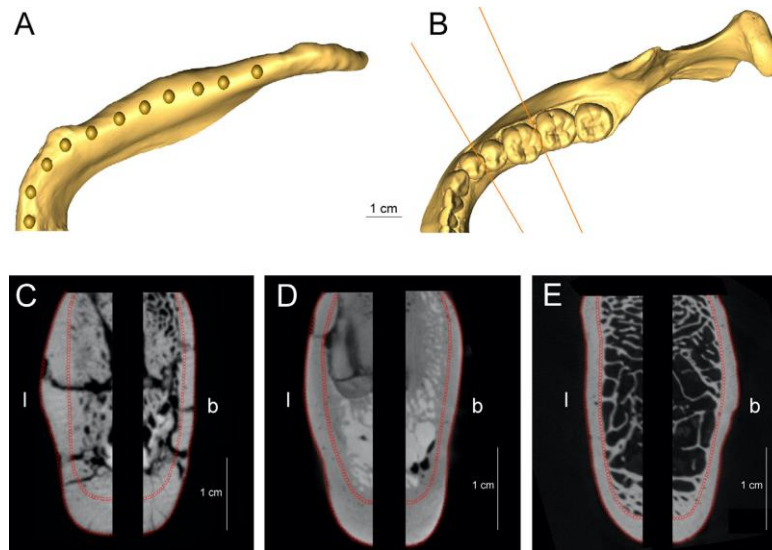
Fig. 2. Position of the semilandmarks on the inferior aspect of the mandible corpus used to fit a reference plane (A), and position of the slices perpendicular to the reference plane and to the mandibular corpus main axis (B), located between the P3 and P4 and M1 and M2. Virtual cross-sections set at the M1/M2 level in Tighenif 1 (C), Tighenif 2 (D) and a modern human (E) showing how the buccal (b) and lingual (l) aspects were delimited for their separate analyses, as well as the position of the semilandmarks placed along the external mandibular surface and on the internal cortical bone margin to assess the cortical bone thickness (CBT).

Fig. 2. Emplacement des points repères sur la partie inférieure de la mandibule utilisés pour positionner le plan de référence (A) et les positions des deux coupes perpendiculaires au plan de référence et à l'axe principal du corps mandibulaire, placées entre la P3 et la P4 ainsi qu'entre la M1 et la M2. Coupes virtuelles au niveau M1/M2 chez Tighenif 1 (C), Tighenif 2 (D) et un humain moderne (E), montrant comment l'aspect buccal (b) et l'aspect lingual (l) ont été délimités pour leur analyse séparée, ainsi que les points repères placés au niveau de la marge externe et interne de l'os cortical, utilisés pour mesurer l'épaisseur de l'os cortical (CBT).

the middle of the corpus until the most inferior point. Thereafter, a first curve was drawn following the external margins of the cortical bone, while a second one was placed along the periosteal cortical bone margins (Fig. 2C–E). An identical number of points for both curves was placed internally for each specimen in order to measure the cortical thickness as the shortest distance between the corresponding external and internal points. These curve points have been transformed into landmark coordinates by multiplying them by the voxel size. Then, a distance matrix was created for each specimen, calculating the distance between each pair of corresponding landmarks. The cortical area (CA, in mm^2) has also been measured on the buccal and lingual compartments with the Avizo 8.1 software.

Cortical bone thickness variation was analyzed on the sections taken along the mandible corpus in the statistical environment R 3.5.3 (R Core Team, 2019). Data were visualized using the package ggplot2 2.2.1 (Wickman, 2016). In order to allow direct comparisons between the fossil specimens and the extant human sample, we calculated a scale-free bi-dimensional Relative Cortical Thickness (2D RCT) index following the same analytical protocol used in Cazenave et al. (2017) for the distal humeral diaphysis. This parameter assesses the amount of cortical bone with respect to the volume occupied by the trabecular one. The RCT index is calculated as the Average Cortical Thickness (2D ACT) multiplied by 100 and divided by the square root of the trabecular area (TBA, in mm^2) (2D RCT = 2D ACT × 100/$TBA^{1/2}$), where 2D ACT is the ratio between cortical area (CA, in mm^2) and the endosteal contour length (ecl, in mm) (2D ACT = CA/ecl, in mm). The 2D RCT calculation was distinctly performed for each lingual and buccal side. The percentages of asymmetry between the P3/P4 and M1/M2 sections, and between the lingual and buccal aspects were calculated on each corpus section with the formula found in Corruccini et al. (2005; buccal-lingual)/((buccal + lingual)/2). For all variables, a number of intra- and inter-observer tests for accuracy run by two independent observers revealed differences less or equal to 5% (e.g., Fiorenza et al., 2019).

Fig. 1. Rendus virtuels de la mandibule Tighenif 1 (A) et de l'hémi-mandibule Tighenif 2 (B) en vues supérieure et latérale. Les coupes virtuelles longitudinales passant au niveau du corps des spécimens Tighenif 1 (C) et Tighenif 2 (D) permettent d'apprécier le degré de préservation de la structure osseuse interne.
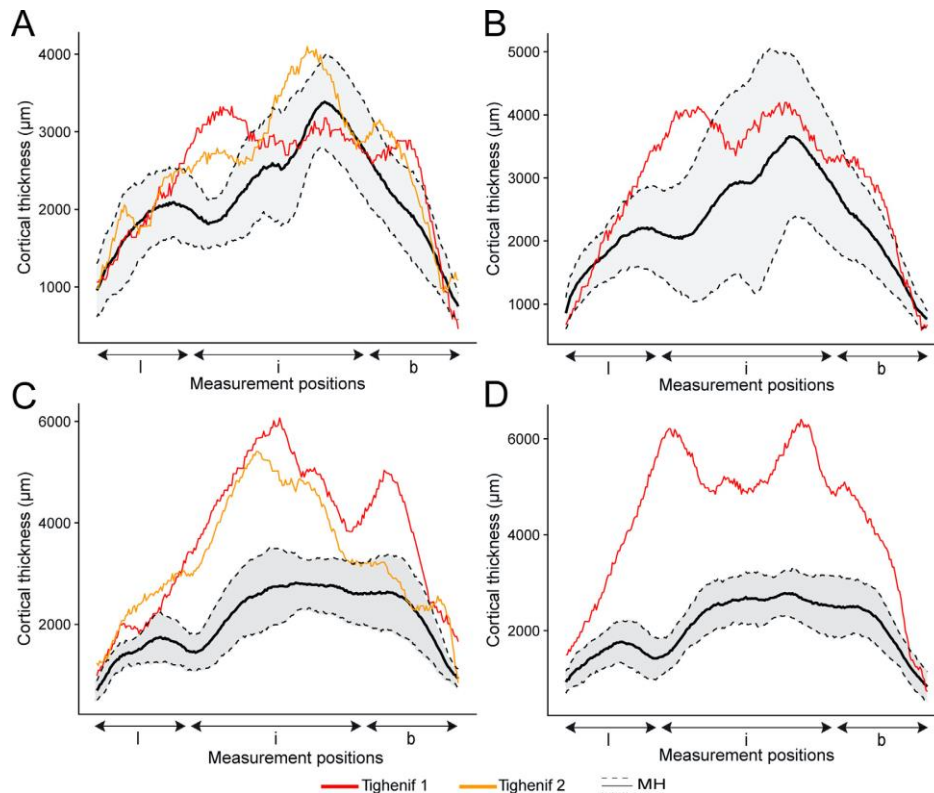
Fig. 3. Variations of CBT (in μm) at P3/P4 and M1/M2 from lingual (l) toward the inferior aspect (i) and to the buccal side (b) in the two Tighenif specimens and in ten modern humans (MH). The average value (dark line) and the variation expressed by plus or minus one standard deviation (grey area) are illustrated for the modern humans. A. Between the P3/P4 on the left side. B. Between the P3/P4 on the right side. C. Between the M1/M2 on the left side. D. Between the M1/M2 on the right side.

Fig. 3. Variations de CBT (en μm) entre P3/P4 et M1/M2 le long de l'aspect lingual (l) jusqu'à la partie inférieure (i) et en remontant vers l'aspect buccal (b) chez les deux fossiles de Tighenif et chez dix humains modernes (MH). La moyenne (ligne noire) ainsi que les variations (aire grise) représentées par plus ou moins un écart-type, sont illustrées pour notre échantillon de référence. A. Entre P3/P4 du côté gauche. B. Entre P3/P4 du côté droit. C. Entre M1/M2 du côté gauche. D. Entre M1/M2 du côté droit.

4. Results

Comparative cortical bone distribution on each bucco-lingual virtual section (respectively at the P3/P4 and M1/M2 levels on right and left parts the mandible corpus; see Fig. 2) was assessed in the two Tighenif specimens (only on the preserved left corpus for Tighenif 2) and extant human sample (Fig. 3A–D).

At the P3/P4 position (Fig. 3A–B), Tighenif 1, Tighenif 2 and extant humans exhibit a similar pattern on the left and right sides. More specifically, the two Algerian specimens mostly fall into the modern human (MH) range, which presents a high variability (meaning that some of MH specimens approximate the Tighenif cortical bone topography at this position). However, there are some exceptions, indeed, Tighenif 1 exceeds the MH range at the infero-lingual aspect on both side and Tighenif 2 displays higher cortical bone than Tighenif 1 and MH at

the inferior aspect. By looking at the cortical area (CA, Table 1), the Tighenif specimens present higher CA than MH. While at the P3/P4 buccal level, Tighenif 2 has substantially higher values than Tighenif 1, the opposite condition is observed lingually. When considering the scale-free bi-dimensional Relative Cortical Thickness index (2D RCT; Table 2) at each P3/P4 section, the two Tighenif specimens display higher values than the average modern human condition. Tighenif 1 2D RCT exceeds that of Tighenif 2, showing its maximal value on the right side. With the CA and 2D RCT measurements, we can also observe different bucco-lingual asymmetry patterns between our specimens (Tables 1 and 3). The Tighenif specimens show a thicker buccal cortical bone, except at the left P3/P4 section for Tighenif 1. Modern humans exhibit the opposite pattern at this position, with a cortical bone thicker lingually than buccally for both right and left sides of the mandible.

Table 1
Cortical area (CA, in mm^2) assessed at the P3/P4 and M1/M2 levels, on the buccal and the lingual aspects, in the two Tighenif specimens and in a selected modern human (MH) sample ($n = 10$). The buccal-to-lingual difference asymmetry was assessed between the sections for each side.

Tableau 1
Aire de l'os cortical mesurée aux niveaux buccal et lingual des P3/P4 et M1/M2 chez les deux spécimens de Tighenif et dans notre échantillon humain (MH) actuel sélectionné ($n = 10$). Le pourcentage de différence a été évalué entre les sections de chaque côté.

	CA (mm^2)			
	Tighenif 1	Tighenif 2	MH	MH range
L				
P3/P4 buccal	85.5	111.6	42.7	22.3–58.2
P3/P4 lingual	91.0	85.1	54.8	28.8–88.2
M1/M2 buccal	112.7	86.0	49.4	22.0–79.3
M1/M2 lingual	101.9	81.9	44.8	26.1–72.0
R				
P3/P4 buccal	115.3		44.8	17.9–71.5
P3/P4 lingual	131.0		59.2	37.5–93.8
M1/M2 buccal	114.1		44.4	19.4–72.8
M1/M2 lingual	111.5		44.9	37.5–93.8
Asymmetry[a]				
P3/P4 left	−6.0%	27.0%	−25.0%	
M1/M2 left	10.0%	5.0%	10.0%	
P3/P4 right	−3.0%		−28.0	
M1/M2 right	2.0%		−1.0%	

[a] Asymmetry percentage assessed with the formula (buccal − lingual)/((buccal − lingual)/2) (Corruccini et al., 2005).

Table 2
2D Relative Cortical Thickness (2D RCT) assessed at the P3/P4 and M1/M2 positions in the two Tighenif specimens and in a modern human (MH) sample ($n = 10$).

Tableau 2
Épaisseur relative corticale 2D (2D RCT) mesurée au niveau des P3/P4 et M1/M2 chez les deux spécimens de Tighenif et dans l'échantillon humain (MH) actuel ($n = 10$).

	2D RCT			
	Tighenif 1	Tighenif 2	MH mean	MH range
L				
P3/P4	12.8	17.4	12.3	9.4–15.5
M1/M2	16.4	17.3	12.5	9.7–18.0
R				
P3/P4	19.7		12.2	9.4–15.5
M1/M2	15.1		12.0	9.7–18.0

Table 3
Buccal-to-lingual difference percentage of the 2D Relative Cortical Thickness (2D RCT) assessed between the P3/P4 and M1/M2 sections for each side in the two Tighenif specimens and in a modern human (MH) sample ($n = 10$).

Tableau 3
Pourcentage de différence entre l'épaisseur relative corticale 2D (2D RCT) buccale et linguale, évalué entre les sections P3/P4 et M1/M2 pour chaque côté chez les deux spécimens de Tighenif et dans l'échantillon humain (MH) actuel ($n = 10$).

	Asymmetry buccal vs. lingual[a]		
	Tighenif 1 (%)	Tighenif 2 (%)	MH mean (%)
L			
P3/P4	−23.0	17.0	−24.0
M1/M2	8.0	5.0	12.0
R			
P3/P4	6.0		−24.0
M1/M2	5.0		−1.0

[a] Asymmetry percentage assessed with the formula (buccal − lingual)/((buccal − lingual)/2) (Corruccini et al., 2005).

At the M1/M2 position, the Tighenif specimens present a similar cortical bone distribution, with a substantially thicker cortical bone than MH (reaching up to nearly three times the average modern human values), except for the left buccal aspect of Tighenif 2, which falls within the modern human range (Fig. 3C–D). Moreover, at the right M1/M2, the Tighenif 1 specimen presents a symmetrical bucco-lingual distribution that differs from that of the right side. The Algerian specimens also exhibit a higher CA compared to the MH range. Tighenif 1 systematically displays substantially higher values than Tighenif 2 for the left side (Table 1). When standardizing through the 2D RCT index (Table 2), the fossils from Tighenif still have a relatively thicker cortical bone than MH, and Tighenif 2 shows a thicker cortical bone than Tighenif 1. The Tighenif specimens display an absolutely and relatively thicker buccal compartment than the lingual one at the M1/M2 level (Tables 1 and 3). Our limited modern human sample shows more variation, with on average a thicker buccal cortical bone on the left side of the mandible, but equivalent values between the buccal and lingual compartments on the right side.

When comparing the P3/P4 and M1/M2 sections, the two fossil specimens exhibit different conditions. Tighenif 1 shows higher CA at the left molar level, while the contrary is observed for Tighenif 2. In addition, the right side Tighenif 1 also shows the opposite condition, with higher CA at the premolar level (Table 1). In modern humans, there is more variation, especially on the buccal aspect, but the lingual CA is on average higher at the premolar level than posteriorly. However, the Tighenif 1 mandible presents thicker cortical bone at the left M1/M2 section than at the left P3/P4 section and the opposite pattern on the right side, whereas Tighenif 2 and MH exhibit equivalent 2D RCT between the two positions (Table 2). The two fossil specimens show higher asymmetry at the left premolar level than posteriorly. The right side of Tighenif 1 displays similar levels of slight buccal asymmetry at both premolar and molar levels. In modern humans, the left and right P3/P4 sections show similarly high magnitudes of asymmetry, comparable to those of the left side of both specimens from Tighenif, but a lower degree of asymmetry at the M1/M2 level.

5. Discussion and conclusions

In this study, we aimed to characterize the post-canine cortical bone thickness (CBT) in the Tighenif 1 and Tighenif 2 mandibular remains. Our results showed that both specimens have comparable absolute and relative CBT and distribution patterns at the P3/P4 and M1/M2 levels. In Tighenif 1, in which both sides of the mandible are preserved, there is a relationship between the relative thick cortical bone at the right P3/P4 level and the important dental occlusal wear found on this side (Arambourg and Hoffstetter, 1963; Zanolli and Mazurier, 2013). This may suggest that the cortical bone topography of this specimen could be biomechanically related to masticatory and/or paramasticatory differential loadings (Daegling and Hotzman, 2003; Fiorenza et al., 2019; Gröning et al., 2012). Recently, Fiorenza et al. (2019) have also found a concordance between wear asymmetry and thicker cortical bone

distribution in the Neanderthal specimen Regourdou 1, likely in relation to the right-handedness and paramasticatory activities previously reported for this individual (Volpato et al., 2012).

There is also a noticeable difference in maximal CBT and distribution pattern on the left buccal side of Tighenif 1 compared with that of Tighenif 2. This localized difference could be due to inter-individual variation (including sexual dimorphism), possibly linked to some subtle expression of the mandibular torus (Arambourg and Hoffstetter, 1963). In addition, it is noteworthy that Tighenif 2 has a CBT mostly equivalent to that of Tighenif 1, but shows less advanced dental occlusal wear (Arambourg and Hoffstetter, 1963; Zanolli and Mazurier, 2013). Thus, it would be too simple to consider that the differences in CBT distributions and the very thick cortical bone in the Tighenif specimens were only explained by a functional response during the masticatory process. It is also important to note that the smaller and less robust specimen Tighenif 2 has been suggested to represent a younger individual than Tighenif 1 and/or could also be a female (Arambourg and Hoffstetter, 1963).

We also highlighted major differences along the post-canine corpus between the two Tighenif specimens and modern humans. Tighenif CBT absolute values and topographic distribution approximate the modern condition at the P3/P4 level (especially on the left side) while they substantially deviate from the modern human pattern posteriorly. In terms of relative values, the 2D RCT index supports the proportionally more robust state of the Tighenif specimens compared with modern humans.

Biomechanical studies of extant human mandibles also suggested that the torsional moments related to masticatory constraints are greatly reduced in the anterior corpus (Hylander, 1984), while lateral transverse bending or "wishboning" stresses increase posteriorly particularly along the lingual margins (Daegling and Hotzman, 2003; Dechow and Hylander, 2000; Demes et al., 1984). The Tighenif mandibles show differences in buccal vs. lingual CBT. Ichim et al. (2006) have suggested that, in modern humans, this asymmetric pattern between buccal and lingual aspects is not related to masticatory strains. Instead, it could result from a retained evolutionary process possibly linked with the reduction of the face and tooth size in *H. sapiens*. In any case, the role and interpretation of this asymmetric mandibular CBT distribution is debated and, as shown in our limited comparative sample, there seems to be some variation that should be investigated further. The two Tighenif specimens exhibit thicker buccal than lingual cortical bone at the post-canine level (except for a single spot at the left P3/P4 section, where the bone is locally fractured and thus may affect the CBT assessment). This condition resembles what has been described for the modern human condition (Daegling and Hotzman, 2003; Dechow and Hylander, 2000; Demes et al., 1984). Martinez-Maza et al. (2011) have also suggested that the buccal side of the mandibular ramus in Neanderthals is affected by higher remodeling activities resulting from mechanical force. This was also evidenced in the Neanderthal specimen Regourdou 1 where the cortical bone under the P3 exhibits an asymmetric pattern in CBT distribution with the left buccal aspect being thicker (Fiorenza et al., 2019).

Substantial size and morphological differences between the fossil specimens from Tighenif and modern human mandibles represent taxonomic features likely reflecting adaptations to withstand biomechanical stresses in relation to the facial architecture (Ledogar et al., 2017; Strait et al., 2010). Such differences could be explained by dissimilarities in physiology. Indeed, numerous hormones are implicated in the systemic control of bone modeling (reshaping of bone through modeling drifts that occur primarily during growth), and remodeling (replacement of old or damaged bone tissue through a process of coupled resorption and formation) (Hublin, 1978, 1986; Kini and Nandeesh, 2012; Raggatt and Partridge, 2010 have argued that many morphological features of *H. erectus*, including cranial superstructures, thick cranial bones, and thick post-cranial cortical bone, could be the result of a single physiological process as a variation in endocrine production). While this may result from an allometric and differential bone growth related to the increase in size and robusticity, it is still unclear whether it could be of adaptive value.

The robusticity of the two Tighenif specimens is associated with the strong development of superstructures such as the sulcus intertoralis, lateral prominence, and the wide extramolar sulcus. In addition, the lateral prominence is positioned between the P3/P4 for Tighenif 1, between the M1/M2 for Tighenif 2 and the mental foramen is found between the P3/P4 for these two African specimens. Moreover, all the premolars from the Tighenif 1 and Tighenif 2 specimens exhibit complex 2R Tomes' root morphologies (Prado-Simón et al., 2012a, 2012b; Zanolli and Mazurier, 2013). Altogether, these morphological differences may have an impact on the CBT assessment, but are also part of the variation characteristic of a taxon. To this date, only a few studies have characterized the internal structure of the mandibular corpus in fossil hominins (Daegling and Grine, 1991; Fiorenza et al., 2019; Zanolli et al., 2017), while the extent of variation of the modern human condition remains to be investigated. Pending future comparisons of the internal bony signature of the Tighenif mandibles with other fossil specimens and larger modern human samples, considering the already proposed mix of features, including the expression of Neanderthal-like features on the external bone morphology and teeth (Mounier et al., 2009; Zanolli et al., 2010; Zanolli and Mazurier, 2013), we hypothesize that the CBT condition in the Tighenif mandible specimens may approximate the Neanderthal pattern, notably at the molar level.

References

Antón, S.C., 2003. Natural history of *Homo erectus*. Yearb. Phys. Anthropol. 46, 126–170.

Antón, S.C., Spoor, F., Fellmann, C.D., Swisher III., C.C., 2007. Defining *Homo erectus*: size considered. In: Henke, W., Tattersall, I. (Eds.), Handbook of Paleoanthropology. Springer, New York, pp. 1655–1695.

Arambourg, C., 1954. L'hominine fossile de Ternifine (Algérie). C. r. hebd. seances Acad. sci. 239, 893–895.

Arambourg, C., 1955. A recent discovery in human paleontology: *Atlanthropus* of Ternifine (Algeria). Am. J. Phys. Anthropol. 13, 191–201.

Arambourg, C., 1957. Récentes découvertes de paléontologie humaine réalisées en Afrique du Nord française (L'*Atlanthropus* de Ternifine – L'Hominien de Casablanca). In: Clarck, J.D., Cole, S. (Eds.), Proceedings of the Third Panafrican Congress on Prehistory. Chatto and Windus, London, pp. 186–194.

Arambourg, C., Hoffstetter, R., 1954. Découverte en Afrique du Nord des restes humains du Paléolithique inférieur. C. r. hebd. seances Acad. sci. 239, 72–74.

Arambourg, C., Hoffstetter, R., 1963. Le gisement de Ternifine. Arch. Inst. Paleontol. Hum. 32, 1–190.

Arribas, A., Palmqvist, P., 1999. On the ecological connection between sabre-tooths and hominids: faunal dispersal events in the lower Pleistocene and a review of the evidence for the first human arrival in Europe. J. Archeol. Sci. 26, 571–585.

Bermúdez de Castro, J.M., Arsuaga, J.L., Carbonell, E., Rosas, A., Maztínez, I., Mosquera, M., 1997. A Hominid from the lower Pleistocene of Atapuerca, Spain: possible ancestor to Neandertals and modern humans. Science 276, 1392–1395.

Bermúdez de Castro, J.M., Martinón-Torres, M., Gómez-Robles, A., Prado, L., Sarmiento, S., 2007. Comparative analysis of the Gran Dolina-TD6 (Spain) and Tighennif (Algeria) hominin mandibles. Bull. Mem. Soc. Anthropol. Paris 19, 149–167.

Bermúdez de Castro, J.M., Martinón-Torres, M., Rosell, J., Blasco, R., Arsuaga, J.L., Carbonell, E., 2016. Continuity *versus* discontinuity of the human settlement of Europe between the late early Pleistocene and the early middle Pleistocene. The mandibular evidence. Quat. Sci. Rev. 153, 51–62.

Cazenave, M., Braga, J., Oettlé, A., Thackeray, J.F., Beer, F., Hoffman, J., Endalamaw, M., Redea, B.E., Puymerail, L., Macchiarelli, R., 2017. Inner structural organization of the distal humerus in *Paranthropus* and *Homo*. C. R. Palevol 16, 521–532.

Corruccini, R.S., Townsend, G.C., Schwerdt, W., 2005. Correspondence between enamel hypoplasia and ondontometric bilateral asymmetry in Australian twins. Am. J. Phys. Anthropol. 126, 177–182.

Daegling, D.J., 1992. Mandibular morphology and diet in the genus *Cebus*. Int. J. Primatol. 13, 545–570.

Daegling, D.J., Grine, F.E., 1991. Compact bone distribution and biomechanics of early hominid mandibles. Am. J. Phys. Anthropol. 86, 321–339.

Daegling, D.J., Grine, F.E., 2006. Mandibular biomechanics and the paleontological evidence for the evolution of human. In: Ungar, P.S. (Ed.), Evolution of the Human Diet: The Know, The Unknown, and the Unknowable. Oxford University Press, New York, pp. 77–105.

Daegling, D.J., Hotzman, J.L., 2003. Functional significance of cortical bone distribution in anthropoid mandibles: an in vitro assessment of bone strain under combined loads. Am. J. Phys. Anthropol. 122, 38–50.

Dechow, P.C., Hylander, W.L., 2000. Elastic properties and masticatory bone stress in the macaque mandible. Am. J. Phys. Anthropol. 112, 557–571.

Demes, B., Preuschoft, H., Wolff, J.E.A., 1984. Stress-strength relationships in the mandibles of hominoids. In: Chivers, D.J., Wood, B.A., Bilsborough, A. (Eds.), Food Acquisition and Processing in Primates. Plenum Press, London, pp. 369–390.

Fajardo, R.J., Ryan, T.M., Kappelman, J., 2002. Assessing the accuracy of high-resolution X-ray computed tomography of primate trabecular bone by comparisons with histological sections. Am. J. Phys. Anthropol. 118, 1–10.

Finlayson, C., 2002. The role of climate in the spatio-temporal pattern of human colonization and extinction in the Pleistocene with specific reference to the Mediterranean Region. In: Ruiz-Zapara, B., et al. (Eds.), Quaternary Climatic Changes and Environmental Crises in the Mediterranean Regions. Universidad de Alcala de Henares, Madrid, pp. 1–8.

Fiorenza, L., Benazzi, S., Kullmer, O., Mazurier, A., Zanolli, C., Macchiarelli, R., 2019. Dental macrowear and cortical bone distribution of the Neanderthal mandible from Regourdou (Dordogne, southwestern France). J. Hum. Evol. 132, 174–188.

Frost, H.M., 1987. Bone "mass" and the "mechanostat": a proposal. Anat. Rec. 219, 1–9.

Frost, H.M., 2003. Bone's mechanostat: a 2003 update. Anat. Rec. 275A, 1081–1101.

Geraads, D., 2016. Pleistocene Carnivora (Mammalia) from Tighenif, Algeria. Gebios 49, 445–458.

Geraads, D., Hublin, J.J., Jaeger, J.J., 1986. The Pleistocene hominid site of Ternifine Algeria: new results on the environment, age, and human industries. Quat. Res. 25, 380–386.

Godinho, R.M., Fitton, L.C., Toro-Ibacache, V., Stringer, C.B., Lacruz, R.S., Bromage, T.G., O'Higgins, P., 2018. The bitting performance of *Homo sapiens* and *Homo heidelbergensis*. J. Hum. Evol. 118, 56–71.

Grine, F.E., Daegling, D.J., 2017. Functional morphology, biomechanics and the retrodiction of early hominin diets. C. R. Palevol 16, 613–631.

Gröning, F., Fagan, M., O'Higgins, P., 2012. Comparing the distribution of strains with the distribution of bone tissue in a human mandible: a finite element study. Anat. Rec. 296, 9–18.

Holmes, M.A., Ruff, C.B., 2011. Dietary effects on development of the human mandibular corpus. Am. J. Phys. Anthropol. 145, 615–628.

Howell, F.C., 1960. European and Northwest African middle Pleistocene hominids. Curr. Anthropol. 1, 195–232.

Hublin, J.-J., (PhD dissertation), 1978. Le torus occipital transverse et les structures associées : évolution dans le genre *Homo*. Université Pierre-et-Marie-Curie, Paris-6, Paris.

Hublin, J.-J., 1986. Some comments on the diagnostic features of *Homo erectus*. Anthropos (Brno) 23, 175–187.

Hylander, W.L., 1984. Stress and strain in the mandibular symphysis of primates: a test of competing hypotheses. Am. J. Phys. Anthropol. 64, 1–46.

Hylander, W.L., 2006. Functional, Anatomy and Biomechanics of the Masticatory Apparatus. In: Temporomandibular Disorders and Evidenced Approach to Diagnosis and Treatment. Quintessence Publishing, New York, pp. 1–34.

Ichim, I., Kieser, J.A., Swain, M.V., 2006. Functional significance of strain distribution in the human mandible under masticatory load: numerical predictions. Arch. Or. Biol. 52, 465–473.

Kini, U., Nandeesh, B.N., 2012. Physiology of bone formation, remodeling and metabolism. In: Fogelman, I., Gnanasegaran, G., Van der Wall, H. (Eds.), Radionuclide and Hybrid Bone Imaging. Springer, Berlin, Heidelberg, pp. 29–57.

L'Abbé, E.N., Loots, M., Meiring, J.H., 2005. The Pretoria bone collection: a modern South African skeletal sample. Homo 56, 197–205.

Ledogar, J.A., Benazzi, S., Smith, A.L., Weber, G.W., Carlson, K.B., Dechow, P.C., Grosse, I.R., Ross, C.F., Richmond, B.G., Wright, B.W., Wang, Q., Byron, C., Carlson, K.J., De Ruiter, D.J., Pryor Mcintosh, L.C., Strait, D.S., 2017. The biomechanics of bony facial "buttresses" in South African austalopiths: an experimental study using finite element analysis. Anat. Rec. 300, 171–195.

Macchiarelli, R., Bayle, P., Bondioli, L., Mazurier, A., Zanolli, C., 2013. From outer to inner structural morphology in dental anthropology. The integration of the third dimension in the visualization and quantitative analysis of fossil remains. In: Scott, G.R., Irish, J.D. (Eds.), Anthropological Perspectives on Tooth Morphology. Genetics, Evolution, Variation. Cambridge University Press, Cambridge, UK, pp.250–277.

Martinez-Maza, C., Rosas, A., García-Vargas, S., Estalrrich, A., de la Rasilla, M., 2011. Bone remodelling in Neanderthal mandibles from the El Sidrón site (Asturias, Spain). Biol. Lett. 7, 593–596.

Mounier, A., 2011. Définition du taxon *Homo heidelbergensis* Schoetensack, 1908 : analyse phénétique du massif facial supérieur des fossiles du genre *Homo* du Pléistocène moyen. Bull. Mem. Soc. Anthropol. Paris 23, 115–151.

Mounier, A., Marchal, F., Condemi, S., 2009. Is *Homo heidelbergensis* a distinct species? New insight on the Mauer mandible. J. Hum. Evol. 56, 219–246.

Pearson, O.M., Lieberman, D.E., 2004. The aging of Wolff's "law": ontogeny and responses to mechanical loading in cortical bone. Am. J. Phys. Anthropol. 125, 63–99.

Prado-Simón, L., Martinón-Torres, M., Baca, P., Gómez-Roblez, A., Lapresa, M., Carbonell, E., Bermúdez de Castro, J.M., 2012a. A morphological study on the tooth roots of the Sima del Enfante mandible (Atapuerca, Spain): a new classification of the teeth – biological and methodological considerations. Anthropol. Sci. 120, 61–72.

Prado-Simón, L., Martinón-Torres, M., Baca, P., Gómez-Roblez, A., Lapresa, M., Carbonell, E., Bermúdez de Castro, J.M., 2012b. Three-dimensional

1082   L. Genochio et al. / C. R. Palevol 18 (2019) 1073–1082

evaluation of root canal morphology in lower second premolars of early and middle Pleistocene human populations from Atapuerca (Burgos, Spain). Am. J. Phys. Anthropol. 147, 452–461.

Raggatt, L.J., Partridge, N.C., 2010. Cellular and molecular mechanisms of bone remodeling. J. Biol. Chem. 285, 25103–25108.

R Core Team, 2019. R: A Language and Environment for Statistical Computing. R Foundation for Statistical Computing, Vienna, Austria (Available at: http://www.R-project.org/).

Rohlf, F.J., 1997. tpsDig: Digitize Landmarks and Outlines. Version 2. 29. Apr 4 (cited 23 Oct 2016. Available at: http://life.bio.sunysb.edu/morph/).

Ruff, C., Holt, B., Trinkaus, E., 2006. Who's afraid of the big bad Wolff?: "Wolff's law" and bone functional adaptation. Am. J. Phys. 126, 484–498.

Sahnouni, M., Parés, J.M., Duval, M., Cáceres, I., Harichane, Z., Van der Made, J., Pérez-González, A., Abdessadok, S., Kandi, N., Derradji, A., Medig, M., Boulaghraif, K., Semaw, S., 2018. 1.9-million- and 2.4-million-year-old artifacts and stone tool-cutmarked bones from Ain Boucherit, Algeria. Science 362, 1297–1301.

Sahnouni, M., Van der Made, J., 2009. The Oldowan in North Africa Within a Biochronological Framework. The Cutting Edge: New Approaches to the Archeology of Human Origins. Stone Age Institute Press, Bloomington, IN, USA, pp. 179–210.

Schneider, C.A., Rasband, W.S., Eliceiri, K.W., 2012. NIH Image to ImageJ: 25 years of image analysis. Nat. Methods 9, 671–675.

Schwartz, J.H., Tattersall, I., 2003. The Human Fossil Record. Craniodental Morphology of Genus Homo (Africa and Asia), vol. 2. Wiley-Liss, Hoboken, NJ, USA.

Schwartz-Dabney, C.A., Dechow, P.C., 2003. Variations in cortical material properties throughout the human dentate mandible. Am. J. Phys Anthropol. 120, 252–277.

Sella-Tunis, T., Pokhojaev, A., Sarig, R., O'Higgins, P., May, H., 2018. Human mandibular shape is associated with masticatory muscle force. Sci. Rep. 8, 6042.

Spoor, C.F., Zonneveld, F.W., Macho, G.A., 1993. Linear measurements of cortical bone and dental enamel by computed tomography: applications and problems. Am. J. Phys. Anthropol. 91, 469–484.

Strait, D.S., Grosse, I.R., Dechow, P.C., Smith, A.L., Wang, Q., Weber, G.W., Neubauer, S., Slice, D.E., Chalk, J., Richmond, B.G., Lucas, P.W., Spencer, M.A., Schrein, C., Wright, B.W., Byron, C., Ross, C.F., 2010. The structural rigidity of the cranium of Australopithecus africanus: implications for diet, dietary adaptations, and the allometry of feeding biomechanics. Anat. Rec. 293, 583–593.

Tillier, A.M., 1980. Les dents d'enfant de Ternifine (Pléistocène moyen d'Algérie). L'Anthropologie 84, 413–421.

Toro-Ibacache, V., Muñoz, V.Z., O'Higgins, P., 2016. The relationship between skull morphology, masticatory muscle force and cranial skeletal deformation during biting. Ann. Anatomy-Anat. Anz. 203, 59–68.

Volpato, V., Macchiarelli, R., Guatelli-Steinberg, D., Fiore, I., Bondioli, L., Frayer, D.W., 2012. Hand to mouth in a Neandertal: right-handedness in Regourdou 1. PLoS One 7, e43949.

Wickman, H., 2016. ggplot2: Elegant Graphics for Data Analysis. Springer-Verlag, New York (Available at: https://ggplot2.tidyverse.org).

Zanolli, C., Mazurier, A., 2013. Endostructural characterization of the H. heidelbergensis dental remains from the early middle Pleistocene site of Tighenif, Algeria. C. R. Palevol 12, 293–304.

Zanolli, C., Bayle, P., Macchiarelli, R., 2010. Tissue proportions and enamel thickness distribution in the early middle Pleistocene human deciduous molars from Tighenif, Algeria. C. R. Palevol 9, 341–348.

Zanolli, C., Dean, M.C., Assefa, Y., Bayle, P., Braga, J., Condemi, S., Endalamaw, M., Engda Redea, B., Macchiarelli, R., 2017. Structural organization and tooth development in a Homo aff. erectus juvenile mandible from the early Pleistocene site of Garba IV at Melka Kunture, Ethiopian highlands. Am. J. Phys. Anthropol. 162, 549–553.

Appendix C. Research Outputs

Articles in peer-reviewed journals

Genochio L., Mazurier A., Dumoncel J., Theye C.E.G., and Zanolli C. 2019. Inner structural organization of the mandibular corpus in the late Early Pleistocene human specimens Tighenif 1 and Tighenif 2. Organisation structurale interne du corps mandibulaire chez les spécimens humains Tighenif 1 et Tighenif 2 du Pléistocène inférieur final. *Comptes Rendus Palevol*, 18: 1073–1082. (Appendix B)

Theye, C.E.G., Hattingh, A., Cracknell, T.J., Oettlé, A.C., Steyn, M. and Vandeweghe, S. 2018. Dento-alveolar measurements and histomorphometric parameters of maxillary and mandibular first molars, using micro-CT. *Clinical Implant Dentistry and Related Research*, 20(4): 550–561. (Appendix A)

Abstracts published in international journals

Theye C.E.G., Steyn M. and Oettlé A.C. 2019. Accuracy and reliability of three-dimensional (3D) macroscopic and microscopic measurements performed on Cone-Beam Computed-Tomography (CBCT) and Micro-Focus X-Ray Computed-Tomography (micro-CT) -based reconstructions of the mandible. Published in: *AACA (American Association of Clinical Anatomists) or BACA (British Association of Clinical Anatomists) Meeting Abstracts - A Selection of Abstracts Presented at the 47th Annual Conference of the Anatomical Society of Southern Africa (ASSA). Clinical Anatomy*.

Theye C., Oettlé A.C. and Steyn M. 2018. Sénescence et perte dentaire : comment la microstructure osseuse de la mandibule est-elle affectée ? Advancing age and tooth loss: how do these variables affect the bony microstructure of the mandible? Published in: *Colloque annuel de la Société d'Anthropologie de Paris, 1843e réunion scientifique. Bulletins et Mémoires de la Société d'Anthropologie de Paris* 30:S9-S31.

Theye C., Oettlé A.C., Steyn M., Cracknell T.J., Hattingh A., Blackbeard G., De Beer F., De Bruyn H., Hoffman J.W. and Vandeweghe S. 2018. Critical dental and periodontal parameters for immediate dental implant placement: a micro-focus X-ray computed tomography (µCT)

study. Published in: *AACA (American Association of Clinical Anatomists) or BACA (British Association of Clinical Anatomists) Meeting Abstracts - A Selection of Abstracts Presented at the 45th Annual Conference of the Anatomical Society of Southern Africa (ASSA). Clinical Anatomy*, 31:E25-E39.

Theye C., Hoffman J.W., De Beer F., Oettlé A.C. & Steyn M. 2018. The effects of aging and tooth loss on the microstructure of the mandible in South Africans. Published in: *AACA (American Association of Clinical Anatomists) or BACA (British Association of Clinical Anatomists) Meeting Abstracts - A Selection of Abstracts Presented at the 44th Annual Conference of the Anatomical Society of Southern Africa (ASSA). Clinical Anatomy,* 31:E11-E24.

Contributions to national and international scientific conferences and meetings

47th Annual Conference of the Anatomical Society of Southern Africa – ASSA (07-10/04/2019, South Africa). Theye C.E.G., Steyn M. & Oettlé A.C. Accuracy and reliability of three-dimensional (3D) macroscopic and microscopic measurements performed on Cone-Beam Computed-Tomography (CBCT) and Micro-Focus X-Ray Computed-Tomography (micro-CT) -based reconstructions of the mandible. *Oral presentation.*

Sefako Makgatho Health Sciences University Research Days (21-23/08/2018, South Africa). Theye C., Oettlé A.C. & Steyn M. Accuracy and reliability of three-dimensional (3D) macroscopic and microscopic measurements performed on cone-beam computed-tomography (CBCT) and micro-focus computed-tomography (micro-CT)-based reconstructions of the mandible. *Poster presentation.*

University of Pretoria Faculty of Health Sciences Research Days (21-22/08/2018, South Africa). Theye C., Oettlé A.C. & Steyn M. Accuracy and reliability of three-dimensional (3D) macroscopic and microscopic measurements performed on cone-beam computed-tomography (CBCT) and micro-focus computed-tomography (micro-CT) -based reconstructions of the mandible. *Oral presentation.*

1843e Journées de la Société d'Anthropologie de Paris – SAP (24-26/01/2018, France). Theye C., Oettlé A.C. & Steyn M. Sénescence et perte dentaire : comment la microstructure osseuse

de la mandibule est-elle affectée ? Advancing age and tooth loss: how do these variables affect the bony microstructure of the mandible? *Oral presentation.*

3rd Conference on Imaging with Radiation – Imgrad2017 (14-15/09/2017, Evolutionary Studies Institute, University of the Witwatersrand, South Africa). <u>Theye C</u>., Oettlé A.C. & Steyn M. Application of Micro-Focus X-Ray Computed-Tomography (X-µCT) to assess maxillofacial skeletal morphology in a South African sample. *Oral presentation.*

University of Pretoria Faculty of Health Sciences Research Days and Sefako Makgatho Health Sciences University Research Days (22-24/08/2017, South Africa). <u>Theye C.</u>, Oettlé A.C., Steyn M., Cracknell T., Hattingh A., Vandewegue S. & De Bruyn H. Three-Dimensional (3D) assessment of critical dento-alveolar parameters for immediate dental implant placement in South Africans. *Poster presentations.*

45th Annual Conference of the Anatomical Society of Southern Africa – ASSA (23-26/04/2017, South Africa). <u>Theye C.</u>, Oettlé A.C., Steyn M., Cracknell T.J., Hattingh A., Blackbeard G., De Beer F., De Bruyn H., Hoffman J.W. & Vandeweghe S. Critical dental and periodontal parameters for immediate dental implant placement: a micro-focus X-ray computed-tomography (µCT) study. *Oral presentation.*

University of Pretoria Faculty of Health Sciences Research Days (23-24/08/2016, South Africa). <u>Theye C.</u>, Oettlé A.C. & Steyn M. Preliminary results of the effects of aging and tooth loss on the microstructure of the mandible in South African males. *Poster presentation.*

44th Annual Conference of the Anatomical Society of Southern Africa – ASSA (8-11/05/2016, South Africa). <u>Theye C.</u>, Hoffman J.W., De Beer F., Oettlé A.C. & Steyn M. The effects of aging and tooth loss on the microstructure of the mandible in South Africans. *Oral presentation.*

3D imaging in a South African context – an AESOP (A European and South African Partnership on Heritage and Past) workshop (12-15/10/2015, University of Pretoria, South Africa). <u>Theye C.</u>, Oettlé A.C. & Steyn M. The effects of aging and tooth loss on the microstructure of the mandible in South Africans. *Oral presentation.*

Appendix D. Scanning parameters

Mandibles scanned by micro-CT

Table D.1. Micro-CT acquisition parameters (resolution in mm, voltage in kV, current in µA) for all the mandibles selected by CT.

MD_ID: individual identification number; RADC: Raymond A. Dart Collection of Modern Human Skeletons, University of the Witwatersrand; PBC: Pretoria Bone Collection, University of Pretoria; Op.: operator; CT: Charlotte Theye.

	MD_ID	Collection	Op.	Resolution	Voltage	Current
1	1904	RADC	CT	0.077	100	100
2	1926	RADC	CT	0.077	100	100
3	2179	RADC	CT	0.076	100	100
4	2187	RADC	CT	0.070	100	100
5	2209	RADC	CT	0.075	100	100
6	2294	RADC	CT	0.076	100	100
7	2331	RADC	CT	0.070	100	100
8	2409	RADC	CT	0.073	100	100
9	2453	RADC	CT	0.070	100	100
10	2657	RADC	CT	0.070	100	100
11	2866	PBC	CT	0.073	100	200
12	2930	RADC	CT	0.070	100	100
13	3046	RADC	CT	0.077	100	100
14	3129	RADC	CT	0.076	100	100
15	3481	RADC	CT	0.070	100	100
16	3603	RADC	CT	0.068	100	100
17	3643	RADC	CT	0.070	100	100
18	3696	RADC	CT	0.071	100	100
19	3773	RADC	CT	0.071	100	100
20	3838	RADC	CT	0.071	100	100
21	3851	RADC	CT	0.070	100	100
22	3865	RADC	CT	0.071	100	100
23	3953	PBC	CT	0.075	100	100
24	4006	PBC	CT	0.071	100	100
25	4139	PBC	CT	0.075	100	100
26	4220	PBC	CT	0.078	100	200
27	4256	PBC	CT	0.075	100	100
28	4364	PBC	CT	0.075	100	100
29	4384	PBC	CT	0.073	100	100

	MD_ID	Collection	Op.	Resolution	Voltage	Current
30	4399	PBC	CT	0.074	100	100
31	4416	PBC	CT	0.071	100	100
32	4417	PBC	CT	0.073	100	100
33	4435	PBC	CT	0.075	100	100
34	4442	PBC	CT	0.075	100	100
35	4448	PBC	CT	0.073	100	200
36	4449	PBC	CT	0.074	100	100
37	4458	PBC	CT	0.077	100	100
38	4537	PBC	CT	0.075	100	100
39	4540	PBC	CT	0.075	100	100
40	4565	PBC	CT	0.075	100	100
41	4578	PBC	CT	0.072	100	100
42	4636	PBC	CT	0.070	100	100
43	4837	PBC	CT	0.078	100	200
44	4853	PBC	CT	0.075	100	100
45	4905	PBC	CT	0.071	100	100
46	4946	PBC	CT	0.075	100	100
47	4956	PBC	CT	0.073	100	200
48	5033	PBC	CT	0.075	100	100
49	5039	PBC	CT	0.075	100	100
50	5056	PBC	CT	0.073	100	100
51	5150	PBC	CT	0.075	100	100
52	5178	PBC	CT	0.071	100	100
53	5203	PBC	CT	0.071	100	100
54	5248	PBC	CT	0.075	100	100
55	5259	PBC	CT	0.075	100	100
56	5304	PBC	CT	0.073	100	100
57	5305	PBC	CT	0.075	100	100
58	5343	PBC	CT	0.076	100	100
59	5345	PBC	CT	0.075	100	100
60	5347	PBC	CT	0.073	100	100
61	5386	PBC	CT	0.071	100	100
62	5446	PBC	CT	0.071	100	100
63	5462	PBC	CT	0.071	100	100

	MD_ID	Collection	Op.	Resolution	Voltage	Current
64	5483	PBC	CT	0.075	100	100
65	5495	PBC	CT	0.076	100	100
66	5575	PBC	CT	0.073	100	100
67	5599	PBC	CT	0.075	100	100
68	5673	PBC	CT	0.078	100	100
69	5681	PBC	CT	0.081	100	100
70	5684	PBC	CT	0.073	100	100
71	5688	PBC	CT	0.078	100	100
72	5692	PBC	CT	0.070	100	100
73	5694	PBC	CT	0.075	100	100
74	5696	PBC	CT	0.072	100	100
75	5697	PBC	CT	0.075	100	100
76	5704	PBC	CT	0.076	100	100
77	5705	PBC	CT	0.073	100	100
78	5710	PBC	CT	0.075	100	100
79	5712	PBC	CT	0.078	100	100
80	5716	PBC	CT	0.073	100	100
81	5717	PBC	CT	0.079	100	100
82	5719	PBC	CT	0.078	100	100
83	5725	PBC	CT	0.075	100	100
84	5728	PBC	CT	0.074	100	100
85	5735	PBC	CT	0.071	100	100
86	5737	PBC	CT	0.076	100	100
87	5743	PBC	CT	0.079	100	100
88	5744	PBC	CT	0.075	100	100
89	5746	PBC	CT	0.079	100	100
90	5747	PBC	CT	0.077	100	100
91	5748	PBC	CT	0.072	100	100
92	5750	PBC	CT	0.077	100	100
93	5752	PBC	CT	0.075	100	100
94	5754	PBC	CT	0.075	100	100
95	5755	PBC	CT	0.081	100	100
96	5756	PBC	CT	0.071	100	100
97	5757	PBC	CT	0.079	100	100

	MD_ID	Collection	Op.	Resolution	Voltage	Current
98	5759	PBC	CT	0.081	100	100
99	5760	PBC	CT	0.075	100	100
100	5761	PBC	CT	0.073	100	200
101	5763	PBC	CT	0.071	100	100
102	5766	PBC	CT	0.073	100	100
103	5768	PBC	CT	0.073	100	100
104	5769	PBC	CT	0.073	100	100
105	5784	PBC	CT	0.077	100	100
106	5785	PBC	CT	0.075	100	200
107	5796	PBC	CT	0.073	100	100
108	5797	PBC	CT	0.073	100	200
109	5800	PBC	CT	0.081	100	100
110	5807	PBC	CT	0.068	100	100
111	5810	PBC	CT	0.073	100	100
112	5812	PBC	CT	0.075	100	100
113	5816	PBC	CT	0.073	100	200
114	5832	PBC	CT	0.075	100	100
115	5837	PBC	CT	0.070	100	100
116	5842	PBC	CT	0.075	100	100
117	5845	PBC	CT	0.066	100	200
118	5848	PBC	CT	0.080	100	100
119	5855	PBC	CT	0.073	100	100
120	5857	PBC	CT	0.080	100	100
121	5860	PBC	CT	0.075	100	100
122	5862	PBC	CT	0.068	100	100
123	5865	PBC	CT	0.077	100	100
124	5867	PBC	CT	0.080	100	100
125	5868	PBC	CT	0.075	100	100
126	5875	PBC	CT	0.080	100	100
127	5880	PBC	CT	0.080	100	200
128	5882	PBC	CT	0.075	100	100
129	5885	PBC	CT	0.070	100	100
130	5886	PBC	CT	0.075	100	100
131	5892	PBC	CT	0.071	100	200

	MD_ID	Collection	Op.	Resolution	Voltage	Current
132	5895	PBC	CT	0.080	100	100
133	5896	PBC	CT	0.071	100	100
134	5903	PBC	CT	0.073	100	100
135	5905	PBC	CT	0.077	100	100
136	5909	PBC	CT	0.080	100	100
137	5912	PBC	CT	0.075	100	100
138	5913	PBC	CT	0.075	100	100
139	5924	PBC	CT	0.075	100	100
140	5925	PBC	CT	0.072	100	100
141	5929	PBC	CT	0.084	100	100
142	5932	PBC	CT	0.073	100	100
143	5942	PBC	CT	0.075	100	100
144	5946	PBC	CT	0.074	100	100
145	5951	PBC	CT	0.075	100	100
146	5953	PBC	CT	0.075	100	100
147	5954	PBC	CT	0.077	100	100
148	5957	PBC	CT	0.070	100	100
149	5958	PBC	CT	0.077	100	100
150	5960	PBC	CT	0.077	100	100
151	5966	PBC	CT	0.075	100	100
152	5975	PBC	CT	0.075	100	100
153	5976	PBC	CT	0.075	100	100
154	5981	PBC	CT	0.074	100	100
155	5982	PBC	CT	0.075	100	100
156	5986	PBC	CT	0.071	100	100
157	5989	PBC	CT	0.075	100	100
158	5990	PBC	CT	0.081	100	100
159	5991	PBC	CT	0.075	100	100
160	5999	PBC	CT	0.073	100	100
161	6002	PBC	CT	0.073	100	100
162	6009	PBC	CT	0.073	100	200
163	6010	PBC	CT	0.077	100	100
164	6011	PBC	CT	0.075	100	100
165	6023	PBC	CT	0.077	100	100

	MD_ID	Collection	Op.	Resolution	Voltage	Current
166	6024	PBC	CT	0.073	100	100
167	6028	PBC	CT	0.073	100	100
168	6030	PBC	CT	0.075	100	100
169	6031	PBC	CT	0.080	100	200
170	6034	PBC	CT	0.075	100	100
171	6035	PBC	CT	0.073	100	100
172	6068	PBC	CT	0.073	100	100
173	6109	PBC	CT	0.073	100	100
174	6145	PBC	CT	0.073	100	100
175	6157	PBC	CT	0.077	100	100
176	6172	PBC	CT	0.073	100	100
177	6187	PBC	CT	0.073	100	200
178	6192	PBC	CT	0.071	100	200
179	6198	PBC	CT	0.071	100	200
180	6215	PBC	CT	0.075	100	100
181	6219	PBC	CT	0.080	100	100
182	6228	PBC	CT	0.084	100	100
183	6229	PBC	CT	0.076	100	100
184	6234	PBC	CT	0.073	100	100
185	6236	PBC	CT	0.075	100	100
186	6237	PBC	CT	0.073	100	100
187	6242	PBC	CT	0.072	100	100
188	6244	PBC	CT	0.080	100	100
189	6248	PBC	CT	0.073	100	100
190	6251	PBC	CT	0.072	100	100
191	6254	PBC	CT	0.071	100	100
192	6256	PBC	CT	0.073	100	100
193	6257	PBC	CT	0.073	100	100
194	6264	PBC	CT	0.075	100	100
195	6274	PBC	CT	0.080	100	100
196	6286	PBC	CT	0.083	100	100
197	6288	PBC	CT	0.077	100	100
198	6289	PBC	CT	0.071	100	100
199	6290	PBC	CT	0.073	100	100

	MD_ID	Collection	Op.	Resolution	Voltage	Current
200	6293	PBC	CT	0.073	100	100
201	6296	PBC	CT	0.075	100	100
202	6307	PBC	CT	0.077	100	100
203	6310	PBC	CT	0.077	100	100
204	6313	PBC	CT	0.080	100	100
205	6315	PBC	CT	0.075	100	100
206	6316	PBC	CT	0.080	100	100
207	6318	PBC	CT	0.077	100	100
208	6319	PBC	CT	0.073	100	100
209	6322	PBC	CT	0.071	100	100
210	6338	PBC	CT	0.075	100	100
211	6339	PBC	CT	0.073	100	100
212	6342	PBC	CT	0.073	100	100
213	6347	PBC	CT	0.071	100	200
214	6358	PBC	CT	0.072	100	100
215	6359	PBC	CT	0.075	100	100
216	6360	PBC	CT	0.075	100	100
217	6364	PBC	CT	0.080	100	100
218	6367	PBC	CT	0.084	100	100
219	6368	PBC	CT	0.080	100	100
220	6369	PBC	CT	0.075	100	200
221	6370	PBC	CT	0.075	100	100
222	6372	PBC	CT	0.073	100	100
223	6374	PBC	CT	0.077	100	100
224	6378	PBC	CT	0.073	100	100
225	6379	PBC	CT	0.077	100	100
226	6388	PBC	CT	0.073	100	100
227	6390	PBC	CT	0.075	100	100
228	6392	PBC	CT	0.084	100	100
229	6395	PBC	CT	0.075	100	100
230	6396	PBC	CT	0.073	100	200
231	6402	PBC	CT	0.073	100	100
232	6407	PBC	CT	0.080	100	100
233	6409	PBC	CT	0.075	100	100

	MD_ID	Collection	Op.	Resolution	Voltage	Current
234	6411	PBC	CT	0.075	100	100
235	6412	PBC	CT	0.075	100	100
236	6425	PBC	CT	0.075	100	100
237	6426	PBC	CT	0.075	100	100
238	6430	PBC	CT	0.075	100	100
239	6432	PBC	CT	0.080	100	100
240	6437	PBC	CT	0.080	100	100
241	6440	PBC	CT	0.075	100	100
242	6444	PBC	CT	0.080	100	100
243	6449	PBC	CT	0.080	100	100
244	6456	PBC	CT	0.075	100	100
245	6458	PBC	CT	0.075	100	100
246	6459	PBC	CT	0.072	100	100
247	6461	PBC	CT	0.072	100	100
248	6463	PBC	CT	0.072	100	100
249	6466	PBC	CT	0.073	100	100
250	6470	PBC	CT	0.073	100	100
251	6481	PBC	CT	0.076	100	100
252	6482	PBC	CT	0.073	100	100
253	6483	PBC	CT	0.073	100	100
254	6487	PBC	CT	0.072	100	100
255	6488	PBC	CT	0.072	100	100
256	6504	PBC	CT	0.080	100	100
257	6512	PBC	CT	0.070	100	100
258	6515	PBC	CT	0.080	100	200
259	6523	PBC	CT	0.075	100	100
260	6524	PBC	CT	0.075	100	100
261	6528	PBC	CT	0.070	100	100
262	7018	PBC	CT	0.084	100	100
263	7022	PBC	CT	0.081	100	100
264	7049	PBC	CT	0.080	100	100
265	7053	PBC	CT	0.075	100	100

Table D.2. Micro-CT acquisition parameters (resolution in mm, voltage in kV, current in µA) for all the mandibles micro-CT-scanned for previous research projects and included in the thesis.

MD_ID: individual identification number; PBC: Pretoria Bone Collection, University of Pretoria; Op.: operator; ACO: Anna C. Oettlé, CS: Clarisa Sutherland.

	MD_ID	Collection	Op.	Resolution	Voltage	Current
1	1636	PBC	ACO	0.089	100	70
2	3094	PBC	ACO	0.098	100	70
3	4968	PBC	ACO	0.097	100	70
4	5007	PBC	ACO	0.095	100	70
5	5012	PBC	ACO	0.098	100	70
6	5020	PBC	ACO	0.097	100	70
7	5057	PBC	ACO	0.073	100	70
8	5086	PBC	ACO	0.091	100	70
9	5177	PBC	ACO	0.093	100	70
10	5250	PBC	ACO	0.097	100	70
11	5256	PBC	ACO	0.095	100	70
12	5285	PBC	ACO	0.097	100	70
13	5296	PBC	ACO	0.095	100	70
14	5315	PBC	ACO	0.093	100	70
15	5358	PBC	ACO	0.090	100	70
16	5378	PBC	ACO	0.097	100	70
17	5383	PBC	ACO	0.089	100	70
18	5407	PBC	ACO	0.094	100	70
19	5454	PBC	ACO	0.091	100	70
20	5463	PBC	ACO	0.095	100	70
21	5476	PBC	ACO	0.094	100	70
22	5526	PBC	ACO	0.097	100	70
23	5573	PBC	ACO	0.076	100	70
24	5576	PBC	ACO	0.089	100	70
25	5614	PBC	ACO	0.078	100	100
26	5657	PBC	ACO	0.089	100	70
27	5661	PBC	ACO	0.090	100	70
28	5679	PBC	ACO	0.106	100	70
29	5693	PBC	ACO	0.102	100	70
30	5772	PBC	ACO	0.095	100	70
31	5792	PBC	ACO	0.102	100	70

	MD_ID	Collection	Op.	Resolution	Voltage	Current
32	5806	PBC	ACO	0.102	100	70
33	5809	PBC	ACO	0.095	100	70
34	5863	PBC	ACO	0.102	100	70
35	5872	PBC	ACO	0.099	100	70
36	5873	PBC	ACO	0.095	100	70
37	5884	PBC	ACO	0.102	100	70
38	5944	PBC	ACO	0.102	100	70
39	6016	PBC	ACO	0.092	100	70
40	6159	PBC	ACO	0.092	100	70
41	6232	PBC	ACO	0.105	100	70
42	6243	PBC	ACO	0.096	100	70
43	6259	PBC	ACO	0.105	100	70
44	6265	PBC	ACO	0.078	100	100
45	6280	PBC	ACO	0.078	100	100
46	6284	PBC	ACO	0.078	100	100
47	6300	PBC	ACO	0.082	100	100
48	6305	PBC	ACO	0.102	100	70
49	6308	PBC	ACO	0.082	100	100
50	6309	PBC	ACO	0.075	100	100
51	6314	PBC	ACO	0.085	100	100
52	6323	PBC	ACO	0.073	100	100
53	6325	PBC	ACO	0.095	100	70
54	6335	PBC	ACO	0.082	100	100
55	6337	PBC	ACO	0.078	100	100
56	6344	PBC	ACO	0.082	100	100
57	6365	PBC	ACO	0.096	100	70
58	6401	PBC	ACO	0.078	100	100
59	6410	PBC	ACO	0.102	100	70
60	6416	PBC	ACO	0.074	100	100
61	6423	PBC	ACO	0.099	100	70
62	6526	PBC	ACO	0.078	100	100
63	6872	PBC	ACO	0.078	100	100
64	7020	PBC	ACO	0.078	100	100
65	5819	PBC	CS	0.075	120	220

	MD_ID	Collection	Op.	Resolution	Voltage	Current
66	5931	PBC	CS	0.075	120	220
67	6011	PBC	CS	0.068	90	120
68	6217	PBC	CS	0.069	120	220
69	6220	PBC	CS	0.073	90	120
70	6225	PBC	CS	0.072	120	220
71	6231	PBC	CS	0.095	90	120
72	6247	PBC	CS	0.070	90	120
73	6252	PBC	CS	0.073	120	220
74	6262	PBC	CS	0.073	120	220
75	6263	PBC	CS	0.069	120	220
76	6265	PBC	CS	0.074	90	120
77	6334	PBC	CS	0.070	90	120
78	6350	PBC	CS	0.074	120	220
79	6353	PBC	CS	0.072	120	220
80	6357	PBC	CS	0.076	120	220
81	6371	PBC	CS	0.068	120	220
82	6376	PBC	CS	0.072	120	220
83	6389	PBC	CS	0.076	120	220
84	6394	PBC	CS	0.072	120	220
85	6403	PBC	CS	0.077	120	220
86	6404	PBC	CS	0.077	120	220
87	6413	PBC	CS	0.073	120	220
88	6429	PBC	CS	0.076	120	220
89	6530	PBC	CS	0.075	120	220
90	6537	PBC	CS	0.082	120	220
91	7019	PBC	CS	0.073	120	220
92	7031	PBC	CS	0.073	120	220

Mandibles scanned by CBCT

Table D.3. CBCT acquisition parameters (resolution in mm, voltage in kV, current in mA, exposure time in ms, field of view FOV in mm) for all the specimens CBCT-scanned at the Oral and Dental Hospital (University of Pretoria).

MD_ID: individual identification number; PBC: Pretoria Bone Collection, University of Pretoria.

	MD_ID	Collection	Resolution	Voltage	Current	Exposure time	FOV
1	5761	PBC	0.200	88	11	12.11	130 x 90
2	6030	PBC	0.200	88	11	12.06	130 x 160
3	6035	PBC	0.200	88	11	12.09	130 x 160
4	6231	PBC	0.200	88	11	12.10	130 x 160
5	6403	PBC	0.200	88	11	12.08	130 x 160
6	6537	PBC	0.200	88	11	12.16	130 x 160
7	5819	PBC	0.200	88	11	12.15	130 x 130
8	5981	PBC	0.200	88	11	12.08	130 x 130
9	6247	PBC	0.200	88	11	12.14	130 x 130
10	6263	PBC	0.200	88	11	12.13	130 x 130
11	6305	PBC	0.200	88	11	12.08	130 x 130
12	6401	PBC	0.200	88	11	12.10	130 x 130
13	5810	PBC	0.200	88	10	12.12	130 x 160
14	5886	PBC	0.200	88	10	12.13	130 x 160
15	5951	PBC	0.200	88	10	12.12	130 x 160
16	5966	PBC	0.200	88	10	12.13	130 x 160
17	5991	PBC	0.200	88	10	12.14	130 x 160
18	6394	PBC	0.200	88	10	12.12	130 x 160
19	4139	PBC	0.200	88	10	12.15	130 x 90
20	5462	PBC	0.200	88	10	12.14	130 x 90
21	5862	PBC	0.200	88	10	12.14	130 x 90
22	5982	PBC	0.200	88	10	12.13	130 x 90
23	6426	PBC	0.200	88	10	12.15	130 x 90
24	7019	PBC	0.200	88	10	12.14	130 x 90

Femora scanned by micro-CT

Table D.4. Micro-CT acquisition parameters (resolution in mm, voltage in kV, current in µA) for all the femora selected by CT.

FEM_ID: individual identification number; PBC: Pretoria Bone Collection, University of Pretoria; Op.: operator; CT: Charlotte Theye.

	FEM_ID	Collection	Op.	Resolution	Voltage	Current
1	4006	PBC	CT	0.0729	100	100
2	4946	PBC	CT	0.0924	100	100
3	5020	PBC	CT	0.0924	100	100
4	5039	PBC	CT	0.0640	100	100
5	5347	PBC	CT	0.0834	100	100
6	5681	PBC	CT	0.0924	100	100
7	5705	PBC	CT	0.0924	100	100
8	5708	PBC	CT	0.0856	100	100
9	5710	PBC	CT	0.0700	100	100
10	5748	PBC	CT	0.0729	100	100
11	5756	PBC	CT	0.0924	100	100
12	5759	PBC	CT	0.0942	100	100
13	5772	PBC	CT	0.0920	100	100
14	5784	PBC	CT	0.1006	100	100
15	5806	PBC	CT	0.0856	100	100
16	5810	PBC	CT	0.0924	100	100
17	5863	PBC	CT	0.1006	100	100
18	5905	PBC	CT	0.0920	100	100
19	5946	PBC	CT	0.0856	100	100
20	5953	PBC	CT	0.0754	100	100
21	5958	PBC	CT	0.0924	100	100
22	5981	PBC	CT	0.0924	100	100
23	5990	PBC	CT	0.0924	100	100
24	6002	PBC	CT	0.0924	100	100
25	6010	PBC	CT	0.0640	100	100
26	6028	PBC	CT	0.0700	100	100
27	6030	PBC	CT	0.0924	100	100
28	6109	PBC	CT	0.0700	100	100
29	6232	PBC	CT	0.0942	100	100
30	6236	PBC	CT	0.0733	100	100

	FEM_ID	Collection	Op.	Resolution	Voltage	Current
31	6237	PBC	CT	0.0733	100	100
32	6244	PBC	CT	0.0700	100	100
33	6247	PBC	CT	0.0924	100	100
34	6274	PBC	CT	0.0942	100	100
35	6284	PBC	CT	0.0924	100	100
36	6288	PBC	CT	0.0942	100	100
37	6310	PBC	CT	0.0700	100	100
38	6313	PBC	CT	0.0856	100	100
39	6339	PBC	CT	0.0856	100	100
40	6344	PBC	CT	0.0924	100	100
41	6359	PBC	CT	0.0733	100	100
42	6365	PBC	CT	0.0700	100	100
43	6367	PBC	CT	0.0942	100	100
44	6368	PBC	CT	0.1006	100	100
45	6378	PBC	CT	0.1006	100	100
46	6426	PBC	CT	0.0942	100	100
47	6449	PBC	CT	0.1006	100	100
48	6482	PBC	CT	0.0856	100	100
49	6488	PBC	CT	0.0729	100	100
50	7049	PBC	CT	0.1006	100	100

Table D.5. Micro-CT acquisition parameters (resolution in mm, voltage in kV, current in µA) for all the femora selected by MC for previous research projects and included in the thesis.

FEM_ID: individual identification number; PBC: Pretoria Bone Collection, University of Pretoria; Op.: operator; MC: Marine Cazenave.

	FEM_ID	Collection	Op.	Resolution	Voltage	Current
1	4220	PBC	MC	0.0750	100	100
2	4926	PBC	MC	0.0689	100	100
3	5155	PBC	MC	0.0757	100	100
4	5626	PBC	MC	0.0757	100	100
5	5767	PBC	MC	0.0689	100	100
6	5618	PBC	MC	0.0750	100	100
7	5878	PBC	MC	0.0689	100	100
8	5957	PBC	MC	0.1000	100	100
9	6064	PBC	MC	0.0649	100	100
10	6068	PBC	MC	0.1000	100	100
11	6177	PBC	MC	0.0888	100	100
12	6192	PBC	MC	0.0757	100	100
13	6293	PBC	MC	0.0689	100	100
14	6314	PBC	MC	0.0757	100	100
15	6338	PBC	MC	0.0689	100	100
16	6390	PBC	MC	0.0849	100	100
17	6512	PBC	MC	0.0888	100	100
18	7028	PBC	MC	0.0772	100	100

Appendix E. Micro-CT analysis of the mandible

Repeatability – ICCs and TEMs

Intra-observer agreement – Bland-Altman plots

Normality – Kernel density plots

Repeatability – ICCs and TEMs

Table E.1. Intra-observer errors estimated on micro-CT-based measurements: ICCs and 95 % Confidence Intervals (CI lower – upper bounds), TEM and %TEM values. Lowest ICCs and largest %TEMs are in bold.

	ICC	95% CI	TEM	%TEM
External distances				
m_h	0.9998	0.9993 – 1.0000	0.031	0.094
a_h	0.9999	0.9998 – 1.0000	0.021	0.064
p_h	0.9999	0.9998 – 1.0000	0.013	0.047
ra_b	1.0000	0.9999 – 1.0000	0.016	0.042
ra_h	1.0000	0.9999 – 1.0000	0.017	0.036
Cortical thicknesses				
m_ba_CtTh	0.9999	0.9997 – 1.0000	0.014	0.488
m_buc_CtTh	**0.9995**	0.9981 – 0.9999	0.013	**0.786**
m_ling_CtTh	0.9996	0.9986 – 0.9999	0.009	0.502
a_ba_CtTh	1.0000	0.9998 – 1.0000	0.012	0.341
a_buc_CtTh	0.9995	0.9983 – 0.9999	0.011	0.534
a_ling_CtTh	0.9995	0.9981 – 0.9999	0.010	0.464
p_ba_CtTh	0.9999	0.9998 – 1.0000	0.007	0.184
p_buc_CtTh	0.9999	0.9995 – 1.0000	0.008	0.339
p_ling_CtTh	0.9998	0.9992 – 0.9999	0.008	0.351
rab_buc_CtTh	**0.9991**	0.9993 – 1.0000	0.009	0.483
rab_ling_CtTh	0.9998	0.9978 – 0.9999	0.013	**0.800**
rah_buc_CtTh	0.9998	0.9966 – 0.9998	0.012	**0.623**
rah_ling_CtTh	**0.9994**	0.9993 – 1.0000	0.008	**0.674**

Intra-observer agreement – Bland-Altman plots

External distances
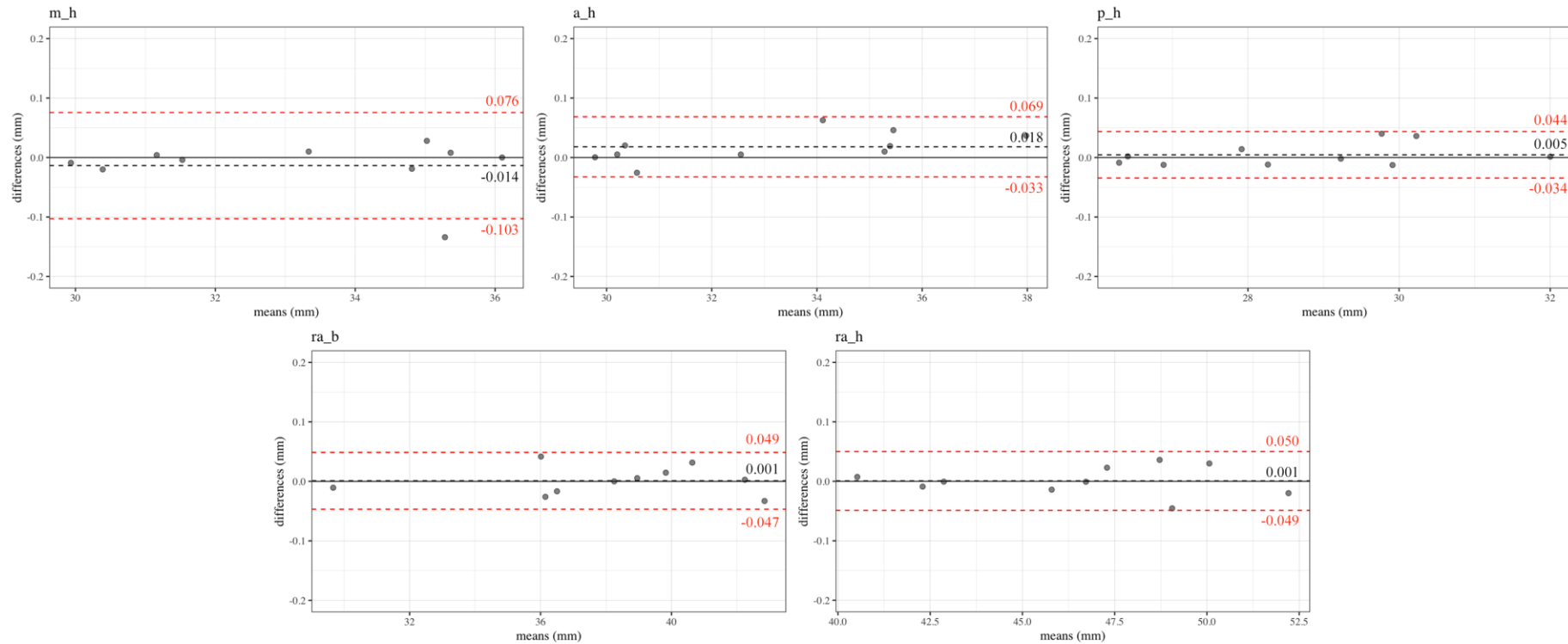
Figure E.1. Bland-Altman plots of the intra-observer agreement for the micro-CT-based external distances recorded on the mandibular corpus: m_h, a_h and p_h (top); and on the mandibular ramus: ra_b and ra_h (bottom). 95% of the measurements are located within the upper and lower limits of agreement (red dashed lines), while the mean of differences is illustrated by the horizontal black dashed line. The vertical y-axis scale is relative to the spread of variations.

Cortical thickness
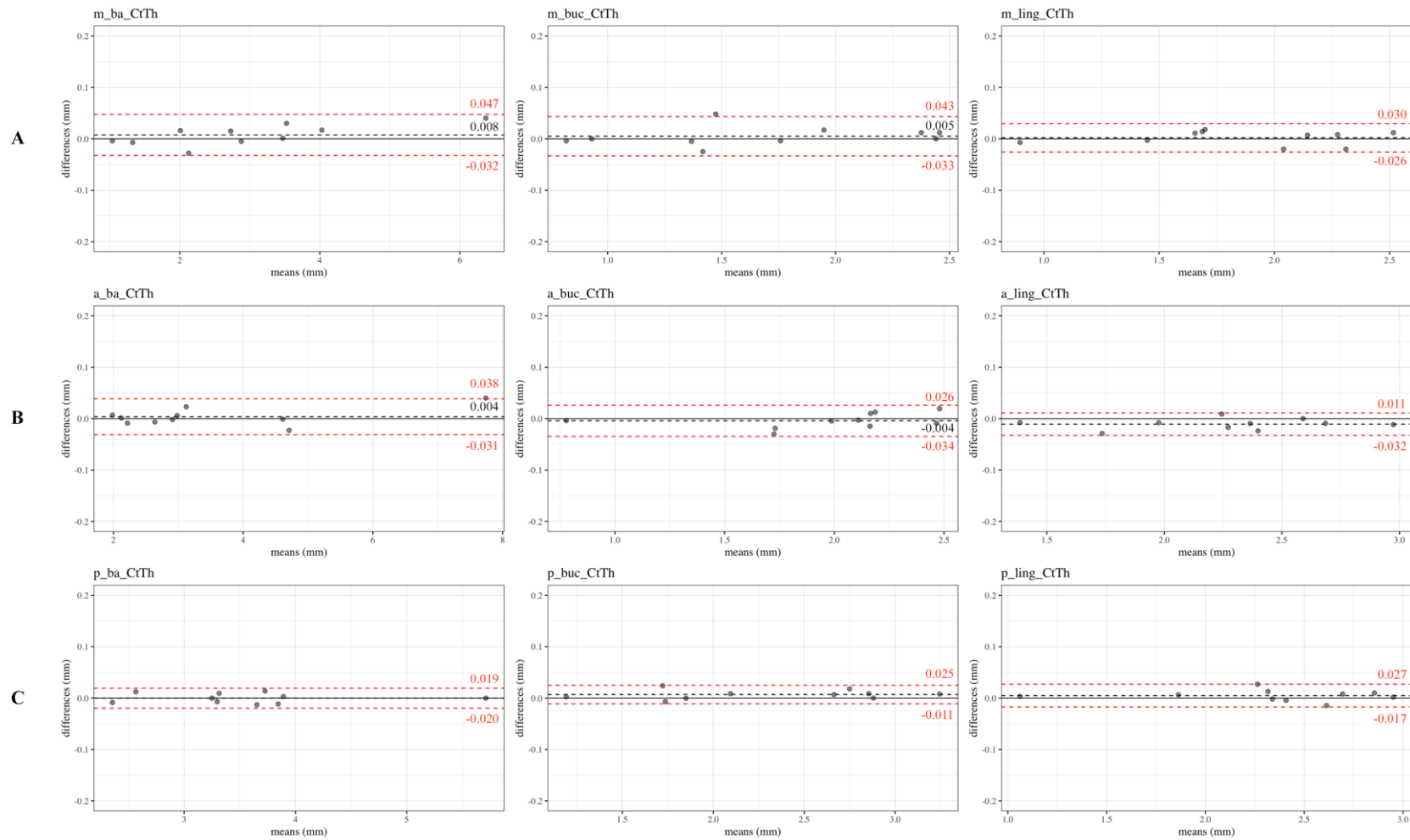
Figure E.2. Bland-Altman plots of the intra-observer agreement for the micro-CT-based cortical thicknesses recorded on the midline [A], anterior [B] and posterior [C] sections, as well as on the ramus breadth [D] and height [E]. 95% of the measurements are located within the upper and lower limits of agreement (red dashed lines), while the mean of differences is illustrated by the horizontal black dashed line. The vertical y-axis scale is relative to the spread of variations. (continued on the next page)
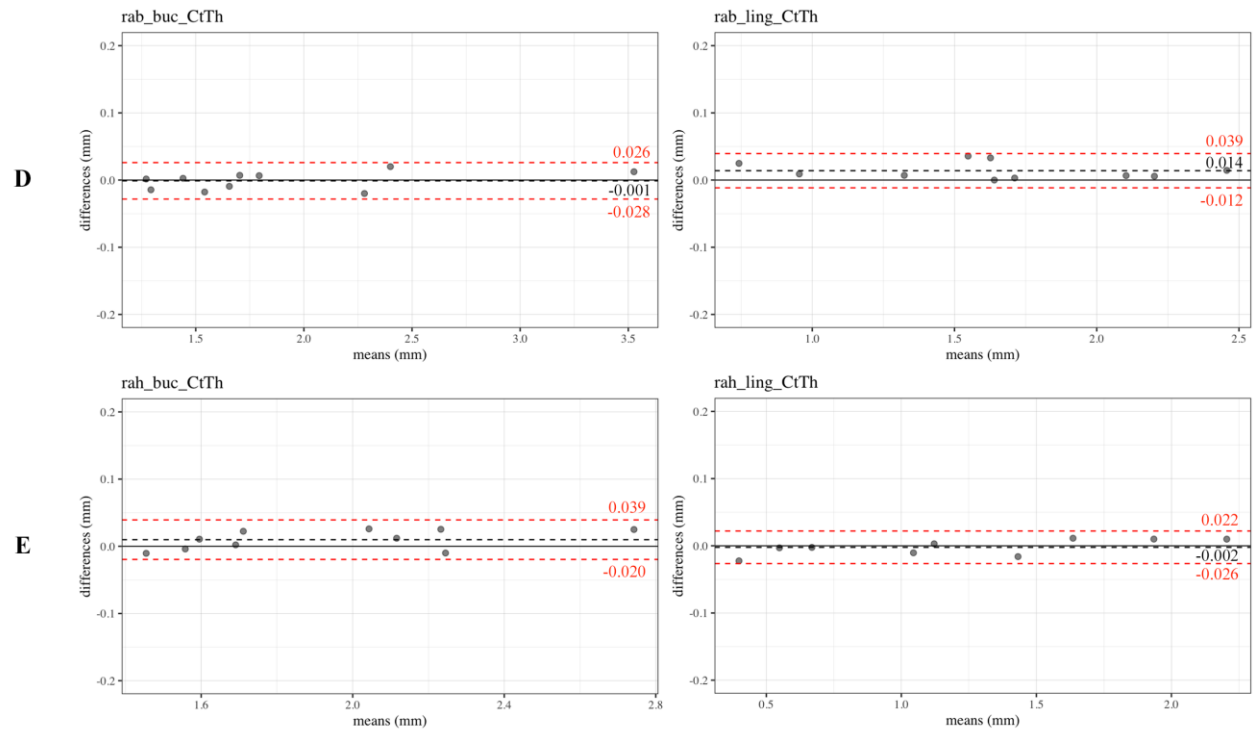
Figure E.2. (continued)

Normality – Kernel density plots

Age
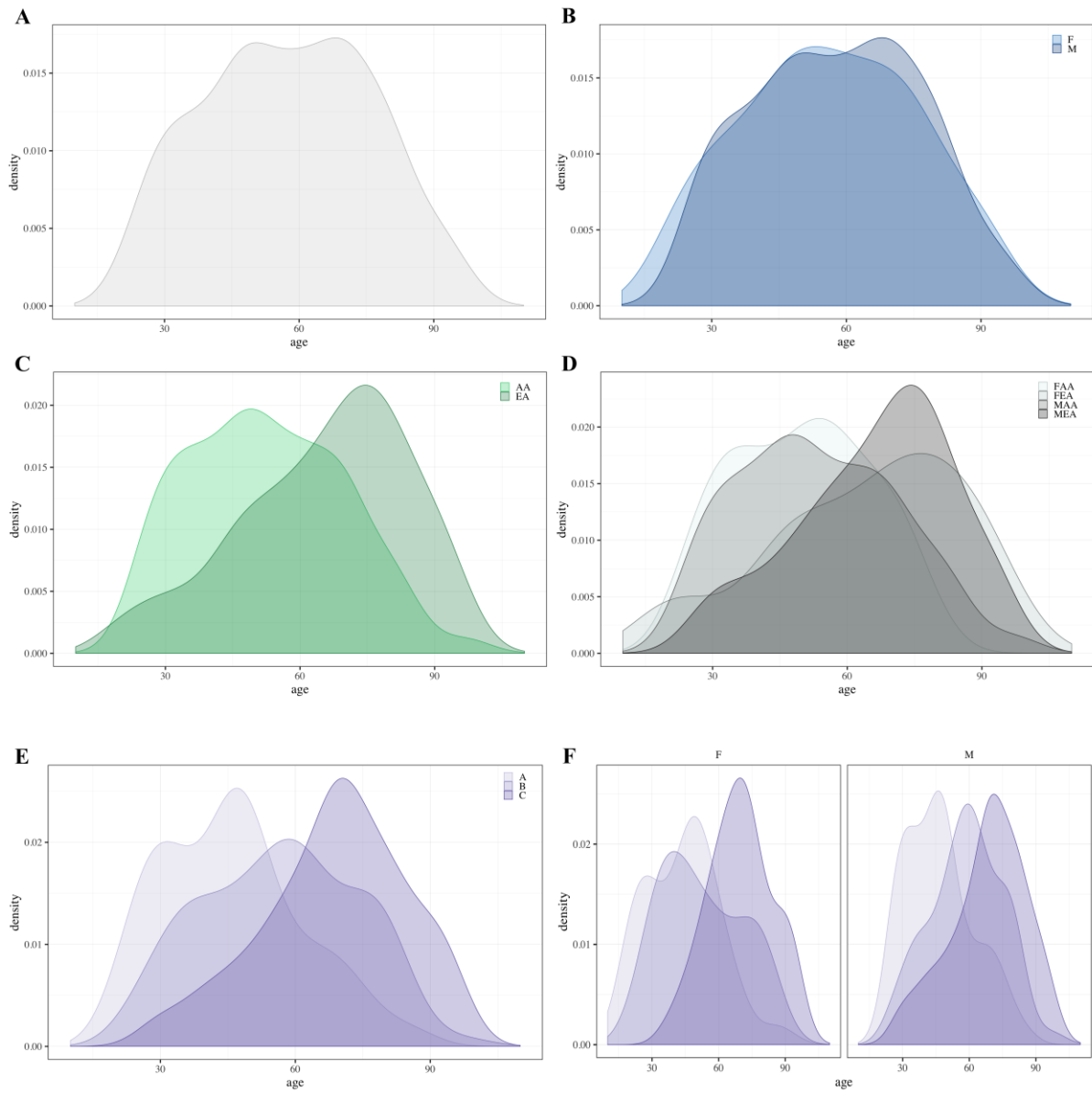
Figure E.3. Kernel density plots of age in the entire sample [A], per sex [B], per ancestry [C], per sex/ancestry [D], per dentition category only [E] or per dentition category within sex [F].
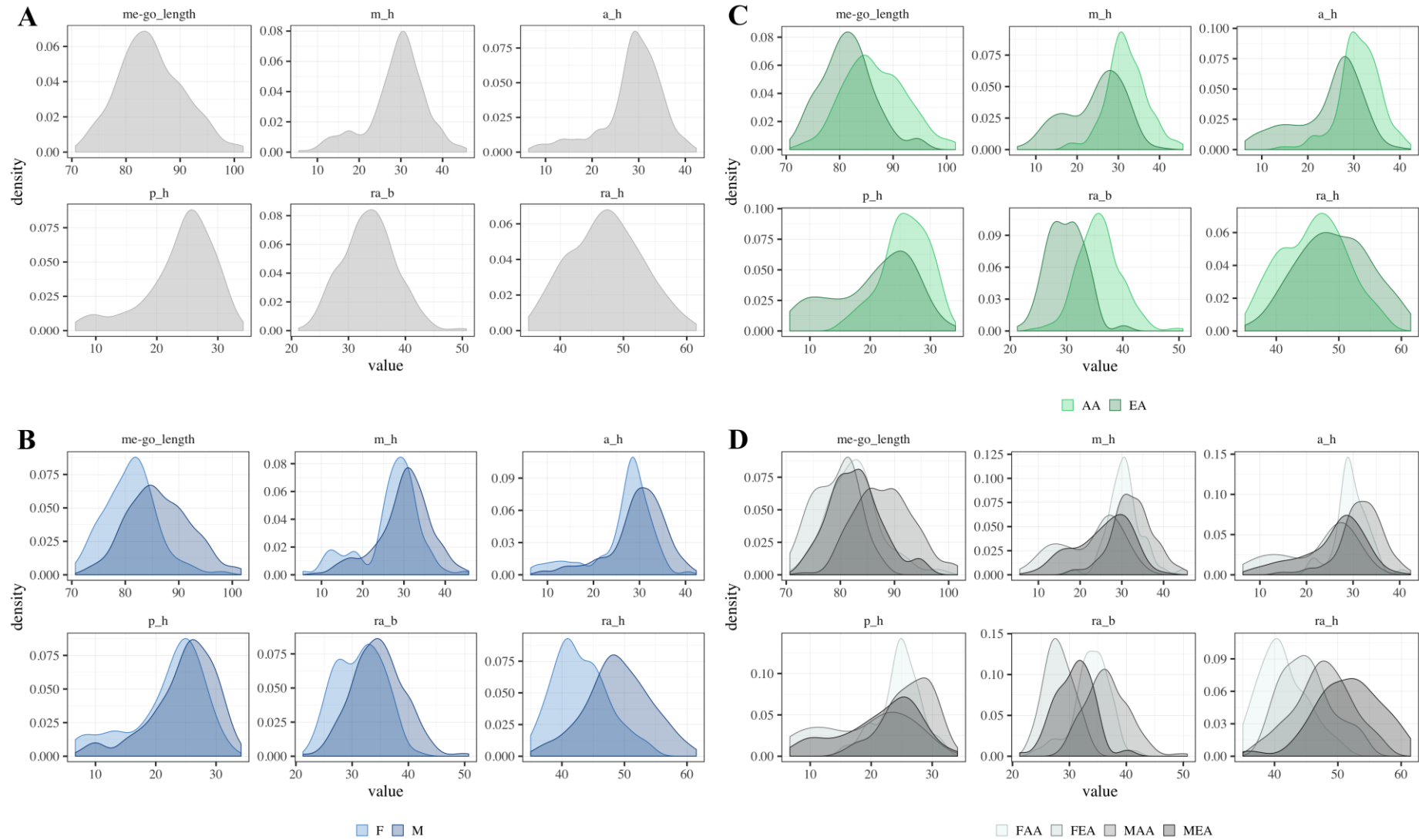
Figure E.4. Kernel density plots of the external distances in the entire sample [A], per sex [B], per ancestry [C] and per sex/ancestry [D].
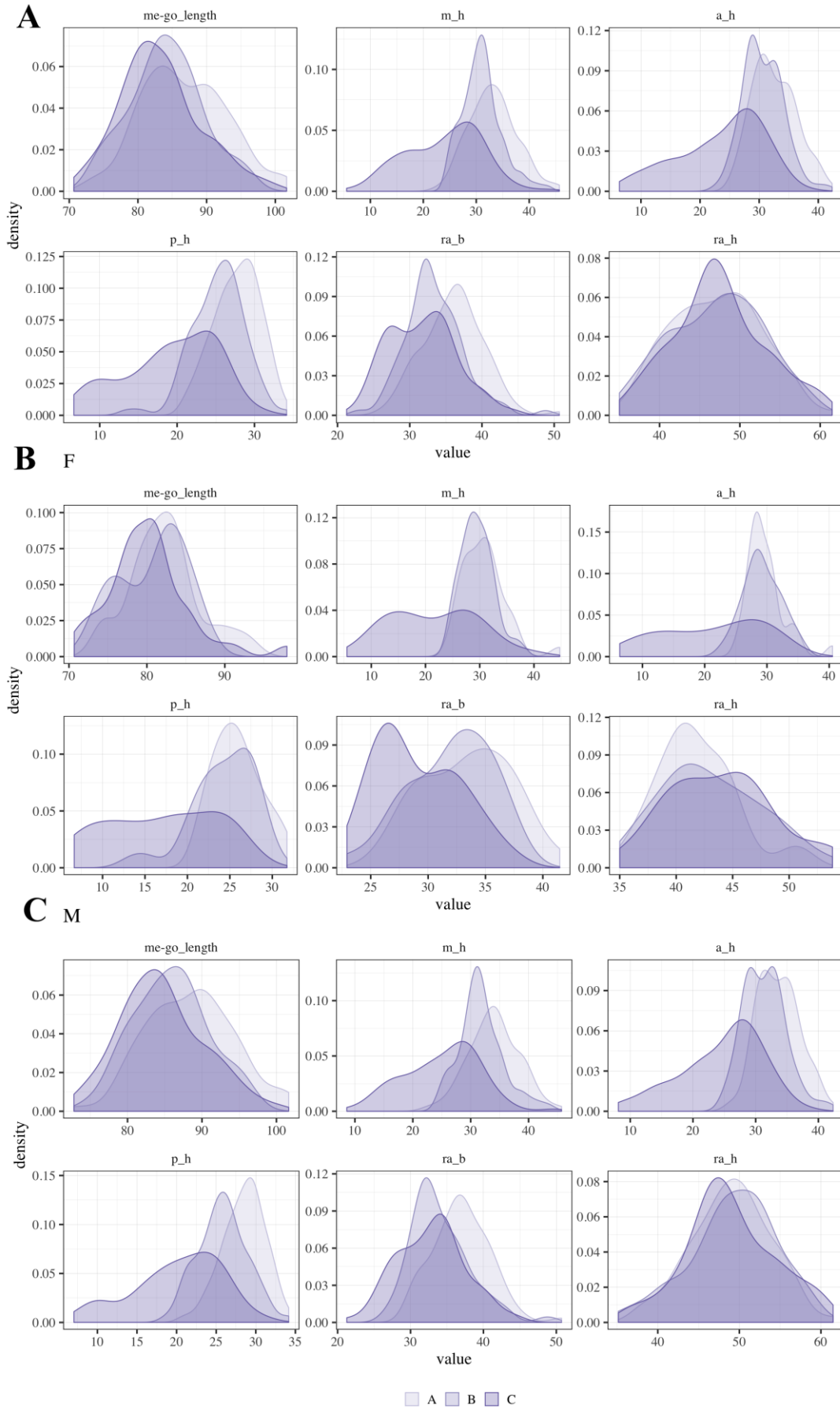
Figure E.5. Kernel density plots of the external distances in the three dentition categories (from light to dark purple) within the entire sample [A], within females [B] and within males [C].
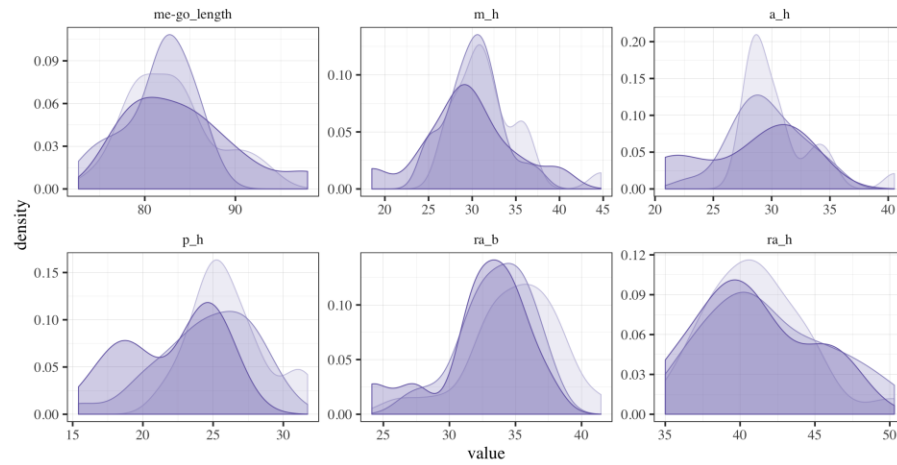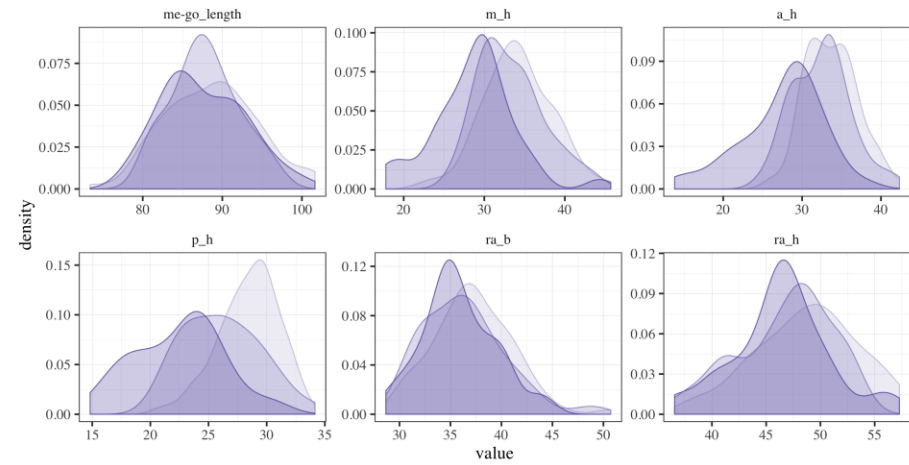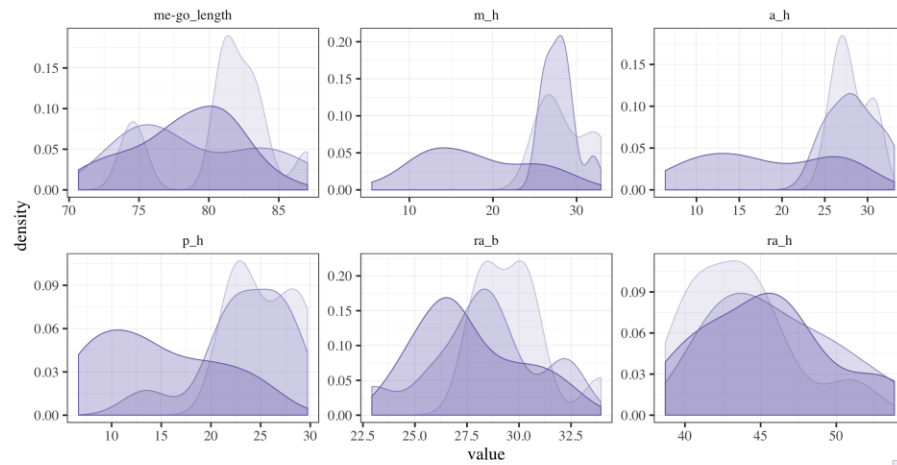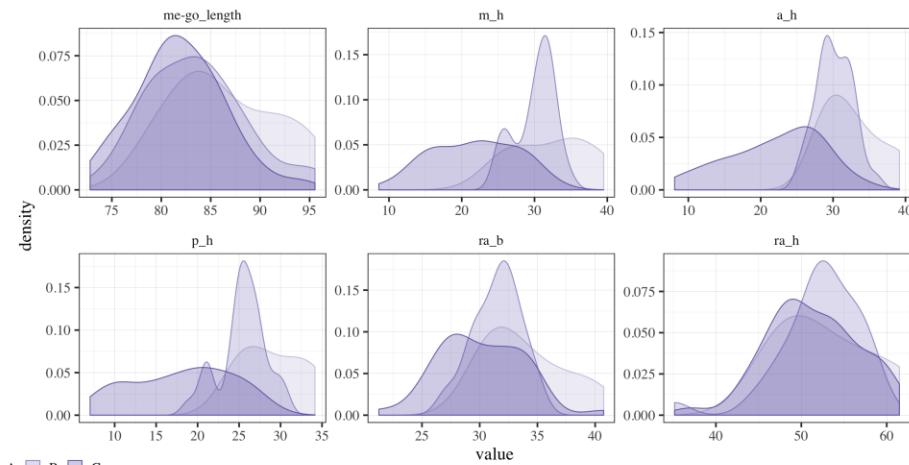
Figure E.6. Kernel density plots of the external distances in the three dentition categories (from light to dark purple) per sex/ancestry: FAA [A], FEA [B], MAA [C] and MEA [D].

Cortical thickness
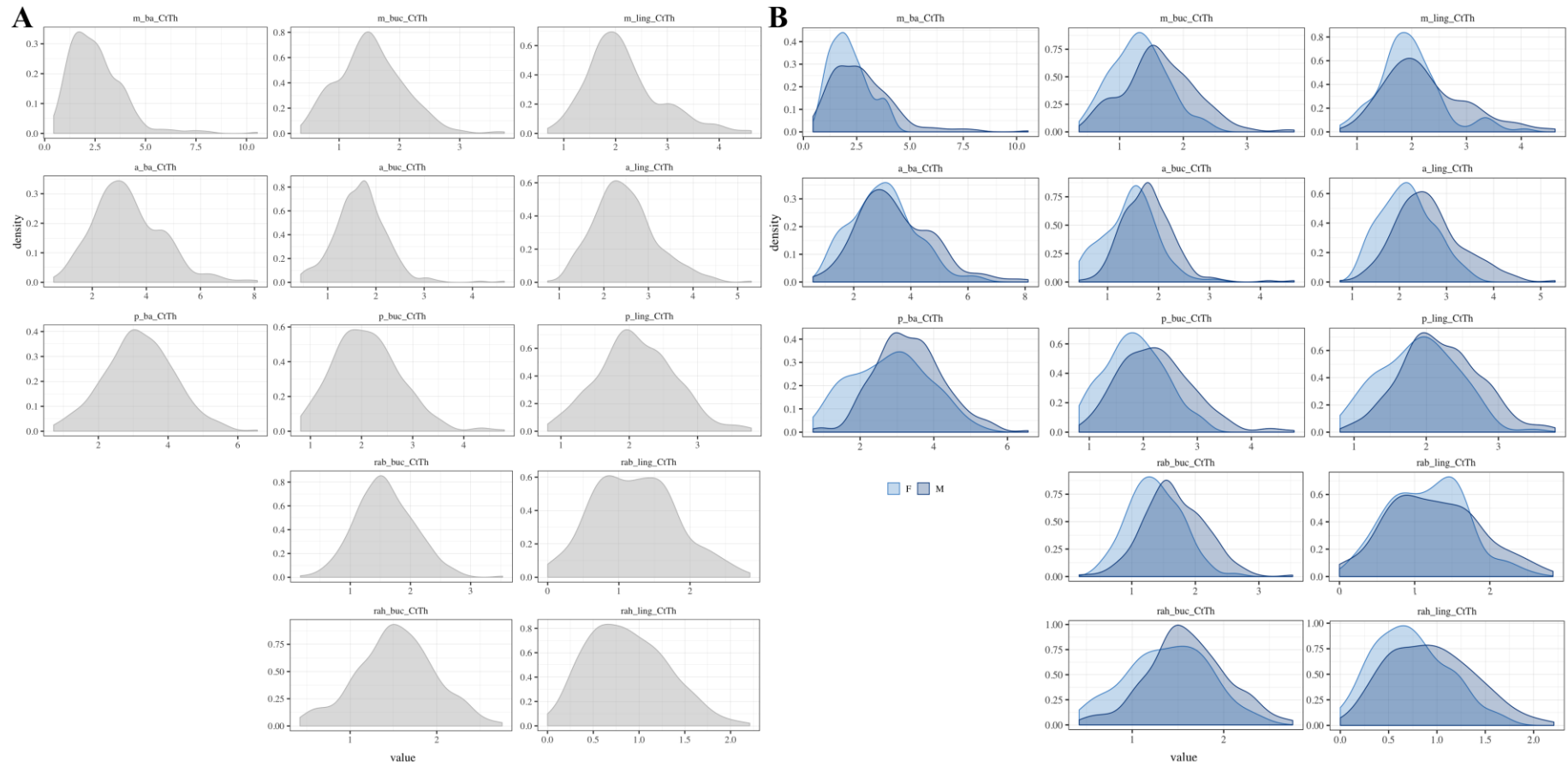
Figure E.7. Kernel density plots of the cortical thicknesses in the entire sample [A], per sex [B], per ancestry [C] and per sex/ancestry [D]. (continued on the next page)

419
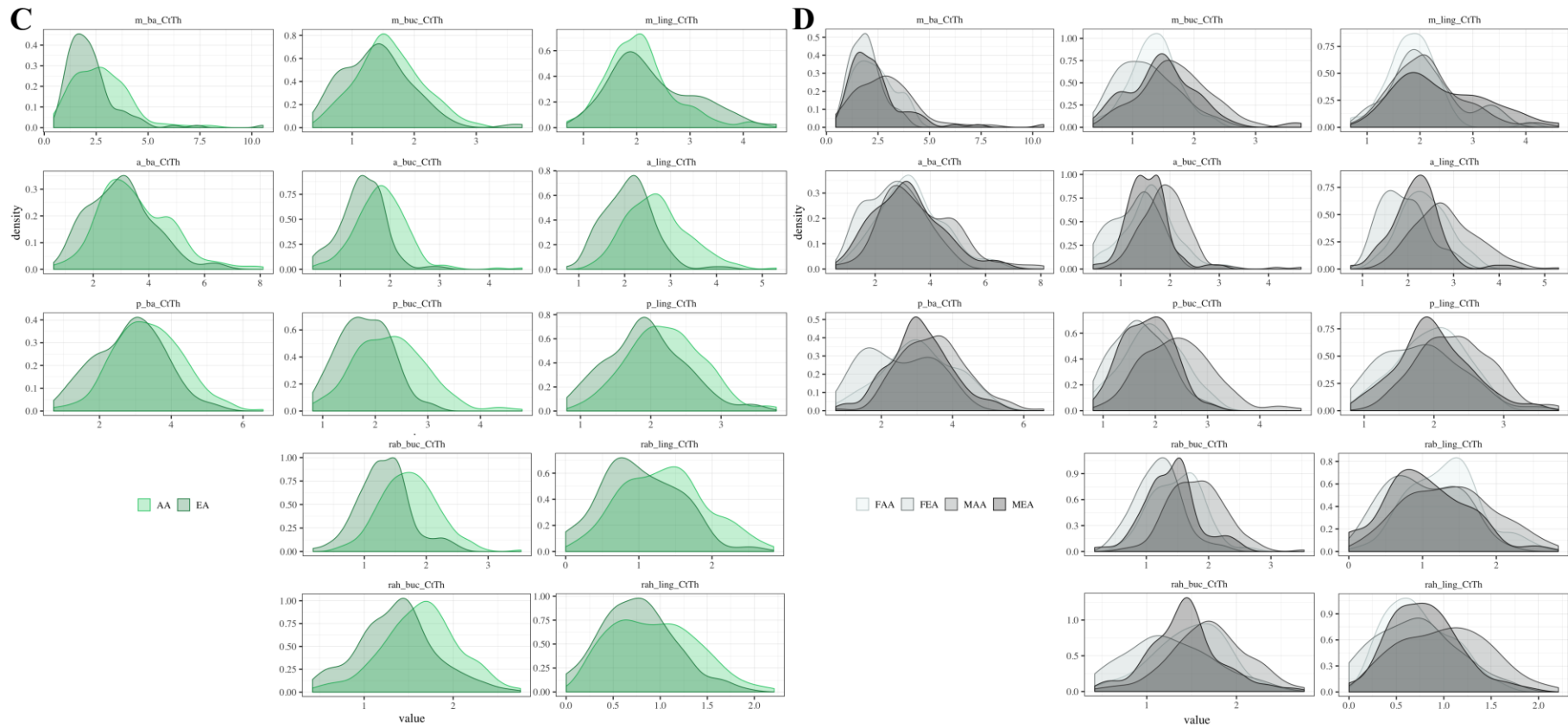
Figure E.7. (continued)
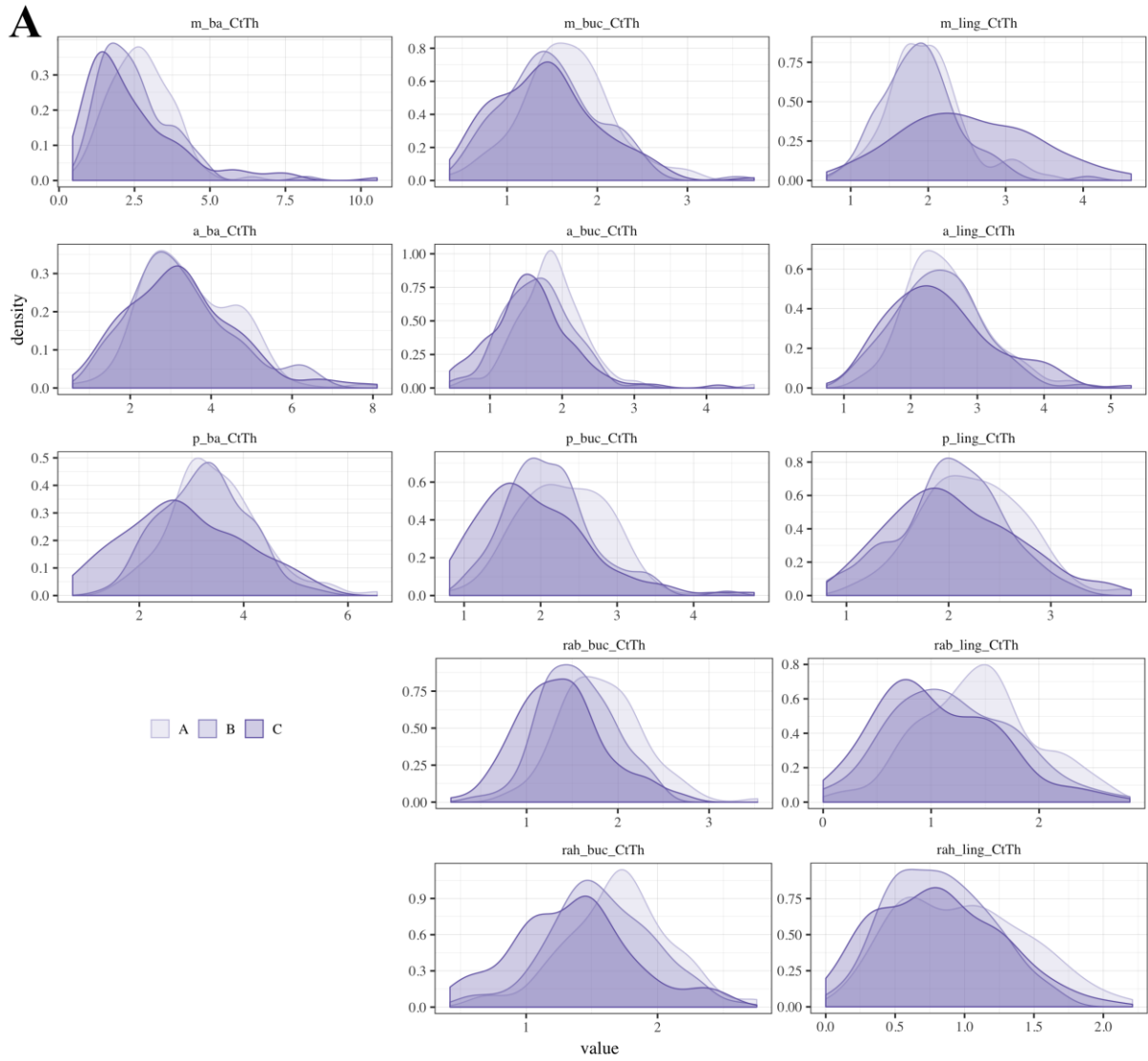
Figure E.8. Kernel density plots of the cortical thicknesses in the three dentition categories (from light to dark purple) within the entire sample [A], within females [B] and within males [C]. (continued on the next page)
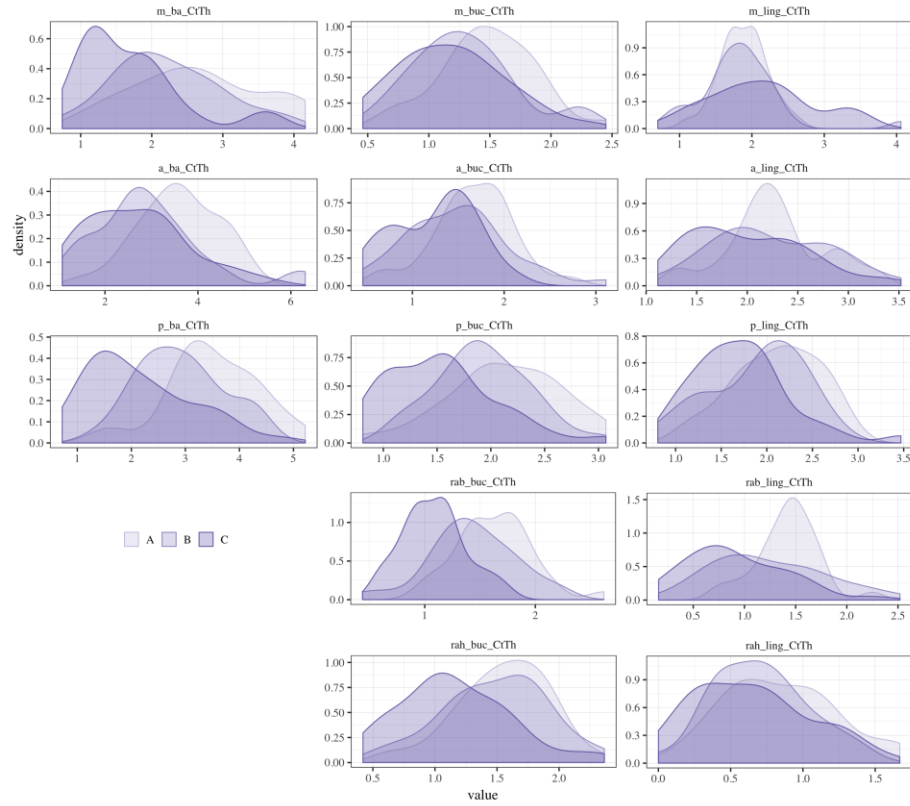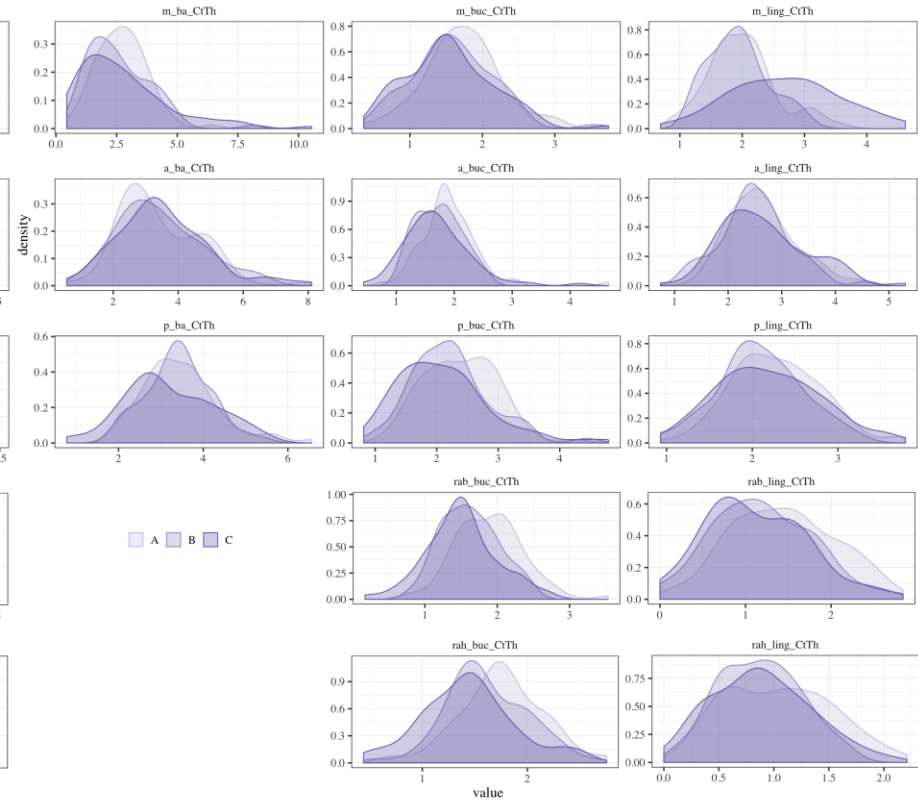
Figure E.8. (continued)
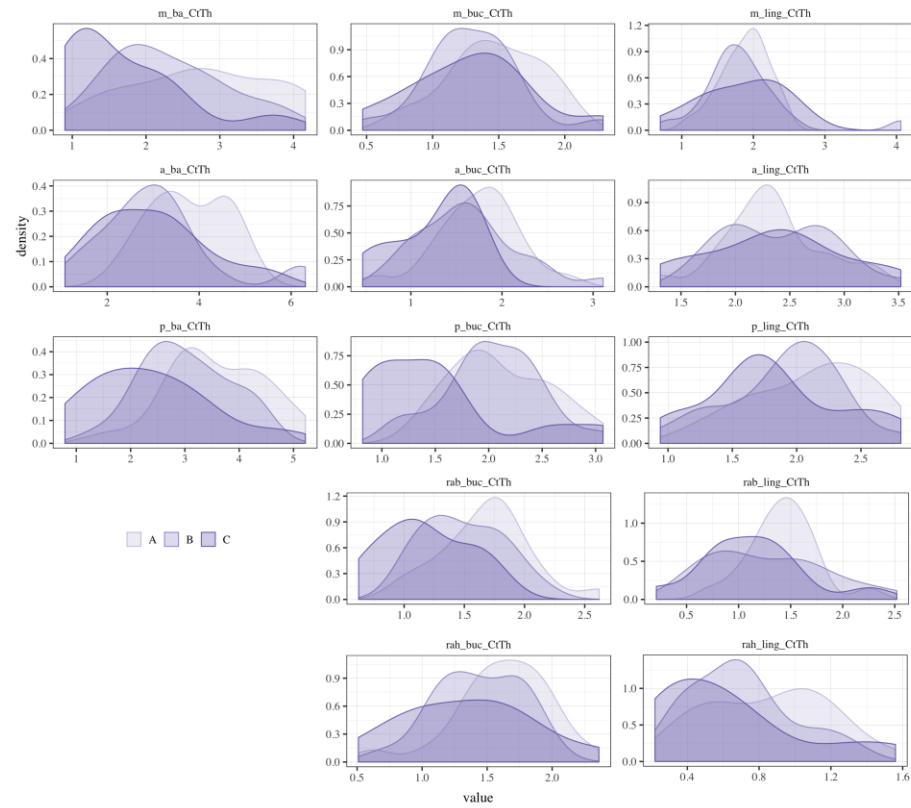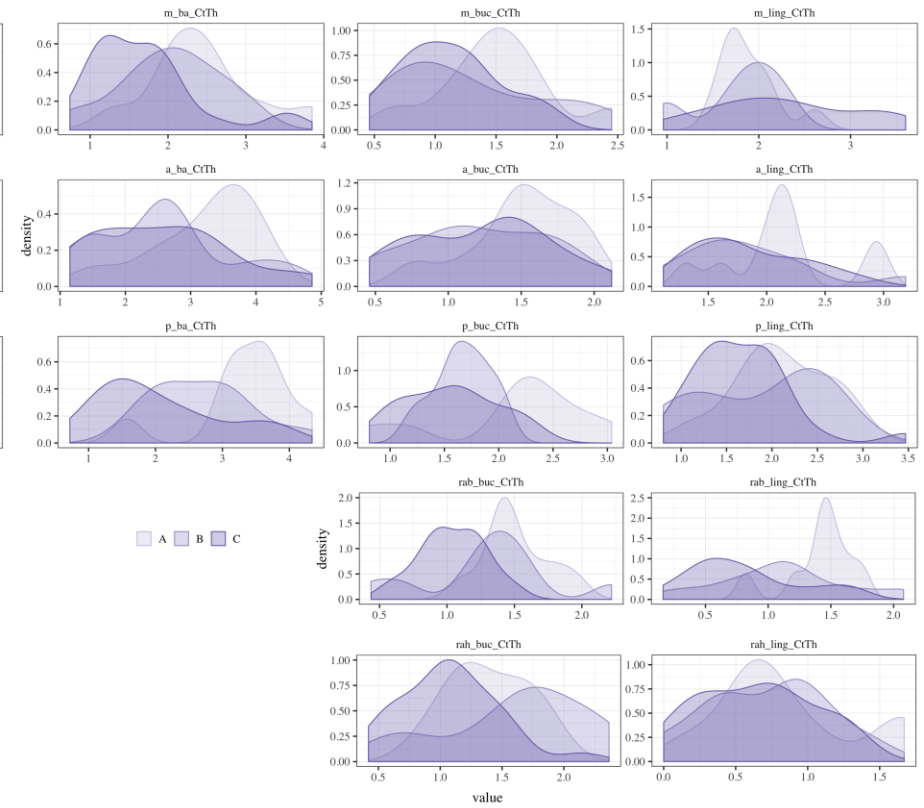
Figure E.9. Kernel density plots of the cortical thicknesses in the three dentition categories (from light to dark purple) within sex/ancestry: FAA [A], FEA [B], MAA [C] and MEA [D]. (continued on the next page)
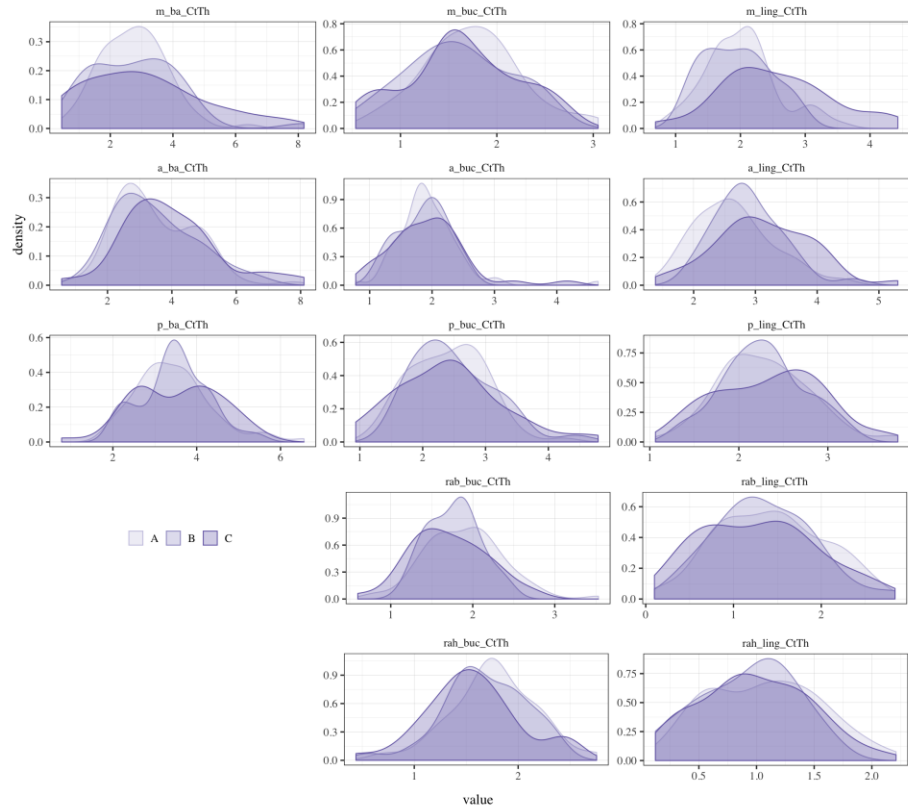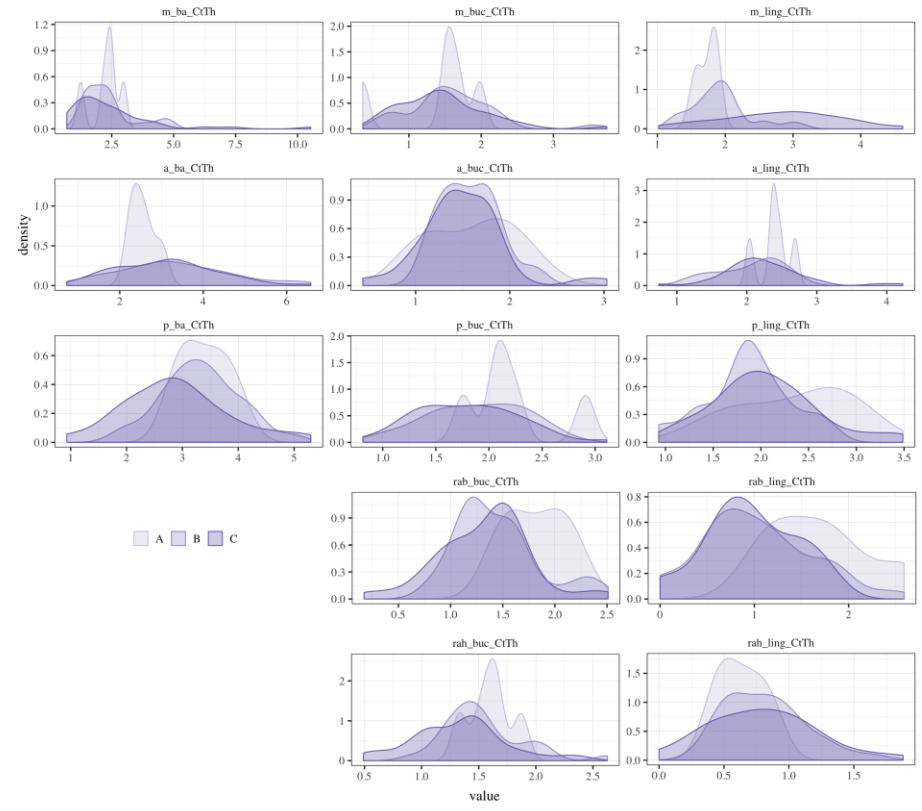
Figure E.9. (continued)

Cortical density
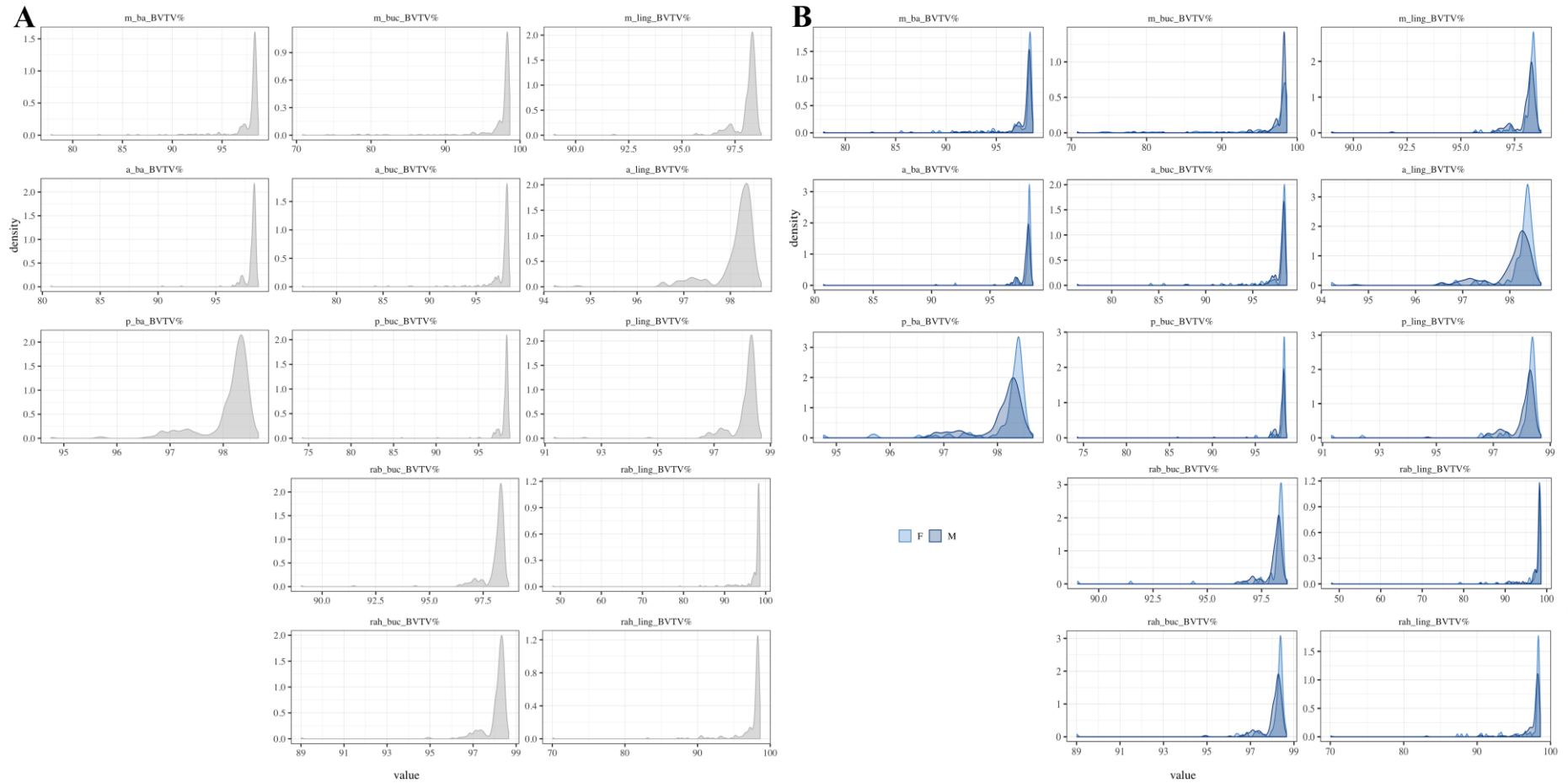
Figure E.10. Kernel density plots of the cortical BV/TV in the entire sample [A] and per sex [B].
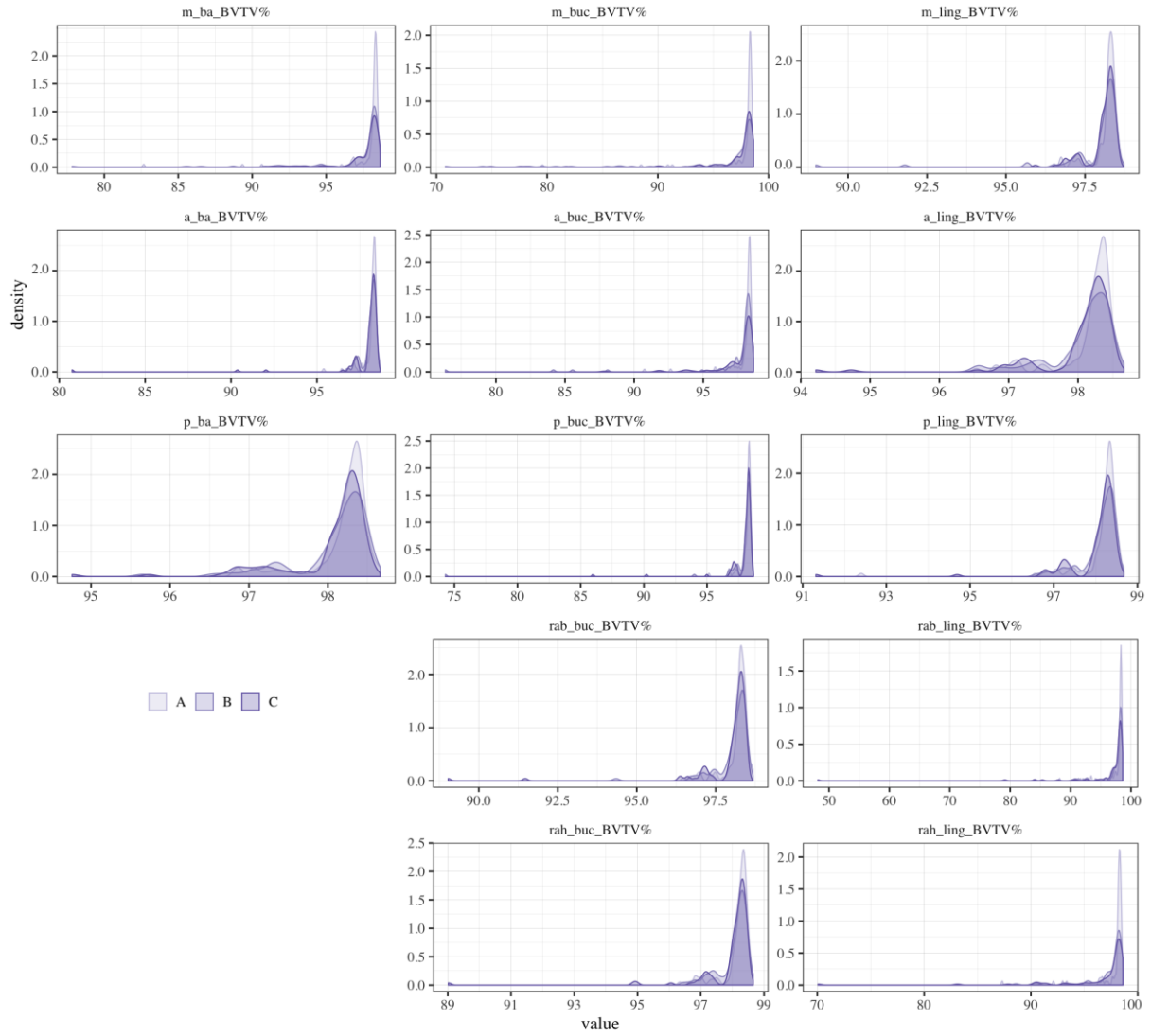
Figure E.11. Kernel density plots of the cortical BV/TV in the three dentition categories (from light to dark purple) within the entire sample.

Appendix F. Micro-CT analysis of the femur

Normality – Kernel density plots

Normality – Kernel density plots

Age

Figure F.1. Kernel density plots of age in the entire femoral sample [A], per sex [B], per ancestry [C] and per sex/ancestry [D].
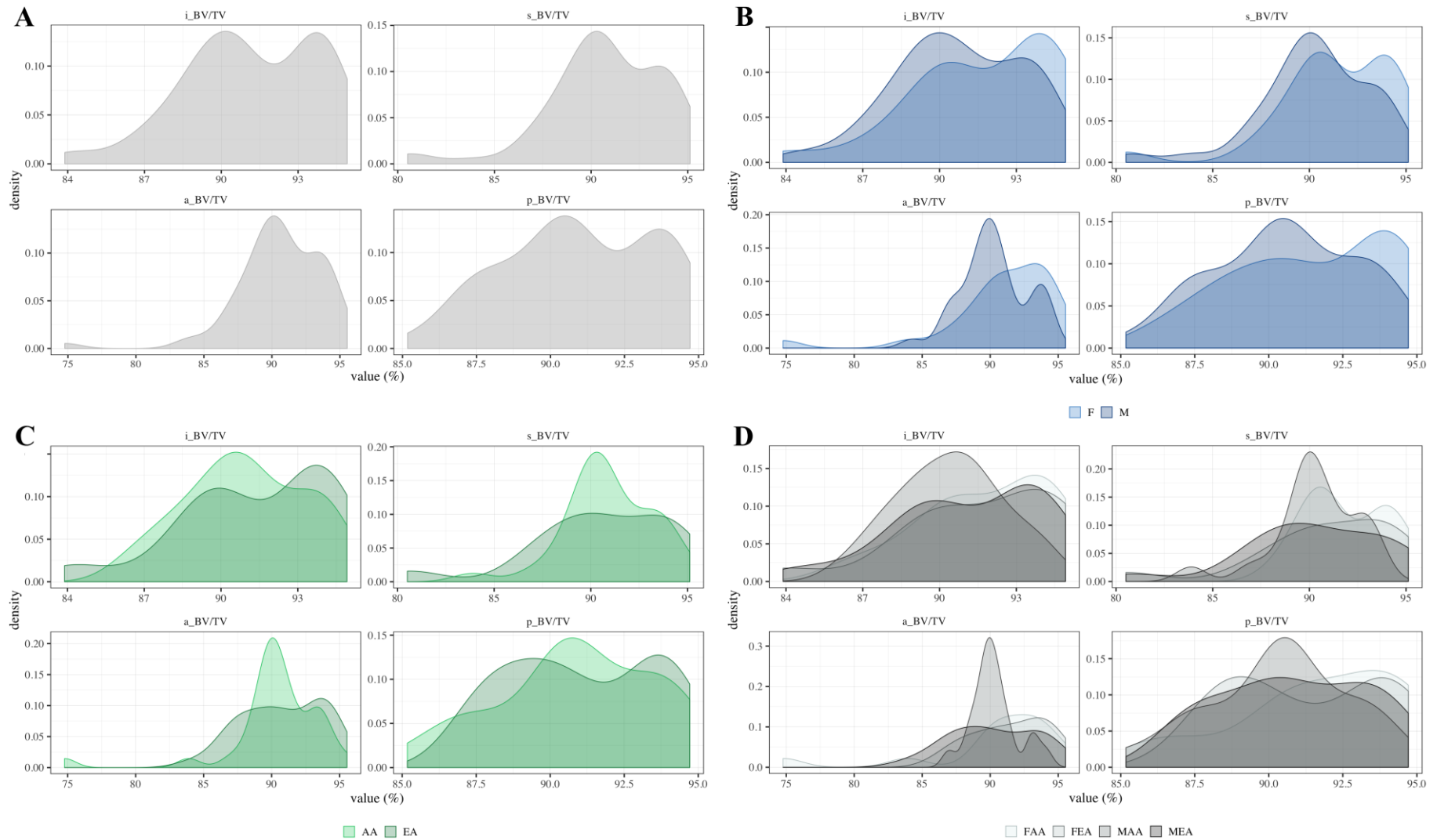
Figure F.2. Kernel density plots of the femoral cortical BV/TV in the entire sample [A], per sex [B], per ancestry [C] and per sex/ancestry [D].

Appendix G. CBCT analysis of the mandible

CBCT intra-observer agreement – Bland-Altman plots

Micro-CT vs. CBCT agreement – Bland-Altman plots

Micro-CT vs. CBCT agreement – Passing-Bablok regressions

CBCT intra-observer agreement – Bland-Altman plots

External distances

Figure G.1. Bland-Altman plots of the intra-observer agreement for the CBCT-based external distances recorded on the mandibular corpus (top): midline (m_h), anterior (a_h) and posterior (p_h) heights; and on the mandibular ramus (bottom): breadth (ra_b) and height (ra_h). 95% of the measurements are located within the upper and lower limits of agreement (red dashed lines), while the mean of differences is illustrated by the horizontal black dashed line. The vertical y-axis scale is relative to the spread of variations.

Cortical thickness
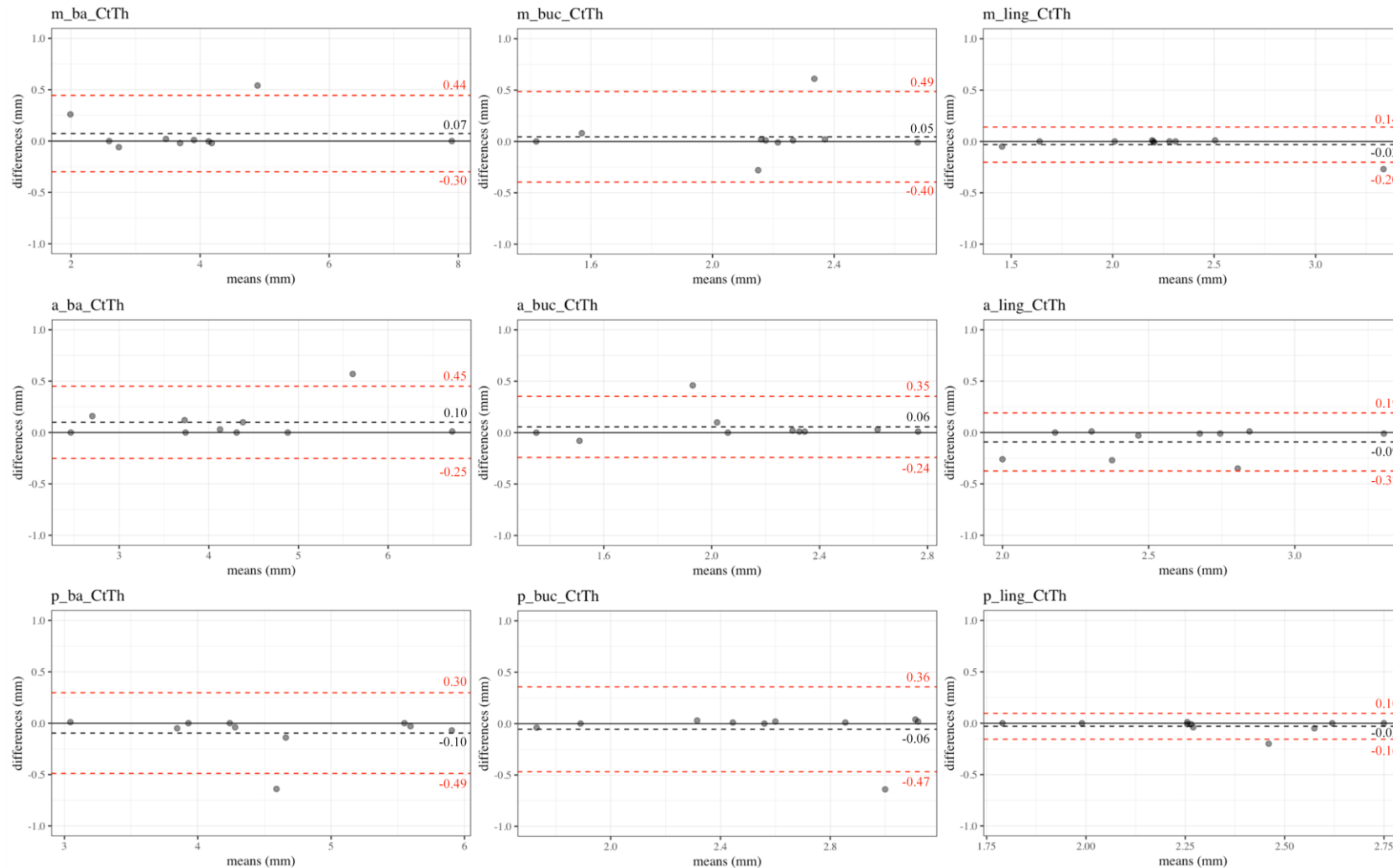

Figure G.2. Bland-Altman plots of the intra-observer agreement for the CBCT-based CtTh recorded on the midline, anterior and posterior sections, as well on the ramus breadth and height. 95% of the measurements are located within the upper and lower limits of agreement (red dashed lines), while the mean of differences is illustrated by the horizontal black dashed line. The vertical y-axis scale is relative to the spread of variations. (continued on the next page)
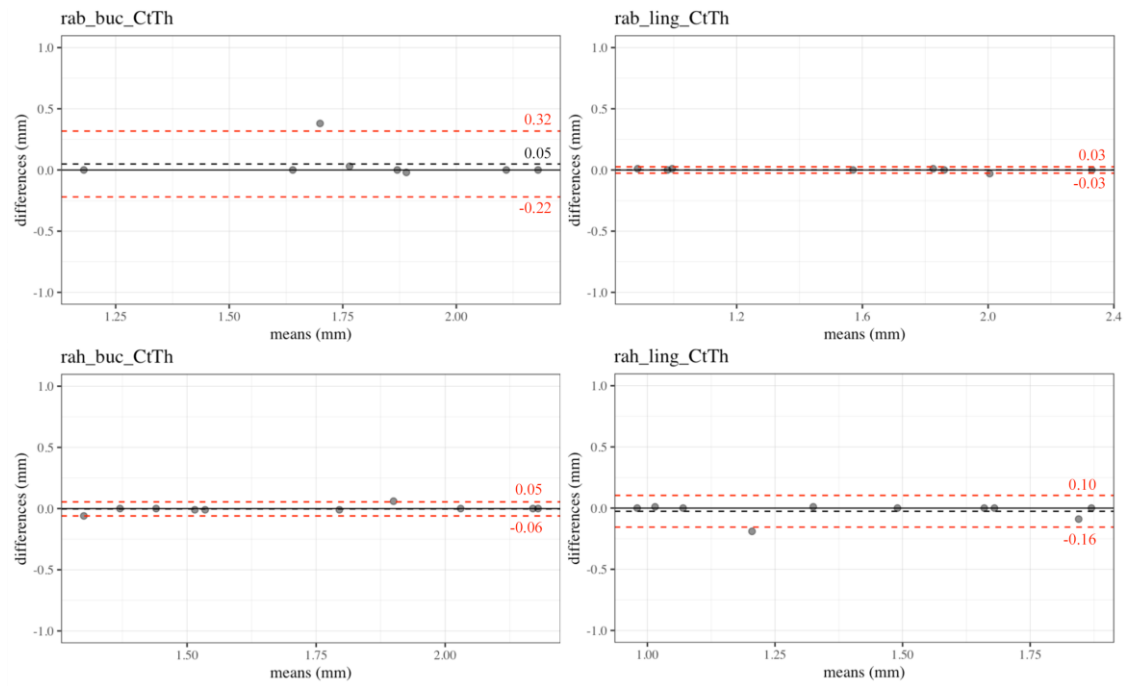
Figure G.2. (continued)

Micro-CT vs. CBCT agreement – Bland-Altman plots

Length of mandibular corpus
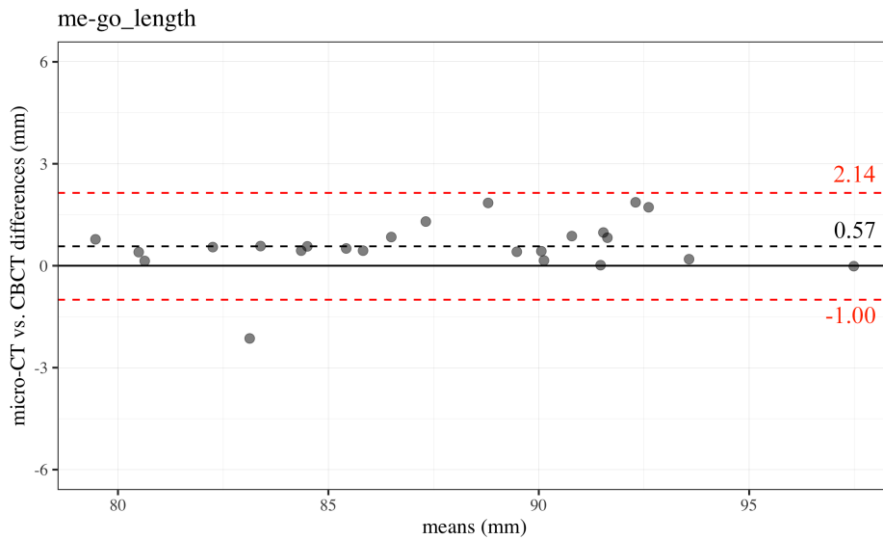
Figure G.3. Bland-Altman plot of micro-CT vs. CBCT mandibular body length. 95% of the measurements are located within the upper and lower limits of agreement (red dashed lines), while the mean of differences is illustrated by the horizontal black dashed line. The vertical y-axis scale is relative to the spread of variations.
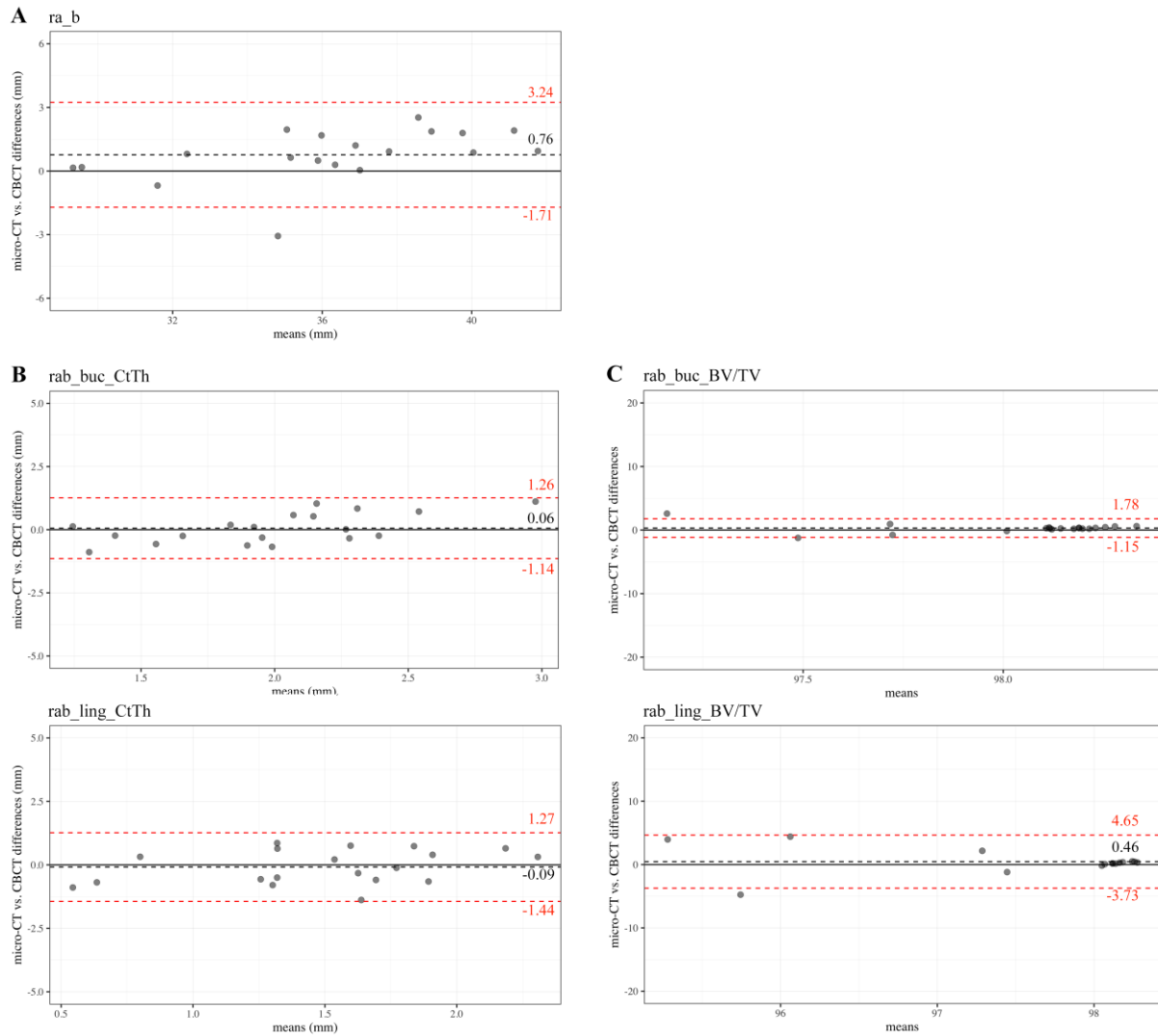
Anterior section
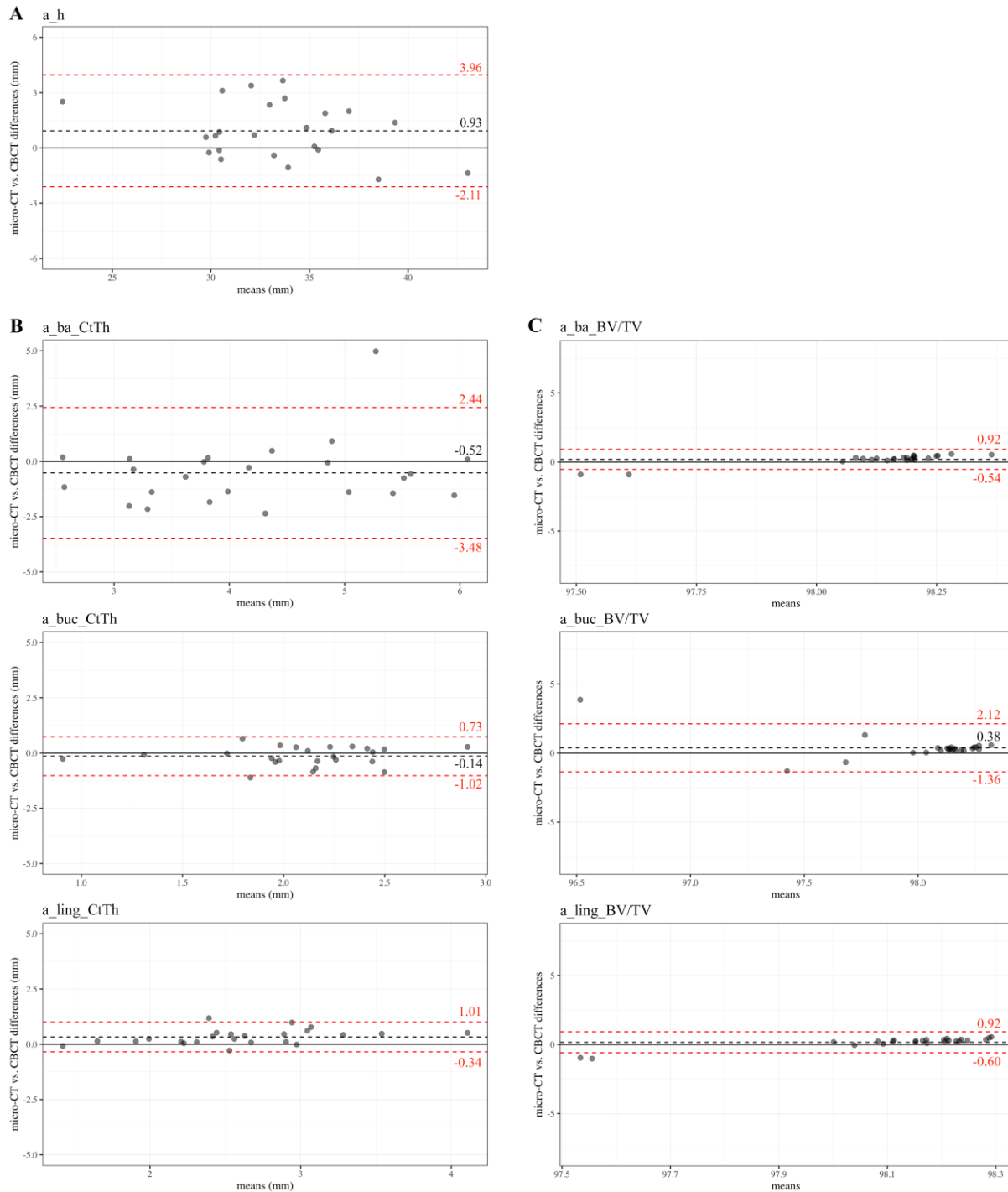
Figure G.4. Bland-Altman plots of the micro-CT vs. CBCT measurements recorded on the anterior section: alveolar height a_h [A], basal, buccal and lingual CtTh [B] and BV/TV [C]. 95% of the measurements are located within the upper and lower limits of agreement (red dashed lines), while the mean of differences is illustrated by the horizontal black dashed line. The vertical y-axis scale is relative to the spread of variations.
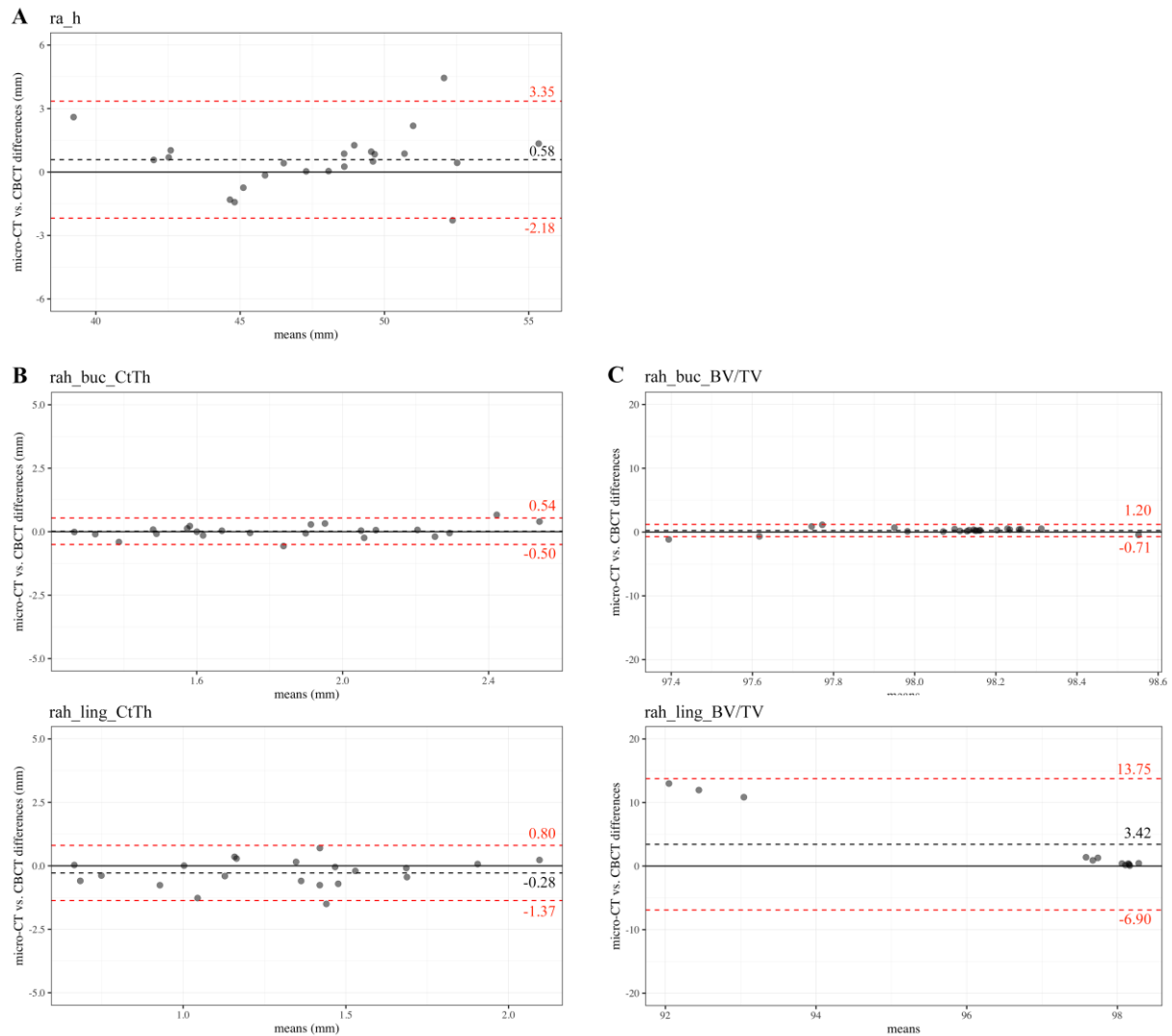
Posterior section
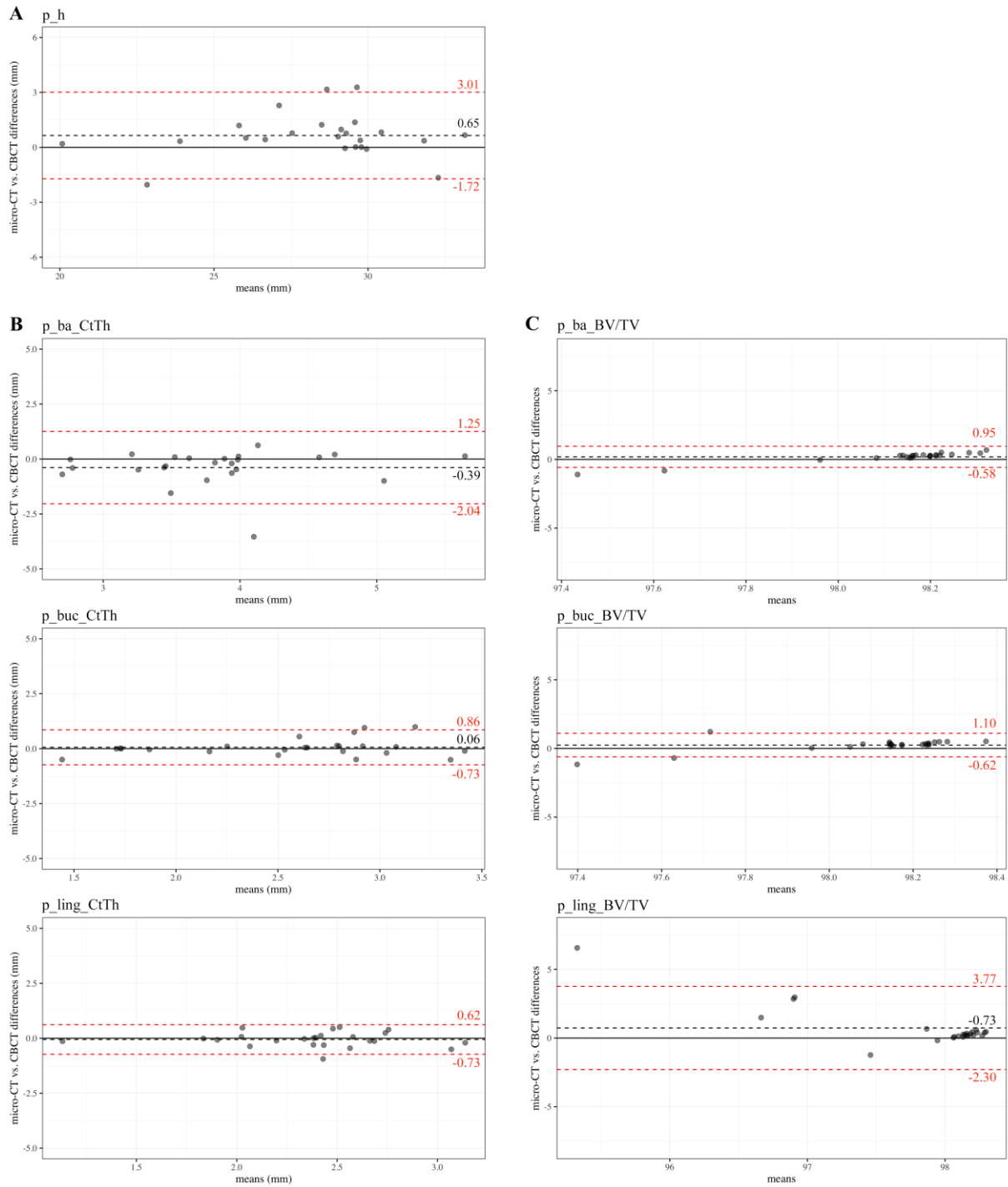
Figure G.5. Bland-Altman plots of the micro-CT vs. CBCT measurements recorded on the posterior section: alveolar height p_h [A], basal, buccal and lingual CtTh [B] and BV/TV [C]. 95% of the measurements are located within the upper and lower limits of agreement (red dashed lines), while the mean of differences is illustrated by the horizontal black dashed line. The vertical y-axis scale is relative to the spread of variations.

Ramus sections

Figure G.6. Bland-Altman plots of the micro-CT vs. CBCT measurements recorded on the ramus breadth section: breadth ra_b [A], buccal and lingual CtTh [B] and BV/TV [C]. 95% of the measurements are located within the upper and lower limits of agreement (red dashed lines), while the mean of differences is illustrated by the horizontal black dashed line. The vertical y-axis scale is relative to the spread of variations.

Figure G.7. Bland-Altman plots of the micro-CT vs. CBCT measurements recorded on the ramus height section: height ra_h [A], buccal and lingual CtTh [B] and BV/TV [C]. 95% of the measurements are located within the upper and lower limits of agreement (red dashed lines), while the mean of differences is illustrated by the horizontal black dashed line. The vertical y-axis scale is relative to the spread of variations.
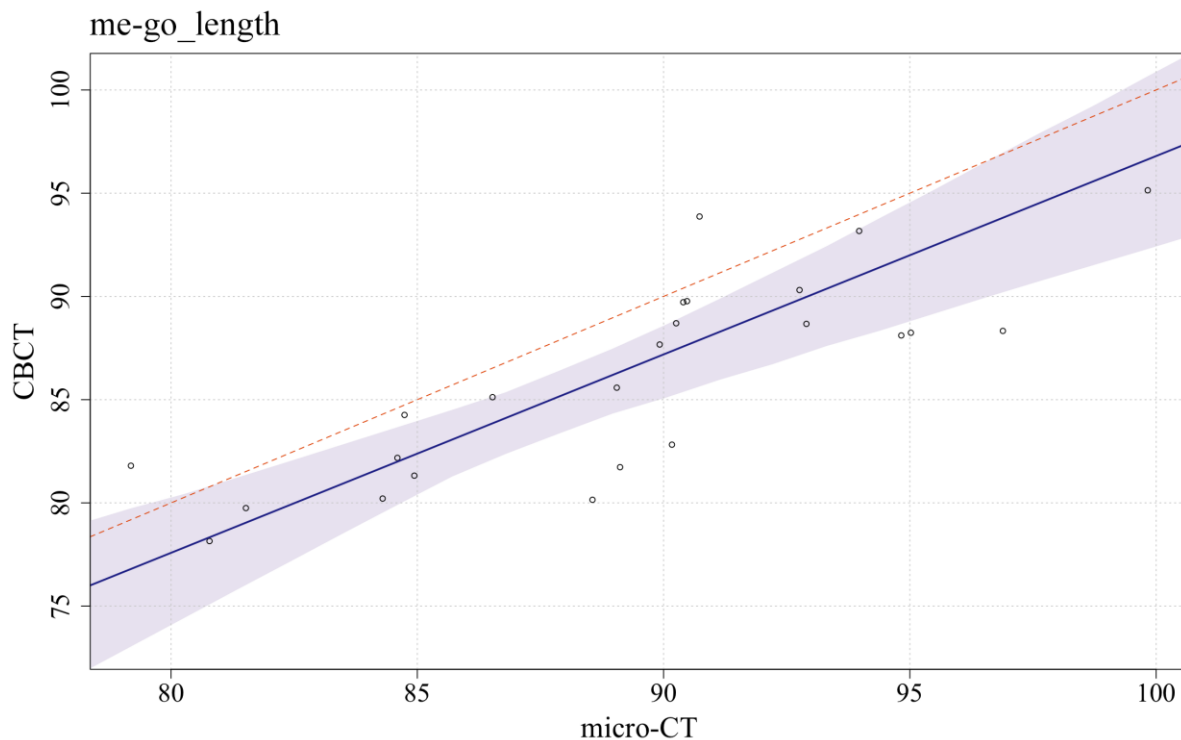
Micro-CT vs. CBCT agreement – Passing-Bablok regressions

Length of mandibular corpus

Figure G.8. Micro-CT vs. CBCT Passing-Bablok regression of the body length. Reference method (x-axis: micro-CT) is plotted against the method tested (y-axis: CBCT) with a regression line (dark purple lines), a 95% confidence area (light purple) and an identity line (x = y, red dashed lines).
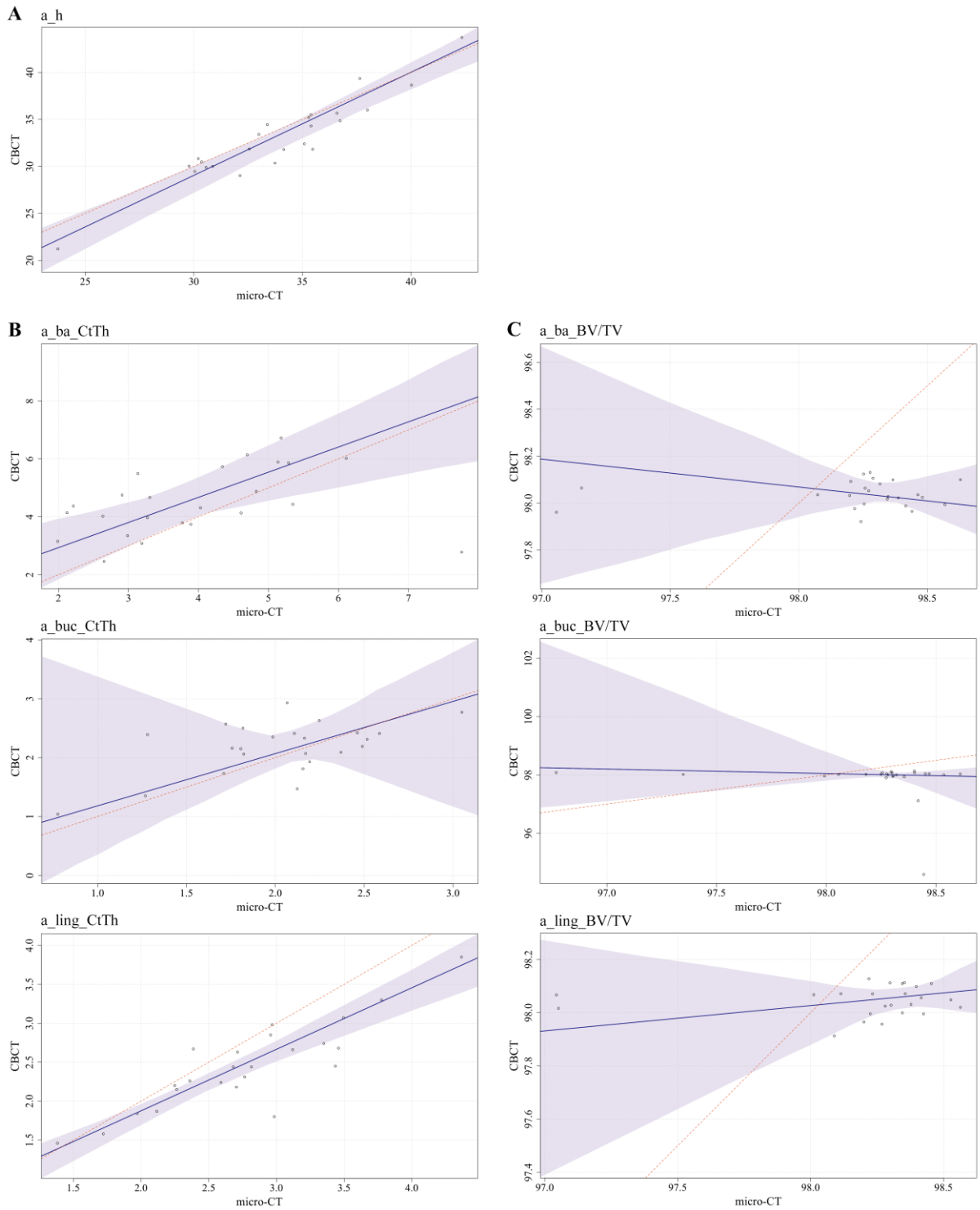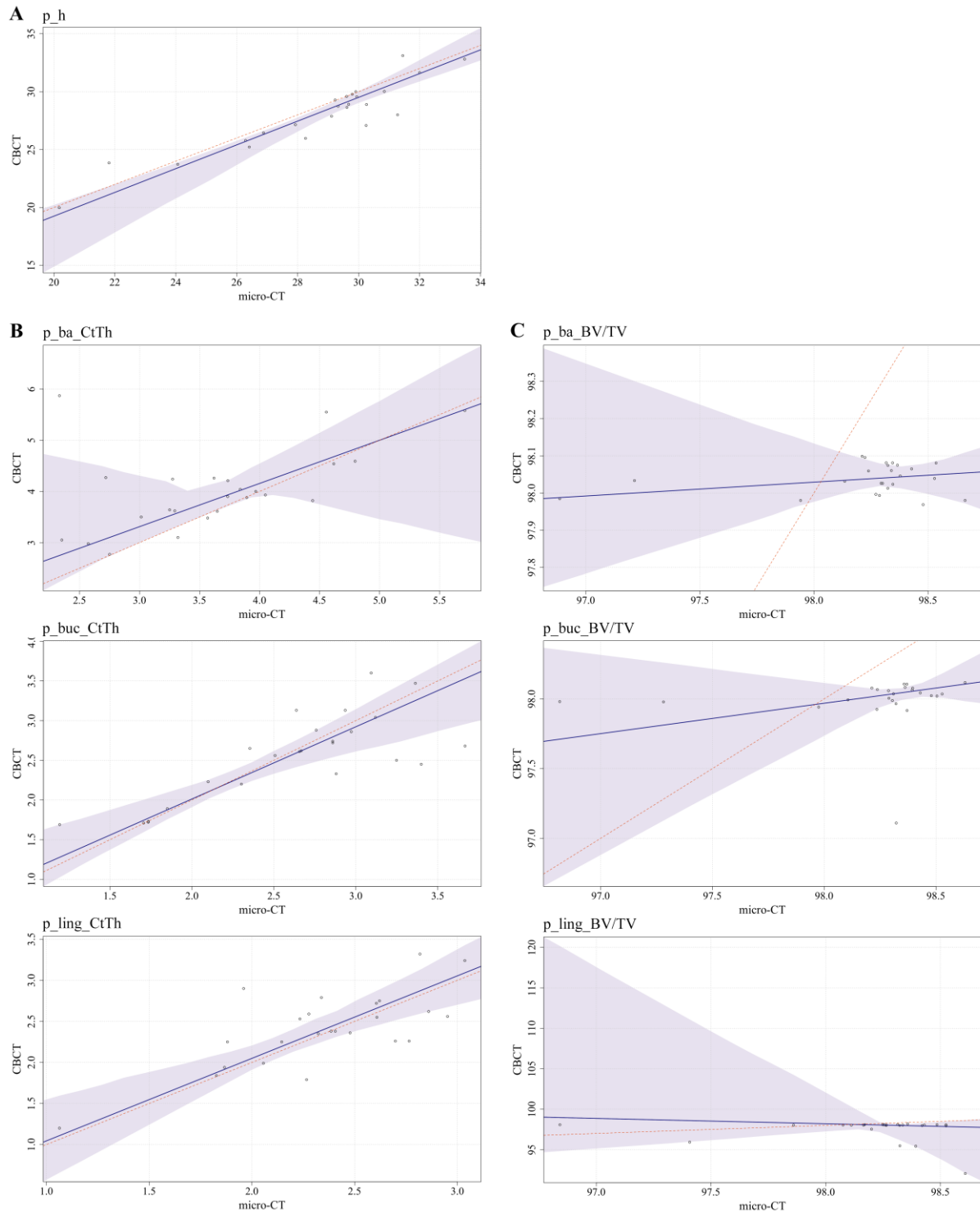
Anterior section

Figure G.9. Micro-CT vs. CBCT Passing-Bablok regressions for the measurements recorded on the anterior section: alveolar height a_h [A], basal, buccal and lingual CtTh [B] and BV/TV [C]. Reference method (x-axis: micro-CT) is plotted against the method tested (y-axis: CBCT) with a regression line (dark purple lines), a 95% confidence area (light purple) and an identity line (x = y, red dashed lines).

Posterior section

Figure G.10. Micro-CT vs. CBCT Passing-Bablok regressions for the measurements recorded on the posterior section: alveolar height p_h [A], basal, buccal and lingual CtTh [B] and BV/TV [C]. Reference method (x-axis: micro-CT) is plotted against the method tested (y-axis: CBCT) with a regression line (dark purple lines), a 95% confidence area (light purple) and an identity line (x = y, red dashed lines).
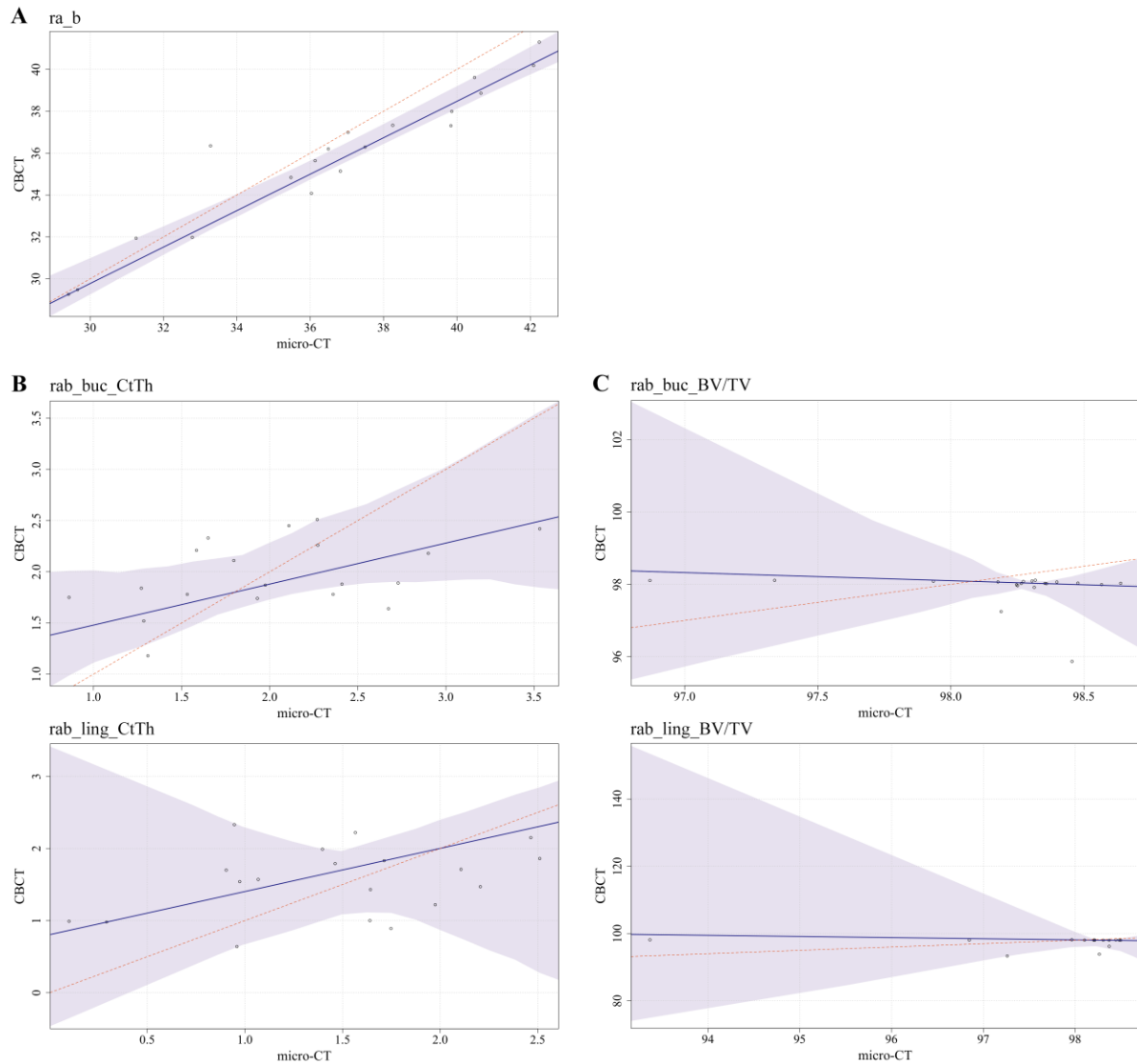
Ramus sections

Figure G.11. Micro-CT vs. CBCT Passing-Bablok regressions for the measurements recorded on the ramus breadth section: breadth [A], buccal and lingual CtTh [B] and BV/TV [C]. Reference method (x-axis: micro-CT) is plotted against the method tested (y-axis: CBCT) with a regression line (dark purple lines), a 95% confidence area (light purple) and an identity line (x = y, red dashed lines).
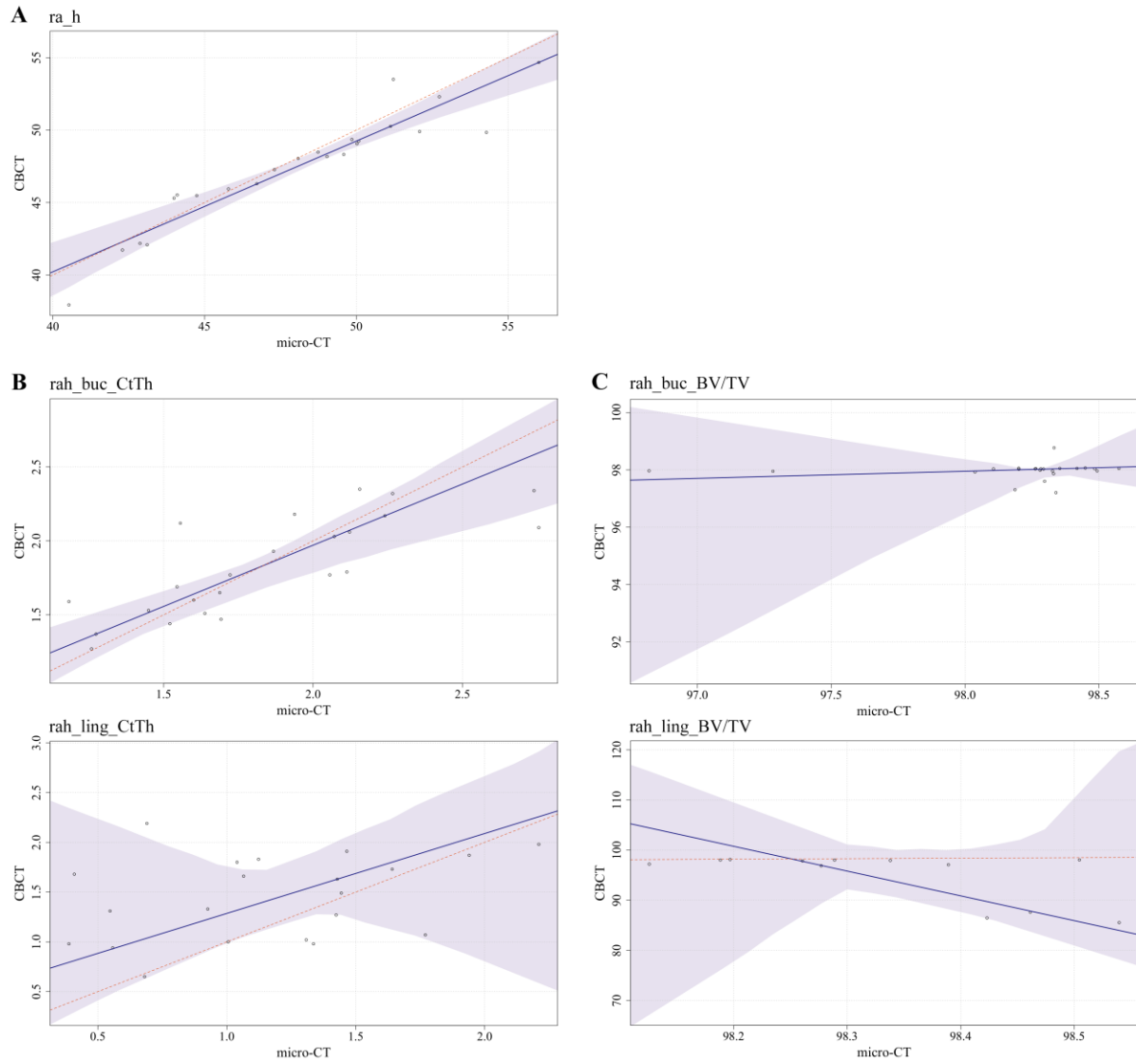
Figure G.12. Micro-CT vs. CBCT Passing-Bablok regressions for the measurements recorded on the ramus height section: height [A], buccal and lingual CtTh [B] and BV/TV [C]. Reference method (x-axis: micro-CT) is plotted against the method tested (y-axis: CBCT) with a regression line (dark purple lines), a 95% confidence area (light purple) and an identity line (x = y, red dashed lines).